

Department of Signal Processing and Acoustics

Advances and New Opportunities in MIMO Radar

Theoretical Analysis and Algorithms

Yongzhe Li

Advances and New Opportunities in MIMO Radar

Theoretical Analysis and Algorithms

Yongzhe Li

A doctoral dissertation completed for the degree of Doctor of Science (Technology) to be defended, with the permission of the Aalto University School of Electrical Engineering, at a public examination held at the lecture hall C, Main building of Aalto University on 18 October 2018 at 12:00.

Aalto University
School of Electrical Engineering
Department of Signal Processing and Acoustics
Signal Processing Group

Supervising professor

Professor Sergiy A. Vorobyov, Aalto University, Finland

Thesis advisor

Professor Sergiy A. Vorobyov, Aalto University, Finland

Preliminary examiners

Professor Yimin D. Zhang, Temple University, USA

Professor Mojtaba Soltanalian, University of Illinois at Chicago, USA

Opponents

Professor Fulvio Gini, University of Pisa, Italy

Professor Christ D. Richmond, Arizona State University, USA

Aalto University publication series

DOCTORAL DISSERTATIONS 201/2018

© 2018 Yongzhe Li

ISBN 978-952-60-8240-0 (printed)

ISBN 978-952-60-8241-7 (pdf)

ISSN 1799-4934 (printed)

ISSN 1799-4942 (pdf)

<http://urn.fi/URN:ISBN:978-952-60-8241-7>

Unigrafia Oy

Helsinki 2018

Finland

Author

Yongzhe Li

Name of the doctoral dissertation

Advances and New Opportunities in MIMO Radar

Publisher School of Electrical Engineering**Unit** Department of Signal Processing and Acoustics**Series** Aalto University publication series DOCTORAL DISSERTATIONS 201/2018**Field of research** Signal Processing Technology**Manuscript submitted** 11 June 2018**Date of the defence** 18 October 2018**Permission to publish granted (date)** 29 August 2018**Language** English **Monograph** **Article dissertation** **Essay dissertation****Abstract**

The thesis focuses on researching the multiple-input multiple-output (MIMO) radar. Particular topics are the study of ambiguity properties by exploiting transmit beamspace (TB) strategies, opportunities and challenges of clutter and jammer suppression in both the conventional and TB-based MIMO radar configurations, waveform designs ensuring good correlation properties, and joint multi-dimensional transmission and receive adaptive design guaranteeing best signal-to-interference-plus-noise ratio performance. A detailed overview of the MIMO radar research related to the above research aspects is presented, including subjects such as waveform(s)/code(s) design, clutter and jammer suppression, TB design, and parameter estimation and detection.

The TB-based MIMO radar AF which deals with the case of far-field targets and narrowband waveforms is proposed. It incorporates the effects of transmit coherent processing gain, waveform diversity, and the array geometry in its definition, and can serve as a generalized AF form for which the phased-array (PA) and conventional MIMO radar AFs are important special cases. It shows interesting relationships with the existing AF results. Furthermore, the maximum achievable "clear region" of the TB-based MIMO radar AF, which is free of sidelobes, is derived, and two limiting cases that help obtain tight bounds for the "clear region" are identified.

For addressing the clutter and jammer suppression problem, a series of reduced-dimensional (RD) spatial and/or temporal adaptive processing algorithms with reasonable complexity are developed, including the space-(fast) time adaptive processing algorithms which can maintain the cold clutter stationarity over the slow time domain, 3D space-time adaptive processing (STAP) algorithms for joint hot and cold clutter mitigation, and RD beamspace and robust beamforming techniques.

Fast and efficient algorithms for generating aperiodic unimodular waveforms with good correlation properties are also proposed. The waveform designs are based on minimizing the integrated sidelobe level (ISL) or weighted ISL (WISL) of waveforms and are formulated as nonconvex quartic optimization problems in frequency domain. By means of the majorization-minimization technique, the quartic problems are then simplified into quadratic ones, where the inherent algebraic structures in the objective functions are exploited. For the WISL minimization based design, an alternative quartic form that allows to apply the quartic-quadratic transformation is additionally derived. The developed algorithms are applicable to large-scale design problems as they have faster convergence speed and lower complexity than the state-of-the-art algorithms.

In addition, an efficient approach for jointly synthesizing the space-(slow) time transmission with unimodular waveforms and designing the receive STAP filter is proposed by means of the minorization-maximization technique. Two cases of known Doppler information and Doppler uncertainty on clutter bins are considered. The proposed algorithms demonstrate good performance with fast convergence speed and low complexity.

Keywords MIMO radar, ambiguity function, clutter and jammer suppression, waveform design**ISBN (printed)** 978-952-60-8240-0**ISBN (pdf)** 978-952-60-8241-7**ISSN (printed)** 1799-4934**ISSN (pdf)** 1799-4942**Location of publisher** Helsinki**Location of printing** Helsinki **Year** 2018**Pages** 260**urn** <http://urn.fi/URN:ISBN:978-952-60-8241-7>

To my family

Preface

The research in the thesis has been carried out at the Department of Signal Processing and Acoustics, Aalto University, Finland, which has been initially funded by China Scholarship Council (CSC) as the visiting doctoral research until March 2015 and ever since then has been fully funded by Aalto University. This work involves the careful academic guidance and strong support from my supervisor at Aalto—Prof. Sergiy A. Vorobyov. I want to express my sincere gratitude to him for his great efforts and complete trust in my research, for sharing his academic experience, and for creating opportunities and freedom of conducting research for me during the past years. I also want to thank Prof. Visa Koivunen, who has been the secondary supervisor during my research visit, for his careful guidance and participation in my early research, and for his support and kind help. I thank both of them for providing me with their strong recommendations.

The research in the thesis also involves the strong support from my Ph.D. supervisor in China—Prof. Zishu He. I want to thank him for his guidance on my previous research on radar signal processing as well as his advice and help when I was pursuing the Ph.D. degree in China and the D.Sc. degree in Finland at the same time. I also want to thank my collaborator Prof. Aboulnasr Hassanien for his professional comments on my research publications and for his strong recommendation.

I would like to thank Prof. Fulvio Gini and Prof. Christ D. Richmond for their precious time and efforts in serving as the opponents, and thank Prof. Yimin D. Zhang and Prof. Mojtaba Soltanalian for their carefully reading the thesis and providing valuable comments as the pre-examiners.

I wish to thank Yuhang Gao and Li Guo in the education office of China's

Embassy in Finland for their kind help and support in life and invitations to many receptions. I also wish to express my gratitude to Dr. Liming Deng and Hua Zheng for their kind help with the procedure of CSC scholarship and full support when they were in the education office in Finland.

I would like to say thanks to my current and former colleagues in the lab for creating wonderful work environment, for sharing culture and experience, and for their all kinds of help. In particular, I want to acknowledge Dr. Jan Oksanen, Dr. Jari Miettinen, Dr. Adriana Chis, Dr. Bica Marian, Dr. Shahab Basiri, Dr. Tuomas Aittomaki, Dr. Mikko Vehkaperä, Dr. Sachin Chaudhari, Dr. Hassan Naseri, Dr. Karthik Upadhya, Henri Hentilä, Elias Raninen, Robin Rajamäki, Emad Mozafari, Eeli Susan, Dr. Pramod Mathecken, Dr. Maarit Melvasalo, Markus Yli-Niemi, Prof. Jorma Skyttä, Prof. Esa Ollila, Prof. Taneli Riihonen, Prof. Stefan Werner, Dr. Jarmo Lunden, and Prof. Risto Wichman. Special thanks go to Prof. Zhipei Sun for his encouragement. Besides, I thank my former colleagues in China.

I want to acknowledge the financial support from Aalto Foundation, Nokia Foundation, and IEEE Signal Processing Society for their grant awards and scholarships. I especially want to thank Kati Voutilainen, Mirja Leppäharju, and Perttu Puska in Aalto ELEC Doctoral School for the help with handling doctoral study related matters.

I would like to thank all the former visiting scholars from China, Dr. Lilong Qin, Rui Gao, Yuanhao Cui, Mingyang Cao, and Dr. Weiyu Zhang, for making my time at Aalto University more enjoyable. Special thanks also go to my friends from the large Chinese student union for organizing various activities and help with finding accommodations.

I thank those people who helped me without informing me of their names.

Finally, I want to express my gratitude to all my family members and relatives. Without the support, understanding, and encouragement of them, the research at Aalto University would not have been possible.

Otaniemi, September 25, 2018,

Yongzhe Li

Contents

Preface	3
Contents	5
List of publications	9
List of symbols	11
List of abbreviations	13
1. Introduction	17
1.1 Motivation of the thesis	17
1.2 Scope and objectives of the thesis	18
1.3 Contributions of the thesis	19
1.4 Author's independent contributions	21
1.5 Structure of the thesis	22
2. Overview of MIMO radar	23
2.1 The concept of MIMO radar	23
2.2 Research on MIMO radar	26
2.2.1 Waveform(s)/code(s) design	28
2.2.2 Clutter and jammer suppression	40
2.2.3 Transmit beamforming/beamspace design	43
2.2.4 Parameter estimation and target detection	45
3. Ambiguity function of the transmit beamspace-based MIMO radar	47

3.1	Radar AF	49
3.1.1	Woodward’s AF	49
3.1.2	Conventional MIMO radar AF	51
3.2	The TB-based MIMO radar AF	53
3.2.1	Signal model	53
3.2.2	Definition, interpretation, and simplifications	54
3.2.3	Relationship with existing AFs	59
3.2.4	Significance	60
3.3	“Clear region” analysis	60
3.3.1	Worst-case bound	61
3.3.2	Best-case bound	63
3.3.3	Further analysis	63
3.4	New TB design strategy	65
4.	Spatial and/or temporal adaptive processing in clutter and jamming suppression	69
4.1	Generalized signal model	73
4.2	Jammer suppression via space-(fast) time adaptive processing in MIMO radar	76
4.2.1	Effect of matched filtering on the correlations of jamming signals	76
4.2.2	Space-(fast) time adaptive processing designs	77
4.3	Joint clutter mitigation and jammer suppression in the TB-based MIMO radar	79
4.3.1	3D STAP design	80
4.3.2	Rank analysis of the TB strategy enabled clutter	80
4.3.3	Computationally efficient 3D STAP method	83
4.4	Spatial adaptive processing for powerful jammer suppression in MIMO radar	84
4.4.1	Reduced dimensional beamspace designs	85
4.4.2	Robust beamforming designs	88
5.	Aperiodic waveform design with good correlation properties	93
5.1	Problem formulation	96

5.2	Fast unimodular waveform designs	97
5.2.1	Fast ISL minimization based design—ISLNew	98
5.2.2	Computational complexity of ISLNew	106
5.2.3	Fast WISL minimization based design—WISLNew	106
5.2.4	Computational complexity of WISLNew	114
5.2.5	Acceleration strategies	115
6.	Joint space-time transmission and adaptive receive filter design	119
6.1	Problem formulation	121
6.2	Joint SST waveform and adaptive receiver design	124
6.2.1	Case I: Known Doppler information on clutter bins	125
6.2.2	Case II: Doppler uncertainties on clutter bins	127
7.	Summary and outlook	131
	References	135
	Publications	159

List of publications

This thesis consists of an overview and of the following publications which are referred to in the text by their Roman numerals.

- I Yongzhe Li**, Sergiy A. Vorobyov and Visa Koivunen. Ambiguity function of the transmit beamspace-based MIMO radar. *IEEE Transactions on Signal Processing*, vol. 63, no. 17, pp. 4445–4457, September 2015.
- II Yongzhe Li**, Sergiy A. Vorobyov and Visa Koivunen. Generalized ambiguity function for the MIMO radar with correlated waveforms. In *IEEE International Conference on Acoustics, Speech, and Signal Processing (ICASSP)*, Florence, Italy, pp. 5302–5306, May 2014.
- III Yongzhe Li**, Sergiy A. Vorobyov and Zishu He. Terrain-scattered jammer suppression in MIMO radar using space-(fast) time adaptive processing. In *IEEE International Conference on Acoustics, Speech, and Signal Processing (ICASSP)*, Shanghai, China, pp. 3026–3030, March 2016.
- IV Yongzhe Li**, Sergiy A. Vorobyov and Zishu He. Joint hot and cold clutter mitigation in the transmit beamspace based MIMO radar. In *IEEE International Conference on Acoustics, Speech, and Signal Processing (ICASSP)*, Brisbane, Australia, pp. 2334–2338, April 2015.
- V Yongzhe Li**, Sergiy A. Vorobyov and Aboulnasr Hassanien. MIMO radar capability on powerful jammers suppression. In *IEEE International Conference on Acoustics, Speech, and Signal Processing (ICASSP)*, Brisbane, Australia, pp. 5277–5281, May 2014.
- VI Yongzhe Li**, Sergiy A. Vorobyov and Aboulnasr Hassanien. Robust

- beamforming for jammers suppression in MIMO radar. In *IEEE Radar Conference*, Cincinnati, OH, USA, pp. 0629–0634, May 2014.
- VII Yongzhe Li** and Sergiy A. Vorobyov. Fast algorithm for designing unimodular waveform(s) with good correlation properties. *IEEE Transactions on Signal Processing*, vol. 66, no. 5, pp. 1197–1212, March 2018.
- VIII Yongzhe Li** and Sergiy A. Vorobyov. Efficient single/multiple unimodular waveform design with low weighted correlations for radar. In *IEEE International Conference on Acoustics, Speech, and Signal Processing (ICASSP)*, New Orleans, LA, USA, pp. 3226–3230, March 2017.
- IX Yongzhe Li**, Sergiy A. Vorobyov and Zishu He. Design of multiple unimodular waveforms with low auto- and cross-correlations for radar via majorization-minimization. In *European Signal Processing Conference (EUSIPCO)*, Budapest, Hungary, pp. 2235–2239., August–September 2016.
- X Yongzhe Li** and Sergiy A. Vorobyov. Joint space-(slow) time transmission with unimodular waveforms and receive adaptive filter design for radar. In *IEEE International Conference on Acoustics, Speech, and Signal Processing (ICASSP)*, Calgary, AB, Canada, pp. 3276–3280, April 2018.

List of symbols

\otimes	Kronecker product
\odot	Element-wise product
$(\cdot)^*$	Conjugate operator
$(\cdot)^T$	Transpose operator
$(\cdot)^H$	Conjugate transpose operator
$ \cdot $	Modulus of a complex value
$\ \cdot\ $	Euclidean norm
$\ \cdot\ _F$	Frobenius norm of a matrix
$[\cdot]_{mi}$	The (m,i) th element of a matrix
$\lfloor \cdot \rfloor$	Floor function
\succeq	Generalized inequality between matrices
$\mathbf{1}_M$	Vector with elements all equal to one
δ_p	Kronecker delta function with respect to the index p
$\lambda_{\max}(\cdot)$	The largest eigenvalue of a matrix
$\arg(\cdot)$	Argument of a complex value
$\text{diag}\{\cdot\}$	Operator that picks up diagonal elements from a matrix and writes them into a vector (for matrix argument) or forms a diagonal matrix with main diagonal entries picked up from a vector (for vector argument)

List of symbols

\mathbf{I}_N	Identity matrix of size $N \times N$
$\max\{\cdot\}$	Maximal element of a vector
$\text{mod}(\cdot, \cdot)$	Modulo operation with the first argument being the dividend
$\text{tr}\{\mathbf{A}\}$	trace of a matrix
$\text{vec}\{\mathbf{A}\}$	Vectorization of a matrix
$\mathfrak{D}(\cdot)$	Diagonalization operator
$\mathcal{D}_p\{\cdot\}$	Operators that picks up the p th off-diagonal ($p = 0$ for the main diagonal) entries from the lower triangular part of a matrix and align them into a vector
$\mathbb{E}\{\cdot\}$	Expectation operator
$\mathcal{U}_p\{\cdot\}$	Operators that picks up the p th off-diagonal ($p = 0$ for the main diagonal) entries from the upper triangular part of a matrix and align them into a vector
$\mathcal{O}(P)$	Order of complexity
$\Re\{\cdot\}$	Real part
$\mathcal{T}\{\cdot\}$	Constructing a Hermitian Toeplitz matrix from a vector that coincides with the first column of the matrix

List of abbreviations

1D	One-dimensional
2D	Two-dimensional
3D	Three-dimensional
AF	Ambiguity function
BPSK	Binary phase shift keying
CA	Cyclic algorithm
CAD	CA-Direct
CAN	CA-New
CDMA	Code division multiple access
CPI	Coherent processing interval
CRB	Cramer-Rao bound
CSM	Cross-spectrum metric
DDMA	Doppler division multiple access
DFT	Discrete Fourier transform
DOA	Direction of arrival
DOF	Degree of freedom
ECM	Electronic counter measure

List of abbreviations

ESPRIT	Estimation of signal parameters via rotational invariance techniques
FDMA	Frequency division multiple access
FFT	Fast Fourier transform
GLRT	Generalized likelihood ratio test
GMTI	Ground moving target indication
GSC	Generalized sidelobe canceler
IFFT	Inverse fast Fourier transform
ISL	Integrated sidelobe level
JDL	Joint domain localized
KA	Knowledge aided
LFM	Linear frequency modulation
MDV	Minimum detectable velocity
MI	Mutual Information
MIMO	Multiple-input multiple-output
MMSE	Minimum mean square error
MSE	Mean square error
MVDR	Minimum variance distortionless response
MaMi	Majorization-minimization
MiMa	Minorization-maximization
OFDM	Orthogonal frequency division multiplexing
OTHR	Over-the-horizon radar
PA	Phased array
PAPR	Peak to average power ratio
PCI	Principal component inverse
PDF	Probability of density function
PRI	Pulse repetition interval

PSD	Power spectral density
PSK	Phase shift keying
QPSK	Quadrature phase shift keying
RCS	Radar cross section
RD	Reduced-dimensional
RIP	Rotational invariance property
RR	Reduced-rank
RTIR	Random target impulse response
SAR	Synthetic aperture radar
SFT	Space-fast time
SFTAP	Space-(fast) time adaptive processing
SIMO	Single-input multiple-output
SINR	Signal to interference plus noise ratio
SNR	Signal to noise ratio
SOI	Sector of interest
SQUAREM	Squared iterative method
SST	Space-(slow) time
STAP	Space time adaptive processing
TB	Transmit beamspace
TDMA	Time division multiple access
WISL	Weighted integrated sidelobe level
WeCAN	Weighted CAN

1. Introduction

1.1 Motivation of the thesis

The multiple-input multiple-output (MIMO) radar configuration has brought new opportunities for radar signal processing because of its transmit diversities [1–18]. By means of transmitting multiple mutually (quasi)-orthogonal or partially correlated waveforms with certain characteristics from colocated antenna arrays, the colocated MIMO radar is capable of gaining many benefits such as improved angular resolution, enhanced parameter identifiability, increased upper limit on the number of resolvable targets, extended aperture by virtual sensor arrays, better slow-moving target detection performance, etc. When the transmit beamforming, or equivalently, the transmit beamspace (TB) design that focuses the transmit energy within a certain spatial region of interest is enforced to MIMO radar, the advantage of enjoying both the transmit diversities and the coherent processing gains is enabled. We term the MIMO radar using TB strategies as the TB-based MIMO radar [19].

The TB-based MIMO radar motivates us to study its resolution ability and further to figure out theoretically how the TB strategies and the number of waveforms affect its resolution performance. Moreover, it motivates us to explore the effect of TB strategies on the clutter subspace and also to explore new opportunities and resolve difficulties in clutter and jammer suppression therein. After all, the coherent processing gain obtained in the TB-based MIMO radar helps only when the clutter and jammers are fully or well suppressed. Since waveforms are inevitably involved in these

issues, we are further motivated to study the topic of waveform design and also to jointly consider it with the design of the space-time adaptive processing (STAP) filter.

1.2 Scope and objectives of the thesis

The thesis focuses on investigating the TB-based MIMO radar performance from the perspective of potential delay-Doppler resolution, finding essential results and properties and therefore comparing with those of the existing radar configurations, proposing meaningful TB strategies/designs, and exploring possible clutter and jammer suppression abilities which may be unique in both the conventional and the TB-based MIMO radars. Furthermore, the thesis aims at studying the design of fast-time or space-(slow) time waveforms in order to facilitate both the conventional and TB-based MIMO radars in dealing with clutter and jammer suppression as well as other applications.

The main objectives of the thesis are summarized as follows.

1. We resort to the tool of ambiguity function (AF) and aim at defining a proper AF for the TB-based MIMO radar configuration. The further goal is to analyze the maximum achievable “clear region” of the defined AF that is free of sidelobes. On the basis of the AF defined for the TB-based MIMO radar, we also seek to devise meaningful TB strategies/designs that lead to good AF sidelobe levels.
2. We seek to find potential opportunities as well as possibly unique abilities of conventional and TB-based the MIMO radars for the purpose of clutter and/or jammer suppression. In particular, the goal is to develop spatial and/or temporal techniques/algorithms which save the computational burden and meanwhile lead to good performance.
3. We aim to design aperiodic unimodular waveforms with good correlation properties, so that the range sidelobe effect can be reduced to the minimum and the clutter and jammer suppression performance can therefore be improved. Consequently, the major interest here is to develop fast and efficient algorithms especially for the case when the

waveform design problem grows to a large scale as the code length and the number of waveforms become large.

4. We also seek to jointly design the space-(slow) time transmission with unimodular waveforms and the receive adaptive filter for MIMO radar. The main objective is to properly design the space-(slow) time waveforms that best match the STAP filter enforced at the receive end, so that the maximum signal-to-interference-plus-noise ratio (SINR) at the output of the STAP filter can be guaranteed. Accordingly, efficient algorithms which shows low computational complexity and have fast convergence speed are required to be devised.

1.3 Contributions of the thesis

The main contributions of the thesis are as follows.

1. On top of Publications I–X included in the thesis, an overview on the MIMO radar research, including the relevant topics that the thesis focuses on, is provided. The overview covers the research of subjects such as waveform design, clutter and jammer suppression, transmit beamforming or TB design, target detection and parameter estimation, etc., in which the corresponding techniques are carefully classified and reviewed. In addition, the newly emerging directions related to the topics reviewed are presented and analyzed with comments.

The corresponding overview is given in Chapter 2.

2. The AF of the TB-based MIMO radar, named as the TB-based MIMO radar AF, for the case of far-field targets and narrow-band waveforms has been proposed, derived, and studied in Publications I and II. The newly defined TB-based MIMO radar AF incorporates the effects of transmit coherent processing gain, waveform diversity, and array geometry. It can serve as a generalized AF form for which the phased-array (PA) and conventional MIMO radar AFs are important special cases. Moreover, it has interesting relationships with the existing AF results including the Woodward's AF and the AFs for conventional PA and MIMO radars. By the identification of two limiting cases

for the TB-based MIMO radar AF, its maximum achievable “clear region” in delay-Doppler domain has been analyzed and has been proved to be in between of the bounds for the two cases. The bound on the “clear region” for the worst case is inversely proportional to the number of transmitted waveforms, while the bound for the best case is independent of that number. In addition, a new TB design based on the TB-based MIMO radar AF has been proposed.

The corresponding results are summarized in Chapter 3.

3. The capability of both the conventional and the TB-based MIMO radars on clutter and jammer suppression has been investigated, and a series of spatial and/or temporal techniques and relevant algorithms have been developed in Publications III–VI. Specifically, two space-(fast) time adaptive processing (SFTAP) algorithms that maintain the stationarity of cold clutter over the slow-time domain have been devised in Publication III for addressing the terrain-scattered jammer suppression problem in conventional MIMO radar, wherein the correlation function of the match-filtered jamming components at the receive end has also been derived. The joint hot and cold clutter mitigation problem in the context of the TB-based MIMO radar has been studied in Publication IV, wherein a three-dimensional (3D) STAP algorithm on the basis of the rank analysis has been developed. Besides, the possibly unique capability of MIMO radar on jammer suppression using spatial processing techniques has been studied in Publications V and VI, wherein reduced-dimensional (RD) beamspace and/or beamforming designs have been developed, with the byproduct of power estimates of interfering sources also obtained.

The corresponding results are summarized in Chapter 4.

4. The aperiodic unimodular waveform design problem with consideration on minimizing the integrated sidelobe level (ISL) and/or weighted ISL (WISL) of waveforms for MIMO radar has been studied in Publications VII–IX, wherein a series of efficient algorithms with fast convergence speed and low computational complexity have been developed. The ISL and WISL minimization based waveform designs are formulated as nonconvex quartic optimization problems and transformed into the frequency domain. By means of the majorization-

minimization (MaMi) technique, the quartic problems are then simplified into quadratic forms, wherein the inherent algebraic structures in the objective functions of these problems are explored and consequently exploited. For the WISL minimization based design problem, an alternative quartic form that allows to apply the quartic-quadratic transformation is additionally derived. The key technical contribution is to design advanced majorization functions which lead to fast convergence speed of the algorithms for generating unimodular waveforms with good correlation properties. A closed-form solution is computed in each iterative procedure of the developed algorithms.

The corresponding results are summarized in Chapter 5.

5. The problem of jointly designing the space-(slow) time (SST) transmission with unimodular waveforms and receive adaptive filter for MIMO radar has been explored in Publication X, wherein an efficient approach to synthesizing the unimodular SST waveforms and the minimum variance distortionless response (MVDR) type receive filter has been proposed. The joint design deals with two cases of known Doppler information and in the presence of Doppler uncertainties on clutter bins, which has been formulated as nonconvex optimization problems. The key technical contribution here is to design proper minorization functions for the formulated composite objectives of the problems, which enable us to solve the joint design problem by means of the minorization-maximization (MiMa) technique with iterative procedures. A closed-form solution is computed in each iterative procedure of the developed algorithms.

The corresponding results are summarized in Chapter 6.

1.4 Author's independent contributions

The main results of the thesis have been published in two journal articles in IEEE TRANSACTIONS ON SIGNAL PROCESSING and eight conference papers (including six publications in IEEE INTERNATIONAL CONFERENCE ON ACOUSTICS, SPEECH AND SIGNAL PROCESSING (ICASSP), and two invited publications in IEEE RADAR CONFERENCE and EUROPEAN SIG-

NAL PROCESSING CONFERENCE (EUSIPCO)). The author of the thesis is responsible for the theoretical studies, algorithm developments, numerical results, and writing the drafts of all the publications included in the thesis (Publications I–X). The co-authors helped with planning the research and revising the publications.

1.5 Structure of the thesis

The thesis consists of seven chapters, which summarize the contributions of ten original publications attached at the end of the thesis (Publications I–X). The attached publications include the original theory, methods and relevant algorithms, and results that are presented in the thesis. The rest of the thesis is organized as follows. In Chapter 2, a detailed overview of the MIMO radar research, including the key concepts and history of MIMO radar and the research (until very recent) on waveform design, clutter and jammer suppression, transmit beamforming or TB design, target detection and parameter estimation, etc., is presented. In Chapter 3, the results on the TB-based MIMO radar AF are presented. In Chapter 4, the spatial and/or temporal processing techniques and relevant algorithms for the clutter and jammer suppression in conventional and TB-based MIMO radars are summarized. The results on aperiodic unimodular waveform design with good correlation properties are presented in Chapter 5, and the results on joint SST transmission and receive adaptive filter design are presented in Chapter 6. Finally, the conclusions of the thesis are given in Chapter 7.

2. Overview of MIMO radar

2.1 The concept of MIMO radar

MIMO radar employs multiple transmit and receive antenna arrays [1–3], with which it emits multiple waveforms or codes at the transmitter and performs a match-filtered or some other processing of the observed echoes at the receiver. In this radar configuration, the transmitted waveforms are normally desired to be mutually orthogonal for any time lag [20], or to have a certain level of partial correlations between each other [5].

The idea of “MIMO” in radar signal processing originates from the development of the “MIMO” technique in communications in the 1990s. In wireless communications [21, 22], “MIMO” enables increased spectral efficiency (i.e., the total number of transmitted information bits per second per Hertz) for a fixed total transmit power, through the use of methods such as space-time coding. Once the channel information is known or estimated from channel observations, the objective in MIMO communications is to adaptively adjust the transmit strategy to improve its throughput performance. By introducing such an idea to radar and letting the radar operate in a “MIMO” configuration, from the perspective of waveform diversity, the concept of MIMO radar emerged.

MIMO communication also overcomes the problem of sensitivity to fading by means of transmitting different streams of information from several decorrelated transmitters. Differing from the conventional single-input-single-output (SISO) communication system that transmits all the energy over a single communication path, MIMO communication allows to exploit

the spatial diversity because signals from different transmitters undergo independent fading, and thus the signal-to-noise ratio (SNR) at the receiver for MIMO communication system does not depend dramatically on the fading in individual channels. Motivated by the spatial diversity idea exploited in MIMO communications, the very early MIMO radar concept has been proposed to overcome target scintillations through decorrelated transmissions.

It is commonly known that the target in radar signal processing is characterized by the radar cross section (RCS) function. For some targets such as the extended ones, their RCS can vary rapidly and significantly due to small changes in the observation angles. Such RCS scintillation leads to signal fading and degrades the radar detection and estimation performance dramatically. To tackle this problem, the idea for MIMO radar consists of placing its transmit antennas in a widely distributed manner, which ensures independent transmission from each antenna. The received signal in MIMO radar is a superposition of the independently faded signals, whose average SNR is therefore approximately constant.

In essence, the transmitted codes in MIMO communications are unknown, but the channels are known or can be estimated. Therefore, the objective of MIMO communications is to extract the transmitted signal from the received observations. In contrast, the emitted waveforms are known in MIMO radar, but the probing environment such as the presence of clutter and jamming signals is typically unknown. The objective of MIMO radar is then to extract the information of potential targets from the received signals. For both MIMO communications and MIMO radar, the common feature is that particular transmit scheme has to be utilized to complete the aforementioned tasks. When it comes to MIMO radar signal processing, the specific goals turn out to be obtaining improved target detection performance [7], enhanced parameter identifiability [9], better angular resolution [2], extended array aperture [23], to name a few.

The earliest protocol of MIMO radar is the *Synthetic pulse and Antenna Radar* (called RIAS in [24]) developed by ONERA in the 1990s. The RIAS radar exploits a sparse circular antenna array for pulse transmission and feeds each elementary antenna with a specific signal. By means of forming multiple beams at the receiver, it can fulfill the goals of omni-directional

long-range air searching and target tracking. It has a low probability of interception because of isotropic radiations. Moreover, it takes advantage of the conventional beamforming techniques to benefit from the radar coherent processing gain. In short, the presence of the RIAS radar has accelerated the emergence of MIMO radar.

The earliest classification of MIMO radar was in terms of the arrangement of antenna arrays, and it divides MIMO radar into two categories [1, ch. 2]. The first category uses widely separated antennas and is termed as statistical MIMO radar (also called distributed MIMO radar) [14], while the second category uses colocated antennas and is termed as coherent MIMO radar (also called colocated MIMO radar) [9].

In statistical MIMO radar, different transmitters and receivers are located at different positions within a certain predefined area, making the observation angles of the target for each transmitter and receiver different from those for the others. This MIMO radar regime aims at obtaining the aforementioned spatial diversity, with the key idea of angular spreading through distributed allocation of both transmit and receive antennas. The echoes received at different receivers then become statistically independent. Both coherent and non-coherent processing can be applied to statistical MIMO radar, and the latter processing is not restricted by synchronizations.

In coherent MIMO radar, the transmit and receive antenna arrays are colocated and share an identical angle of the target in the far field. Judging from the way of antenna allocation, the colocated MIMO radar regime does not differ from conventional radars, and it also allows separating transmit and receive arrays into sub-arrays. However, the waveform diversity exploited by MIMO radar distinguishes it from conventional radars and brings the benefit of generating extra degrees of freedom (DOFs). It potentially leads to superiorities over the conventional radars in terms of many aspects, such as angular resolution, parameter identifiability, clutter and jammer suppression, array aperture, etc. Many signal processing techniques that have been developed in conventional radars, including beamforming and coherent processing techniques, are still valid and can be easily applied to colocated MIMO radar.

From the perspective of radiating and receiving sites, statistical MIMO

radar can be viewed as a generic multistatic radar, while coherent MIMO radar can be considered as a generic monostatic radar. With more findings on MIMO radar, many other classifications have appeared, depending on the aspects of interest. For example, MIMO radars can be divided into narrow-band and wide-band MIMO radars [25, 26] in terms of the bandwidth, conventional and hybrid phased-MIMO radars [17, 27] in terms of the way of transmission, and MIMO synthetic aperture radar (SAR) [28], MIMO over-the-horizon radar (OTHR) [29], and other types of MIMO radars in terms of different applications.

2.2 Research on MIMO radar

MIMO radar has attracted significant interest over the past decade, and it continues to gain plenty of attention. Although the history of it is only one decade or so, its relevant research area has already expanded to almost every sub-field of radar signal processing.

According to the publicly available literature, the earliest work on MIMO radar dates back to the year of 2003 when authors from MIT Lincoln Laboratory first introduced the concept of MIMO to radar signal processing in the ASILOMAR CONFERENCE ON SIGNALS, SYSTEMS, AND COMPUTERS [2]. Since then, the research on coherent MIMO radar has been developing. In [2], a MIMO model has been built for radar, based on which the advantages with respect to DOFs and resolution of MIMO radar over the conventional single-input multiple-output (SIMO) radar have been discussed in the context of the ground moving target indication (GMTI) application. This MIMO radar signal model has been compared with that of MIMO communications. In another early work [30], which appeared in the same year, the issue of applying multifunctional digital arrays for the purpose of enabling wide angular coverage in the MIMO mode has been researched. It has been reported therein that the integration time and the radar radiation energy can be managed by the proposed array technique.

The original intention of Lincoln Laboratory's early work on MIMO radar was to investigate its ability of detecting slow-moving targets in the presence of strong clutter. Their GMTI study has shown that coherent MIMO

radar is capable of achieving better resolution and slow-moving target detection performance compared to conventional SIMO radars. These performance improvements are attributed to the extra DOFs and the extended array aperture in MIMO radar. However, they are affected by the quality of transmitted waveforms. The nonorthogonality and poor sidelobe levels of waveforms can severely degrade the clutter mitigation (and/or jammer suppression) performance. Unfortunately, ideally orthogonal waveforms for any time lag do not exist.

A variant of MIMO radar was proposed in both the IEEE RADAR CONFERENCE and the ASILOMAR CONFERENCE ON SIGNALS, SYSTEMS, AND COMPUTERS in 2004 [3, 31], which initialized the research on statistical MIMO radar. The work of [3] has proposed to use widely separated antennas for addressing the problem of RCS scintillation, which enables the radar to obtain independent received signals, and therefore, to improve its target detection and parameter estimation performance. The performance analysis of MIMO radar in terms of the Cramer-Rao bound (CRB) for direction of arrival (DOA) estimation has been presented in [3], while the exploitation of spatial diversity for improving the target detection performance has been studied in [31]. An optimal Neyman-Pearson detector has been developed in the latter.

Since then, many valuable results on MIMO radar have been obtained and reported in a great quantity of literature. Coherent MIMO radar has been shown to be able to obtain improved spatial or angular resolution, enhanced parameter identifiability, increased upper limit on the number of detectable targets, extended array aperture, better clutter and jammer suppression performance, and other advantages [9, 15, 23, 32]. Statistical MIMO radar has been shown to be able to obtain better performance of target detection and localization, enhanced ability of overcoming RCS scintillations, and improved parameter estimation among other benefits. These advantages have been partially discussed by two overview papers [9, 14] in IEEE SIGNAL PROCESSING MAGAZINE and the major early results on MIMO radar have been reviewed by the book [1].

Motivated by the aforementioned groundbreaking work, the research on MIMO radar has been expanded into nearly every branch of conventional radar signal processing. Until now, the relevant research fields on MIMO

radar include waveform/code design, transmit beamforming or TB design, clutter and jammer suppression, parameter estimation and target detection, target tracking [33, 34], DOA estimation [35], MIMO compressive sensing [36, 37], MIMO OTHR [29, 38], MIMO SAR [28, 39, 40], MIMO radar-communication coexistence [41–43], experiments on MIMO radar [16, 30, 32], etc.

It would be nearly impossible to provide a full overview on all these subjects. Instead, we hereby present a comprehensive overview on the first four subjects, while the others will be reviewed only briefly. It can be foreseen that more research branches of MIMO radar will appear in the coming future, or the MIMO radar concept will be replaced by some other new ideas. In any case, MIMO radar has already become the foundation of new developments for radar signal processing.

2.2.1 Waveform(s)/code(s) design

Waveform design has been a research problem of significant interest over several decades [12, 13, 20, 33, 44–130]. It has been widely used in many applications such as radar, active sensing, communications, etc. The waveform design methods for MIMO radar have been in development ever since the emergence of the MIMO radar concept. In MIMO radar, a set of waveforms has to be designed, which is critically different from the single-waveform design for SIMO radars. These waveforms need to satisfy some particular conditions, for example, the constraints of mutual orthogonality, constant envelope of waveform elements, low correlation or sidelobe level (or low peak sidelobe level (PSL)), “excellent” AF, spectral nulling, etc. Moreover, the challenge of jointly designing waveforms for MIMO radar while at the same time considering some other aspects, such as the receive filter design for certain applications, also appears. In addition, if the code length and/or the number of waveforms are required to be significantly large, the resulting problem size of the waveform design for MIMO radar will grow to a large scale.

In existing literature on MIMO radar waveform design, the most commonly used approach is to generate the desirable set of waveforms on the basis of some specific criteria. Such criteria normally depend on the appli-

cations that are studied or the aspects that the design focuses on. Among them, the widely used criteria include the minimization of auto- and/or cross-correlation (or sidelobe) levels, maximization of SINR, optimization of AF shaping, minimization of CRB, maximization of mutual information (MI) or entropy, and minimization of mean square error (MSE). Using these criteria, the waveform designs for MIMO radar are typically formulated as optimization problems, and they can be solved by convex optimization techniques (with off-the-shelf solvers) if they can be cast as convex problems. Once the design encounters difficult constraints on some particular aspects of waveforms, the resulting problems can become non-convex and have to be solved by suitable algorithms that need to be designed. Although there exist other MIMO radar waveform design approaches, such as methods structured using existing waveforms with simple phase rotations (or with whatever small modifications), they turn out to be non-competitive for achieving desirable waveform properties and therefore are rarely reported.

The early stage of relevant work on waveform design focused on designing fast-time waveforms for MIMO radar in order to achieve various desirable properties. This type of waveform design improves only the quality of waveforms since the receiver of MIMO radar is fixed to be the matched filter (bank). In the corresponding publicly available literature, the earliest waveform design for MIMO radar dates back to the work of [20] in 2004. Statistical optimization methods that are based on simulated annealing and genetic algorithms have been proposed for generating orthogonal polyphase coded waveforms therein. Despite having been specially developed for netted radars, these methods can be directly applied to both the statistical and coherent MIMO radar configurations.

Another early work on MIMO radar waveform design has been reported in [51], in which two optimal strategies, including one in wide-band for imaging and the other in narrow-band for clutter-free angle estimation, have been studied. In the latter optimal strategy, CRB has been introduced to MIMO radar waveform design for the first time. The work of [51] has been extended to the general case of multiple targets and in the presence of spatially colored interference and noise in [63], and the minimization of the trace, determinant, and largest eigenvalue of the CRB matrix have been respectively used in the CRB minimization based waveform design

criteria therein. Like [51] and [63], the CRB minimization based MIMO radar waveform design with respect to parameter estimation has been also studied in [88], wherein the waveform is obtained from the minimization of the Bayesian CRB or the Reuven-Messer bound for parameter estimation. It is worth noting that these CRB minimization based waveform design works for MIMO radar have verified the fact that the CRB for parameter estimation is related to the waveform covariance matrix.

The minimization or controlling of the auto- and cross-correlation levels (or equivalently, the sidelobe levels) of waveforms has been commonly used in MIMO radar waveform design. Using this approach, the waveform design problem turns out to involve a particular metric that is related to waveform correlation or sidelobe levels. This metric can be a certain aspect of the waveform covariance matrix (such as its trace or determinant), the ISL (i.e., the sum of the auto- and cross-correlation levels), the WISL (i.e., ISL after weighting on correlations at different time lags), or the modification of ISL/WISL. Given the number of waveforms and the code length, there exists a lower bound on the ISL for aperiodic waveforms with constant envelopes [84, ch. 4]. Once either of both becomes significantly large, the resulting problem size will grow to a large scale. Therefore, the developments of fast and computationally efficient algorithms have been the focus of this type of waveform design.

The correlation/sidelobe minimization based waveform design for MIMO radar has been initiated for the purpose of transmit beamforming through partial waveform correlations. The relevant results for this approach have been reported initially in [5] and later in [54, 59, 65]. These works have all dealt with designing the waveform covariance matrix and meanwhile enforcing constraints on its correlation levels in order to obtain desirable transmit beampatterns and therefore synthesize waveforms. A random signaling based method for code/sequence synthesis has been presented in [59], while a cyclic algorithm (CA) has been proposed for the signal synthesis in [65]. The main idea of CA is to find the solution to the design problem in an alternating manner when multiple (normally two) sets of variables are updated cyclically until convergence. It has been developed especially for addressing waveform designs formulated as nonconvex problems with very difficult constraints.

The CA method has attracted significant attention and later has been developed into more advanced versions in [66]. Three algorithms, namely, CA-New (CAN), Weighted CAN (WeCAN), and CA-Direct (CAD), respectively, have been proposed for the MIMO radar waveform design in [66], and they have been the extended versions of the algorithms developed in [67] for single-waveform design.

The CAN and WeCAN algorithms deal with the ISL and WISL minimizations of waveforms, respectively, while the CAD algorithm deals with a particular case of the WISL minimization. For WeCAN, a meaningful example is the case when only partial sidelobes next to the mainlobe of waveform correlations need to be controlled. In this situation, deep notches corresponding to these sidelobes can be formed for some mitigation purposes. Both the CAN and WeCAN algorithms resort to transforming the minimization problems to the frequency domain, but the CAD algorithm does not. The major difference between CAN and WeCAN is that the former considers the correlations for all time lags while the latter concentrates on the correlations only for the time lags of interest by applying predefined weights. They both seek to save the computational burden through exploiting the fast Fourier transform (FFT) or the inverse FFT (IFFT). In theory, all these algorithms have the ability to generate unimodular waveform sets with arbitrary code length.

The benchmark CAN and WeCAN algorithms have attracted plenty of attention. They have been competitive for unimodular waveform design with emphasis on achieving good correlation properties for MIMO radar until the recent emergence of some more advanced algorithms. One major limitation for CAN and WeCAN is that they can become time consuming when the number of waveforms and/or the code length are large, and they can cost several hours or even days of elapsed time. For WeCAN, the additional limitation is that the weighting matrix has to be positive semidefinite.

To tackle the aforementioned difficulties that CAN and WeCAN face, the works of [105, 111, 123, 126] have resorted to the MaMi technique [131]. Three MaMi based algorithms that cope with the ISL, complementary ISL, and WISL minimization based unimodular waveform designs for MIMO radar have been proposed in [105], whose less advanced variants

for single-waveform case have been reported in [95, 106]. The work of [126] has presented two more advanced MaMi based algorithms compared to the ones in [105] for addressing the ISL and WISL minimization based unimodular waveform design problems, respectively.

Despite also transforming the waveform design problems to the frequency domain and exploiting FFT or IFFT to save computations, the aforementioned MaMi based algorithms can significantly outperform CAN and WeCAN, mainly because of their rapid convergence speed after applying efficient acceleration schemes. The major challenges for the MaMi based algorithm developments are formulating the problems into proper forms and elaborating competitive majorization functions. It is worth noting that the MaMi framework has been used earlier in the single-waveform design work [87], whose principal objective is to improve the detection performance of multi-static radar with clutter environment.

In addition to the aforementioned works, the correlation/sidelobe minimization based design has been also applied to space-time coding in MIMO radar [16, 64, 71, 75, 82]. In [64] and [82], multiple types of coding techniques such as code division multiple access (CDMA), time division multiple access (TDMA), and frequency division multiple access (FDMA) have been studied, and the concept of “cancellation ratio” has been presented in the latter for evaluating the clutter mitigation performance after applying these techniques to MIMO radar. In [16], a coding strategy, which obtains mutual orthogonality of waveforms through phase coding for slow-time pulses and therefore allows using classical fast-time waveforms, has been proposed for the first time. This coding technique has been termed as Doppler division multiple access (DDMA) therein. In the work of [71], the idea of using space-time coding to mitigate waveform cross-correlations in MIMO radar has been considered, and four types of space-time codes as well as the conditions of removing waveform cross-correlations have been presented therein.

In general, these space-time coding techniques have drawbacks when applied to MIMO radar. For example, the FDMA signals can only occupy a certain bandwidth, while the TDMA and DDMA signals are limited by the pulse repetition interval (PRI). Furthermore, only one TDMA signal can be transmitted within the same time interval.

A second way for designing MIMO radar waveforms is the information theoretic approach, which typically involves the study of MI and/or entropy. The relevant works can be found in [12, 13, 33, 70, 73, 79, 83, 97, 120], with the basic idea originating from the work of [47] that has been reported in the 1990s. In some of these works, such as [12, 13, 79], the MSE criterion has also been used.

The work of [13] has proposed to design minimax robust waveforms for MIMO radar target detection and identification on the basis of minimum MI and minimum MSE (MMSE) principles, where the case of uncertain target power spectral density (PSD) with known upper and lower bounds has been studied. The same criteria have been used in [12] for MIMO radar waveform design with extended (i.e., non-point) targets whose scattering characteristics have been modeled by a random target impulse response (RTIR). The waveforms have been designed through maximizing the MI between the RTIR and the radar echo or through minimizing the MSE in estimating the RTIR therein. The methods of [13] and [12] have also been implemented by means of alternating projection with iterations which later has been studied in [70].

Using the information theoretic criteria, [73] and [83] have studied the waveform design problem for MIMO radar in the presence of colored noise. Two waveform design strategies have been proposed in [73], wherein the first one is based on the same MI criterion as in [13] and the second one is based on maximizing the relative entropy of two hypotheses (specifically, cases with and without target presence in the clutter environment). This work has been extended to deal with both the clutter and interference in [97] for MIMO radar detection, wherein the relative entropy based criterion has also been used for the waveform design and the resulting nonconvex problem has been tackled by means of the MiMa technique. Using also MiMa, the work of [120] has proposed an information theoretic (MI based) approach to designing robust constrained codes for MIMO radar, wherein the problem has been studied in the presence of the signal-dependent interference and target mobility with some practical constraints such as the energy constraint, peak-to-average-power ratio (PAPR) [80], similarity constraint [69], etc.

In essence, the key ideas of the aforementioned information theoretic

MIMO radar waveform designs are similar. The typical approach is to select a specific information theoretic quantity that is related to waveforms as the objective for optimization, and then to formulate the waveform design problem into a certain form based on the application under consideration. The major difference between these designs lies in the nature of the environment that has been considered, while the minor differences are determined by the applications studied as well as the waveform constraints introduced.

Taking [33] for example, it has focused on designing optimal orthogonal frequency division multiplexing (OFDM) signals for the application of low-grazing angle tracking in MIMO radar, where the MI between the state and measurement vectors at the next pulse duration has been maximized. Note that the MIMO OFDM signals, which usually occupy a large bandwidth and can have a large time-bandwidth product, belong to the category of wide-band waveforms in MIMO radar. They are generally easy to obtain and implement, whose example can also be found in [98].

A third direction for MIMO radar waveform design has been established through the optimization of AF shaping, i.e., from the perspective of good AF matching (to the ideal shape). The relevant works have been reported in [11, 19, 26, 62, 112–114, 132–134].

The work of [62] has proposed an algorithm for designing frequency-hopping waveforms through analyzing the properties of MIMO radar AF, whose basic idea is to optimize an objective function that is constructed from the AF and seek to reduce the AF sidelobe levels. The work of [113] has exploited the same idea to design frequency-hopping waveforms for MIMO radar with arbitrary antenna separations. In [112] and [114], the AF shaping based design strategy has been applied to designing sub-chirp waveforms and complex sequences for MIMO radar, respectively. Typically, these AF shaping based waveform designs exploit the relationship between the MIMO radar AF and the waveforms or codes that need to be designed. In such designs, the optimization of the AF related objective function contributes to optimizing the waveforms, and the quality of the optimized waveforms depends on how the AF is defined and how the objective function is constructed from the AF.

Strictly speaking, the works of [11, 19, 26, 132–134] do not involve direct

waveform designs for the MIMO radar. Instead, they are more closely related to the AF definitions, analyses, and designs. The main reason for listing them here is because they provide important insights into the AF shaping based waveform designs for MIMO radar. It is intuitive that AF is an efficient tool for evaluating the radar resolution performance from the nature of the transmitted waveforms, array aperture utilized, and other aspects. For MIMO radar with multi-waveform transmission, the desirable AF is to contain an impulse-like peak at the mainlobe and to have almost zero-level sidelobes elsewhere.

In other words, the optimal MIMO radar AF should be thumbtack-shaped. In [11], the well-known Woodward's AF [135–138] has been introduced to MIMO radar, wherein the MIMO radar AF and its four simplified forms for different scenarios have been presented. A similar form of the AF in [11] has been given in [62], in which the AF properties have been analyzed and subsequently exploited for waveform design. The work of [132] has proposed another MIMO radar AF form, which exhibits higher sidelobe levels compared to the AF in [11] and is more suitable for statistical MIMO radar. It has also analyzed the maximum achievable “clear region” of the proposed MIMO radar AF. In [133] and [19], the AF for the TB-based MIMO radar has been defined, and the latter has presented relevant “clear region” analysis and has proposed a TB design that leads to lower AF sidelobes. In [26], the ultra-wideband MIMO radar AF has been introduced.

A fourth way for designing MIMO radar waveforms is to maximize the SINR (or to minimize the SINR loss). The relevant works have been reported in [55, 60, 68, 93]. In the early work of [55], a MIMO radar waveform design procedure, which is based on the statistics of the extended target and the clutter, has been developed through maximizing the SINR at the detector output. The optimal waveform design in [55] requires the knowledge of both the target and the clutter, while the suboptimal designs therein require only one of two or both. Another early work of [68] has also studied the waveform design problem in the presence of extended target and clutter, and iterative algorithms have been proposed to guarantee the SINR improvement at each iteration.

The SINR maximization based waveform design in MIMO radar typically involves jointly designing the multi-waveform transmission (in fast-time

domain) and the receive adaptive filter, which has attracted significant interest in recent years. The main motivation of this joint design is to deal with some difficult/harsh environments that involve the clutter with different characteristics and/or active jamming. In order to fulfill the goal, the receiver has to be flexible, adaptive, and jointly optimized with the transmitted waveforms. Therefore, the designing focus shifts to the so-called mismatched filter design. In a few reported papers in the publicly available literature, such design has also been termed as instrumental variable filter design [60, 61].

Normally, the joint waveform transmission and receive filter design problems are nonconvex, but they can be solved in a cyclic manner. Most of the reported works adopt an MVDR type solution for fixed waveforms when developing cyclic algorithms. However, the technical difficulties lie in guaranteeing fast SINR performance improvements through iterations and ensuring low computational complexity per iteration. Towards this end, the work of [60] has presented an algorithm for synthesizing constant-modulus transmit signals with consideration on their correlation levels, wherein the instrumental variable approach has been applied to the design of the receive filter for solving the range compression problem in MIMO radar imaging.

Other works on the joint transmission and receive filter design for MIMO radar reported recently, such as [93, 94, 100, 100, 127, 128], either deal with the case of point target and signal dependent clutter, or more commonly, focus on solving the joint design problem with different practical constraints on waveforms. For example, the work of [93] has presented a sequential optimization algorithm, and the works of [127] and [128] have proposed MaMi and MiMa based algorithms. Different types of constraints, such as similarity, constant-modulus, spectral controlling, and PAPR, have been considered therein.

The works on the SINR maximization based joint transmission and receive filter design for MIMO radar have stimulated the very recent emergence of another research sub-division on waveform design, that is, the joint element-space/space-time transmission and element-space/STAP receive filter design. Here, we term them as the multi-dimensional joint transmission and receive filter designs. The basic idea of this research is

to extend the aforementioned joint transmission and receive filter design problem to space-time transmission and/or multi-dimensional STAP, so that the benefits introduced by both the multi-waveform diversity and the STAP can be enjoyed by MIMO radar. The principal reason for explaining the potential performance improvements lies in the fact that MIMO radar introduces extra DOFs compared to conventional radar configurations, and they can be additionally exploited.

In essence, the multi-dimensional joint transmission and receive filter design is the same as the previous SINR maximization based joint design. They only differ in the dimensions of the transmission and/or the receive filter. Through properly and jointly designing the waveforms and/or the STAP filter, the output SINR performance can be guaranteed to be optimal. The multi-dimensional joint designs for MIMO radar can be found in [116, 122, 129]. The work of [116] has studied the joint design problem to enhance the slow-moving target detection performance in the presence of both the clutter and jamming signals, and it has proposed a cyclic method for addressing the joint design problem. The work of [122] has dealt with the joint SST transmission and STAP filter design problem in the presence of the signal dependent clutter, and it has transferred the corresponding problem to sub-problems that are either convex or solvable in polynomial time. Similarity and constant-modulus constraints on waveforms have been considered therein. The work of [129] has also studied the joint SST transmission and STAP filter design problem and has incorporated the extra DOFs introduced by transmit waveform diversity into the STAP. A more general signal model has been presented and a MiMa based algorithm for addressing the design problem with unimodular waveform constraints has been proposed therein. Both [122] and [129] have considered two cases of known Doppler information and Doppler uncertainties on clutter bins.

The newly emerging research on multi-dimensional joint transmission and receive filter design in MIMO radar originates from the joint design of the single-waveform transmission (in fast- or slow-time domain) and the receive adaptive filter (or the Doppler filter with robustness). Corresponding works have been reported in [61, 81, 86, 96, 108, 110]. We omit the detailed overview on these works here but briefly conclude that the joint design of the transmission and receive filter allows us to obtain transmit

waveforms with various constraints and meanwhile to deal with Doppler or STAP related issues.

The multi-dimensional joint design research indicates that the waveform design can relate to the issue of STAP in MIMO radar [119], whereas it rarely establishes a relationship with the STAP in conventional radars that deal with a single waveform. The extension of STAP to MIMO radar allows for more flexibility, for example, it enables to exploit more DOFs. However, this newly emerging research can also become challenging. The main issue is that we have to develop computationally fast and efficient algorithms for solving the joint design problems which are typically non-convex, with problem size of large scale.

Note that the interest in developing multi-dimensional joint transmission and receive adaptive filter in MIMO radar is also generated by the practical need, especially for the case of considering slow-time transmissions. In this case, the focus is on synthesizing slow-time waveforms for inter-pulse coding at the transmitter, which typically copes with some Doppler-related issues such as uncertainty, and also for achieving enhanced resolution and/or superior detection performance.

Besides, as mentioned in the beginning of the overview on waveform design, there exist works that synthesize waveforms on the basis of their correlation matrices. We term them as the correlation matrix based MIMO radar waveform designs. Most of the correlation matrix based waveform designs are indirect, which first generate the waveform covariance matrix using some specific methods, and then synthesize waveforms based on the devised covariance matrix. In contrast, a few of the correlation matrix based designs directly incorporate the required correlation information into devising waveforms for MIMO radar. The relevant works can be found in [5, 59, 65, 78, 92, 124, 125].

The works of [5, 59, 65, 124] have exploited the indirect way of waveform design and the first three of them have been reviewed earlier, while the works of [78, 92, 124, 125] have employed the direct way. In [78], two algorithms for generating the finite alphabet constant envelope waveforms have been presented, wherein the first one provides a closed-form solution for mapping Gaussian random variables to binary phase shift keying (BPSK) and quadrature phase shift keying (QPSK) waveforms, and the sec-

and one provides a generalized solution for synthesizing BPSK signals for MIMO radar. Similar methods that map Gaussian variables to phase shift keying (PSK) signals as in [78] have been presented in [92] for generating PSK, pulse amplitude modulation, and quadrature amplitude modulation waveforms. In [124], a discrete Fourier transform (DFT) based closed-form solution for finding the waveform correlation matrix and then synthesizing the finite alphabet constant envelope waveforms has been presented. In addition, an alternating direction method of multipliers based algorithm has been presented in the work of [125] for addressing the correlation matrix based waveform design problem with constant modulus constraints.

The above-mentioned correlation matrix based MIMO radar waveform design has been developed primarily for transmit beampattern matching in MIMO radar. It is understandable that the waveforms in this class are no longer mutually orthogonal. Normally, they are partially correlated and their partial correlations are used for achieving desirable beampatterns or some other goals for MIMO radar. In general, the indirect approach to synthesizing waveforms is more commonly used and widely applied, and the resulting design problems, with various waveform constraints, are commonly solved using optimization techniques. While the direct designs, especially the ones using off-the-shelf waveform strategies such as linear frequency modulation (LFM), BPSK, and QPSK signals, are relatively easier to develop, however, they have very limited applications.

In addition to the MIMO radar waveform designs developed on the basis of the aforementioned criteria that have been identified, there also exist other works which depend on specific applications, scenarios, or operating modes of interest of MIMO radar. For instance, waveforms have to be designed adaptively in accordance with the varying environment, target positions, and/or SNRs. We refer interested readers to [64, 72, 88, 130] for examples and more details. The waveforms also have to be properly designed for applications of MIMO OTHR [29, 38, 56] and MIMO SAR [28, 139, 140]. Other examples include waveform designs for radar-communication coexistence [43], spectrum control, frequency agility and/or Doppler tolerant scenarios [115], cognitive (or other knowledge aided) MIMO radar applications, etc. Generally speaking, these waveform design works either use off-the-shelf radar waveforms/codes (e.g., PSK, LFM,

or OFDM signal possibly with some modifications), or exploit waveform optimization approaches that have been reviewed earlier. We omit the detailed overview on this topic and refer interested readers to the works listed in the review and references therein.

2.2.2 Clutter and jammer suppression

Another important topic of MIMO radar research is the clutter and jammer suppression [2, 8, 15, 16, 18, 32, 141–165], which has also attracted a lot of interest over the past decade. In the publicly available literature on this topic, the relevant works mainly deal with the research subdivisions including MIMO GMTI [16, 32, 146, 147, 159, 165], MIMO STAP [15, 142, 155], rank estimation and reduction of the clutter covariance matrix [15, 144, 148], and designs of clutter and jammer suppression algorithms [15, 156, 157].

A large part of the GMTI research for MIMO radar has been done by Lincoln Laboratory, including both the theoretical [2, 16, 146] and experimental studies [32, 147]. In the earliest work of [16], a GMTI example has been briefly introduced to MIMO radar, whose purpose is to show that extending the conventional radar configurations to MIMO mode has the benefits of bringing extra DOFs. Such GMTI technique later has been introduced to the concept of coherent MIMO radar in [16], wherein the GMTI performance has been compared with that of the conventional radar, and the theoretical bounds on the angle estimation and MDV for MIMO GMTI have been presented. The work of [146] has been concerned with the limitations of waveforms that have been commonly used for MIMO GMTI radar, in which the drawback of constructing waveforms from frequency shifting techniques has been discussed and the function of SNR loss with respect to waveform characteristics has been introduced.

The study on MIMO GMTI has also been explored through experiments. In [32] and [147], an airborne MIMO radar testbed operating at S-band with six transmit and eight receive independent channels has been reported, wherein the MIMO GMTI has been tested using TDMA/DDMA waveforms and compared with the GMTI in SIMO radar. Indeed, the earliest relevant experiment dates back to the work of [30] reported in

2003, which has also been conducted in Lincoln Laboratory and paved the way for the MIMO GMTI experiments in [32] and [147]. An experimental MIMO radar with reconfigurable antennas operating at L-band through four independent transmitters and receivers, which is referred to as multifunctional digital array radar, has been reported therein.

The main results obtained in the MIMO GMTI study are that the improvements on SINR for clutter mitigation and MDV for slow-moving target detection can be achieved. The research therein has shown that such improvements result from the extended aperture of MIMO radar, which indeed indicates the potential improvement on the spatial resolution of MIMO radar. Because of this, the slow-moving targets can be identified with higher accuracy in severe clutter environment, and more competitive MDV can be obtained for MIMO radar. However, the performance of MIMO GMTI is subject to the transmitted waveforms in MIMO radar. It has been pointed out in [147] and [146] that the non-ideal orthogonality of waveforms may increase the rank of the clutter covariance matrix for a fixed Doppler cell in MIMO GMTI. The challenge is that (pulse-repeated) waveforms that are ideally orthogonal at every time lag do not exist [146]. To tackle this difficulty, either advanced waveforms with satisfying orthogonality property or some other signal strategies such as TDMA, FDMA, or DDMA should be developed.

Another important technique for clutter and jammer suppression is the MIMO STAP, which has usually been exploited in MIMO GMTI as well. The MIMO STAP is essential to the clutter and jammer suppression in MIMO radar since the interfering environment can be varying and uncertain. Moreover, the nonadaptive or even the adaptive techniques that exploit processing only in single spatial or temporal domain turn out to be not competitive for the clutter and jammer suppression. Therefore, the multi-dimensional MIMO STAP techniques become necessary.

In the early work of [15], a subspace based MIMO STAP method that can avoid calculating the inverse of a large-dimensional covariance matrix through separately estimating the clutter and jammer-plus-noise covariance matrices has been proposed. The clutter subspace therein has been related to the MIMO radar geometry and represented through the offline calculation of prolate spheroidal wave functions [166–168], there-

fore, its construction is independent of the received data observations of MIMO radar. The work of [155] has introduced the joint domain localized processing method [169] to MIMO STAP, wherein the received spatio-temporal data has been transformed to the angle-Doppler domain using joint transmit-receive beamforming and two-dimensional (2D) DFT techniques, and a multi-stage Wiener filter based algorithm with automatic stage selection and reduced complexity has been proposed for the MIMO STAP conducted in localized sub angle-Doppler domain.

Indeed, the STAP technique has been fully studied in conventional radars, for which many meaningful results such as the fully and partially adaptive, RD, reduced-rank (RR), and knowledge-aided (KA) STAP techniques have been obtained over the past several decades [170–174].¹ The reason why the conventional radar STAP has been extended to MIMO radar is mainly because that extra DOFs can be introduced by the diversities of transmitted waveforms, transmit beamspace, and some other aspects in MIMO radar. These extra DOFs enable MIMO STAP to have the potential of filtering out more clutter subspace but with little SINR loss. On the other hand, they also increase the complexity of MIMO STAP, which has become a challenging issue for MIMO STAP and consequently requires the developments of new advanced algorithms.

The study on the clutter rank estimation for MIMO radar has also been carried out. The work of [15] has extended the clutter rank estimation rule for PA radar, i.e., the well-known Brennan's rule [170, 171, 175] to MIMO radar. The result therein has shown that the transmit waveform diversity in MIMO radar also contributes to the clutter rank, whose extent is determined by the aperture ratio between transmit and receive arrays. The work of [148] has analyzed the clutter rank in terms of clutter covariance matrix, wherein the transmitted waveforms of MIMO radar are not strictly constrained to be perfectly orthogonal and the clutter rank has been shown to have relationship with both the rank and structure of the waveform covariance matrix. The MIMO radar clutter rank estimation in the presence of multipath ground clutter has been studied in [144], wherein the transmit-receive directionality spectrum has been employed

¹The overview on the fundamental results of conventional radar STAP is given in the introduction of Chapter 4.

for the rank analysis.

The issue of jammer suppression has also been studied for MIMO radar. It has been incorporated in the MIMO STAP study conducted in [15], wherein the diagonal structure of the jammer covariance matrix has been exploited for developing the STAP algorithm. The works of [156] and [157] have studied the problem of terrain-scattered jammer suppression and have proposed RD beamspace designs or robust beamforming techniques, wherein the spatial signature difference between the echoes of targets and jamming sources has been explored and therefore employed.

2.2.3 Transmit beamforming/beamspace design

Beamforming is another important research aspect in MIMO radar. Among all relevant subjects, transmit beamforming or TB design [5, 10, 17, 25, 27, 35, 54, 59, 65, 89, 101, 176–210] is the most popular.

The study on transmit beamforming dates back to the year of 2004 when the work of [5] was published, wherein a gradient search based method for achieving or approximating the desired transmit beampattern by means of partial signal correlations has been proposed. This type of transmit beamforming technique allows for an arbitrary waveform cross-correlation matrix, and it has been further studied in [59] which has resorted to constrained optimization for obtaining the correlation matrix. The work of [10] has modified the beampattern matching criterion of [5] and has proposed a semidefinite quadratic programming approach [211, 212] for solving the design problem in polynomial time, wherein several beampattern matching criteria including the maximization of the incident power on multiple targets with known/unknown locations, the minimization of the beampattern sidelobe levels, and the minimization of the matching difference have been proposed.

There also have been ways of designing the waveform correlation matrix to achieve or match desired transmit beampatterns [185, 190, 194, 195]. The main difference among them is actually they have different goals. For example, the ripples within the energy-focusing region and the transition bandwidth of the beampattern have been mainly considered in [190], while the gain of SINR and the reduction of sidelobes that the beampattern

can obtain have been studied in [195]. Besides, some of these works have proposed to implement transmit beamforming via unconstrained designs with/without closed-form solutions [185, 194].

In contrast to the waveform correlation matrix based designs reviewed above, researchers have also devised techniques that have exploited beamforming vectors for achieving the same goal. Relevant works can be found in [35, 183, 184, 186, 188]. In this type of design, initially orthogonal waveforms are assumed, and their correlations (or equivalently, the correlated waveforms) are generated through the TB matrix that needs to be designed. In essence, this TB matrix based design is equivalent to the waveform cross-correlation matrix based design, but it is more flexible and can be easily implemented through convex optimization techniques.

A significant fraction of the aforementioned methods have been designed for the purpose of facilitating direction finding or achieving superior DOA estimation performance [35, 183, 184, 188]. In [184], two transmit energy focusing strategies have been proposed, wherein the first pursues to find the orthogonal basis of TB in terms of subspace decomposition, while the second casts the design as a convex problem that involves desired phase rotations for DOA estimation using estimation of signal parameters via rotational invariance techniques (ESPRIT). It has shown that superior DOA estimation performance compared to the conventional MIMO radar with no TB designs can be obtained, and the proper selection of the TB matrix as well as its size can lead to an optimum/lowest CRB of DOA estimation. In [35], the TB design that enables search-free ESPRIT DOA estimation has been proposed, wherein a specific structure that separates the TB matrix into two conjugate flipped parts for maintaining the rotational invariance property (RIP) [213, 214] and therefore enables superior DOA estimation performance compared to that of [184] has been imposed. In addition, the TB matrix based design has been generalized to 2D transmit-array applications in [191, 192], which has been shown to be also efficient in terms of DOA estimation.

In addition to the waveform correlation matrix or the TB matrix based designs, the transmit beamforming in MIMO radar has also been implemented through subarrays or subapertures [17, 182, 187]. In [17], the concept of phased-MIMO radar configuration, which enjoys the advan-

tages of both PA and conventional MIMO radar configurations by means of partitioning the transmit array into several uniform or overlapped subarrays, has been proposed. In phased-MIMO radar configuration, different subarrays independently emits mutually orthogonal waveforms with each operating in a PA mode, therefore, the benefits of both the waveform diversity and the coherent processing gain can be achieved. Not that introducing subarrays into conventional MIMO radar can reduce the coherent processing time required by pulse Doppler processing.

In addition to the aforementioned techniques, the transmit beamforming in MIMO radar has also been extended to other categories such as the time-division transmit beamforming [89].

2.2.4 Parameter estimation and target detection

There also have been many works on MIMO radar parameter estimation and target detection [6, 7, 97, 99, 215–243]. The relevant studies have been reported in [6] and [7] in 2006. The work of [6] has improving the detection performance by means of exploiting the spatial diversity of target for statistical MIMO radar, wherein the effect of slow fluctuations of the target reflection cross section have been fully studied and the optimal Neyman-Pearson-type detector has been shown to consist of noncoherent processing of the outputs at the receiver. The work of [7] has analyzed the performance of target detection, angular estimation accuracy, and angular resolution for MIMO radar, wherein the generalized likelihood ratio test (GLRT) target detection, maximum likelihood direction estimation as well as its CRB have been derived in the presence of an arbitrary signal coherence matrix.

Among the aforementioned works, some of them have dealt with moving target detection and its parameter estimation, with relevant works reported in [222, 230, 232, 234]. The work of [222] has investigated the moving target detection problem in Gaussian noise and homogeneous clutter, wherein the GLRT detector has been developed and the (widely separated) MIMO radar approach has been shown to be more suitable for coping with targets with small radial velocities, especially for scenarios that the colocated approach fails to separate the moving target from clutter. Other

works on MIMO radar GLRT detection have been considered in [230] and [234], in both of which the constant false alarm rate has been achieved. The work of [232] has studied the parameter estimation problem of moving targets for noncoherent MIMO radar, wherein an approach that makes use of the phase information associated with each transmit-receive path has been proposed.

There also have been works dealing with the problem of joint parameter estimation and target detection [223, 233], the sensitivity analysis of detection [229], and the detection in the presence of phase synchronization mismatch [224] or heterogeneous environment [225] for MIMO radar. Some studies on MIMO radar target detection have also been extended to passive MIMO mode [236, 237].

3. Ambiguity function of the transmit beamspace-based MIMO radar

In conventional radar theory, the AF stands for the time response of a filter matched to a signal of given finite energy when the signal is received with a time delay and a Doppler shift [44, ch. 3], which has been a major tool for analyzing and evaluating signals for radar. The radar AF was originally proposed as a useful concept to describe the properties of a radar modulation in 1953 [135, ch. 7], and since then it has been subjected to considerable further studies and developments [136–138]. This concept, which is referred to as the Woodward’s AF, has been widely employed in the evaluation of the resolution performance and ambiguities with respect to different ranges and Doppler frequencies for single-waveform radar transmission.

Since the concept of MIMO radar was proposed [2, 3], the configuration of conventional radar has been conceptually updated. Different from the routine with single-waveform transmission in conventional radars, MIMO radar exploits multiple waveforms that are typically desirable to be orthogonal to each other (at any time lag). This leads to the difficulty that the well-known Woodward’s AF [136] cannot be directly applied to evaluate the ambiguity properties of these waveforms as well as the resulting resolution performance for MIMO radar. In this situation, new AF definitions have to be developed. Such issue has been studied in [11] and [132], wherein two types of MIMO radar AFs have been proposed. A similar AF form motivated by the work of [11] has been presented in [62], wherein the properties of MIMO radar AF have been fully studied. Here we refer interested readers to the overview on the AF shaping based waveform design in Chapter 2 for more details.

When transmit beamforming techniques or TB strategies are enabled in MIMO radar, i.e., the TB-based MIMO radar is used, as explained in Chapter 1 and also in the overview on TB designs in Chapter 2, the benefits of coherent processing gain and transmit waveform diversities can both be enjoyed. The potential advantage is that an improved SNR/SINR can be obtained, provided that the TB strategy is properly designed and the required processing is thoroughly conducted. The relevant examples typically include SNR improvement over a wide range for super-resolution DOA estimation and the SINR improvement in some clutter and jammer suppression applications, to name a few.

The TB-based MIMO radar configuration leads to emitting non-orthogonal or correlated waveforms from different antenna elements (i.e., in element space), and its performance can be flexibly affected by the TB strategies that are exploited [19]. As for the resolution performance and ambiguity properties of the TB-based MIMO radar, they are not only subject to the transmitted waveforms and the array geometry as investigated in [11], but also are determined by a factor that is related to the TB strategies and therefore needs to be identified. However, the AFs developed for conventional MIMO radars in [11, 62, 132] are no longer suitable for serving as the AF for the TB-based MIMO radar. Consequently, a new AF form that incorporates the effect of the TB processing needs to be defined, and if possible, such AF definition is also expected to be generic and flexibly suitable for existing radar configurations.

While defining the TB-based MIMO radar AF, we are also motivated by the research on Woodward's AF and the AFs of conventional MIMO radars to investigate the maximum achievable "clear region" of the defined AF [244]. Conducting theoretical analysis on the "clear region" of the TB-based MIMO radar AF enables us to see how large the region in delay-Doppler domain that is free of sidelobes can be obtained. However, calculating the "clear region" of the AF is a difficult task, and it typically does not allow for achieving a closed-form solution. Therefore, we have to derive as tight bounds as possible for the "clear region" analysis of the TB-based MIMO radar AF. On the other hand, we also expect that such theoretical analysis can provide insights into devising new TB strategies. Corresponding results are reviewed in the rest of this chapter.

3.1 Radar AF

The Radar AF originates from the theory of matched filter. For a certain matched filter, the impulse response of it is defined by a particular signal, to which the filter is matched. The result of matching is that the maximum SNR can be achieved at the output of the filter. Due to the importance of the time and Doppler processing in radar signal processing, the matched-filter response to a time-delayed and Doppler-shifted signal usually serves as the prototype of the radar AF.

3.1.1 Woodward's AF

The Woodward's AF has been used in conventional radar signal processing for the evaluation of single-waveform transmission, and it has been defined as [44, 136, 138]

$$|\chi(\tau, f_d)| \triangleq \left| \int_{-\infty}^{\infty} u(t)u^*(t + \tau)\exp\{j2\pi f_d t\} dt \right| \quad (3.1)$$

where τ and f_d are the time delay and Doppler shift parameters, respectively, and $u(t)$ is the complex envelop of the tested signal with respect to the time index t . Note that positive τ implies a target is farther from the radar than the reference position ($\tau = 0$), while positive f_d means that the target is moving towards the radar [44, ch. 3]. Without loss of generality, $u(t)$ is normalized to have unit energy, i.e., $\int_{-\infty}^{\infty} |u(t)|^2 dt = 1$.

The following important properties hold for Woodward's AF.

- i) The maximum value occurs at the origin, i.e.,

$$|\chi(\tau, f_d)| \leq |\chi(0, 0)| = 1. \quad (3.2)$$

- ii) The volume under Woodward's AF is constant, i.e.,

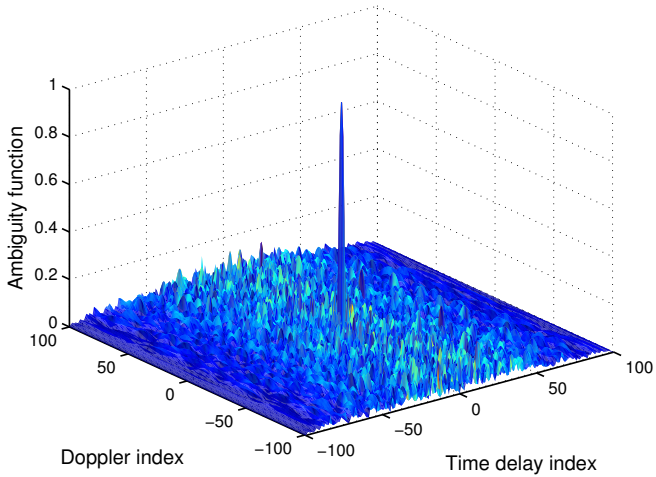
$$\int_{-\infty}^{\infty} \int_{-\infty}^{\infty} |\chi(\tau, f_d)|^2 d\tau df_d = 1. \quad (3.3)$$

- iii) Woodward's AF is symmetric with respect to the origin, i.e.,

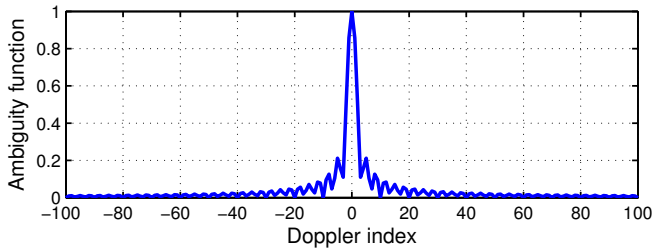
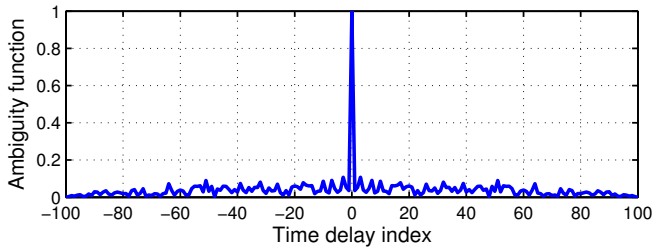
$$|\chi(-\tau, -f_d)| = |\chi(\tau, f_d)|. \quad (3.4)$$

- iv) LFM effect: if the complex envelope of the signal $u(t)$ has an AF $|\chi(\tau, f_d)|$, namely,

$$u(t) \Leftrightarrow |\chi(\tau, f_d)| \quad (3.5)$$



(a) 3D AF



(b) 2D AF cuts

Figure 3.1. Woodward’s AF and its zero-delay and zero-Doppler cuts for a single polyphase coded waveform. The maximum magnitude of the AF in this example is normalized to 1.

then the LFM signal $u(t) \exp\{j\pi kt^2\}$ leads to the AF $|\chi(\tau, f_d - k\tau)|$, i.e.,

$$u(t) \exp\{j\pi kt^2\} \Leftrightarrow |\chi(\tau, f_d - k\tau)|. \quad (3.6)$$

It is also interesting to see the zero-Doppler and zero-delay cuts of Wood-

ward's AF, as shown in Fig. 3.1 for example, since both cuts have meaningful implications. Inserting $f_d = 0$ into (3.1), the zero-Doppler cut of Woodward's AF can be expressed as

$$|\chi(\tau, 0)| = \left| \int_{-\infty}^{\infty} u(t)u^*(t + \tau) dt \right| \triangleq |R(\tau)| \quad (3.7)$$

where $R(\tau)$ is the auto-correlation function of $u(t)$. Therefore, the zero-Doppler cut of Woodward's AF is the auto-correlation of the evaluated signal.

Similarly, inserting $\tau = 0$ into (3.1), the zero-delay cut of the Woodward's AF can be expressed as

$$|\chi(0, f_d)| = \left| \int_{-\infty}^{\infty} |u(t)|^2 e^{j2\pi f_d t} dt \right|. \quad (3.8)$$

The expression (3.8) implies that the zero-delay cut of the Woodward's AF is the Fourier transform of the squared magnitude of the evaluated signal.

3.1.2 Conventional MIMO radar AF

The Woodward's AF can not be straightforwardly applied to MIMO radar simply because of its multiple-waveform transmission feature. As a result, a newly defined AF has to be developed for the MIMO radar configuration. Moreover, this AF definition needs to efficiently characterize the local and/or global resolution properties of the set of transmitted waveforms in MIMO radar.

There have been existing AF developments for the conventional MIMO radar configuration, which have been reported in [11, 62, 132]. The work of [11] defines the MIMO radar AF in the following form

$$\begin{aligned} \chi(\Theta, \Theta') \triangleq & \left| \sum_{n=1}^N \sum_{m'=1}^M \sum_{m=1}^M \int_{-\infty}^{\infty} \phi_m(t - \tau_{m,n}(\mathbf{p})) \phi_{m'}^*(t - \tau_{m',n}(\mathbf{p}')) \right. \\ & \times \exp\{-j2\pi\tau_{m,n}(\mathbf{p})(f_c + f_{m,n}(\Theta))\} \exp\{j2\pi\tau_{m',n}(\mathbf{p}')(f_c + f_{m',n}(\Theta'))\} \\ & \left. \times \exp\{j2\pi(f_{m,n}(\Theta) - f_{m',n}(\Theta'))t\} dt \right|^2 \end{aligned} \quad (3.9)$$

where M and N are respectively the numbers of transmit and receive antenna elements, $\phi_m(t - \tau_{m,n}(\mathbf{p}))$ and $\phi_{m'}(t - \tau_{m',n}(\mathbf{p}'))$ are the time-delayed

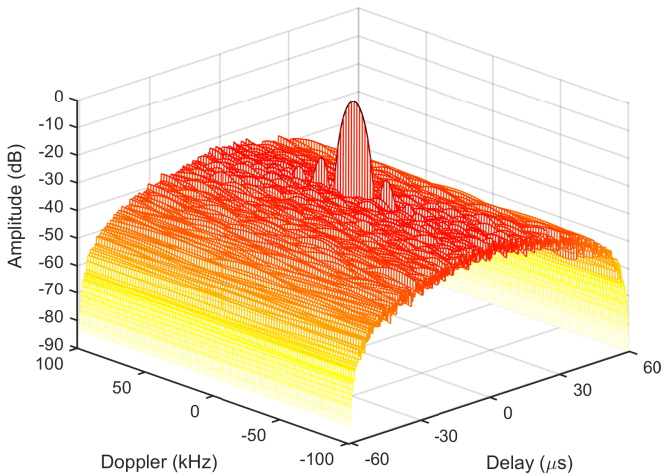


Figure 3.2. The square-summation-form AF defined for the conventional MIMO radar. Here $M = 8$ single-pulse polyphase-coded waveforms of code length 512 are employed for plotting the AF, and the maximum magnitude of the AF is normalized to 0 dB. High relative sidelobe levels of this square-summation-form AF appear in the Doppler-delay domain.

versions of the m th and m' th transmitted waveforms $\phi_m(t)$ and $\phi_{m'}(t)$ with $\tau_{m,n}(\mathbf{p})$ and $\tau_{m',n}(\mathbf{p}')$ being the (m, n) th and (m', n) th transmit-receive-path time delays associated with the target positions \mathbf{p} and \mathbf{p}' , respectively, $f_{m,n}(\Theta)$ and $f_{m',n}(\Theta')$ are Doppler frequencies associated with the target parameters Θ and Θ' for respectively, the (m, n) th and (m', n) th transmit-receive paths, and f_c is the carrier frequency.

A second AF development for the conventional MIMO radar has been defined in [132] in the following form

$$|\chi(\tau, f_d)|^2 \triangleq \sum_{m=1}^M \sum_{m'=1}^M \left| \int_{-\infty}^{\infty} \phi_m(t) \phi_{m'}^*(t + \tau) e^{j2\pi f_d t} dt \right|^2 \quad (3.10)$$

whose parameters are the same as those in (3.9). We term this AF definition as the “*square-summation-form*” MIMO radar AF and show one example of it in Fig. 3.2.

A third AF development for the conventional MIMO radar has been defined in [62], which takes similar form as the definition in [11]. We therefore omit presenting its explicit expression here. Note that there also exist other AF definitions for the conventional MIMO radar, for example, the wide-band-case MIMO radar AF has been also defined in [11]. Here, we focus on the narrow-band case for the MIMO radar AF.

The contributions in Publications I and II are reviewed in the following.

3.2 The TB-based MIMO radar AF

3.2.1 Signal model

Let us start from considering a colocated MIMO radar system equipped with M transmit and N receive antenna elements. Both the transmit and receive arrays are assumed to be closely located, and thus, sharing the same spatial angle for any target in the far field. In the context of the conventional MIMO radar, the complex envelopes of the transmitted waveforms can be modeled as

$$s_m(t) = \sqrt{\frac{E}{M}} \phi_m(t), \quad m = 1, 2, \dots, M \quad (3.11)$$

where E is the total transmit energy within one radar pulse, t is the continuous fast-time index, i.e., time within the pulse, and $\phi_m(t)$ is the m th baseband waveform which is orthogonal to the others. Without loss of generality, these baseband waveforms are assumed to have unit energy within a radar pulse of duration T , which can be formally expressed as

$$\int_T |\phi_m(t)|^2 dt = 1, \quad m = 1, 2, \dots, M. \quad (3.12)$$

Different from the conventional MIMO radar with omni-directional transmissions, the TB-based MIMO radar illuminates transmit energy towards a spatial sector-of-interest (SOI) through beaming. In this radar configuration, K (in general, $K \leq M$) initially orthogonal waveforms are transmitted, and each corresponds to a synthesized transmit beam that illuminates a certain area within the SOI. By means of synthesizing K transmit beams, the SOI can be fully covered. Normally, the SOI needs to be predetermined or estimated, depending on specific applications that are studied. For example, the spatial directions or the range of it can be estimated with low resolution and complexity. Using such principle, the signal radiated through the k th beam can be modeled as

$$s_k(t) = \sqrt{\frac{E}{K}} \mathbf{c}_k^T \mathbf{a}(\theta) \phi_k(t), \quad k = 1, \dots, K \quad (3.13)$$

where $\mathbf{a}(\theta) \in \mathbb{C}^{M \times 1}$ is the transmit steering vector for the spatial direction θ , and $\mathbf{c}_k \in \mathbb{C}^{M \times 1}$ is the k th transmit beamforming vector, whose elements construct the k th column of the TB matrix $\mathbf{C} \in \mathbb{C}^{M \times K}$ defined as follows

$$\mathbf{C} \triangleq [\mathbf{c}_1, \dots, \mathbf{c}_K]. \quad (3.14)$$

Denoting the m th element of \mathbf{c}_k as c_{mk} , the signal radiated from the m th transmit antenna can be expressed as

$$\tilde{s}_m(t) = \sqrt{\frac{E}{K}} \sum_{k=1}^K c_{mk} \phi_k(t), \quad m = 1, \dots, M. \quad (3.15)$$

The model (3.15) serves as the foundation of the TB-based MIMO radar AF, which is to be reviewed in the latter part of this chapter.

3.2.2 Definition, interpretation, and simplifications

In order to define the AF for the TB-based MIMO radar, the most common scenario of far-field targets and narrow-band waveforms has been considered. In the context of the TB-based MIMO radar, the received signal of a target with location vector \mathbf{p} at the j th receive antenna element before demodulation to the base band can be expressed as

$$\tilde{r}_j(t, \mathbf{p}) = \sum_{m=1}^M \alpha_{mj} \tilde{s}_m(t - \tau_{mj}(\mathbf{p})) \exp\{j2\pi f_c(t - \tau_{mj}(\mathbf{p}))\} + \tilde{z}_j(t) \quad (3.16)$$

where α_{mj} and $\tau_{mj}(\mathbf{p})$ are respectively the complex reflection coefficient of the target and the two-way time delay resulting from the target position \mathbf{p} , both associated with the (m, j) th transmit-receive channel, $\tilde{s}_m(t - \tau_{mj}(\mathbf{p}))$ is the time-delayed version of $\tilde{s}_m(t)$ defined in (3.15), f_c is the operating frequency, and $\tilde{z}_j(t)$ is the correspondingly observed noise.

Inserting (3.15) into (3.16) and incorporating the effect of target Doppler, after demodulation to the based band, the received signal can then be rewritten as

$$\begin{aligned} \hat{r}_j(t, \Theta) = & \sqrt{\frac{E}{K}} \sum_{m=1}^M \sum_{k=1}^K \alpha_{mj} c_{mk} \phi_k(t - \tau_{mj}(\mathbf{p})) \exp\{-j2\pi \tau_{mj}(\mathbf{p})(f_c + f_{mj}(\Theta))\} \\ & \times \exp\{j2\pi f_{mj}(\Theta)t\} + z_j(t) \end{aligned} \quad (3.17)$$

where $f_{mj}(\Theta)$ is the target Doppler shift associated with the (m, j) th transmit-receive channel, with the parameter Θ used for brevity denoting

the set that consists of both the location and velocity parameters of the target, and $z_j(t)$ is the noise signal observed at the j th receive antenna element after demodulation, which is assumed to be white Gaussian with power σ_z^2 .

At the receive end, a bank of matched filters is applied to the received signal based on the principle that the optimal detector is a filter matched to a specific set of target parameters. For the TB-based MIMO radar studied here, the received signal $\hat{r}_j(t, \Theta)$ in (3.17) is matched to each of the original waveforms $\{\phi_k(t)\}_{k=1}^K$ with a specific target parameter Θ' , denoted by $\{\phi_k(t, \Theta')\}_{k=1}^K$. The match-filtered signal component associated with the i th ($1 \leq i \leq K$) waveform can be expressed as

$$\begin{aligned}
 \bar{r}_{ji}(\Theta, \Theta') &= \int \hat{r}_j(t, \Theta) \phi_i^*(t, \Theta') dt \\
 &= \sqrt{\frac{E}{K}} \sum_{m=1}^M \sum_{k=1}^K \alpha_{mj} \int c_{mk} \phi_k(t - \tau_{mj}(\mathbf{p})) \phi_i^*(t - \tau_{q(i)j}(\mathbf{p}')) \\
 &\quad \times \exp\{-j2\pi\tau_{mj}(\mathbf{p})(f_c + f_{mj}(\Theta))\} \exp\{j2\pi\tau_{q(i)j}(\mathbf{p}')(f_c + f_{q(i)j}(\Theta'))\} \\
 &\quad \times \exp\{j2\pi(f_{mj}(\Theta) - f_{q(i)j}(\Theta'))t\} dt + \bar{z}_{ji}(t) \\
 &\triangleq \bar{r}'_{ji}(\Theta, \Theta') + \bar{z}_{ji}(t)
 \end{aligned} \tag{3.18}$$

where $q(i)$ is the subscript that denotes the index of the equivalent transmit phase center for the i th waveform, $\bar{r}'_{ji}(\Theta, \Theta')$ used for brevity stands for the noise-free match-filtered signal, and $\bar{z}_{ji}(t)$ is the corresponding noise.

The TB-based MIMO radar AF has been defined as the square of the coherent summation of all noise-free match-filtered pairs $\{(j, i)\}_{j=1, i=1}^{N, K}$ at the output, which is mathematically expressed as

$$\begin{aligned}
 \chi(\Theta, \Theta') &\triangleq \left| \sum_{j=1}^N \sum_{i=1}^K \bar{r}'_{ji}(\Theta, \Theta') \right|^2 \\
 &= \left| \sqrt{\frac{E}{K}} \sum_{j=1}^N \sum_{i=1}^K \sum_{m=1}^M \sum_{k=1}^K \alpha_{mj} \int c_{mk} \phi_k(t - \tau_{mj}(\mathbf{p})) \phi_i^*(t - \tau_{q(i)j}(\mathbf{p}')) \right. \\
 &\quad \times \exp\{-j2\pi\tau_{mj}(\mathbf{p})(f_c + f_{mj}(\Theta))\} \exp\{j2\pi\tau_{q(i)j}(\mathbf{p}')(f_c + f_{q(i)j}(\Theta'))\} \\
 &\quad \left. \times \exp\{j2\pi(f_{mj}(\Theta) - f_{q(i)j}(\Theta'))t\} dt \right|^2.
 \end{aligned} \tag{3.19}$$

The above AF definition takes a complex form and has been simplified as

$$\chi(\Theta, \Theta') = \left| \sum_{j=1}^N \sum_{i=1}^K \sum_{m=1}^M \alpha_{mj} [\mathbf{R}]_{mi}(\Theta, \Theta', \mathbf{C}, j) \exp\{-j2\pi\tau_{mj}(\mathbf{p})(f_c + f_{mj}(\Theta))\} \right. \\ \left. \times \exp\{j2\pi\tau_{q(i)j}(\mathbf{p}')(f_c + f_{q(i)j}(\Theta'))\} \right|^2. \quad (3.20)$$

via introducing the matrix $\mathbf{R} \in \mathbb{C}^{M \times K}$ whose (m, i) th element is given by

$$[\mathbf{R}]_{mi}(\Theta, \Theta', \mathbf{C}, j) \triangleq \sqrt{\frac{E}{K}} \sum_{k=1}^K c_{mk} \int \phi_k(t - \tau_{mj}(\mathbf{p})) \phi_k^*(t - \tau_{q(i)j}(\mathbf{p}')) \\ \times \exp\{j2\pi(f_{mj}(\Theta) - f_{q(i)j}(\Theta'))t\} dt. \quad (3.21)$$

Remark 1. The AF expression in (3.20) consists of the square of summation terms, and each term involves two important components. One is the match-filtered component conveyed by \mathbf{R} in (3.21), representing the properties of waveforms (correlation levels together with Doppler tolerance). The other is composed of the last two exponential terms in (3.20), standing for the phase shift information introduced by target position and motions.

Remark 2. The AF expression in (3.20) can also be interpreted as follows. The m th transmit antenna emits a compound signal resulting from the K initially orthogonal waveforms windowed by the elements of the m th row of \mathbf{C} . Moreover, the properties of the initial K waveforms are transformed to those of the compound signals launched from the M antennas after applying the TB strategy. This interpretation highlights the most significant difference between the TB-based MIMO radar AF and the conventional MIMO radar AF.

Remark 3. The phase shift information in (3.20) is useful for evaluating coherent processing properties introduced by the array geometry and the radar configuration. With the proper design of the TB matrix \mathbf{C} and the transmit phase centers, the AF expression in (3.20) can serve as a generalized AF for existing radar configurations.

The AF expression in (3.20) has been further simplified into the following compact form

$$\chi(\Theta, \Theta') = |\mathbf{a}_R^H(\Theta) \mathbf{a}_R(\Theta')|^2 |\mathbf{a}_T^H(\Theta) \bar{\mathbf{R}}(\Delta\tau, \Delta f_d, \mathbf{C}) \mathbf{a}_{TE}(\Theta')|^2 \quad (3.22)$$

via the matrix $\bar{\mathbf{R}}(\Delta\tau, \Delta f_d, \mathbf{C}) \in \mathbb{C}^{M \times K}$ whose (m, i) th element is given by

$$[\bar{\mathbf{R}}]_{mi}(\Delta\tau, \Delta f_d, \mathbf{C}) = \sqrt{\frac{E}{K}} \sum_{k=1}^K c_{mk} \int \phi_k(t) \phi_i^*(t - \Delta\tau) \exp\{j2\pi\Delta f_d t\} dt \quad (3.23)$$

and three steering vectors (i.e., the transmit, receive, and equivalent transmit ones) defined respectively as follows

$$\mathbf{a}_T(\Theta) \triangleq [\exp\{\tilde{\mathbf{u}}^T(\Theta)\mathbf{q}_{T,1}\}, \dots, \exp\{\tilde{\mathbf{u}}^T(\Theta)\mathbf{q}_{T,M}\}]^T \quad (3.24)$$

$$\mathbf{a}_R(\Theta) \triangleq [\exp\{\tilde{\mathbf{u}}^T(\Theta)\mathbf{q}_{R,1}\}, \dots, \exp\{\tilde{\mathbf{u}}^T(\Theta)\mathbf{q}_{R,N}\}]^T \quad (3.25)$$

$$\mathbf{a}_{TE}(\Theta) \triangleq [\exp\{\tilde{\mathbf{u}}^T(\Theta)\mathbf{q}_{TE,1}\}, \dots, \exp\{\tilde{\mathbf{u}}^T(\Theta)\mathbf{q}_{TE,K}\}]^T. \quad (3.26)$$

Here, $\Delta\tau \triangleq \tau(\mathbf{p}) - \tau(\mathbf{p}')$, $\Delta f_d \triangleq f(\Theta) - f(\Theta')$, $\tilde{\mathbf{u}}(\Theta) \triangleq j2\pi(f_c + f(\Theta))\mathbf{u}(\Theta)/c$ with $\mathbf{u}(\Theta)$ being the unit-norm directional vector pointing from the transmit/receive array to the target identified by the parameter Θ and c being the speed of light, and $\{\mathbf{q}_{T,m}\}_{m=1}^M$, $\{\mathbf{q}_{R,n}\}_{n=1}^N$, and $\{\mathbf{q}_{TE,k}\}_{k=1}^K$ are the antenna element locations of the transmit array, receive array, and equivalent transmit phase centers in 3D Cartesian coordinate system, respectively.

The effect of the target reflection coefficient α_{mj} has been ignored (or equivalently, normalized to 1) in (3.22). It does not affect the AF since the contributions associated with the transmit-receive channels to the AF are constant at any time t for the case of far-field targets and narrow-band waveforms. These contributions remain constant even for the scenario with multiple pulses and inter-pulse varying target reflection coefficients, provided that no range folding occurs.

Introducing the matrix $\bar{\chi}(\Delta\tau, \Delta f_d) \in \mathbb{C}^{K \times K}$ whose (k, k') th element is defined by

$$[\bar{\chi}]_{kk'}(\Delta\tau, \Delta f_d) = \int \phi_k(t) \phi_{k'}^*(t - \Delta\tau) \exp\{j2\pi\Delta f_d t\} dt \quad (3.27)$$

and using (3.23), the AF in (3.22) has been finally rewritten as

$$\chi(\Theta, \Theta') = \frac{E}{K} |\mathbf{a}_R^H(\Theta) \mathbf{a}_R(\Theta')|^2 |\mathbf{a}_T^H(\Theta) \mathbf{C} \bar{\chi}(\Delta\tau, \Delta f_d) \mathbf{a}_{TE}(\Theta')|^2 \quad (3.28)$$

where the parameters $\Delta\tau$ and Δf_d depend on Θ and Θ' . One simulated example of the TB-based MIMO radar AF is shown in Fig. 3.3.

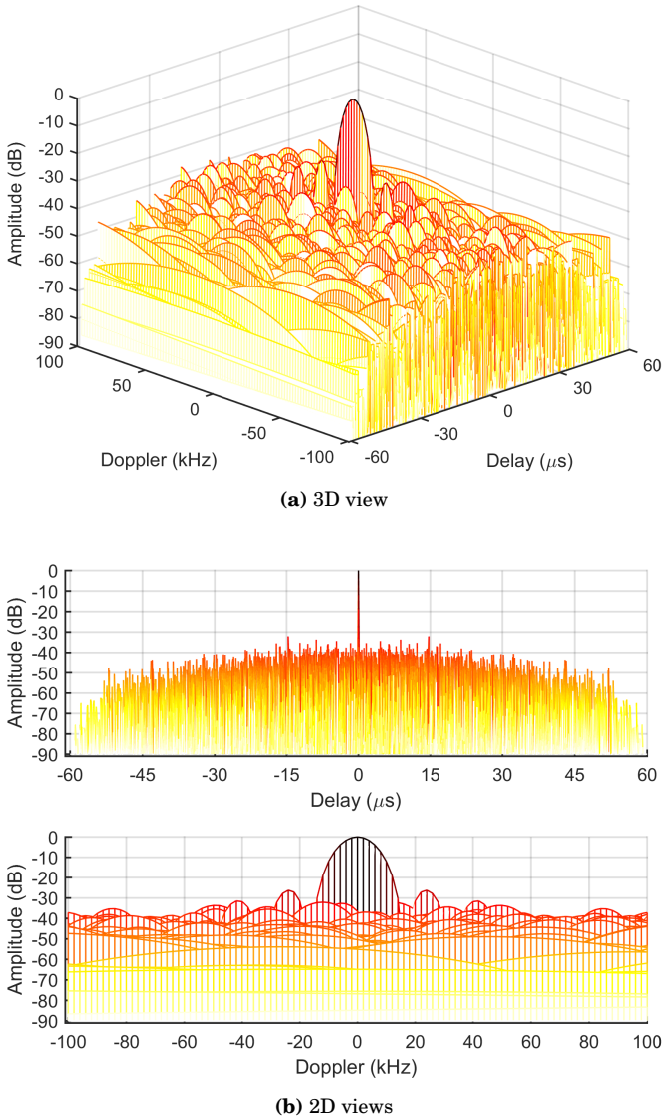


Figure 3.3. The TB-based MIMO radar AF versus delays and Doppler. Here $M = 8$, $N = 8$, $E = M$, and $K = 4$ single-pulse waveforms of code length 512 have been used: The pulse width, time-bandwidth product, and sampling rate are $T_p = 60 \mu\text{s}$, $BT_p = 256$, and $f_s = 2B$, respectively. The TB matrix \mathbf{C} is designed by focusing transmit energy within $[-15^\circ, 15^\circ]$ with a 10° transition band on both sides and absolute normalized sidelobe levels lower than 0.38. The AF mainlobe has been normalized to 0 dB. (a) 3D view of AF and (b) 2D views of the AF. Low AF sidelobes are obtained in the Doppler-delay domain using the TB-based MIMO radar AF, and they spread rather than focus. The Doppler sidelobes are relatively high because of no controlling.

3.2.3 Relationship with existing AFs

A. Relationship with Woodward's AF

The last product term in the AF expression in (3.28) implies that the original transmit steering vector $\mathbf{a}_T(\Theta) \in \mathbb{C}^{M \times 1}$ is transformed to $\tilde{\mathbf{a}}_T(\Theta) \triangleq \mathbf{C}^H \mathbf{a}_T(\Theta) \in \mathbb{C}^{K \times 1}$, and both the transformed and equivalent transmit steering vectors impact the Woodward's AF matrix for the K waveforms (auto- and cross-AFs). Equivalently, it can be understood that the Woodward's AFs are windowed by the joint effect of coherent processing gains and equivalent transmit phases. To be specific, the AF quantity $[\bar{\chi}]_{kk'}(\Delta\tau, \Delta f_d)$ associated with the k th and k' th waveforms is windowed by the product of the k th coherent processing gain (quantified by $\mathbf{a}_T^H(\Theta)\mathbf{c}_k$) and the k' th phase term of $\mathbf{a}_{TE}(\Theta')$.

B. Relationship with the conventional MIMO radar AF

If the number of waveforms K increases to M , \mathbf{C} is simply equal to the identity matrix $\mathbf{I}_M \in \mathbb{C}^{M \times M}$, and the equivalent transmit phase centers are chosen as positions of the M transmit antennas, then the AF in (3.28) becomes the following form

$$\chi_{\text{MIMO}}(\Theta, \Theta') = \frac{E}{M} |\mathbf{a}_R^H(\Theta)\mathbf{a}_R(\Theta')|^2 |\mathbf{a}_T^H(\Theta)\bar{\chi}(\Delta\tau, \Delta f_d)\mathbf{a}_T(\Theta')|^2 \quad (3.29)$$

which takes the same form as the AF in [11] except for the magnitude term that represents the general expression of transmit power allocation for the conventional MIMO radar, and they become identical when $E = M$. Moreover, the AF in (3.28) is compatible with the conventional MIMO radar with K uniform subarrays [27] if \mathbf{C} is properly designed as a block diagonal matrix and the phase centers of the subarrays are chosen.

C. Relationship with the PA radar AF

If the number of waveforms K decreases to 1, \mathbf{C} shrinks to a single beamforming vector that is denoted by \mathbf{w} , and the equivalent transmit phase center is chosen as the position of a reference transmit antenna element, then the AF in (3.28) takes the following form

$$\chi_{\text{PA}}(\Theta, \Theta') = E |\mathbf{a}_R^H(\Theta)\mathbf{a}_R(\Theta')|^2 |\mathbf{a}_T^H(\Theta)\mathbf{w}\bar{\chi}(\Delta\tau, \Delta f_d)|^2 \quad (3.30)$$

where $\bar{\chi}(\Delta\tau, \Delta f_d)$ is Woodward's AF for the only waveform in PA radar, and the equivalent transmit phase center is a scalar with unit modulus.

3.2.4 Significance

Since the newly defined TB-based MIMO radar AF establishes connections with existing AFs, it therefore can serve as a generalized AF form for which the PA and conventional MIMO radar AFs are important special cases. The common characteristics of the TB-based MIMO radar AF and existing AFs are that they are all developed on the basis of Woodward's AF and their definitions are related to the match-filtered outputs.

When it comes to the comparison with the “*square-summation-form*” MIMO radar AF in [132], the TB-based MIMO radar AF uniquely incorporates the phase shift information introduced by the array geometry and the relative motion between the target and the antenna array. Moreover, the TB-based MIMO radar AF evaluates the square of the sum of all auto- and cross-AFs for the K waveforms, which potentially leads to lower relative sidelobe levels than the “*square-summation-form*” MIMO radar AF. This advantage results from the inherent structure of the AF expression and the waveform orthogonality that has been used.

3.3 “Clear region” analysis

The “clear region” of an AF denotes the volume-clearance area in its Doppler-delay domain that is free of sidelobes. In the following, the “clear region” analysis for the TB-base MIMO radar AF is reviewed.

The Siebert's self-transform property for Woodward's AF given by the following equality [137]

$$|\bar{\chi}(\sigma, \nu)|^2 = \iint_{-\infty}^{\infty} |\bar{\chi}(\tau, f_d)|^2 \exp\{-j2\pi\nu\tau + j2\pi f_d\sigma\} d\tau df_d \quad (3.31)$$

has been used to conduct the analysis, where σ and ν are two introduced variables. Based on this property, the self-transform of the TB-based MIMO radar AF $\chi(\Theta, \Theta')$ can be expressed as

$$f(\sigma, \nu) = \iint_{-\infty}^{\infty} \chi(\Theta, \Theta') \exp\{-j2\pi\nu\Delta\tau + j2\pi\Delta f_d\sigma\} d\Delta\tau d\Delta f_d. \quad (3.32)$$

It generally cannot be guaranteed that $f(\sigma, \nu)$ is non-negative since the expansion of $\chi(\Theta, \Theta')$ normally contains negative terms, which disobeys the non-negative condition required by (3.31). To tackle this issue and see how large the maximum achievable “clear region” of the TB-based MIMO radar AF is, the derivation of the “clear region” bounds have been resorted, and two limiting cases that both enable $f(\sigma, \nu)$ to be non-negative have been identified.

The first limiting case has considered only the squared AF terms in the expansion of (3.28), which has been shown to lead to the smallest “clear region” and the highest relative sidelobe levels. We term this case as the “worst” case. In contrast, the second limiting case has ignored the cross-AF components in the expansion of (3.28), which has been shown to lead to the largest “clear region” of the TB-based MIMO radar AF. We name this case as the “best” case. However, it can never be reached due to multi-waveform transmission in the TB-based MIMO radar.

The actual maximum achievable “clear region” of the TB-based MIMO radar AF is in between of the bounds for both limiting cases, and it depends on the level of the non-squared terms of the AF expansion windowed by coherent processing gains and equivalent transmit phase terms.

3.3.1 Worst-case bound

We first define the volume of the TB-based MIMO radar AF over the integration region A as

$$V_{\text{TB}}(A) \triangleq \iint_A \chi(\Theta, \Theta') \, d\Delta\tau \, d\Delta f_d. \quad (3.33)$$

To find the maximum achievable sidelobe-free area in the Doppler-delay domain for the worst case, the following relaxed volume conditions with respect to the auto- and cross-AFs

$$\begin{cases} \iint_A |[\bar{\chi}]_{jj}(\tau, f_d)|^2 \, d\tau \, df_d \simeq \iint_{(0,0)} |[\bar{\chi}]_{jj}(\tau, f_d)|^2 \, d\tau \, df_d \triangleq V_j \\ \iint_A |[\bar{\chi}]_{jk, j \neq k}(\tau, f_d)|^2 \, d\tau \, df_d \simeq 0 \end{cases} \quad (3.34)$$

are specified. For simplicity, the K waveforms are assumed to share the same bandwidth and time duration here, which means that the integration of the auto-AF for each waveform over the region A has a fixed volume V_0 , i.e., $V_j = V_0, \forall j \in \{1, \dots, K\}$.

Under the assumption that A is convex, symmetric around the origin, and furthermore contains a delta function at the origin, the volume for the worst case, denoted by $V_{\text{TB}}^{\text{I}}(A)$, satisfies the following inequality

$$\begin{aligned}
 V_{\text{TB}}^{\text{I}}(A) &> \frac{1}{4}C(A) \lim_{A' \rightarrow 0} V_{\text{TB}}^{\text{I}'}(A') \\
 &= \frac{1}{4}C(A) \frac{N^2 \left(\sum_{k=1}^K \sum_{j=1}^K |\Upsilon_k \mathbf{a}_{\text{TE}}(j)|^2 \right)}{|\mathbf{a}_{\text{R}}^{\text{H}}(\Theta) \mathbf{a}_{\text{R}}(\Theta')|^2 \left(\sum_{k=1}^K |\Upsilon_k|^2 \right)} V_K \\
 &= \frac{1}{4}C(A) \frac{N^2 K}{|\mathbf{a}_{\text{R}}^{\text{H}}(\Theta) \mathbf{a}_{\text{R}}(\Theta')|^2} V_K \tag{3.35}
 \end{aligned}$$

where $C(A)$ denotes the area of A , $\Upsilon_k \triangleq \mathbf{a}_{\text{T}}^{\text{H}}(\Theta) \mathbf{c}_k$ stands for the k th coherent processing gain, V_K is the volume approximation for the worst-case scenario after substituting (3.28) to (3.33), which is given by

$$V_K = \frac{E}{K} |\mathbf{a}_{\text{R}}^{\text{H}}(\Theta) \mathbf{a}_{\text{R}}(\Theta')|^2 \left(\sum_{k=1}^K |\Upsilon_k|^2 \right) V_0 \tag{3.36}$$

and $V_{\text{TB}}^{\text{I}'}(A')$ represents the transformation given as follows

$$\begin{aligned}
 V_{\text{TB}}^{\text{I}'}(A') &\triangleq \iint_{A'} \chi(\Theta, \Theta') \psi(\Delta\tau, \Delta f_d) \, d\Delta\tau \, d\Delta f_d \\
 &= \frac{E}{K} \iint_{A'} |\mathbf{a}_{\text{R}}^{\text{H}}(\Theta) \mathbf{a}_{\text{R}}(\Theta')|^2 \sum_{k=1}^K \sum_{j=1}^K |\Upsilon_k \mathbf{a}_{\text{TE}}(j)|^2 \\
 &\quad \times [\bar{\chi}]_{kk}^*(\Delta\tau, \Delta f_d) [\bar{\chi}]_{jj}(\Delta\tau, \Delta f_d) \Psi(\Delta\tau, \Delta f_d) \, d\Delta\tau \, d\Delta f_d \tag{3.37}
 \end{aligned}$$

with $\psi(\Delta\tau, \Delta f_d)$ being any quadratically integrable function and $\Psi(\Delta\tau, \Delta f_d)$ being its Fourier transform. Here, the latter equality of (3.37) is derived using the aforementioned Siebert's self-transform property (3.31) and the Parseval's theorem.

Using (3.35) and considering the “ η -clear” area (convex and symmetric) associated with $\chi(\Theta, \Theta') \leq \eta$, the worst-case “clear region” of the TB-based MIMO radar AF is bounded by

$$C_{\text{TB}}^{\text{I}}(A) \leq \frac{4V_K}{\frac{N^2 K}{|\mathbf{a}_{\text{R}}^{\text{H}}(\Theta) \mathbf{a}_{\text{R}}(\Theta')|^2} V_K - 4\eta} \tag{3.38}$$

if and only if

$$\eta < \frac{N^2 K V_K}{4 |\mathbf{a}_{\text{R}}^{\text{H}}(\Theta) \mathbf{a}_{\text{R}}(\Theta')|^2}. \tag{3.39}$$

3.3.2 Best-case bound

Under the same conditions as listed in the worst case, the volume for the best-case, denoted by $V_{\text{TB}}^{\text{II}}(A)$, satisfies the following inequality

$$\begin{aligned} V_{\text{TB}}^{\text{II}}(A) &> \frac{1}{4}C(A) \lim_{A' \rightarrow 0} V_{\text{TB}}^{\text{II}'}(A') \\ &= \frac{1}{4}C(A) \frac{N^2 \left(\sum_{k=1}^K |\Upsilon_k|^2 \right)}{|\mathbf{a}_R^{\text{H}}(\Theta) \mathbf{a}_R(\Theta')|^2 \left(\sum_{k=1}^K |\Upsilon_k|^2 \right)} V_K \\ &= \frac{1}{4}C(A) \frac{N^2}{|\mathbf{a}_R^{\text{H}}(\Theta) \mathbf{a}_R(\Theta')|^2} V_K \end{aligned} \quad (3.40)$$

where V_K is the volume approximation for the best-case scenario that has the same expression as in (3.36), and $V_{\text{TB}}^{\text{II}'}(A')$ is the transformation that is obtained similarly to (3.37) and takes the form

$$\begin{aligned} V_{\text{TB}}^{\text{II}'}(A') &\triangleq \iint_A \chi(\Theta, \Theta') \psi(\Delta\tau, \Delta f_d) d\Delta\tau d\Delta f_d \\ &= \frac{E}{K} \iint_{A'} |\mathbf{a}_R^{\text{H}}(\Theta) \mathbf{a}_R(\Theta')|^2 \sum_{k=1}^K |\Upsilon_k|^2 |\bar{\chi}]_{kk}(\Delta\tau, \Delta f_d)|^2 \Psi(\Delta\tau, \Delta f_d) d\Delta\tau d\Delta f_d. \end{aligned} \quad (3.41)$$

Using (3.40) and considering the “ η -clear” area (convex and symmetric) associated with $\chi(\Theta, \Theta') \leq \eta$, the best-case “clear region” of the TB-based MIMO radar AF is bounded by

$$C_{\text{TB}}^{\text{II}}(A) \leq \frac{4V_K}{\frac{N^2}{|\mathbf{a}_R^{\text{H}}(\Theta) \mathbf{a}_R(\Theta')|^2} V_K - 4\eta} \quad (3.42)$$

if and only if

$$\eta < \frac{N^2 V_K}{4 |\mathbf{a}_R^{\text{H}}(\Theta) \mathbf{a}_R(\Theta')|^2}. \quad (3.43)$$

3.3.3 Further analysis

The worst- and best-case “clear region” bounds in (3.38) and (3.42) are related to the array configurations, and they are inversely proportional to the quantity $N^2/|\mathbf{a}_R^{\text{H}}(\Theta) \mathbf{a}_R(\Theta')|^2$. The largest bound for each occurs when this quantity decreases to 1, as long as the η -level condition is guaranteed. Both bounds are also related to the volume approximation V_K in (3.36)

which depends on the coherent processing gains obtained in the TB-based MIMO radar through the TB matrix.

Under the condition specified in the previous subsection, the worst-case bound has been shown to be independent of the coherent processing gains, but it depends on (to be specific, is inversely proportional to) the number of waveforms K . In this sense, it is similar to the case of the conventional MIMO radar AF with K mutually orthogonal waveforms emitting from K transmit antenna elements. In other words, the worst-case “clear region” of the TB-based MIMO radar AF is inversely proportional to the number of orthogonal waveforms (or beams) K , but not the number of transmit antenna elements M . On the contrary, the best-case bound indicates that the ideal “clear region” for the TB-based MIMO radar AF is independent of the number of waveforms, and it is equivalent to the case of the PA radar AF with single-waveform transmission.

Note that the maximum achievable “clear region” of the TB-based MIMO radar AF differs from those obtained by the PA and conventional MIMO radar AFs. The PA and conventional MIMO radars have their own fixed forms of TB matrices and therefore result in constant volume approximations of V_K under the specified conditions. The worst maximum achievable “clear region” obtained by the latter is approximately $1/M$ of that obtained by the former. However, the TB-based MIMO radar enables the maximum achievable “clear region” of its AF to become varying within the range of the two obtained bounds.

Note also that there exists a trade-off between the maximum achievable “clear region” and the waveform diversity for the TB-based MIMO radar AF. The reason is that a smaller number of waveforms K leads to a larger “clear region” according to the worst-cased bound, but it reduces the waveform diversity. Such trade-off can possibly be found through the evaluation of the TB-based MIMO radar AF once the radar configuration and target parameters are selected.

Finally, it is worth mentioning that large “clear region” under the “ η -clear” condition may be obtained for the TB-based MIMO radar AF. One can resort to the range-Doppler sidelobes mitigation techniques such as the receiver instrumental variable filter [60, 245, 246] applied at the receive end. However, the attainable “clear region” depends on the exact level of

sidelobe mitigation.

3.4 New TB design strategy

The existing TB strategies are typically designed on the basis of incorporating only the spatial information, which mainly contributes to the zero-Doppler-delay cut of the TB-based MIMO radar AF. In order to gain improvements from the perspectives of large “clear region” and good AF shaping, we have proposed to control the relative sidelobe levels of the TB-based MIMO radar AF by enforcing additional constraints on different Doppler and delay bins when designing the TB matrix \mathbf{C} . For example, if the relative AF sidelobes within the Doppler SOI \mathfrak{F} and the delay SOI \mathfrak{D} are kept below a certain level, the AF shaping based TB strategy can be designed as follows

$$\min_{\mathbf{C}} \max_i \left\| \mathbf{C}^H \mathbf{a}_T(\boldsymbol{\theta}_i) \odot \mathbf{a}_{TE}(\boldsymbol{\theta}_i) - \mathbf{d}(\boldsymbol{\theta}_i) \right\|, \boldsymbol{\theta}_i \in \boldsymbol{\Omega}, i = 1, \dots, I \quad (3.44a)$$

$$\text{s.t.} \quad \left\| \mathbf{C}^H \mathbf{a}_T(\bar{\boldsymbol{\theta}}_j) \odot \mathbf{a}_{TE}(\bar{\boldsymbol{\theta}}_j) \right\| \leq \gamma, \bar{\boldsymbol{\theta}}_j \in \bar{\boldsymbol{\Omega}}, j = 1, \dots, J \quad (3.44b)$$

$$\left| \mathbf{a}_T^H(\boldsymbol{\vartheta}_0, f_d^0) \mathbf{C} \bar{\chi}((\Delta\tau)_p, (\Delta f_d)_q) \mathbf{a}_{TE}(\boldsymbol{\vartheta}_{\tilde{i}}, (f_d)_q) \right| \leq \delta \quad (3.44c)$$

$$(\Delta\tau)_p \in \mathfrak{D}, p = 1, \dots, P$$

$$(\Delta f_d)_q \in \mathfrak{F}, q = 1, \dots, Q$$

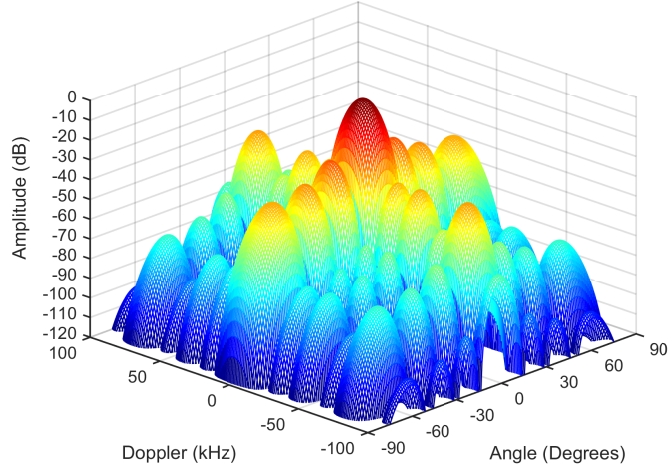
$$\boldsymbol{\vartheta}_{\tilde{i}} \in \tilde{\boldsymbol{\Omega}}, \tilde{i} = 1, \dots, \tilde{I}$$

$$\mathbf{a}_T^H(\boldsymbol{\vartheta}_0, f_d^0) \mathbf{C} \mathbf{a}_{TE}(\boldsymbol{\vartheta}_0, f_d^0) = K \quad (3.44d)$$

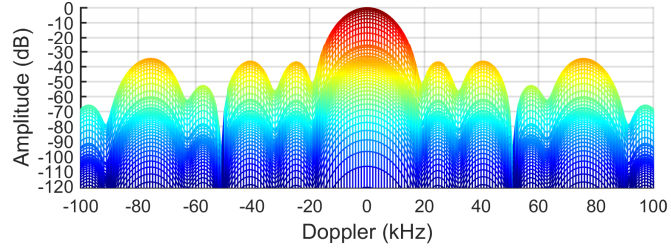
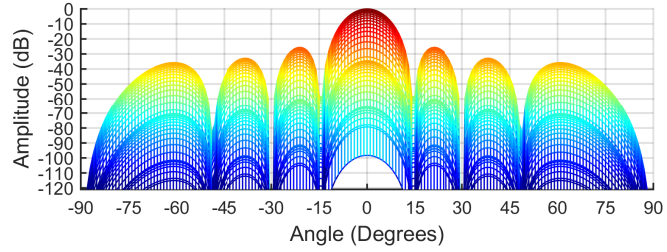
where $\boldsymbol{\vartheta}_0$ and f_d^0 are respectively the spatial angular vector and the Doppler frequency of the target, $\mathbf{d}(\boldsymbol{\theta}_i) \in \mathbb{C}^{K \times 1}$ is the presumed vector that guarantees the TB property, $\boldsymbol{\Omega}$ is the SOI approximated by I grids of spatial directions, $\bar{\boldsymbol{\Omega}}$ and $\tilde{\boldsymbol{\Omega}}$ combine the continuum of the out-of-sector region that lies outside $\boldsymbol{\Omega}$ and the spatial region of interest for AF sidelobe suppression using J and \tilde{I} grids of spatial directions, respectively, $\{(\Delta\tau)_p \in \mathfrak{D}, p = 1, \dots, P\}$ and $\{(\Delta f_d)_q \in \mathfrak{F}, q = 1, \dots, Q\}$ are grids of delay and Doppler used to approximate the SOIs \mathfrak{D} and \mathfrak{F} by finite numbers of P and Q delay and Doppler bins, respectively, $(f_d)_q \triangleq (\Delta f_d)_q + f_d^0$, and δ is the parameter of user choice that characterizes the sidelobe levels of the

AF in the intersection of \mathfrak{D} , \mathfrak{F} , and $\tilde{\Omega}$. Given the set of waveforms and the parameters $((\Delta\tau)_p, (\Delta f_d)_q)$, $p \in \{1, \dots, P\}$ and $q \in \{1, \dots, Q\}$, the matrix $\bar{\chi}((\Delta\tau)_p, (\Delta f_d)_q)$ in (3.44) can be easily obtained from (3.27).

Here in the proposed TB design (3.44), the objective function ensures transmit energy focusing towards the SOI, the first and second constraints deal with the beampattern sidelobe mitigation outside the spatial SOI and the control on AF sidelobes for the Doppler and delay regions of interest, and the third is the energy constraint enforced to the TB matrix \mathbf{C} . We show a simulated example of TB-based MIMO radar AF associated with the proposed TB design in Fig. 3.4.



(a) 3D view of the AF



(b) 2D views of the AF

Figure 3.4. The TB-based MIMO radar AF (versus angles and Doppler) associated with the proposed TB design (3.44). Here $M = 8$, $N = 8$, $E = M$, and $K = 4$ single-pulse waveforms of code length 512 have been used: The pulse width, time-bandwidth product, and sampling rate are $T_p = 60 \mu\text{s}$, $BT_p = 256$, and $f_s = 2B$, respectively. The spatial SOI is $[-15^\circ, 15^\circ]$, and a 10° transition band on both sides is assumed. Other parameters are: $\gamma = 0.1$, $\delta = 0.3$, $\vartheta_0 = 0$, $f_d^0 = 0$. The AF mainlobe has been normalized to 0 dB. (a) 3D view of AF and (b) 2D views of the AF. The relative sidelobe levels of AF in sub Doppler domain $[-30 \text{ kHz}, -18 \text{ kHz}] \cup [18 \text{ kHz}, 30 \text{ kHz}]$ along the spatial direction $\theta = 0^\circ$ are suppressed to below -38 dB, which demonstrates the trade-off between Doppler and spatial processing in the TB-based MIMO radar.

4. Spatial and/or temporal adaptive processing in clutter and jamming suppression

Clutter mitigation and jammer suppression are two problems that play critically important roles in radar signal processing [247–252]. The radar system radiates energy towards special directions where potential targets are located using some transmission strategies and completes the goals of target detection and corresponding parameter estimation in terms of the echoes that has been received. The backscattered radar signal, which can be reflected from the land or ocean surface, specific barriers in the probing environment, clouds and hailstones, etc., is referred to as clutter [170], [171, ch. 3], [253, ch. 2].

In essence, the clutter can be calculated as a superposition of signals backscattered from multiple point-like scatters in the environment, with each one having its own independent spatial and Doppler information. Some clutter generated from particular environments such as grass, ocean, and atmosphere can even show statistics with specific distributions determined by measurements.

The radar system also receives signals radiated from interfering sources such as hostile jamming stations, communication (or other radar) systems using the same frequency band, and other non-intentional disrupt radiations. These non-radar radiated signals, especially the intentional and deliberate transmissions or retransmissions of amplitude, phase, frequency, or otherwise modulated intermittent, or other type signals such as noise, transmitted with the purpose of impairing, deceiving, exploiting, masking, or degrading the radar receive system, is referred to as jammer [253, ch. 24], [254, ch. VIII].

There exist many types of jamming signals. In general, they can be di-

vided into two categories of active or passive jammers from the perspective of radiating sources. From the interfering manner standpoint, they can also be divided into two categories of suppressive and deceptive jammers. The common jammer examples include (barrage, spot, or swept) noise jamming, chaff, decoy, and various deceptive jammers. In radar signal processing, the aforementioned jamming measures are usually taken by hostile forces for degrading the performance of electromagnetic systems, and they are termed as electronic countermeasure (ECM) [255, 256].

In some radar literature, the radar-radiation-resulted clutter is known as “cold clutter”, while the multipath interference such as terrain-scattered jamming is known as “hot clutter” [247–251]. Normally, potential targets are severely submerged in the hot and/or cold clutter as well as jamming environment, and the resulting problem is that both the clutter and jammer have detrimental effect on radar functions of detecting ranges, estimating velocities, and tracking targets, unless efficient mitigation techniques are put into effect. Consequently, the implementation of clutter and jammer suppression, synchronously or sequentially, becomes necessary in radar signal processing.

Under the condition that potential target(s) can be separated from clutter and jamming signals through spatial direction or Doppler frequency, the one-dimension (1D) spatial or temporal processing is sufficient to accomplish the clutter and jammer mitigation goal. The corresponding techniques include (element-space) beamforming, beamspace processing, and Doppler processing, possibly with robustness and adaptiveness [170].

Once the targets cannot be separated through 1D spatial or temporal processing, the 2D STAP has to be used. The principle of STAP is to adaptively or dynamically adjust the 2D space-time filter response so that the output SINR can be maximized in order to improve the target detection performance [173, 174]. Depending on the application that is studied, the 1D spatial/temporal and 2D STAP techniques can involve fast-time and slow-time domains which respectively correspond to range and Doppler bins. Essentially, all existing clutter and jammer mitigation techniques boil down to 1D or multi-dimension filter processing.

Over the past several decades, the problems of clutter mitigation and jammer suppression have been fully studied and significant progress has

been achieved, especially due to the rapid development of PA radar technology [175, 257–264]. Nonadaptive techniques, however, turn out to be uncompetitive since the clutter and jamming signals are normally varying and uncertain. Many well known techniques, such as Wiener filtering [263, 264], generalized sidelobe canceler (GSC) [258], MVDR beamforming [213], STAP, etc., have been developed with adaptiveness and/or robustness during the past forty years.

The aforementioned adaptive techniques can face the difficulty of heavy computational complexity in the case of large spatial and temporal data size, which triggers the developments of RD and RR algorithms [170–173, 260]. In radar signal processing, the RD and RR strategies are particularly necessary for the large-dimensional STAP due to the limitation of fully adaptive STAP in real-time applications. Towards this end, partially adaptive STAP [170, ch. 4], [264], element/beam-space pre-Doppler/post-Doppler STAP [170, ch. 5, ch. 6], and knowledge-aided STAP [174] techniques have been devised. Among various different applications, the study of clutter and jammer suppression in the context of airborne radar system has attracted significant interest.

The difficulty of clutter mitigation increases in particular when the radar array is downward looking. In this situation, the airborne radar system faces strong homogeneous or heterogeneous clutter echoes from the ground and objects therein. In general, the subspace of homogeneous clutter is related to the array aperture and can be estimated and identified. It enables and accelerates the developments of RD and RR strategies for airborne clutter mitigation. The well known Brennan's rule [175] provides the earliest proof for the clutter rank estimation in conventional radar signal processing.

As for the jamming, though dependent on the radar platform that is exploited, the existence of the jammer inevitably aggravates the difficulty of clutter and jammer suppression further. Indeed, many subtopics around airborne radar clutter and jammer suppression, for example, the beam-pattern design, pulsed operation, effect of range and Doppler ambiguities, imaging, and ground moving target indication (GMTI), have been consequently investigated. The corresponding classical algorithms that have been developed include principal component inverse (PCI) [265], cross-

spectrum metric (CSM) [260], joint domain localized (JDL) processing techniques [259], etc.

As the concept of MIMO radar emerged and its potential advantages over conventional PA radar were discovered, researchers started to investigate the issue of clutter and jammer suppression for MIMO radar. Technically, almost all the clutter and jammer suppression techniques developed for the conventional PA radar can be applied to MIMO radar directly or after some slight modifications. Then the relevant research question is that whether a better clutter and jammer suppression can be achieved by exploiting the MIMO radar configuration. To answer this question, many studies have been conducted during the last decade. We refer interested readers to the overview on MIMO radar clutter and jammer suppression in Chapter 2.

One important reason for performing such study is that MIMO radar, compared to PA radar, is capable of providing more DOFs introduced by the transmit waveform and/or beamspace diversities [2, 15]. It enables extended (equivalent) array aperture [23]. If necessary, the long integration time can also be used, which enables us to have more flexibilities to filter out clutter and jammer subspace with little effect on the output SINR. The potential advantage is that it may achieve the superiority that the PA radar can never reach without any additional cost on hardware. In particular, the flexibly adjustable design of TB strategies in MIMO radar may allow to improve the clutter and jammer suppression performance from the standpoint of coherent processing gain.

Another important reason for studying the impacts of MIMO radar configuration on clutter mitigation and jammer suppression is that MIMO radar enables improved spatial resolution and enhanced parameter identifiability performance [9], which can improve the possibility of distinguishing the potential target from clutter and jamming signals. When it comes to the GMTI application, the superiority becomes that a better minimum detectable velocity (MDV) can be attained [16].

However, the clutter mitigation and jammer suppression problems in the context of MIMO radar are challenging. The extra DOFs introduced by the MIMO radar increase the rank of the clutter and jamming subspace, making the suppression techniques more complicated with higher complexity. Moreover, the challenge is also to deal with the multiple-waveform

transmission in MIMO radar. Note that waveforms which are absolutely orthogonal to each other at any time lag do not exist [146], and the non-ideal orthogonality of waveforms leads to mismatches after pulse compression. Consequently, the clutter rank in the covariance matrix associated with a given single Doppler cell is increased for some particular waveforms, which can also degrade the performance of GMTI applications.

The above-mentioned challenges stimulate us to develop advanced techniques for MIMO radar clutter and jammer suppression, and if possible, to make use of the unique characteristics and capabilities of MIMO radar. Towards this end, we conduct the clutter mitigation and jammer suppression for MIMO radar using spatial and/or temporal adaptive processing techniques.

The results to be reviewed mainly focus on the aspects listed as follows.

1. Build the generalized signal model adapting to multiple radar configurations and meanwhile considering the effect of waveforms.
2. Develop possibly efficient spatial processing techniques by virtue of the unique spatial structure of MIMO radar.
3. Devise simple robust spatial processing techniques that facilitate estimating the DOA and the power of interfering sources.
4. Find spatial and temporal adaptive processing techniques in the context of the TB-based MIMO radar.

4.1 Generalized signal model

Let us start by considering the TB-based MIMO radar configuration, where the radar is equipped with a transmit array of M and a receive array of N antenna elements. Both arrays are colocated so that they lead to a monostatic setup which shares an identical spatial angle for a far-field target. Without loss of generality, we assume that K ($K \leq M$) transmit beams are synthesized by means of the TB matrix $\mathbf{C} \in \mathbb{C}^{M \times K}$. Moreover, let us denote $\phi(t) = [\phi_1(t), \dots, \phi_K(t)]^T \in \mathbb{C}^{K \times 1}$ as the vector of envelopes for the transmitted waveforms at the given fast time t , with each waveform having unit energy within one slow-time pulse interval of duration T_p . Ideally, these K transmitted waveforms are expected to be mutually orthogonal at

any time lag.

The general space-(fast and slow) time signal model for the vector of the receive array observations, denoted by $\mathbf{x}(t, \tau) \in \mathbb{C}^{N \times 1}$, can be expressed as

$$\mathbf{x}(t, \tau) = \mathbf{x}_t(t, \tau) + \mathbf{x}_c(t, \tau) + \mathbf{x}_j(t, \tau) + \mathbf{x}_n(t, \tau) \quad (4.1)$$

where t and τ denote respectively the fast- and slow-time indices, and $\mathbf{x}_t(t, \tau) \in \mathbb{C}^{N \times 1}$, $\mathbf{x}_c(t, \tau) \in \mathbb{C}^{N \times 1}$, $\mathbf{x}_j(t, \tau) \in \mathbb{C}^{N \times 1}$, and $\mathbf{x}_n(t, \tau) \in \mathbb{C}^{N \times 1}$ stand for the received signals of the target, clutter, jammer, and noise, respectively, which are assumed to be uncorrelated to each other.

The received target and backscattered radar clutter signals can be respectively expressed as

$$\mathbf{x}_t(t, \tau) = \sqrt{\frac{E}{K}} \alpha_t D_t(\tau) ((\mathbf{C}^H \mathbf{a}(\theta_t))^T \phi(t - \zeta_0)) \mathbf{b}(\theta_t) \quad (4.2)$$

$$\mathbf{x}_c(t, \tau) = \sqrt{\frac{E}{K}} \sum_{i=1}^{N_c} \xi_i D_i(\tau) ((\mathbf{C}^H \mathbf{a}(\theta_i))^T \phi(t - \zeta_0)) \mathbf{b}(\theta_i) \quad (4.3)$$

where E is the transmit energy, ζ_0 is the fast-time delay of the range of interest consisting of N_c patches, θ_t and θ_i , α_t and ξ_i , and $D_t(\tau)$ and $D_i(\tau)$ are the pairs of spatial angles, complex reflection coefficients, and Doppler shifts for the target and the i th clutter patch, respectively, and $\mathbf{a}(\theta)$ and $\mathbf{b}(\theta)$ are the transmit and receive array steering vectors, respectively.

The received jamming observations can be expressed as

$$\mathbf{x}_j(t, \tau) = \sum_{j=1}^J \sum_{p=1}^P \beta_{j,p} s_j(t - \zeta_0 - \zeta_p, \tau) \mathbf{b}(\vartheta_{j,p}) \quad (4.4)$$

where $\{s_j(t, \tau)\}_{j=1}^J$ is the set of J arbitrarily independent jamming signals, with each assumed to propagate through P independent paths that are caused by direct, specular and diffuse scatters, ζ_p is the fast-time delay of the p th path, $\beta_{j,p}$ and $\vartheta_{j,p}$ are the magnitude of the j th jamming signal propagated through the p th path and the corresponding spatial angle, respectively. In addition, the received noise observation is assumed to be white and Gaussian distributed.

At the receiving end, a filterbank that consists of the K transmitted waveforms is used for extracting the waveform characteristics from the received data $\mathbf{x}(t, \tau)$. After extracting (i.e., match-filtering) the receive data

at the fast-time index ζ and then stacking the results into a column vector, the output at the receiver, denoted by $\mathbf{y}(\zeta, \tau) \in \mathbb{C}^{KN \times 1}$, can be expressed as

$$\begin{aligned} \mathbf{y}(\zeta, \tau) &= \text{vec} \left(\int_{T_p} \mathbf{x}(t, \tau) \boldsymbol{\phi}^H(t - \zeta) dt \right) \\ &\triangleq \mathbf{y}_t(\zeta, \tau) + \mathbf{y}_c(\zeta, \tau) + \mathbf{y}_j(\zeta, \tau) + \mathbf{y}_n(\zeta, \tau) \end{aligned} \quad (4.5)$$

where $\mathbf{y}_t(\zeta, \tau) \in \mathbb{C}^{KN \times 1}$, $\mathbf{y}_c(\zeta, \tau) \in \mathbb{C}^{KN \times 1}$, $\mathbf{y}_j(\zeta, \tau) \in \mathbb{C}^{KN \times 1}$, and $\mathbf{y}_n(\zeta, \tau) \in \mathbb{C}^{KN \times 1}$ are respectively the match-filtered target, clutter, jamming, and noise components expressed as

$$\mathbf{y}_t(\zeta, \tau) = \sqrt{\frac{E}{K}} \alpha_t D_t(\tau) \mathbf{u}(\theta_t, \zeta) \otimes \mathbf{b}(\theta_t) \quad (4.6)$$

$$\mathbf{y}_c(\zeta, \tau) = \sqrt{\frac{E}{K}} \sum_{i=1}^{N_c} \xi_i D_i(\tau) \mathbf{u}(\theta_i, \zeta) \otimes \mathbf{b}(\theta_i) \quad (4.7)$$

$$\mathbf{y}_j(\zeta, \tau) = \sum_{j=1}^J \sum_{p=1}^P \beta_{j,p} \boldsymbol{\eta}_{j,p}(\zeta, \tau) \otimes \mathbf{b}(\vartheta_{j,p}) \quad (4.8)$$

and

$$\mathbf{y}_n(\zeta, \tau) = \text{vec} \left(\int_{T_p} \mathbf{x}_n(\zeta, \tau) \boldsymbol{\phi}^H(t - \zeta) dt \right). \quad (4.9)$$

Here, $\mathbf{u}(\theta, \zeta) \in \mathbb{C}^{K \times 1}$ and $\boldsymbol{\eta}_{j,p}(\zeta, \tau) \in \mathbb{C}^{K \times 1}$ are respectively the synthesized beamspace steering vector with consideration of the waveform effect that is characterized by the waveform covariance matrix $\mathbf{R}_\phi(\zeta) \in \mathbb{C}^{K \times K}$ and the match-filtered jamming signal component, which take the forms given as follows

$$\mathbf{u}(\theta, \zeta) \triangleq \mathbf{R}_\phi^T(\zeta) \mathbf{C}^H \mathbf{a}(\theta) \quad (4.10)$$

$$\mathbf{R}_\phi(\zeta) \triangleq \int_{T_p} \boldsymbol{\phi}(t) \boldsymbol{\phi}^H(t - \zeta + \zeta_0) dt \quad (4.11)$$

$$\boldsymbol{\eta}_{j,p}(\zeta, \tau) \triangleq \int_{T_p} s_j(t - \zeta_0 - \zeta_p, \tau) \boldsymbol{\phi}^*(t - \zeta) dt \quad (4.12)$$

Note that (4.5) serves as a generalized signal model. Given properly designed beamspace matrix \mathbf{C} for $\mathbf{u}(\theta, \zeta)$, the explicit expressions for the target and clutter models in (4.6) and (4.7) can be adapted to the PA, MIMO, TB-based MIMO, and many other possible monostatic radar configurations.

4.2 Jammer suppression via space-(fast) time adaptive processing in MIMO radar

Let us take the conventional MIMO radar for example, i.e., choose $K = M$ and $\mathbf{C} = \mathbf{I}_M$ in the generalized signal models (4.6)–(4.9). The interest here is to study the suppression of the terrain-scattered jammer, or to be specific, to study the barrage noise jamming suppression in MIMO radar. Such jammer suppression is not supposed to affect the stationarity of clutter so that a subsequent procedure of cascaded clutter mitigation can be applied.

In order to study the effect of matched filtering on jamming signals, the temporal cross-correlations and space-time covariance matrix with respect to a certain transmitted waveform after matched filtering have been derived in Publication III. The characteristic of the derived match-filtered jamming signals have been used in developing SFTAP techniques for the terrain-scattered jammer suppression. Moreover, both the waveform-introduced range sidelobes and stationarity of cold clutter over different pulse intervals have been considered in the proposed SFTAP designs.

4.2.1 Effect of matched filtering on the correlations of jamming signals

The barrage noise jamming signals $s_j(t, \tau)$, $j = 1, \dots, J$ are independently generated from stationary white random processes. Therefore, it is necessary to first perform correlation analysis on the match-filtered vector $\boldsymbol{\eta}_{j,p}(\zeta, \tau)$ in (4.8) since it is the only term determining the correlation property of the jamming components.

The analysis has shown that the temporal cross-correlation matrix of $\boldsymbol{\eta}_{j,p}(\zeta, \tau)$, denoted by $\mathbf{R}_{j,p,j',p'}^{\boldsymbol{\eta}}(\zeta, \zeta', \tau, \tau') \in \mathbb{C}^{M \times M}$, can be derived as

$$\begin{aligned} \mathbf{R}_{j,p,j',p'}^{\boldsymbol{\eta}}(\zeta, \zeta', \tau, \tau') &\triangleq \mathbb{E}\{\boldsymbol{\eta}_{j,p}(\zeta, \tau)\boldsymbol{\eta}_{j',p'}^H(\zeta', \tau')\} \\ &= \mathbb{E}\left\{\iint_{T_p} \iint_{T_p} s_j(t - \zeta_0 - \zeta_p, \tau) s_{j'}^*(u - \zeta_0 - \zeta_{p'}, \tau') \boldsymbol{\phi}^*(t - \zeta) \boldsymbol{\phi}^T(u - \zeta') dt du\right\} \\ &= S_j(f_c) \delta_{jj'} \delta_{\tau\tau'} \mathbf{R}_{\boldsymbol{\phi}}^T(\zeta_p - \zeta_{p'} + \zeta' - \zeta + \zeta_0) \end{aligned} \quad (4.13)$$

where $S_j(f_c)$ is the jamming PSD at carrier frequency f_c , and $\delta_{jj'}$ and $\delta_{\tau\tau'}$ are both Kronecker delta functions.

The significance of (4.13) is that it establishes the relationship with the waveform covariance matrix after matched filtering. Given the jamming

signal, the temporal correlation matrix in (4.13) for a fixed pulse is guaranteed to be nonzero once the term $\zeta_p - \zeta_{p'} + \zeta' - \zeta$ is equal to zero. Such temporal correlation analysis is the foundation for further analyzing the space-time covariance matrix of the match-filtered jamming components.

On the basis of the above result, the space-time covariance matrix of the match-filtered jamming components, denoted by $\mathbf{R}_j(\zeta, \zeta', \tau, \tau') \in \mathbb{C}^{MN \times MN}$, has been derived as

$$\begin{aligned}
 \mathbf{R}_j(\zeta, \zeta', \tau, \tau') &\triangleq \mathbb{E}\{\mathbf{y}_j(\zeta, \tau)\mathbf{y}_j^H(\zeta', \tau')\} \\
 &= \sum_{j=1}^J \sum_{j'=1}^J \sum_{p=1}^P \sum_{p'=1}^P \beta_{j,p}\beta_{j',p'}^* \mathbf{R}_{j,p,j',p'}^\eta(\zeta, \zeta', \tau, \tau') \otimes (\mathbf{b}(\vartheta_{j,p})\mathbf{b}^H(\vartheta_{j',p'})) \\
 &= S_j(f_c)\delta_{\tau\tau'} \sum_{j=1}^J \sum_{p=1}^P \sum_{p'=1}^P \beta_{j,p}\beta_{j,p'}^* \mathbf{R}_\phi^T(\zeta_p - \zeta_{p'} + \zeta' - \zeta + \zeta_0) \otimes (\mathbf{b}(\vartheta_{j,p})\mathbf{b}^H(\vartheta_{j,p'})).
 \end{aligned} \tag{4.14}$$

The result in (4.14) enables us to quantify the effect of matched filtering in MIMO radar on the jamming components. Note that the jamming signals after matched filtering remain to be uncorrelated over the slow-time domain in MIMO radar. However, their correlation levels over the fast-time domain have been changed, and the corresponding extent is related to the frequency of multipath occurrence. The analysis here implies that the terrain-scattered jamming in MIMO radar can be suppressed by means of properly designed SFTAP techniques.

4.2.2 Space-(fast) time adaptive processing designs

The analysis of jamming components after matched filtering shows that the correlations in spatial and fast-time domains exist, which can be exploited for the purpose of terrain-scattered jammer suppression. Since the clutter signals are correlated in slow-time domain, the mitigation of them has to be cascaded with the suppression of jamming signals if the problem size is not allowed to increase significantly. In this case, the key technical issue is to keep the clutter stationarity over slow-time domain after conducting the jammer suppression. The potential benefit of doing so is that a direct slow-time Doppler processing can then be used.

Towards this end, two SFTAP designs have been proposed. The first one

has been shown to lead to a close-form solution, which has been formulated as the following optimization problem

$$\min_{\mathbf{w}(\tau)} \quad \mathbf{w}^H(\tau) \mathbf{R}_{\text{jn}} \mathbf{w}(\tau) \quad (4.15\text{a})$$

$$\text{s.t.} \quad \mathbf{w}^H(\tau) \mathbf{s}_t(\theta_t) = 1 \quad (4.15\text{b})$$

$$\frac{\mathbf{w}^H(\tau) \mathbf{R}_c(\tau) \mathbf{w}(\tau)}{\mathbf{w}^H(0) \mathbf{R}_c(\tau) \mathbf{w}(0)} = 1 \quad (4.15\text{c})$$

$$\mathbf{w}^H(\tau) \tilde{\mathbf{u}}(\zeta_0, \theta_t) = 0 \quad (4.15\text{d})$$

where $\mathbf{s}_t(\theta_t) \in \mathbb{C}^{MNQ \times 1}$ is the target steering vector with Q fast-time taps exploited, $\mathbf{w}(\tau) \in \mathbb{C}^{MNQ \times 1}$ and $\mathbf{R}(\tau) \in \mathbb{C}^{MNQ \times MNQ}$ are respectively the adaptive weight vector and the clutter covariance matrix for the τ th (first index starting from 0) slow-time pulse, $\mathbf{R}_{\text{jn}} \in \mathbb{C}^{MNQ \times MNQ}$ is the jammer-pulse-noise covariance matrix, and

$$\tilde{\mathbf{u}}(\zeta_0, \theta_t) \triangleq [0, \mathbf{u}^T(\zeta_0 + 1, \theta_t), \dots, \mathbf{u}^T(\zeta_0 + Q - 1, \theta_t)]^T \otimes \mathbf{b}(\theta_t) \quad (4.16)$$

with $\mathbf{u}(\zeta, \theta_t)$ defined in (4.10).

Note that (4.15) deals with the SFTAP design problem for each transmitted pulse since the Doppler information of clutter signals changes over slow-time domain. The clutter stationarity is guaranteed by the constraint (4.15c), and the attenuation of range sidelobes is enabled by (4.15d). The close-form solution to (4.15) is given by

$$\mathbf{w}(\tau) = (\mathbf{R}_{\text{jn}} + \lambda \mathbf{R}_c(\tau))^{-1} \mathbf{v}(\zeta_0, \theta_t) (\mathbf{v}^H(\zeta_0, \theta_t) (\mathbf{R}_{\text{jn}} + \lambda \mathbf{R}_c(\tau))^{-1} \mathbf{v}(\zeta_0, \theta_t))^{-1} \mathbf{e} \quad (4.17)$$

where $\mathbf{v}(\zeta_0, \theta_t) \triangleq [\mathbf{s}_t(\theta_t), \tilde{\mathbf{u}}(\zeta_0, \theta_t)]$, $\mathbf{e} \triangleq [1, 0]^T$, and λ is determined by the smallest eigenvalue of the matrix $\mathbf{R}_c^{-1/2}(\tau) \mathbf{R}_{\text{jn}} \mathbf{R}_c^{-1/2}(\tau) / (\mathbf{w}^H(0) \mathbf{R}_c(\tau) \mathbf{w}(0))$ that is supposed to be positive definite. The solution (4.17) is valid only when the matrix inverse in (4.17) exists. In practice, the clutter and jamming-plus-noise covariance matrices have to be estimated. We can also resort to the estimation strategies developed in the conventional PA radar, for example, the methods in [250] and references therein.

The second SFTAP design has been proposed on the basis of the first one. It allows for a larger feasibility set through relaxation of the latter two

constrains in (4.15), and therefore, can avoid the possibility of non-existing solution to (4.15). Mathematically, it has been formulated as

$$\min_{\mathbf{w}(\tau)} \quad \mathbf{w}^H(\tau) \mathbf{R}_{\text{jn}} \mathbf{w}(\tau) \quad (4.18a)$$

$$\text{s.t.} \quad \mathbf{w}^H(\tau) \mathbf{s}_t(\theta_t) = 1 \quad (4.18b)$$

$$\|\mathbf{w}^H(\tau) \mathbf{R}_c^{1/2}(\tau) - \mathbf{w}^H(0) \mathbf{R}_c^{1/2}(\tau)\| \leq \epsilon \quad (4.18c)$$

$$|\mathbf{w}^H(\tau) \tilde{\mathbf{u}}(\zeta_0, \theta_t)| \leq \gamma \quad (4.18d)$$

where $\epsilon \geq 0$ is the parameter that bounds the difference of clutter distortions after adaptive processing, and $\gamma \geq 0$ is the parameter of user choice characterizing the worst acceptable range sidelobe mitigation levels.

Once either of the two proposed SFTAP designs is applied to the received data of the MIMO radar, the slow-time adaptive Doppler processing can therefore be performed.

4.3 Joint clutter mitigation and jammer suppression in the TB-based MIMO radar

If higher computational complexity is permitted by the hardware of radar system, the clutter mitigation and jammer suppression can be conducted at the same time. In this case, the proposed SFTAP design needs to be expanded to space-(fast and slow) time adaptive processing, i.e., the 3D STAP comes into effect.

The motivation here is to investigate the joint clutter mitigation and terrain scattered jammer suppression problem in the context of the TB-based MIMO radar. Provided that the clutter and jammers can be well suppressed simultaneously, we have the opportunity to additionally enjoy and efficiently exploit the benefits of transmit processing gain and waveform diversity obtained by the TB-based MIMO radar.

The key issue here is to formulate the 3D STAP problem for the TB-based MIMO radar and then develop efficient techniques for solving the problem. Such study also triggers the clutter rank analysis since the configuration of the TB-based MIMO radar differs from that of the PA and conventional MIMO radar configurations. Therefore, the interest is also to explore the

clutter rank for the sake of developing simple and computationally efficient 3D STAP algorithms.

In the following, the results reported in Publication IV are reviewed.

4.3.1 3D STAP design

The joint clutter mitigation and jammer suppression in the TB-based MIMO radar has been formulated as the following 3D STAP problem

$$\begin{aligned} \min_{\mathbf{w}} \quad & \mathbf{w}^H \mathbf{R}_y \mathbf{w} \\ \text{s.t.} \quad & \mathbf{w}^H \mathbf{s}_t(\bar{Q}, f_s(\theta_t), f_d(\theta_t)) = 1 \end{aligned} \quad (4.19)$$

where $\mathbf{R}_y \in \mathbb{C}^{QLKN \times QLKN}$ is the clutter-jammer-plus-noise covariance matrix (calculated via Q fast-time and L slow-time taps), and $\mathbf{s}_t(\bar{Q}, f_s(\theta_t), f_d(\theta_t))$ is the steering vector of the target expressed as

$$\mathbf{s}_t(\bar{Q}, f_s(\theta_t), f_d(\theta_t)) \triangleq \mathbf{e}_{\bar{Q}} \otimes \mathbf{d}(\theta_t) \otimes \mathbf{u}(\theta_t, \bar{Q}) \otimes \mathbf{b}(\theta_t) \quad (4.20)$$

with $\bar{Q} \triangleq (Q + 1)/2$, $\mathbf{e}_{\bar{Q}} \in \mathbb{C}^{Q \times 1}$ being a vector of all zeros except the \bar{Q} th entry replaced by 1, and $f_s(\theta_t)$ and $f_d(\theta_t)$ being the spatial and Doppler frequencies of the target, respectively.

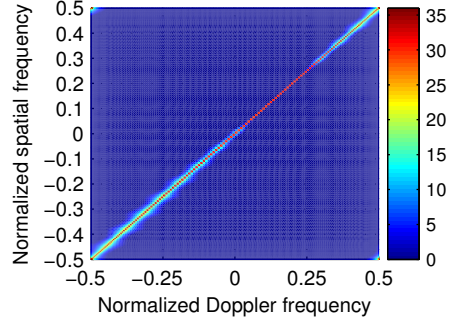
The 3D STAP problem (4.19) leads to the following MVDR solution

$$\mathbf{w} = \frac{\mathbf{R}_y^{-1} \mathbf{s}_t(\bar{Q}, f_s(\theta_t), f_d(\theta_t))}{\mathbf{s}_t^H(\bar{Q}, f_s(\theta_t), f_d(\theta_t)) \mathbf{R}_y^{-1} \mathbf{s}_t(\bar{Q}, f_s(\theta_t), f_d(\theta_t))} \quad (4.21)$$

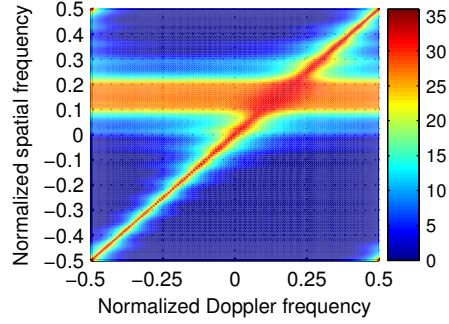
which can cause heavy computational burden if we directly calculate the $QLKN$ -dimensional matrix inverse. Therefore, the issue of efficiently computing the solution (4.21) has to be further studied, which is to be reviewed in the following subsections.

4.3.2 Rank analysis of the TB strategy enabled clutter

In the TB-based MIMO radar, the TB matrix $\mathbf{C} \in \mathbb{C}^{M \times K}$ is normally designed in advance, which mainly depends on the knowledge of the SOI. The possible byproduct of applying the TB matrix is the attenuation of sidelobe levels and the possibility of flexibly choosing the beamspace dimension K , provided that the illuminating beams guarantee the coverage over the whole SOI.



(a) Spectrum with clutter subspace only



(b) Spectrum with clutter and jammer space

Figure 4.1. Clutter spectrum with and without the presence of jamming subspace in the TB-based MIMO radar. Here $M = 16$ transmit and $N = 5$ receive antenna elements are used, $K = 4$ transmit beams are synthesized for the coverage of SOI $[10^\circ, 25^\circ]$, and $L = 5$ slow-time pulses are exploited. The clutter to noise ratio (CNR) and jammer to noise ratio (JNR) are both set to 50 dB.

Since the clutter results from the radar radiated signals, the spatial structure of it is partially determined by the TB matrix C . When clutter mitigation is taken into consideration in the TB-based MIMO radar, the clutter subspace can be expanded and therefore become difficult to separate from the jammer-plus-noise space because of the TB strategy. In this case, the difficulty of developing efficient 3D STAP technique is even increased. A simulated example of the clutter spectrum with and without the presence of jamming subspace in the context of the TB-based MIMO radar is shown in Fig. 4.1. It can be seen that the cold clutter ridge concentrates on the region of SOI, meaning that more cold clutter energy is focused because of the TB strategy. When the jamming subspace is present, the region of

SOI is completely contaminated, and all the Doppler frequencies of this region are occupied. Moreover, the clutter ridge spreads at a certain extent, meaning that the potential target can be submerged in the harsh hybrid clutter.

To alleviate the restriction, the TB strategy that enables an approximation of linear phase rotations among transmit beams has been proposed as a valid approach. Mathematically, the desired approximation can be expressed as

$$\mathbf{C}^H \mathbf{a}(\theta_b) \simeq \mathbf{g}(\theta_b) \triangleq \left[e^{j\mu_1(f_s(\theta_b))}, \dots, e^{j\mu_K(f_s(\theta_b))} \right]^T, \quad b = 1, \dots, B \quad (4.22)$$

where $\mu_i(f_s(\theta_b))$, $i = 1, \dots, K$ are the uniform linear functions of the spatial frequency $f_s(\theta_b)$ and B is the number of angular grids for SOI approximation. The meaning of (4.22) is to simply enforce approximately the structure of linear phase in the pseudo-element space spanned by $\mathbf{g}(\theta_b)$. Hence, the well-known Brennan's rule on clutter rank estimation can be used for analyzing the rank of the TB enabled clutter subspace.

The clutter covariance matrix, denoted by $\mathbf{R}_c \in \mathbb{C}^{QLKN \times QLKN}$, has been shown to have a block diagonal structure, and its rank is characterized by the quantity r_c given as follows

$$r_c \triangleq Q \lceil N + \rho(K - 1) + \eta(L - 1) \rceil \quad (4.23)$$

where ρ denotes the ratio between the synthesized transmit aperture (associated with $\mathbf{g}(\theta)$) and the receive one and η stands for the ratio between radar movement within one pulse and the neighbor receive antenna element space.

There may exist other good TB strategies that even enable lower clutter rank. However, it is hard/impossible to come up to an *a priori* best choice of the TB strategy in general because many other aspects have to be simultaneously considered, such as the out-of-sector sidelobe attenuation extent, the mainlobe ripples, etc.

For the jamming studied here, its covariance matrix, denoted by $\mathbf{R}_h \in \mathbb{C}^{QLKN \times QLKN}$, has been found to take the following form

$$\mathbf{R}_h = \mathbf{R}_Q \otimes (\mathbf{I}_{LK} \otimes \mathbf{R}_N) \quad (4.24)$$

where $\mathbf{R}_Q \in \mathbb{C}^{Q \times Q}$ is the fast-time Toeplitz cross-correlation matrix dependent on the bandwidth of the jamming signal, and $\mathbf{R}_N \in \mathbb{C}^{N \times N}$ is a

spatial covariance matrix of the jamming multipath. The matrix \mathbf{R}_h has been shown to generally have the rank of QLK times that of \mathbf{R}_N , and it has also been shown to have $Q \times Q$ space-(slow) time diagonal blocks.

The noise covariance matrix, denoted by $\mathbf{R}_z \in \mathbb{C}^{QLKN \times QLKN}$, generally has full rank and takes the form $\mathbf{R}_z = \sigma_z^2 \tilde{\mathbf{R}}_Q \otimes \mathbf{I}_{LKN}$ with $\tilde{\mathbf{R}}_Q \in \mathbb{C}^{Q \times Q}$ being the fast-time cross-correlation matrix of noise caused by range sidelobes.

4.3.3 Computationally efficient 3D STAP method

Recall that the solution (4.21) to the 3D STAP problem needs calculating the inverse of the high-dimensional clutter-jammer-plus-noise covariance matrix. To tackle this difficulty, a computationally efficient method for obtaining the 3D STAP weight vector has been proposed in Publication IV, whose main ideas are summarized as follows.

The inverse of the original covariance matrix has been developed into several parts that involve both the inverse of the jammer-plus-noise covariance matrix and the inverse of clutter-related matrices. The calculation of the former inverse has exploited the special structure of the jammer and noise covariance matrices, while the calculation of the latter inverses have exploited the results of the clutter rank analysis and has manipulated with the clutter subspace. Specifically, using the theory of clutter rank approximation, the latter clutter-related matrix inverses have been converted to simple calculations with respect to the receive data observations and the jammer-plus-noise covariance matrices. As a result, the calculation of the original $QLKN$ -dimensional matrix inverse has been simplified into the calculations of lower-dimensional matrix inverse as well as some matrix-vector products.

In the proposed 3D STAP method, the covariance matrix estimation has also been performed. It is worth noting that the jammer-plus-noise covariance matrix can be estimated by switching the radar system to the mode of passive receiving. For the terrain-scatter jamming signals studied here, the jammer-plus-noise covariance matrix can be estimated efficiently in this way because the jamming signals are wide-sense stationary over the temporal domain. Here, we show the simulated SINR performance of the proposed 3D STAP algorithm as well as its superiority over the

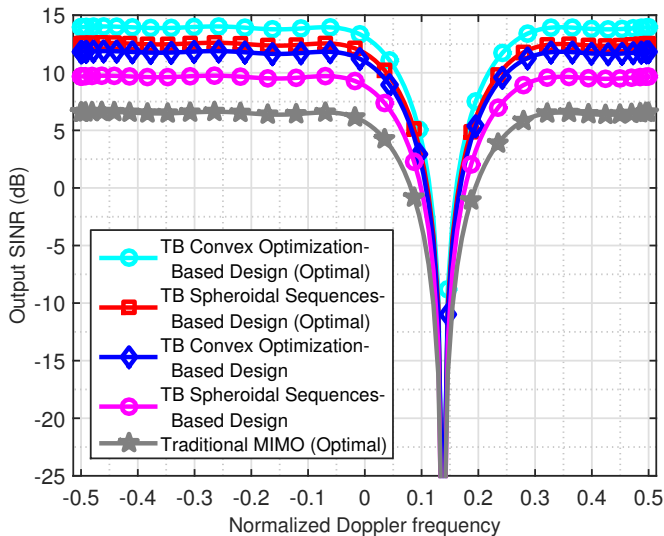


Figure 4.2. The SINR performance versus normalized Doppler frequencies. Here $M = 16$ transmit and $N = 5$ receive antenna elements are used, $K = 4$ transmit beams are synthesized, and $L = 5$ slow-time pulses are exploited. The SNR, CNR, and JNR are set to 0 dB, 50 dB, and 50 dB, respectively. The mark “Optimal” in difference cases means that the output SINRs are calculated using known clutter and jammer covariance matrices.

conventional MIMO STAP in Fig. 4.2.

4.4 Spatial adaptive processing for powerful jammer suppression in MIMO radar

The interest here is to investigate the possible capability of MIMO radar on powerful jammer suppression using only spatial processing techniques. The clutter signals are secondary in this study, therefore, are classified as signals from interfering sources. In this case, the signal model of clutter is similar to that of desired targets. Hence, the general models in (4.6) and (4.7) for both the target and clutter have been combined (see (4.25) in the following), and the Doppler information and sidelobes of waveform correlations after matched filtering therein have been ignored. The remaining parameters in the general models have been chosen as $E = M$ and $C = \mathbf{I}_M$.

4.4.1 Reduced dimensional beamspace designs

Let us assume that L targets including the desired and interfering sources are present in the background of noise. In the presence of J powerful jammers, the simplified signal model can be expressed as

$$\mathbf{y}(\tau) = \sum_{l=1}^L \alpha_l(\tau) \mathbf{v}(\theta_l) + \sum_{j=1}^J \beta_j(\tau) \tilde{\mathbf{v}}(\theta_j) + \tilde{\mathbf{z}}(\tau) \quad (4.25)$$

where $\beta_j(\tau)$ is the signal of the j th jammer, θ_j is the presumed spatial angle associated with the j th jammer, and $\mathbf{v}(\theta_l)$ and $\tilde{\mathbf{v}}(\theta_j)$ are the virtual steering vectors of the l th target and the j th jammer, respectively.

The following scenario is of interest here. That is, the desired targets are assumed to be located within the SOI where powerful jamming sources are also present. Both the targets and jammers may even have the same spatial angles, while the interfering sources are located outside the SOI. In general, both the in-sector jamming and the out-of-sector interfering sources are unknown.

Let $\mathbf{B} \in \mathbb{C}^{MN \times D}$ be the RD beamspace matrix that transforms the original data vector $\mathbf{y}(\tau) \in \mathbb{C}^{MN \times 1}$ to a new data vector of length D , denoted by $\tilde{\mathbf{y}}(\tau) \in \mathbb{C}^{K \times 1}$, which is expressed in the following form

$$\tilde{\mathbf{y}}(\tau) = \mathbf{B}^H \mathbf{y}(\tau) \quad (4.26)$$

whose covariance matrix is expressed as

$$\begin{aligned} \mathbf{R}_{\tilde{\mathbf{y}}} &\triangleq \mathbb{E}\{\tilde{\mathbf{y}}(\tau) \tilde{\mathbf{y}}^H(\tau)\} = \mathbf{B}^H \mathbb{E}\{\mathbf{y}(\tau) \mathbf{y}^H(\tau)\} \mathbf{B} \\ &\triangleq \mathbf{B}^H \mathbf{R}_{\mathbf{y}} \mathbf{B} \end{aligned} \quad (4.27)$$

where $\mathbf{R}_{\mathbf{y}} \in \mathbb{C}^{MN \times MN}$ denotes the covariance matrix of the original received data $\mathbf{y}(\tau)$.

The main idea of conducting RD beamspace designs is to preserve desired signal energy received within the SOI, and to simultaneously attenuate the energy of the in-sector jamming and out-of-sector interfering sources. The essential meaning of these RD beamspace processing techniques is to significantly reduce the computational burden and meanwhile to achieve good suppression performance.

Technically, a quiescent response beamspace matrix denoted by \mathbf{B}_q , which ensures the preservation of energy received within the desired SOI, has

been achieved by exploiting certain beamspace design techniques. For example, the spheroidal sequences based methods [184, 266] can be used to implement transmit energy focusing. Then, the robust/adaptive RD beamspace processing has been proposed, aiming at preserving the desired signal components while suppressing the in-sector powerful jammers and/or filtering out the interfering components that come from the outside of SOI. Trade-offs between the in-sector source distortion and the out-of-sector source attenuation have been made while imposing a constraint used to nullify the jammers.

A. The first beamspace design

The first solution is to upper-bound the acceptable difference between the desired and quiescent response beamspace matrices while maximizing the worst-case in-sector jammers suppression. Additionally, the out-of-sector sidelobes can be kept below a certain level to insure interference attenuation. The corresponding optimization problem can be written as

$$\begin{aligned} \min_{\mathbf{B}} \max_i \quad & \|\mathbf{B}^H \tilde{\mathbf{v}}(\theta_i)\|, \theta_i \in \Omega, i = 1, \dots, Q \\ \text{s.t.} \quad & \|\mathbf{B} - \mathbf{B}_q\|_F \leq \varepsilon \\ & \|\mathbf{B}^H \tilde{\mathbf{v}}(\bar{\theta}_k)\| \leq \gamma, \bar{\theta}_k \in \bar{\Omega}, k = 1, \dots, K \end{aligned} \quad (4.28)$$

where $\varepsilon > 0$ is the parameter that bounds the in-sector signal distortion caused by the beamspace matrix \mathbf{B} as compared to \mathbf{B}_q , $\gamma > 0$ is the parameter of the user choice that characterizes the worst acceptable out-of-sector attenuation, $\bar{\Omega}$ combines a continuum of all out-of-sector directions, and $\{\theta_i \in \Omega, i = 1, \dots, Q\}$ and $\{\bar{\theta}_k \in \bar{\Omega}, k = 1, \dots, K\}$ are grids of angles used to approximate the SOI Ω and the out-of-sector $\bar{\Omega}$ by finite numbers Q and K of directions, respectively.

B. The second beamspace design

An alternative robust approach is to minimize the difference between the desired and quiescent response beamspace matrices while keeping the in-sector jammers suppression higher than a certain desired level and, if needed, keeping the out-of-sector attenuation to an acceptable level. Hence,

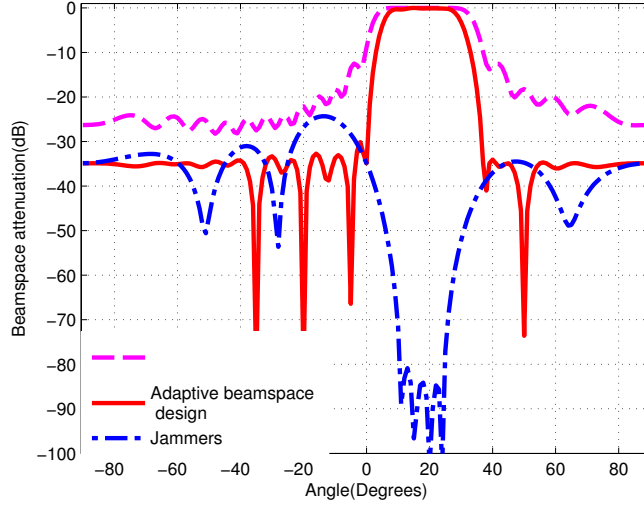


Figure 4.3. Normalized beamspace attenuation versus angles using the third design (4.30). Here $M = 16$ transmit and $N = 8$ receive antenna elements and beamspace dimension of $D = 7$ are exploited. The SOI is $\Omega = [10^\circ, 25^\circ]$ and the out-of-sector area is $\bar{\Omega} = [-90^\circ, 0^\circ] \cup [35^\circ, 90^\circ]$. Four interfering sources are located at $\theta = -35^\circ, -20^\circ, -5^\circ$, and 50° , respectively, with interference-to-noise ratio (INR) set to 40 dB. The powerful jammers are assumed to be uniformly distributed within the SOI spaced 1° apart from each other, whose jammer-to-noise ratio (JNR) is set to 50 dB. Other parameters are: $\gamma = 0.2$, $\delta = 0.1$, and $\epsilon = 1.467$.

the corresponding optimization problem can be written as

$$\begin{aligned}
 \min_{\mathbf{B}} \quad & \|\mathbf{B} - \mathbf{B}_q\|_F \\
 \text{s.t.} \quad & \|\mathbf{B}^H \tilde{\mathbf{v}}(\theta_i)\| \leq \delta, \theta_i \in \Omega, i = 1, \dots, Q \\
 & \|\mathbf{B}^H \mathbf{v}(\bar{\theta}_k)\| \leq \gamma, \bar{\theta}_k \in \bar{\Omega}, k = 1, \dots, K
 \end{aligned} \tag{4.29}$$

where $\delta > 0$ is the parameter that characterizes the worst acceptable level of the jamming power radiation in the SOI Ω . The last set of constraints in (4.28) and (4.29) are needed only if there are interfering sources located in the out-of-sector area.

C. The third beamspace design

A third approach is to develop a data-adaptive beamspace design, which is particularly important when the jammers and/or the interfering sources are varying. In order to adaptively cancel out both types of sources, the data-adaptive formulation can be developed by minimizing the output

power of the transformed vector $\tilde{\mathbf{y}}(\tau)$, and the corresponding data-adaptive beamspace design can be cast as

$$\begin{aligned} \min_{\mathbf{B}} \quad & \text{tr}\{\mathbf{B}^H \mathbf{R}_y \mathbf{B}\} \\ \text{s.t.} \quad & \|\mathbf{B} - \mathbf{B}_q\|_F \leq \varepsilon \\ & \|\mathbf{B}^H \tilde{\mathbf{v}}(\theta_i)\| \leq \delta, \theta_i \in \Omega, i = 1, \dots, Q \\ & \|\mathbf{B}^H \tilde{\mathbf{v}}(\bar{\theta}_k)\| \leq \gamma, \bar{\theta}_k \in \bar{\Omega}, k = 1, \dots, K. \end{aligned} \quad (4.30)$$

Fig. 4.3 shows the performance of the third proposed RD beamspace techniques on the attenuation of powerful jammers.

4.4.2 Robust beamforming designs

A. The first beamforming design

The first beamforming design is for the case when all the in-sector jammers are known, for example, they may be estimated beforehand using certain methods. To achieve the goal of jammer suppression, deep null notches should be formed towards the spatial directions of the jammers while maintaining distortionless response towards the direction of the target(s). Thus, the corresponding optimization problem can be written as

$$\min_{\mathbf{w}} \quad \mathbf{w}^H \mathbf{R} \mathbf{w} \quad (4.31a)$$

$$\text{s.t.} \quad \mathbf{w}^H \mathbf{v}(\theta_t) = 1 \quad (4.31b)$$

$$\mathbf{w}^H \tilde{\mathbf{v}}(\theta_j) = 0, j = 1, \dots, J \quad (4.31c)$$

where \mathbf{R} is the covariance matrix of the interference plus jammer and noise and \mathbf{w} is the designed beamforming weight vector.

B. The second beamforming design

The second beamforming design is based on the general case that the in-sector jammers and the out-of-sector interfering sources are unknown. Deep null notches should be formed towards all the possible directions of the jammers and, if needed, the out-of-sector interfering source attenuation should be kept to an acceptable level. Hence, the corresponding

optimization problem can be written as

$$\min_{\mathbf{w}} \quad \mathbf{w}^H \mathbf{R} \mathbf{w} \quad (4.32a)$$

$$\text{s.t.} \quad \mathbf{w}^H \mathbf{v}(\theta_t) = 1 \quad (4.32b)$$

$$|\mathbf{w}^H \tilde{\mathbf{v}}(\theta_i)| \leq \delta, \theta_i \in \Omega, i = 1, \dots, Q \quad (4.32c)$$

$$|\mathbf{w}^H \mathbf{v}(\bar{\theta}_k)| \leq \gamma, \bar{\theta}_k \in \bar{\Omega}, k = 1, \dots, K \quad (4.32d)$$

where the parameters used here are the same as used in the RD beamspace designs in the previous subsection.

C. Power estimates of sources

The standard MVDR beamforming problem, i.e., the problem (4.31) without the constraint (4.31c), yields the estimate of the source power σ_0^2 as

$$\sigma_0^2 = \frac{1}{\mathbf{v}^H(\theta_t) \mathbf{R}^{-1} \mathbf{v}(\theta_t)} \quad (4.33)$$

which is derived from its closed-form solution.

However, powerful jamming source that locates at the same direction as the desired target results in severe performance degradation of the standard MVDR beamforming technique. It becomes even worse when the knowledge of $\mathbf{v}(\theta_t)$ is imprecise because the standard MVDR beamformer attempts to suppress the desired target as if it was an interfering source. This happens in practice especially when there are array calibration errors and mismatches between the presumed and actual target steering vectors.

The power estimates of sources have been started from deriving the closed-form solution of a simplified version of the problem in (4.32). For the sake of simplifying the derivation, the out-of-sector interfering source attenuation constraint (4.32d) therein has been ignored. In this situation, the optimization problem (4.32) without (4.32d) has been rewritten in the following form

$$\begin{aligned} \min_{\mathbf{w}} \quad & \mathbf{w}^H \mathbf{R} \mathbf{w} \\ \text{s.t.} \quad & \mathbf{w}^H \mathbf{v}(\theta_t) = 1 \\ & \|\mathbf{w}^H \tilde{\mathbf{V}}\|_{\infty} \leq \delta \end{aligned} \quad (4.34)$$

where $\tilde{\mathbf{V}} \in \mathbb{C}^{MN \times Q}$ is constructed as $\tilde{\mathbf{V}} \triangleq [\tilde{\mathbf{v}}(\theta_1), \dots, \tilde{\mathbf{v}}(\theta_Q)]$.

Incorporating the mismatching information with the assumption that the mismatch between the actual target steering vector $\mathbf{v}(\theta)$ and the presumed target steering vector $\tilde{\mathbf{v}}(\theta)$ is bounded as $\|\tilde{\mathbf{v}}(\theta) - \mathbf{v}(\theta)\|^2 \leq \epsilon$, where ϵ is the given parameter that characterizes the worst allowable mismatch. Using also the fact that $\|\mathbf{w}^H \tilde{\mathbf{V}}\|_\infty \geq \|\mathbf{w}^H \tilde{\mathbf{V}}\|/\sqrt{MN}$, the optimization problem (4.34) can be approximated by the following

$$\begin{aligned} \min_{\mathbf{w}} \quad & \mathbf{w}^H \mathbf{R} \mathbf{w} \\ \text{s.t.} \quad & \mathbf{w}^H \tilde{\mathbf{v}}(\theta_t) = 1 \\ & \|\mathbf{w}^H \tilde{\mathbf{V}}\|^2 \leq \tilde{\delta} \end{aligned} \quad (4.35)$$

where $\tilde{\delta} \triangleq MN\delta^2$ is the new parameter that characterizes the worst acceptable level of the in-sector jamming power radiation for the second constraint in (4.34).

Until now, the method of Lagrangian multipliers can be resorted for deriving a closed-form solution to (4.35), so that the power estimates of sources can be obtained. In the following, the Lagrangian multipliers based power estimates are briefly reviewed.

The Lagrangian of the optimization problem (4.35), denoted by $L(\mathbf{w}, \lambda, \mu)$, has been defined as

$$L(\mathbf{w}, \lambda, \mu) = \mathbf{w}^H \mathbf{R} \mathbf{w} + \lambda \left(\|\mathbf{w}^H \tilde{\mathbf{V}}\|^2 - \tilde{\delta} \right) + \mu \left(-\Re\{\mathbf{w}^H \tilde{\mathbf{v}}(\theta_t)\} + 1 \right) \quad (4.36)$$

where $\lambda > 0$ and μ are the real-valued Lagrange multipliers. After introducing $\mathbf{R}_{\tilde{\mathbf{v}}} \triangleq \tilde{\mathbf{V}} \tilde{\mathbf{V}}^H$, it has been rewritten into the following form

$$L(\mathbf{w}, \lambda, \mu) = \mathbf{w}^H \mathbf{R} \mathbf{w} + \lambda \left(\mathbf{w}^H \mathbf{R}_{\tilde{\mathbf{v}}} \mathbf{w} - \tilde{\delta} \right) + \mu \left(-\Re\{\mathbf{w}^H \tilde{\mathbf{v}}(\theta_t)\} + 1 \right) \quad (4.37)$$

which satisfies the inequality $L(\mathbf{w}, \lambda, \mu) \leq \mathbf{w}^H \mathbf{R} \mathbf{w}$ for any \mathbf{w} in the feasible set defined by the constraints in (4.35). The equality $L(\mathbf{w}, \lambda, \mu) = \mathbf{w}^H \mathbf{R} \mathbf{w}$ holds on the boundary of the feasible set.

Based on the Lagrangian above, the solution to (4.35) has been derived in terms of two conditions. The first condition has been described by

$$\frac{\tilde{\mathbf{v}}^H(\theta_t) \mathbf{R}^{-1} \mathbf{R}_{\tilde{\mathbf{v}}} \mathbf{R}^{-1} \tilde{\mathbf{v}}(\theta_t)}{[\tilde{\mathbf{v}}^H(\theta_t) \mathbf{R}^{-1} \tilde{\mathbf{v}}(\theta_t)]^2} \leq \tilde{\delta} \quad (4.38)$$

which leads to the following solution

$$\bar{\mathbf{w}} = \frac{\mathbf{R}^{-1} \tilde{\mathbf{v}}(\theta_t)}{\tilde{\mathbf{v}}^H(\theta_t) \mathbf{R}^{-1} \tilde{\mathbf{v}}^H(\theta_t)}. \quad (4.39)$$

While the second condition has been described by

$$\frac{\bar{\mathbf{v}}^H(\theta_t)\mathbf{R}^{-1}\mathbf{R}_{\bar{\mathbf{v}}}\mathbf{R}^{-1}\bar{\mathbf{v}}(\theta_t)}{[\bar{\mathbf{v}}^H(\theta_t)\mathbf{R}^{-1}\bar{\mathbf{v}}(\theta_t)]^2} > \bar{\delta} \quad (4.40)$$

which leads to the solution given by

$$\bar{\mathbf{w}} = \frac{(\mathbf{R} + \bar{\lambda}\mathbf{R}_{\bar{\mathbf{v}}})^{-1}\bar{\mathbf{v}}(\theta_t)}{\bar{\mathbf{v}}(\theta_t)^H(\mathbf{R} + \bar{\lambda}\mathbf{R}_{\bar{\mathbf{v}}})^{-1}\bar{\mathbf{v}}(\theta_t)} \quad (4.41)$$

where $\bar{\lambda} > 0$ is the Lagrangian multiplier in (4.37) which can be obtained numerically using any efficient searching algorithm.

Using the above two solutions (4.39) and (4.40), the power estimate has been derived into the following generalized form

$$\bar{\sigma}_0^2 = \frac{\bar{\mathbf{v}}(\theta_t)^H(\mathbf{R} + \bar{\lambda}\mathbf{R}_{\bar{\mathbf{v}}})^{-1}\mathbf{R}(\mathbf{R} + \bar{\lambda}\mathbf{R}_{\bar{\mathbf{v}}})^{-1}\bar{\mathbf{v}}(\theta_t)}{\left[\bar{\mathbf{v}}(\theta_t)^H(\mathbf{R} + \bar{\lambda}\mathbf{R}_{\bar{\mathbf{v}}})^{-1}\bar{\mathbf{v}}(\theta_t)\right]^2} \quad (4.42)$$

which has also addressed the case under the first condition by switching $\bar{\lambda}$ to zero. We refer readers to Publication VI for the details of derivations to the results reviewed above. The corresponding beamforming performance and power estimates of an simulated example are shown in Figs. 4.4 and 4.5, respectively.

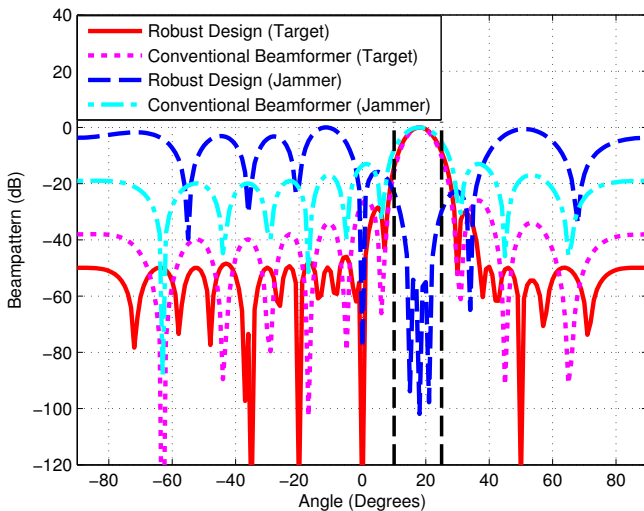


Figure 4.4. Normalized beampatterns versus angles for unknown in-sector jammers and out-of-sector interfering sources via the proposed robust beamforming technique. Here $M = 10$ transmit and $N = 10$ receive antenna elements are used. The SOI is $\Omega = [10^\circ, 25^\circ]$ and the out-of-sector area is $\bar{\Omega} = [-90^\circ, 0^\circ] \cup [35^\circ, 90^\circ]$. Four interfering sources are located at $\theta = -35^\circ, -20^\circ, 0^\circ$, and 50° , respectively, with INR set to 40 dB. Three jamming sources with DOAs $15^\circ, 18^\circ$, and 21° are present and the JNR is set to 50 dB.

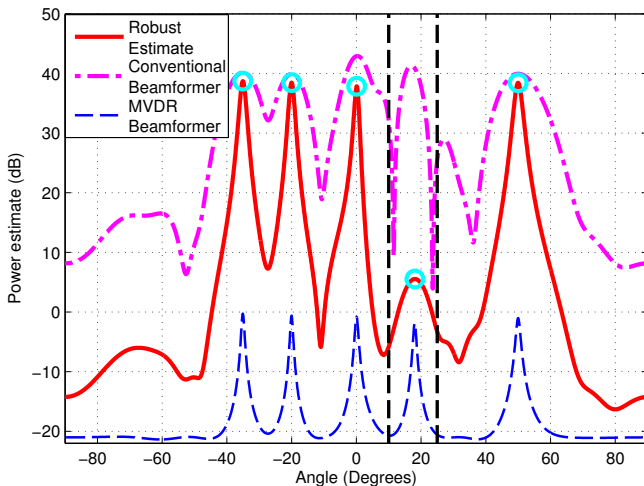


Figure 4.5. Power estimates versus angle for unknown in-sector jammers and out-of-sector interfering sources. The parameters used here is the same as in Fig. 4.4.

5. Aperiodic waveform design with good correlation properties

Waveform or code design has been the research field of significance over several decades. It is of crucial importance in many applications such as radar signal processing [10, 12, 20, 45, 47, 60, 62, 66, 67, 69, 74, 80, 84–86, 109], active sensing [28, 81, 140], communications [22], etc. As the exact form of signaling strategy, the characteristics of waveforms as well as their quality can affect the system performance a lot. The technical developments on waveform design, therefore, have always been driven by new coming applications and their various purposes, making the research on waveform design never to become complete.

The waveform or coding strategies have been studied and developed in radar signal processing since the 1930s when the earliest radar system started to emerge [85]. After that, waveforms have been fully explored for radar, which leads to the publication of several books particularly for radar signals [44, 46, 74, 84, 85]. Different types of waveforms or codes such as frequency modulated and phase coded ones have been developed over the past decades, among which the well-known examples include the LFM, OFDM, Costa, Barker, P1, P2, P4, Zadoff-Chu, maximal length sequence (also called M-sequence [48, 49]), Kasami, and Gold waveforms or sequences [44].

It has been widely realized that waveforms play an essential role in radar signal processing since “excellent” waveforms can ensure higher localization accuracy [7], enhanced resolution capability [60], and improved delay-Doppler ambiguity of the potential target [19]. Moreover, waveforms designed with robustness and/or adaptiveness can also guarantee the low possibility of interception and the capability of dealing with harsh

environments which involves heterogeneous clutter as well as active and hostile jammers [45].

Since the concept of “MIMO” was introduced to radar from communication in 2004, the topic of waveform design has even attracted more attention. The significant difference between MIMO radar waveform design and that of conventional radars lies in the waveform diversity, that is, a set of waveforms with desirable properties has to be generated in the context of the former.

For a large portion of the MIMO radar research, the harsh requirement, in theory, is that the transmitted waveforms should be mutually orthogonal at each time lag in order to extract the information associated with transmit diversity at the receiver. In other words, they are required to have perfect auto- and cross-correlation properties with emitted waveforms mutually uncorrelated to any time-delayed replica of them, which means that the target located at the range bin of interest can be easily extracted after matched filtering, while the sidelobes from other range bins are unable to attenuate it. Although it is impossible to implement the absolute waveform orthogonality, the auto- and cross-correlation levels of waveforms in MIMO radar are preferred to be as low as possible. Poor correlation properties result in the leakage of the match-filtered target and clutter energy to neighboring range bins, in consequence, the SNR loss and range sidelobes that significantly degrade MIMO radar performance occur.

The relevant question is that why we bother to devise complex approach for generating the set of waveforms but not to simply use the off-the-shelf ones with possibly slight modifications. For example, we can construct the set of waveforms for MIMO radar from a family of balanced Gold codes [50] generated by modulo-2 addition of two M-sequences. The answer is that it is of significant interest and practical importance to design MIMO radar waveforms with low aperiodic correlations, especially to design waveforms with arbitrary phases and constant modulus at each of their elements. We refer interested readers to the overview on correlation minimization based waveform design in Chapter 2 for more details with respect to this issue.

Designing aperiodic poly-phase waveforms in MIMO radar is more difficult than designing periodic ones. The correlations of the latter are symmetric with respect to time lags, and therefore, only half of them (with

known locations) need to be considered. On the contrary, the entire correlation sidelobes have to be dealt with for minimizing aperiodic correlations. Furthermore, the correlation levels associated with the maximal-length time lags on both sides (i.e., $-p + 1$ and $p - 1$ for code length p) can not be minimized because of constant magnitude (always equal to one for unimodular waveforms). Despite difficult, the benefit introduced by aperiodic waveform design is that they allow arbitrary phase values for any code length and any number of waveforms in the set. This potentially enables more DOFs, and thus, larger feasibility set for the waveform design problem. When a larger search space (or feasible region) is available, there are more possibilities for finding a better solution to the waveform design problem that is normally non-convex than it would be by searching within a fixed discrete/binary set only.

The main concern of designing aperiodic unimodular waveforms with good correlation properties for MIMO radar is the computational complexity of the developed algorithms. As reviewed in Chapter 2 for the correlation minimization based MIMO radar waveform designs, the algorithms devised for the non-convex design problems often resort to iterative procedures. Hence, the main interest turns out to be the reduction of both the computational burden per iteration and the number of iterations required for convergence. In other words, algorithms that show fast convergence speed/rate and have low complexity need to be developed.

The additional difficulty is that the problem size for waveform designs in MIMO radar quickly grows to a large scale with the increase of code length and the number of waveforms. However, they are typically non-convex especially when difficult constraints are enforced, and therefore, they cannot be solved by classical large-scale optimization algorithms developed for convex problems with relatively simple objectives and constraints [267]. Although the analytical bounds on convergence rate may be hard/impossible to derive even for some existing large-scale convex optimization algorithms, designing algorithms with provably faster convergence speed to tolerance than that of the other algorithms is possible and of high practical importance.

5.1 Problem formulation

Consider designing a set of M waveforms for a MIMO radar or communication system. Each waveform in the set is of code length P and has constant modulus, and the M waveforms are expected to be mutually orthogonal.¹ The whole waveform matrix, denoted by $\mathbf{Y} \in \mathbb{C}^{P \times M}$, is defined as

$$\mathbf{Y} \triangleq [\mathbf{y}_1, \dots, \mathbf{y}_M] \quad (5.1)$$

whose m th column $\mathbf{y}_m \in \mathbb{C}^{P \times 1}$ stands for the waveform vector launched from the m th antenna of the MIMO radar or communication system. The p th element of \mathbf{y}_m takes the following form

$$y_m(p) = e^{j\psi_m(p)}, \quad m \in \{1, \dots, M\}; \quad p \in \{1, \dots, P\} \quad (5.2)$$

where $\psi_m(p)$ denotes the phase of the unimodular waveform element $y_m(p)$, taking arbitrary value from the interval $[-\pi, \pi]$. When the number of emitted waveforms M reduces to one, the waveform matrix \mathbf{Y} becomes a column vector of length P .

In order to evaluate the quality of the waveforms from the perspective of correlation or sidelobe levels, the ISL and WISL metrics [67] can be exploited. The ISL for the set of waveforms $\{y_m(p)\}_{m=1, p=1}^{M, P}$, denoted by ζ , is given as

$$\zeta = \sum_{m=1}^M \sum_{\substack{p=-P+1 \\ p \neq 0}}^{P-1} |r_{mm}(p)|^2 + \sum_{m=1}^M \sum_{\substack{m'=1 \\ m' \neq m}}^M \sum_{p=-P+1}^{P-1} |r_{mm'}(p)|^2 \quad (5.3)$$

were

$$r_{mm'}(p) \triangleq \sum_{k=p+1}^P y_m(k) y_{m'}^*(k-p) = (r_{m'm}(-p))^* \\ m, m' \in \{1, \dots, M\}; \quad p \in \{1, \dots, P-1\} \quad (5.4)$$

is the cross-correlation between the m th and m' th waveforms at the p th time lag. Note that the first term on the right-hand side of (5.3) is the superposition of the auto-correlation levels, while the second term represents the superposition of the cross-correlation levels of the waveforms.

¹Absolutely orthogonal waveform set, i.e., orthogonal at any time lag, does not exist. Here it means that the waveforms are expected to be as orthogonal as possible.

The WISL metric for the set of waveforms $\{y_m(p)\}_{m=1,p=1}^{M,P}$, denoted by ζ_w , is given as

$$\zeta_w = \sum_{m=1}^M \sum_{\substack{p=-P+1 \\ p \neq 0}}^{P-1} \gamma_p^2 |r_{mm}(p)|^2 + \sum_{m=1}^M \sum_{\substack{m'=1 \\ m' \neq m}}^M \sum_{p=-P+1}^{P-1} \gamma_p^2 |r_{mm'}(p)|^2 \quad (5.5)$$

where $\{\gamma_p\}_{p=-P+1}^{P-1}$ are the corresponding weights for controlling the auto- and cross-correlation levels associated with different time lags, which are real-valued and symmetric, i.e., $\gamma_p = \gamma_{-p}, \forall p \in \{1, \dots, P-1\}$. If the weight γ_p equals zeros, it means that the correlation levels associated with the p th time lag are not controlled. Note that the WISL metric ζ_w in (5.5) coincides with the ISL metric ζ in (5.3) when all the ISL controlling weights take value 1.

The objective of the waveform design problem then can be stated as synthesizing unimodular and mutually orthogonal waveforms $\{y_m(p)\}_{m=1,p=1}^{M,P}$, which have as good as possible correlation or weighted correlation levels.

In terms of the ISL metric in (5.3) and the WISL metric in (5.5), the ISL and WISL minimization based unimodular waveform designs can be written as the following optimization problems

$$\begin{aligned} \min_{\mathbf{Y}} \quad & \zeta \\ \text{s.t.} \quad & |y_m(p)| = 1, \quad m = 1, \dots, M; \quad p = 1, \dots, P \end{aligned} \quad (5.6)$$

and

$$\begin{aligned} \min_{\mathbf{Y}} \quad & \zeta_w \\ \text{s.t.} \quad & |y_m(p)| = 1, \quad m = 1, \dots, M; \quad p = 1, \dots, P \end{aligned} \quad (5.7)$$

respectively, where the constraints in each optimization problem ensure the constant-modulus property for each waveform element, while the mutual orthogonality of the waveforms is guaranteed by the corresponding objective.

5.2 Fast unimodular waveform designs

This section reviews the solutions to the problems of the ISL and the WISL minimization based unimodular waveform designs. These solutions are

summaries of the results in Publications VII–IX. The MaMi technique is exploited in solving both problems.

5.2.1 Fast ISL minimization based design—ISLNew

The ISL ζ in (5.3) sums up the power of all correlation terms (i.e., sidelobe levels). In order to minimize this quantity which serves as the objective in (5.6), proper transformations and other algebraic manipulations need to be done to convert it into a simplified form. Specifically, we rewrite the ISL into a compact matrix-expressed form, apply frequency-domain transformations, and rewrite the ISL as a quartic form. Moreover, a quartic-quadratic transformation is then applied to the obtained quartic form, in which the MaMi technique is exploited twice. The devised strategy finally results in a simple iterative algorithm for solving the non-convex problem (5.6) of the ISL minimization based waveform design, with closed-form solution of low complexity at each iteration.

In for following, the key transformations and algebraic manipulations used for deriving the ISL minimization problem are briefly reviewed. Most of the details can be found in Publications VII and IX.

Let

$$\mathbf{R}_p \triangleq \begin{bmatrix} r_{11}(p) & r_{12}(p) & \dots & r_{1M}(p) \\ r_{21}(p) & r_{22}(p) & \dots & r_{2M}(p) \\ \vdots & \vdots & \ddots & \vdots \\ r_{M1}(p) & \dots & \dots & r_{MM}(p) \end{bmatrix}, p = -P + 1, \dots, 0, \dots, P - 1 \quad (5.8)$$

be the waveform correlation matrices whose elements have been defined in (5.4). In terms of \mathbf{R}_p , the ISL ζ in (5.3) can therefore be rewritten in the following compact form

$$\zeta = \sum_{p=-P+1}^{P-1} \|\mathbf{R}_p - P\mathbf{I}_M\delta_p\|^2. \quad (5.9)$$

Despite taking a brief summation form that involves squared norms, (5.9) is not a direct expression of the ISL ζ with respect to the overall waveform matrix \mathbf{Y} (or its simple stacking versions). Thus, a frequency-domain transformation of (5.9) is needed. After the transformation and also after

performing some derivations, the ISL ζ can be expressed as [66]

$$\zeta = \frac{1}{2P} \sum_{p=1}^{2P} \|\tilde{\mathbf{y}}(\omega_p) \tilde{\mathbf{y}}^H(\omega_p) - P \mathbf{I}_M\|^2 \quad (5.10)$$

where

$$\tilde{\mathbf{y}}(\omega_p) \triangleq \sum_{n=1}^P \tilde{\mathbf{y}}_n e^{-j\omega_p n}, \quad \omega_p \triangleq \frac{2\pi}{2P} p \quad (5.11)$$

$$\tilde{\mathbf{y}}_n \triangleq [y_1(n), \dots, y_M(n)]^T. \quad (5.12)$$

Expanding the norm and using the fact that $\tilde{\mathbf{y}}^H(\omega_p) \tilde{\mathbf{y}}(\omega_p) = \|\tilde{\mathbf{y}}(\omega_p)\|^2$, the ISL ζ in (5.10) can be further rewritten as

$$\zeta = \frac{1}{2P} \sum_{p=1}^{2P} \left(\|\tilde{\mathbf{y}}(\omega_p)\|^4 - 2P \|\tilde{\mathbf{y}}(\omega_p)\|^2 + P^2 M \right). \quad (5.13)$$

Introducing the vectors $\mathbf{y} \in \mathbb{C}^{MP \times 1}$ and $\mathbf{a}_p \in \mathbb{C}^{P \times 1}$, and the matrix $\mathbf{A}_p \in \mathbb{C}^{MP \times M}$, defined respectively as

$$\mathbf{y} \triangleq \text{vec}(\mathbf{Y}) = [\mathbf{y}_1^T, \dots, \mathbf{y}_M^T]^T \quad (5.14)$$

$$\mathbf{a}_p \triangleq [1, e^{j\omega_p}, \dots, e^{j(P-1)\omega_p}]^T, \quad p = 1, \dots, 2P \quad (5.15)$$

$$\mathbf{A}_p \triangleq \mathbf{I}_M \otimes \mathbf{a}_p, \quad p = 1, \dots, 2P \quad (5.16)$$

and using the fact that $\tilde{\mathbf{y}}(\omega_p) = \mathbf{A}_p^H \mathbf{y}$, the ISL ζ in (5.13) can be rewritten as

$$\zeta = \frac{1}{2P} \sum_{p=1}^{2P} \left((\mathbf{y}^H \mathbf{A}_p \mathbf{A}_p^H \mathbf{y})^2 - 2P (\mathbf{y}^H \mathbf{A}_p \mathbf{A}_p^H \mathbf{y}) + P^2 M \right). \quad (5.17)$$

It is straightforward to see that the ISL in (5.17) now takes a direct form with respect to \mathbf{y} , in which the summation for the second term is constant, i.e.,

$$\sum_{p=1}^{2P} \mathbf{y}^H \mathbf{A}_p \mathbf{A}_p^H \mathbf{y} = \mathbf{y}^H \left(\sum_{p=1}^{2P} \mathbf{A}_p \mathbf{A}_p^H \right) \mathbf{y} = 2P \|\mathbf{y}\|^2 = 2MP^2 \quad (5.18)$$

where the properties

$$\sum_{p=1}^{2P} \mathbf{A}_p \mathbf{A}_p^H = 2P \mathbf{I}_{MP} \quad (5.19)$$

$$\|\mathbf{y}\|^2 = MP \quad (5.20)$$

are employed for deriving the second and third equalities. The details of the proof can be found in Publication VII.

Ignoring the summations of the second and third terms in (5.17), which are constant and therefore immaterial for optimization, the ISL minimization based waveform design problem (5.6) can be rewritten as

$$\begin{aligned} \min_{\mathbf{y}} \quad & \sum_{p=1}^{2P} (\mathbf{y}^H \mathbf{A}_p \mathbf{A}_p^H \mathbf{y})^2 \\ \text{s.t.} \quad & |\mathbf{y}(p')| = 1, \quad p' = 1, \dots, MP \end{aligned} \quad (5.21)$$

where the summing components in the objective function are the squares of a quadratic term with respect to \mathbf{y} . As a result, the objective of (5.21) takes a quartic form, to which the following quartic-quadratic transformation is applied

$$\begin{aligned} \sum_{p=1}^{2P} (\mathbf{y}^H \mathbf{A}_p \mathbf{A}_p^H \mathbf{y})^2 &= \sum_{p=1}^{2P} \left(\text{tr} \{ \tilde{\mathbf{Y}}^H \mathbf{A}_p \mathbf{A}_p^H \} \right)^2 \\ &= \sum_{p=1}^{2P} \left(\text{vec}(\tilde{\mathbf{Y}}) \right)^H \text{vec}(\mathbf{A}_p \mathbf{A}_p^H) \left(\text{vec}(\mathbf{A}_p \mathbf{A}_p^H) \right)^H \text{vec}(\tilde{\mathbf{Y}}) \\ &= \left(\text{vec}(\tilde{\mathbf{Y}}) \right)^H \Phi \text{vec}(\tilde{\mathbf{Y}}) \end{aligned} \quad (5.22)$$

where $\tilde{\mathbf{Y}} \in \mathbb{C}^{MP \times MP}$ and $\Phi \in \mathbb{C}^{M^2 P^2 \times M^2 P^2}$ are newly introduced matrices, respectively defined as

$$\tilde{\mathbf{Y}} \triangleq \mathbf{y} \mathbf{y}^H \quad (5.23)$$

$$\Phi \triangleq \sum_{p=1}^{2P} \text{vec}(\mathbf{A}_p \mathbf{A}_p^H) \left(\text{vec}(\mathbf{A}_p \mathbf{A}_p^H) \right)^H. \quad (5.24)$$

The following equalities

$$\mathbf{y}^H \mathbf{A}_p \mathbf{A}_p^H \mathbf{y} = \text{tr} \{ \tilde{\mathbf{Y}}^H \mathbf{A}_p \mathbf{A}_p^H \} = \left(\text{vec}(\tilde{\mathbf{Y}}) \right)^H \text{vec}(\mathbf{A}_p \mathbf{A}_p^H) \quad (5.25)$$

obtained from the elementary properties of the trace and vectorization operations, have been used for deriving the equalities in (5.22).

Then, the facts therein, the problem (5.21) can be further rewritten as

$$\min_{\tilde{\mathbf{Y}}} \quad \left(\text{vec}(\tilde{\mathbf{Y}}) \right)^H \Phi \text{vec}(\tilde{\mathbf{Y}}) \quad (5.26a)$$

$$\text{s.t.} \quad \tilde{\mathbf{Y}} = \mathbf{y} \mathbf{y}^H \quad (5.26b)$$

$$|\mathbf{y}(p')| = 1, \quad p' = 1, \dots, MP. \quad (5.26c)$$

Note that the newly obtained objective (5.26a) takes a quadratic form with respect to the intermediate matrix variable $\tilde{\mathbf{Y}}$.

In order to tackle the non-convex problem (5.26), we also do some algebraic manipulations with the quadratic-form objective and the associated constraints, so that the optimization problem is converted to one that allows for simple closed-form solutions. Toward this end, the MaMi technique is used.

Before proceeding, the following general theoretical result used later is presented.

Lemma 5.1. *If a real-valued function $f(\mathbf{x})$ with respect to complex variable \mathbf{x} is second-order differentiable, and there is a matrix $\mathbf{G} \succeq 0$ satisfying the generalized inequality $\nabla^2 f(\mathbf{x}) \preceq \mathbf{G}$ for all \mathbf{x} , then for each point \mathbf{x}_0 , the following convex quadratic function*

$$g(\mathbf{x}) = f(\mathbf{x}_0) + \Re\{\nabla^H f(\mathbf{x}_0)(\mathbf{x} - \mathbf{x}_0)\} + \frac{1}{2}(\mathbf{x} - \mathbf{x}_0)^H \mathbf{G}(\mathbf{x} - \mathbf{x}_0) \quad (5.27)$$

majorizes $f(\mathbf{x})$ at \mathbf{x}_0 .²

Proof. The proof is given in [126]. □

The following corollary will be needed.

Corollary 5.1.1. *If $f(\mathbf{x})$ takes a quadratic form, i.e., $f(\mathbf{x}) = \mathbf{x}^H \mathbf{Q} \mathbf{x}$, then the following explicit function*

$$g(\mathbf{x}) = \frac{1}{2} \mathbf{x}^H \mathbf{G} \mathbf{x} + \mathbf{x}_0^H \left(\frac{1}{2} \mathbf{G} - \mathbf{Q} \right) \mathbf{x}_0 + 2 \Re \left\{ \mathbf{x}_0^H \left(\mathbf{Q} - \frac{1}{2} \mathbf{G} \right) \mathbf{x}_0 \right\} \quad (5.28)$$

can serve as the majorant of $f(\mathbf{x})$.

Proof. Substituting the explicit expressions of the quadratic function $f(\mathbf{x})$ and its gradient $\nabla f(\mathbf{x}_0)$ at \mathbf{x}_0 , i.e., $\nabla f(\mathbf{x}_0) = 2\mathbf{Q}\mathbf{x}_0$, to (5.27), after some straightforward algebraic manipulations, the majorant (5.28) is obtained. □

One simple way for selecting the matrix \mathbf{G} is to choose it as a diagonal matrix such that the first summing term of (5.28) becomes constant. Here, we choose \mathbf{G} to be an identity matrix magnified by the largest eigenvalue of Φ , i.e., $\mathbf{G} \triangleq \lambda_{\max}(\Phi) \mathbf{I}_{M^2 P^2} \in \mathbb{C}^{M^2 P^2 \times M^2 P^2}$. With such selection of \mathbf{G} , the

²The one-dimension version of Lemma 5.1 appears in [268] as Theorem 3.1.

generalized inequality $\mathbf{G} \succeq \Phi$ is guaranteed to hold. By means of (5.28), we can obtain the majorant of the objective function (5.26a) as follows

$$g_1(\tilde{\mathbf{Y}}, \tilde{\mathbf{Y}}^{(k)}) = \frac{\lambda_{\max}(\Phi)}{2} (\text{vec}(\tilde{\mathbf{Y}}))^H \text{vec}(\tilde{\mathbf{Y}}) + (\text{vec}(\tilde{\mathbf{Y}}^{(k)}))^H \left(\frac{\lambda_{\max}(\Phi)}{2} \mathbf{I}_{M^2 P^2} - \Phi \right) \times \text{vec}(\tilde{\mathbf{Y}}^{(k)}) + 2\Re \left\{ (\text{vec}(\tilde{\mathbf{Y}}))^H \left(\Phi - \frac{\lambda_{\max}(\Phi)}{2} \mathbf{I}_{M^2 P^2} \right) \text{vec}(\tilde{\mathbf{Y}}^{(k)}) \right\} \quad (5.29)$$

where $\tilde{\mathbf{Y}}^{(k)} \triangleq \mathbf{y}^{(k)} (\mathbf{y}^{(k)})^H \in \mathbb{C}^{MP \times MP}$ is obtained at the k th iteration with $\mathbf{y}^{(k)} \triangleq \text{vec}\{\mathbf{Y}^{(k)}\} \in \mathbb{C}^{MP \times 1}$.

The first summing term on the right hand side of (5.29) is constant due to the following facts

$$(\text{vec}(\tilde{\mathbf{Y}}))^H \text{vec}(\tilde{\mathbf{Y}}) = \|\mathbf{y}\|^4 = M^2 P^2 \quad (5.30)$$

$$\lambda_{\max}(\Phi) = 2MP^2 \quad (5.31)$$

where (5.30) is proved using the equalities

$$\text{vec}(\tilde{\mathbf{Y}}) = \text{vec}(\mathbf{y}\mathbf{y}^H) = (\mathbf{y}^T \otimes \mathbf{I}_{MP})^H \mathbf{y}. \quad (5.32)$$

and the constant-modulus and mutual orthogonality properties of desired waveforms, while the proof of (5.31) is given in the appendix of Publication VII. Moreover, since $\tilde{\mathbf{Y}}^{(k)}$ and $\lambda_{\max}(\Phi)$ are known, the second summing term is also known. These two constant terms are immaterial for optimization. Therefore, ignoring them, the majorization problem for (5.26) can be written as

$$\begin{aligned} \min_{\tilde{\mathbf{Y}}} \quad & (\text{vec}(\tilde{\mathbf{Y}}))^H (\Phi - MP^2 \mathbf{I}_{M^2 P^2}) \text{vec}(\tilde{\mathbf{Y}}^{(k)}) \\ \text{s.t.} \quad & \tilde{\mathbf{Y}} = \mathbf{y}\mathbf{y}^H \\ & |\mathbf{y}(p')| = 1, \quad p' = 1, \dots, MP. \end{aligned} \quad (5.33)$$

Using the definition (5.24) and the properties (5.32) and also the equality

$$\text{vec}(\mathbf{A}_p \mathbf{A}_p^H) = (\mathbf{A}_p^T \otimes \mathbf{I}_{MP})^H \text{vec}(\mathbf{A}_p) \quad (5.34)$$

the objective function in (5.33), denoted hereafter as obj^a , can be expanded

as

$$\begin{aligned} \text{obj}^a &= \sum_{p=1}^{2P} \left(\mathbf{y}^H (\mathbf{y}^T \otimes \mathbf{I}_{MP}) (\mathbf{A}_p^T \otimes \mathbf{I}_{MP})^H \text{vec}(\mathbf{A}_p) (\text{vec}(\mathbf{A}_p))^H (\mathbf{A}_p^T \otimes \mathbf{I}_{MP}) \right. \\ &\quad \left. \times ((\mathbf{y}^{(k)})^T \otimes \mathbf{I}_{MP})^H \mathbf{y}^{(k)} \right) - MP^2 \mathbf{y}^H (\mathbf{y}^T \otimes \mathbf{I}_{MP}) ((\mathbf{y}^{(k)})^T \otimes \mathbf{I}_{MP})^H \mathbf{y}^{(k)}. \end{aligned} \quad (5.35)$$

Applying the mixed-product property of the Kronecker product to obj^a in (5.35), we can further derive the objective of (5.33) as

$$\begin{aligned} \text{obj}^a &= \sum_{p=1}^{2P} \mathbf{y}^H ((\mathbf{y}^T \mathbf{A}_p^*) \otimes \mathbf{I}_{MP}) \text{vec}(\mathbf{A}_p) (\text{vec}(\mathbf{A}_p))^H ((\mathbf{A}_p^T (\mathbf{y}^{(k)})^*) \otimes \mathbf{I}_{MP}) \mathbf{y}^{(k)} \\ &\quad - MP^2 \mathbf{y}^H (\mathbf{y}^T (\mathbf{y}^{(k)})^*) \mathbf{y}^{(k)}. \end{aligned} \quad (5.36)$$

Here, it is straightforward to check that the equality

$$((\mathbf{y}^T \mathbf{A}_p^*) \otimes \mathbf{I}_{MP}) \text{vec}(\mathbf{A}_p) = \mathbf{A}_p \mathbf{A}_p^H \mathbf{y} \quad (5.37)$$

holds. Applying this equality to (5.36), we can rewrite the objective of (5.33) as

$$\begin{aligned} \text{obj}^a &= \sum_{p=1}^{2P} \mathbf{y}^H \mathbf{A}_p ((\mathbf{y}^{(k)})^H \mathbf{A}_p \mathbf{A}_p^H \mathbf{y}^{(k)}) \mathbf{A}_p^H \mathbf{y} - MP^2 \mathbf{y}^H (\mathbf{y}^{(k)} (\mathbf{y}^{(k)})^H) \mathbf{y} \\ &= \mathbf{y}^H (\mathbf{A} \mathbf{\Lambda}^{(k)} \mathbf{A}^H - MP^2 \mathbf{y}^{(k)} (\mathbf{y}^{(k)})^H) \mathbf{y} \end{aligned} \quad (5.38)$$

where the matrices $\mathbf{A} \in \mathbb{C}^{MP \times 2MP}$ and $\mathbf{\Lambda}^{(k)} \in \mathbb{C}^{2MP \times 2MP}$ and the vector $\boldsymbol{\mu}^{(k)} \in \mathbb{C}^{2P \times 1}$ are defined as³

$$\mathbf{A} \triangleq [\mathbf{A}_1, \dots, \mathbf{A}_{2P}] \quad (5.39)$$

$$\mathbf{\Lambda}^{(k)} \triangleq \text{diag}\{\boldsymbol{\mu}^{(k)} \otimes \mathbf{1}_M\} \quad (5.40)$$

$$\boldsymbol{\mu}^{(k)} \triangleq |\tilde{\mathbf{A}}^H \mathbf{Y}^{(k)}|^2 \mathbf{1}_M \quad (5.41)$$

respectively, with $\tilde{\mathbf{A}} \triangleq [\mathbf{a}_1, \dots, \mathbf{a}_{2P}] \in \mathbb{C}^{P \times 2P}$.

Using (5.38), the problem (5.33) can be rewritten as

$$\begin{aligned} \min_{\mathbf{y}} \quad & \mathbf{y}^H (\mathbf{A} \mathbf{\Lambda}^{(k)} \mathbf{A}^H - MP^2 \mathbf{y}^{(k)} (\mathbf{y}^{(k)})^H) \mathbf{y} \\ \text{s.t.} \quad & |\mathbf{y}(p')| = 1, \quad p' = 1, \dots, MP. \end{aligned} \quad (5.42)$$

³In (5.41), $|\cdot|$ is applied to a matrix argument, which means that the magnitude is found for each element of the matrix, that is, the element-wise magnitude.

Algorithm 1 The ISL Minimization-Based Algorithm—ISLNew

```

1:  $k \leftarrow 0$ ,  $\mathbf{Y} \leftarrow$  unimodular sequence matrix with random phases.
2: repeat
3:   procedure ISLNEW( $\mathbf{Y}^{(k)}$ )
4:      $\boldsymbol{\mu}^{(k)} = |\tilde{\mathbf{A}}^H \mathbf{Y}^{(k)}|^2 \mathbf{1}_M$ 
5:      $\mathbf{v}^{(k)} = -\tilde{\mathbf{A}} \left( \boldsymbol{\mu}^{(k)} - \frac{1}{2} (\mu_{\max}^{(k)} + M^2 P^2) \mathbf{1}_{2P} \right)$ 
6:      $\mathbf{T}^{(k)} = \mathcal{T} \{ \mathbf{v}^{(k)} \}$ 
7:      $[\mathbf{Y}]_{m,p} = e^{j \cdot \arg([\mathbf{T}^{(k)} \mathbf{Y}^{(k)}]_{m,p})}$ ,  $\forall m, \forall p$ 
8:      $k \leftarrow k + 1$ 
9:   end procedure
10: until convergence

```

The objective function of (5.42) takes a quadratic form, which enables us to apply the majorant (5.28) again. Substituting the matrix $\mathbf{G} \triangleq \mu_{\max}^{(k)} \mathbf{A} \mathbf{A}^H \in \mathbb{C}^{2MP \times 2MP}$ into (5.28), (5.38) can be majorized by

$$\begin{aligned}
g_2(\mathbf{y}, \mathbf{y}^{(k)}) &= \frac{1}{2} \mu_{\max}^{(k)} \mathbf{y}^H \mathbf{A} \mathbf{A}^H \mathbf{y} + (\mathbf{y}^{(k)})^H (MP^2 \mathbf{y}^{(k)} (\mathbf{y}^{(k)})^H \\
&\quad - \mathbf{A} (\boldsymbol{\Lambda}^{(k)} - \frac{1}{2} \mu_{\max}^{(k)} \mathbf{I}_{2MP}) \mathbf{A}^H) \mathbf{y}^{(k)} + 2 \Re \{ \mathbf{y}^H (\mathbf{A} (\boldsymbol{\Lambda}^{(k)} \\
&\quad - \frac{1}{2} \mu_{\max}^{(k)} \mathbf{I}_{2MP}) \mathbf{A}^H - MP^2 \mathbf{y}^{(k)} (\mathbf{y}^{(k)})^H) \mathbf{y}^{(k)} \} \quad (5.43)
\end{aligned}$$

where the scaling factor $\mu_{\max}^{(k)} \triangleq \max \{ \boldsymbol{\mu}^{(k)} \}$ ensures that the generalized inequality $\mathbf{G} \succeq \mathbf{A} \boldsymbol{\Lambda}^{(k)} \mathbf{A}^H$ holds.

The first two terms in (5.43) are constant due to the facts that

$$\mathbf{A} \mathbf{A}^H = \sum_{p=1}^{2P} \mathbf{A}_p \mathbf{A}_p^H = 2P \mathbf{I}_{MP} \quad (5.44)$$

$$\mathbf{y}^H \mathbf{y} = (\mathbf{y}^{(k)})^H \mathbf{y}^{(k)} = \|\mathbf{y}\|^2 = MP \quad (5.45)$$

where (5.44) follows from the structure of \mathbf{A}_p and (5.45) results from the mutual orthogonality and constant-modulus properties of designed waveforms. They are immaterial for optimization and can be ignored. Therefore, we can further rewrite the majorized problem for (5.42) as

$$\min_{\mathbf{y}} \mathbf{y}^H \left(\mathbf{A} (\boldsymbol{\Lambda}^{(k)} - \frac{1}{2} \mu_{\max}^{(k)} \mathbf{I}_{2MP}) \mathbf{A}^H - M^2 P^3 \mathbf{I}_{MP} \right) \mathbf{y}^{(k)}$$

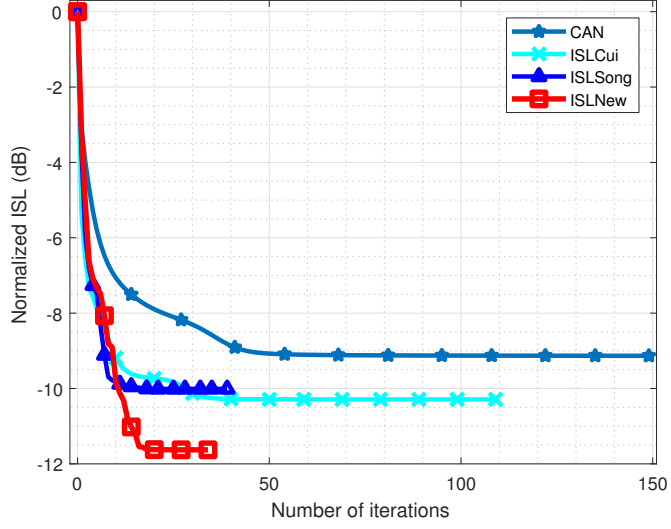


Figure 5.1. Convergence evaluations of algorithms developed for ISL minimization: Normalized ISL values versus the number of iterations for $M = 1$ unimodular waveform of code length $P = 32$. Here the legends 'CAN', 'ISLSong' and 'ISLCui' respectively stand for the corresponding algorithms developed in [66], [105], and [121], and 'ISLNew' denotes the ISL minimization based algorithm reviewed in this chapter.

$$\text{s.t. } |\mathbf{y}(p')| = 1, \quad p' = 1, \dots, MP. \quad (5.46)$$

Using (5.45) again, the problem (5.46) can be equivalently rewritten as

$$\begin{aligned} \min_{\mathbf{Y}} \quad & \|\mathbf{Y} - \mathbf{T}^{(k)}\mathbf{Y}^{(k)}\| \\ \text{s.t.} \quad & |[\mathbf{Y}]_{m,p}| = 1, \quad m = 1, \dots, M; \quad p = 1, \dots, P \end{aligned} \quad (5.47)$$

where the matrix $\mathbf{T}^{(k)} \triangleq \mathcal{T}\{\mathbf{v}^{(k)}\} \in \mathbb{C}^{P \times P}$ is a Hermitian Toeplitz matrix constructed from the vector

$$\mathbf{v}^{(k)} \triangleq -\tilde{\mathbf{A}}\left(\boldsymbol{\mu}^{(k)} - \frac{1}{2}(\mu_{\max}^{(k)} + M^2 P^2)\mathbf{1}_{2P}\right). \quad (5.48)$$

The problem (5.47) has the following closed-form solution

$$[\mathbf{Y}]_{m,p} = \exp\left\{j \cdot \arg\left([\mathbf{T}^{(k)}\mathbf{Y}^{(k)}]_{m,p}\right)\right\}, \quad \forall m, \forall p. \quad (5.49)$$

Finally, the ISL minimization-based unimodular waveform design algorithm is summarized in Algorithm 1. Fig. 5.1 shows the convergence speed performance of the proposed Algorithm 1.

5.2.2 Computational complexity of ISLNew

In terms of the per iteration computational complexity of Algorithm 1, the straightforward calculation of $\boldsymbol{\mu}^{(k)}$ according to (5.41) requires $2MP(P+1)$ operations, the calculation of $\mathbf{v}^{(k)}$ costs $2P^2$ operations, while computing the matrix-to-matrix product $\mathbf{T}^{(k)}\mathbf{Y}^{(k)}$ in (5.49) needs MP^2 operations.

Consequently, the total computations require $(3M+2)P^2 + 2MP$ operations. However, $\boldsymbol{\mu}^{(k)}$ and $\mathbf{v}^{(k)}$ can be computed by means of the FFT at the order of complexity $\mathcal{O}(MP \log P)$ and $\mathcal{O}(P \log P)$, respectively. Similarly, using the Toeplitz structure of $\mathbf{T}^{(k)}$, the product $\mathbf{T}^{(k)}\mathbf{Y}^{(k)}$ can also be calculated at a reduced complexity $\mathcal{O}(MP \log P)$, which is the highest in Algorithm 1. Therefore, the order of computational complexity of Algorithm 1 is $\mathcal{O}(MP \log P)$, which is nearly linear in the dimension of the problem, as required in large-scale optimization.

5.2.3 Fast WISL minimization based design—WISLNew

The WISL in (5.5) can be written in the matrix form as follows

$$\zeta_w = \gamma_0^2 \|\mathbf{R}_0 - P\mathbf{I}_M\|^2 + \sum_{\substack{p=-P+1 \\ p \neq 0}}^{P-1} \gamma_p^2 \|\mathbf{R}_p\| \quad (5.50)$$

where \mathbf{R}_p , $p \in \{-P+1, \dots, P-1\}$ is defined in (5.8).

Expressing (5.50) in frequency domain yields [66]

$$\zeta_w = \frac{1}{2P} \sum_{p=1}^{2P} \|\Psi(\omega_p) - \gamma_0 P\mathbf{I}_M\|^2 \quad (5.51)$$

where the weighted spectral density matrix $\Psi(\omega_p) \in \mathbb{C}^{M \times M}$ is defined as

$$\Psi(\omega_p) \triangleq \sum_{p=-P+1}^{P-1} \gamma_p \mathbf{R}_p e^{-j\omega_p n}, \quad \omega_p \triangleq \frac{2\pi}{2P} p. \quad (5.52)$$

Let us define the weighting matrix $\Gamma \in \mathbb{C}^{P \times P}$ which has Toeplitz structure and is constructed by the weights $\{\gamma_p\}_{p=-P+1}^{P-1}$ as follows

$$\Gamma \triangleq \begin{bmatrix} \gamma_0 & \gamma_1 & \dots & \gamma_{P-1} \\ \gamma_{-1} & \gamma_0 & \ddots & \vdots \\ \vdots & \ddots & \ddots & \gamma_1 \\ \gamma_{-P+1} & \dots & \gamma_{-1} & \gamma_0 \end{bmatrix}. \quad (5.53)$$

Using (5.53), $\Psi(\omega_p)$ in (5.52) can be rewritten in the vector-matrix form as

$$\begin{aligned}\Psi(\omega_p) &= \mathbf{Y}^H(\text{diag}\{\mathbf{a}_p\})^H \Gamma \text{diag}\{\mathbf{a}_p\} \mathbf{Y} \\ &= \mathbf{Y}^H((\mathbf{a}_p \mathbf{a}_p^H) \odot \Gamma) \mathbf{Y}.\end{aligned}\quad (5.54)$$

Inserting (5.54) into (5.51), the WISL ζ_w can be expressed as

$$\zeta_w = \frac{1}{2P} \sum_{p=1}^{2P} \|\mathbf{Y}^H((\mathbf{a}_p \mathbf{a}_p^H) \odot \Gamma) \mathbf{Y} - \gamma_0 P \mathbf{I}_M\|^2. \quad (5.55)$$

Expanding the squared norm of (5.55) yields

$$\begin{aligned}\zeta_w &= \frac{1}{2P} \sum_{p=1}^{2P} \left(\|\mathbf{Y}^H((\mathbf{a}_p \mathbf{a}_p^H) \odot \Gamma) \mathbf{Y}\|^2 + \gamma_0^2 M P^2 \right. \\ &\quad \left. - 2\gamma_0 P \text{tr}\{\mathbf{Y}^H((\mathbf{a}_p \mathbf{a}_p^H) \odot \Gamma) \mathbf{Y}\} \right)\end{aligned}\quad (5.56)$$

where the second term of (5.56) is constant, and the third one can be proved to be constant by using the facts

$$\begin{aligned}\sum_{p=1}^{2P} \text{tr}\{\mathbf{Y}^H((\mathbf{a}_p \mathbf{a}_p^H) \odot \Gamma) \mathbf{Y}\} &= \text{tr}\left\{\mathbf{Y}^H\left(\left(\sum_{p=1}^{2P} \mathbf{a}_p \mathbf{a}_p^H\right) \odot \Gamma\right) \mathbf{Y}\right\} \\ &= 2P \text{tr}\{\mathbf{Y}^H(\mathbf{I}_P \odot \Gamma) \mathbf{Y}\} = 2\gamma_0 P \|\mathbf{Y}\|^2 = 2\gamma_0 M P^2.\end{aligned}\quad (5.57)$$

Here, the fact $\text{tr}\{\mathbf{Y}^H \mathbf{Y}\} = \|\mathbf{Y}\|^2 = MP$ resulting from mutual orthogonality and constant modulus property of designed waveforms and also the fact $\sum_{p=1}^{2P} \mathbf{a}_p \mathbf{a}_p^H = 2P \mathbf{I}_P$ are used.

Therefore, the second and third terms of (5.56) are immaterial for optimization and can be ignored. With this observation, the WISL minimization problem (5.7) can be rewritten as

$$\min_{\mathbf{Y}} \sum_{p=1}^{2P} \|\mathbf{Y}^H((\mathbf{a}_p \mathbf{a}_p^H) \odot \Gamma) \mathbf{Y}\|^2 \quad (5.58a)$$

$$\text{s.t. } |y_m(p)| = 1, \quad m = 1, \dots, M; \quad p = 1, \dots, P. \quad (5.58b)$$

Despite taking a quartic form with squared norm in (5.58a), the Hadamard product of two matrices appears under the Frobenius norm there, and the resulting matrix turns out to be complex. Directly expanding the squared norm will not help us to rewrite (5.58a) into a proper quartic form with

respect to \mathbf{y} . Hence, we need to convert (5.58a) into an alternative quartic form which allows us to apply the quartic-quadratic transformation.

Towards this end, we consider the eigenvalue decomposition of the weighting matrix Γ , which in general may be indefinite expressed as

$$\Gamma = \sum_{k=1}^K \lambda_k \mathbf{q}_k \mathbf{q}_k^H = \sum_{k=1}^K \mathbf{u}_k \mathbf{v}_k^H \quad (5.59)$$

where λ_k (real-valued) and \mathbf{q}_k are the k th eigenvalue and eigenvector, respectively, \mathbf{u}_k and \mathbf{v}_k are respectively defined as

$$\mathbf{u}_k \triangleq \sqrt{\lambda_k} \mathbf{q}_k \quad (5.60)$$

$$\mathbf{v}_k \triangleq \begin{cases} \mathbf{u}_k, & \text{if } \lambda_k \geq 0 \\ -\mathbf{u}_k, & \text{otherwise} \end{cases} \quad (5.61)$$

and K is the rank of Γ .

Inserting (5.59) into (5.58a) and expanding the Frobenius norm, the objective function (5.58a), called hereafter as obj^b , can be rewritten as

$$\text{obj}^b = \sum_{p=1}^{2P} \sum_{k=1}^K \sum_{k'=1}^K \left| (\mathbf{v}_{k'} \odot \mathbf{a}_p)^H \mathbf{Y} \mathbf{Y}^H (\mathbf{u}_k \odot \mathbf{a}_p) \right|^2. \quad (5.62)$$

Applying the property

$$\mathbf{Y}^H (\mathbf{u}_k \odot \mathbf{a}_p) = (\mathbf{I}_M \otimes (\mathbf{a}_p \odot \mathbf{u}_k))^T \mathbf{y}^* \quad (5.63)$$

which also holds if \mathbf{u}_k is replaced by $\mathbf{v}_{k'}$, to (5.62) together with the mixed-product property of the Kronecker product, the objective (5.58a) can be rewritten as

$$\begin{aligned} \text{obj}^b &= \sum_{p=1}^{2P} \sum_{k=1}^K \sum_{k'=1}^K \left| \mathbf{y}^H (\mathbf{I}_M \otimes ((\mathbf{a}_p \mathbf{a}_p^H) \odot (\mathbf{u}_k \mathbf{v}_{k'}^H))) \mathbf{y} \right|^2 \\ &= \sum_{p=1}^{2P} \sum_{k=1}^K \sum_{k'=1}^K \left(\mathbf{y}^H \left((\mathbf{A}_p \mathbf{A}_p^H) \odot \Gamma_{kk'}^{\text{real}} \right) \mathbf{y} \right)^2 + \left(\mathbf{y}^H \left((\mathbf{A}_p \mathbf{A}_p^H) \odot \Gamma_{kk'}^{\text{img}} \right) \mathbf{y} \right)^2 \end{aligned} \quad (5.64)$$

where $\Gamma_{kk'}^{\text{real}} \in \mathbb{C}^{MP \times MP}$ and $\Gamma_{kk'}^{\text{img}} \in \mathbb{C}^{MP \times MP}$ are both Hermitian matrices defined as

$$\Gamma_{kk'}^{\text{real}} \triangleq \mathbf{I}_M \otimes \frac{\mathbf{u}_k \mathbf{v}_{k'}^H + \mathbf{v}_{k'} \mathbf{u}_k^H}{2} \quad (5.65)$$

$$\Gamma_{kk'}^{\text{img}} \triangleq \mathbf{I}_M \otimes \frac{\mathbf{u}_k \mathbf{v}_{k'}^H - \mathbf{v}_{k'} \mathbf{u}_k^H}{2i} \quad (5.66)$$

with $i \triangleq \sqrt{-1}$.

Utilizing (5.64), the problem (5.58) can be rewritten as

$$\begin{aligned} \min_{\mathbf{y}} \quad & \sum_{p=1}^{2P} \sum_{k=1}^K \sum_{k'=1}^K \left(\mathbf{y}^H \left((\mathbf{A}_p \mathbf{A}_p^H) \odot \mathbf{\Gamma}_{kk'}^{\text{real}} \right) \mathbf{y} \right)^2 + \left(\mathbf{y}^H \left((\mathbf{A}_p \mathbf{A}_p^H) \odot \mathbf{\Gamma}_{kk'}^{\text{img}} \right) \mathbf{y} \right)^2 \\ \text{s.t.} \quad & |\mathbf{y}(p')| = 1, \quad p' = 1, \dots, MP. \end{aligned} \quad (5.67)$$

The objective function in (5.67) takes a proper quartic form with respect to \mathbf{y} which enables us to apply the quartic-quadratic transformation and design a fast algorithm on the basis of MaMi technique.

Similar to the quartic-quadratic transformation in (5.22), the objective of (5.67), denoted for brevity as obj^c , can be rewritten as

$$\begin{aligned} \text{obj}^c &= \sum_{p=1}^{2P} \left(\text{tr} \left\{ \tilde{\mathbf{Y}}^H \left((\mathbf{A}_p \mathbf{A}_p^H) \odot \mathbf{\Gamma}_{kk'}^{\text{real}} \right) \right\} \right)^2 + \left(\text{tr} \left\{ \tilde{\mathbf{Y}}^H \left((\mathbf{A}_p \mathbf{A}_p^H) \odot \mathbf{\Gamma}_{kk'}^{\text{img}} \right) \right\} \right)^2 \\ &= (\text{vec}(\tilde{\mathbf{Y}}))^H \tilde{\mathbf{\Phi}} \text{vec}(\tilde{\mathbf{Y}}) \end{aligned} \quad (5.68)$$

where and $\tilde{\mathbf{\Phi}} \in \mathbb{C}^{M^2 P^2 \times M^2 P^2}$ is defined as

$$\tilde{\mathbf{\Phi}} \triangleq \bar{\mathbf{\Phi}} \odot \bar{\mathbf{\Gamma}} \quad (5.69)$$

with

$$\bar{\mathbf{\Phi}} \triangleq \sum_{p=1}^{2P} \text{vec}(\mathbf{A}_p \mathbf{A}_p^H) (\text{vec}(\mathbf{A}_p \mathbf{A}_p^H))^H \quad (5.70)$$

$$\bar{\mathbf{\Gamma}} \triangleq \sum_{k=1}^K \sum_{k'=1}^K \text{vec}(\mathbf{\Gamma}_{kk'}^{\text{real}}) (\text{vec}(\mathbf{\Gamma}_{kk'}^{\text{real}}))^H + \text{vec}(\mathbf{\Gamma}_{kk'}^{\text{img}}) (\text{vec}(\mathbf{\Gamma}_{kk'}^{\text{img}}))^H. \quad (5.71)$$

Utilizing (5.68), the optimization problem (5.67) can be rewritten as

$$\begin{aligned} \min_{\tilde{\mathbf{Y}}} \quad & (\text{vec}(\tilde{\mathbf{Y}}))^H \tilde{\mathbf{\Phi}} \text{vec}(\tilde{\mathbf{Y}}) \\ \text{s.t.} \quad & \tilde{\mathbf{Y}} = \mathbf{y} \mathbf{y}^H \\ & |\mathbf{y}(p')| = 1, \quad p' = 1, \dots, MP \end{aligned} \quad (5.72)$$

where the objective takes a quadratic form, to which a majorant can be applied.

Yet before applying the majorization procedure, we present the following result that will be used later.

Lemma 5.2. *Given a set of $N \times 1$ arbitrary complex vectors $\{\mathbf{d}_k\}_{k=1}^K$ and an $N \times N$ arbitrary Hermitian matrix \mathbf{H} , the following generalized inequality*

$$\sum_{k=1}^K (\mathbf{d}_k \mathbf{d}_k^H) \odot \mathbf{H} \preceq \lambda_{\max}(\mathbf{H}) \mathbf{D} \quad (5.73)$$

holds, where $\mathbf{D} \triangleq \text{diag}\left\{\sum_{k=1}^K |\mathbf{d}_k(1)|^2, \dots, \sum_{k=1}^K |\mathbf{d}_k(N)|^2\right\}$.

Proof: The proof is given in Publication VII. \square

Applying Lemma 5.2 by taking $\mathbf{d}_k = \text{vec}(\mathbf{A}_p \mathbf{A}_p^H)$, $\mathbf{H} = \bar{\Gamma}$, and $K = 2P$, the following generalized inequality

$$\bar{\Phi} \odot \bar{\Gamma} \preceq \lambda_{\max}(\bar{\Gamma}) \text{diag}\{\bar{\Phi}\} \quad (5.74)$$

is guaranteed, with $\lambda_{\max}(\bar{\Gamma}) = M \lambda_{\max}^2(\Gamma)$ (see Appendix A in Publication VII for the proof). Note that for the majorization function computation it is more efficient in terms of the computational complexity to approximate $\lambda_{\max}(\Gamma)$ by any matrix norm of Γ . In addition, the elements of $\bar{\Phi}$ on the main diagonal equal either zero or $2P$. For this reason, the matrix $\text{diag}\{\bar{\Phi}\}$ in (5.74) can be replaced with an identity matrix magnified by $2P$ without disobeying the generalized inequality.

Using (5.28) by applying $\mathbf{G} \triangleq \lambda_{\bar{\Phi}} \mathbf{I}_{M^2 P^2}$ with $\lambda_{\bar{\Phi}} \triangleq 2P \lambda_{\max}(\bar{\Gamma})$ so that $\mathbf{G} \succeq \bar{\Phi}$ is guaranteed, the objective of (5.72) can be majorized by

$$\begin{aligned} \tilde{g}_1(\tilde{\mathbf{Y}}, \tilde{\mathbf{Y}}^{(k)}) &= \frac{\lambda_{\bar{\Phi}}}{2} (\text{vec}(\tilde{\mathbf{Y}}))^H \text{vec}(\tilde{\mathbf{Y}}) + (\text{vec}(\tilde{\mathbf{Y}}^{(k)}))^H \left(\frac{\lambda_{\bar{\Phi}}}{2} \mathbf{I}_{M^2 P^2} - \bar{\Phi} \right) \\ &\quad \times \text{vec}(\tilde{\mathbf{Y}}^{(k)}) + 2\Re \left\{ (\text{vec}(\tilde{\mathbf{Y}}))^H \left(\bar{\Phi} - \frac{\lambda_{\bar{\Phi}}}{2} \mathbf{I}_{M^2 P^2} \right) \text{vec}(\tilde{\mathbf{Y}}^{(k)}) \right\}. \end{aligned} \quad (5.75)$$

The first and second terms in (5.75) are constant because of the property (5.30) and known $\tilde{\mathbf{Y}}^{(k)}$, which are therefore immaterial for optimization. Ignoring these terms, (5.72) can be majorized by the problem

$$\min_{\tilde{\mathbf{Y}}} (\text{vec}(\tilde{\mathbf{Y}}))^H \left(\bar{\Phi} - \frac{\lambda_{\bar{\Phi}}}{2} \mathbf{I}_{M^2 P^2} \right) \text{vec}(\tilde{\mathbf{Y}}^{(k)}) \quad (5.76a)$$

$$\text{s.t. } \tilde{\mathbf{Y}} = \mathbf{y} \mathbf{y}^H \quad (5.76b)$$

$$|\mathbf{y}(p')| = 1, \quad p' = 1, \dots, MP. \quad (5.76c)$$

To further simplify (5.76a), the following result that relates Hadamard to Kronecker products is needed.

Lemma 5.3. *Given two matrices \mathbf{F} and \mathbf{C} of the same size $N \times N$ and the $N \times N^2$ selection matrix $\mathbf{E} = [\bar{\mathbf{E}}_1, \dots, \bar{\mathbf{E}}_N]$ with $\bar{\mathbf{E}}_n$ being the n th $N \times N$ block matrix composed of all zeros except the n th element on the main diagonal equaling 1, i.e., $[\bar{\mathbf{E}}_n]_{n,n} = 1$, the following equality*

$$\mathbf{F} \circ \mathbf{C} = \mathbf{E}(\mathbf{C} \otimes \mathbf{F})\mathbf{E}^H \quad (5.77)$$

holds. Under the condition that \sqrt{N} is an integer, $\bar{\mathbf{E}}_n$ can be decomposed as

$$\bar{\mathbf{E}}_n = \hat{\mathbf{E}}_{u(n)} \otimes \hat{\mathbf{E}}_{v(n)} \quad (5.78)$$

where the matrices $\hat{\mathbf{E}}_{u(n)}$ and $\hat{\mathbf{E}}_{v(n)}$ are constructed in the same way as $\bar{\mathbf{E}}_n$, but have the reduced size $\sqrt{N} \times \sqrt{N}$, and

$$u(n) \triangleq \left\lfloor \frac{n-1}{\sqrt{N}} \right\rfloor + 1, \quad n = 1, \dots, N \quad (5.79)$$

$$v(n) \triangleq \text{mod}(n-1, \sqrt{N}) + 1, \quad n = 1, \dots, N \quad (5.80)$$

are respectively the column and row indices of the element in a $\sqrt{N} \times \sqrt{N}$ matrix corresponding to the unique linear index n in its column-wise vectorization.

Proof. The proof of (5.77) appears in Lemma 1 of [269]. The remaining results (5.78)–(5.80) are the elementary properties of the selection matrix. The proof is complete. \square

Applying Lemma 5.3 by taking $\mathbf{F} = \bar{\Phi}$, $\mathbf{C} = \bar{\Gamma}$, and $N = M^2 P^2$, and inserting (5.69) into (5.76a), the objective function (5.76a), denoted for brevity as obj^d , can be rewritten as

$$\begin{aligned} \text{obj}^d &= (\text{vec}(\tilde{\mathbf{Y}}))^H \left(\mathbf{E}(\bar{\Gamma} \otimes \bar{\Phi})\mathbf{E}^H - \frac{\lambda_{\bar{\Phi}}}{2} \mathbf{I}_{M^2 P^2} \right) \text{vec}(\tilde{\mathbf{Y}}^{(k)}) \\ &= (\text{vec}(\tilde{\mathbf{Y}}))^H \left(\sum_{n=1}^{M^2 P^2} \sum_{n'=1}^{M^2 P^2} [\bar{\Gamma}]_{n,n'} \bar{\mathbf{E}}_n \bar{\Phi} \bar{\mathbf{E}}_{n'}^H \right) \text{vec}(\tilde{\mathbf{Y}}^{(k)}) \\ &\quad - \frac{\lambda_{\bar{\Phi}}}{2} (\text{vec}(\tilde{\mathbf{Y}}))^H \text{vec}(\tilde{\mathbf{Y}}^{(k)}) \end{aligned} \quad (5.81)$$

where the latter expression in (5.81) is obtained from expanding the Kronecker product in the prior one.

Using (5.71) and (5.78), and applying the properties (5.32) and (5.34), (5.81) can be further rewritten as

$$\begin{aligned} \text{obj}^d &= \sum_{p=1}^{2P} \sum_{n=1}^{M^2 P^2} \sum_{n'=1}^{M^2 P^2} [\bar{\Gamma}]_{n,n'} \mathbf{y}^H (\mathbf{y}^T \otimes \mathbf{I}_{MP}) (\hat{\mathbf{E}}_{u(n)} \otimes \hat{\mathbf{E}}_{v(n)}) (\mathbf{A}_p^T \otimes \mathbf{I}_{MP})^H \\ &\quad \times \text{vec}(\mathbf{A}_p) (\text{vec}(\mathbf{A}_p))^H (\mathbf{A}_p^T \otimes \mathbf{I}_{MP}) (\hat{\mathbf{E}}_{u(n')} \otimes \hat{\mathbf{E}}_{v(n')})^H ((\mathbf{y}^{(k)})^T \otimes \mathbf{I}_{MP})^H \mathbf{y}^{(k)} \\ &\quad - \frac{\lambda_{\bar{\Phi}}}{2} \mathbf{y}^H (\mathbf{y}^T \otimes \mathbf{I}_{MP}) ((\mathbf{y}^{(k)})^T \otimes \mathbf{I}_{MP})^H \mathbf{y}^{(k)}. \end{aligned} \quad (5.82)$$

Applying the property

$$((\mathbf{y}^T \hat{\mathbf{E}}_{u(n)} \mathbf{A}_p^*) \otimes \hat{\mathbf{E}}_{v(n)}) \text{vec}(\mathbf{A}_p) = \hat{\mathbf{E}}_{v(n)} \mathbf{A}_p \mathbf{A}_p^H \hat{\mathbf{E}}_{u(n)} \mathbf{y} \quad (5.83)$$

and the mixed-product property of Kronecker product to (5.82), we obtain

$$\begin{aligned} \text{obj}^d &= \mathbf{y}^H \left(\sum_{p=1}^{2P} \sum_{n=1}^{M^2 P^2} \sum_{n'=1}^{M^2 P^2} [\bar{\Gamma}]_{n,n'} \hat{\mathbf{E}}_{v(n)} \mathbf{A}_p \left((\mathbf{y}^{(k)})^H \hat{\mathbf{E}}_{u(n')} \right. \right. \\ &\quad \left. \left. \times \mathbf{A}_p \mathbf{A}_p^H \hat{\mathbf{E}}_{v(n')} \mathbf{y}^{(k)} \right) \mathbf{A}_p^H \hat{\mathbf{E}}_{u(n)} - \frac{\lambda_{\bar{\Phi}}}{2} \mathbf{y}^{(k)} (\mathbf{y}^{(k)})^H \right) \mathbf{y} \\ &= \mathbf{y}^H \left(\mathbf{B}^{(k)} - \frac{\lambda_{\bar{\Phi}}}{2} \mathbf{y}^{(k)} (\mathbf{y}^{(k)})^H \right) \mathbf{y} \end{aligned} \quad (5.84)$$

where $\mathbf{y}^{(k)} \triangleq \text{vec}\{\mathbf{Y}^{(k)}\}$ and the Hermitian matrix $\mathbf{B}^{(k)} \in \mathbb{C}^{MP \times MP}$ consisting of M^2 blocks is defined as

$$\mathbf{B}^{(k)} \triangleq \begin{bmatrix} \mathbf{B}_{11}^{(k)} & \cdots & \mathbf{B}_{1M}^{(k)} \\ \vdots & \ddots & \vdots \\ \mathbf{B}_{M1}^{(k)} & \cdots & \mathbf{B}_{MM}^{(k)} \end{bmatrix}. \quad (5.85)$$

Here, the (m, m') th block element $\mathbf{B}_{mm'}^{(k)} \in \mathbb{C}^{P \times P}$, denoted by

$$\mathbf{B}_{mm'}^{(k)} = 2P\mathcal{T} \left(\boldsymbol{\rho}_{mm'}^{(k)}, \boldsymbol{\eta}_{mm'}^{(k)} \right) \quad (5.86)$$

is a Toeplitz matrix whose first row and column respectively coincide with the vectors $\boldsymbol{\rho}_{mm'}^{(k)} \in \mathbb{C}^{P \times 1}$ and $\boldsymbol{\eta}_{mm'}^{(k)} \in \mathbb{C}^{P \times 1}$, whose $(p+1)$ th $(0 \leq p \leq P-1)$ elements of are given by

$$\boldsymbol{\rho}_{mm'}^{(k)}(p+1) \triangleq \begin{cases} \gamma_p^2 \mathbf{1}_{P-p}^T \mathcal{U}_p(\mathbf{Z}_{mm'}^{(k)}), & p \in \Omega \\ 0, & p \in \bar{\Omega} \end{cases} \quad (5.87)$$

$$\boldsymbol{\eta}_{mm'}^{(k)}(p+1) \triangleq \begin{cases} \gamma_p^2 \mathbf{1}_{P-p}^T \mathcal{D}_p(\mathbf{Z}_{mm'}^{(k)}), & p \in \Omega \\ 0, & p \in \bar{\Omega} \end{cases} \quad (5.88)$$

respectively, where $\mathbf{Z}_{mm'}^{(k)} \triangleq \mathbf{y}_m^{(k)} (\mathbf{y}_{m'}^{(k)})^H$, and

$$\Omega \triangleq \{0\} \cup \{p | \gamma_p \neq 0, p > 0\} \quad (5.89)$$

$$\bar{\Omega} \triangleq \{p | \gamma_p = 0, p > 0\} \quad (5.90)$$

are the set of non-negative indices associated with the non-zero ISL controlling weights (always including index $p = 0$ for simplicity) and the complementary set of Ω with the full set defined as $[0, P - 1]$, respectively.

Note that the meanings of (5.87) and (5.88) are that the non-zero elements of $\rho_{mm'}^{(k)}$ and $\eta_{m,m'}^{(k)}$ are respectively expressed by the sum of the off-diagonal elements in the upper and lower triangular parts of $\mathbf{Z}_{mm'}^{(k)}$ magnified by γ_p^2 . Using (5.87) and (5.88), the calculations for zero-valued elements can be avoided. Note also that $\mathbf{B}_{mm'}^{(k)} = (\mathbf{B}_{m'm}^{(k)})^H$, therefore, only the upper (or lower) triangular part of $\mathbf{B}^{(k)}$ needs to be determined.

Considering that (5.84) takes a quadratic form, the majorant of (5.28) can be applied again, where $\mathbf{G} \triangleq \tau^{(k)} \mathbf{I}_{MP}$ with $\tau^{(k)}$ being a scaling factor, such that $\mathbf{G} \succeq \mathbf{Q}$ is guaranteed for (5.28). Here, any norm of the following matrix

$$\mathbf{Q}^{(k)} \triangleq \mathbf{B}^{(k)} - \frac{\lambda_{\Phi}}{2} \mathbf{y}^{(k)} (\mathbf{y}^{(k)})^H \quad (5.91)$$

can be used as an estimation for $\tau^{(k)}$, for the reason that any norm of a matrix serves as the upper bound on its the largest eigenvalue.

Using the above selection of \mathbf{G} , the majorant of (5.84) can be written as

$$\begin{aligned} \tilde{g}_2(\mathbf{y}, \mathbf{y}^{(k)}) &= \frac{\tau^{(k)}}{2} \mathbf{y}^H \mathbf{y} + (\mathbf{y}^{(k)})^H \left(\frac{\tau^{(k)} + MP \lambda_{\Phi}}{2} \mathbf{I}_{MP} - \mathbf{B}^{(k)} \right) \mathbf{y}^{(k)} \\ &\quad + 2\Re \left\{ \mathbf{y}^H \left(\mathbf{B}^{(k)} - \frac{\tau^{(k)} + MP \lambda_{\Phi}}{2} \mathbf{I}_{MP} \right) \mathbf{y}^{(k)} \right\}. \end{aligned} \quad (5.92)$$

Similar to (5.43), the first two terms of (5.92) are constant and therefore immaterial for optimization. Ignoring these two terms, we can express the majorization problem for (5.76) as

$$\begin{aligned} \min_{\mathbf{y}} \quad & \mathbf{y}^H \left(\mathbf{B}^{(k)} - \frac{\tau^{(k)} + MP \lambda_{\Phi}}{2} \mathbf{I}_{MP} \right) \mathbf{y}^{(k)} \\ \text{s.t.} \quad & |\mathbf{y}(p')| = 1, p' = 1, \dots, MP. \end{aligned} \quad (5.93)$$

Due to the constant-modulus property of \mathbf{y} , (5.93) is equivalent to

$$\begin{aligned} \min_{\mathbf{y}} \quad & \|\mathbf{y} - \mathbf{z}^{(k)}\|^2 \\ \text{s.t.} \quad & |\mathbf{y}(p')| = 1, p' = 1, \dots, MP \end{aligned} \quad (5.94)$$

Algorithm 2 The WISL Minimization-Based Algorithm—WISLNew

```

1:  $k \leftarrow 0, \mathbf{y} \leftarrow$  unimodular sequence with random phases.
2:  $\lambda_{\tilde{\Phi}} \triangleq 2MP\lambda_{\max}^2(\Gamma)$ 
3: repeat
4:   procedure WISLNEW( $\mathbf{y}^{(k)}$ )
5:     Calculate  $\boldsymbol{\rho}_{mm'}^{(k)}, \boldsymbol{\eta}_{mm'}^{(k)}$  via (5.87) and (5.88),
6:        $m = 1, \dots, M; m' = m, \dots, M.$ 
7:      $\mathbf{B}_{mm'}^{(k)} = \left(\mathbf{B}_{m'm}^{(k)}\right)^H = 2P\mathcal{T}\left(\boldsymbol{\rho}_{mm'}^{(k)}, \boldsymbol{\eta}_{mm'}^{(k)}\right),$ 
8:        $m = 1, \dots, M; m' = m, \dots, M.$ 
9:     Construct  $\mathbf{B}^{(k)}$  via (5.85)
10:     $\tau^{(k)} = \|\mathbf{B}^{(k)} - \frac{1}{2}\lambda_{\tilde{\Phi}}\mathbf{Y}^{(k)}(\mathbf{y}^{(k)})^H\|$ 
11:     $\mathbf{z}^{(k)} = \left(\frac{1}{2}(\tau^{(k)} + MP\lambda_{\tilde{\Phi}})\mathbf{I}_{MP} - \mathbf{B}^{(k)}\right)\mathbf{y}^{(k)}$ 
12:     $\mathbf{y}^{(k+1)}(p') = e^{j\arg(\mathbf{z}^{(k)}(p'))}, p' = 1, \dots, MP$ 
13:     $k \leftarrow k + 1$ 
14:   end procedure
15: until convergence

```

where $\mathbf{z}^{(k)} \triangleq ((\tau^{(k)} + MP\lambda_{\tilde{\Phi}})\mathbf{I}_{MP}/2 - \mathbf{B}^{(k)})\mathbf{y}^{(k)}$. Finally, (5.94) can be solved in closed form as

$$\mathbf{y}(p') = \exp\{j \cdot \arg(\mathbf{z}^{(k)}(p'))\}, p' = 1, \dots, MP. \quad (5.95)$$

Reshaping the obtained waveform vector \mathbf{y} into the matrix \mathbf{Y} , the designing procedure is completed. The WISL minimization-based unimodular waveform design algorithm is summarized in Algorithm 2. Fig. 5.2 shows the convergence speed performance of the proposed Algorithm 2, and Fig. 5.3 shows the correlation properties of the WISL minimization based waveform design.

5.2.4 Computational complexity of WISLNew

In order to find the computational complexity of Algorithm 2, we assume that the set Ω consists of N_P ($0 < N_P \leq P$) elements. It can be seen that both $\boldsymbol{\rho}_{mm'}^{(k)}$ in (5.87) and $\boldsymbol{\eta}_{mm'}^{(k)}$ in (5.88) can be calculated with at most $N_P P$

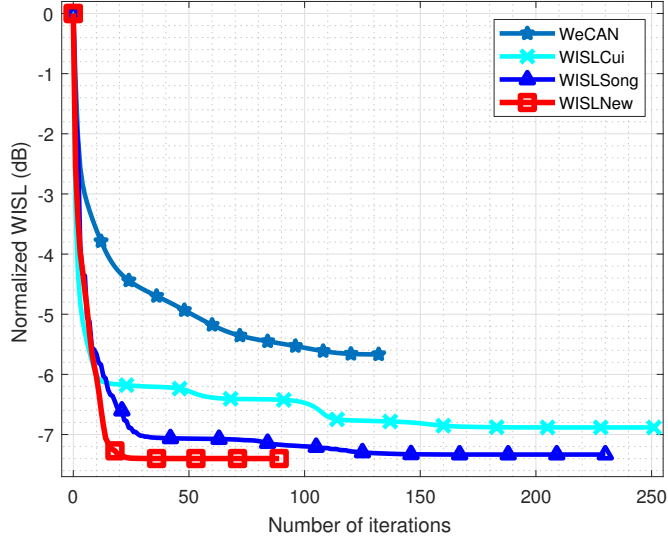


Figure 5.2. Convergence evaluations of algorithms developed for WISL minimization: Normalized WISL values versus the number of iterations for $M = 2$ unimodular waveforms of code length $P = 32$. Here the legends ‘WeCAN’, ‘WISLSong’ and ‘WISLCui’ respectively stand for the corresponding algorithms developed in [66], [105], and [121], and ‘WISLNew’ denotes the WISL minimization based algorithm reviewed in this chapter.

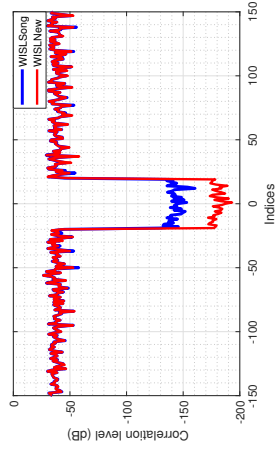
operations if the covariance matrix $\mathbf{Z}_{mm'}^{(k)}$ is given. The calculation of $\mathbf{Z}_{mm'}^{(k)}$ costs P^2 operations. Note that we only need to perform calculations for the subscripts $m = 1, \dots, M$ and $m' = m, \dots, M$, and then repeat the above summarized calculations $M(M - 1)/2$ times. Finally, the calculation of the vector $\mathbf{z}^{(k)}$ needs $M^2 P^2$ operations. Consequently, the total number of operations is upper bounded by $((3M^2 - M)P^2 + (M^2 - M)N_P P)/2$. In other words, the computational complexity of Algorithm 2 is at most $\mathcal{O}((M - 1)MP^2)$ which is smaller than quadratic in the problem size, and therefore suitable for large-scale optimization.

5.2.5 Acceleration strategies

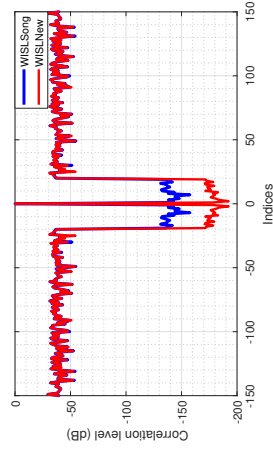
There exist accelerated schemes for MaMi, such as the squared iterative method (SQUAREM) of [270], which can be straightforwardly applied to speed up Algorithms 1 and 2. The SQUAREM scheme is an extension of the scalar Steffensen type method [271], [272] to vector fixed-point iteration empowered with the idea of “squaring” [273]. It is an “off-the-shelf”

acceleration method that requires nothing extra to the parameter updating rules of an original algorithm, except possibly the computationally cheap projection to feasibility set, and it is guaranteed to converge [107, 270].

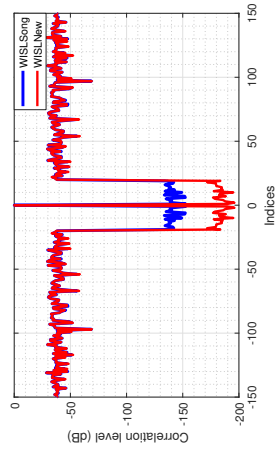
Different stopping criteria can be employed in Algorithms 1 and 2. For example, it can be the absolute ISL/WISL difference between the current and previous iterations normalized by the initial ISL/WISL, or it can be the norm of the difference between the waveform matrices obtained at the current and previous iterations.



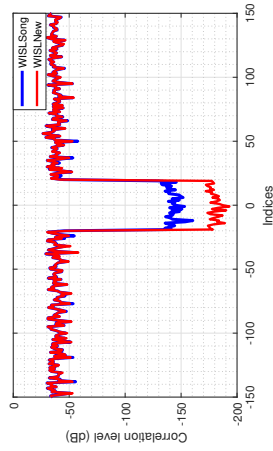
(b) Cross-correlation between the first and second designed waveforms.



(d) Auto-correlation of the second designed waveform.



(a) Auto-correlation of the first designed waveform.



(c) Cross-correlation between the second and first designed waveforms.

Figure 5.3. Correlation property evaluation of the designed waveforms for the WISL minimization-based designs. Here $M = 2$ waveforms of large code length $P = 4096$ are generated. Correlation results with respect to time lags only within the range $[-150, 150]$ are shown.

6. Joint space-time transmission and adaptive receive filter design

Waveform design has been the research field of significant interest over several decades [44–47, 74, 84, 85]. As reviewed in Chapter 2, many existing works focus on the design of fast-time waveform(s) in order to achieve various desirable properties [12, 62, 66, 67, 123], such as minimum ISL or WISL (or good correlation properties), mutual orthogonality, good AF shaping, maximum MI, constant envelope, etc. Typically, these works focus on improving the waveform quality itself when the receiver is fixed as the matched filter. Corresponding waveform designs use the fact that the matched filter can be implemented based on the correlation between the waveform and its delayed replica.

However, in harsh environments involving heterogeneous clutter with Doppler uncertainties and/or active jamming, the receiver should be flexibly adaptive, and therefore, joint transmission and receive filter design (JTRFD) becomes necessary. The resulting focus then shifts to the so-called mismatched filter design, which adds flexibility as it enables to consider constraints that are difficult to address otherwise. In essence, it makes receive filter to become generally mismatched mainly because of trading off the SNR in order to improve the SINR. The corresponding techniques for this design are usually developed on the basis of alternating optimization with MVDR filter design involved.

Recent works on JTRFD [60, 61, 81, 86, 96, 110, 122] can be divided into two categories. The first category concentrates on designing fast-time waveform transmission and receive filter with particular constraints on waveform characteristics, which essentially trade off the SNR for signal-to-clutter-plus-noise ratio [60, 61, 81]. The methods of this category generally

do not consider Doppler information processing. Differing from the first category, the methods in the second category focus on synthesizing slow-time waveforms (for inter-pulse coding) at transmission while jointly enforcing the receive adaptive filter [86, 96, 110, 122]. As a result, they have the potential of coping with Doppler related issues, such as uncertainty, and therefore, can offer enhanced resolution, superior detection, etc.

For the joint designs that deal with difficult constraints in both categories, the resulting optimization problems are usually nonconvex. When the number of waveforms and the size of filter increase to become large, the problem size can also grow to a large scale. To tackle these issues, the developments of fast and efficient algorithms are highly needed.

As we have already seen that MIMO radar enables transmit waveform/beam-space diversity and thus introduce extra DOFs compared to conventional radars, it naturally motivates us to implement the JTRFD in the context of MIMO radar and to see the resulting performance improvement. When it comes to receive filter, we have also seen that the multi-dimensional STAP filter enables superiority on clutter and jammer suppression and therefore leads to advanced output SINR performance. This also motivates us to extend the JTRFD to incorporate multi-dimensional STAP filter. However, involving both the MIMO architecture and the STAP filter make the JTRFD challenging since the increase of either size can result in a large-scale problem size of JTRFD. Such challenge further necessitates the developments of optimization algorithms that are fast and computationally efficient.

Typically, the problems of JTRFD for MIMO radar with STAP filters are nonconvex and have to be solved in cyclic manner. When fixing the multi-waveform transmission for the developments of cyclic algorithms, the common strategy use is to obtain an MVDR type solution to the problem by means of certain reformulations and manipulations. The major technical difficulty lies in ensuring fast SINR performance improvements in terms of iterations and meanwhile guaranteeing low computational complexity per iteration. We refer interested readers to the overview on SINR maximization based waveform design, in particular, the multi-dimensional joint transmission and receive filter design in Chapter 2 for more details.

6.1 Problem formulation

Consider an airborne colocated MIMO radar equipped with M transmit and N receive antenna elements. Within one radar coherent processing interval (CPI), a train of L pulses encoded by an independent slow-time waveform, denoted by $\phi_m \triangleq [\phi_{m,1}, \dots, \phi_{m,L}]^T \in \mathbb{C}^{L \times 1}$, is launched at the m th, $m \in \{1, \dots, M\}$ transmit element. Moreover, an independent fast-time waveform of length P , denoted by $\mathbf{s}_m \in \mathbb{C}^{P \times 1}$ for the m th antenna, is repeatedly used for all intra-pulse modulations.

We denote the space-(slow) time (SST) and space-(fast) time (SFT) waveform matrices for transmission as $\Phi \triangleq [\phi_1, \dots, \phi_M]^T \in \mathbb{C}^{M \times L}$ and $\mathbf{S} \triangleq [\mathbf{s}_1, \dots, \mathbf{s}_M]^T \in \mathbb{C}^{M \times P}$, respectively, and define $\mathbf{R}_S^{(p)} \triangleq \mathbf{S} \mathbf{J}_p \mathbf{S}^H \in \mathbb{C}^{M \times M}$ as the waveform covariance matrix (for pulse compression in fast time domain) at time lag p ($0 \leq p \leq P-1$). Here $\mathbf{J}_p \in \mathbb{C}^{P \times P}$ is the p th lower shift matrix whose (i, j) th, $i, j \in \{1, \dots, P\}$ entry is expressed by

$$[\mathbf{J}_p]_{i,j} \triangleq \begin{cases} 1, & \text{if } i - j = p \\ 0, & \text{otherwise.} \end{cases} \quad (6.1)$$

At the receive end, the intra-pulse compression is applied to the receiver, i.e., the received signal is match-filtered to \mathbf{S} at the time lag p ($p = 0$ for the target). Stacking the match-filtered data into a vector, the received target vector $\mathbf{y}_t \in \mathbb{C}^{MNL \times 1}$ can be expressed as

$$\mathbf{y}_t = \alpha_t \mathbf{a}_R(\theta_t) \otimes \mathcal{D}(\mathbf{d}(f_t)) \otimes ((\mathbf{R}_S^{(0)})^T \mathcal{D}(\mathbf{a}_T(\theta_t))) \phi \quad (6.2)$$

where α_t , θ_t , and f_t denote the complex reflection coefficient, azimuth angle, and normalized Doppler frequency of the target, respectively, $\mathbf{a}_T(\theta_t)$, $\mathbf{a}_R(\theta_t)$, and $\mathbf{d}(f_t)$ are respectively the transmit, receive, and Doppler steering vectors, and $\phi \triangleq \text{vec}(\Phi) \in \mathbb{C}^{ML \times 1}$ is the vectorized version of Φ .

The observed clutter is a superposition of echoes from different scatters which are assumed to be uncorrelated between each other. Suppose that there are N_r ($N_r \leq L$) range rings interfering with the range-azimuth bin of interest where the target locates, and each range ring consists of N_c discrete azimuth bins. Thus, the match-filtered clutter vector $\mathbf{y}_c \in \mathbb{C}^{MNL \times 1}$ at the receive end can be expressed as

$$\mathbf{y}_c = \sum_{i=0}^{N_r-1} \sum_{i'=1}^{N_c} \xi_{ii'} \mathbf{a}_R(\theta_{ii'}) \otimes (\mathbf{J}_{i'} \mathcal{D}(\mathbf{d}(f_{ii'}))) \otimes ((\mathbf{R}_S^{(p)})^T \mathcal{D}(\mathbf{a}_T(\theta_{ii'}))) \phi \quad (6.3)$$

where $\theta_{ii'}$, $f_{ii'}$, and $\xi_{ii'}$ respectively denote the azimuth angle, normalized Doppler frequency, and complex reflection coefficient with zero mean for the (i, i') th range-azimuth bin.

The overall match-filtered received data vector $\mathbf{y} \in \mathbb{C}^{MNL \times 1}$ including the target, clutter, and jamming plus noise can be expressed as

$$\mathbf{y} = \mathbf{y}_t + \mathbf{y}_c + \mathbf{y}_{j+n} \quad (6.4)$$

where $\mathbf{y}_{j+n} \in \mathbb{C}^{MNL \times 1}$ is the jamming plus noise vector assumed to be independent of the target and clutter components, with covariance matrix denoted by $\mathbf{R}_{j+n} \triangleq \mathbb{E}\{\mathbf{y}_{j+n}\mathbf{y}_{j+n}^H\}$.

To simplify the notations, the received target vector \mathbf{y}_t in (6.2) can be further expressed as $\mathbf{y}_t = \alpha_t \mathbf{T}_t \phi$ by means of the matrix $\mathbf{T}_t \in \mathbb{C}^{MNL \times ML}$ defined as follows

$$\mathbf{T}_t \triangleq \mathbf{a}_R(\theta_t) \otimes \mathfrak{D}(\mathbf{d}(f_t)) \otimes ((\mathbf{R}_S^{(0)})^T \mathfrak{D}(\mathbf{a}_T(\theta_t))) \quad (6.5)$$

and the received clutter vector \mathbf{y}_c in (6.3) can be further expressed as

$$\mathbf{y}_c = \sum_{i'=0}^{N_r-1} \sum_{i=1}^{N_c} \xi_{ii'} \tilde{\mathbf{T}}_{ii'}^{(p)} ((\mathbf{d}(f_{ii'}) \otimes \mathbf{1}_M) \odot \phi) \quad (6.6)$$

$$= \sum_{i'=0}^{N_r-1} \sum_{i=1}^{N_c} \xi_{ii'} \mathbf{T}_{ii'}^{(p)} \phi \quad (6.7)$$

with the matrices $\tilde{\mathbf{T}}_{ii'}^{(p)} \in \mathbb{C}^{MNL \times ML}$ and $\mathbf{T}_{ii'}^{(p)} \in \mathbb{C}^{MNL \times ML}$ defined as

$$\tilde{\mathbf{T}}_{ii'}^{(p)} \triangleq \mathbf{a}_R(\theta_{ii'}) \otimes \mathbf{J}_{i'} \otimes ((\mathbf{R}_S^{(p)})^T \mathfrak{D}(\mathbf{a}_T(\theta_{ii'}))) \quad (6.8)$$

$$\begin{aligned} \mathbf{T}_{ii'}^{(p)} &\triangleq \tilde{\mathbf{T}}_{ii'}^{(p)} \mathfrak{D}(\mathbf{d}(f_{ii'}) \otimes \mathbf{1}_M) \\ &= \mathbf{a}_R(\theta_{ii'}) \otimes (\mathbf{J}_{i'} \mathfrak{D}(\mathbf{d}(f_{ii'}))) \otimes ((\mathbf{R}_S^{(p)})^T \mathfrak{D}(\mathbf{a}_T(\theta_{ii'}))). \end{aligned} \quad (6.9)$$

Let us consider both cases with known and unknown Doppler information on clutter bins.

In the case of known Doppler information on clutter bins, the normalized Doppler frequency $f_{ii'}$ in (6.3) is fixed. While in the case of Doppler uncertainties on clutter bins, $f_{ii'}$ is uncertain, but rather distributed in an uncertainty interval $[\bar{f}_{ii'} - \epsilon_{ii'}/2, \bar{f}_{ii'} + \epsilon_{ii'}/2]$ with known probability density function (PDF). Here, $\bar{f}_{ii'}$ denotes the mean, and $\epsilon_{ii'}$ is the associated bounding parameter.

Based on (6.7), the clutter covariance matrix $\mathbf{R}_c \triangleq \mathbb{E}\{\mathbf{y}_c \mathbf{y}_c^H\} \in \mathbb{C}^{MNL \times MNL}$ for the case of known Doppler, denoted as \mathbf{R}_c^I , can be expressed as

$$\mathbf{R}_c^I = \sum_{i'=0}^{N_r-1} \sum_{i=1}^{N_c} \sigma_{ii'}^2 \mathbf{T}_{ii'}^{(p)} \boldsymbol{\phi} \boldsymbol{\phi}^H (\mathbf{T}_{ii'}^{(p)})^H \quad (6.10)$$

with $\sigma_{ii'}^2 \triangleq \mathbb{E}\{|\xi_{ii'}|^2\}$ being the variance of the reflection coefficient $\xi_{ii'}$. Using (6.6), the clutter covariance matrix \mathbf{R}_c for the case of unknown Doppler, denoted as \mathbf{R}_c^H , can be expressed as

$$\mathbf{R}_c^H = \sum_{i'=0}^{N_r-1} \sum_{i=1}^{N_c} \sigma_{ii'}^2 \tilde{\mathbf{T}}_{ii'}^{(p)} (\boldsymbol{\phi} \boldsymbol{\phi}^H) \odot (\boldsymbol{\Upsilon}_{ii'} \otimes \mathbf{1}_M \mathbf{1}_M^T) (\tilde{\mathbf{T}}_{ii'}^{(p)})^H \quad (6.11)$$

where $\boldsymbol{\Upsilon}_{ii'} \in \mathbb{C}^{L \times L}$ is a matrix determined by the PDF of $f_{ii'}$. For example, in the case of uniform distribution, $\boldsymbol{\Upsilon}_{ii'}$ is Hermitian with the (l, l') th element expressed as [86]

$$[\boldsymbol{\Upsilon}_{ii'}]_{ll'} = \exp\{j2\pi \bar{f}_{ii'}(l - l')\} \cdot \frac{\sin \pi \epsilon_{ii'}(l - l')}{\pi \epsilon_{ii'}(l - l')}, \quad \forall l, l' \in \{1, \dots, L\}. \quad (6.12)$$

The STAP filter that aims at maximizing the output SINR is applied to the received data vector \mathbf{y} in (6.4). With the weight vector of the STAP filter, denoted by $\mathbf{w} \in \mathbb{C}^{MNL \times 1}$, the SINR at the output can be expressed as

$$\zeta = \frac{|\alpha_t|^2 \cdot |\mathbf{w}^H \mathbf{T}_t \boldsymbol{\phi}|^2}{\mathbf{w}^H (\mathbf{R}_c + \mathbf{R}_{j+n}) \mathbf{w}}. \quad (6.13)$$

We consider the problem when both the SST waveform $\boldsymbol{\phi}$ and the STAP filter \mathbf{w} are to be jointly designed. Moreover, we enforce the constraint that the waveform(s) have constant modulus. With the joint design of the slow-time transmission and STAP filter, the objective of maximizing the output SINR in (6.13) is achieved. Here, we are interested in the case that the SFT waveform matrix \mathbf{S} is known, that is, the set of fast-time covariances $\{\mathbf{R}_S^p\}_{p=0}^{P-1}$ is known.

On the basis of (6.13), we can write the joint design problem as

$$\begin{aligned} & \max_{\boldsymbol{\phi}, \mathbf{w}} \quad \zeta \\ & \text{s.t.} \quad |\boldsymbol{\phi}(n)| = 1, \quad n = 1, \dots, ML \end{aligned} \quad (6.14)$$

where the constraints ensure the constant-modulus property of the slow-time waveforms.

6.2 Joint SST waveform and adaptive receiver design

Given ϕ in (6.13), the solution of the problem (6.14) with respect to \mathbf{w} can be easily found, and it obeys the MVDR expression as follows

$$\mathbf{w}_{\text{opt}}(\phi) = \frac{(\mathbf{R}_c + \mathbf{R}_{j+n})^{-1} \mathbf{T}_t \phi}{\phi^H \mathbf{T}_t^H (\mathbf{R}_c + \mathbf{R}_{j+n})^{-1} \mathbf{T}_t \phi}. \quad (6.15)$$

Inserting (6.15) into (6.13), the SINR ζ can therefore be rewritten as

$$\zeta = |\alpha_t|^2 \cdot \phi^H \mathbf{T}_t^H (\mathbf{R}_c + \mathbf{R}_{j+n})^{-1} \mathbf{T}_t \phi. \quad (6.16)$$

Replacing ζ with the explicit expression given by (6.16), the optimization problem (6.14) can be rewritten as

$$\begin{aligned} \max_{\phi} \quad & \phi^H \mathbf{T}_t^H (\mathbf{R}_c + \mathbf{R}_{j+n})^{-1} \mathbf{T}_t \phi \\ \text{s.t.} \quad & |\phi(n)| = 1, \quad n = 1, \dots, ML. \end{aligned} \quad (6.17)$$

Note that the argument of (6.17) is ϕ only, and the objective in (6.17) is a composite function of both ϕ and $\mathbf{R}_c \in \{\mathbf{R}_c^I, \mathbf{R}_c^{II}\}$ where \mathbf{R}_c is also a function of ϕ .

To solve (6.17), we resort to MiMa technique. The key idea is to properly design minorization functions for the objective of (6.17), and apply MiMa technique a number of times to come up to a closed-form solution of a minimization problem needed. While designing the minorization function, the algebraic structure of the objective function is explored and utilized, so that the resulting rewritten problems can contain standard forms leading to computationally cheap solutions. Before applying the MiMa procedure, we present the following result to be used later.

Lemma 6.1. *The objective in (6.17) is minorized by the following function*

$$\begin{aligned} g_1(\phi, \phi^{(k)}) = & (\phi^{(k)})^H \Psi(\phi^{(k)}) \phi^{(k)} + 2\Re \left\{ (\phi^{(k)})^H (\Psi(\phi^{(k)}))^H (\phi - \phi^{(k)}) \right\} \\ & - (\phi^{(k)})^H \mathbf{T}_t^H (\Omega(\phi^{(k)}))^H (\mathbf{R}_c(\phi) - \mathbf{R}_c(\phi^{(k)})) \Omega(\phi^{(k)}) \mathbf{T}_t \phi^{(k)} \end{aligned} \quad (6.18)$$

where $\phi^{(k)} \in \mathbb{C}^{ML \times 1}$ is the SST waveform vector obtained at iteration k , and $\Omega(\phi^{(k)}) \in \mathbb{C}^{MNL \times MNL}$ and $\Psi(\phi^{(k)}) \in \mathbb{C}^{ML \times ML}$ are both functions of

$\phi^{(k)}$, respectively defined as

$$\Omega(\phi^{(k)}) \triangleq (\mathbf{R}_c(\phi^{(k)}) + \mathbf{R}_{j+n})^{-1} \quad (6.19)$$

$$\Psi(\phi^{(k)}) \triangleq \mathbf{T}_t^H \Omega(\phi^{(k)}) \mathbf{T}_t. \quad (6.20)$$

Proof. Using Taylor's theorem and applying the first order expansion to the objective function in (6.17), it can be straightforwardly proved after some elementary derivations that (6.18) minorizes the objective in (6.17). The proof is complete. \square

6.2.1 Case I: Known Doppler information on clutter bins

Recall that in the case of known Doppler information on clutter bins, the resulting clutter covariance matrix \mathbf{R}_c takes the form $\mathbf{R}_c = \mathbf{R}_c^I$ given by (6.10). Inserting the explicit expression of \mathbf{R}_c^I into (6.18) for Lemma 6.1, after some elementary algebraic derivations, the minorization function for the objective in (6.17) can be rewritten as

$$\begin{aligned} g_1^I(\phi, \phi^{(k)}) &= (\phi^{(k)})^H \Psi^I(\phi^{(k)}) \phi^{(k)} + 2\Re\left\{ (\phi^{(k)})^H (\Psi^I(\phi^{(k)}))^H (\phi - \phi^{(k)}) \right\} \\ &\quad - \phi^H \mathbf{E}_c^I(\phi^{(k)}) \phi + (\phi^{(k)})^H \mathbf{E}_c^I(\phi^{(k)}) \phi^{(k)} \end{aligned} \quad (6.21)$$

with $\Psi^I(\phi^{(k)}) \in \mathbb{C}^{ML \times ML}$ and $\mathbf{E}_c^I(\phi^{(k)}) \in \mathbb{C}^{ML \times ML}$ respectively defined as

$$\Psi^I(\phi^{(k)}) \triangleq \mathbf{T}_t^H \Omega^I(\phi^{(k)}) \mathbf{T}_t \quad (6.22)$$

$$\mathbf{E}_c^I(\phi^{(k)}) \triangleq \sum_{i'=0}^{N_T-1} \sum_{i=1}^{N_c} \sigma_{ii'}^2 (\mathbf{T}_{ii'}^{(p)})^H \Omega^I(\phi^{(k)}) \mathbf{T}_t \phi^{(k)} (\phi^{(k)})^H \mathbf{T}_t^H (\Omega^I(\phi^{(k)}))^H \mathbf{T}_{ii'}^{(p)}. \quad (6.23)$$

via the matrix $\Omega^I(\phi^{(k)}) \in \mathbb{C}^{MNL \times MNL}$ given by

$$\Omega^I(\phi^{(k)}) \triangleq (\mathbf{R}_c^I(\phi^{(k)}) + \mathbf{R}_{j+n})^{-1}. \quad (6.24)$$

Note that for given $\phi^{(k)}$, the first and last terms of (6.21) are fixed. The second term takes a linear form in ϕ , while the third term is a quadratic form with respect to ϕ . Therefore, we can apply a proper minorization again to the quadratic form.

Before proceeding with the further minorization of (6.21), we present the following result.

Lemma 6.2. Given $\phi^{(k)}$, the quadratic function $f(\phi) = -\phi^H \mathbf{E}_c^I(\phi^{(k)}) \phi$ with respect to ϕ is minorized by

$$\begin{aligned} \tilde{g}(\phi, \phi^{(k)}) &= -\frac{1}{2} \phi^H \mathbf{G}^{(k)} \phi - (\phi^{(k)})^H \left(\frac{1}{2} \mathbf{G}^{(k)} - \mathbf{E}_c^I(\phi^{(k)}) \right) \phi^{(k)} \\ &\quad - 2\Re \left\{ \phi^H \left(\mathbf{E}_c^I(\phi^{(k)}) - \frac{1}{2} \mathbf{G}^{(k)} \right) \phi^{(k)} \right\} \end{aligned} \quad (6.25)$$

where the matrix $\mathbf{G}^{(k)} \in \mathbb{C}^{ML \times ML}$ satisfies the condition that the generalized inequality $\mathbf{G}^{(k)} \succeq \mathbf{E}_c^I(\phi^{(k)})$ holds.

Proof. The minimization of $f(\phi)$ is equivalent to the majorization of $-f(\phi) = \phi^H \mathbf{E}_c^I(\phi^{(k)}) \phi$, and the proof for the majorization given in this quadratic form has been presented in Corollary 5.1.1 of Chapter 5. Replacing \mathbf{x} with ϕ and \mathbf{Q} with $\mathbf{E}_c^I(\phi^{(k)})$ therein, (6.25) is proved. The proof is complete. \square

Applying Lemma 6.2 to (6.21), after some derivations, the minorization function $g_1^I(\phi, \phi^{(k)})$ can be rewritten as

$$\begin{aligned} g_2^I(\phi, \phi^{(k)}) &= -\frac{1}{2} \phi^H \mathbf{G}^{(k)} \phi - 2\Re \left\{ \phi^H \left(\mathbf{E}_c^I(\phi^{(k)}) - \frac{1}{2} \mathbf{G}^{(k)} - \Psi^I(\phi^{(k)}) \right) \phi^{(k)} \right\} \\ &\quad + (\phi^{(k)})^H \left(2\mathbf{E}_c^I(\phi^{(k)}) - \Psi^I(\phi^{(k)}) - \frac{1}{2} \mathbf{G}^{(k)} \right) \phi^{(k)}. \end{aligned} \quad (6.26)$$

Choosing $\mathbf{G}^{(k)}$ as a diagonal matrix with properly selected magnitude such that $\mathbf{G}^{(k)} \succeq \mathbf{E}_c^I(\phi^{(k)})$ is guaranteed. For example, $\mathbf{G}^{(k)}$ can be designed as $\mathbf{G}^{(k)} = \lambda^{(k)} \mathbf{I}_{ML}$ with $\lambda^{(k)}$ being the largest eigenvalue of $\mathbf{E}_c^I(\phi^{(k)})$. Due to the mutual orthogonality and unit-modulus properties of the slow-time waveform vector ϕ , it is straightforward to see that the first term of (6.26) under such selection of $\mathbf{G}^{(k)}$ becomes constant.

Ignoring the first term and also the third one, which are irrelevant to ϕ , in (6.26), the minorization problem for (6.17) can be written as

$$\begin{aligned} \max_{\phi} \quad & -\Re \left\{ \phi^H \left(\mathbf{E}_c^I(\phi^{(k)}) - \frac{1}{2} \mathbf{G}^{(k)} - \Psi^I(\phi^{(k)}) \right) \phi^{(k)} \right\} \\ \text{s.t.} \quad & |\phi(n)| = 1, \quad n = 1, \dots, ML. \end{aligned} \quad (6.27)$$

Note that the objective function in (6.27) takes a linear form in ϕ . Since ϕ needs to be unimodular, the problem (6.27) can therefore be written into the following equivalent form

$$\begin{aligned} \min_{\phi} \quad & \|\phi - \tau_1^{(k)}\| \\ \text{s.t.} \quad & |\phi(n)| = 1, \quad n = 1, \dots, ML \end{aligned} \quad (6.28)$$

where $\tau_{\mathbf{I}}^{(k)} \in \mathbb{C}^{ML \times 1}$ is defined as

$$\tau_{\mathbf{I}}^{(k)} \triangleq \left(\mathbf{E}_{\mathbf{c}}^{\mathbf{I}}(\phi^{(k)}) - \frac{1}{2} \mathbf{G}^{(k)} - \Psi^{\mathbf{I}}(\phi^{(k)}) \right) \phi^{(k)}. \quad (6.29)$$

Problem (6.28) leads to the closed-form solution given as

$$\phi(n) = \exp \left\{ j \cdot \arg \left(\tau_{\mathbf{I}}^{(k)}(n) \right) \right\}, \quad n = 1, \dots, ML. \quad (6.30)$$

6.2.2 Case II: Doppler uncertainties on clutter bins

Recall that in the case of Doppler uncertainties on clutter bins, the resulting clutter covariance matrix takes the form $\mathbf{R}_{\mathbf{c}} = \mathbf{R}_{\mathbf{c}}^{\mathbf{II}}$ given by (6.11). In this case, directly inserting the explicit expression of $\mathbf{R}_{\mathbf{c}}^{\mathbf{II}}$ into (6.18) for Lemma 6.1 cannot help in rewriting the minorization function into a proper form like (6.21). The reason is that the Hadamard product appears in the expression of $\mathbf{R}_{\mathbf{c}}^{\mathbf{II}}$, and we have to deal with it. To tackle this difficulty, we need to convert $\mathbf{R}_{\mathbf{c}}^{\mathbf{II}}$ in (6.11) to an alternative expression, so that the corresponding minorization function can contain stand quadratic form that enables further minorization.

Towards this end, we first consider the eigen decomposition of $\Upsilon_{ii'}$ involved in $\mathbf{R}_{\mathbf{c}}^{\mathbf{II}}$, which in general is expressed as

$$\Upsilon_{ii'} = \sum_{k=1}^{K^{(ii')}} \lambda_k^{(ii')} \mathbf{q}_k^{(ii')} (\mathbf{q}_k^{(ii')})^{\mathbf{H}} = \sum_{k=1}^{K_{ii'}} \mathbf{u}_k^{(ii')} (\mathbf{u}_k^{(ii')})^{\mathbf{H}} \quad (6.31)$$

where $\lambda_k^{(ii')}$ (real-valued) and $\mathbf{q}_k^{(ii')}$ are the k th eigenvalue and eigenvector, respectively, $K^{(ii')}$ is the rank of $\Upsilon_{ii'}$, and $\mathbf{u}_k^{(ii')} \triangleq \sqrt{\lambda_k^{(ii')}} \mathbf{q}_k^{(ii')} \in \mathbb{C}^{L \times 1}$.

Based on (6.31), $\mathbf{R}_{\mathbf{c}}^{\mathbf{II}}$ in (6.11) can be rewritten as

$$\mathbf{R}_{\mathbf{c}}^{\mathbf{II}} = \sum_{i'=0}^{N_{\mathbf{r}}-1} \sum_{i=1}^{N_{\mathbf{c}}} \sum_{k=1}^{K_{ii'}} \sigma_{ii'}^2 \tilde{\mathbf{T}}_{ii'}^{(p)} \mathbf{D}_k^{(ii')} \phi \phi^{\mathbf{H}} (\mathbf{D}_k^{(ii')})^{\mathbf{H}} (\tilde{\mathbf{T}}_{ii'}^{(p)})^{\mathbf{H}} \quad (6.32)$$

with the diagonal matrix $\mathbf{D}_k^{(ii')} \in \mathbb{C}^{ML \times ML}$ defined as

$$\mathbf{D}_k^{(ii')} \triangleq \mathfrak{D} \left(\mathbf{u}_k^{(ii')} \otimes \mathbf{1}_M \right). \quad (6.33)$$

Inserting (6.32) into (6.18) for Lemma 6.1, after some elementary algebraic manipulations, the objective of (6.17) for the uncertain Doppler case is minorized by

$$\begin{aligned} g_{\mathbf{I}}^{\mathbf{II}}(\phi, \phi^{(k)}) &= (\phi^{(k)})^{\mathbf{H}} \Psi^{\mathbf{II}}(\phi^{(k)}) \phi^{(k)} + 2\Re \left\{ (\phi^{(k)})^{\mathbf{H}} (\Psi^{\mathbf{II}}(\phi^{(k)}))^{\mathbf{H}} (\phi - \phi^{(k)}) \right\} \\ &\quad - \phi^{\mathbf{H}} \mathbf{E}_{\mathbf{c}}^{\mathbf{II}}(\phi^{(k)}) \phi + (\phi^{(k)})^{\mathbf{H}} \mathbf{E}_{\mathbf{c}}^{\mathbf{II}}(\phi^{(k)}) \phi^{(k)} \end{aligned} \quad (6.34)$$

Algorithm 3 Joint Design Algorithm

- 1: Initialization: $\phi^{(0)}$; $\text{mod} \in \{\text{I}, \text{II}\}$
 - 2: **repeat** procedure with respect to $\phi^{(k)}$
 - 3: Calculate $\mathbf{\Omega}^{\text{mod}}(\phi^{(k)})$, $\mathbf{\Psi}^{\text{mod}}(\phi^{(k)})$, $\mathbf{E}_c^{\text{mod}}(\phi^{(k)})$
 - 4: Construct $\mathbf{G}^{(k)}$ via $\mathbf{E}_c^{\text{mod}}(\phi^{(k)})$
 - 5: $\tau_{\text{mod}}^{(k)} \triangleq (\mathbf{E}_c^{\text{mod}}(\phi^{(k)}) - \frac{1}{2}\mathbf{G}^{(k)} - \mathbf{\Psi}^{\text{mod}}(\phi^{(k)}))\phi^{(k)}$
 - 6: $\phi(n) = \exp\{j \cdot \arg(\tau_{\text{mod}}^{(k)}(n))\}$, $n = 1, \dots, ML$
 - 7: $k \leftarrow k + 1$
 - 8: **until** convergence
 - 9: Calculate \mathbf{w}_{opt} , and $\phi_{\text{opt}} = \phi^{(k+1)}$
-

with $\mathbf{\Psi}^{\text{II}}(\phi^{(k)})$ and $\mathbf{E}_c^{\text{II}}(\phi^{(k)})$ respectively defined as

$$\mathbf{\Psi}^{\text{II}}(\phi^{(k)}) \triangleq \mathbf{T}_t^{\text{H}} \mathbf{\Omega}^{\text{II}}(\phi^{(k)}) \mathbf{T}_t \quad (6.35)$$

$$\begin{aligned} \mathbf{E}_c^{\text{II}}(\phi^{(k)}) \triangleq & \sum_{i'=0}^{N_c-1} \sum_{i=1}^{N_c} \sum_{k=1}^{K_{ii'}} \sigma_{ii'}^2 (\mathbf{D}_k^{(ii')})^{\text{H}} (\mathbf{T}_{ii'}^{(p)})^{\text{H}} \mathbf{\Omega}^{\text{II}}(\phi^{(k)}) \\ & \times \mathbf{T}_t \phi^{(k)} (\phi^{(k)})^{\text{H}} \mathbf{T}_t^{\text{H}} (\mathbf{\Omega}^{\text{II}}(\phi^{(k)}))^{\text{H}} \mathbf{T}_{ii'}^{(p)} \mathbf{D}_k^{(ii')} \end{aligned} \quad (6.36)$$

via the matrix $\mathbf{\Omega}^{\text{II}}(\phi^{(k)})$ given by

$$\mathbf{\Omega}^{\text{II}}(\phi^{(k)}) \triangleq (\mathbf{R}_c^{\text{II}}(\phi^{(k)}) + \mathbf{R}_{j+n})^{-1}. \quad (6.37)$$

Similar to the previous known Doppler case, applying Lemma 6.2 to the third (quadratic) term of $g_1^{\text{II}}(\phi, \phi^{(k)})$ by replacing the matrices $\mathbf{E}_c^{\text{I}}(\phi^{(k)})$ and $\mathbf{\Psi}^{\text{I}}(\phi^{(k)})$ therein with $\mathbf{E}_c^{\text{II}}(\phi^{(k)})$ and $\mathbf{\Psi}^{\text{II}}(\phi^{(k)})$, respectively, (6.34) can be further minorized by

$$\begin{aligned} g_2^{\text{II}}(\phi, \phi^{(k)}) = & -\frac{1}{2} \phi^{\text{H}} \mathbf{G}^{(k)} \phi - 2\Re \left\{ \phi^{\text{H}} \left(\mathbf{E}_c^{\text{II}}(\phi^{(k)}) - \frac{1}{2} \mathbf{G}^{(k)} - \mathbf{\Psi}^{\text{II}}(\phi^{(k)}) \right) \phi^{(k)} \right\} \\ & + (\phi^{(k)})^{\text{H}} \left(2\mathbf{E}_c^{\text{II}}(\phi^{(k)}) - \mathbf{\Psi}^{\text{II}}(\phi^{(k)}) - \frac{1}{2} \mathbf{G}^{(k)} \right) \phi^{(k)}. \end{aligned} \quad (6.38)$$

With proper selection of the matrix $\mathbf{G}^{(k)}$ such as the routine used in the previous case, the first two terms of (6.38) become constant and therefore can be excluded from optimization as immaterial. As a result, the

minorization problem for (6.17) can be written as

$$\begin{aligned} \max_{\phi} \quad & -\Re\left\{\phi^H\left(\mathbf{E}_c^{\text{II}}(\phi^{(k)}) - \frac{1}{2}\mathbf{G}^{(k)} - \Psi^{\text{II}}(\phi^{(k)})\right)\phi^{(k)}\right\} \\ \text{s.t.} \quad & |\phi(n)| = 1, \quad n = 1, \dots, ML \end{aligned} \quad (6.39)$$

and solved in closed-form as

$$\phi(n) = \exp\left\{j \cdot \arg\left(\tau_{\text{II}}^{(k)}(n)\right)\right\}, \quad n = 1, \dots, ML \quad (6.40)$$

with $\tau_{\text{II}}^{(k)} \in \mathbb{C}^{ML \times 1}$ defined as

$$\tau_{\text{II}}^{(k)} \triangleq \left(\mathbf{E}_c^{\text{II}}(\phi^{(k)}) - \frac{1}{2}\mathbf{G}^{(k)} - \Psi^{\text{II}}(\phi^{(k)})\right)\phi^{(k)}. \quad (6.41)$$

It is worth noting that the solution given in (6.40) boils down to (6.30) when the conditions $\mathbf{u}_k^{(ii')} = \mathbf{d}(f_{ii'})$ and $K^{(ii')} = 1$, $\forall i, i'$ are both satisfied. In this situation, the Doppler uncertainties on clutter bins do not exist, which results in the same clutter covariance matrix as in the previous case. Hence, the solution obtained for the Doppler uncertainty case incorporates that for the Doppler known case. However, the Doppler uncertainty case causes a lot more computations.

The corresponding algorithm for joint SST waveform and receive filter design in term of the two aforementioned cases is summarized in Algorithm 3, where two modes account for both cases.

The algorithm summarized Algorithm 3 can be accelerated using, for example, the squared iterative method (SQUAREM) of [270], the backtracking line search method (BLSM) [274], etc. The SINR performance of the proposed Algorithm 3 for the two joint designs is shown Figs. 6.1 and 6.2, respectively.

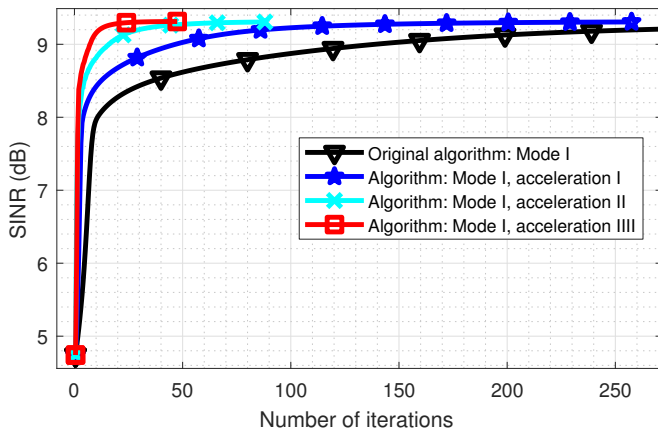


Figure 6.1. Output SINR performance of the developed algorithm versus the number of iterations for the case of known Doppler information on clutter bins. Here $M = 4$ transmit and $N = 3$ receive receive antenna elements spaced half wavelength apart from each other and $L = 20$ pulses within one CPI are used. Other parameters are: $\theta_t = 10^\circ$, $f_t = 0.13$, SNR = 10 dB, and stopping tolerance 10^{-8} . Homogeneous clutter environment composed of $N_r = 10$ range rings interfering with the range-azimuth bin of interest with each separated into $N_c = 181$ patches is considered, and the CNR for each clutter bin is set to 40 dB. Accelerations I: SQUAREM; II: BLSM; III: Combination of I and II.

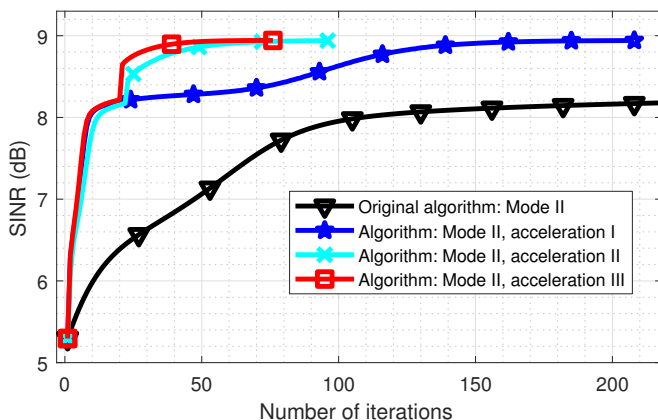


Figure 6.2. Output SINR performance of the developed algorithm versus the number of iterations for the case of Doppler uncertainties on clutter bins. Discrete heterogeneous clutter environment composed of $N_r = 10$ range rings with each having $N_c = 3$ sources randomly distributed within sectors $[-50^\circ, -30^\circ]$, $[-20^\circ, 10^\circ]$, and $[25^\circ, 35^\circ]$ is considered. Doppler uncertainty parameters are: $f_{ii'} = 0$, and $\epsilon_{ii'} = 0.35$. The CNR for each clutter bin is set to 50 dB. Other parameters are the same as used in the known Doppler case.

7. Summary and outlook

The thesis has made several advances in the research area of signal processing for MIMO radar. Particularly, ambiguity properties of MIMO radar exploiting TB strategies have been analysed, opportunities and challenges of clutter and jammer suppression with both the conventional and TB-based MIMO radar configurations have been investigated, and waveform designs ensuring good correlation or weighted correlation properties and joint multi-dimensional waveform transmission and receive adaptive design guaranteeing best SINR performance have been developed.

The TB-based MIMO radar AF has been proposed and ambiguity properties of the MIMO radar with TB designs have been investigated. A series of spatial and/or temporal adaptive processing algorithms with RD (in elementspace/beamspace) and reasonable computational burden, fast algorithms for generating unimodular waveforms with good correlation properties and low complexity, and a novel algorithm for the joint multi-dimensional transmission and receive STAP filter design have been developed. The corresponding results have been presented in Chapters 3, 4, 5, and 6 of the thesis, respectively. In addition, a detailed overview of the MIMO radar research with a focus on the above-mentioned studies has been given in Chapter 2, where the history, the concept of MIMO radar, the relevant major existing results on waveform(s)/code(s) design, interference suppression, transmit beamforming or TB strategy design, parameter estimation and detection, and the newly emerging research directions on MIMO radar have been reviewed and analyzed.

- **The TB-based MIMO radar AF**

The AF for the TB-based MIMO radar configuration, termed as the

TB-based MIMO radar AF, has been proposed in Publications I and II, while the corresponding main results have been reviewed in the thesis. The TB-based MIMO radar AF deals with the case of far-field targets and narrowband waveforms, and has incorporated the effects of transmit coherent processing gain, waveform diversity, and the array geometry in its definition. It can serve as a generalized AF form for which the PA and conventional MIMO radar AFs are important special cases. Moreover, it reveals interesting relationships with the existing AF results including the Woodward's AF and the AFs for PA and conventional MIMO radars. Furthermore, the maximal achievable "clear region" in delay-Doppler domain of the TB-based MIMO radar AF, i.e., the region free of sidelobes, has been analyzed. Two limiting cases which help to obtain tight close-form bounds for the "clear region" analysis have been identified.

The theoretical analysis on the "clear region" of the TB-based MIMO radar AF has shown that the bound on the "clear region" for the worst case is inversely proportional to the number of transmitted waveforms, while the bound for the best case is independent of that number. The actual maximal achievable "clear region" of the TB-based MIMO radar AF is in between of the bounds for the two limiting cases. Consequently, there exist a trade-off between the maximal "clear region" and the waveform and beamspace diversity in the TB-based MIMO radar. In addition, a new TB design strategy has been devised and it has been shown to have the ability of reducing the AF sidelobes.

- **Spatial and/or temporal processing techniques**

The capability, opportunities, and challenges of the conventional and TB-based MIMO radars in dealing with the clutter and jammer suppression problems have been also reserached in the thesis, and a series of spatial and/or temporal processing algorithms with RD (in elementspace/beamspace) have been developed in Publications III–VI.

First, two SFTAP algorithms have been proposed for addressing the terrain-scattered jammer suppression problem in conventional MIMO radar in Publication III, where the first one leads to a close-form solution while the second one allows a larger feasibility set through relaxation of the constraints in the first. They have shown to have the ability of maintaining the cold clutter stationarity over slow time domain. In addition to these

results, the effect of match filtering on the correlation function of jamming signals has been studied.

Second, a 3D STAP algorithm has been proposed for the joint hot and cold clutter mitigation in the TB-based MIMO radar in Publication IV, where the algorithm has been developed on the basis of rank analysis on clutter subspace. A valid approach of TB strategy design, which enables the approximation of linear phase rotations among transmit beams and facilitates the rank analysis, is also proposed.

Third, three RD beamspace designs with adaptiveness and two robust beamforming designs with robustness have been developed to demonstrate unique capabilities of MIMO radar on powerful jammer suppression in Publications V and VI. An efficient power estimates of desired and interfering sources in the presence of powerful jammers and non-ideal factors have been derived there as well.

The general conclusion on the above-mentioned results is that there exist new opportunities in conventional and the TB-based MIMO radars for clutter and jammer suppression using spatial and/or temporal adaptive processing techniques including multi-dimensional STAP. With properly designed STAP techniques, an improved SINR performance can be obtained in the context of the TB-based MIMO radar. On the other hand, challenges such as computation burden also exist, which requires the developments of specialized algorithms with low complexity.

- **ISL and WISL minimization based waveform designs**

In Publications VII–IX, new computationally efficient algorithms for generating aperiodic unimodular waveforms with good correlation properties have been developed. The waveform designs have been conducted based on the minimization of the ISL and WISL of waveforms. The algorithms in Publications VIII and IX have been the early versions of the ones in Publication VII, which deal with WISL and ISL minimizations, respectively.

The ISL and WISL minimization based waveform designs have been formulated as nonconvex quartic optimization problems in frequency domain. By means of MaMi technique, the quartic problems have then been simplified into quadratic problems, where the inherent algebraic structures in the objective functions of these problems have been exploited in the algo-

rithms. In the case of designing the WISL minimization based waveforms, an alternative quartic form that allows to apply the quartic-quadratic transformation has been additionally derived. Moreover, closed-form solution has been found at each iteration of the iterative procedures developed. The ISL and WISL minimization based waveform design algorithms have been applicable to large-scale unimodular waveform design problems as they have been proved to have lower or comparable computational burden (analyzed theoretically) and faster convergence speed (confirmed by comprehensive simulations) than the state-of-the-art algorithms. In addition, the waveforms designed by the developed algorithms have demonstrated better correlation properties compared to their counterparts.

- **Joint SST transmission and STAP filter design**

Finally, the thesis has also reviewed our main results of the algorithm development for joint design of SST transmission with unimodular waveforms and receive adaptive filter for MIMO radar in Publication X. An efficient approach for jointly synthesizing the unimodular SST waveforms and the MVDR type STAP filter has been proposed. In our study we have dealt with two cases of known Doppler information and the presence of Doppler uncertainties on clutter bins. The corresponding problems have been formulated as nonconvex optimization problems with composite objective functions. In order to address the non-convex problems, the MiMa technique has been used. Advanced minorizing surrogates have been devised so that the non-convex problems have been converted to minimization problems which are easy to solve by iterative procedures. Closed form solution has been enabled at each iteration of the iterative procedures. Moreover, the proposed algorithms have demonstrated good performance and have shown fast convergence speed and low complexity.

In the future, the research reviewed in Chapter 6 is to be continued, for which more advanced algorithms are to be developed. Moreover, the scenarios studied therein will be extended to more generalized cases. Besides, the clutter and jammer suppression research in Chapter 4 is to relate to the research of waveform design and joint waveform transmission and receive filter design in Chapters 5 and 6.

References

- [1] J. Li and P. Stoica, *MIMO Radar Signal Processing*. NY, USA: Wiley, 2009.
- [2] D. W. Bliss and K. W. Forsythe, "Multiple-input multiple-output (MIMO) radar and imaging: Degrees of freedom and resolution," in *Proceedings of Asilomar Conference on Signals, Systems, and Computers*, vol. 1, Pacific Grove, CA, USA, November 2003, pp. 54–59.
- [3] E. Fishler, A. Haimovich, R. S. Blum, D. Chizhik, L. Cimini, and R. Valenzuela, "MIMO radar: An idea whose time has come," in *Proceedings of IEEE Radar Conference*, Honolulu, HI, USA, April 2004, pp. 71–78.
- [4] K. W. Forsythe, D. W. Bliss, and G. S. Fawcett, "Multiple-input multiple-output (MIMO) radar: Performance issues," in *Proceedings of Asilomar Conference on Signals, Systems, and Computers*, vol. 1, Pacific Grove, CA, USA, November 2004, pp. 310–315.
- [5] D. R. Fuhrmann and G. San Antonio, "Transmit beamforming for MIMO radar systems using partial signal correlation," in *Proceedings of Asilomar Conference on Signals, Systems, and Computers*, vol. 1, Pacific Grove, CA, USA, November 2004, pp. 295–299.
- [6] E. Fishler, A. Haimovich, R. S. Blum, L. Cimini, D. Chizhik, and R. Valenzuela, "Spatial diversity in radars—Models and detection performance," *IEEE Transactions on Signal Processing*, vol. 54, no. 3, pp. 823–838, March 2006.
- [7] I. Bekkerman and J. Tabrikian, "Target detection and localization using MIMO radar and sonars," *IEEE Transactions on Signal Processing*, vol. 54, no. 10, pp. 3873–3883, October 2006.
- [8] V. F. Mecca, D. Ramakrishnan, and J. L. Krolik, "MIMO radar space-time adaptive processing for multipath clutter mitigation," in *Proceedings of IEEE Workshop on Sensor Array and Multichannel Signal Processing (SAM)*, Waltham, MA, USA, July 2006, pp. 249–253.
- [9] J. Li and P. Stoica, "MIMO radar with colocated antennas," *IEEE Signal Processing Magazine*, vol. 24, no. 5, pp. 106–114, September 2007.

- [10] P. Stoica, J. Li, and Y. Xie, "On probing signal design for MIMO radar," *IEEE Transactions on Signal Processing*, vol. 55, no. 8, pp. 4151–4161, August 2007.
- [11] G. San Antonio, D. R. Fuhrmann, and F. C. Robey, "MIMO radar ambiguity functions," *IEEE Journal of Selected Topics in Signal Processing*, vol. 1, no. 1, pp. 167–177, June 2007.
- [12] Y. Yang and R. S. Blum, "MIMO radar waveform design based on mutual information and minimum mean-square error estimation," *IEEE Transactions on Aerospace and Electronic Systems*, vol. 43, no. 1, pp. 330–343, January 2007.
- [13] Y. Yang and R. S. Blum, "Minimax robust mimo radar waveform design," *IEEE Journal of Selected Topics in Signal Processing*, vol. 1, no. 1, pp. 147–155, 2007.
- [14] A. M. Haimovich, R. S. Blum, and L. J. Cimini, "MIMO radar with widely separated antennas," *IEEE Signal Processing Magazine*, vol. 24, no. 1, pp. 116–129, January 2008.
- [15] C.-Y. Chen and P. P. Vaidyanathan, "MIMO radar space-time adaptive processing using prolate spheroidal waveform functions," *IEEE Transactions on Signal Processing*, vol. 56, no. 2, pp. 623–635, February 2008.
- [16] D. W. Bliss, K. W. Forsythe, S. K. Davis, G. S. Fawcett, D. J. Rabideau, L. L. Horowitz, and S. Kraut, "GMTI MIMO radar," in *Proceedings of International Waveform Diversity and Design Conference (WDD)*, Kissimmee, FL, USA, February 2009, pp. 118–122.
- [17] A. Hassanien and S. A. Vorobyov, "Phased-MIMO radar: A tradeoff between phased-array and MIMO radars," *IEEE Transactions on Signal Processing*, vol. 58, no. 6, pp. 3137–3151, June 2010.
- [18] X. Song, P. Willett, S. Zhou, and P. B. Luh, "The MIMO radar and jammer games," *IEEE Transactions on Signal Processing*, vol. 60, no. 2, pp. 687–699, February 2012.
- [19] Y. Li, S. A. Vorobyov, and V. Koivunen, "Ambiguity function of the transmit beamspace-based MIMO radar," *IEEE Transactions on Signal Processing*, vol. 63, no. 17, pp. 4445–4457, September 2015, [Publication I].
- [20] H. Deng, "Polyphase code design for orthogonal netted radar systems," *IEEE Transactions on Signal Processing*, vol. 52, no. 11, pp. 3126–3135, November 2004.
- [21] V. Tarokh, N. Seshadri, and A. R. Calderbank, "Space-time codes for high data rate wireless communication: Performance criterion and code construction," *IEEE Transactions on Information Theory*, vol. 44, no. 2, pp. 744–765, March 1998.

- [22] D. Tse and P. Viswanath, *Fundamentals of wireless communication*. Cambridge, U.K.: Cambridge University Press, 2005.
- [23] D. J. Rabideau, "MIMO radar aperture optimization," Lincoln Laboratory, Massachusetts Institute of Technology, Lexington, MA, USA, Tech. Rep., January 2011.
- [24] J.-M. Colin, "Phased array radars in France: Present and future," in *Proc. IEEE Int. Symp. Phased Array Syst. and Technology*, Boston, MA, USA, October 1996, pp. 458–462.
- [25] H. He, P. Stoica, and J. Li, "Wideband MIMO systems: Signal design for transmit beampattern synthesis," *IEEE Transactions on Signal Processing*, vol. 59, pp. 618–628, November 2011.
- [26] H. Yan, G. Shen, R. Zetik, O. Hirsch, and R. S. Thoma, "Ultra-wideband MIMO ambiguity function and its factorability," *IEEE Transactions on Geoscience and Remote Sensing*, vol. 51, no. 1, pp. 504–519, January 2013.
- [27] D. R. Fuhrmann, J. P. Browning, and M. Rangaswamy, "Signaling strategies for the hybrid MIMO phased-array radar," *IEEE Journal of Selected Topics in Signal Processing*, vol. 4, no. 1, pp. 66–78, September 2010.
- [28] G. Krieger, "MIMO-SAR: Opportunities and pitfalls," *IEEE Transactions on Geoscience and Remote Sensing*, vol. 52, no. 5, pp. 2628–2645, May 2014.
- [29] Y. I. Abramovich, G. J. Frazer, and B. A. Johnson, "Principles of mode-selective MIMO OTHR," *IEEE Transactions on Aerospace and Electronic Systems*, vol. 49, no. 3, pp. 1839–1868, July 2013.
- [30] D. J. Rabideau. and P. Parker, "Ubiquitous MIMO multifunction digital array radar," in *Proceedings of Asilomar Conference on Signals, Systems, and Computers*, vol. 1, Pacific Grove, CA, USA, November 2003, pp. 1057–1064.
- [31] E. Fishler, A. Haimovich, R. Blum, R. Cimini, D. Chizhik, and R. Valenzuela, "Performance of MIMO radar systems: Advantages of angular diversity," in *Proceedings of Asilomar Conference on Signals, Systems, and Computers*, vol. 1, Pacific Grove, CA, USA, 7-10 Nov. 2004 2004, pp. 305–309.
- [32] J. Kantor. and S. K. Davis, "Airborne GMTI using MIMO techniques," in *Proceedings of IEEE Radar Conference*, Washington, DC, USA, May 2010, pp. 1344–1349.
- [33] S. Sen and A. Nehorai, "OFDM MIMO radar with mutual-information waveform design for low-grazing angle tracking," *IEEE Transactions on Signal Processing*, vol. 58, no. 6, pp. 3152–3162, June 2010.
- [34] J. Yan, B. Jiu, H. Liu, B. Chen, and Z. Bao, "Prior knowledge-based simultaneous multibeam power allocation algorithm for cognitive multiple targets tracking in clutter," *IEEE Transactions on Signal Processing*, vol. 63, pp. 512–527, November 2015.

- [35] A. Khabbazibasmenj, A. Hassanien, S. A. Vorobyov, and M. W. Morency, "Efficient transmit beamspace design for search-free based DOA estimation in MIMO radar," *IEEE Transactions on Signal Processing*, vol. 62, no. 6, pp. 1490–1500, March 2014.
- [36] Y. Yu, A. P. Petropulu, and H. V. Poor, "MIMO radar using compressive sampling," *IEEE Journal of Selected Topics in Signal Processing*, vol. 4, no. 1, pp. 146–163, February 2010.
- [37] M. Rossi, A. M. Haimovich, and Y. C. Eldar, "Spatial compressive sensing for MIMO radar," *IEEE Transactions on Signal Processing*, vol. 62, no. 2, pp. 419–430, January 2014.
- [38] G. J. Frazer, Y. I. Abramovich, and B. A. Johnson, "Spatially waveform diverse radar: Perspectives for high frequency OTHR," in *Proceedings of IEEE Radar Conference*, 4 2007, pp. 385–390.
- [39] B. Correll, "Efficient spotlight SAR MIMO linear collection configurations," *IEEE Journal of Selected Topics in Signal Processing*, vol. 4, no. 1, pp. 33–39, February 2010.
- [40] W.-Q. Wang, "MIMO SAR imaging: Potential and challenges," *IEEE Aerospace and Electronics Systems Magazine*, vol. 28, pp. 18–23, August 2013.
- [41] A. Hassanien, M. G. Amin, Y. D. Zhang, and F. Ahmad, "Dual-function radar-communications: Information embedding using sidelobe control and waveform diversity," *IEEE Transactions on Signal Processing*, vol. 64, no. 8, pp. 2168–2181, April 2016.
- [42] B. Li, A. P. Petropulu, and W. Trappe, "Optimum co-design for spectrum sharing between matrix completion based MIMO radars and a MIMO communication system," *IEEE Transactions on Signal Processing*, vol. 64, no. 17, pp. 4562–4575, September 2016.
- [43] B. Li and A. P. Petropulu, "Joint transmit designs for coexistence of mimo wireless communications and sparse sensing radars in clutter," *IEEE Transactions on Aerospace and Electronic Systems*, vol. 53, no. 6, pp. 2846–2864, 2017.
- [44] N. Levanon and E. Mozeson, *Radar Signals*. Hoboken, NJ, USA: Wiley, 2004.
- [45] D. DeLong and E. M. Hofstetter, "On the design of optimum radar waveforms for clutter rejection," *IEEE Transactions on Information Theory*, vol. 13, no. 3, pp. 454–463, July 1967.
- [46] C. E. Cook and M. Bernfeld, *Radar Signals—An introduction to theory and application*. Newyork, NJ, USA: Academic Press, 1967.

- [47] M. R. Bell, "Information theory and radar waveform design," *IEEE Transactions on Information Theory*, vol. 39, no. 5, pp. 1578–1597, September 1993.
- [48] E. H. Dinan and B. Jabbari, "Spreading codes for direct sequence CDMA and wideband CDMA cellular networks," *IEEE Communications Magazine*, vol. 36, no. 9, pp. 48–54, September 1998.
- [49] S. W. Golomb, *Shift register sequences*. San Francisco, CA, USA: Holden-Day, 1967.
- [50] R. H. S. Boztas and P. V. Kumar, "4-phase sequences with near-optimum correlation properties," *IEEE Transactions on Information Theory*, vol. 38, no. 3, pp. 1101–1113, May 1992.
- [51] K. W. Forsythe and D. W. Bliss, "Waveform correlation and optimization issues for MIMO radar," in *Proceedings of Asilomar Conference on Signals, Systems, and Computers*, Pacific Grove, CA, USA, October 2005, pp. 1306–1310.
- [52] B. Liu, Z. He, J. Zeng, and B. Liu, "Polyphase orthogonal code design for MIMO radar systems," in *Proceedings of CIE Radar Conference*, Shanghai, China, October 2006, pp. 1–4.
- [53] Y. Yang and R. S. Blum, "Waveform design for MIMO radar based on mutual information and minimum mean-square error estimation," in *Proceedings of 40th Annual Conference on Information Sciences and Systems*, Princeton, NJ, USA, March 2006, pp. 111–116.
- [54] P. Stoica, J. Li, X. Zhu, and B. Guo, "Waveform synthesis for diversity-based transmit beampattern design," in *Proceedings of IEEE Workshop on Statistical Signal Processing (SSP)*, Madison, WI, USA, August 2007, pp. 473–477.
- [55] B. Friedlander, "Waveform design for mimo radars," *IEEE Transactions on Aerospace and Electronic Systems*, vol. 43, no. 3, pp. 1227–1238, July 2007.
- [56] G. J. Frazer, B. A. Johnson, and Y. I. Abramovich, "Orthogonal waveform support in MIMO HF OTH radars," in *Proceedings of International Waveform Diversity and Design Conference (WDD)*, June 2007, pp. 423–427.
- [57] B. Liu, Z. He, and Q. He, "Optimization of orthogonal discrete frequency-coding waveform based on modified genetic algorithm for MIMO radar," in *Proceedings of International Conference on Communications, Circuits and Systems (ICCCAS)*, Kokura, Japan, 2007, pp. 966–970.
- [58] C. Y. Chen, "MIMO radar ambiguity optimization using frequency-hopping waveforms," in *Proceedings of Asilomar Conference on Signals, Systems, and Computers*, Pacific Grove, CA, USA, 2007, pp. 192–196.

- [59] D. R. Fuhrmann and G. San Antonio, "Transmit beamforming for MIMO radar systems using signal cross-correlation," *IEEE Transactions on Aerospace and Electronic Systems*, vol. 44, no. 1, pp. 171–186, 2008.
- [60] J. Li, P. Stoica, and X. Zheng, "Signal synthesis and receiver design for MIMO radar imaging," *IEEE Transactions on Signal Processing*, vol. 56, no. 8, pp. 3959–3968, August 2008.
- [61] P. Stoica, J. Li, and M. Xue, "Transmit codes and receive filters for radar," *IEEE Signal Processing Magazine*, vol. 25, no. 6, pp. 94–109, November 2008.
- [62] C.-Y. Chen and P. P. Vaidyanathan, "MIMO radar ambiguity properties and optimization using frequency-hopping waveforms," *IEEE Transactions on Signal Processing*, vol. 56, no. 12, pp. 5926–5936, December 2008.
- [63] J. Li, L. Xu, P. Stoica, K. W. Forsythe, and D. W. Bliss, "Range compression and waveform optimization for MIMO radar: A Cramér-Rao bound based study," *IEEE Transactions on Signal Processing*, vol. 56, no. 1, pp. 218–232, January 2008.
- [64] D. J. Rabideau, "Adaptive MIMO radar waveforms," in *Proceedings of IEEE Radar Conference*, Rome, Italy, May 2008, pp. 1–6.
- [65] P. Stoica, J. Li, and X. Zhu, "Waveform synthesis for diversity-based transmit beampattern design," *IEEE Transactions on Signal Processing*, vol. 56, no. 6, pp. 2593–2598, 2008.
- [66] H. Hao, P. Stoica, and J. Li, "Designing unimodular sequences sets with good correlations—Including an application to MIMO radar," *IEEE Transactions on Signal Processing*, vol. 57, no. 11, pp. 4391–4405, November 2009.
- [67] P. Stoica, H. He, and J. Li, "New algorithms for designing unimodular sequences with good correlation properties," *IEEE Transactions on Signal Processing*, vol. 57, no. 4, pp. 1415–1425, April 2009.
- [68] C.-Y. Chen and P. P. Vaidyanathan, "MIMO radar waveform optimization with prior information of the extended target and clutter," *IEEE Transactions on Signal Processing*, vol. 57, no. 9, pp. 3533–3544, September 2009.
- [69] A. De Maio, S. D. Nicola, Y. Huang, Z.-Q. Luo, and S. Zhang, "Design of phase codes for radar performance optimization with a similarity constraint," *IEEE Transactions on Signal Processing*, vol. 57, no. 2, pp. 610–621, February 2009.
- [70] Y. Yang, R. S. Blum, Z. He, and D. R. Fuhrmann, "MIMO radar waveform design via alternating projection," *IEEE Transactions on Signal Processing*, vol. 58, no. 3, pp. 1440–1445, March 2010.

- [71] X. Song, S. Zhou, and P. Willett, "Reducing the waveform cross correlation of MIMO radar with space-time coding," *IEEE Transactions on Signal Processing*, vol. 58, no. 8, pp. 4213–4224, August 2010.
- [72] J. Zhang, H. Wang, and X. Zhu, "Adaptive waveform design for separated transmit/receive ULA-MIMO radar," *IEEE Transactions on Signal Processing*, vol. 58, no. 9, pp. 4936–4942, September 2010.
- [73] B. Tang, J. Tang, and Y. Peng, "MIMO radar waveform design in colored noise based on information theory," *IEEE Transactions on Signal Processing*, vol. 58, no. 9, pp. 4684–4697, September 2010.
- [74] M. C. Wicks, E. L. Mokole, S. D. Blunt, R. S. Schneible, and V. J. Amuso, *Principles of Waveform Diversity and Design*. Raleigh, NC, USA: SciTech Publishing, 2010.
- [75] G. H. Jajamovich, M. Lops, and X. Wang, "Space-time coding for MIMO radar detection and ranging," *IEEE Transactions on Signal Processing*, vol. 58, pp. 6195–6206, September 2010.
- [76] H. He, P. Stoica, and J. Li, "Wideband MIMO waveform design for transmit beampattern synthesis," in *Proceedings of International Waveform Diversity and Design Conference (WDD)*, Niagara Falls, ON, Canada, August 2010, pp. 000 006–000 010.
- [77] E. Grossi, M. Lops, and L. Venturino, "Robust waveform design for MIMO radars," *IEEE Transactions on Signal Processing*, vol. 59, no. 7, pp. 3262–3271, July 2011.
- [78] S. Ahmed, J. S. Thompson, Y. R. Petillot, and B. Mulgrew, "Finite alphabet constant-envelope waveform design for MIMO radar," *IEEE Transactions on Signal Processing*, vol. 59, no. 11, pp. 5326–5337, November 2011.
- [79] T. Naghibi and F. Behnia, "MIMO radar waveform design in the presence of clutter," *IEEE Transactions on Aerospace and Electronic Systems*, vol. 47, no. 2, pp. 770–781, 2011.
- [80] A. De Maio, Y. Huang, M. Piezzo, S. Zhang, and A. Farina, "Design of optimized radar codes with a peak to average power ratio constraint," *IEEE Transactions on Signal Processing*, vol. 59, no. 6, pp. 2683–2697, June 2011.
- [81] P. Stoica, H. He, and J. Li, "Optimization of the receive filter and transmit sequence for active sensing," *IEEE Transactions on Signal Processing*, vol. 60, no. 4, pp. 1730–1740, April 2012.
- [82] D. J. Rabideau, "Mimo radar waveforms and cancellation ratio," *IEEE Transactions on Aerospace and Electronic Systems*, vol. 48, no. 2, pp. 1167–1178, 2012.
- [83] B. Tang, J. Tang, and Y. Peng, "Waveform optimization for MIMO radar in colored noise: Further results for estimation-oriented criteria," *IEEE Transactions on Signal Processing*, vol. 60, no. 3, pp. 1517–1522, March 2012.

- [84] H. He, J. Li, and P. Stoica, *Waveform design for active sensing systems: A computational Approach*. Cambridge, U.K.: Cambridge University Press, 2012.
- [85] A. D. Fulvio Gini and L. Patton, *Waveform Design and Diversity for Advanced Radar Systems*. Herts, U.K.: The Institution of Engineering and Technology, 2012.
- [86] A. Aubry, A. De Maio, A. Farina, and M. Wicks, "Knowledge-aided (potentially cognitive) transmit signal and receive filter design in signal-dependent clutter," *IEEE Transactions on Aerospace and Electronic Systems*, vol. 49, no. 1, pp. 93–117, January 2013.
- [87] M. M. Naghsh, M. Hashemi, S. Shahbazpanahi, M. Soltanalian, and P. Stoica, "Majorization-minimization technique for multi-static radar code design," in *Proceedings of European Signal Processing Conference*, Palais Des Congres, Marrakech, September 2013, pp. 1–5.
- [88] W. Huleihel, J. Tabrikian, and R. Shavit, "Optimal adaptive waveform design for cognitive MIMO radar," *IEEE Transactions on Signal Processing*, vol. 61, no. 20, pp. 5075–5089, October 2013.
- [89] A. Duly, D. J. Love, and J. V. Krogmeier, "Time-division beamforming for MIMO radar waveform design," *IEEE Transactions on Aerospace and Electronic Systems*, vol. 49, no. 2, pp. 1210–1223, April 2013.
- [90] G. Babur, O. A. Krasnov, A. Yarovoy, and P. Aubry, "Nearly orthogonal waveforms for MIMO FMCW radar," *IEEE Transactions on Aerospace and Electronic Systems*, vol. 49, pp. 1426–1437, July 2013.
- [91] W. Rowe, P. Stoica, and J. Li, "Spectrally constrained waveform design," *IEEE Signal Processing Magazine*, vol. 31, no. 3, pp. 157–162, May 2014.
- [92] S. Jardak, S. Ahmed, and M.-S. Alouini, "Generation of correlated finite alphabet waveforms using Gaussian random variables," *IEEE Transactions on Signal Processing*, vol. 62, no. 17, pp. 4587–4596, September 2014.
- [93] G. Cui, H. Li, and M. Rangaswamy, "MIMO radar waveform design with constant modulus and similarity constraints," *IEEE Transactions on Signal Processing*, vol. 62, no. 2, pp. 343–353, January 2014.
- [94] S. M. Karbasi, A. Aubry, A. D. Maio, and M. H. Bastani, "Robust transmit code and receive filter design for extended targets in clutter," *IEEE Transactions on Signal Processing*, vol. 63, no. 8, pp. 1965–1976, April 2015.
- [95] J. Song, P. Babu, and D. P. Palomar, "Optimization methods for designing sequences with low autocorrelation sidelobes," *IEEE Transactions on Signal Processing*, vol. 63, no. 15, pp. 3998–4009, August 2015.
- [96] A. Aubry, A. De Maio, and M. M. Naghsh, "Optimizing radar waveform and Doppler filter bank via generalized fractional programming," *IEEE Journal of Selected Topics in Signal Processing*, vol. 9, no. 8, pp. 1387–1399, December 2015.

- [97] T. Bo, M. M. Naghsh, and T. Jun, "Relative entropy-based waveform design for mimo radar detection in the presence of clutter and interference," *IEEE Transactions on Signal Processing*, vol. 63, no. 14, pp. 3783–3796, 2015.
- [98] W.-Q. Wang, "Large time-bandwidth product MIMO radar waveform design based on chirp rate diversity," *IEEE Sensors Journal*, vol. 15, no. 2, pp. 1027–1034, February 2015.
- [99] B. Jiu, H. Liu, X. Wang, L. Zhang, Y. Wang, and B. Chen, "Knowledge-based spatial-temporal hierarchical mimo radar waveform design method for target detection in heterogeneous clutter zone," *IEEE Transactions on Signal Processing*, vol. 63, no. 3, pp. 543–554, February 2015.
- [100] W. Zhu and J. Tang, "Robust design of transmit waveform and receive filter for colocated mimo radar," *IEEE Signal Processing Letters*, vol. 22, no. 11, pp. 2112–2116, July 2015.
- [101] L. Guo, D. Hai, B. Himed, M. Tan, and G. Zhe, "Waveform optimization for transmit beamforming with MIMO radar antenna arrays," *IEEE Transactions on Antennas and Propagation*, vol. 63, no. 2, pp. 543–552, February 2015.
- [102] O. Aldayel, V. Monga, and M. Rangaswamy, "SQR: Successive QCQP refinement for MIMO radar waveform design under practical constraints," in *Proceedings of Asilomar Conference on Signals, Systems, and Computers*, Pacific Grove, CA, USA, November 2015, pp. 85–89.
- [103] S. Sun and A. P. Petropulu, "Waveform design for MIMO radars with matrix completion," *IEEE Journal of Selected Topics in Signal Processing*, vol. 9, pp. 1400–1414, August 2015.
- [104] S. Imani and S. A. Ghorashi, "Transmit signal and receive filter design in co-located MIMO radar using a transmit weighting matrix," *IEEE Signal Processing Letters*, vol. 22, pp. 1521–1524, March 2015.
- [105] J. Song, P. Babu, and D. P. Palomar, "Sequence set design with good correlations properties via Majorization-Mimimization," *IEEE Transactions on Signal Processing*, vol. 64, no. 11, pp. 2866–2879, June 2016.
- [106] J. Song, P. Babu, and D. P. Palomar, "Sequence design to minimize the weighted integrated and peak sidelobe levels," *IEEE Transactions on Signal Processing*, vol. 64, no. 8, pp. 2051–2064, April 2016.
- [107] L. Zhao, J. Song, P. Babu, and D. P. Palomar, "A unified framework for low autocorrelation sequence design via Majorization-Mimimization," *IEEE Transactions on Signal Processing*, vol. 65, no. 2, pp. 438–453, January 2017.
- [108] P. Setlur and M. Rangaswamy, "Waveform design for radar STAP in signal dependent interference," *IEEE Transactions on Signal Processing*, vol. 53, no. 1, pp. 19–34, January 2016.

- [109] S. D. Blunt and E. L. Mokole, "Overview of radar waveform diversity," *IEEE Aerospace and Electronics Systems Magazine*, vol. 31, no. 11, pp. 2–42, November 2016.
- [110] A. Aubry, A. De Maio, Y. Huang, and M. Piezzo, "Robust design of radar Doppler filters," *IEEE Transactions on Signal Processing*, vol. 64, no. 22, pp. 5848–5860, November 2016.
- [111] Y. Li, S. A. Vorobyov, and Z. He, "Design of multiple unimodular waveforms with low auto- and cross-correlations for radar via majorization-minimization," in *Proceedings of European Signal Processing Conference*, Budapest, Hungary, Aug.–Sep. 2016, pp. 2235–2239, [Publication IX].
- [112] G. Zhao, Y. Fu, L. Nie, and Z. Zhuang, "Optimal sub-chirp combination waveform design based on mimo sar general ambiguity function," in *2016 IEEE International Geoscience and Remote Sensing Symposium (IGARSS)*, July 2016, pp. 1118–1121.
- [113] A. Guruswamy and R. Blum, "Ambiguity optimization for frequency-hopping waveforms in mimo radars with arbitrary antenna separations," *IEEE Signal Processing Letters*, vol. 23, no. 9, pp. 1231–1235, 2016.
- [114] F. Arlery, R. Kassab, U. Tan, and F. Lehmann, "Efficient optimization of the ambiguity functions of multi-static radar waveforms," in *2016 17th International Radar Symposium (IRS)*, May 2016, pp. 1–6.
- [115] U. Majumder, M. R. Bell, and M. Rangaswamy, "Design and analysis of radar waveforms achieving transmit and receive orthogonality," *IEEE Transactions on Aerospace and Electronic Systems*, vol. 52, no. 3, pp. 1056–1066, 2016.
- [116] B. Tang and J. Tang, "Joint design of transmit waveforms and receive filters for mimo radar space time adaptive processing," *IEEE Transactions on Signal Processing*, vol. PP, no. 99, pp. 1–1, 2016.
- [117] T. Aittomaki and V. Koivunen, "Radar waveform sidelobe level optimality and sampling," *IEEE Signal Processing Letters*, vol. 23, pp. 371–375, January 2016.
- [118] S. Zhou, H. Liu, and H. Z. H. Su, "Doppler sensitivity of MIMO radar waveforms," *IEEE Transactions on Aerospace and Electronic Systems*, vol. 52, no. 5, pp. 2091–2110, October 2016.
- [119] S. D. Blunt, J. Metcalf, J. Jakabosky, J. Stiles, and B. Himed, "Multi-waveform space-time adaptive processing," *IEEE Transactions on Aerospace and Electronic Systems*, vol. 53, no. 1, pp. 385–404, February 2017.
- [120] M. M. Naghsh, M. Modarres-Hashemi, M. A. Kerahroodi, and E. H. M. Alian, "An information theoretic approach to robust constrained code design for mimo radars," *IEEE Transactions on Signal Processing*, vol. 65, no. 14, pp. 3647–3661, 2017.

- [121] G. Cui, X. Yu, M. Piezzo, and L. Kong, "Constant modulus sequence set design with good correlation properties," *Signal Process.*, vol. 139, pp. 75–85, October 2017.
- [122] G. Cui, X. Yu, V. Carotenuto, and L. Kong, "Space-time transmit code and receive filter design for colocated MIMO radar," *IEEE Transactions on Signal Processing*, vol. 65, no. 5, pp. 1116–1129, March 2017.
- [123] Y. Li and S. A. Vorobyov, "Efficient single/multiple unimodular waveform design with low weighted correlations," in *Proceedings of IEEE International Conference on Acoustics, Speech, and Signal Processing (ICASSP)*, New Orleans, USA, March 2017, [Publication VIII].
- [124] T. Bouchoucha, S. Ahmed, T. Al-Naffouri, and M. S. Alouini, "DFT-based closed-form covariance matrix and direct waveforms design for MIMO radar to achieve desired beampatterns," *IEEE Transactions on Signal Processing*, vol. 65, no. 8, pp. 2104–2113, April 2017.
- [125] Z. Cheng, Z. He, S. Zhang, and J. Li, "Constant modulus waveform design for mimo radar transmit beampattern," *IEEE Transactions on Signal Processing*, vol. 65, no. 18, pp. 4912–4923, September 2017.
- [126] Y. Li and S. A. Vorobyov, "Fast algorithms for designing unimodular waveform(s) with good correlation properties," *IEEE Transactions on Signal Processing*, vol. 66, no. 5, pp. 1197–1212, March 2018, [Publication VII].
- [127] L. Zhao and D. P. Palomar, "Maximin joint optimization of transmitting code and receiving filter in radar and communications," *IEEE Transactions on Signal Processing*, vol. 65, no. 4, pp. 850–863, February 2017.
- [128] L. Wu, P. Babu, and D. P. Palomar, "Transmit waveform/receive filter design for mimo radar with multiple waveform constraints," *IEEE Transactions on Signal Processing*, vol. 66, no. 6, pp. 1526–1540, March 2018.
- [129] Y. Li and S. A. Vorobyov, "Joint space-(slow) time transmission with unimodular waveforms and receive adaptive filter design for radar," in *Proceedings of IEEE International Conference on Acoustics, Speech, and Signal Processing (ICASSP)*, Calgary, AB, Canada, April 2018, pp. 3276–3280, [Publication X].
- [130] S. Herbert, J. R. Hopgood, and B. Mulgrew, "MMSE adaptive waveform design for active sensing with applications to MIMO radar," *IEEE Transactions on Signal Processing*, vol. 66, no. 5, pp. 1361–1373, March 2018.
- [131] D. R. Hunter and K. Lange, "A tutorial on MM algorithms," *Amer. Statist.*, vol. 58, no. 1, pp. 30–37, February 2004.
- [132] Y. I. Abramovich and G. J. Frazer, "Bounds on the volume and height distributions for the MIMO radar ambiguity function," *IEEE Signal Processing Letters*, vol. 15, pp. 505–508, 2008.

- [133] Y. Li, S. A. Vorobyov, and V. Koivunen, "Generalized ambiguity function for the MIMO radar with correlated waveforms," in *Proceedings of IEEE International Conference on Acoustics, Speech, and Signal Processing (ICASSP)*, Florence, Italy, May 2014, pp. 5302–5306, [Publication II].
- [134] B. Shtarkalev and B. Mulgrew, "Effects of FDMA/TDMA orthogonality on the gaussian pulse train MIMO ambiguity function," *IEEE Signal Processing Letters*, vol. 22, no. 2, pp. 153–157, February 2015.
- [135] P. M. Woodward, *Probability and information theory with application to radar*. Oxford, UK: Pergamon Press, 1953.
- [136] P. M. Woodward, "Radar ambiguity analysis," Royal Radar Establishment, Ministry of Technology, Malvern, Worecs., Technical Report 731, February 1967.
- [137] W. M. Siebert, "Studies of Woodward's uncertainty function," Electronics Research Laboratory, Massachusetts Institute of Technology, Cambridge Massachusetts, MA, USA, Quarterly Progress Report, April 1958.
- [138] A. I. Sinsky and C. P. Wang, "Standardization of the definition of the radar ambiguity function," *IEEE Transactions on Aerospace and Electronic Systems*, vol. AES-10, no. 4, pp. 532–533, July 1974.
- [139] J. Li, X. Zheng, and P. Stoica, "MIMO SAR imaging: Signal synthesis and receiver design," in *Proc. IEEE Int. Workshop. on Computational Advances in Multi-Sensor Adaptive Processing*, St. Thomas, VI, USA, December 2007, pp. 89–92.
- [140] W.-Q. Wang and J. Cai, "MIMO SAR using chirp diverse waveform for wide-swath remote sensing," *IEEE Transactions on Aerospace and Electronic Systems*, vol. 48, no. 4, pp. 3171–3185, October 2012.
- [141] C.-Y. Chen and P. Vaidyanathan, "Beamforming issues in modern MIMO radars with doppler," in *Proceedings of Asilomar Conference on Signals, Systems, and Computers*, Pacific Grove, CA, USA, October/November 2006, pp. 41–45.
- [142] V. F. Mecca and J. L. Krolik, "Slow-time MIMO STAP with improved power efficiency," in *Proceedings of Asilomar Conference on Signals, Systems, and Computers*, Pacific Grove, CA, USA, November 2007, pp. 202–206.
- [143] V. F. Mecca, J. L. Krolik, and F. C. Robey, "Beamspace slow-time MIMO radar for multipath clutter mitigation," in *Proceedings of IEEE International Conference on Acoustics, Speech, and Signal Processing (ICASSP)*, Las Vegas, NV, USA, March/April 2008, pp. 2313–2316.
- [144] V. F. Mecca and J. L. Krolik, "MIMO enabled multipath clutter rank estimation," in *Proceedings of IEEE Radar Conference*, Pasadena, CA, USA, May 2009, pp. 1–6.

- [145] G. Wang and Y. Lu, "Clutter rank of MIMO radar with a special class of waveforms," in *Proceedings of International Waveform Diversity and Design Conference (WDD)*, Kissimmee, FL, USA, February 2009, pp. 108–112.
- [146] K. W. Forsythe and D. W. Bliss, "MIMO radar waveform constraints for GMTI," *IEEE Journal of Selected Topics in Signal Processing*, vol. 4, no. 1, pp. 21–32, February 2010.
- [147] J. M. Kantor and D. W. Bliss, "Clutter covariance matrices for GMTI MIMO radar," in *Proceedings of Asilomar Conference on Signals, Systems, and Computers*, Pacific Grove, CA, USA, November 2010, pp. 1821–1826.
- [148] G. Wang and Y. Lu, "Clutter rank of STAP in MIMO radar with waveform diversity," *IEEE Transactions on Signal Processing*, vol. 58, no. 2, pp. 938–943, February 2010.
- [149] Y. I. Abramovich, G. J. Frazer, and B. A. Johnson, "Noncausal adaptive spatial clutter mitigation in monostatic MIMO radar: Fundamental limitations," *IEEE Journal of Selected Topics in Signal Processing*, vol. 4, no. 1, pp. 40–54, February 2010.
- [150] W. Roberts, P. Stoica, J. Li, T. Yardibi, and F. A. Sadjadi, "Iterative adaptive approaches to MIMO radar imaging," *IEEE Journal of Selected Topics in Signal Processing*, vol. 4, pp. 5–20, January 2010.
- [151] G. Hickman and J. L. Krolik, "MIMO GMTI radar with multipath clutter suppression," in *Proceedings of IEEE Workshop on Sensor Array and Multichannel Signal Processing (SAM)*, Jerusalem, Israel, October 2010, pp. 65–68.
- [152] R. Fa and R. C. De Lamare, "Knowledge-aided reduced-rank STAP for MIMO radar based on joint iterative constrained optimization of adaptive filters with multiple constraints," in *Proceedings of IEEE International Conference on Acoustics, Speech, and Signal Processing (ICASSP)*, Dallas, TX, USA, March 2010, pp. 2762–2765.
- [153] R. Boyer, "Performance bounds and angular resolution limit for the moving colocated MIMO radar," *IEEE Transactions on Signal Processing*, vol. 59, pp. 1539–1552, December 2011.
- [154] J. Wu, T. Wang, L. Zhang, and Z. Bao, "Range-dependent clutter suppression for airborne sidelooking radar using MIMO technique," *IEEE Transactions on Aerospace and Electronic Systems*, vol. 48, pp. 3647–3654, October 2012.
- [155] H. Li, Y. Li, and Z. He, "MIMO radar clutter mitigation based on joint beamforming and joint domain localized processing," *EURASIP journal on wireless communications and networking (Radar and sonar networks topic)*, vol. 1, pp. 1–10, April 2013.
- [156] Y. Li, S. A. Vorobyov, and A. Hassanien, "MIMO radar capability on powerful jammers suppression," in *Proceedings of IEEE International Conference on*

- Acoustics, Speech, and Signal Processing (ICASSP)*, Florence, Italy, May 2014, pp. 5277–5281, [Publication V].
- [157] Y. Li, S. A. Vorobyov, and A. Hassanien, “Robust beamforming for jammers suppression in MIMO radar,” in *Proceedings of IEEE Radar Conference*, Cincinnati, OH, USA, May 2014, pp. 0629–0634, [Publication VI].
- [158] T. K. Sjögren, V. T. Vu, M. I. Pettersson, F. Wang, D. J. G. Murdin, A. Gustavsson, and L. M. Ulander, “Suppression of clutter in multichannel SAR GMTI,” *IEEE Transactions on Geoscience and Remote Sensing*, vol. 52, pp. 4005–4013, September 2014.
- [159] T. K. Sjögren, V. T. Vu, M. I. Pettersson, F. Wang, D. J. G. Murdin, A. Gustavsson, and L. M. H. Ulander, “Suppression of clutter in multichannel SAR GMTI,” *IEEE Transactions on Geoscience and Remote Sensing*, vol. 52, no. 7, pp. 4005–4013, July 2014.
- [160] Y. Li, S. A. Vorobyov, and Z. He, “Joint hot and cold clutter mitigation in the transmit beamspace-based MIMO radar,” in *Proceedings of IEEE International Conference on Acoustics, Speech, and Signal Processing (ICASSP)*, Brisbane, Australia, April 2015, pp. 2334–2338, [Publication IV].
- [161] G. Marino, D. Tarchi, V. Kyovtorov, J. Figueiredo-Morgado, and P. F. Sammartino, “Concept and performance analysis of melissa MIMO GMTI,” in *Proceedings of IEEE International Geoscience and Remote Sensing Symposium (IGRSS)*, Milan, Italy, July 2015, pp. 3251–3254.
- [162] X. Jingwei, Z. Shengqi, and L. Guisheng, “Space-time-range adaptive processing for airborne radar systems,” *IEEE Sensors Journal*, vol. 15, no. 3, pp. 1602–1610, October 2015.
- [163] K. Bell, J. Johnson, C. Baker, G. Smith, and M. Rangaswamy, “Bistatic coherent MIMO clutter rank analysis,” in *Proceedings of European Signal Processing Conference*, Nice, France, August/September 2015, pp. 519–523.
- [164] W. Feng, Y. Zhang, and X. He, “Clutter rank estimation for reduce-dimension space-time adaptive processing mimo radar,” *IEEE Sensors Journal*, vol. 17, no. 2, pp. 238–239, January 2017.
- [165] Y. Huang, G. Liao, J. Xu, J. Li, and D. Yang, “GMTI and parameter estimation for MIMO SAR system via fast interferometry RPCA method,” *IEEE Transactions on Geoscience and Remote Sensing*, vol. 56, no. 3, pp. 1774–1787, March 2018.
- [166] D. Slepian and H. O. Pollak, “Prolate spheroidal wave functions, fourier analysis and uncertainty—I,” *The Bell System Technical Journal*, pp. 43–63, January 1961.
- [167] D. Slepian and H. O. Pollak, “Prolate spheroidal wave functions, fourier analysis and uncertainty—II,” *The Bell System Technical Journal*, pp. 65–84, January 1961.

- [168] D. Slepian and H. O. Pollak, "Prolate spheroidal wave functions, fourier analysis and uncertainty—III: The dimension of the space of essentially time- and band-limited signals," *The Bell System Technical Journal*, pp. 1295–1336, July 1962.
- [169] H. Wang and L. Cai, "On adaptive spatial-temporal processing for airborne surveillance radar systems," *IEEE Transactions on Aerospace and Electronic Systems*, vol. 30, no. 3, pp. 660–670, July 1994.
- [170] J. Ward, "Space-time adaptive processing for airborne radar," Lincoln Laboratory, Massachusetts Institute of Technology, Lexington Massachusetts, MA, USA, Technical Report 1015, December 1994.
- [171] R. Klemm, *Principles of space-time adaptive processing*, 3rd ed. London, UK: The Institution of Engineering Technology, 2006.
- [172] J. R. Guerci, *Space-time adaptive processing for radar*. Norwood, MA, USA: Artech House, 2003.
- [173] W. L. Melvin, "A STAP overview," *IEEE Aerospace and Electronics Systems Magazine*, vol. 19, no. 1, pp. 19–35, January 2004.
- [174] W. Melvin, M. Wicks, P. Antonik, Y. Salama, P. Li, and H. Schuman, "Knowledge-based space-time adaptive processing for airborne early warning radar," *IEEE Aerospace and Electronics Systems Magazine*, vol. 13, no. 4, pp. 37–42, April 1998.
- [175] L. E. Brennan and L. Reed, "Theory of adaptive radar," *IEEE Transactions on Aerospace and Electronic Systems*, no. 2, pp. 237–252, March 1973.
- [176] G. San Antonio and D. R. Fuhrmann, "Beampattern synthesis for wideband MIMO radar systems," in *Proceedings of International Workshop on Computational Advances in Multi-Sensor Adaptive Processing (CAMSAP)*, Puerto Vallarta, Mexico, 2005, pp. 105–108.
- [177] T. Aittomaki and V. Koivunen, "Signal covariance matrix optimization for transmit beamforming in MIMO radars," in *Proceedings of Asilomar Conference on Signals, Systems, and Computers*, Pacific Grove, CA, November 2007, pp. 182–186.
- [178] T. Aittomaki and V. Koivunen, "Low-complexity method for transmit beamforming in MIMO radars," in *Proceedings of IEEE International Conference on Acoustics, Speech, and Signal Processing (ICASSP)*, vol. II, Honolulu, HI, UAS, April 2007, pp. 305–308.
- [179] G. Frazer, Y. Abramovich, and B. A. Johnson, "Use of adaptive non-causal transmit beamforming in OTHR: Experimental results," in *Proceedings of IEEE Radar Conference*, Adelaide, SA, Australia, 2008, pp. 311–316.
- [180] A. Hassanien and S. A. Vorobyov, "Transmit/receive beamforming for MIMO radar with colocated antennas," in *Proceedings of IEEE International Conference on Acoustics, Speech, and Signal Processing (ICASSP)*, Taipei, Taiwan, 2009, pp. 2089–2092.

- [181] A. Hassanien and S. A. Vorobyov, "Why the phased-MIMO radar outperforms the phased-array and MIMO radars," in *Proceedings of European Signal Processing Conference*, Aalborg, Denmark, August 2010, pp. 1234–1238.
- [182] H. Li and B. Himed, "Transmit subaperturing for MIMO radars with colocated antennas," *IEEE Journal of Selected Topics in Signal Processing*, vol. 4, no. 1, pp. 55–65, February 2010.
- [183] A. Khabbazibasmenj, S. A. Vorobyov, and A. Hassanien, "Transmit beamspace design for direction finding in colocated MIMO radar with arbitrary receive array," in *Proceedings of IEEE International Conference on Acoustics, Speech, and Signal Processing (ICASSP)*, Prague, Czech Republic, May 2011, pp. 2784–2787.
- [184] A. Hassanien and S. A. Vorobyov, "Transmit energy focusing for DOA estimation in MIMO radar with colocated antennas," *IEEE Transactions on Signal Processing*, vol. 59, no. 6, pp. 2669–2682, June 2011.
- [185] S. Ahmed, J. S. Thompson, Y. R. Petillot, and B. Mulgrew, "Unconstrained synthesis of covariance matrix for MIMO radar transmit beampattern," *IEEE Transactions on Signal Processing*, vol. 59, no. 8, pp. 3837–3849, August 2011.
- [186] B. Friedlander, "On transmit beamforming for MIMO radar," *IEEE Transactions on Aerospace and Electronic Systems*, vol. 48, no. 4, pp. 3376–3388, October 2012.
- [187] D. Wilcox and M. Sellathurai, "On MIMO radar subarrayed transmit beamforming," *IEEE Transactions on Signal Processing*, vol. 60, no. 4, pp. 2076–2081, April 2012.
- [188] A. Khabbazibasmenj, S. A. Vorobyov, A. Hassanien, and M. W. Morency, "Transmit beamspace design for direction finding in colocated MIMO radar with arbitrary receive array and even number of waveforms," in *Proceedings of Asilomar Conference on Signals, Systems, and Computers*, Pacific Grove, CA, November 2012, pp. 1307–1311.
- [189] G. Hua and S. S. Abeysekera, "Colocated MIMO radar transmit beamforming using orthogonal waveforms," in *Proceedings of IEEE International Conference on Acoustics, Speech, and Signal Processing (ICASSP)*, Kyoto, Japan, 2012, pp. 2453–2456.
- [190] G. Hua and S. S. Abeysekera, "MIMO radar transmit beampattern design with ripple and transition band control," *IEEE Transactions on Signal Processing*, vol. 61, no. 11, pp. 2963–2974, June 2013.
- [191] A. Hassanien, M. W. Morency, A. Khabbazibasmenj, S. A. Vorobyov, J.-Y. Park, and S.-J. Kim, "Two-dimensional transmit beamforming for MIMO radar with sparse symmetric arrays," in *Proceedings of IEEE Radar Conference*, Ottawa, ON, Canada, April–May 2013, pp. 1–6.

- [192] A. Hassanien, S. A. Vorobyov, and J.-Y. Park, "Joint transmit array interpolation and transmit beamforming for source localization in MIMO radar with arbitrary arrays," in *Proceedings of IEEE International Conference on Acoustics, Speech, and Signal Processing (ICASSP)*, Vancouver, BC, Canada, May 2013, pp. 4139–4143.
- [193] W.-Q. Wang, "Phased-MIMO radar with frequency diversity for range-dependent beamforming," *IEEE Sensors Journal*, vol. 13, pp. 1320–1328, December 2013.
- [194] J. Lipor, S. Ahmed, and M.-S. Alouini, "Fourier-based transmit beampattern design using MIMO radar," *IEEE Transactions on Signal Processing*, vol. 62, no. 9, pp. 2226–2235, May 2014.
- [195] S. Ahmed and M.-S. Alouini, "MIMO-radar waveform covariance matrix for high SINR and low side-lobe levels," *IEEE Transactions on Signal Processing*, vol. 62, no. 8, pp. 2056–2065, April 2014.
- [196] S. Ahmed and M.-S. Alouini, "MIMO radar transmit beampattern design without synthesising the covariance matrix," *IEEE Transactions on Signal Processing*, vol. 62, no. 9, pp. 2278–2289, May 2014.
- [197] J. Liu, H. Li, and B. Himed, "Joint optimization of transmit and receive beamforming in active arrays," *IEEE Signal Processing Letters*, vol. 21, pp. 39–42, November 2014.
- [198] M. Soltanalian, H. Hu, and P. Stoica, "Single-stage transmit beamforming design for MIMO radar," *Signal Process.*, vol. 102, pp. 132–138, September 2014.
- [199] H. Xu, R. S. Blum, J. Wang, and J. Yuan, "Colocated MIMO radar waveform design for transmit beampattern formation," *IEEE Transactions on Aerospace and Electronic Systems*, vol. 51, no. 2, pp. 1558–1568, 2015.
- [200] H. Xu, J. Wang, J. Yuan, and X. Shan, "Colocated MIMO radar transmit beamspace design for randomly present target detection," *IEEE Signal Processing Letters*, vol. 22, pp. 828–832, November 2015.
- [201] A. Hassanien, S. A. Vorobyov, and A. Khabbazibasmenj, "Transmit radiation pattern invariance in MIMO radar with application to DOA estimation," *IEEE Signal Processing Letters*, vol. 22, pp. 1609–1613, March 2015.
- [202] G. Hua and S. S. Abeysekera, "Robust transmit beampattern design for uniform linear arrays using correlated LFM waveforms," in *Proceedings of IEEE International Conference on Acoustics, Speech, and Signal Processing (ICASSP)*, Brisbane, QLD, Australia, 2015, pp. 2504–2508.
- [203] S. Sun and A. P. Petropulu, "On transmit beamforming in MIMO radar with matrix completion," in *Proceedings of IEEE International Conference on Acoustics, Speech, and Signal Processing (ICASSP)*, Brisbane, QLD, Australia, 2015, pp. 2774–2778.

References

- [204] X. Zhang, Z. He, L. Rayman-Bacchus, and J. Yan, "MIMO radar transmit beampattern matching design," *IEEE Transactions on Signal Processing*, vol. 63, pp. 2049–2056, January 2015.
- [205] W. Khan, I. M. Qureshi, A. Basit, and M. Zubair, "Hybrid phased MIMO radar with unequal subarrays," *IEEE Antennas and Wireless Propagation Letters*, vol. 14, pp. 1702–1705, April 2015.
- [206] A. Aubry, A. De Maio, and Y. Huang, "PSL-based beampattern design for MIMO radar systems," in *Proceedings of IEEE Radar Conference*, Arlington, VA, USA, 2015, pp. 0231–0236.
- [207] A. Aubry, A. De Maio, and Y. Huang, "MIMO radar beampattern design via PSL/ISL optimization," *IEEE Transactions on Signal Processing*, vol. 64, pp. 3955–3967, March 2016.
- [208] O. Aldayel, V. Monga, and M. Rangaswamy, "Tractable MIMO beampattern design under constant modulus waveform constraint," in *Proceedings of IEEE Radar Conference*, Philadelphia, PA, USA, May 2016, pp. 1–6.
- [209] P. M. McCormick, S. D. Blunt, and J. G. Metcalf, "Joint spectrum/beam-pattern design of wideband FM MIMO radar emissions," in *Proceedings of IEEE Radar Conference*, Philadelphia, PA, USA, 5 2016, pp. 1–6.
- [210] Y. Wang, G. Huang, and W. Li, "Transmit beampattern design in range and angle domains for mimo frequency diverse array radar," *IEEE Antennas and Wireless Propagation Letters*, vol. 16, no. 99, pp. 1003–1006, 2017.
- [211] Z.-Q. Luo, W.-K. Ma, A. M.-C. So, Y. Ye, and S. Zhang, "Semidefinite relaxation of quadratic optimization problems," *IEEE Signal Processing Magazine*, vol. 27, no. 3, pp. 20–34, 2010.
- [212] S. Boyd and L. Vandenberghe, *Convex optimization*. New York, NY, USA: Cambridge University Press, 2004.
- [213] H. L. Van Trees, *Optimum array processing*. New York, NY, USA: Wiley, 2002.
- [214] G. Xu, S. D. Silverstein, R. H. Roy, and T. Kailath, "Beamspace ESPRIT," *IEEE Transactions on Signal Processing*, vol. 42, no. 2, pp. 349–356, February 1994.
- [215] N. A. Goodman and D. Bruyere, "Optimum and decentralized detection for multistatic airborne radar," *IEEE Transactions on Aerospace and Electronic Systems*, vol. 43, August 2007.
- [216] J. Li, P. Stoica, L. Xu, and W. Roberts, "On parameter identifiability of MIMO radar," *IEEE Signal Processing Letters*, vol. 14, pp. 968–971, November 2007.

- [217] N. H. Lehmann, E. Fishler, A. M. Haimovich, R. S. Blum, D. Chizhik, L. J. Cimini, and R. A. Valenzuela, "Evaluation of transmit diversity in MIMO-radar direction finding," *IEEE Transactions on Signal Processing*, vol. 55, pp. 2215–2225, April 2007.
- [218] A. De Maio, M. Lops, and L. Venturino, "Diversity-integration tradeoffs in MIMO detection," *IEEE Transactions on Signal Processing*, vol. 56, no. 10, pp. 5051–5061, Oct 2008.
- [219] L. Xu, J. Li, and P. Stoica, "Target detection and parameter estimation for MIMO radar systems," *IEEE Transactions on Aerospace and Electronic Systems*, vol. 44, October 2008.
- [220] C. Du, J. S. Thompson, and Y. Petillot, "Predicted detection performance of MIMO radar," *IEEE Signal Processing Letters*, vol. 15, pp. 83–86, January 2008.
- [221] J. Tang, N. Li, Y. Wu, and Y. Peng, "On detection performance of MIMO radar: A relative entropy-based study," *IEEE Signal Processing Letters*, vol. 16, pp. 184–187, February 2009.
- [222] Q. He, N. H. Lehmann, R. S. Blum, and A. M. Haimovich, "MIMO radar moving target detection in homogeneous clutter," *IEEE Transactions on Aerospace and Electronic Systems*, vol. 46, no. 3, pp. 1290–1301, July 2010.
- [223] A. Tajer, G. H. Jajamovich, X. Wang, and G. V. Moustakides, "Optimal joint target detection and parameter estimation by MIMO radar," *IEEE Journal of Selected Topics in Signal Processing*, vol. 4, no. 1, pp. 127–145, February 2010.
- [224] M. Akcakaya and A. Nehorai, "MIMO radar detection and adaptive design under a phase synchronization mismatch," *IEEE Transactions on Signal Processing*, vol. 58, no. 10, pp. 4994–5005, October 2010.
- [225] C. Chong, F. Pascal, J. Ovarlez, and M. Lesturgie, "MIMO radar detection in non-Gaussian and heterogeneous clutter," *IEEE Journal of Selected Topics in Signal Processing*, vol. 4, no. 1, pp. 115–126, February 2010.
- [226] S. Gogineni and A. Nehorai, "Polarimetric MIMO radar with distributed antennas for target detection," *IEEE Transactions on Signal Processing*, vol. 58, no. 3, pp. 1689–1697, March 2010.
- [227] Q. He, R. S. Blum, and A. M. Haimovich, "Noncoherent MIMO radar for location and velocity estimation: More antennas means better performance," *IEEE Transactions on Signal Processing*, vol. 58, no. 7, pp. 3661–3680, July 2010.
- [228] Q. He and R. S. Blum, "Diversity gain for MIMO Neyman-Pearson signal detection," *IEEE Transactions on Signal Processing*, vol. 59, no. 3, pp. 869–881, March 2011.

- [229] M. Akcakaya and A. Nehorai, "MIMO radar sensitivity analysis for target detection," *IEEE Transactions on Signal Processing*, vol. 59, no. 7, pp. 3241–3250, July 2011.
- [230] P. Wang, H. Li, and B. Himed, "Moving target detection using distributed MIMO radar in clutter with nonhomogeneous power," *IEEE Transactions on Signal Processing*, vol. 59, no. 10, pp. 4809–4820, October 2011.
- [231] M. Akcakaya and A. Nehorai, "Adaptive MIMO radar design and detection in compound-gaussian clutter," *IEEE Transactions on Aerospace and Electronic Systems*, vol. 47, pp. 2200–2207, July 2011.
- [232] A. Hassanien, S. A. Vorobyov, and A. B. Gershman, "Moving target parameters estimation in non-coherent MIMO radar systems," *IEEE Transactions on Signal Processing*, vol. 60, no. 5, pp. 2354–2361, May 2012.
- [233] G. V. Moustakides, G. H. Jajamovich, A. Tajer, and X. Wang, "Joint detection and estimation: Optimum tests and applications," *IEEE Transactions on Information Theory*, vol. 58, no. 7, pp. 4215–4229, July 2012.
- [234] P. Wang, H. Li, and B. Himed, "A parametric moving target detector for distributed MIMO radar in non-homogeneous environment," *IEEE Transactions on Signal Processing*, vol. 61, no. 9, pp. 2282–2294, May 2013.
- [235] S. Zhou and H. Liu, "Space-partition-based target detection for distributed MIMO radar," *IEEE Transactions on Aerospace and Electronic Systems*, vol. 49, pp. 2717–2729, October 2013.
- [236] D. E. Hack, L. K. Patton, B. Himed, and M. A. Saville, "Detection in passive MIMO radar networks," *IEEE Transactions on Signal Processing*, vol. 62, no. 11, pp. 2999–3012, June 2014.
- [237] D. E. Hack, L. K. Patton, B. Himed, and M. A. Saville, "Centralized passive MIMO radar detection without direct-path reference signals," *IEEE Transactions on Signal Processing*, vol. 62, no. 11, pp. 3013–3023, June 2014.
- [238] H. Liu, S. Zhou, H. Su, and Y. Yu, "Detection performance of spatial-frequency diversity MIMO radar," *IEEE Transactions on Aerospace and Electronic Systems*, vol. 50, pp. 3137–3155, December 2014.
- [239] A. Khawar, A. Abdelhadi, and C. Clancy, "Target detection performance of spectrum sharing MIMO radars," *IEEE Sensors Journal*, vol. 15, pp. 4928–4940, April 2015.
- [240] W. Liu, Y. Wang, J. Liu, W. Xie, H. Chen, and W. Gu, "Adaptive detection without training data in colocated MIMO radar," *IEEE Transactions on Aerospace and Electronic Systems*, vol. 51, pp. 2469–2479, September 2015.
- [241] M. Park and H. S. Lee, "Adaptive selection method for generalized likelihood ratio test," *IEEE Transactions on Aerospace and Electronic Systems*, vol. 51, pp. 2615–2626, October 2015.

- [242] Q. Hu, H. Su, S. Zhou, Z. Liu, and J. Liu, "Target detection in distributed MIMO radar with registration errors," *IEEE Transactions on Aerospace and Electronic Systems*, vol. 52, pp. 438–450, April 2016.
- [243] H. Yang and J. Chun, "An improved algebraic solution for moving target localization in noncoherent MIMO radar systems," *IEEE Transactions on Signal Processing*, vol. 64, pp. 258–270, September 2016.
- [244] R. Price and E. Hofstetter, "Bounds on the volume and height distributions of the ambiguity function," *IEEE Transactions on Information Theory*, vol. 11, no. 2, pp. 207–214, April 1965.
- [245] C. Ma, T. S. Yeo, C. S. Tan, Y. Qiang, and T. Zhang, "Receiver design for MIMO radar range sidelobes suppression," *IEEE Transactions on Signal Processing*, vol. 58, no. 10, pp. 5469–5474, October 2010.
- [246] G. Hua and S. S. Abeysekera, "Receiver design for range and sidelobe suppression using MIMO and phased-array radar," *IEEE Transactions on Signal Processing*, vol. 61, no. 6, pp. 1315–1326, March 2013.
- [247] L. J. Griffiths, "Linear constraints in hot clutter cancellation," in *Proceedings of IEEE International Conference on Acoustics, Speech, and Signal Processing (ICASSP)*, Atlanta, GA, USA, May 1996, pp. 1181–1184.
- [248] R. L. Fante and J. A. Torres, "Cancellation of dissuse jammer multipath by an airborne adaptive radar," *IEEE Transactions on Aerospace and Electronic Systems*, vol. 31, no. 2, pp. 805–820, April 1995.
- [249] P. M. Techau, J. R. Guerci, T. H. Slocumb, and L. J. Griffiths, "Performance bounds for hot and cold clutter mitigation," *IEEE Transactions on Aerospace and Electronic Systems*, vol. 35, no. 4, pp. 1235–1265, October 1999.
- [250] Y. I. Abramovich, N. K. Spencer, S. J. Anderson, and A. Y. Gorokhov, "Stochastic-constraints method in nonstationary hot-clutter cancellation—Part I: Fundamentals and supervised training applications," *IEEE Transactions on Aerospace and Electronic Systems*, vol. 34, no. 4, pp. 1271–1291, October 1998.
- [251] Y. I. Abramovich, N. K. Spencer, and S. J. Anderson, "Stochastic-constraints method in nonstationary hot-clutter cancellation—Part II: Unsupervised training applications," *IEEE Transactions on Aerospace and Electronic Systems*, vol. 36, no. 1, pp. 132–150, January 2000.
- [252] D. J. Rabideau, "Clutter and jammer multipath cancellation in airborne adaptive radar," *IEEE Transactions on Aerospace and Electronic Systems*, vol. 36, no. 2, pp. 565–583, April 2000.
- [253] M. I. Skolnik, *Radar handbook*, 3rd ed. New York, NY, USA: McGraw-Hill, 2008.
- [254] G. W. Stimson, *Introduction to airborne radar*, 2nd ed. New Jersey, NY, USA: SciTech Publishing Inc., 1998.

References

- [255] N.-J. Li and Y.-T. Zhang, "A survey of radar ecm and eccm," *IEEE Transactions on Aerospace and Electronic Systems*, vol. 31, no. 3, pp. 1110–1120, July 1995.
- [256] A. Graham, *Communications, Radar and Electronic Warfare*. West Sussex, U.K.: Wiley, 2011.
- [257] I. S. Reed, J. D. Mallett, and L. E. Brennan, "Rapid convergence rate in adaptive arrays," *IEEE Transactions on Aerospace and Electronic Systems*, no. 6, pp. 853–863, November 1974.
- [258] K. Buckley and L. Griffiths, "An adaptive generalized sidelobe canceller with derivative constraints," *IEEE Transactions on Antennas and Propagation*, vol. 34, no. 3, pp. 311–319, March 1986.
- [259] H. Wang and L. Cai, "On adaptive spatial-temporal processing for airborne surveillance radar systems," *IEEE Transactions on Aerospace and Electronic Systems*, vol. 30, no. 3, pp. 660–670, July 1994.
- [260] J. S. Goldstein and I. S. Reed, "Theory of partially adaptive radar," *IEEE Transactions on Aerospace and Electronic Systems*, vol. 33, no. 4, pp. 1309–1325, October 1997.
- [261] W. L. Melvin, "Space-time adaptive radar performance in heterogeneous clutter," *IEEE Transactions on Aerospace and Electronic Systems*, vol. 36, no. 2, pp. 621–633, April 2000.
- [262] J. R. Guerci, J. S. Goldstein, and I. S. Reed, "Optimal and adaptive reduced-rank stap," *IEEE Transactions on Aerospace and Electronic Systems*, vol. 36, no. 2, pp. 647–663, April 2000.
- [263] J. S. Goldstein, I. S. Reed, and L. L. Scharf, "A multistage representation of the wiener filter based on orthogonal projections," *IEEE Transactions on Information Theory*, vol. 44, no. 7, pp. 2943–2959, November 1998.
- [264] J. S. Goldstein, I. S. Reed, and P. A. Zulch, "Multistage partially adaptive stap cfar detection algorithm," *IEEE Transactions on Aerospace and Electronic Systems*, vol. 35, no. 2, pp. 645–661, 1999.
- [265] A. Haimovich, "The eigencanceler: Adaptive radar by eigenanalysis methods," *IEEE Transactions on Aerospace and Electronic Systems*, vol. 32, no. 2, pp. 532–542, April 1996.
- [266] A. Hassanien, S. A. Elkader, A. B. Gershman, and K. M. Wong, "Convex optimization based beamspace preprocessing with an improved robustness against out-of-sector sources," *IEEE Transactions on Signal Processing*, vol. 54, no. 5, pp. 1587–1595, May 2006.
- [267] Y. Nesterov, *Introductory lectures on convex optimization: A basic course*. Norwell, MA, USA: Kluwer Academic Publishers, 2004.

- [268] J. D. Leeuw. (2003, June) Quadratic majorization. [Online]. Available: http://gifi.stat.ucla.edu/janspubs/2003/notes/deleeuw_U_03c.pdf
- [269] S. Liu and G. Trenkler, "Hadamard, Khatri-Rao, Kronecker and other matrix products," *International Journal of Information and Systems Sciences*, vol. 4, no. 1, pp. 160–177, 2008.
- [270] R. Varadhan and C. Roland, "Simple and globally convergent methods for accelerating the convergence of any EM algorithm," *Scandinavian Journal of Statistics*, vol. 35, no. 2, pp. 335–353, 2008.
- [271] P. Henrici, *Elements of Numerical Analysis*. New York: John Wiley, 1964.
- [272] A. Cordero, J. L. Hueso, E. Martinez, and J. R. Torregrosa, "Steffensen type methods for solving nonlinear equations," *Journal of Computational and Applied Mathematics*, vol. 236, no. 12, pp. 3058–3064, June 2012.
- [273] M. Raydan and B. F. Svaiter, "Relaxed steepest descent and Cauchy-Barzilai-Borwein method," *Computational Optimization and Applications*, vol. 21, no. 2, pp. 155–167, February 2002.
- [274] J. Nocedal and S. Wright, *Numerical Optimization*, 2nd ed. New York, NY, USA: Springer, 2000.

Publication I

Yongzhe Li, Sergiy A. Vorobyov and Visa Koivunen. Ambiguity function of the transmit beamspace-based MIMO radar. *IEEE Transactions on Signal Processing*, vol. 63, no. 17, pp. 4445–4457, September 2015.

© 2015 IEEE.

Reprinted with permission.

Ambiguity Function of the Transmit Beamspace-Based MIMO Radar

Yongzhe Li, *Student Member, IEEE*, Sergiy A. Vorobyov, *Senior Member, IEEE*, and Visa Koivunen, *Fellow, IEEE*

Abstract—In this paper, we derive an ambiguity function (AF) for the transmit beamspace (TB)-based MIMO radar for the case of far-field targets and narrow-band waveforms. The effects of transmit coherent processing gain and waveform diversity are incorporated into the AF definition. To cover all the phase information conveyed by different factors, we introduce the equivalent transmit phase centers. The newly defined AF serves as a generalized AF form for which the phased-array (PA) and traditional MIMO radar AFs are important special cases. We establish relationships among the defined TB-based MIMO radar AF and the existing AF results, including the Woodward's AF, the AFs defined for traditional colocated MIMO radar, and also the PA radar AF, respectively. Moreover, we compare the TB-based MIMO radar AF with the square-summation-form AF definition and identify two limiting cases to bound its “clear region” in Doppler-delay domain that is free of sidelobes. Corresponding bounds for these two cases are derived, and it is shown that the bound for the worst case is inversely proportional to the number of transmitted waveforms K , whereas the bound for the best case is independent of K . The actual “clear region” of the TB-based MIMO radar AF depends on the array configuration and is in between of the worst- and best-case bounds. We propose a new TB design strategy to reduce the levels of the AF sidelobes and show in simulations that proper design of the TB matrix leads to reduction of the relative sidelobe levels of the TB-based MIMO radar AF.

Index Terms—Ambiguity function (AF), clear region, generalized AF, MIMO radar, transmit beamspace (TB).

I. INTRODUCTION

THE multiple-input multiple-output (MIMO) radar has become the focus of intensive research in recent years [1]–[10]. It has been shown that the traditional MIMO radar with colocated antenna elements provides many benefits such

Manuscript received July 29, 2014; revised January 05, 2015, March 23, 2015, and May 20, 2015; accepted May 20, 2015. Date of publication June 01, 2015; date of current version July 21, 2015. The associate editor coordinating the review of this manuscript and approving it for publication was Dr. Branko Ristic. This work was supported in part by the Finnish Defense Research Agency. Y. Li was also supported by China Scholarship Council (CSC) and the Fundamental Research Funds for the Central Universities of China under Contract ZYGX2010YB007. Some of the preliminary and relevant results on AF for MIMO radar with correlated waveforms have been presented at the IEEE International Conference on Acoustics, Speech, and Signal Processing (ICASSP), Florence, Italy, 2014.

Y. Li is with the Department of Signal Processing and Acoustics, Aalto University, FI-00076 Aalto, Finland, and also with the Department of Electronic Engineering, University of Electronic Science and Technology of China, Chengdu, 611731, China (e-mail: lyzlyz888@gmail.com; yongzhe.li@aalto.fi).

S. A. Vorobyov and V. Koivunen are with the Department of Signal Processing and Acoustics, Aalto University, FI-00076 Aalto, Finland (e-mail: svor@ieee.org; visa.koivunen@aalto.fi).

Color Versions of one or more of the figures in this paper are available online at <http://ieeexplore.ieee.org>.

Digital Object Identifier 10.1109/TSP.2015.2439241

as increased upper limit on the number of resolvable targets [1], improved parameter identifiability and angular resolution [3], extended array aperture by virtual sensors [6], opportunity for improved clutter mitigation [8], [11], and capability on suppressing jammers [12], [13]. Moreover, the techniques that aim at combining the benefits of the traditional MIMO radar and the well developed phased-array (PA) radar have emerged in the past few years [14]–[23]. These techniques, namely, transmit beamspace (TB) design techniques, trade off the omnidirectional transmission of mutually orthogonal waveforms to higher transmit coherent processing gain in MIMO radar. For example, the work of [14] attempts to simultaneously incorporate the benefits of waveform diversity and transmit coherent processing gain by separating the transmit antenna array into several uniform subarrays, and enabling each one to perform as a PA. Unlike [14], the TB-based MIMO radar (see for example [15]) focuses the energy of multiple transmitted orthogonal waveforms within a certain spatial sector where a target is likely to be located using beamspace design techniques. In this radar configuration, beams that fully cover the sector-of-interest are synthesized at the transmitting end. Each beam associated with a certain orthogonal waveform is implemented via the whole transmit array of the TB-based MIMO radar. The essence of it is to find the jointly optimal scheme that achieves improved signal-to-noise ratio (SNR) together with increased aperture by means of TB processing techniques [15]–[23]. For example, it allows to achieve transmit coherent processing gain or desired beampattern by appropriate design of waveform correlation matrix [16], [17].

In comparison to the traditional MIMO radar, one verified benefit of the TB-based MIMO radar is the superior direction-of-arrival (DOA) estimation performance in a wide range of SNRs [15], [19], [20]. Based on classic MUSIC [24] or ESPRIT [25] approaches, multiple efficient algorithms that facilitate DOA estimation can be developed. Moreover, the Cramér-Rao bound (CRB) derived for the TB-based MIMO radar in [15] demonstrates that it can achieve a lower CRB with fewer waveforms than the traditional MIMO radar with full waveform diversity, and the lowest CRB can be achieved with proper TB design. This leads to emitting non-orthogonal or correlated waveforms from different transmit antenna elements. To study the performance of these actually emitted waveforms as well as the resolution performance of the TB-based MIMO radar system, it is essential to employ ambiguity function (AF) [26]–[33] for the performance evaluation.

The well-known Woodward's AF [26]–[29], which characterizes the resolution property in Doppler-delay domain for narrow-band waveforms, has served as a starting point for the

works on the traditional MIMO radar AF [31]–[33]. It has been extended to the traditional MIMO radar setup in [31] for the first time, and four AF simplifications corresponding to different scenarios have been derived there. Some properties of the traditional MIMO radar AF have been studied in [32]. Another AF definition for the traditional MIMO radar which does not consider the phase information, has been introduced in [33]. However, with the development of TB design techniques, which allow for non-orthogonal or correlated waveforms to be emitted from each transmit antenna element, the traditional MIMO radar AFs are no longer applicable to the TB-based MIMO radar. This motivates us to derive the AF for the TB-based MIMO radar and investigate how it behaves. Moreover, in-depth study of the TB-based MIMO radar AF also provides insights into the clutter/interference mitigation in airborne/spaceborne MIMO radar system with TB design. On the other hand, it is known that the so-called “clear region” [28], [29] denotes the volume-clearance area in Doppler-delay domain which is free of sidelobes. It serves as a measure to determine how close to the ideal thumbtack-shape AF one can come. It is also of great significance for the TB-based MIMO radar AF analysis to see how large its “clear region” is. The work in [33] defines the traditional MIMO radar AF as the sum of the squared noise-free outputs after matched filtering to the waveforms. Based on this definition the “clear region” bound is derived. Such bound is also important to derive for the TB-based MIMO radar AF.

In this paper, we derive the AF for the TB-based MIMO radar, and it serves as a generalized AF form for which the existing traditional MIMO radar AF and PA radar AF are important special cases.¹ The effects of both transmit coherent processing gain and waveform diversity are considered when defining the new AF for the TB-based MIMO radar, and the phase information conveyed by multiple factors such as array geometry and relative motion is incorporated. Our newly defined AF deals with fewer transmitted waveforms as compared to the traditional MIMO radar configuration where different waveform is launched from each antenna. It will be shown to contribute to achieving lower relative sidelobe levels by the new AF. Considering that it is impossible to give an exact “clear region” bound for the TB-based MIMO radar AF because the self-transform [28] of the TB-based MIMO radar AF can not guarantee the non-negativity in general, we identify two limiting cases to conduct the analysis.

The main contributions of this paper are as follows:

- We introduce a new AF definition for the TB-based MIMO radar for the case of far-field targets and narrow-band waveforms. Equivalent transmit phase centers are introduced in the definition as well.
- We show that the TB-based MIMO radar AF is a generalization of AF for many well-known radar configurations such as the PA radar, the traditional MIMO radar (with sub-arrays), and the TB-based MIMO radar, by properly selecting the TB matrix and the equivalent transmit phase centers.

- We establish relationships among the defined TB-based MIMO radar AF and other existing AFs in the literature including the well-known Woodward’s AF, the traditional MIMO radar AF, and the PA radar AF, respectively.
- We compare the newly defined TB-based MIMO radar AF with the square-summation-form AF [33], and propose a TB design strategy to reduce the relative sidelobe levels of the TB-based MIMO radar AF.
- We identify the worst and the best limiting cases for the TB-based MIMO radar AF, and derive the corresponding “clear region” bounds.

The rest of the paper is organized as follows. In Section II, the signal models for the traditional and the TB-based MIMO radars are briefly introduced as well as some preliminaries about the TB matrix design. In Section III, we present the definition of the TB-based MIMO radar AF and establish connections to the previous AF works. A new TB design strategy that enables lower relative AF sidelobe levels is proposed in this section. The “clear region” analysis for the TB-based MIMO radar AF is given in Section IV. In Section V, simulation results corresponding to different types of radar AFs are provided. Optimized polyphase-coded sequences [35] with single pulse are employed as the transmitted waveforms. Finally, conclusions are drawn in Section VI.

II. SIGNAL MODEL AND PRELIMINARIES

Consider a colocated MIMO radar system with a transmit array of M antenna elements and a receive array of N antenna elements. Both the transmit and receive arrays are assumed to be closely located, therefore, they share an identical spatial angle for a far-field target. In the context of the traditional MIMO radar, the complex envelope of the waveforms emitted by the transmit antenna elements can be modeled as

$$s_m(\tilde{t}) = \sqrt{\frac{E}{M}} \phi_m(\tilde{t}), \quad m = 1, 2, \dots, M \quad (1)$$

where E is the total transmit energy within one radar pulse, \tilde{t} is the continuous fast-time index, i.e., time within the pulse, and $\phi_m(\tilde{t})$ is the m th orthogonal baseband waveform. Without loss of generality, we assume that the transmitted waveforms are normalized to have unit energy, i.e.,

$$\int_{T_p} |\phi_m(\tilde{t})|^2 d\tilde{t} = 1, \quad m = 1, 2, \dots, M \quad (2)$$

where T_p is the time duration of the pulse, and $|\cdot|$ stands for the absolute value operation.

Assuming that L targets are present, the $N \times 1$ received complex signal vector can be expressed as

$$\mathbf{x}(t, \varsigma) = \sum_{l=1}^L r_l(t, \varsigma) \mathbf{b}(\theta_l) + \mathbf{z}(t, \varsigma) \quad (3)$$

where t is the continuous fast-time index for the received signal, ς is the slow-time index, i.e., the pulse number, $\mathbf{b}(\theta_l)$ is the

¹Some of the preliminary and relevant results on AF for MIMO radar with correlated waveforms have been presented in [34].

steering vector of the receive array associated with the l th target, $\mathbf{z}(t, \varsigma)$ is the $N \times 1$ zero-mean white Gaussian noise, and

$$r_l(t, \varsigma) = \sqrt{\frac{E}{M}} \alpha_l(\varsigma) D_l(\varsigma) \mathbf{a}^T(\theta_l) \boldsymbol{\phi}(t) \quad (4)$$

is the echo of radar return due to the l th target located at the spatial direction θ_l . In (4), $\alpha_l(\varsigma)$, $D_l(\varsigma)$, $\mathbf{a}(\theta_l)$, and θ_l are respectively the complex reflection coefficient, the phase due to Doppler, the steering vector of transmit array, and the spatial angle all associated with the l th target, $\boldsymbol{\phi}(t) \triangleq [\phi_1(t), \dots, \phi_M(t)]^T$ is the $M \times 1$ waveform vector, and $(\cdot)^T$ stands for the transpose operation. The reflection coefficient $\alpha_l(\varsigma)$ is assumed to be constant over the whole radar coherent processing interval. The phase term $D_l(\varsigma)$ is assumed to be constant for any give t during the ς th pulse, i.e., slow-moving targets are assumed.

At the receiving end, the $N \times 1$ component of the received data (4) due to the m th waveform is extracted by employing the matched filtering technique, i.e.,

$$\mathbf{x}_m(\varsigma) \triangleq \int_{T_p} \mathbf{x}(t, \varsigma) \phi_m^*(t) dt, \quad m = 1, \dots, M \quad (5)$$

where $(\cdot)^*$ is the conjugation operator. By stacking all the filtered components (5) into a column vector, we can obtain the following $MN \times 1$ virtual data vector

$$\begin{aligned} \mathbf{y}_{\text{MIMO}}(\varsigma) &\triangleq [\mathbf{x}_1^T(\varsigma), \dots, \mathbf{x}_M^T(\varsigma)]^T \\ &= \sqrt{\frac{E}{M}} \sum_{l=1}^L \alpha_l(\varsigma) D_l(\varsigma) \mathbf{u}_{\text{MIMO}}(\theta_l) + \tilde{\mathbf{z}}(\varsigma) \end{aligned} \quad (6)$$

where $\mathbf{u}_{\text{MIMO}} \triangleq \mathbf{a}(\theta) \otimes \mathbf{b}(\theta)$ is the $MN \times 1$ virtual steering vector, $\tilde{\mathbf{z}}(\varsigma)$ is the $MN \times 1$ noise term whose covariance is given by $\sigma_z^2 \mathbf{I}_{MN}$, and \otimes denotes the Kronecker product.

In the TB-based MIMO radar system, K (in general, $K \leq M$) initially orthogonal waveforms are transmitted [15]. For each waveform, a transmit beam that illuminates a certain area within the pre-determined spatial angular sector-of-interest Ω is formed. The K synthesized transmit beams are designed to fully cover the spatial sector Ω . Thus, in the context of the TB-based MIMO radar, the signal radiated towards the target located at the spatial direction θ via the k th transmit beam can be modeled as [15]

$$s_k(t) = \sqrt{\frac{E}{K}} \mathbf{c}_k^T \mathbf{a}(\theta) \phi_k(t), \quad k = 1, \dots, K \quad (7)$$

where \mathbf{c}_k is the k th column vector of the $M \times K$ TB matrix \mathbf{C} with \mathbf{C} being defined as

$$\mathbf{C} \triangleq [\mathbf{c}_1, \dots, \mathbf{c}_K]. \quad (8)$$

Technically, each column of \mathbf{C} that is composed of M elements is carefully designed to form a certain transmit beam within the sector-of-interest Ω , and the k th orthogonal waveform is emitted through the k th synthesized transmit beam. Therefore,

by denoting the m th element of \mathbf{c}_k as c_{mk} , the signal $\tilde{s}_m(t)$ radiated from the m th transmit antenna element can be expressed as

$$\tilde{s}_m(t) = \sqrt{\frac{E}{K}} \sum_{k=1}^K c_{mk} \phi_k(t), \quad m = 1, \dots, M. \quad (9)$$

There are many ways of designing the TB matrix \mathbf{C} . For example, one way is to maximize (or keep fixed) the energy transmitted within the sector-of-interest Ω while minimizing (or keeping fixed) the energy transmitted in the out-of-sector area at the same time [15]. Mathematically, the constrained optimization problem for finding \mathbf{C} can be expressed as

$$\begin{aligned} \min_{\mathbf{C}} \max_i &\| \mathbf{C}^H \mathbf{a}(\theta_i) - \mathbf{d}(\theta_i) \|^2, \quad \theta_i \in \Omega, i = 1, \dots, I \\ \text{s.t.} &\| \mathbf{C}^H \mathbf{a}(\theta_j) \|^2 \leq \gamma, \quad \bar{\theta}_j \in \bar{\Omega}, j = 1, \dots, J \end{aligned} \quad (10)$$

where $\mathbf{d}(\theta)$ is the presumed vector of size $K \times 1$ that guarantees the desired property of transmit beamforming, $\bar{\Omega}$ combines a continuum of all out-of-sector directions that lie outside Ω , γ is the parameter of user choice that characterizes the worst acceptable level of transmit power leakage in the out-of-sector region, I and J are the numbers of grids of angles within and outside the sector-of-interest Ω , respectively, $(\cdot)^H$ is the conjugate transpose operator, and $\|\cdot\|$ is the Euclidean norm. The correlated waveforms $\mathbf{S}(t) \triangleq [\tilde{s}_1(t), \dots, \tilde{s}_M(t)]$ can also be designed directly [36]. To achieve good Doppler tolerance of the waveforms, spectral constraints can be enforced in the designing process [37]. In essence, both the TB matrix design and the direct correlated waveforms design can be understood as achieving an optimal (in some pre-determined sense) mixing matrix \mathbf{R}_d that can be expressed as $\mathbf{R}_d = \mathbf{C}\mathbf{C}^H$ or as $\mathbf{R}_d = \mathbb{E}\{\mathbf{S}(t)\mathbf{S}^H(t)\}$ with $\mathbb{E}\{\cdot\}$ standing for the expectation operation. In contrast to designing the mixing matrix \mathbf{R}_d directly [16], the TB-based approach enables us to investigate the AF of the TB-based MIMO radar.

III. THE TB-BASED MIMO RADAR AF

In this section, we first introduce the AF of the TB-based MIMO radar, then we establish relationships among the so-defined AF and the previous works on AF including the well-known Woodward's AF, the traditional MIMO radar AF, and the PA radar AF.

As it has been shown in the previous section, K orthogonal waveforms/beams versus M transmit antenna elements are employed in the TB-based MIMO radar, and generally, K is much less than M . Thus, the situation when it is required to alternate between the beamspace and the element space occurs. The K initial waveforms in the beamspace correspond to M compound waveforms in the element space. Generally, these M compound waveforms are correlated to each other, which is achieved by the TB matrix \mathbf{C} . When it comes to the introduction of AF for the TB-based MIMO radar, we aim at obtaining an expression which separates the characteristics of the K initial waveforms and the effect of correlation due to the TB matrix \mathbf{C} . To achieve this, we start from the beamspace waveforms $\phi_k(t)$, $k = 1, \dots, K$, and follow the element space signal model (9).

One more benefit due to this routine is that no changes need to be done at the receiver, i.e., a regular bank of matched filters matching to the waveforms $\phi_k(t)$, $k = 1, \dots, K$ can still be used.

A. AF Definition and Implication

We consider the most common radar scenario of far-field targets and narrow-band waveforms, and assume that the TB-based MIMO radar is operating at the frequency f_c . For a point target located at the position \mathbf{p} , the received signal at the j th receive antenna element before demodulation to the base band can be written as

$$\tilde{r}_j(t, \mathbf{p}) = \sum_{m=1}^M \alpha_{mj} \tilde{s}_m(t - \tau_{mj}(\mathbf{p})) \times \exp \{j2\pi f_c(t - \tau_{mj}(\mathbf{p}))\} + \tilde{z}_j(t) \quad (11)$$

where α_{mj} is the complex reflection coefficient for the (m, j) th transmit-receive channel, $\tau_{mj}(\mathbf{p})$ is the two-way time delay of the (m, j) th transmit-receive channel due to the target location at \mathbf{p} , $\tilde{s}_m(t - \tau_{mj}(\mathbf{p}))$ is the time-delayed version of $\tilde{s}_m(t)$ that has been defined in (9), and $\tilde{z}_j(t)$ is the noise observed by the j th receive antenna element.

Let us assume that the target is moving, and its velocity and moving direction are depicted by the vector \mathbf{v} . For the sake of brevity, we exploit Θ to denote the target parameter which contains the information of the target position \mathbf{p} and the velocity vector \mathbf{v} . Considering the effect of target motion on Doppler in (11) and using also (9), the received signal after performing demodulation to the baseband can be expressed as

$$\hat{r}_j(t, \Theta) = \sqrt{\frac{E}{K}} \sum_{m=1}^M \sum_{k=1}^K \alpha_{mj} c_{mk} \phi_k(t - \tau_{mj}(\mathbf{p})) \times \exp \{-j2\pi \tau_{mj}(\mathbf{p})(f_c + f_{mj}(\Theta))\} \times \exp \{j2\pi f_{mj}(\Theta)t\} + z_j(t) \quad (12)$$

where $f_{mj}(\Theta)$ is the Doppler shift of the target due to the (m, j) th transmit-receive channel and $z_j(t)$ is the white

Gaussian noise with power σ_z^2 observed at the j th receive antenna element after demodulation.

At the receiving end, a bank of matched filters is employed due to the fact that the received signal is a sum of the reflected echoes associated with the known transmitted waveforms. The optimal detector is a filter matched to a specific set of target parameters. Therefore, by matched filtering $\hat{r}_j(t, \Theta)$ to each of the waveforms $\phi_k(t)$, $k = 1, \dots, K$ with a specific target parameter Θ' , namely, $\phi_k(t, \Theta')$, $k = 1, \dots, K$, the received signal component associated with the i th transmitted waveform can be obtained as (13), shown at the bottom of this page, where $q(i)$ is the equivalent transmit phase center for the i th transmitted waveform and $\tilde{z}_{ji}(t)$ is the noise after matched filtering.

Let us define the AF as the square of coherent summation of all the noise-free matched filtering output pairs (j, i) , $j = 1, \dots, N$ and $i = 1, \dots, K$. Thus, the AF of the TB-based MIMO radar can be mathematically expressed as (14), shown at the bottom of this page. Introducing an $M \times K$ matrix \mathbf{R} whose (m, i) th element is defined as

$$\begin{aligned} [\mathbf{R}]_{mi}(\Theta, \Theta', \mathbf{C}, j) \\ \triangleq \sqrt{\frac{E}{K}} \sum_{k=1}^K c_{mk} \int \phi_k(t - \tau_{mj}(\mathbf{p})) \phi_i^*(t - \tau_{q(i)j}(\mathbf{p}')) \\ \times \exp \{j2\pi (f_{mj}(\Theta) - f_{q(i)j}(\Theta'))t\} dt \end{aligned} \quad (15)$$

the TB-based MIMO radar AF (14) can be simplified as

$$\begin{aligned} \chi(\Theta, \Theta') = \left| \sum_{j=1}^N \sum_{i=1}^K \sum_{m=1}^M \alpha_{mj} [\mathbf{R}]_{mi}(\Theta, \Theta', \mathbf{C}, j) \right. \\ \times \exp \{-j2\pi \tau_{mj}(\mathbf{p})(f_c + f_{mj}(\Theta))\} \\ \left. \times \exp \{j2\pi \tau_{q(i)j}(\mathbf{p}')(f_c + f_{q(i)j}(\Theta'))\} \right|^2. \end{aligned} \quad (16)$$

The TB-based MIMO radar AF (16) is composed of square of summation terms, and each summation term contains two

$$\begin{aligned} \bar{r}_{ji}(\Theta, \Theta') = \int \hat{r}_j(t, \Theta) \phi_i^*(t, \Theta') dt = \sqrt{\frac{E}{K}} \sum_{m=1}^M \sum_{k=1}^K \alpha_{mj} \int c_{mk} \phi_k(t - \tau_{mj}(\mathbf{p})) \phi_i^*(t - \tau_{q(i)j}(\mathbf{p}')) \\ \exp \{-j2\pi \tau_{mj}(\mathbf{p})(f_c + f_{mj}(\Theta))\} \exp \{j2\pi \tau_{q(i)j}(\mathbf{p}')(f_c + f_{q(i)j}(\Theta'))\} \exp \{j2\pi (f_{mj}(\Theta) - f_{q(i)j}(\Theta'))t\} dt + \tilde{z}_{ji}(t) \\ \triangleq \bar{r}'_{ji}(\Theta, \Theta') + \tilde{z}_{ji}(t) \end{aligned} \quad (13)$$

$$\begin{aligned} \chi(\Theta, \Theta') \triangleq \left| \sum_{j=1}^N \sum_{i=1}^K \bar{r}'_{ji}(\Theta, \Theta') \right|^2 = \left| \sqrt{\frac{E}{K}} \sum_{j=1}^N \sum_{i=1}^K \sum_{m=1}^M \sum_{k=1}^K \alpha_{mj} \int c_{mk} \phi_k(t - \tau_{mj}(\mathbf{p})) \phi_i^*(t - \tau_{q(i)j}(\mathbf{p}')) \right. \\ \left. \times \exp \{-j2\pi \tau_{mj}(\mathbf{p})(f_c + f_{mj}(\Theta))\} \exp \{j2\pi \tau_{q(i)j}(\mathbf{p}')(f_c + f_{q(i)j}(\Theta'))\} \exp \{j2\pi (f_{mj}(\Theta) - f_{q(i)j}(\Theta'))t\} dt \right|^2 \end{aligned} \quad (14)$$

more components in addition to the complex reflection coefficient part. One is the match-filtered component denoted by the matrix \mathbf{R} that has been expressed by (15), which stands for the effect of waveform properties, i.e., the auto- and cross-correlations of the transmitted waveforms, and their Doppler tolerance. The other component is composed of the last two exponential terms in (16), and it stands for the phase shift information due to the relative target position and motion with respect to the transmit and receive arrays. The TB-based MIMO radar AF (16) can also be understood as follows. The m th transmit antenna element emits a compound signal that contains all the K orthogonal waveforms, and these waveforms are windowed by the elements of the m th row in the TB matrix \mathbf{C} . Consequently, the matrix \mathbf{R} should be of size $M \times K$, meaning that the TB matrix \mathbf{C} has been employed to transform the original $K \times K$ matrix of waveform properties to \mathbf{R} . This presents the most significant difference that distinguishes the TB-based MIMO radar AF from the traditional MIMO radar AF. Therefore, the AF defined in [31] is not applicable to the TB-based MIMO radar.

The main objective of incorporating phase shift information in (16) is for taking into account the property of coherent processing introduced by the colocated array geometry and the specific radar configuration. Therefore, if the i th equivalent transmit phase center is selected to be the position of the i th transmit antenna element, it matches the way of processing in the traditional MIMO radar. If the position of the first (or the reference) transmit antenna element is selected, then it matches the case in the PA radar. The equivalent transmit phase centers of the TB-based MIMO radar depend on the exact form of the TB matrix \mathbf{C} . By properly designing the matrix \mathbf{C} and the equivalent transmit phase centers, the AF (16) can serve as the AF of the PA, the traditional MIMO, and the TB-based MIMO radars. Hence, it can be viewed as a generalized AF form for the currently existing radar configurations.

B. Relationships With Other AFs

The standard assumption of far-field targets and narrow-band waveforms is used in this paper. The antenna elements of the transmit and receive arrays have locations $\{\mathbf{q}_{T,1}, \dots, \mathbf{q}_{T,M}\}$ and $\{\mathbf{q}_{R,1}, \dots, \mathbf{q}_{R,N}\}$ in three-dimensional Cartesian coordinate system, respectively. The equivalent transmit phase centers are assumed to have locations $\{\mathbf{q}_{TE,1}, \dots, \mathbf{q}_{TE,K}\}$. Here $\mathbf{q}_{T,i}$, $i = 1, \dots, M$; $\mathbf{q}_{R,i}$, $i = 1, \dots, N$; and $\mathbf{q}_{TE,i}$, $i = 1, \dots, K$ are all 3×1 vectors. In addition, we let $\mathbf{u}(\Theta)$ be a unit-norm direction vector pointing from the transmit/receive array to the target identified by the parameter Θ .

We can neglect the effect of target reflection coefficients for different transmit-receive channels, i.e., assume that all α_{mj} are equal to one. This assumption is valid because the contributions of transmit-receive channels to the TB-based MIMO radar AF are constant at any given time t under the standard case of far-field targets and narrow-band waveforms. The effect of α_{mj} on the TB-based MIMO radar AF is still constant even when considering multiple pulses and inter-pulse varying target reflection coefficients if wide pulse is employed and no range folding [32] occurs. Then the AF (16) can be simplified as

$$\chi(\Theta, \Theta') = |\mathbf{a}_R^H(\Theta)\mathbf{a}_R(\Theta')|^2 |\mathbf{a}_T^H(\Theta)\bar{\mathbf{R}}\mathbf{a}_{TE}(\Theta')|^2 \quad (17)$$

where the (m, i) th element of the $M \times K$ matrix $\bar{\mathbf{R}}$ is expressed as

$$\begin{aligned} [\bar{\mathbf{R}}]_{mi}(\Delta\tau, \Delta f_d, \mathbf{C}) \\ = \sqrt{\frac{E}{K}} \sum_{k=1}^K c_{mk} \int \phi_k(t)\phi_i^*(t - \Delta\tau) \exp\{j2\pi\Delta f_d t\} dt. \end{aligned} \quad (18)$$

Here also $\Delta\tau \triangleq \tau(\mathbf{p}) - \tau(\mathbf{p}')$, $\Delta f_d \triangleq f(\Theta) - f(\Theta')$, and

$$\mathbf{a}_T(\Theta) \triangleq [\exp\{\tilde{\mathbf{u}}^T(\Theta)\mathbf{q}_{T,1}\}, \dots, \exp\{\tilde{\mathbf{u}}^T(\Theta)\mathbf{q}_{T,M}\}]^T \quad (19)$$

$$\mathbf{a}_R(\Theta) \triangleq [\exp\{\tilde{\mathbf{u}}^T(\Theta)\mathbf{q}_{R,1}\}, \dots, \exp\{\tilde{\mathbf{u}}^T(\Theta)\mathbf{q}_{R,N}\}]^T \quad (20)$$

$$\mathbf{a}_{TE}(\Theta) \triangleq [\exp\{\tilde{\mathbf{u}}^T(\Theta)\mathbf{q}_{TE,1}\}, \dots, \exp\{\tilde{\mathbf{u}}^T(\Theta)\mathbf{q}_{TE,K}\}]^T \quad (21)$$

are the $M \times 1$ transmit steering vector, the $N \times 1$ receive steering vector, and the $K \times 1$ equivalent transmit steering vector, respectively, with $\tilde{\mathbf{u}}(\Theta) \triangleq j2\pi f'(\Theta) \cdot \mathbf{u}(\Theta)/c$ and $f'(\Theta) \triangleq f_c + f(\Theta)$. The dependence of $\bar{\mathbf{R}}$ on $\Delta\tau$, Δf_d , and \mathbf{C} is not shown in (17) for brevity, and the subscript indices for τ and f are omitted since we consider the case of far-field target and narrow-band waveforms.

It is known that the Woodward's AF for a single waveform $u(t)$ can be expressed as

$$\bar{\chi}(\tau, f_d) = \int u(t)u^*(t - \tau) \exp\{j2\pi f_d t\} dt. \quad (22)$$

Based on this expression, we can define the $K \times K$ matrix $\bar{\chi}(\tau, f_d)$ as the AF matrix of the K orthogonal waveforms for the TB-based MIMO radar. The (j, k) th element of $\bar{\chi}(\tau, f_d)$ is given by

$$[\bar{\chi}]_{jk}(\tau, f_d) = \int \phi_j(t)\phi_k^*(t - \tau) \exp\{j2\pi f_d t\} dt. \quad (23)$$

Using (18) and (23), the AF (17) can be expressed as

$$\begin{aligned} \chi(\Theta, \Theta') = \frac{E}{K} |\mathbf{a}_R^H(\Theta)\mathbf{a}_R(\Theta')|^2 \\ \times |\mathbf{a}_T^H(\Theta)\mathbf{C}\bar{\chi}(\Delta\tau, \Delta f_d)\mathbf{a}_{TE}(\Theta')|^2 \end{aligned} \quad (24)$$

where $\bar{\chi}(\Delta\tau, \Delta f_d)$ is the $K \times K$ matrix whose elements are obtained from (23) by changing the parameters τ and f_d into $\Delta\tau$ and Δf_d , respectively. Realizing that $\Delta\tau$ and Δf_d depend on Θ and Θ' , we employ these two parameters to denote the TB-based MIMO radar AF. In the following, we show how the derived AF is a generalization of the widely used AF results for different radar configurations.

Equation (24) establishes the connection between the TB-based MIMO radar AF and the well known Woodward's AF. The TB matrix \mathbf{C} transforms the original transmit steering vector of length M into a new one of length K . Both the transformed and the equivalent transmit steering vectors are acting on the Woodward's AF matrix of the K waveforms, representing both the transmit coherent processing gain and the waveform diversity. Equivalently, we can say that each AF is windowed by the product of a transmit coherent processing

gain and an equivalent transmit phase term. To be precise, for the j th and k th waveforms, the quantity $[\bar{\chi}(\Delta\tau, \Delta f_d)]_{jk}$, $j, k \in \{1, \dots, K\}$ is windowed by the product of the j th transmit coherent processing gain, namely, $\Upsilon_j \triangleq \mathbf{a}_T^H(\Theta)\mathbf{c}_j$ and the k th equivalent transmit phase term which is denoted by the k th element of $\mathbf{a}_{TE}(\Theta')$.

Equation (24) establishes the connection between the TB-based MIMO radar AF and the traditional MIMO radar AF. If the number of transmitted waveforms K is increased to M , \mathbf{C} is simply the $M \times M$ identity matrix \mathbf{I}_M , and the equivalent transmit phase centers are selected to be the positions of the M individual transmit antenna elements, then the TB-based MIMO radar AF (24) becomes the following form

$$\chi_{\text{MIMO}}(\Theta, \Theta') = \frac{E}{M} |\mathbf{a}_R^H(\Theta)\mathbf{a}_R(\Theta')|^2 \times |\mathbf{a}_T^H(\Theta)\bar{\chi}(\Delta\tau, \Delta f_d)\mathbf{a}_T(\Theta')|^2 \quad (25)$$

which denotes the traditional MIMO radar AF and has exactly the same form as the AF definition in [31] except for the magnitude term. This term represents the general expression of the transmit power allocation for the traditional MIMO radar. Therefore, if E is selected to be equal to M , the expression (25) and the definition of AF in [31] have identical expressions. Furthermore, the TB-based MIMO radar AF (24) also shows compatibility with the traditional MIMO radar with K uniform subarrays [14], if \mathbf{C} is properly designed to be a block diagonal TB matrix whose block diagonal elements are associated with the subarrays. The equivalent phase centers in this case are selected as the centers of subarrays.

Equation (24) also establishes the connection between the TB-based MIMO radar AF and the PA radar AF. If the number of transmitted waveforms K is decreased to 1, \mathbf{C} becomes just a beamforming weight vector \mathbf{w} , and the equivalent transmit phase center is selected to be the first (or the reference) transmit antenna. Then the TB-based MIMO radar AF takes the following form

$$\chi_{\text{PA}}(\Theta, \Theta') = E |\mathbf{a}_R^H(\Theta)\mathbf{a}_R(\Theta')|^2 |\mathbf{a}_T^H(\Theta)\mathbf{w}\bar{\chi}(\Delta\tau, \Delta f_d)|^2 \quad (26)$$

where the Woodward's AF $\bar{\chi}(\Delta\tau, \Delta f_d)$ for the only transmitted waveform in the PA radar is obtained from (22) by changing the parameters τ and f_d into $\Delta\tau$ and Δf_d , respectively. Considering that the magnitude of the equivalent transmit phase center in the PA mode is constant, it can be neglected when deriving (26). Consequently, the TB-based MIMO radar AF defined in this paper serves as a universal AF definition for the traditional MIMO radar (with subarrays) and the PA radar. Moreover, this generalized AF definition can be expressed using the Woodward's AF matrix which links it to the Woodward's AF.

It is also worth noticing the difference between the TB-based MIMO radar AF and the traditional MIMO radar AF in [33] which defines it as the sum of squared match-filtered outputs of employed waveforms. The TB-based MIMO radar AF (24) incorporates phase shift information introduced by the array geometry and the relative motion between the target and the array, and furthermore exploits the square of summation of

all the auto- and cross-AF terms of the K waveforms as the TB-based MIMO radar AF metric. This operation enables it to obtain lower relative sidelobe levels in the Doppler-delay domain than that of the AF in [33]. The reason lies in the mathematical expression itself and the waveform orthogonality. In a word, the existing AF definitions in [31] and [33] for the traditional MIMO radar and the AF defined here for the TB-based MIMO radar all adopt the matched-filtering-based definition, and they are developed on the basis of the Woodward's AF. To distinguish from the former two AFs, the TB-based MIMO radar AF addresses the situation that deals with waveform correlations.

C. New TB Design

The existing TB strategies are designed based on zero-Doppler and zero-delay AF cut, i.e., only spatial information is incorporated in the designs. Therefore, we can also control the relative sidelobe levels of the TB-based MIMO radar AF by enforcing additional constraints on different Doppler and delay bins during the design process of the TB matrix \mathbf{C} . For example, if the relative sidelobes of the TB-based MIMO radar AF within certain Doppler and delay sectors-of-interest \mathfrak{F} and \mathfrak{D} are desired to be kept below a certain level, the TB strategy (10) can be redesigned by solving the following optimization problem

$$\min_{\mathbf{C}} \max_i \|\mathbf{C}^H \mathbf{a}_T(\theta_i) \odot \mathbf{a}_{TE}(\theta_i) - \mathbf{d}(\theta_i)\| \quad (27a)$$

$$\begin{aligned} & \theta_i \in \Omega, i = 1, \dots, I \\ \text{s.t. } & \|\mathbf{C}^H \mathbf{a}_T(\bar{\theta}_j) \odot \mathbf{a}_{TE}(\bar{\theta}_j)\| \leq \gamma \quad (27b) \\ & \bar{\theta}_j \in \bar{\Omega}, j = 1, \dots, J \end{aligned}$$

$$\begin{aligned} & |\mathbf{a}_T^H(\vartheta_0, f_d^0) \mathbf{C} \\ & \times \bar{\chi}((\Delta\tau)_p, (\Delta f_d)_q) \mathbf{a}_{TE}(\vartheta_{\tilde{i}}, (f_d)_q)| \leq \delta \quad (27c) \end{aligned}$$

$$(\Delta\tau)_p \in \mathfrak{D}, p = 1, \dots, P$$

$$(\Delta f_d)_q \in \mathfrak{F}, q = 1, \dots, Q$$

$$\vartheta_{\tilde{i}} \in \tilde{\Omega}, \tilde{i} = 1, \dots, \tilde{I}$$

$$\mathbf{a}_T^H(\vartheta_0, f_d^0) \mathbf{C} \mathbf{a}_{TE}(\vartheta_0, f_d^0) = K \quad (27d)$$

where ϑ_0 and f_d^0 are respectively the spatial angular vector and the Doppler frequency of the target, $\tilde{\Omega}$ combines the spatial region of interest where the AF sidelobes need to be suppressed using \tilde{I} grids of spatial directions $\{\vartheta_{\tilde{i}} \in \tilde{\Omega}, \tilde{i} = 1, \dots, \tilde{I}\}$, $\{(\Delta\tau)_p \in \mathfrak{D}, p = 1, \dots, P\}$ and $\{(\Delta f_d)_q \in \mathfrak{F}, q = 1, \dots, Q\}$ are grids of delay and Doppler used to approximate the sectors-of-interest \mathfrak{D} and \mathfrak{F} by finite numbers of P and Q delay and Doppler bins, respectively, $(f_d)_q \triangleq (\Delta f_d)_q + f_d^0$, and δ is the parameter of user choice that characterizes the sidelobe levels of the AF in the intersection of \mathfrak{D} , \mathfrak{F} , and $\tilde{\Omega}$. It is worth noting that for a certain set of designed waveforms and a fixed group of parameters $\{(\Delta\tau)_p, (\Delta f_d)_q\}$, $p \in \{1, \dots, P\}$ and $q \in \{1, \dots, Q\}$, the matrix $\bar{\chi}((\Delta\tau)_p, (\Delta f_d)_q)$ in (27) can be easily known from (23). This motivates us to further explore the "clear region" bound of the TB-based MIMO radar AF which is studied in the next section.

IV. “CLEAR REGION” ANALYSIS OF THE TB-BASED MIMO RADAR AF

The Siebert’s self-transform property [29] expressed by the following equality

$$|\bar{\chi}(\sigma, \nu)|^2 = \iint_{-\infty}^{\infty} |\bar{\chi}(\tau, f_d)|^2 \exp\{-j2\pi\nu\tau + j2\pi f_d\sigma\} d\tau df_d \quad (28)$$

holds for the Woodward’s AF, and it is required that the transform (28) be non-negative when conducting the “clear region” analysis [28]. Here $\bar{\chi}(\sigma, \nu)$ is the new Woodward’s AF generated from (22) by replacing the parameters τ and f_d with σ and ν , respectively. In the context of the TB-based MIMO radar, let $f(\sigma, \nu)$ denote the self-transform of its AF $\chi(\Theta, \Theta')$, i.e.,

$$f(\sigma, \nu) = \iint_{-\infty}^{\infty} \chi(\Theta, \Theta') \times \exp\{-j2\pi\nu\Delta\tau + j2\pi\Delta f_d\sigma\} d\Delta\tau d\Delta f_d. \quad (29)$$

Normally, the TB-based MIMO radar AF (24) has negative terms in its expansion.² Therefore, the transform (29) contains negative terms. Realizing this fact, it becomes clear that in general it is not guaranteed that $f(\sigma, \nu)$ is non-negative. However, it is needed in order to derive the “clear region” bound of the TB-based MIMO radar AF. Hence, to see how large the maximum achievable “clear region” of the TB-based MIMO radar AF is, we identify two limiting cases which both enable $f(\sigma, \nu)$ to be non-negative. In the first case, we only consider the squared AF terms in the expansion of (24). It is later shown that this case achieves the smallest “clear region” and has high relative sidelobe levels. Thus, it can be considered as the worst case for the “clear region” bound of the TB-based MIMO radar AF defined in this paper. In the second case, we assume that all the cross-AFs of the K waveforms are zero, i.e., we ignore the effects of the components in the AF expansion of (24) that are associated with the sidelobes resulting from different pairs of waveforms. This case represents the best situation for the “clear region” bound of the TB-based MIMO radar AF. However, it can never be achieved because in general more than one waveforms is transmitted in the TB-based MIMO radar system. The actual maximum achievable “clear region” bound of the TB-based MIMO radar AF is in between that of these two cases, and it depends on the level of the non-squared terms of the AF expansion which are windowed by the transmit coherent processing gains and the equivalent transmit phase terms.

In the remaining part of this section, we analyze the worst- and best-case “clear region”. We first derive the bounds for these two cases, then we conduct the analysis based on these two bounds. The superscripts $(\cdot)^I$ and $(\cdot)^{II}$ are used for de-

noting the quantities with respect to the worst- and best-cases, respectively.

A. Worst-Case Bound

In the worst case, in order to find the maximum achievable sidelobe-free area in Doppler-delay domain, we specify the relaxed conditions on the auto- and cross-AFs in (30), shown at the bottom of this page, where A denotes the convex and centrosymmetric region of integration in the Doppler-delay plane. Here, we define the volume of the TB-based MIMO radar AF over the integral region A as

$$V_{\text{TB}}(A) \triangleq \iiint_A \chi(\Theta, \Theta') d\Delta\tau d\Delta f_d. \quad (31)$$

In the following derivation, we assume that all the K waveforms are sharing the same bandwidth and time duration, meaning that the integration of the auto-AF for each waveform over region A has a fixed volume V_0 , i.e., $V_j = V_0, \forall j \in \{1, \dots, K\}$. By substituting (24) into (31), the volume of the TB-based MIMO radar AF for the worst-case scenario can be expressed as

$$V_{\text{TB}}^I(A) \simeq \frac{E}{K} |\mathbf{a}_R^H(\Theta) \mathbf{a}_R(\Theta')|^2 \iint_A \left(\sum_{k=1}^K |\Upsilon_k|^2 \right) \times |\bar{\chi}]_{kk}(\Delta\tau, \Delta f_d)|^2 d\Delta\tau d\Delta f_d \\ = \frac{E}{K} |\mathbf{a}_R^H(\Theta) \mathbf{a}_R(\Theta')|^2 \left(\sum_{k=1}^K |\Upsilon_k|^2 \right) V_0 \quad (32)$$

$$\triangleq V_K \quad (33)$$

where $\Upsilon_k \triangleq \mathbf{a}_T^H(\Theta) \mathbf{c}_k$, $k \in \{1, \dots, K\}$ is the k th transmit coherent processing gain that has been defined before.

Employing the Siebert’s self-transform property (28) and Parseval’s theorem, under the condition that $\psi(\tau, f_d)$ is any quadratically integrable function whose Fourier transform is

$$\Psi(\tau, f_d) = \iint_{-\infty}^{\infty} \psi(\sigma, \nu) \exp\{-j2\pi\nu\tau + j2\pi f_d\sigma\} d\sigma d\nu \quad (34)$$

the following transform

$$\iint_A \chi(\Theta, \Theta') \psi(\Delta\tau, \Delta f_d) d\Delta\tau d\Delta f_d \\ = \frac{E}{K} \iint_{A'} |\mathbf{a}_R^H(\Theta) \mathbf{a}_R(\Theta')|^2 \\ \times \sum_{k=1}^K \sum_{j=1}^K |\Upsilon_k [\mathbf{a}_{\text{TE}}]_j(\Theta')|^2 |\bar{\chi}]_{kk}^*(\Delta\tau, \Delta f_d) \\ \times |\bar{\chi}]_{jj}(\Delta\tau, \Delta f_d) \Psi(\Delta\tau, \Delta f_d) d\Delta\tau d\Delta f_d \\ \triangleq V_{\text{TB}}^I(A') \quad (35)$$

holds.

Under the assumption that A is convex, symmetric around the origin, and furthermore contains a delta function at the origin,

²In general, the AF (24) can contain negative sub-terms introduced by the expansion of the second product term.

$$\left\{ \iint_A |\bar{\chi}]_{jj}(\tau, f_d)|^2 d\tau df_d \simeq \iint_{(0,0)} |\bar{\chi}]_{jj}(\tau, f_d)|^2 d\tau df_d \triangleq V_j \right. \\ \left. \iint_A |\bar{\chi}]_{jk, j \neq k}(\tau, f_d)|^2 d\tau df_d \simeq 0 \right. \quad (30)$$

it can be shown using the approach in [28] that the following inequality

$$\begin{aligned} V_{\text{TB}}^{\text{I}}(A) &> \frac{1}{4}C(A) \lim_{A' \rightarrow 0} V_{\text{TB}}^{\text{I}'}(A') \\ &= \frac{1}{4}C(A) \frac{N^2 \left(\sum_{k=1}^K \sum_{j=1}^K |\Upsilon_k[\mathbf{a}_{\text{TE}}]_j(\boldsymbol{\Theta}')|^2 \right)}{|\mathbf{a}_{\text{R}}^{\text{H}}(\boldsymbol{\Theta})\mathbf{a}_{\text{R}}(\boldsymbol{\Theta}')|^2 \left(\sum_{k=1}^K |\Upsilon_k|^2 \right)} V_K \\ &= \frac{1}{4}C(A) \frac{N^2 K}{|\mathbf{a}_{\text{R}}^{\text{H}}(\boldsymbol{\Theta})\mathbf{a}_{\text{R}}(\boldsymbol{\Theta}')|^2} V_K \end{aligned} \quad (36)$$

holds, where $C(A)$ denotes the area of A , and V_K is defined in (33).

Based on (36) and considering the “ η -clear” area that is convex and symmetric around the origin with $\chi(\boldsymbol{\Theta}, \boldsymbol{\Theta}') \leq \eta$, we obtain that the following inequality for the worst-case “clear region” of the TB-based MIMO radar AF

$$C_{\text{TB}}^{\text{I}}(A) \leq \frac{4V_K}{\frac{N^2 K}{|\mathbf{a}_{\text{R}}^{\text{H}}(\boldsymbol{\Theta})\mathbf{a}_{\text{R}}(\boldsymbol{\Theta}')|^2} V_K - 4\eta} \quad (37)$$

which holds if and only if

$$\eta < \frac{N^2 K V_K}{4 |\mathbf{a}_{\text{R}}^{\text{H}}(\boldsymbol{\Theta})\mathbf{a}_{\text{R}}(\boldsymbol{\Theta}')|^2}. \quad (38)$$

B. Best-Case Bound

In the best case, based on the same assumptions for the transmitted waveforms as made in the worst-case, and using also (24), (31) can be expressed as

$$V_{\text{TB}}^{\text{H}}(A) = V_{\text{TB}}^{\text{I}}(A) \simeq V_K. \quad (39)$$

Similarly, the following transform

$$\begin{aligned} &\iint_A \chi(\boldsymbol{\Theta}, \boldsymbol{\Theta}') \psi(\Delta\tau, \Delta f_d) d\Delta\tau d\Delta f_d \\ &= \frac{E}{K} \iint_{A'} |\mathbf{a}_{\text{R}}^{\text{H}}(\boldsymbol{\Theta})\mathbf{a}_{\text{R}}(\boldsymbol{\Theta}')|^2 \sum_{k=1}^K |\Upsilon_k|^2 \\ &\quad \times |\tilde{\mathbf{x}}|_{kk}(\Delta\tau, \Delta f_d)|^2 \Psi(\Delta\tau, \Delta f_d) d\Delta\tau d\Delta f_d \\ &\triangleq V_{\text{TB}}^{\text{H}'}(A') \end{aligned} \quad (40)$$

holds.

Under the same condition as applied in the worst case, it can be shown that the following inequality

$$\begin{aligned} V_{\text{TB}}^{\text{H}}(A) &> \frac{1}{4}C(A) \lim_{A' \rightarrow 0} V_{\text{TB}}^{\text{H}'}(A') \\ &= \frac{1}{4}C(A) \frac{N^2 \left(\sum_{k=1}^K |\Upsilon_k|^2 \right)}{|\mathbf{a}_{\text{R}}^{\text{H}}(\boldsymbol{\Theta})\mathbf{a}_{\text{R}}(\boldsymbol{\Theta}')|^2 \left(\sum_{k=1}^K |\Upsilon_k|^2 \right)} V_K \\ &= \frac{1}{4}C(A) \frac{N^2}{|\mathbf{a}_{\text{R}}^{\text{H}}(\boldsymbol{\Theta})\mathbf{a}_{\text{R}}(\boldsymbol{\Theta}')|^2} V_K \end{aligned} \quad (41)$$

holds.

Based on (41) and considering the “ η -clear” area that is convex and symmetric around the origin for $\chi(\boldsymbol{\Theta}, \boldsymbol{\Theta}') \leq \eta$, we

obtain the following inequality for the best-case “clear region” of the TB-based MIMO radar AF

$$C_{\text{TB}}^{\text{H}}(A) \leq \frac{4V_K}{\frac{N^2}{|\mathbf{a}_{\text{R}}^{\text{H}}(\boldsymbol{\Theta})\mathbf{a}_{\text{R}}(\boldsymbol{\Theta}')|^2} V_K - 4\eta} \quad (42)$$

which holds if and only if

$$\eta < \frac{N^2 V_K}{4 |\mathbf{a}_{\text{R}}^{\text{H}}(\boldsymbol{\Theta})\mathbf{a}_{\text{R}}(\boldsymbol{\Theta}')|^2}. \quad (43)$$

C. Discussion

The worst- and best-case “clear region” bounds in (37) and (42) which correspond to the two identified limiting cases indicate that they depend on the array configuration, and the quantity $N^2/|\mathbf{a}_{\text{R}}^{\text{H}}(\boldsymbol{\Theta})\mathbf{a}_{\text{R}}(\boldsymbol{\Theta}')|^2$ makes these two bounds variable. The smaller the quantity is, the larger the maximum possible “clear region” bound can be obtained. The largest bound is achieved when this quantity is decreased to 1 as long as the η -level condition is guaranteed.

The “clear region” bound for the worst case indicates that the worst achievable “clear region” of the TB-based MIMO radar AF is independent of the transmit coherent gains, however, it depends on the number of transmitted waveforms K under the condition that the emitted waveforms share the same characteristic parameters and have the same properties. In this sense, it is similar to the case of the traditional MIMO radar AF with K mutually orthogonal waveforms that has been given in [33]. However, the worst-case bound derived here clarifies that the worst-case “clear region” of the TB-based MIMO radar AF is inversely proportional to the number of orthogonal waveforms K (or the number of beams), but not the number of transmit antenna elements M . Contrarily, the best-case “clear region” bound indicates that the ideal “clear region” for the TB-based MIMO radar AF is independent of the waveform number K , and it is equivalent to the case of the PA radar AF with a single waveform that has been shown in [28].

It is worth noting from analyzing (32) that V_K defined in (33) is partially determined by the sum of squared magnitudes of the transmit coherent processing gains Υ_k , $k = 1, \dots, K$, which means that it is subjected to the TB matrix \mathbf{C} employed by the TB-based MIMO radar system. This quantity, together with the one resulted from the receive array geometry, determines how small the η -level can be for the TB-based MIMO radar AF. The PA radar and the traditional MIMO radar have their own fixed forms of TB matrices, therefore, their AFs achieve fixed values of volume V_K under the conditions (30). Different from the former two, the TB-based MIMO radar uses its own TB matrix \mathbf{C} , which makes its maximum “clear region” varying in the range bounded by the worst- and best-case bounds. This leads to significant differences between the results achieved for the traditional MIMO radar AF in [33] and that achieved for the TB-based MIMO radar AF.

The actual maximum achievable “clear region” of the TB-based MIMO radar AF is bounded on both sides by the two identified limiting cases. The worst-case bound becomes larger as K decreases. Consequently, there exists a tradeoff between the maximum achievable “clear region” and the waveform

diversity for the TB-based MIMO radar AF. Once the desired radar system and target parameters are selected, the TB-based MIMO radar AF can be evaluated directly using its definition (16) or simplification (24). This facilitates the radar designer to find the best tradeoff. The worst- and best-case bounds derived in (37) and (42) also implicate that the traditional MIMO radar AF achieves the worst maximum achievable “clear region”, and it is approximately $1/M$ that of the PA radar, which agrees with the result of [33]. It is clear that the maximum achievable “clear region” of the TB-based MIMO radar AF is in between that of the PA and traditional MIMO radar cases.

In reality, orthogonal waveforms for all time delays and Doppler shifts do not exist [38]. Indeed, the TB-based MIMO radar makes it relatively easier to achieve waveforms with better orthogonality because fewer waveforms are needed, provided that the degrees of freedom are enough. The above “clear region” analysis is essentially the way to investigate the non-orthogonal effects of the K original waveforms employed in the TB-based MIMO radar, which is highly related to sidelobe analysis. There exist waveform design methods based on minimizing or explicitly constraining the sidelobe levels of the transmitted waveforms [32], [39], [40] and other design methods such as the ones based on time/Doppler division [38] or space-time coding [41]–[43]. Hence, large “clear region” under the “ η -clear” condition can be achieved. To further obtain a larger “clear region” for the TB-based MIMO radar AF, one can resort to the range-Doppler sidelobes mitigation techniques. For example, receiver instrumental variable filter [40], [44], [45] can be employed at the receiving end to suppress the sidelobes. However, the attainable “clear region” depends on the exact sidelobe mitigation level.

V. SIMULATION RESULTS

In this section, we provide numerical examples to demonstrate the AFs for different radar configurations using the generalized TB-based MIMO radar AF definition given in this paper. We also present comparisons to the AF metric of [33].

Throughout the simulations, we assume that uniform linear arrays of $M = 8$ omni-directional transmit antenna elements and $N = 8$ omni-directional receive antenna elements spaced half a wavelength apart from each other are used. Both the transmit and receive arrays are located on the x -axis with their centers at the origin. The total transmit energy E is fixed to be equal to the number of transmit antenna elements M . Optimized polyphase-coded waveforms [35] of code length 512 are used. We employ a single pulse for simulating the AF, and the pulse width T_p is selected to be $60 \mu\text{s}$. The time-bandwidth product BT_p is set to be equal to 256, and the sampling rate f_s is selected to be two times of the bandwidth, i.e., $f_s = 2B$. We fix both target parameters Θ (with zero Doppler) and Θ' in the x - y plane, and the latter is varying. We show all together four examples, and in the first two examples, both parameters are set to share the same spatial angle $\theta = 0^\circ$. While in the last two examples, both parameters are set to share the same delay $\tau = 0$, but Θ' is allowed to have different spatial angles. The maximum magnitudes of all the simulated AFs are normalized to 1, thus, the mainlobes of all simulated AFs are 0 dB.

For the TB-based MIMO radar configuration, we select the spatial sector-of-interest as $\Omega = [-15^\circ, 15^\circ]$ with a 10° wide transition band on each side. The transmit energy is focused within Ω and it is radiated via $K = 4$ transmit beams. Two TB design strategies are used in the simulations. One is the TB design (10) which is used in the second and third examples, and the other is the TB design (27) which is used in the first and last examples. For the TB design (10), the desired vector $\mathbf{d}(\theta)$ is selected as³ $\mathbf{d}(\theta) \triangleq [\exp\{\mu_1(\theta)\}, \dots, \exp\{\mu_4(\theta)\}]^T$ where $\mu_k(\theta)$, $k \in \{1, \dots, 4\}$ is the k th linear function of the spatial angle θ . The parameter γ of this design that controls the level of radiated power outside Ω is selected differently in the second and third examples. For the TB design (27), the desired vector $\mathbf{d}(\theta)$ is selected as the same in (10), and the Doppler domain $\Delta f_d = [-30 \text{ kHz}, -18 \text{ kHz}] \cup [18 \text{ kHz}, 30 \text{ kHz}]$ at the spatial direction of $\theta = 0^\circ$ is selected to be controlled. Other parameters of this design are respectively selected as $\gamma = 0.1$, $\delta = 0.3$, $\vartheta = 0^\circ$, and $f_d^0 = 0 \text{ kHz}$. We use the CVX MATLAB toolbox [48] to solve both TB optimization design problems in the simulations.

In the first example, we show the square-summation-form MIMO radar AF metric defined in [33] (see Fig. 1(a)), and compare its zero-delay and zero-Doppler cuts to that of the MIMO radar AF for $\mathbf{C} = \mathbf{I}$ and the TB-based MIMO radar AF for the proposed design of \mathbf{C} by (27) (see Fig. 1(b)). It can be seen from Fig. 1 that the relative sidelobe levels of the square-summation-form AF are highly concentrated and of arched shape over the delay domain. For example, it can be viewed from delay domain that all AF sidelobes in the range of delays within $[-15 \mu\text{s}, 15 \mu\text{s}]$ are above -42 dB , and the highest level of sidelobes around the AF mainlobe reaches approximately -32 dB . From the comparison results of the zero-delay and zero-Doppler cuts of AF, it can be seen (see Fig. 1(b)) that spreading relative sidelobes are obtained using the latter two AFs, and their levels are lower than that of the square-summation-form AF. The MIMO radar AF for $\mathbf{C} = \mathbf{I}$ boils down to the MIMO radar AF defined in [31] because no TB processing is applied. To maintain good Doppler tolerance, we can enforce spectral constraints [37] in addition to ensuring good waveform correlation (i.e., zero-Doppler cut of AF) property when designing the waveforms. For the TB-based MIMO radar, we also have the choice to control Doppler sidelobe levels by designing the TB matrix. It can also be seen from Fig. 1(b) that the Doppler relative sidelobe levels are suppressed to about -40 dB . Indeed, this example implicates that the square-summation-form AF metric obtains worse “clear region” than that of the AF defined in this paper for a given allowable sidelobe level limit η . In other words, the sidelobe level limit for the AF of [33] can only be set to a relatively high value.

In the second example, we show the TB-based MIMO radar AF versus delays and Doppler (see Fig. 2) where the TB design strategy (10) is employed. The target velocity is not needed when carrying out the optimization process, thus we employ the spatial angle θ to replace Θ in all the steering vectors. The parameter γ is selected to be 0.38. The figure shows the 3D (full

³For such $\mathbf{d}(\theta)$, the rotational invariance property (RIP) [46], [47] is guaranteed that may be desirable in DOA estimation applications [19], [20].

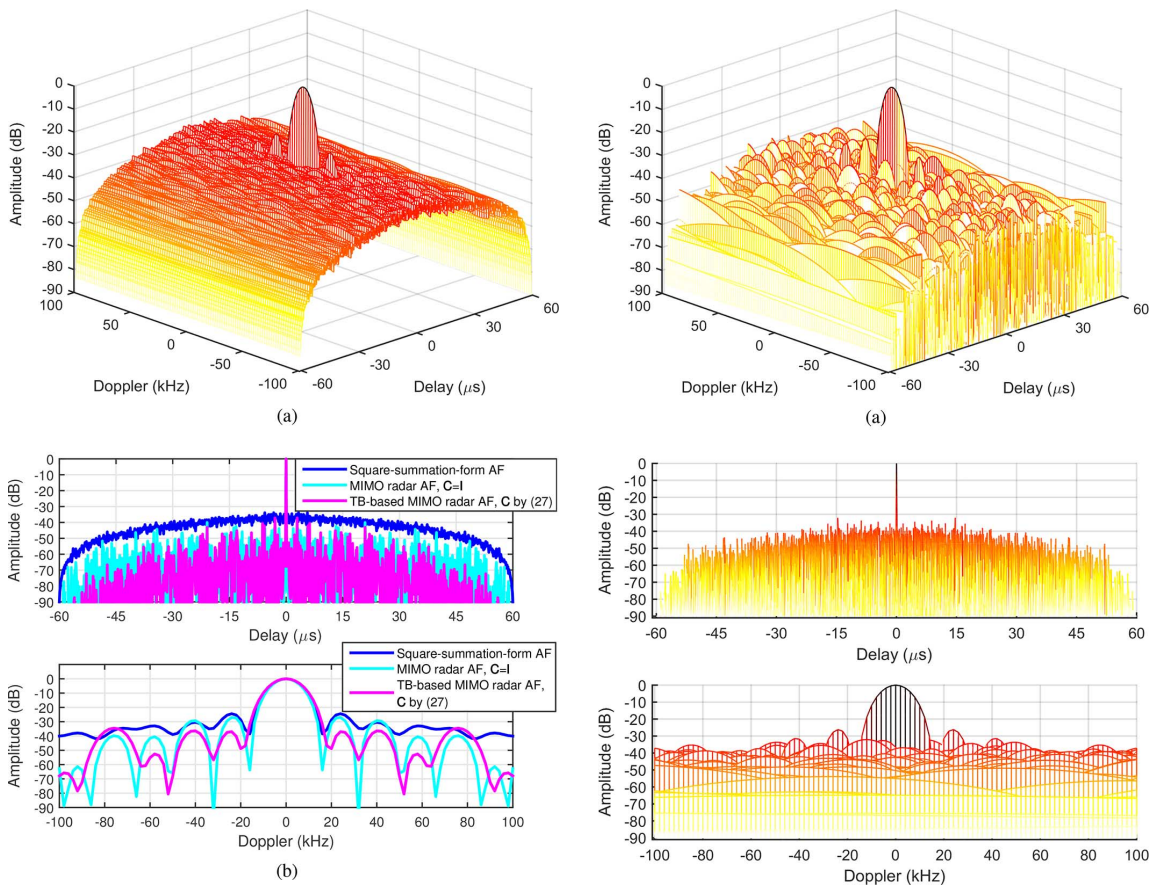


Fig. 1. Comparison to the square-summation-form MIMO radar AF of [33]. Here $M = 8$, $N = 8$, and $E = M$. (a) 3D view of the square-summation-form MIMO radar AF and (b) Zero-delay and zero-Doppler cuts of the square-summation-form MIMO radar AF, the MIMO radar AF for $\mathbf{C} = \mathbf{I}$, and the TB-based MIMO radar AF for the proposed design of \mathbf{C} by (27). The total 8 single-pulse polyphase-coded waveforms of code length 512 are used for the square-summation-form MIMO radar AF and the MIMO radar AF for $\mathbf{C} = \mathbf{I}$, and the first $K = 4$ waveforms are used for the TB-based MIMO radar AF for design of \mathbf{C} by (27): $T_p = 60 \mu\text{s}$, $BT_p = 256$, and $f_s = 2B$. High relative sidelobe levels are obtained in Doppler-delay domain using the square-summation-form AF, and they are highly concentrated and of arched shape over the delay domain (e.g., the range $[-42 \text{ dB}, -32 \text{ dB}]$ of AF amplitudes versus the delay interval $[-15 \mu\text{s}, 15 \mu\text{s}]$). Spreading relative sidelobes (with nulls) are obtained using the latter two AFs, and their levels are lower than that of the square-summation-form AF. The MIMO radar AF for $\mathbf{C} = \mathbf{I}$ boils down to the existing MIMO radar AF defined in [31] because no TB processing is applied. The relative sidelobe levels of the sub Doppler domain $[-30 \text{ kHz}, -18 \text{ kHz}] \cup [18 \text{ kHz}, 30 \text{ kHz}]$ is controlled to approach -40 dB for the TB-based MIMO radar AF for design of \mathbf{C} by (27). The square-summation-form AF metric of [33] shows the worst “clear region”.

view) result in the first subfigure, and the 2D (side view) result in the second subfigure. It can be seen from both subfigures that the relative sidelobes of the TB-based MIMO radar AF occupy a certain large range, i.e., they spread rather than focus. From the view of delay domain, it can be seen that the major sidelobes around the AF mainlobe concentrate on the level of -50 dB . While from the view of Doppler domain, it can be seen that the average level of major sidelobes is about -40 dB . The worst

Fig. 2. The TB-based MIMO radar AF (versus delays and Doppler) associated with the TB design (10). Here $M = 8$, $N = 8$, $K = 4$, and $E = M$. The first 4 out of 8 single-pulse polyphase-coded waveforms of code length 512 are used: $T_p = 60 \mu\text{s}$, $BT_p = 256$, and $f_s = 2B$. (a) 3D view of AF and (b) 2D views of the AF. Low relative sidelobe levels are achieved in Doppler-delay domain using this AF, and the relative sidelobes spread rather than focus. The average relative sidelobe levels can be seen lower than that present in the previous example. Doppler relative sidelobe levels are high because no control is implemented.

sidelobe level from this view is about -27 dB , which is because the convex optimization based TB design (10) does not consider the factor of Doppler processing.

In the third example, we show the TB-based MIMO radar AF versus Doppler and spatial angles (see Fig. 3). The convex optimization based strategy (10) is used to design \mathbf{C} . All other simulation parameters are the same as in the previous example except the parameter γ which is selected as 0.2. To better display the results, we remove all the sidelobes that are below -120 dB . The 3D and 2D results are shown in the first and second subfigures, respectively. It can be seen from the 3D subfigure that the TB-based MIMO radar AF has lower sidelobe levels versus angles than that versus Doppler. From the view of angle, the AF in fact shows the beam pattern of the TB-based MIMO radar system, and the highest relative sidelobe level in this view is

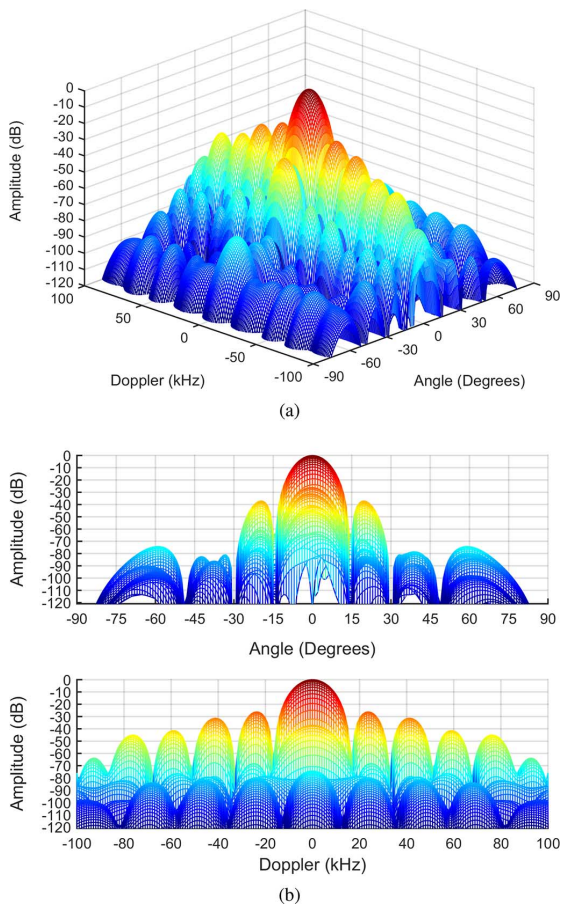


Fig. 3. The TB-based MIMO radar AF (versus angles and Doppler) associated with the TB design (10). Here $M = 8$, $N = 8$, $K = 4$, and $E = M$. The first 4 single-pulse polyphase-coded waveforms of code length 512 are used: $T_p = 60 \mu\text{s}$, $BT_p = 256$, and $f_s = 2B$. (a) 3D view of AF and (b) 2D views of the AF. The information of transmit energy focusing within the spatial sector $[-15^\circ, 15^\circ]$ is conveyed by the result. Low relative sidelobe levels of the AF are achieved in Doppler-angle domain. Due to the reason that the used TB design does not consider the effect of Doppler processing, some relative sidelobe levels along the spatial direction $\theta = 0^\circ$ are still high.

about -28 dB. From the view of Doppler, the worst relative sidelobe level reaches about -27 dB. As the same in the previous example, this level is relatively high due to the reason that the design of the TB matrix does not consider the factor of Doppler processing.

In the last example, we show the TB-based MIMO radar AF versus Doppler and spatial angles using the proposed TB design strategy (27) (see Fig. 4). We aim at suppressing the relative Doppler sidelobe levels of AF in the range $[-30 \text{ kHz}, -18 \text{ kHz}] \cup [18 \text{ kHz}, 30 \text{ kHz}]$ at the spatial direction of $\theta = 0^\circ$. To better display the results, we remove the sidelobes that are below -120 dB. It can be seen from the 2D subfigure that the worst sidelobe level in the desired Doppler range is well suppressed to below -38 dB, and the worst sidelobe level in the whole Doppler domain which is far away from the AF

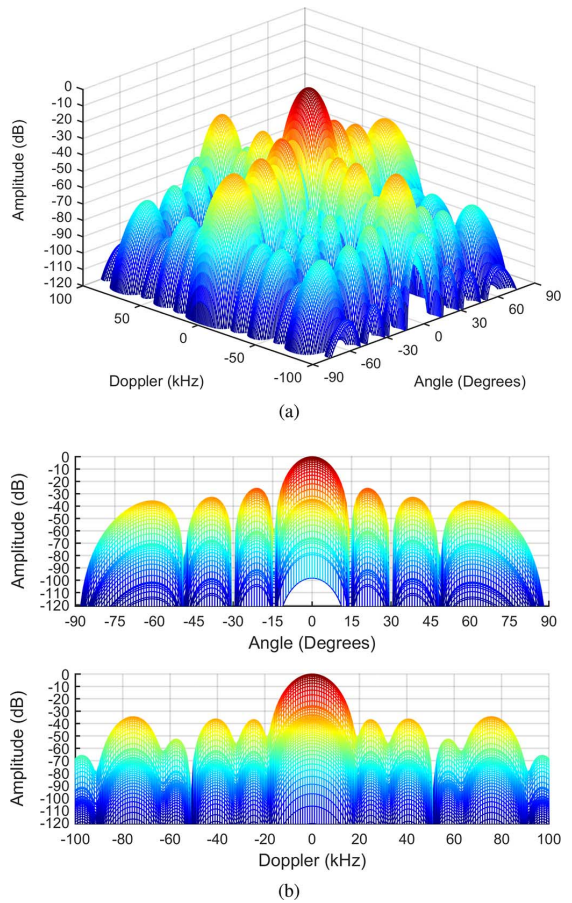


Fig. 4. The TB-based MIMO radar AF (versus angles and Doppler) associated with the proposed TB design (27). Here $M = 8$, $N = 8$, $K = 4$, and $E = M$. The first 4 single-pulse polyphase-coded waveforms are used: $T_p = 60 \mu\text{s}$, $BT_p = 128$, and $f_s = 2B$. (a) 3D view of AF and (b) 2D views of the AF. The relative sidelobe levels of AF in sub Doppler domain $[-30 \text{ kHz}, -18 \text{ kHz}] \cup [18 \text{ kHz}, 30 \text{ kHz}]$ along the spatial direction $\theta = 0^\circ$ are artificially controlled by the proposed TB design, and they are well suppressed to below -38 dB which in fact demonstrates the tradeoff between Doppler and spatial processing in the TB-based MIMO radar.

mainlobe is about -35 dB. Because there is no constraint on the sidelobe levels versus other angles except $\theta = 0^\circ$ in (27), the worst sidelobe level in the whole spatial domain increases to about -26 dB. The result shown in this example, indeed, is the tradeoff between Doppler and spatial processing for the TB-based MIMO radar AF, and it newly verifies the validity of tradeoffs in the TB-based MIMO radar [49].

VI. CONCLUSION

In this paper, we have derived the AF for the recently proposed TB-based MIMO radar (namely, the TB-based MIMO radar AF) which allows obtaining waveform diversity and transmit coherent processing gains over a pre-defined angular sector simultaneously. Our definition is very general and contains the AFs for the PA, traditional MIMO, and TB-based

MIMO radars as important special cases under the standard assumption of far-field targets and narrow-band waveforms. This newly defined AF deals with less number of transmitted waveforms than the number of transmit antennas as compared to the standard MIMO radar configuration where different waveform is launched from each antenna. It has been shown to contribute to achieving lower relative AF sidelobe levels. Relationships among the TB-based MIMO radar AF defined in this paper and the previous AF works including the Woodward's AF, the AF defined for the traditional colocated MIMO radar, and the PA radar AF, have been established, respectively. We have compared our newly defined TB-based MIMO radar AF with the existing traditional MIMO radar AF, and have proposed a new TB design in order to give better relative AF sidelobe levels. Two limiting cases are identified to bound the "clear region" of the TB-based MIMO radar AF, and corresponding bounds for these two cases have been derived, respectively. We have also shown that the "clear region" for the worst bounding case is inversely proportional to the number of transmitted waveforms K , while the one for the best bounding case is independent of K . The "clear region" of the TB-based MIMO radar AF, which depends on the array configuration, is in between that of the worst and best cases. We have shown in the simulation results that the square-summation-form AF leads to higher relative AF sidelobe levels than that of the TB-based MIMO radar AF. Moreover, using the proposed convex optimization TB design, the levels can be further reduced.

REFERENCES

- [1] J. Li and P. Stoica, *MIMO Radar Signal Processing*. New York, NY, USA: Wiley, 2009.
- [2] A. M. Haimovich, R. S. Blum, and L. J. Cimini, "MIMO radar with widely separated antennas," *IEEE Signal Process. Mag.*, vol. 24, no. 1, pp. 116–129, Jan. 2008.
- [3] J. Li and P. Stoica, "MIMO radar with colocated antennas," *IEEE Signal Process. Mag.*, vol. 24, no. 5, pp. 106–114, Sep. 2007.
- [4] E. Fishler, A. Haimovich, R. S. Blum, L. Cimini, D. Chizhik, and R. Valenzuela, "Spatial diversity in radars—Models and detection performance," *IEEE Trans. Signal Process.*, vol. 54, no. 3, pp. 823–838, Mar. 2006.
- [5] E. Fishler, A. Haimovich, R. S. Blum, D. Chizhik, L. Cimini, and R. Valenzuela, "MIMO radar: An idea whose time has come," in *Proc. IEEE Radar Conf.*, Honolulu, HI, USA, Apr. 2004, pp. 71–78.
- [6] D. W. Bliss and K. W. Forsythe, "Multiple-input multiple-output MIMO radar and imaging: Degrees of freedom and resolution," in *Proc. Asilomar Conf. Signals, Syst., Comput.*, Pacific Grove, CA, USA, Nov. 2003, vol. 1, pp. 54–59.
- [7] I. Bekkerman and J. Tabrikian, "Target detection and localization using MIMO radar and sonars," *IEEE Trans. Signal Process.*, vol. 54, no. 10, pp. 3873–3883, Oct. 2006.
- [8] Y. I. Abramovich, G. J. Frazer, and B. A. Johnson, "Noncausal adaptive spatial clutter mitigation in monostatic MIMO radar: Fundamental limitations," *IEEE J. Sel. Topics Signal Process.*, vol. 4, no. 1, pp. 40–54, Feb. 2010.
- [9] J. Li, X. Zheng, and P. Stoica, "MIMO SAR imaging: Signal synthesis and receiver design," in *Proc. IEEE Int. Workshop. Comput. Adv. Multi-Sensor Adapt. Process.*, St. Thomas, VI, Dec. 2007, pp. 89–92.
- [10] G. Krieger, "MIMO-SAR: Opportunities and pitfalls," *IEEE Trans. Geosci. Remote Sens.*, vol. 52, no. 5, pp. 2628–2645, May 2014.
- [11] Y. Li, S. A. Vorobyov, and Z. He, "Joint hot and cold clutter mitigation in the transmit beamspace-based MIMO radar," in *Proc. IEEE Int. Conf. Acoust., Speech, Signal Process. (ICASSP)*, Brisbane, Australia, Apr. 2015, pp. 2334–2338.
- [12] Y. Li, S. A. Vorobyov, and A. Hassaniien, "MIMO radar capability on powerful jammers suppression," in *Proc. IEEE Int. Conf. Acoust., Speech, Signal Process. (ICASSP)*, Florence, Italy, May 2014, pp. 5277–5281.
- [13] Y. Li, S. A. Vorobyov, and A. Hassaniien, "Robust beamforming for jammers suppression in MIMO radar," in *Proc. IEEE Radar Conf.*, Cincinnati, OH, USA, May 2014, pp. 0629–0634.
- [14] D. R. Fuhrmann, J. P. Browning, and M. Rangaswamy, "Signaling strategies for the hybrid MIMO phased-array radar," *IEEE J. Sel. Topics Signal Process.*, vol. 4, no. 1, pp. 66–78, Sep. 2010.
- [15] A. Hassaniien and S. A. Vorobyov, "Transmit energy focusing for DOA estimation in MIMO radar with colocated antennas," *IEEE Trans. Signal Process.*, vol. 59, no. 6, pp. 2669–2682, June 2011.
- [16] D. R. Fuhrmann and G. San Antonio, "Transmit beamforming for MIMO radar systems using signal cross-correlation," *IEEE Trans. Aerosp. Electron. Syst.*, vol. 44, no. 1, pp. 171–186, Jan. 2008.
- [17] P. Stoica, J. Li, and Y. Xie, "On probing signal design for MIMO radar," *IEEE Trans. Signal Process.*, vol. 55, no. 8, pp. 4151–4161, Aug. 2007.
- [18] A. Hassaniien and S. A. Vorobyov, "Phased-MIMO radar: A tradeoff between phased-array and MIMO radars," *IEEE Trans. Signal Process.*, vol. 58, no. 6, pp. 3137–3151, June 2010.
- [19] A. Khabbazbasmenj, A. Hassaniien, S. A. Vorobyov, and M. W. Morency, "Efficient transmit beamspace design for search-free based DOA estimation in MIMO radar," *IEEE Trans. Signal Process.*, vol. 62, no. 6, pp. 1490–1500, Mar. 2014.
- [20] A. Khabbazbasmenj, S. A. Vorobyov, A. Hassaniien, and M. W. Morency, "Transmit beamspace design for direction finding in colocated MIMO radar with arbitrary receive array and even number of waveforms," in *Proc. Asilomar Conf. Signals, Syst., Comput.*, Pacific Grove, CA, USA, Nov. 2012, pp. 1307–1311.
- [21] A. Khabbazbasmenj, S. A. Vorobyov, and A. Hassaniien, "Transmit beamspace design for direction finding in colocated MIMO radar with arbitrary receive array," in *Proc. IEEE Int. Conf. Acoust., Speech, Signal Process. (ICASSP)*, Prague, Czech Republic, May 2011, pp. 2784–2787.
- [22] T. Aittomaki and V. Koivunen, "Low-complexity method for transmit beamforming in MIMO radars," in *Proc. IEEE Int. Conf. Acoust., Speech, Signal Process. (ICASSP)*, Honolulu, HI, USA, Apr. 2007, vol. II, pp. 305–308.
- [23] T. Aittomaki and V. Koivunen, "Signal covariance matrix optimization for transmit beamforming in MIMO radars," in *Proc. Asilomar Conf. Signals, Syst., Comput.*, Pacific Grove, CA, USA, Nov. 2007, pp. 182–186.
- [24] R. O. Schmidt, "Multiple emitter location and signal parameter estimation," *IEEE Trans. Antennas Propag.*, vol. 34, no. 3, pp. 276–280, Mar. 1986.
- [25] R. Roy and T. Kailath, "ESPRIT—Estimation of signal parameters via rotational invariance techniques," *IEEE Trans. Acoust., Speech, Signal Process.*, vol. 37, no. 7, pp. 984–995, July 1989.
- [26] P. M. Woodward, *Probability and Information Theory With Application to Radar*. Oxford, U.K.: Pergamon, 1953.
- [27] P. M. Woodward, "Radar ambiguity analysis," Royal Radar Establishment Ministry of Technology, Malvern, Worcestershire, U.K., RRE Technical Note, Feb. 1967.
- [28] R. Price and E. Hofstetter, "Bounds on the volume and height distributions of the ambiguity function," *IEEE Trans. Inf. Theory*, vol. 11, no. 2, pp. 207–214, Apr. 1965.
- [29] W. M. Siebert, "Studies of Woodward's uncertainty function," Electronics Res. Lab., M.I.T., Cambridge, MA, USA, Quart. Progress Rep., Apr. 1958.
- [30] R. O. Harger, "An optimum design of ambiguity function, antenna pattern, and signal for side-looking radars," *IEEE Trans. Mil. Electron.*, vol. 9, no. 3, pp. 264–278, July 1965.
- [31] G. San Antonio, D. R. Fuhrmann, and F. C. Robey, "MIMO radar ambiguity functions," *IEEE J. Sel. Topics Signal Process.*, vol. 1, no. 1, pp. 167–177, Jun. 2007.
- [32] C.-Y. Chen and P. P. Vaidyanathan, "MIMO radar ambiguity properties and optimization using frequency-hopping waveforms," *IEEE Trans. Signal Process.*, vol. 56, no. 12, pp. 5926–5936, Dec. 2008.
- [33] Y. I. Abramovich and G. J. Frazer, "Bounds on the volume and height distributions for the MIMO radar ambiguity function," *IEEE Signal Process. Lett.*, vol. 15, pp. 505–508, 2008.

- [34] Y. Li, S. A. Vorobyov, and V. Koivunen, "Generalized ambiguity function for the MIMO radar with correlated waveforms," in *Proc. IEEE Int. Conf. Acoust., Speech, Signal Process. (ICASSP)*, Florence, Italy, May 2014, pp. 5302–5306.
- [35] N. Levanon and E. Mozeson, *Radar Signals*. Hoboken, NJ, USA: Wiley, 2004.
- [36] M. Soltanalian, H. Hu, and P. Stoica, "Single-stage transmit beamforming design for MIMO radar," *Signal Process.*, vol. 102, pp. 132–138, Mar. 2014.
- [37] W. Rowe, P. Stoica, and J. Li, "Spectrally constrained waveform design," *IEEE Signal Process. Mag.*, vol. 31, no. 3, pp. 157–162, May 2014.
- [38] K. W. Forsythe and D. W. Bliss, "MIMO radar waveform constraints for GMTI," *IEEE J. Sel. Topics Signal Process.*, vol. 4, no. 1, pp. 21–32, Feb. 2010.
- [39] Y. Yang and R. S. Blum, "MIMO radar waveform design based on mutual information and minimum mean-square error estimation," *IEEE Trans. Aerosp. Electron. Syst.*, vol. 43, no. 1, pp. 330–343, Jan. 2007.
- [40] J. Li, P. Stoica, and X. Zheng, "Signal synthesis and receiver design for MIMO radar imaging," *IEEE Trans. Signal Process.*, vol. 56, no. 8, pp. 3959–3968, Aug. 2008.
- [41] H. Deng, "Polyphase code design for orthogonal netted radar systems," *IEEE Trans. Signal Process.*, vol. 52, no. 11, pp. 3126–3135, Nov. 2004.
- [42] D. J. Rabideau, "Adaptive MIMO radar waveforms," in *Proc. IEEE Radar Conf.*, Rome, Italy, May 2008, pp. 1–6.
- [43] X. Song, S. Zhou, and P. Willett, "Reducing the waveform cross correlation of MIMO radar with space-time coding," *IEEE Trans. Signal Process.*, vol. 58, no. 8, pp. 4213–4224, Aug. 2010.
- [44] C. Ma, T. S. Yeo, C. S. Tan, Y. Qiang, and T. Zhang, "Receiver design for MIMO radar range sidelobe suppression," *IEEE Trans. Signal Process.*, vol. 58, no. 10, pp. 5469–5474, Oct. 2010.
- [45] G. Hua and S. S. Abeysekera, "Receiver design for range and sidelobe suppression using MIMO and phased-array radar," *IEEE Trans. Signal Process.*, vol. 61, no. 6, pp. 1315–1326, Mar. 2013.
- [46] H. L. Van Trees, *Optimum Array Processing*. New York, NY, USA: Wiley, 2002.
- [47] G. Xu, S. D. Silverstein, R. H. Roy, and T. Kailath, "Beamspace ESPRIT," *IEEE Trans. Signal Process.*, vol. 42, no. 2, pp. 349–356, Feb. 1994.
- [48] M. Grant and S. Boyd, CVX: Matlab software for disciplined convex programming, ver. 2.1, Sep. 2014 [Online]. Available: <http://cvxr.com/cvx>
- [49] S. A. Vorobyov and M. Lops, "Tradeoffs in MIMO radar," in *Tutorial in 8th IEEE Sensor Array and Multichannel Signal Process. Workshop*, A Coruña, Spain, Jun. 2014 [Online]. Available: http://www.gtcc.udc.es/sam2014/images/sam2014/tutorials/slides_tutorial_tradeoffs_mimo_radar_sam_2014_v2.pdf



Yongzhe Li (S'12) received his B.Eng. degree in electronic engineering in 2008 from University of Electronic Science and Technology of China (UESTC), Chengdu, China.

He is currently finalizing his D.Sc. degree at the Department of Signal Processing and Acoustics, Aalto University, Finland and Ph.D. degree at the Department of Electronic Engineering, UESTC, China. His research interests include statistical and array signal processing, radar signal processing, and optimization.

Mr. Li is a recipient of the Distinguished Graduate Award of UESTC in 2008 and the State Scholarship of China Scholarship Council (CSC) from 2013 to 2015.



Sergiy A. Vorobyov (M'02–SM'05) received the M.Sc. and Ph.D. degrees in systems and control from Kharkiv National University of Radio Electronics, Ukraine, in 1994 and 1997, respectively.

He is a Professor with the Department of Signal Processing and Acoustics, Aalto University, Finland. He has been previously with the University of Alberta, Alberta, Canada as an Assistant Professor from 2006 to 2010, Associate Professor from 2010 to 2012, and became Full Professor there in 2012. Since his graduation, he also held various research and faculty

positions at Kharkiv National University of Radio Electronics, Ukraine; the Institute of Physical and Chemical Research (RIKEN), Japan; McMaster University, Canada; Duisburg-Essen University and Darmstadt University of Technology, Germany; and the Joint Research Institute between Heriot-Watt University and Edinburgh University, U.K. He has also held short-term visiting positions at Technion, Haifa, Israel and Ilmenau University of Technology, Ilmenau, Germany. His research interests include statistical and array signal processing; optimization and linear algebra methods in signal processing, communications, and machine learning; sparse signal processing; estimation and detection theory; sampling theory; multi-antenna, large, cooperative, and cognitive systems.

Dr. Vorobyov is a recipient of the 2004 IEEE Signal Processing Society Best Paper Award, the 2007 Alberta Ingenuity New Faculty Award, the 2011 Carl Zeiss Award (Germany), the 2012 NSERC Discovery Accelerator Award, and other awards. He served as an Associate Editor for the IEEE TRANSACTIONS ON SIGNAL PROCESSING from 2006 to 2010 and for the IEEE TRANSACTIONS ON SIGNAL PROCESSING LETTERS from 2007 to 2009. He was a member of the Sensor Array and Multi-Channel Signal Processing Committee of the IEEE Signal Processing Society from 2007 to 2012. He is a member of the Signal Processing for Communications and Networking Committee since 2010. He has served as the Track Chair for Asilomar 2011, Pacific Grove, CA, the Technical Co-Chair for IEEE CAMSAP 2011, Puerto Rico, and the Tutorial Chair for ISWCS 2013, Ilmenau, Germany.



Visa Koivunen (F'11) received his D.Sc. (EE) degree with honors from the University of Oulu, Department of Electrical Engineering. He received the *primus doctor* (best graduate) award among the doctoral graduates in years 1989–1994. He is a member of Eta Kappa Nu. From 1992 to 1995 he was a visiting researcher at the University of Pennsylvania, Philadelphia, USA. Years 1997–1999 he was faculty at Tampere UT. Since 1999 he has been a full Professor of Signal Processing at Aalto University (formerly known as Helsinki Univ of

Technology), Finland. He received the Academy professor position. He was one of the Principal Investigators in SMARAD Center of Excellence in Research nominated by the Academy of Finland. Years 2003–2006 he has been also adjunct full professor at the University of Pennsylvania, Philadelphia, USA. During his sabbatical term year 2007 he was a Visiting Fellow at Princeton University, NJ, USA. He has also been a part-time Visiting Fellow at Nokia Research Center (2006–2012). He spent a sabbatical at Princeton University for the full academic year 2013–2014.

Dr. Koivunen's research interest include statistical, communications, sensor array and multichannel signal processing. He has published about 350 papers in international scientific conferences and journals. He co-authored the papers receiving the best paper award in IEEE PIMRC 2005, EUSIPCO'2006, EUCAP (European Conference on Antennas and Propagation) 2006 and COCORA 2012. He has been awarded the IEEE Signal Processing Society best paper award for the year 2007 (with J. Eriksson). He served as an associate editor for IEEE SIGNAL PROCESSING LETTERS, IEEE TRANSACTIONS ON SIGNAL PROCESSING, *Signal Processing* and *Journal of Wireless Communication and Networking*. He is co-editor for IEEE JSTSP special issue on Smart Grids and a member of editorial board for *IEEE Signal Processing Magazine*. He has been a member of the IEEE SPS technical committees SPCOM-TC and SAM-TC. He was the general chair of the IEEE SPAWC conference 2007 conference in Helsinki, Finland, June 2007. He is the Technical Program Chair for the IEEE SPAWC 2015 as well as Array Processing track chair for 2014 Asilomar conference. He is the recipient of the EURASIP Technical Achievement Award in 2015.

Publication II

Yongzhe Li, Sergiy A. Vorobyov and Visa Koivunen. Generalized ambiguity function for the MIMO radar with correlated waveforms. In *IEEE International Conference on Acoustics, Speech, and Signal Processing (ICASSP)*, Florence, Italy, pp. 5302–5306, May 2014.

© 2014 IEEE.

Reprinted with permission.

GENERALIZED AMBIGUITY FUNCTION FOR THE MIMO RADAR WITH CORRELATED WAVEFORMS

Yongzhe Li^{*†}, Sergiy A. Vorobyov^{†‡}, and Visa Koivunen[†]

^{*}Dept. EE, University of Electronic Science and Technology of China, Chengdu, 611731, China

[†]Dept. Signal Processing and Acoustics, Aalto University, PO Box 13000, FI-00076 Aalto, Finland

[‡]Dept. Electrical and Computer Engineering, University of Alberta, Edmonton, AB T6G 2V4, Canada

Emails: lyzlyz888@gmail.com/yongzhe.li@aalto.fi, svor@ieee.org, visa.koivunen@aalto.fi

ABSTRACT

An ambiguity function (AF) for the multiple-input multiple-output (MIMO) radar with correlated waveforms is derived. It serves as a generalized AF for which the phased-array and the traditional MIMO radar AFs are important special cases. A simplified expression for the AF for the case of far-field targets and narrow-band waveforms is also derived. We establish relationships between the generalized MIMO radar AF metric and the previous works on AF including the Woodward's AF and the AF defined for the traditional colocated MIMO radar. Moreover, we compare the AF of the MIMO radar with correlated waveforms with the squared-summation-form AF definition. Simulation results show that the generalized MIMO radar AF achieves lower relative sidelobe level with proper design of the waveform correlation matrix or, equivalently, the transmit beamspace matrix.

Index Terms— Ambiguity function, correlated waveforms, generalized, MIMO radar, transmit beamspace.

1. INTRODUCTION

Recently, the multiple-input multiple-output (MIMO) radar has become the focus of intensive research [1]–[3]. Despite the benefits due to the use of waveform diversity [3], the traditional MIMO radar with colocated transmit antenna elements suffers from the loss of coherent processing gain that can be achieved in the phased-array (PA) radar system [4]. The transmit beampattern can be formed by designing a proper correlation matrix for the waveforms at the transmitter [5]–[7]. Such waveform correlation matrix design can be simplified to transmit beamspace (TB) matrix design (see for example [8]). It allows to achieve the coherent processing gain by focusing the energy of multiple transmitted orthogonal waveforms within a certain angular sector where a target is likely to be

located using beamforming techniques [4], [8]. For the MIMO radar systems, accurate estimation and detection capabilities are critically important. For example, one important task is to estimate the direction-of-arrivals of potential targets utilizing the extra degrees-of-freedom offered by the MIMO radar. To efficiently characterize the resolution performance, ambiguity function (AF) [9]–[13] can be employed. There are some works on the traditional MIMO radar AF [11]–[13], and their starting point is the well-known Woodward's AF [9], [10]. The research questions of great significance are to see how the AF of the MIMO radar with correlated waveforms behaves, and what the relationships with the previous works on AF are.

In this paper, we define the AF for the MIMO radar with correlated waveforms, in which the phase shift information conveyed by the target echo is contained. This phase shift results from the array geometry and the relative position between the target and the transmit/receive colocated array. Equivalent phase centers are used for its calculation. Moreover, we derive a simplified AF expression for the case of far-field targets and narrow-band waveforms. Based on this expression relationships between the AF of the MIMO radar with correlated waveforms and the previous works on AF are established. It can be utilized as a generalized AF for the PA and traditional MIMO radars, as well as the MIMO radar with correlated waveforms. We propose a method to reduce the relative sidelobe level of the AF and compare it with the traditional MIMO radar AF defined in [13] by simulations.

2. SIGNAL MODEL

Consider a colocated MIMO radar system with a transmit array of M antenna elements and a receive array of N antenna elements. The complex envelope of the transmitted waveforms in the case of the traditional MIMO radar can be modeled as $s_m(t) = \sqrt{E/M}\phi_m(t)$, $m = 1, 2, \dots, M$ where E is the total transmit energy, t is the continuous time index, i.e., time within the pulse, and $\phi_m(t)$ is the m th orthogonal baseband waveform. Without loss of generality, we assume that the transmitted waveforms are normalized to have unit-energy, i.e., $\int_T |\phi_m(t)|^2 dt = 1$, $m = 1, 2, \dots, M$ where T is the time

Y. Li's work is supported by China Scholarship Council while he is visiting Aalto University, and by the Fundamental Research Funds for the Central Universities of China under Contract ZYGX2010YB007, and the National Nature Science Foundation of China under Grant 61032010. This work is also supported in part by the Natural Science and Engineering Research Council (NSERC), Canada.

duration of the pulse.

In the MIMO radar with correlated waveforms formulated using the TB matrix design, K (in general, $K \leq M$) initially orthogonal waveforms are transmitted. For each waveform, a transmit beam is formed by illuminating a particular area within an angular sector Ω . The signal radiated towards the target that is located at the spatial direction θ via the k th transmit beam can be modeled as [8]

$$s_k(t) = \sqrt{\frac{E}{K}} \mathbf{c}_k^T \mathbf{a}(\theta) \phi_k(t), \quad k = 1, 2, \dots, K \quad (1)$$

where $\mathbf{a}(\theta)$ is the transmit array steering vector, \mathbf{c}_k denotes the k th column of the $M \times K$ TB matrix \mathbf{C} which is defined as $\mathbf{C} \triangleq [\mathbf{c}_1, \dots, \mathbf{c}_K]$, and $(\cdot)^T$ stands for the transpose operation. Each column of \mathbf{C} with M elements is designed to form a certain transmit beam within the sector-of-interest Ω , and it corresponds to one of the K transmitted waveforms. Let c_{mk} be the m th element of \mathbf{c}_k , then the signal $\tilde{s}_m(t)$ radiated by the m th antenna element can be expressed as

$$\tilde{s}_m(t) = \sqrt{\frac{E}{K}} \sum_{k=1}^K c_{mk} \phi_k(t), \quad m = 1, \dots, M. \quad (2)$$

The transmitted energy focused within the sector-of-interest Ω can be maximized by properly designing the TB matrix \mathbf{C} .

3. GENERALIZED MIMO RADAR AF WITH CORRELATED WAVEFORMS

3.1. AF Definition

Let a point target be described by the parameter Θ which contains the information of the target position vector \mathbf{p} and the velocity vector \mathbf{v} . Based on (2), the received signal at the j th receive antenna element after demodulation to the base band can be written as (3), shown at the bottom of this

page. Here α_{mj} denotes the complex reflection coefficient for the (m, j) th transmit-receive channel, $\tau_{mj}(\mathbf{p})$ is the two-way time delay due to a target located at \mathbf{p} , f_c is the operating frequency, $f_{mj}(\Theta)$ is the Doppler shift associated with the (m, j) th transmit-receive channel for the target characterized by the parameter Θ and $z_j(t)$ is the white Gaussian noise observed at the j th receive antenna element with power σ_z^2 .

At the receiving end, $\hat{r}_j(t, \Theta)$ is matched to each of the waveforms $\phi_k(t)$, $k = 1, \dots, K$ with a specific target parameter Θ' due to the fact that it is composed of the cumulative echoes of the known transmitted waveforms. Thus, the received signal component $\bar{r}'_{ji}(\Theta, \Theta')$ that is associated with the i th transmitted waveform can be obtained as (4), shown at the bottom of this page. Here $(\cdot)^*$ is the conjugate operator, $q(i)$ is the equivalent phase center for the i th transmitted waveform and $\bar{z}_{ji}(t)$ is the noise after matched filtering.

We define the AF as the square of the coherent summation of all noise-free matched filtering outputs $\bar{r}'_{ji}(\Theta, \Theta')$, $j = 1, \dots, N$ and $i = 1, \dots, K$. Then the AF of the MIMO radar with correlated waveforms can be mathematically expressed as (5), shown at the bottom of this page. Let us introduce an $M \times K$ matrix \mathbf{R} whose (m, i) th element is defined as (6), shown at the bottom of the next page. Using (6), the AF (5) can be expressed in a simplified form as (7), shown at the bottom of the next page.

The AF (7) is composed of summation terms, and each term contains two more components in addition to the complex reflection coefficient. One is the matched-filtered component denoted by (6), which stands for the effect of waveform correlation. The other is composed of the last two exponential terms in (7), which stands for the phase shift information caused by the relative position and velocity of the target with respect to the array geometry. It can also be understood as follows. The m th transmit antenna element emits a signal that is composed of all the K initially orthogonal waveforms windowed by the elements of the m th row in the TB matrix \mathbf{C} . Thus, the TB

$$\hat{r}_j(t, \Theta) = \sqrt{\frac{E}{K}} \sum_{m=1}^M \sum_{k=1}^K \alpha_{mj} c_{mk} \phi_k(t - \tau_{mj}(\mathbf{p})) \exp\{-j2\pi\tau_{mj}(\mathbf{p})(f_c + f_{mj}(\Theta))\} \exp\{j2\pi f_{mj}(\Theta)t\} + z_j(t) \quad (3)$$

$$\begin{aligned} \bar{r}'_{ji}(\Theta, \Theta') &= \int \hat{r}_j(t, \Theta) \phi_i^*(t, \Theta') dt = \sqrt{\frac{E}{K}} \sum_{m=1}^M \sum_{k=1}^K \alpha_{mj} \int c_{mk} \phi_k(t - \tau_{mj}(\mathbf{p})) \phi_i^*(t - \tau_{q(i)j}(\mathbf{p}')) \\ &\times \exp\{-j2\pi\tau_{mj}(\mathbf{p})(f_c + f_{mj}(\Theta))\} \exp\{j2\pi\tau_{q(i)j}(\mathbf{p}')(f_c + f_{q(i)j}(\Theta'))\} \exp\{j2\pi(f_{mj}(\Theta) - f_{q(i)j}(\Theta'))t\} dt \\ &+ \bar{z}_{ji}(t) \triangleq \bar{r}'_{ji}(\Theta, \Theta') + \bar{z}_{ji}(t) \end{aligned} \quad (4)$$

$$\begin{aligned} \chi(\Theta, \Theta') &\triangleq \left| \sum_{j=1}^N \sum_{i=1}^K \bar{r}'_{ji}(\Theta, \Theta') \right|^2 = \left| \sqrt{\frac{E}{K}} \sum_{j=1}^N \sum_{i=1}^K \sum_{m=1}^M \sum_{k=1}^K \alpha_{mj} \int c_{mk} \phi_k(t - \tau_{mj}(\mathbf{p})) \phi_i^*(t - \tau_{q(i)j}(\mathbf{p}')) \right. \\ &\times \exp\{-j2\pi\tau_{mj}(\mathbf{p})(f_c + f_{mj}(\Theta))\} \exp\{j2\pi\tau_{q(i)j}(\mathbf{p}')(f_c + f_{q(i)j}(\Theta'))\} \exp\{j2\pi(f_{mj}(\Theta) - f_{q(i)j}(\Theta'))t\} dt \left. \right|^2 \end{aligned} \quad (5)$$

matrix \mathbf{C} is playing a role of transforming the original $K \times K$ waveform covariance matrix to the $M \times K$ matrix \mathbf{R} . The main purpose of adding the phase shift information in (7) is to incorporate the property of coherent processing introduced by the array configuration. By properly designing the matrix \mathbf{C} and selecting the equivalent phase centers, the AF (7) can serve also as the AF for the PA and traditional MIMO radars.

3.2. Far-Field Targets and Narrow-Band Waveforms

One most common scenario that radar systems deal with is the case of far-field targets and narrow-band waveforms. The effect of the complex reflection coefficients in different transmit-receive channels can be neglected in this case because the contributions of different transmit-receive channels to the generalized MIMO radar AF are constant at any given time t . They remain constant even when considering multiple pulses and inter-pulse varying reflection coefficients, if long pulse width is employed and no range folding occurs [12].

Assume that the antenna elements of the transmit and receive arrays have locations $\{\mathbf{q}_{T,1}, \dots, \mathbf{q}_{T,M}\}$ and $\{\mathbf{q}_{R,1}, \dots, \mathbf{q}_{R,N}\}$, respectively, and the equivalent phase centers have locations $\{\mathbf{q}_{TE,1}, \dots, \mathbf{q}_{TE,K}\}$ whose elements are vectors in three-dimensional Cartesian coordinates. Let $\mathbf{u}(\Theta)$ be a unit-norm steering vector pointing from the transmit/receive array to the target with parameter Θ . Then the AF (7) can be simplified as

$$\chi(\Theta, \Theta') = |\mathbf{a}_R^H(\Theta) \mathbf{a}_R(\Theta')|^2 |\mathbf{a}_T^H(\Theta) \bar{\mathbf{R}} \mathbf{a}_{TE}(\Theta')|^2 \quad (8)$$

where the (m, i) th element of the $M \times K$ matrix $\bar{\mathbf{R}}$ is expressed as

$$\begin{aligned} [\bar{\mathbf{R}}]_{mi}(\Delta\tau, \Delta f_d, \mathbf{C}) & \quad (9) \\ &= \sqrt{\frac{E}{K}} \sum_{k=1}^K c_{mk} \int \phi_k(t) \phi_k^*(t - \Delta\tau) \exp\{j2\pi\Delta f_d t\} dt \end{aligned}$$

and $(\cdot)^H$ denotes the conjugate transpose. Here also $\Delta\tau \triangleq \tau(\mathbf{p}) - \tau(\mathbf{p}')$, $\Delta f_d \triangleq f(\Theta) - f(\Theta')$, and $\mathbf{a}_T(\Theta) \triangleq [\exp\{\tilde{\mathbf{u}}^T(\Theta) \mathbf{q}_{T,1}\}, \dots, \exp\{\tilde{\mathbf{u}}^T(\Theta) \mathbf{q}_{T,M}\}]^T$, $\mathbf{a}_R(\Theta) \triangleq [\exp\{\tilde{\mathbf{u}}^T(\Theta) \mathbf{q}_{R,1}\}, \dots, \exp\{\tilde{\mathbf{u}}^T(\Theta) \mathbf{q}_{R,N}\}]^T$, $\mathbf{a}_{TE}(\Theta) \triangleq [\exp\{\tilde{\mathbf{u}}^T(\Theta) \mathbf{q}_{TE,1}\}, \dots, \exp\{\tilde{\mathbf{u}}^T(\Theta) \mathbf{q}_{TE,K}\}]^T$ are the $M \times 1$ transmit array steering vector, the $N \times 1$ receive array

steering vector, and the $K \times 1$ equivalent transmit array steering vector, respectively, with $\tilde{\mathbf{u}}(\Theta) \triangleq j2\pi f'(\Theta) \cdot \mathbf{u}(\Theta)/c$ and $f'(\Theta) \triangleq f_c + f(\Theta)$. The dependence of $\bar{\mathbf{R}}$ from $\Delta\tau, \Delta f_d$, and \mathbf{C} is not shown in (8) for brevity, and the subscript indices for τ and f are omitted for the far-field narrow-band case.

3.3. Relationships With Other AFs

Let the $K \times K$ matrix $\bar{\chi}(\tau, f_d)$ be the AF matrix of the K orthogonal waveforms, whose (j, k) th element is given by

$$[\bar{\chi}]_{jk}(\tau, f_d) = \int \phi_j(t) \phi_k^*(t - \tau) \exp\{j2\pi f_d t\} dt. \quad (10)$$

Using (9) and (10), the simplified AF (8) can be expressed as

$$\begin{aligned} \chi(\Theta, \Theta') &= \frac{E}{K} |\mathbf{a}_R^H(\Theta) \mathbf{a}_R(\Theta')|^2 \quad (11) \\ &\quad \times |\mathbf{a}_T^H(\Theta) \mathbf{C} \bar{\chi}(\Delta\tau, \Delta f_d) \mathbf{a}_{TE}(\Theta')|^2 \end{aligned}$$

where $\bar{\chi}(\Delta\tau, \Delta f_d)$ is the $K \times K$ matrix whose elements are given by (10). Considering that $\Delta\tau$ and Δf_d depend on Θ and Θ' , we employ these two parameters to denote the AF of the MIMO radar with correlated waveforms.

Equation (11) establishes the connection between the generalized MIMO radar AF and the well known Woodward's AF. If the number of transmitted waveforms K is increased to M , \mathbf{C} is simply the identity matrix \mathbf{I}_M , and the equivalent phase centers are selected to be the positions of the M transmit antenna elements, then the AF (11) becomes

$$\begin{aligned} \chi_{\text{MIMO}}(\Theta, \Theta') &= \frac{E}{M} |\mathbf{a}_R^H(\Theta) \mathbf{a}_R(\Theta')|^2 \quad (12) \\ &\quad \times |\mathbf{a}_T^H(\Theta) \bar{\chi}(\Delta\tau, \Delta f_d) \mathbf{a}_T(\Theta')|^2. \end{aligned}$$

Expression (12) denotes the traditional MIMO radar AF and has the same form as the definition in [11] except for the magnitude term. This term represents the general expression of the transmit power allocation for the traditional MIMO radar. Therefore, if E is selected to be equal to M , then the expression (12) and the AF definition [11] have identical expressions. Furthermore, the generalized MIMO radar AF (11) is also related to the traditional MIMO radar AF with K uniform subarrays [14]. In this case, \mathbf{C} is designed as a block diagonal matrix whose block elements are associated with the

$$[\mathbf{R}]_{mi}(\Theta, \Theta', \mathbf{C}, j) \triangleq \sqrt{\frac{E}{K}} \sum_{k=1}^K c_{mk} \int \phi_k(t - \tau_{mj}(\mathbf{p})) \phi_k^*(t - \tau_{q(i)j}(\mathbf{p}')) \exp\{j2\pi(f_{mj}(\Theta) - f_{q(i)j}(\Theta'))t\} dt \quad (6)$$

$$\begin{aligned} \chi(\Theta, \Theta') & \quad (7) \\ &= \left| \sum_{j=1}^N \sum_{i=1}^K \sum_{m=1}^M \alpha_{mj} [\mathbf{R}]_{mi}(\Theta, \Theta', \mathbf{C}, j) \exp\{-j2\pi\tau_{mj}(\mathbf{p})(f_c + f_{mj}(\Theta))\} \exp\{j2\pi\tau_{q(i)j}(\mathbf{p}')(f_c + f_{q(i)j}(\Theta'))\} \right|^2 \end{aligned}$$

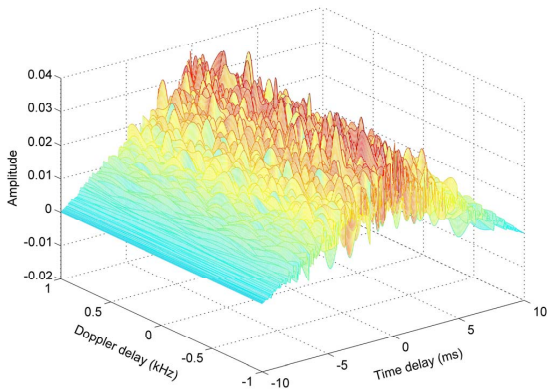


Fig. 1. Difference between the AF (8) and that defined in [13].

subarrays. The corresponding equivalent phase centers are selected as the centers of the subarrays. When K is selected as 1, the generalized MIMO radar AF (11) also boils down to the PA radar AF. Consequently, the AF defined in this paper serves as a unified definition of AF, and it links to the Woodward's AF by using the expression of the Woodward's AF matrix.

For the MIMO radar with correlated waveforms, if each coherent processing gain $\Upsilon_j \triangleq \mathbf{a}_T^H(\Theta)\mathbf{c}_j$, $j \in \{1, \dots, K\}$ is designed to have constant magnitude, then the rotational invariance property [15], [16] holds. Hence, we can design the TB matrix \mathbf{C} to guarantee that the j th coherent processing gain and the j th element of the equivalent transmit array steering vector have opposite phases, i.e., $\angle \Upsilon_j = -\angle \mathbf{a}_{TE,j}(\Theta)$, $j \in \{1, \dots, K\}$, in order to reduce the effect of the relative sidelobes of the generalized MIMO radar AF.

4. SIMULATION RESULTS

Throughout our simulations, we assume uniform linear arrays of $M = 8$ omni-directional transmit antennas and $N = 8$ receive antennas spaced half a wavelength apart. Both the transmit and receive arrays are located at the same position on the x -axis. The total transmit energy is fixed to $E = M$. Polyphase-coded sequences [17] are employed as the transmitted waveforms. The code length of each waveform is 256. We employ a single pulse whose pulse width is selected to be $T = 10$ ms to simulate the AF. The time-bandwidth product is set to be $BT = 128$, and the sampling rate is set to be $f_s = 2B$. Two targets are assumed to be located on the y -axis, sharing the same spatial angle $\theta = 0^\circ$. The simulated AFs for the case of far-field targets and narrow-band waveforms are normalized to their maximal value.

In the first example, we investigate the difference between the generalized MIMO radar AF metric defined in this paper and the AF metric defined in [13]. 8 waveforms for the traditional MIMO radar case are employed, and the TB matrix \mathbf{C} is given as the identity matrix \mathbf{I}_M . It can be seen that the differ-

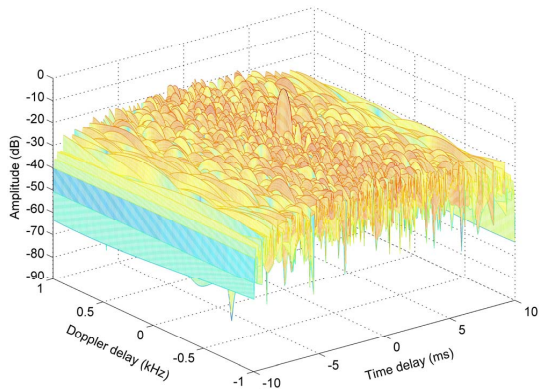


Fig. 2. Generalized MIMO radar AF with 4 waveforms.

ences are nearly all above zero, which means that the relative sidelobe level of the AF in [13] is higher than that obtained using the AF (8). The largest difference of the relative sidelobe level reaches 4% of the normalized AF metric peak (i.e., 1), demonstrating that the AF (8) gives a better relative sidelobe level than that in [13]. This means that the maximum possible region which is free of sidelobes achieved in the generalized AF for the MIMO radar with correlated waveforms is always larger than that achieved in the AF in [13].

In the second example, we present the generalized MIMO radar AF with $K = 4$ waveforms. The first 4 waveforms used in the first example are exploited. The TB matrix \mathbf{C} of size 8×4 is designed to meet the aforementioned condition that the rotational invariance property at the receive array holds. It can be seen that the mainlobe peak of the generalized MIMO radar AF is obtained at the point $(0, 0)$, i.e., no time and Doppler delays for the two targets. The relative sidelobe level of the generalized MIMO radar AF in this case ranges from -50 dB to -20 dB. The thumbtack shape of the AF clearly demonstrates how the AF of the generalized MIMO radar with 4 orthogonal transmitted waveforms behaves.

5. CONCLUSIONS

We have derived the AF for the MIMO radar with correlated waveforms that facilitates obtaining waveform diversity and coherent processing gain simultaneously. Our definition generalizes the AFs for the PA and traditional MIMO radars, as well as the AF of the MIMO radar with correlated waveforms. A simplified AF expression for the case of far-field targets and narrow-band waveforms is obtained. We have established the relationships between the generalized AF defined in this paper and the previous works on AF including the Woodward's AF and the AF for the traditional MIMO radar. It is shown that the proposed generalized MIMO radar AF can achieve lower relative sidelobe level by properly designing the TB matrix or, equivalently, the waveform correlation matrix.

6. REFERENCES

- [1] J. Li and P. Stoica, *MIMO Radar Signal Processing*. New York: Wiley, 2009.
- [2] A. M. Haimovich, R. S. Blum, and L. J. Cimini, "MIMO radar with widely separated antennas," *IEEE Signal Processing Magaz.*, vol. 24, no. 1, pp. 116–129, Jan. 2008.
- [3] J. Li and P. Stoica, "MIMO radar with colocated antennas," *IEEE Signal Processing Magaz.*, vol. 24, no. 5, pp. 106–114, Sep. 2007.
- [4] A. Hassanien and S. A. Vorobyov, "Phased-MIMO radar: A tradeoff between phased-array and MIMO radars," *IEEE Trans. Signal Processing*, vol. 58, no. 6, pp. 3137–3151, June 2010.
- [5] D. R. Fuhrmann and G. S. Antonio, "Transmit beamforming for MIMO radar systems using signal cross-correlation," *IEEE Trans. Aerosp. Electron. Syst.*, vol. 44, no. 1, pp. 171–186, Jan. 2008.
- [6] P. Stoica, J. Li and Y. Xie, "On probing signal design for MIMO radar," *IEEE Trans. Signal Processing*, vol. 55, no. 8, pp. 4151–4161, Aug. 2007.
- [7] T. Aittomaki and V. Koivunen, "Low-complexity method for transmit beamforming in MIMO radars," in *Proc. IEEE Int. Conf. Acoust., Speech, Signal Processing*, Honolulu, Hawaii, Apr. 2007, pp. II-305–II-308.
- [8] A. Hassanien and S. A. Vorobyov, "Transmit energy focusing for DOA estimation in MIMO radar with colocated antennas," *IEEE Trans. Signal Processing*, vol. 59, no. 6, pp. 2669–2682, June 2011.
- [9] R. Price and E. Hofstetter, "Bounds on the volume and height distributions of the ambiguity function," *IEEE Trans. Information Theory*, vol. 11, no. 2, pp. 207–214, Apr. 1965.
- [10] W. M. Siebert, "Studies of Woodward's uncertainty function," Electronics Research Lab., M.I.T., Cambridge Massachusetts, MA, Quarterly Progress Rep., Apr. 15, 1958, pp. 90–94.
- [11] G. S. Antonio, D. R. Fuhrmann and F. C. Robey, "MIMO Radar Ambiguity Functions," *IEEE Journal Selected Topics Signal Processing*, vol. 1, no. 1, pp. 167–177, June 2007.
- [12] C-Y. Chen and P. P. Vaidyanathan, "MIMO radar ambiguity properties and optimization using frequency-hopping waveforms," *IEEE Trans. Signal Processing*, vol. 56, no. 12, pp. 5926–5936, Dec. 2008.
- [13] Y. I. Abramovich and G. J. Frazer, "Bounds on the Volume and Height Distributions for the MIMO Radar Ambiguity Function," *IEEE Signal Processing Letters*, vol. 15, pp. 505–508, 2008.
- [14] D. R. Fuhrmann, J. P. Browning, and M. Rangaswamy, "Signaling strategies for the hybrid MIMO phased-array radar," *IEEE J. Sel. Topics Signal Processing*, vol. 4, no. 1, pp. 66–78, Feb. 2010.
- [15] A. Khabbazibasmenj, S. A. Vorobyov, A. Hassanien, and M. W. Morency, "Transmit beamspace design for direction finding in colocated MIMO radar with arbitrary receive array and even number of waveforms," in *Proc. Asilomar Conf. Signals, Syst., Comput.*, Asilomar, Pacific Grove, CA, USA, Nov. 2012, pp. 1307–1311.
- [16] A. Khabbazibasmenj, S. A. Vorobyov, and A. Hassanien, "Transmit beamspace design for direction finding in colocated MIMO radar with arbitrary receive array," in *Proc. IEEE Int. Conf. Acoust., Speech, Signal Processing*, Prague, Czech Republic, May 2011, pp. 2784–2787.
- [17] N. Levanon and E. Mozeson, *Radar Signals*. Hoboken, NJ, USA: Wiley, 2004.

Publication III

Yongzhe Li, Sergiy A. Vorobyov and Zishu He. Terrain-scattered jammer suppression in MIMO radar using space-(fast) time adaptive processing. In *IEEE International Conference on Acoustics, Speech, and Signal Processing (ICASSP)*, Shanghai, China, pp. 3026–3030, March 2016.

© 2016 IEEE.

Reprinted with permission.

TERRAIN-SCATTERED JAMMER SUPPRESSION IN MIMO RADAR USING SPACE-(FAST) TIME ADAPTIVE PROCESSING

Yongzhe Li^{†‡}, Sergiy A. Vorobyov[†], and Zishu He[‡]

[†]Dept. Signal Processing and Acoustics, Aalto University, P.O. Box 13000, FI-00076 Aalto, Finland

[‡]Dept. EE, University of Electronic Science and Technology of China, Chengdu, 611731, China

Emails: lyzlyz888@gmail.com/yongzhe.li@aalto.fi, svor@ieee.org, zshe@uestc.edu.cn

ABSTRACT

We address the problem of terrain-scattered jammer suppression in multiple-input multiple-output (MIMO) radar using space-(fast) time adaptive processing (SFTAP). The correlation function of jamming components after matched filtering at the receiving end of MIMO radar is derived, and its relationship to the correlation matrix of the transmitted waveforms is established. This correlation function serves as a theoretical measure of evaluating the matched filtering effect on the received jamming signals. We propose a minimum variance distortionless response (MVDR) type SFTAP design by taking into account the factors of waveform-introduced range sidelobes and cold clutter stationarity over different pulse intervals. A closed-form solution to this design is derived by means of the method of Lagrange multipliers. We also propose a relaxed SFTAP design by modifying the constraints of the MVDR type design. Both proposed SFTAP designs can support further slow-time Doppler processing procedure. Simulation results show the validity of our SFTAP designs.

Index Terms—Jammer suppression, MIMO radar, space-(fast) time adaptive processing (SFTAP).

1. INTRODUCTION

The multiple-input multiple-output (MIMO) radar has become a research field of significant interest in recent years [1]–[12]. Many benefits enabled by MIMO radar such as improved parameter identifiability and angular resolution [1], extended array aperture by virtual sensors [4], and increased opportunities for clutter and jammer mitigation [5], [13]–[15] have been explored. One of the most important factors that contribute to these benefits is the significantly increased number of degrees of freedom (DOFs) [4], which motivates researchers to use this characteristic in various classic topics that have been studied for phased-array radar. The terrain-scattered or diffuse jamming multipath suppression [16]–[20] in the presence of backscattered radar ground clutter (i.e., cold clutter) is an important example of such research topics. Jamming signals can be scattered off greatly when the surface of the ground region becomes diffuse, which results in strong correlations of jamming signals over fast-time domain. Therefore,

fast-time processing or space-time adaptive processing (STAP) techniques [21], [22] are needed.

Since pure mutual orthogonality of multiple waveforms does not exist in MIMO radar [10], [12], it is necessary to study the effect of matched filtering on the received jamming signals before applying STAP techniques. Despite of the opportunity introduced by the extra DOFs, MIMO radar also faces the challenge of significantly increased computational burden. Therefore, it is worth developing proper STAP techniques for MIMO radar. Three-dimensional STAP dealing with joint clutter mitigation has been studied in [15]. Here we develop two-dimensional space-(fast) time adaptive processing (SFTAP) techniques for jammer suppression, through which the cold clutter stationarity can be maintained.

In this paper, we study the problem of terrain-scattered jammer suppression using SFTAP approach and derive a correlation function of the match-filtered jamming components which establishes relationship to the correlation matrix of the transmitted waveforms. This correlation function can serve as a measure of evaluating the matched filtering effect on the received jamming signals. We consider two important factors including range sidelobes resulted from the actual transmitted waveforms and the cold clutter stationarity over different pulse intervals. For a certain pulse, we null the range sidelobes resulted from the transmitted waveforms towards the target direction, and enable the stationarity of the output cold clutter by enforcing its output power to be equal to that of the starting pulse. Based on this idea, a minimum variance distortionless response (MVDR) type SFTAP design is proposed. We derive a closed-form solution to the design utilizing the method of Lagrange multipliers. Considering that a closed-form solution does not always exist, especially when the weight vector subspace defined by the constraints of the design is empty, we propose an alternative SFTAP design by relaxing equality constraints into inequality ones.

2. SIGNAL MODEL

Consider a colocated MIMO radar system equipped with a transmit array of M antenna elements and a receive array of N antenna elements. Both arrays are assumed to be closely located so that they share an identical spatial angle for a far-

field target. Let $\phi(t) \triangleq [\phi_1(t), \dots, \phi_M(t)]^T$ be the $M \times 1$ vector that contains the complex envelopes of the transmitted waveforms $\phi_i(t)$, $i = 1, \dots, M$ for a given fast time t where $(\cdot)^T$ is the transpose operator. Each waveform has unit energy over the whole pulse duration T_p . The general model for the $N \times 1$ vector of the receive array observations at the fast time t within the τ th pulse can be expressed as

$$\mathbf{x}(t, \tau) = \mathbf{x}_t(t, \tau) + \mathbf{x}_c(t, \tau) + \mathbf{x}_j(t, \tau) + \mathbf{x}_n(t, \tau) \quad (1)$$

where the components on the right hand side, which are all $N \times 1$ vectors, denote the received signals of the target, clutter, jamming, and noise, respectively. These components are generally uncorrelated to each other. The target and backscattered radar clutter are expressed as¹

$$\mathbf{x}_t(t, \tau) = \sqrt{\frac{E}{M}} \alpha_t D_t(\tau) (\mathbf{a}^T(\theta_t) \phi(t - \zeta_0)) \mathbf{b}(\theta_t) \quad (2)$$

$$\mathbf{x}_c(t, \tau) = \sqrt{\frac{E}{M}} \sum_{i=1}^{N_c} \xi_i D_i(\tau) (\mathbf{a}^T(\theta_i) \phi(t - \zeta_0)) \mathbf{b}(\theta_i) \quad (3)$$

respectively, where E is the transmit energy, ζ_0 is the fast-time delay of the range of interest which is separated into N_c patches, θ_t and θ_i are spatial angles of the target and the i th clutter patch, respectively, α_t and ξ_i are the complex reflection coefficients of the target and the i th clutter patch, respectively, $D_t(\tau)$ and $D_i(\tau)$ are respectively the Doppler shifts of the target and the i th clutter patch, and $\mathbf{a}(\theta)$ and $\mathbf{b}(\theta)$ are the transmit and receive antenna array steering vectors for a spatial angle θ , respectively.

Let $s_j(t, \tau)$, $j = 1, \dots, J$ be the jamming signals, each of which is assumed to be independent of the others and propagated through P independent propagation paths (enabled by diffuse scatters) generally including the direct, specular, and diffuse ones. Then the vector of received jamming observations can be expressed as

$$\mathbf{x}_j(t, \tau) = \sum_{j=1}^J \sum_{p=1}^P \beta_{j,p} s_j(t - \zeta_0 - \zeta_p, \tau) \mathbf{b}(\vartheta_{j,p}) \quad (4)$$

where ζ_p is the fast-time delay associated with the p th propagation path, $\beta_{j,p}$ is the magnitude of the reflected jamming signal, and $\vartheta_{j,p}$ is the corresponding spatial angle, both associated with the p th propagation path due to the j th jammer. The received noise component $\mathbf{x}_n(t, \tau)$ is assumed to be white and Gaussian distributed.

After matched filtering the received data $\mathbf{x}(t, \tau)$ to the M transmitted waveforms at the fast-time index ζ and stacking the filtered outputs into one column vector, the resulting $MN \times 1$ virtual data vector $\mathbf{y}(\zeta, \tau)$ can be obtained as

$$\mathbf{y}(\zeta, \tau) = \text{vec} \left(\int_{T_p} \mathbf{x}(t, \tau) \phi^H(t - \zeta) dt \right) \triangleq \mathbf{y}_t(\zeta, \tau) + \mathbf{y}_c(\zeta, \tau) + \mathbf{y}_j(\zeta, \tau) + \mathbf{y}_n(\zeta, \tau) \quad (5)$$

¹We assume here that the cold clutter signal is stationary for a given range bin and the information of target signal is perfectly known or detectable. The case that their distortions due to strongly glistening surface occur (see for example [23]), and hence requires robust processing [24], is not considered.

where the filtered target, clutter, and jamming components $\mathbf{y}_t(\zeta, \tau)$, $\mathbf{y}_c(\zeta, \tau)$, and $\mathbf{y}_j(\zeta, \tau)$ are respectively expressed as

$$\mathbf{y}_t(\zeta, \tau) = \sqrt{\frac{E}{M}} \alpha_t D_t(\tau) (\mathbf{R}_\phi^T(\zeta) \mathbf{a}(\theta_t)) \otimes \mathbf{b}(\theta_t) \quad (6)$$

$$\mathbf{y}_c(\zeta, \tau) = \sqrt{\frac{E}{M}} \sum_{i=1}^{N_c} \xi_i D_i(\tau) (\mathbf{R}_\phi^T(\zeta) \mathbf{a}(\theta_i)) \otimes \mathbf{b}(\theta_i) \quad (7)$$

$$\mathbf{y}_j(\zeta, \tau) = \sum_{j=1}^J \sum_{p=1}^P \beta_{j,p} \boldsymbol{\eta}_{j,p}(\zeta, \tau) \otimes \mathbf{b}(\vartheta_{j,p}) \quad (8)$$

with the $M \times M$ waveform correlation matrix $\mathbf{R}_\phi(\zeta)$ and the $M \times 1$ match-filtered vector $\boldsymbol{\eta}_{j,p}(\zeta, \tau)$ that is associated with the p th propagation path of the j th jamming signal defined as $\mathbf{R}_\phi(\zeta) \triangleq \int_{T_p} \phi(t) \phi^H(t - \zeta + \zeta_0) dt$ and $\boldsymbol{\eta}_{j,p}(\zeta, \tau) \triangleq \int_{T_p} s_j(t - \zeta_0 - \zeta_p, \tau) \phi^*(t - \zeta) dt$. Moreover, $\mathbf{y}_n(\zeta, \tau) \triangleq \text{vec}(\int_{T_p} \mathbf{x}_n(t, \tau) \phi^H(t - \zeta) dt)$. Here $(\cdot)^*$, $(\cdot)^H$, \otimes , and $\text{vec}(\cdot)$ are conjugate, Hermitian transpose, Kronecker product, and stacking operators, respectively.

3. JAMMER SUPPRESSION VIA SFTAP

We first derive correlations of jamming signals after matched filtering in order to show that the match-filtered jamming components with respect to a certain transmitted waveform in MIMO radar are correlated to each other over fast-time domain. This characteristic can be used by SFTAP techniques for the terrain-scattered jammer suppression. Then we present two SFTAP designs for jammer suppression, where the waveform-introduced range sidelobes and stationarity of cold clutter over different pulse intervals are both considered.

3.1. Correlations of Jamming Components

Let us consider the commonly used barrage noise jamming signals, i.e., $s_j(t, \tau)$, $j = 1, \dots, J$ are mutually independent stationary white random processes which satisfy

$$\mathbb{E}\{s_j(t, \tau) s_{j'}^*(t', \tau')\} = S_j(f_c) \delta_{jj'} \delta(t - t') \delta_{\tau\tau'} \quad (9)$$

where $S_j(f_c)$ is the jamming power spectral density at carrier frequency f_c , $\delta(\cdot)$ and $\delta_{jj'}$ (also $\delta_{\tau\tau'}$) are Dirac and Kronecker delta functions, respectively, and $\mathbb{E}\{\cdot\}$ is the expectation operator. New subscript j' and parameters t' and τ' are introduced in (9) in order to distinguish from j , t , and τ , respectively.

First, we perform correlation analysis on the match-filtered vector $\boldsymbol{\eta}_{j,p}(\zeta, \tau)$ in (8) which is the only term that determines the correlation property of the jamming component. The $M \times M$ correlation matrix of $\boldsymbol{\eta}_{j,p}(\zeta, \tau)$ can be derived as

$$\begin{aligned} \mathbf{R}_{j,p,j',p'}^{\boldsymbol{\eta}}(\zeta, \zeta', \tau, \tau') &\triangleq \mathbb{E}\{\boldsymbol{\eta}_{j,p}(\zeta, \tau) \boldsymbol{\eta}_{j',p'}^H(\zeta', \tau')\} \\ &= \mathbb{E}\left\{ \int_{T_p} \int_{T_p} s_j(t - \zeta_0 - \zeta_p, \tau) s_{j'}^*(u - \zeta_0 - \zeta_{p'}, \tau') \right. \\ &\quad \left. \times \phi^*(t - \zeta) \phi^T(u - \zeta') dt du \right\} \\ &= S_j(f_c) \delta_{jj'} \delta_{\tau\tau'} \mathbf{R}_\phi^T(\zeta_p - \zeta_{p'} + \zeta' - \zeta + \zeta_0). \end{aligned} \quad (10)$$

For a certain jamming signal and an identical pulse, the correlation matrix (10) is guaranteed to be nonzero on condition that the term $\zeta_p - \zeta_{p'} + \zeta' - \zeta$ equals zero. Based on (10) and also using (8), the $MN \times MN$ correlation matrix of the jamming signal can be derived as

$$\begin{aligned} \mathbf{R}_j(\zeta, \zeta', \tau, \tau') &\triangleq \mathbb{E}\{\mathbf{y}_j(\zeta, \tau)\mathbf{y}_j^H(\zeta', \tau')\} \\ &= \sum_{j=1}^J \sum_{j'=1}^J \sum_{p=1}^P \sum_{p'=1}^P \beta_{j,p}\beta_{j',p'}^* \mathbf{R}_{j,p,j',p'}^n(\zeta, \zeta', \tau, \tau') \\ &\quad \otimes (\mathbf{b}(\vartheta_{j,p})\mathbf{b}^H(\vartheta_{j',p'})) \\ &= S_j(f_c)\delta_{\tau\tau'} \sum_{j=1}^J \sum_{p=1}^P \sum_{p'=1}^P \beta_{j,p}\beta_{j',p'}^* \\ &\quad \times \mathbf{R}_\phi^T(\zeta_p - \zeta_{p'} + \zeta' - \zeta + \zeta_0) \otimes (\mathbf{b}(\vartheta_{j,p})\mathbf{b}^H(\vartheta_{j',p'})). \end{aligned} \quad (11)$$

Note that the relationship between the correlation matrix of transmitted waveforms and that of jamming signals after matched filtering is established in (11). Thus, the effect of matched filtering on jamming signals can be measured by (11). Indeed, the correlation property of jamming signals over fast-time domain is not destroyed by matched filtering, and their correlation levels depend on the occurrence frequency of multipath. Due to the correlations in both fast-time and spatial domains, jamming signals can be suppressed using proper SFTAP designs which will be presented in the following.

3.2. SFTAP Designs

Let us assume that Q fast-time taps (i.e., range bins) are available. We stack all the Q taps of data vectors associated with the τ th pulse, namely, $\mathbf{y}(\zeta, \tau)$, $\zeta = \zeta_0, \dots, \zeta_0 + Q - 1$ (see (5)), into an $MNQ \times 1$ virtual data vector $\mathbf{y}(\tau)$, i.e.,

$$\mathbf{y}(\tau) \triangleq [\mathbf{y}^T(\zeta_0, \tau), \dots, \mathbf{y}^T(\zeta_0 + Q - 1, \tau)]^T \quad (12)$$

$$= \mathbf{y}_t(\tau) + \mathbf{y}_c(\tau) + \mathbf{y}_j(\tau) + \mathbf{y}_n(\tau) \quad (13)$$

where $\mathbf{y}_t(\tau)$, $\mathbf{y}_c(\tau)$, $\mathbf{y}_j(\tau)$, and $\mathbf{y}_n(\tau)$ are formed by means of the same stacking way as $\mathbf{y}(\tau)$ in (12).

Using (13) and realizing that clutter, jammer, and noise signals are independent of each other, the $MNQ \times MNQ$ target-free covariance matrix of $\mathbf{y}(\tau)$ can be expressed as

$$\begin{aligned} \mathbf{R}_y(\tau) &\triangleq \mathbb{E}\{\mathbf{y}_c(\tau)\mathbf{y}_c^H(\tau)\} + \mathbb{E}\{\mathbf{y}_j(\tau)\mathbf{y}_j^H(\tau)\} \\ &\quad + \mathbb{E}\{\mathbf{y}_n(\tau)\mathbf{y}_n^H(\tau)\} \\ &= \mathbf{R}_c(\tau) + \mathbf{R}_j + \mathbf{R}_n \triangleq \mathbf{R}_c(\tau) + \mathbf{R}_{jn} \end{aligned} \quad (14)$$

where $\mathbf{R}_c(\tau)$, \mathbf{R}_j , and \mathbf{R}_n are covariance matrices of clutter, jamming, and noise signals, respectively, and $\mathbf{R}_{jn} \triangleq \mathbf{R}_j + \mathbf{R}_n$. Note that only the clutter covariance matrix depends on the slow-time index τ . Jamming covariance does not depend on τ due to the result of (11). We refer readers to [17] (and references therein) for practical estimation of covariance matrices.

For the τ th pulse, the SFTAP aims at finding an adaptive filter which minimizes the output interference power without attenuating that of the target so that the output signal-to-jammer-plus-noise ratio (SJNR) is maximized. The key issue

lies in the stationarity of cold clutter over different pulse intervals after processing. Well maintained clutter stationarity enables direct application of slow-time Doppler processing. Realizing this, we propose the following SFTAP design, i.e.,

$$\min_{\mathbf{w}(\tau)} \mathbf{w}^H(\tau)\mathbf{R}_{jn}\mathbf{w}(\tau) \quad (15a)$$

$$\text{s.t.} \quad \mathbf{w}^H(\tau)\mathbf{s}_t(\theta_t) = 1 \quad (15b)$$

$$\frac{\mathbf{w}^H(\tau)\mathbf{R}_c(\tau)\mathbf{w}(\tau)}{\mathbf{w}^H(0)\mathbf{R}_c(\tau)\mathbf{w}(0)} = 1 \quad (15c)$$

$$\mathbf{w}^H(\tau)\tilde{\mathbf{u}}(\zeta_0, \theta_t) = 0 \quad (15d)$$

where $\mathbf{s}_t(\theta_t)$ is the $MNQ \times 1$ target steering vector, $\mathbf{w}(0)$ is the $MNQ \times 1$ adaptive weight vector for the first pulse (indexed by $\tau = 0$), and $\tilde{\mathbf{u}}(\zeta_0, \theta_t) \triangleq [0, \mathbf{u}^T(\zeta_0 + 1, \theta_t), \dots, \mathbf{u}^T(\zeta_0 + Q - 1, \theta_t)]^T$ with $\mathbf{u}(\zeta, \theta_t)$ defined as $\mathbf{u}(\zeta, \theta_t) \triangleq (\mathbf{R}_\phi^T(\zeta)\mathbf{a}(\theta_t) \otimes \mathbf{b}(\theta_t))$. Note that (15) deals with the SFTAP design problem for each transmitted pulse since the Doppler information of clutter signals changes over slow-time domain. The constraint (15c) ensures to keep the cold clutter stationarity, and (15d) accounts for the attenuation of sidelobes at range bins other than the one where the target is located.

Let $\mathbf{v}(\zeta_0, \theta_t) \triangleq [\mathbf{s}_t(\theta_t), \tilde{\mathbf{u}}(\zeta_0, \theta_t)]$ and $\mathbf{e} \triangleq [1, 0]^T$. Using the method of Lagrange multipliers, the solution to the optimization problem (15) can be derived as

$$\begin{aligned} \mathbf{w}(\tau) &= (\mathbf{R}_{jn} + \lambda\mathbf{R}_c(\tau))^{-1}\mathbf{v}(\zeta_0, \theta_t)(\mathbf{v}^H(\zeta_0, \theta_t) \\ &\quad \times (\mathbf{R}_{jn} + \lambda\mathbf{R}_c(\tau))^{-1}\mathbf{v}(\zeta_0, \theta_t))^{-1}\mathbf{e} \end{aligned} \quad (16)$$

where λ is determined by the smallest eigenvalue of the matrix $\mathbf{R}_c^{-1/2}(\tau)\mathbf{R}_{jn}\mathbf{R}_c^{-1/2}(\tau)/(\mathbf{w}^H(0)\mathbf{R}_c(\tau)\mathbf{w}(0))$. The solution (16) exists on condition that the subspace of adaptive weights defined by constraints of (15) is nonempty. Consequently, λ should guarantee the existence of the matrix inverse in (16) and also this matrix should not be indefinite.

In practice, we can relax the latter two constraints of (15). One way is to upper-bound the difference between roots of the nominator and denominator in (15c), and meanwhile keep the range sidelobe levels towards the target direction lower than a reasonable level. The corresponding relaxed design can be cast as the following optimization problem, i.e.,

$$\min_{\mathbf{w}(\tau)} \mathbf{w}^H(\tau)\mathbf{R}_{jn}\mathbf{w}(\tau) \quad (17a)$$

$$\text{s.t.} \quad \mathbf{w}^H(\tau)\mathbf{s}_t(\theta_t) = 1 \quad (17b)$$

$$\|\mathbf{w}^H(\tau)\mathbf{R}_c^{1/2}(\tau) - \mathbf{w}^H(0)\mathbf{R}_c^{1/2}(\tau)\| \leq \epsilon \quad (17c)$$

$$|\mathbf{w}^H(\tau)\tilde{\mathbf{u}}(\zeta_0, \theta_t)| \leq \gamma \quad (17d)$$

where $\epsilon \geq 0$ is the parameter that bounds the adaptive output of clutter distortion caused by the achieved weight vector $\mathbf{w}(\tau)$ as compared to the $\mathbf{w}(0)$, $\gamma \geq 0$ is the parameter of user choice that characterizes the worst acceptable range sidelobes towards the target direction, and $\|\cdot\|$ and $|\cdot|$ denote the Euclidean norm and the absolute value, respectively. Note that (17) is convex and can be efficiently solved. For given value of γ , the feasibility of (17) can be guaranteed if $\epsilon \geq \epsilon_{\min}$ where ϵ_{\min} is the minimum value of the output clutter distortion associated with the calculation under constraints (17b) and (17d).

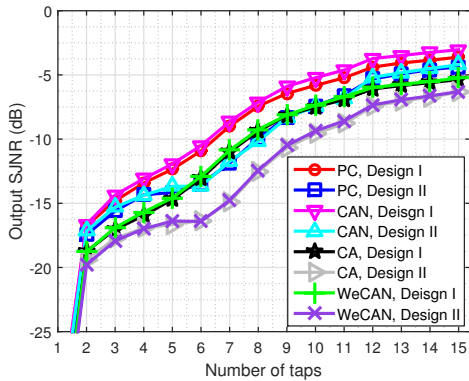


Fig. 1. SJNR performance versus taps.

4. SIMULATION RESULTS

We use uniform linear arrays equipped with $M = 8$ transmit and $N = 8$ receive antenna elements spaced half a wavelength apart from each other. The transmit energy is set as $E = M$, and the moving speed of the radar platform is 125 m/s. Each radar coherent processing interval is assumed to consist of 10 pulses. We consider the scenario that $P = 19$ diffuse multipath due to the presence of $J = 1$ jamming source occurs, and the multipath is uniformly distributed within $[-9^\circ, 9^\circ]$. Both the jammer-to-noise ratio (JNR) (for each path) and the clutter-to-noise ratio (CNR) are assumed to be 30 dB. The signal-to-noise ratio (SNR) of the target located at the spatial direction $\theta_t = 0^\circ$ is 0 dB. We utilize 4 sets of unimodular waveforms including the polyphase-coded (PC) [25], the cyclic algorithm (CA)-based, cyclic algorithm new (CAN)-based, and weighted cyclic algorithm new (WeCAN)-based waveforms [7] to evaluate the performance of the two proposed SFTAP designs. The code length of each waveform is 256. We select parameters $\epsilon = 0.2$ and $\gamma = 0.001$ for the design (17). The CVX MATLAB package is used to solve the optimization problems (15) and (17).

In our first example, we evaluate the output SJNR performance versus the employed number of temporal taps for different waveforms. It can be seen that the output SJNR performance improves when the number of employed fast-time taps is increased. The case with one single temporal tap, i.e., the suppression without fast-time processing, shows the worst SJNR performance (less than -35 dB), meaning that fast-time processing is vital for the suppression of jamming signals. For either of the two SFTAP designs, it can be seen that the output SJNR performance differs with respect to different sets of waveforms, and the largest performance gap for a certain number of temporal taps goes larger than 6 dB. This indeed verifies the effects of matched filtering on jammer suppression in the context of different sets of waveforms. It can be seen that the PC and CAN-based waveforms (which show similar

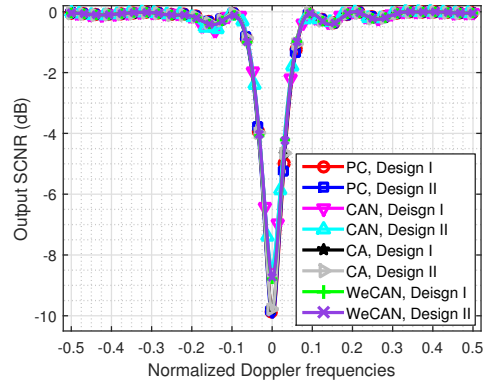


Fig. 2. SCNR performance versus normalized Doppler.

SJNR performance) outperform the other two sets of waveforms. For a certain set of waveforms, it can be seen that the SFTAP design (15) generally outperforms the design (17).

In our second example, we evaluate the output signal-to-clutter-plus-noise ratio (SCNR) performance of slow-time Doppler processing, i.e., adaptive processing after applying the proposed SFTAP designs. We employ 12 temporal taps for both SFTAP designs, and select other parameters to have the same values as the previous example. The remarkable result of this example is that the SFTAP designs associated with different sets of waveforms show similar slow-time Doppler processing performance, i.e., the slow-time Doppler processing which follows the jammer suppression over fast-time domain is no longer sensitive to the employed waveforms, and both SFTAP designs show almost the same output SCNR performance. This example verifies that the stationarity of cold clutter is well maintained by the proposed SFTAP designs.

5. CONCLUSION

We have addressed the problem of terrain-scattered jammer suppression in MIMO radar utilizing SFTAP techniques. The correlation function of match-filtered jamming components has been derived, which establishes connections with the correlation matrix of the transmitted waveforms. It serves as a measure of evaluating the matched filtering effect on the received jamming signals. We have proposed an MVDR type SFTAP design in which the waveform-introduced range sidelobes towards the target direction and the cold clutter stationarity over different pulse intervals have been considered. A closed-form solution to the proposed design has been derived. We have also proposed a relaxed SFTAP design by replacing the equality constraints of the MVDR type design with inequality constraints. The proposed SFTAP designs have shown the ability to maintain cold clutter stationarity and further support slow-time Doppler processing. Simulation results have verified the validity of the proposed designs.

6. REFERENCES

- [1] J. Li and P. Stoica, *MIMO Radar Signal Processing*. New York, NY, USA: Wiley, 2009.
- [2] J. Li and P. Stoica, "MIMO radar with colocated antennas," *IEEE Signal Process. Mag.*, vol. 24, no. 5, pp. 106–114, Sep. 2007.
- [3] A. M. Haimovich, R. S. Blum, and L. J. Cimini, "MIMO radar with widely separated antennas," *IEEE Signal Process. Mag.*, vol. 24, no. 1, pp. 116–129, Jan. 2008.
- [4] D. W. Bliss and K. W. Forsythe, "Multiple-input multiple-output MIMO radar and imaging: Degrees of freedom and resolution," in *Proc. Asilomar Conf. Signals, Syst., Comput.*, vol. 1, Pacific Grove, CA, USA, Nov. 2003, pp. 54–59.
- [5] C.-Y. Chen and P. P. Vaidyanathan, "MIMO radar space-time adaptive processing using prolate spheroidal waveform functions," *IEEE Trans. Signal Process.*, vol. 56, no. 2, pp. 623–635, Feb. 2008.
- [6] G. San Antonio, D. R. Fuhrmann, and F. C. Robey, "MIMO radar ambiguity functions," *IEEE J. Sel. Topics Signal Process.*, vol. 1, no. 1, pp. 167–177, Jun. 2007.
- [7] H. Hao, P. Stoica, and J. Li, "Designing unimodular sequences sets with good correlations—Including an application to MIMO radar," *IEEE Trans. Signal Process.*, vol. 57, no. 11, pp. 4391–4405, Nov. 2009.
- [8] A. Hassanien and S. A. Vorobyov, "Phased-MIMO radar: A tradeoff between phased-array and MIMO radars," *IEEE Trans. Signal Process.*, vol. 58, no. 6, pp. 3137–3151, Jun. 2010.
- [9] A. Hassanien and S. A. Vorobyov, "Transmit energy focusing for DOA estimation in MIMO radar with colocated antennas," *IEEE Trans. Signal Process.*, vol. 59, no. 6, pp. 2669–2682, Jun. 2011.
- [10] K. W. Forsythe and D. W. Bliss, "MIMO radar waveform constraints for GMTI," *IEEE J. Sel. Topics Signal Process.*, vol. 4, no. 1, pp. 21–32, Feb. 2010.
- [11] Q. He, N. H. Lehmann, R. S. Blum, and A. M. Haimovich, "MIMO radar moving target detection in homogeneous clutter," *IEEE Trans. Aerosp. Electron. Syst.*, vol. 46, no. 3, pp. 1290–1301, Jul. 2010.
- [12] Y. Li, S. A. Vorobyov, and V. Koivunen, "Ambiguity function of the transmit beamspace-based MIMO radar," *IEEE Trans. Signal Process.*, vol. 63, no. 17, pp. 4445–4457, Sep. 2015.
- [13] Y. Li, S. A. Vorobyov, and A. Hassanien, "MIMO radar capability on powerful jammers suppression," in *Proc. IEEE Int. Conf. Acoust., Speech, Signal Process. (ICASSP)*, Florence, Italy, May 2014, pp. 5277–5281.
- [14] Y. Li, S. A. Vorobyov, and A. Hassanien, "Robust beamforming for jammers suppression in MIMO radar," in *Proc. IEEE Radar Conf.*, Cincinnati, OH, USA, May 2014, pp. 0629–0634.
- [15] Y. Li, S. A. Vorobyov, and Z. He, "Joint hot and cold clutter mitigation in the transmit beamspace-based MIMO radar," in *Proc. IEEE Int. Conf. Acoust., Speech, Signal Process. (ICASSP)*, Brisbane, Australia, Apr. 2015, pp. 2334–2338.
- [16] R. L. Fante and J. A. Torres, "Cancellation of dissuade jammer multipath by an airborne adaptive radar," *IEEE Trans. Aerosp. Electron. Syst.*, vol. 31, no. 2, pp. 805–820, Apr. 1995.
- [17] Y. I. Abramovich, N. K. Spencer, S. J. Anderson, and A. Y. Gorokhov, "Stochastic-constraints method in nonstationary hot-clutter cancellation—Part I: Fundamentals and supervised training applications," *IEEE Trans. Aerosp. Electron. Syst.*, vol. 34, no. 4, pp. 1271–1291, Oct. 1998.
- [18] Y. I. Abramovich, N. K. Spencer, and S. J. Anderson, "Stochastic-constraints method in nonstationary hot-clutter cancellation—Part II: Unsupervised training applications," *IEEE Trans. Aerosp. Electron. Syst.*, vol. 36, no. 1, pp. 132–150, Jan. 2000.
- [19] P. M. Techau, J. R. Guerci, T. H. Slocumb, and L. J. Griffiths, "Performance bounds for hot and cold clutter mitigation," *IEEE Trans. Aerosp. Electron. Syst.*, vol. 35, no. 4, pp. 1235–1265, Oct. 1999.
- [20] D. J. Rabideau, "Clutter and jammer multipath cancellation in airborne adaptive radar," *IEEE Trans. Aerosp. Electron. Syst.*, vol. 36, no. 2, pp. 565–583, Apr. 2000.
- [21] R. Klemm, *Principles of space-time adaptive processing*, 3rd ed. London, UK: The Institution of Elect. Eng., 2006.
- [22] J. Ward, "Space-time adaptive processing for airborne radar," MIT Lincoln Lab., Lexington Massachusetts, MA, USA, Tech. Rep. 1015, Dec. 1994.
- [23] A. Aubry, A. De Maio, G. Foglia, and D. Orlando, "Difuse multipath exploitation for adaptive radar detection," *IEEE Trans. Signal Process.*, vol. 63, no. 5, pp. 1268–1281, Mar. 2015.
- [24] S. A. Vorobyov, A. B. Gershman, and Z.-Q. Luo, "Robust adaptive beamforming using worst-case performance optimization: A solution to the signal mismatch problem," *IEEE Trans. Signal Process.*, vol. 51, no. 2, pp. 313–324, Feb. 2003.
- [25] N. Levanon and E. Mozeson, *Radar Signals*. Hoboken, NJ, USA: Wiley, 2004.

Publication IV

Yongzhe Li, Sergiy A. Vorobyov and Zishu He. Joint hot and cold clutter mitigation in the transmit beamspace based MIMO radar. In *IEEE International Conference on Acoustics, Speech, and Signal Processing (ICASSP)*, Brisbane, Australia, pp. 2334–2338, April 2015.

© 2015 IEEE.

Reprinted with permission.

JOINT HOT AND COLD CLUTTER MITIGATION IN THE TRANSMIT BEAMSPACE-BASED MIMO RADAR

Yongzhe Li^{†‡}, Sergiy A. Vorobyov[‡], and Zishu He[†]

[†]Dept. EE, University of Electronic Science and Technology of China, Chengdu, 611731, China

[‡]Dept. Signal Processing and Acoustics, Aalto University, P.O. Box 13000, FI-00076 Aalto, Finland

Emails: lyzlyz888@gmail.com/yongzhe.li@aalto.fi, svor@ieee.org, zshe@uestc.edu.cn

ABSTRACT

In this paper, the problem of joint hot and cold clutter mitigation in the context of transmit beamspace (TB)-based multiple-input multiple-output (MIMO) radar is studied. The TB-based MIMO radar enables special spatio-temporal structure and low rank of clutter covariance matrices. To efficiently mitigate the hot clutter such as terrain scattered multipath jamming concentrated in the sector-of-interest and the enhanced cold clutter due to transmit energy focusing, we resort to three-dimensional (3D) space-time adaptive processing (STAP) technique. A new 3D STAP method is proposed, which significantly reduces the computational complexity. We show from interference mitigation perspective that the TB-based MIMO radar enables superior output signal-to-interference-plus-noise ratio to that of its traditional MIMO radar counterpart.

Index Terms—Colocated MIMO radar, joint clutter mitigation, space-time adaptive processing (STAP), transmit beamspace (TB).

1. INTRODUCTION

The multiple-input multiple-output (MIMO) radar has become a research field of significant interest in recent years [1]–[15]. Transmit beamforming techniques have been employed to achieve desired beampattern (possibly flat) that covers a certain spatial sector of interest (SOI) [5]–[10]. Additional benefit in terms of signal-to-noise ratio (SNR) gain can be obtained if much less number of waveforms than that employed in the traditional MIMO radar are used [8], i.e., transmit coherent processing gain [7] and waveform diversity [1] are jointly achieved. Superior direction-of-arrival estimation performance, for example, can be achieved in the presence of only noise due to this core feature [8], [10]. Moreover, flexible correlated waveforms are also allowed to be emitted [13]. Such advantages motivate us to further investigate the question on how the transmit beamspace (TB)-based MIMO radar behaves in the environment when both interference and noise are present. The situation of special interest is when hot clutter [16] and cold clutter [17] are both present simultaneously. Cold clutter energy is concentrated within the SOI, and terrain

scattered multipath or diffuse jamming that represents the hot clutter occupying the whole SOI can further have a significant impact on the performance of the TB-based MIMO radar. Different from the clutter mitigation in the phased-array (PA) radar [18]–[22], the TB-based MIMO radar enables special spatio-temporal structure and low rank of clutter covariance matrices due to its TB strategy [8], [10]. To the best of our knowledge, the potential of the TB-based MIMO radar on joint clutter mitigation has not been studied previously.

In this paper, we aim at studying and verifying benefits of the TB-based MIMO radar from the perspective of clutter mitigation. Motionless hot clutter such as terrain scattered multipath or diffuse jamming together with ground reflected cold clutter are both involved in the interference environment. We resort to three-dimensional (3D) space-time adaptive processing (STAP) technique to achieve the mitigation goal. Utilizing the special spatio-temporal structure produced by the TB strategy as well as the low-rank and block diagonal hot and cold clutter covariance matrices, we propose a new 3D STAP method with low computational complexity. Passive receiving and off-line clutter subspace calculation with respect to (w.r.t.) radar geometry are used in this method. We show that the TB-based MIMO radar enables superior output signal-to-interference-plus-noise ratio (SINR) to that of its traditional MIMO radar counterpart under efficient clutter mitigation.

2. SIGNAL MODEL

Consider an airborne colocated MIMO radar system with a transmit array of M antenna elements and a receive array of N antenna elements. Both arrays are assumed to be closely located, therefore, they share an identical spatial angle for a far-field target. In the context of the TB-based MIMO radar, K (in general, $K \leq M$) initially orthogonal waveforms are transmitted via K synthesized transmit beams [8]. Let $\phi(t) = [\phi_1(t), \dots, \phi_K(t)]^T$ be the $K \times 1$ vector of the transmitted waveform values for a given fast time t where $(\cdot)^T$ stands for the transpose operation. We assume that the transmitted waveforms are orthogonal to each other over the time interval of radar pulse duration T_p . The signal radiated towards the spatial direction θ through the k th transmit beam can be

Y. Li's work is supported by China Scholarship Council (CSC).

modeled as [8]

$$s_k(t) = \sqrt{\frac{E}{K}} (\mathbf{c}_k^H \mathbf{a}(\theta)) \phi_k(t), \quad k = 1, \dots, K \quad (1)$$

where E is the total transmit energy, $\mathbf{a}(\theta)$ is the transmit antenna array steering vector, \mathbf{c}_k is the k th unit-norm column vector of the $M \times K$ TB matrix \mathbf{C} which is defined as $\mathbf{C} \triangleq [\mathbf{c}_1, \dots, \mathbf{c}_K]$, and $(\cdot)^H$ stands for the Hermitian transpose. From the elementspace perspective, one of the possible transmit schemes is to individually emit the following compound waveforms by the M transmit antenna elements [23]

$$\tilde{s}_m(t) = \sqrt{\frac{E}{K}} \sum_{k=1}^K c_k^m \phi_k(t), \quad m = 1, \dots, M \quad (2)$$

where c_k^m is the m th element of \mathbf{c}_k .

Let us assume that one radar coherent processing interval (CPI) contains L pulses, and the ground range (ring) of interest (ROI) is separated into N_c ($N_c \gg KNL$) patches. The number of J independent motionless jammers is present, and the jamming signal (to be specific, barrage noise) generated by each hostile jammer is propagated through P independent propagation paths which generally include the direct, specular, and diffuse ones. Thus, in the presence of the target and for the τ th pulse, the $N \times 1$ complex vector of array observations from the ROI can be expressed as

$$\begin{aligned} \mathbf{x}(t, \tau) = & \sqrt{\frac{E}{K}} \alpha_t D_t(\tau) \left((\mathbf{C}^H \mathbf{a}(\theta_t))^T \phi(t - \zeta_0) \right) \mathbf{b}(\theta_t) \\ & + \sqrt{\frac{E}{K}} \sum_{i=1}^{N_c} \xi_i D_i(\tau) \left((\mathbf{C}^H \mathbf{a}(\theta_i))^T \phi(t - \zeta_0) \right) \mathbf{b}(\theta_i) \\ & + \sum_{j=1}^J \sum_{p=1}^P \beta_j^p s_j^p(t - \zeta_0, \tau) \mathbf{b}(\vartheta_j^p) + \mathbf{z}(t, \tau) \end{aligned} \quad (3)$$

where t and τ are respectively the fast- and slow-time indices, ζ_0 is the fast-time delay of the ROI, θ_t , θ_i , and ϑ_j^p are spatial angles of the target, the i th clutter patch, and the p th scatter associated with the j th jamming source, respectively, α_t , ξ_i , and β_j^p are the complex reflection coefficients of the target, the i th clutter patch, and the j th jamming source associated with the p th propagation path with variances σ_α^2 , $\sigma_{\xi_i}^2$, and $\sigma_{\beta_{j,p}}^2$, respectively, $D_t(\tau)$ and $D_i(\tau)$ are respectively the Doppler shifts of the target and the i th clutter patch introduced by the relative motions w.r.t. the radar platform, $s_j^p(t, \tau)$ is the j th jamming signal through the p th propagation path (i.e., a time delayed version of the j th original jamming signal) at the fast-time index t and the slow-time index τ , $\mathbf{b}(\theta)$ is the receive antenna array steering vector, and $\mathbf{z}(t, \tau)$ is the $N \times 1$ white Gaussian noise term.

By match filtering the receive data $\mathbf{x}(t, \tau)$ to the K original orthogonal waveforms at the fast-time index ζ (matched filtering of the ROI occurs at ζ_0) and stacking the filtered outputs for all slow-time pulses, the $LKN \times 1$ virtual data vector

can be obtained as

$$\begin{aligned} \mathbf{y}(\zeta) = & \text{vec} \left(\int_{T_p} \mathbf{x}(t, \tau) \phi^H(t - \zeta) dt \right)_{\tau=1, \dots, L} \\ = & \sqrt{\frac{E}{K}} \alpha_t \mathbf{d}(\theta_t) \otimes \mathbf{u}(\theta_t, \zeta) \otimes \mathbf{b}(\theta_t) \\ & + \sqrt{\frac{E}{K}} \sum_{i=1}^{N_c} \xi_i \mathbf{d}(\theta_i) \otimes \mathbf{u}(\theta_i, \zeta) \otimes \mathbf{b}(\theta_i) \\ & + \sum_{j=1}^J \sum_{p=1}^P \beta_j^p \boldsymbol{\eta}_j^p(\zeta) \otimes \mathbf{b}(\vartheta_j^p) + \bar{\mathbf{z}}(\zeta) \end{aligned} \quad (4)$$

$$\triangleq \mathbf{y}_t(\zeta) + \mathbf{y}_c(\zeta) + \mathbf{y}_h(\zeta) + \bar{\mathbf{z}}(\zeta) \quad (5)$$

where $\mathbf{u}(\theta, \zeta) \triangleq \mathbf{R}_\phi^T(\zeta) (\mathbf{C}^H \mathbf{a}(\theta))$ with $\mathbf{R}_\phi(\zeta)$ being defined as $\mathbf{R}_\phi(\zeta) \triangleq \int_{T_p} \phi(t) \phi^H(t - \zeta + \zeta_0) dt$, $\mathbf{d}(\theta)$ is the Doppler steering vector, $\boldsymbol{\eta}_j^p(\zeta)$ is a $LKN \times 1$ vector associated with the p th propagation of the j th jamming signal with its τ th $K \times 1$ component being defined as $\boldsymbol{\eta}_j^p(\zeta, \tau) \triangleq \int_{T_p} s_j^p(t - \zeta_0, \tau) \phi^H(t - \zeta) dt$, $\bar{\mathbf{z}}(\zeta)$ is the stacked noise term whose covariance is denoted by $\sigma_z^2 \mathbf{I}_{LKN}$ with \mathbf{I}_{LKN} being the identity matrix of size $LKN \times LKN$, $\text{vec}(\cdot)$ is the operator that stacks the columns of a matrix into one column vector, and \otimes denotes the Kronecker product. Note that $\mathbf{y}_t(\zeta)$, $\mathbf{y}_c(\zeta)$, and $\mathbf{y}_h(\zeta)$ are used in (5) to denote the space-(slow) time virtual data vectors of the target, the cold clutter, and the hot clutter filtered at the fast-time index ζ , respectively, and they are assumed to be not correlated with each other.

3. JOINT CLUTTER MITIGATION IN THE TB-BASED MIMO RADAR

Let us consider the worst situation that most jamming signals resulted by terrain scatters or multipath propagations impinge on the receiver within the whole pre-determined SOI Ω where the target is also located. This means that strong correlations among multipath jamming signals in fast-time domain may occur. To facilitate the mitigation, we assume that the jamming sources are motionless, i.e., no Doppler shift is introduced into the hot clutter signal for each terrain scatter or multipath propagation. In what follows, we first formulate the 3D STAP problem for the TB-based MIMO radar system followed by the rank analysis of the hot and cold clutter covariance matrices, then we present the proposed 3D STAP method.

3.1. 3D STAP Formulation and Clutter Rank Analysis

In 3D STAP, the number of Q (assume to be an odd number) fast-time taps (i.e., range bins) is employed in addition to the previously defined $LKN \times 1$ virtual space-(slow) time data vector. By stacking $\mathbf{y}(\zeta)$, $\zeta = \zeta_0 - \bar{Q}, \dots, \zeta_0 + \bar{Q}$ in (5), the $QLKN \times 1$ virtual data vector \mathbf{y} can be obtained as

$$\begin{aligned} \mathbf{y} \triangleq & [\mathbf{y}^T(\zeta_0 - \bar{Q}), \dots, \mathbf{y}^T(\zeta_0 + \bar{Q})]^T \quad (6) \\ = & \mathbf{y}_t + \mathbf{y}_c + \mathbf{y}_h + \bar{\mathbf{z}} \quad (7) \end{aligned}$$

where $\tilde{Q} \triangleq (Q - 1)/2$ and \mathbf{y}_t , \mathbf{y}_c , \mathbf{y}_h , and $\tilde{\mathbf{z}}$ are formed using the same way as \mathbf{y} in (6) with the same size $QLKN \times 1$.

Using (7), the target-free interference covariance matrix of the virtual data vector \mathbf{y} is defined as

$$\begin{aligned} \mathbf{R}_y &\triangleq \mathbb{E}\{\mathbf{y}\mathbf{y}^H\} = \mathbb{E}\{\mathbf{y}_c\mathbf{y}_c^H\} + \mathbb{E}\{\mathbf{y}_h\mathbf{y}_h^H\} + \mathbb{E}\{\tilde{\mathbf{z}}\tilde{\mathbf{z}}^H\} \\ &\triangleq \mathbf{R}_c + \mathbf{R}_h + \mathbf{R}_z \end{aligned} \quad (8)$$

where \mathbf{R}_c , \mathbf{R}_h , and \mathbf{R}_z stand for the covariance matrices of the cold clutter, the hot clutter, and the noise, respectively, and $\mathbb{E}\{\cdot\}$ is the expectation operator.

The objective of the 3D STAP is to find an adaptive filter (with a $QLKN \times 1$ weight vector \mathbf{w}) that maximizes the output SINR. This filter can be obtained by solving the following minimum variance distortionless response (MVDR) type optimization problem

$$\begin{aligned} \min_{\mathbf{w}} \quad & \mathbf{w}^H \mathbf{R}_y \mathbf{w} \\ \text{s.t.} \quad & \mathbf{w}^H \mathbf{s}_t(\tilde{Q}, f_s(\theta_t), f_d(\theta_t)) = 1 \end{aligned} \quad (9)$$

where $f_s(\theta_t)$ and $f_d(\theta_t)$ are the spatial and the Doppler frequencies of the target, respectively, and $\mathbf{s}_t(\tilde{Q}, f_s(\theta_t), f_d(\theta_t))$ is the target steering vector which can be expressed as

$$\mathbf{s}_t(\tilde{Q}, f_s(\theta_t), f_d(\theta_t)) \triangleq \mathbf{e}_{\tilde{Q}} \otimes \mathbf{d}(\theta_t) \otimes \mathbf{u}(\theta_t, \tilde{Q}) \otimes \mathbf{b}(\theta_t) \quad (10)$$

with $\tilde{Q} \triangleq (Q + 1)/2$ and $\mathbf{e}_{\tilde{Q}}$ being a $Q \times 1$ all-zero vector except the \tilde{Q} th entry replaced by 1.

The MVDR problem (9) leads to the following solution [24]

$$\mathbf{w} = \frac{\mathbf{R}_y^{-1} \mathbf{s}_t(\tilde{Q}, f_s(\theta_t), f_d(\theta_t))}{\mathbf{s}_t^H(\tilde{Q}, f_s(\theta_t), f_d(\theta_t)) \mathbf{R}_y^{-1} \mathbf{s}_t(\tilde{Q}, f_s(\theta_t), f_d(\theta_t))}. \quad (11)$$

Let us take the TB strategy that aims at approximating linear phase rotations among the K transmit beams for example, i.e., $\mathbf{C}^H \mathbf{a}(\theta_b) \simeq \mathbf{g}(\theta_b) \triangleq [e^{j\mu_1(f_s(\theta_b))}, \dots, e^{j\mu_K(f_s(\theta_b))}]^T$, $b = 1, \dots, B$ where $\mu_i(f_s(\theta_b))$, $i = 1, \dots, K$ are uniform linear functions of the spatial frequency $f_s(\theta_b)$, and B is the number of angular grids used for approximating the SOI Ω .

The matrix \mathbf{R}_c takes the form $\mathbf{R}_c = \text{diag}\{\mathbf{R}_{c,-\tilde{Q}}, \dots, \mathbf{R}_{c,\tilde{Q}}\}$ where $\text{diag}\{\cdot\}$ stands for the diagonalization operation and $\mathbf{R}_{c,q}$, $q \in \{-\tilde{Q}, \dots, \tilde{Q}\}$ is the $LKN \times LKN$ space-(slow) time cold clutter covariance matrix for the q th range bin whose rank is $r_0 \triangleq \lceil N + \rho(K - 1) + \eta(L - 1) \rceil$. Here ρ is the ratio between the synthesized transmit aperture (i.e., the one associated with $\mathbf{g}(\theta)$) and the receive one, η is the ratio between radar movement in one pulse and the neighbour receive antenna element space, and $\lceil \cdot \rceil$ is the ceiling function. Thus, the rank of \mathbf{R}_c is $r_c \triangleq Q \lceil N + \rho(K - 1) + \eta(L - 1) \rceil$. Considering that hot clutter is not correlated to pulses and assuming that TB processing does not affect its wide stationarity, the matrix \mathbf{R}_h takes the form $\mathbf{R}_h = \mathbf{R}_Q \otimes (\mathbf{I}_{LK} \otimes \mathbf{R}_N)$ where \mathbf{R}_Q is a $Q \times Q$ fast-time Toeplitz cross-correlation matrix which is dependent on the bandwidth of jamming signal,

and \mathbf{R}_N is an $N \times N$ spatial covariance matrix of jamming multipath. Generally, \mathbf{R}_h has a rank that is QLK times rank of \mathbf{R}_N , however, it contains $Q \times Q$ space-(slow) time diagonal blocks. The noise covariance matrix \mathbf{R}_z takes the form $\mathbf{R}_z = \sigma_z^2 \mathbf{R}_Q \otimes \mathbf{I}_{LKN}$ where \mathbf{R}_Q is a $Q \times Q$ fast-time cross-correlation matrix of noise resulted by range sidelobes.

Note that \mathbf{R}_h is in general a function of the fast time t , and it differs for different pulses if motions of jamming sources are considered. Although 3D STAP is still effective, here we aim at presenting the potential of the TB-based MIMO radar in motionless hot clutter environment.

3.2. Proposed 3D STAP Method

Let us deal with the case when range sidelobes are well controlled or negligible¹ and no overlap occurs in fast-time sampling. Thus, \mathbf{R}_z becomes an identity matrix of size $QLKN \times QLKN$, i.e., $\mathbf{R}_z = \sigma_z^2 \mathbf{I}_{QLKN}$. Let $\mathbf{R}_{h\tilde{z}} \triangleq \mathbf{R}_h + \mathbf{R}_z$, then $\mathbf{R}_{h\tilde{z}}$ can be expressed as

$$\mathbf{R}_{h\tilde{z}} = \mathbf{R}_Q \otimes (\mathbf{I}_{LK} \otimes \tilde{\mathbf{R}}_N) - \sigma_z^2 \tilde{\mathbf{R}}_Q \otimes \mathbf{I}_{LKN} \quad (12)$$

where $\tilde{\mathbf{R}}_N \triangleq \mathbf{R}_N + \sigma_z^2 \mathbf{I}_N$, and $\tilde{\mathbf{R}}_Q$ is identical to \mathbf{R}_Q except for the main diagonal elements which are replaced by zeros. Block diagonal property of \mathbf{R}_h is preserved in $\mathbf{R}_{h\tilde{z}}$.

Since the matrices $\mathbf{R}_{c,q}$, $q = -\tilde{Q}, \dots, \tilde{Q}$ share the same clutter rank r_0 , there exists an $r_0 \times r_0$ matrix Λ_q for the q th sub clutter covariance matrix which satisfies $\mathbf{R}_{c,q} \simeq \mathbf{S}_q \Lambda_q \mathbf{S}_q^H$. The quality of this approximation depends on the ratio $\gamma = \sum_{k=1}^{r_0} \lambda_k^q / \sum_{k=1}^{LKN} \lambda_k^q$ where λ_k^q is the k th eigenvalue of $\mathbf{R}_{c,q}$ whose eigenvalues are ordered in decreasing manner. Let us define the cold clutter subspace as $\mathbf{S}_c \triangleq \text{diag}\{\mathbf{S}_{-\tilde{Q}}, \dots, \mathbf{S}_{\tilde{Q}}\}$, then the whole cold clutter matrix \mathbf{R}_c can be expressed as $\mathbf{R}_c \simeq \mathbf{S}_c \Lambda \mathbf{S}_c^H$ where Λ is an $r_c \times r_c$ matrix. The overall clutter covariance matrix \mathbf{R}_y can then be re-expressed as

$$\mathbf{R}_y \simeq \mathbf{R}_{h\tilde{z}} + \mathbf{S}_c \Lambda \mathbf{S}_c^H. \quad (13)$$

The expression (13) leads to the following inversion

$$\mathbf{R}_y^{-1} \simeq \mathbf{R}_{h\tilde{z}}^{-1} - \mathbf{R}_{h\tilde{z}}^{-1} \mathbf{S}_c (\Lambda^{-1} + \mathbf{S}_c^H \mathbf{R}_{h\tilde{z}}^{-1} \mathbf{S}_c)^{-1} \mathbf{S}_c^H \mathbf{R}_{h\tilde{z}}^{-1} \quad (14)$$

where the matrix inversion lemma is used in the derivation, and the inverse of $\mathbf{R}_{h\tilde{z}}$ can be achieved by the following approximation

$$\begin{aligned} \mathbf{R}_{h\tilde{z}}^{-1} &\simeq \sum_{k=0}^{\kappa} \sigma_z^{2k} \left(\mathbf{R}_Q^{-1} \otimes \mathbf{I}_{LK} \otimes \tilde{\mathbf{R}}_N^{-1} \right) \\ &\quad \times \left(\mathbf{R}_Q^{-1} \tilde{\mathbf{R}}_Q \right)^k \otimes \mathbf{I}_{LK} \otimes \tilde{\mathbf{R}}_N^{-k} \end{aligned} \quad (15)$$

with κ being the order of Taylor expansion for the inverse of (12), if the corresponding convergence condition is satisfied. It only requires calculating the inverse of \mathbf{R}_Q and $\tilde{\mathbf{R}}_N$.

¹ This can be achieved by employing waveforms with good correlation properties or by artificially controlling the sidelobe levels within a certain range of fast time. The corresponding range-Doppler "clear region" is between that of the PA and traditional MIMO radar cases, depending on the number of the synthesized transmit beams K [13], [23].

Using (13) and also (8), the matrix \mathbf{A} can be obtained as

$$\mathbf{A} = \mathbf{R}_{\tilde{\mathbf{y}}} - \mathbf{U}^H \mathbf{R}_{\mathbf{h}\tilde{\mathbf{z}}}\mathbf{U} \quad (16)$$

where $\mathbf{U} \triangleq \text{diag}\{\mathbf{S}_{-\tilde{Q}}(\mathbf{S}_{-\tilde{Q}}^H \mathbf{S}_{-\tilde{Q}})^{-1}, \dots, \mathbf{S}_{\tilde{Q}}(\mathbf{S}_{\tilde{Q}}^H \mathbf{S}_{\tilde{Q}})^{-1}\}$ and $\mathbf{R}_{\tilde{\mathbf{y}}} \triangleq \mathbb{E}\{\tilde{\mathbf{y}}\tilde{\mathbf{y}}^H\}$ with $\tilde{\mathbf{y}} \triangleq \mathbf{U}^H \mathbf{y}$.

One way to obtain the q th clutter subspace \mathbf{S}_q is to span using N_c space-(slow) time antenna array steering vectors of the q th range bin. Hence, the 3D STAP solution can be achieved by substituting (14) into (11). In practice, $\tilde{\mathbf{R}}_N$ is estimated using the $N \times 1$ target and clutter free signals at the receiver by switching radar to the passive receive mode, \mathbf{R}_Q is estimated based on fast-time samples, and $\mathbf{R}_{\tilde{\mathbf{y}}}$ is estimated using the transformed 3D samples $\tilde{\mathbf{y}}$.

4. SIMULATION RESULTS

We use uniform linear arrays of half wavelength spaced $M = 16$ transmit and $N = 5$ receive antenna elements. The total transmit energy is set to be $E = M$. We select $\Omega = [10^\circ, 25^\circ]$ as the SOI and 10° width as the transition band for the TB-based MIMO radar. This leads to a minimum selection of $K = 4$ waveforms according to the procedure in [8]. The radar platform is assumed to be moving with a velocity of 125 m/s, and there are $L = 5$ pulses in one CPI with pulse repetition frequency being $f_r = 500$ Hz. The target is located at $\theta_t = 16^\circ$ and has a relative Doppler $f_d = 0.14$. We assume that 100 diffuse scatters are uniformly distributed within Ω for each range bin. The hot and cold clutter-to-noise ratios are both set to be 50 dB, and the SNR (before processing) is 0 dB. We select $Q = 3$ range bins due to high correlation of multipath jamming, and the target is located at the middle one.

In the first example, we show the high-resolution clutter spectra of the ROI (see Fig. 1). The spectra are defined as $P(f_s, f_d) \triangleq (\mathbf{s}^H(f_s, f_d)\mathbf{R}_{\tilde{\mathbf{y}}}^{-1}\mathbf{s}(f_s, f_d))^{-1}$ [22] where $\mathbf{s}(f_s, f_d)$ is the space-(slow) time antenna array steering vector achieved from (10) by enforcing $Q = 1$. Fig. 1(a) shows the clutter spectra when only cold clutter is present. It can be seen that the cold clutter ridge concentrates on the region of SOI, meaning that more cold clutter energy is focused because of the TB strategy. The off-ridge area is clean. Fig. 1(b) shows the case when hot clutter is also present. It can be seen that the region of SOI ($f_s \in [0.09, 0.21]$) is completely contaminated by the hot clutter, and all the Doppler frequencies of this region are occupied. Moreover, the ridge of the cold clutter spreads at a certain extent. This means that if potential target is present in this area, it is submerged in harsh hybrid clutter.

In the second example, we evaluate the output SINR performance of clutter mitigation (see Fig. 2). The SINR is defined as $\text{SINR} = \sigma_\alpha^2 E \mathbf{w}^H \mathbf{s}_t \mathbf{s}_t^H \mathbf{w} / K \mathbf{w}^H \mathbf{R}_{\tilde{\mathbf{y}}} \mathbf{w}$. We employ 10 samples to estimate \mathbf{R}_Q and $\tilde{\mathbf{R}}_N$, and 30 samples to estimate $\mathbf{R}_{\tilde{\mathbf{y}}}$ when evaluating the SINR performance of the TB-based MIMO radar with spheroidal sequences-based and convex optimization-based TB designs (see [8]) using the proposed 3D

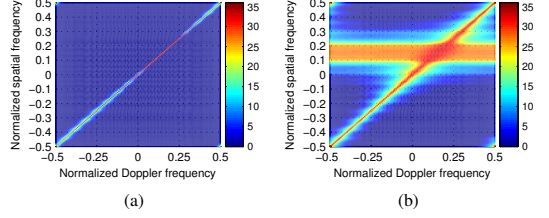


Fig. 1. Clutter spectra of the TB-based MIMO radar.

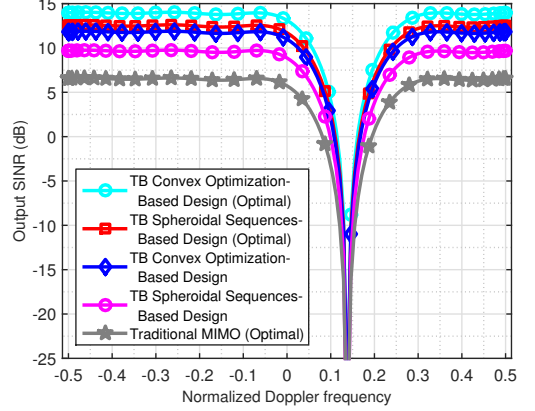


Fig. 2. SINR performance versus Doppler frequencies.

STAP method. The optimal output SINR associated with the former TB design is about 1 dB better than that associated with the latter one. It can be seen that the proposed method shows good clutter mitigation performance for both TB designs. The convex optimization-based design gives better (about 2 dB) SINR than the spheroidal sequences-based one, meaning that proper TB design is prone to achieve good clutter mitigation performance. The optimal SINR of the TB-based MIMO radar is about 6~7 dB higher than that of the traditional MIMO radar because of the energy focusing in the TB designs.

5. CONCLUSIONS

We have considered the problem of joint hot and cold clutter mitigation in the context of the TB-based MIMO radar which has not been studied before. The energy of the cold clutter is shown to be focused in this type of radar configuration, while the hot clutter contaminates the whole SOI. 3D STAP technique has been employed to mitigate the hybrid clutter. We have formulated the STAP problem and analyzed the rank of the hot and cold clutter covariance matrices. By utilizing the low-rank and block diagonal properties of the clutter covariance matrices, a new 3D STAP method with lower computational complexity has been developed. It has been also shown that the TB-based MIMO radar enables superior output SINR to that of its traditional MIMO radar counterpart.

6. REFERENCES

- [1] J. Li and P. Stoica, "MIMO radar with colocated antennas," *IEEE Signal Process. Mag.*, vol. 24, no. 5, pp. 106–114, Sep. 2007.
- [2] A. M. Haimovich, R. S. Blum, and L. J. Cimini, "MIMO radar with widely separated antennas," *IEEE Signal Process. Mag.*, vol. 24, no. 1, pp. 116–129, Jan. 2008.
- [3] E. Fishler, A. Haimovich, R. S. Blum, L. Cimini, D. Chizhik, and R. Valenzuela, "Spatial diversity in radars—Models and detection performance," *IEEE Trans. Signal Process.*, vol. 54, no. 3, pp. 823–838, Mar. 2006.
- [4] C.-Y. Chen and P. P. Vaidyanathan, "MIMO radar space-time adaptive processing using prolate spheroidal wave-form functions," *IEEE Trans. Signal Process.*, vol. 56, no. 2, pp. 623–635, Feb. 2008.
- [5] D. R. Fuhrmann and G. San Antonio, "Transmit beamforming for MIMO radar systems using signal cross-correlation," *IEEE Trans. Aerosp. Electron. Syst.*, vol. 44, no. 1, pp. 171–186, Jan. 2008.
- [6] P. Stoica, J. Li, and Y. Xie, "On probing signal design for MIMO radar," *IEEE Trans. Signal Process.*, vol. 55, no. 8, pp. 4151–4161, Aug. 2007.
- [7] A. Hassanien and S. A. Vorobyov, "Phased-MIMO radar: A tradeoff between phased-array and MIMO radars," *IEEE Trans. Signal Process.*, vol. 58, no. 6, pp. 3137–3151, Jun. 2010.
- [8] A. Hassanien and S. A. Vorobyov, "Transmit energy focusing for DOA estimation in MIMO radar with colocated antennas," *IEEE Trans. Signal Process.*, vol. 59, no. 6, pp. 2669–2682, Jun. 2011.
- [9] B. Friedlander, "On transmit beamforming for MIMO radar," *IEEE Trans. Aerosp. Electron. Syst.*, vol. 48, no. 4, pp. 3376–3388, Oct. 2012.
- [10] A. Khabbazi-basmenj, A. Hassanien, S. A. Vorobyov, and M. W. Morency, "Efficient transmit beamspace design for search-free based DOA estimation in MIMO radar," *IEEE Trans. Signal Process.*, vol. 62, no. 6, pp. 1490–1500, Mar. 2014.
- [11] V. F. Mecca, D. Ramakrishnan, and J. L. Krolik, "MIMO radar space-time adaptive processing for multipath clutter mitigation," in *Proc. IEEE Sensor Array Multichannel Signal Process. Workshop*, Waltham, MA, Jul. 2006, pp. 249–253.
- [12] Q. He, N. H. Lehmann, R. S. Blum, and A. M. Haimovich, "MIMO radar moving target detection in homogeneous clutter," *IEEE Trans. Aerosp. Electron. Syst.*, vol. 46, no. 3, pp. 1290–1301, Jul. 2010.
- [13] Y. Li, S. A. Vorobyov, and V. Koivunen, "Generalized ambiguity function for the MIMO radar with correlated waveforms," in *Proc. IEEE Int. Conf. Acoust., Speech, Signal Process. (ICASSP)*, Florence, Italy, May 2014, pp. 5322–5326.
- [14] Y. Li, S. A. Vorobyov, and A. Hassanien, "MIMO radar capability on powerful jammers suppression," in *Proc. IEEE Int. Conf. Acoust., Speech, Signal Process. (ICASSP)*, Florence, Italy, May 2014, pp. 5277–5281.
- [15] Y. Li, S. A. Vorobyov, and A. Hassanien, "Robust beamforming for jammers suppression in MIMO radar," in *Proc. IEEE Radar Conf.*, Cincinnati, OH, May 2014, pp. 0629–0634.
- [16] L. J. Griffiths, "Linear constraints in hot clutter cancellation," in *Proc. IEEE Int. Conf. Acoust., Speech, Signal Process. (ICASSP)*, Atlanta, GA, May 1996, pp. 1181–1184.
- [17] J. Ward, "Space-time adaptive processing for airborne radar," MIT Lincoln Lab., Lexington Massachusetts, MA, Technical Rep. 1015, Dec. 1994.
- [18] R. L. Fante and J. A. Torres, "Cancellation of disuse jammer multipath by an airborne adaptive radar," *IEEE Trans. Aerosp. Electron. Syst.*, vol. 31, no. 2, pp. 805–820, Apr. 1995.
- [19] Y. I. Abramovich, N. K. Spencer, S. J. Anderson, and A. Y. Gorokhov, "Stochastic-constraints method in non-stationary hot-clutter cancellation—Part I: Fundamentals and supervised training applications," *IEEE Trans. Aerosp. Electron. Syst.*, vol. 34, no. 4, pp. 1271–1291, Oct. 1998.
- [20] P. M. Techau, J. R. Guerci, T. H. Slocumb, and L. J. Griffiths, "Performance bounds for hot and cold clutter mitigation," *IEEE Trans. Aerosp. Electron. Syst.*, vol. 35, no. 4, pp. 1235–1265, Oct. 1999.
- [21] W. L. Melvin, "A STAP overview," *IEEE Trans. Aerosp. Electron. Syst.*, vol. 19, no. 1, pp. 19–35, Jan. 2004.
- [22] R. Klemm, *Principles of space-time adaptive processing*, 3rd ed. London, United Kingdom: The Institution of Electrical Engineering and Technology, 2006.
- [23] Y. Li, S. A. Vorobyov, and V. Koivunen, "Ambiguity function of the transmit beamspace-based MIMO radar," *IEEE Trans. Signal Process.*, revised, Jan. 2015.
- [24] H. L. Van Trees, *Optimum array processing*. New York: Wiley, 2002.

Publication V

Yongzhe Li, Sergiy A. Vorobyov and Aboulnasr Hassanien. MIMO radar capability on powerful jammers suppression. In *IEEE International Conference on Acoustics, Speech, and Signal Processing (ICASSP)*, Brisbane, Australia, pp. 5277–5281, May 2014.

© 2014 IEEE.

Reprinted with permission.

MIMO RADAR CAPABILITY ON POWERFUL JAMMERS SUPPRESSION

Yongzhe Li^{*†}, Sergiy A. Vorobyov^{†‡}, and Aboulnasr Hassanien[‡]

^{*}Dept. EE, University of Electronic Science and Technology of China, Chengdu, 611731, China

[†]Dept. Signal Processing and Acoustics, Aalto University, PO Box 13000, FI-00076 Aalto, Finland

[‡]Dept. Electrical and Computer Engineering, University of Alberta, Edmonton, AB T6G 2V4, Canada

Emails: lyzlyz888@gmail.com/yongzhe.li@aalto.fi, svor@ieee.org, hassanien@ieee.org

ABSTRACT

The problem of jammers suppression in colocated multiple-input multiple-output (MIMO) radar is considered. We resort to reduced dimension (RD) beamspace designs with robustness/adaptiveness to achieve the goal of efficient jammers suppression. Specifically, our RD beamspace techniques aim at designing optimal beamspace matrices based on reasonable tradeoffs between the desired in-sector source distortion and the powerful jammer (possibly in-sector) attenuation when conducting the jammers suppression. These designs are cast as convex optimization problems which are derived using second-order cone programming. Meanwhile, we study the MUSIC-based direction-of-arrival estimation performance of the proposed beamspace designs by comparing to the conventional algorithms. Moreover, we demonstrate that the capability of efficient powerful in-sector jammers suppression using these designs is unique in MIMO radar.

Index Terms— Beamspace design, colocated MIMO radar, convex optimization, jammers suppression, robustness.

1. INTRODUCTION

The recently emerging concept of multiple-input multiple-output (MIMO) radar has become the focus of intensive research [1]–[4]. It has been shown that MIMO radar with colocated antennas has advantages over phased-array (PA) radar such as improved parameter identifiability and angular resolution, increased upper limit on the number of detectable targets, and extended array aperture by virtual sensors [3]. Beamforming techniques have been employed in colocated MIMO radar to achieve coherent processing gain or desirable beampatterns [5]–[9]. Space-time adaptive processing techniques have also been exploited to mitigate clutter [10], [11]. One issue that is of great importance for colocated MIMO radar is to suppress the jamming signals which are typical interfering sources that

take the form of high-power transmission and hence result in impairing the receive system. Terrain-scattered jamming occurs when the high-power jammer transmits its energy to ground, and it reflects the energy in a dispersive manner. Thus the jamming appears at the receive array as distributed source. This scenario becomes quite complicated when the jamming impinges on the receive array within the same spatial domain as the desired source [12]. To the best of our knowledge, the capability of efficient suppression on powerful jammers for MIMO radar has not been studied in previous works.

In this paper, we utilize robust/adaptive techniques to implement the suppression of powerful jammers in the context of MIMO radar with colocated antennas. We show that in MIMO radar the echoes reflected from the targets and the intentionally radiated jamming signals have different spatial signatures even if they impinge on the receive array from the same spatial angle. Using this observation, we provide a category of beamspace processing methods which employ mathematical optimization techniques to design the beamspace matrices by making tradeoffs among the in-sector source distortion, the in-sector powerful jammers suppression, and the out-of-sector interference attenuation. These matrices are of reduced dimension (RD), which saves the computational burden. We propose to incorporate robustness/adaptiveness against both the unknown in-sector jammers and the out-of-sector interference, and further cast the designs as convex optimization problems. The MUSIC-based direction-of-arrival (DOA) estimation performance of these designs is investigated.

2. SIGNAL MODEL

Consider a MIMO radar system equipped with colocated arrays which contain M transmit antenna elements and N receive antenna elements. We assume that both the transmit and receive arrays are close enough to each other such that they share the same spatial angle of a far-field target. Let $\Phi(t) = [\phi_1(t), \dots, \phi_M(t)]^T$ be the $M \times 1$ vector that contains the complex envelopes of the transmitted waveforms $\phi_i(t)$, $i = 1, \dots, M$ which are assumed to be orthogonal, i.e., $\int_{T_p} \phi_i(t)\phi_j^*(t)dt = \delta(i-j)$, $i, j = 1, \dots, M$ where T_p is the pulse duration and $\delta(\cdot)$ is the Kronecker delta func-

Y. Li's work is supported by China Scholarship Council while he is visiting Aalto University, and by the Fundamental Research Funds for the Central Universities of China under Contract ZYGX2010YB007, and the National Nature Science Foundation of China under Grant 61032010. This work is also supported in part by the Natural Science and Engineering Research Council (NSERC), Canada.

tion. Here $(\cdot)^T$ and $(\cdot)^*$ stand for the transpose and complex conjugate operations, respectively.

Let us assume that L targets including the desired and interfering sources are present in the background of noise. The $N \times 1$ complex vector of the received observations can be expressed as

$$\mathbf{x}(t, \tau) = \sum_{l=1}^L \alpha_l(\tau) [\mathbf{a}^T(\theta_l) \Phi(t)] \mathbf{b}(\theta_l) + \mathbf{z}(t, \tau) \quad (1)$$

where τ is the slow time index, i.e., the pulse number, $\alpha_l(\tau)$ is the reflection coefficient of the l th source with variance σ_α^2 , θ_l is the spatial angle associated with the l th source, $\mathbf{a}(\theta)$ and $\mathbf{b}(\theta)$ are the steering vectors of the transmit and receive arrays, respectively, and $\mathbf{z}(t, \tau)$ is the $N \times 1$ zero-mean white Gaussian noise term.

By matched filtering the received data to the M transmitted orthogonal waveforms at the receiving end, the $MN \times 1$ virtual data vector can be obtained as

$$\begin{aligned} \mathbf{y}(\tau) &= \text{vec} \left(\int_{T_p} \mathbf{x}(t, \tau) \Phi^H(t) dt \right) \\ &= \sum_{l=1}^L \alpha_l(\tau) [\mathbf{a}(\theta_l) \otimes \mathbf{b}(\theta_l)] + \tilde{\mathbf{z}}(\tau) \end{aligned} \quad (2)$$

where $\text{vec}(\cdot)$ is the operator that stacks the columns of a matrix into one column vector, \otimes denotes the Kronecker product, $(\cdot)^H$ stands for the Hermitian transpose, and $\tilde{\mathbf{z}}(\tau) = \text{vec}(\int_{T_p} \mathbf{z}(t, \tau) \Phi^H(t) dt)$ is the $MN \times 1$ noise term whose covariance is given by $\sigma_z^2 \mathbf{I}_{MN}$ with \mathbf{I}_{MN} denoting the identity matrix of size $MN \times MN$.

In the presence of powerful jammers, the signal model (2) can be rewritten as

$$\mathbf{y}(\tau) = \sum_{l=1}^L \alpha_l(\tau) \mathbf{v}(\theta_l) + \sum_{j=1}^J \beta_j(\tau) \tilde{\mathbf{v}}(\theta_j) + \tilde{\mathbf{z}}(\tau) \quad (3)$$

where $\beta_j(\tau)$ is the signal of the j th jammer, θ_j is the presumed spatial angle associated with the j th jammer, J is the number of jammers, and $\mathbf{v}(\theta_l) \triangleq \mathbf{a}(\theta_l) \otimes \mathbf{b}(\theta_l)$ and $\tilde{\mathbf{v}}(\theta_j) \triangleq \mathbf{1}_M \otimes \mathbf{b}(\theta_j)$ are the virtual steering vectors of the l th target and the j th jammer, respectively, with $\mathbf{1}_M$ denoting the $M \times 1$ vector of all ones. The reason that the virtual steering vector of the jammer contains $\mathbf{1}_M$ is because the terrain-scattered jammer does not originate from the MIMO radar transmit array and, therefore, does not depend on its transmit array steering vector.

3. SUPPRESSION OF POWERFUL JAMMERS

We assume that the desired targets are located within a known angular sector Θ [8] where powerful jamming sources are also present and can even have the same spatial angles as the targets. In what follows, we first introduce the beamspace

signal model and present the MUSIC-based beamspace DOA estimator. Then, we propose three RD beamspace designs with robustness/adaptiveness against the in-sector jammers and the out-of-sector interfering sources whose performance is evaluated using the MUSIC-based DOA estimation.

3.1. MUSIC-Based Beamspace DOA Estimator

Let \mathbf{B} be the $MN \times D$ ($D \ll MN$) RD beamspace matrix that transforms the original $MN \times 1$ received data vector $\mathbf{y}(\tau)$ to a new data snapshot $\tilde{\mathbf{y}}(\tau)$ of size $D \times 1$, i.e.,

$$\tilde{\mathbf{y}}(\tau) = \mathbf{B}^H \mathbf{y}(\tau). \quad (4)$$

Using (4), the covariance matrix of the reduced size vector $\tilde{\mathbf{y}}(\tau)$ can be expressed as

$$\mathbf{R}_{\tilde{\mathbf{y}}} \triangleq \mathbb{E} \{ \tilde{\mathbf{y}}(\tau) \tilde{\mathbf{y}}^H(\tau) \} = \mathbf{B}^H \mathbf{R}_{\mathbf{y}} \mathbf{B} \quad (5)$$

where $\mathbf{R}_{\mathbf{y}} \triangleq \mathbb{E} \{ \mathbf{y}(\tau) \mathbf{y}^H(\tau) \}$ denotes the covariance matrix of the original received data with $\mathbb{E} \{ \cdot \}$ denoting the expectation operation. In practice, (5) is usually estimated using P available sampling snapshots and thus it can be expressed as

$$\hat{\mathbf{R}}_{\tilde{\mathbf{y}}} = \frac{1}{P} \sum_{\tau=1}^P \tilde{\mathbf{y}}(\tau) \tilde{\mathbf{y}}^H(\tau). \quad (6)$$

Under the condition that all the jamming and interfering sources are well suppressed by the beamspace processing, the eigendecomposition of (6) can be denoted as

$$\hat{\mathbf{R}}_{\tilde{\mathbf{y}}} = \mathbf{E}_s \mathbf{\Lambda}_s \mathbf{E}_s^H + \mathbf{E}_n \mathbf{\Lambda}_n \mathbf{E}_n^H \quad (7)$$

where the $L_d \times L_d$ diagonal matrix $\mathbf{\Lambda}_s$ contains the largest (signal subspace) eigenvalues and the columns of the $D \times L_d$ matrix \mathbf{E}_s are the corresponding eigenvectors with L_d being the number of the desired targets within Θ . Similarly, the $(D - L_d) \times (D - L_d)$ diagonal matrix $\mathbf{\Lambda}_n$ contains the smallest (noise subspace) eigenvalues while the $D \times (D - L_d)$ matrix \mathbf{E}_n is built from the corresponding eigenvectors.

Applying the principle of the elementspace MUSIC estimator [13], we can obtain the beamspace spectral-MUSIC DOA estimator as

$$f(\theta) = \frac{\mathbf{v}^H(\theta) \mathbf{B} \mathbf{B}^H \mathbf{v}(\theta)}{\mathbf{v}^H(\theta) \mathbf{B} \mathbf{Q} \mathbf{B}^H \mathbf{v}(\theta)} \quad (8)$$

where $\mathbf{Q} \triangleq \mathbf{E}_n \mathbf{E}_n^H = \mathbf{I}_D - \mathbf{E}_s \mathbf{E}_s^H$ is the projection matrix onto the noise subspace.

3.2. Beamspace Design With Robustness/Adaptiveness

We assume that the interfering sources are present outside Θ and consider the general case that both the in-sector jamming and the out-of-sector interfering sources are unknown.

To efficiently suppress the unknown jammers and interference, we resort to RD beamspace design techniques to

achieve the goal and later use the beamspace designs for the MUSIC-based DOA estimation. Specifically, these designs are expected to preserve desired signal energy received within the sector-of-interest (SOI) Θ , and to attenuate in-sector jammers and out-of-sector interference simultaneously. It is worth noting that these techniques significantly reduce the computational burden, and performing DOA estimation in beamspace leads to performance improvements such as enhanced source resolution, reduced DOA estimation bias, and reduced sensitivity to array calibration errors.

Technically, we first exploit the spheroidal sequences based methods [8], [14] to achieve a quiescent response beamspace matrix which ensures the preservation of energy received within the desired sector Θ . Then, we propose to design robust/adaptive RD beamspace processing, aiming at preserving the desired signal components while suppressing the in-sector powerful jammers and/or filtering out the interfering components that come from outside Θ . In other words, tradeoffs between the in-sector source distortion and the out-of-sector source attenuation are made while imposing a novel constraint used to nullify the jammers. It naturally leads to the robustness/adaptiveness against the unknown jammers. For example, we consider the case of distributed jammers that are located within the desired sector Θ . Although these jamming signals overlap with the desired sector, they can still be cancelled out by imposing the additional constraint.

For our beamspace designs, the beamspace dimension D depends on the width of Θ , and it can be obtained based on the principle that D should not be smaller than the number of the largest eigenvalues of the matrix $\mathbf{A} \triangleq \int_{\Theta} \mathbf{v}^H(\theta)\mathbf{v}(\theta)d\theta$ while simultaneously requires their sum to exceed a certain percentage (e.g., 99%) of the total sum of all eigenvalues. When the MUSIC-based DOA estimation is applied, D also needs to be no smaller than the number of the desired targets.

The first solution is to upper-bound the acceptable difference between the desired and quiescent response beamspace matrices while maximizing the worst-case in-sector jammers suppression. Additionally, the out-of-sector sidelobes can be kept below a certain level to insure interference attenuation. The corresponding optimization problem can be written as

$$\begin{aligned} \min_{\mathbf{B}} \max_i & \|\mathbf{B}^H \tilde{\mathbf{v}}(\theta_i)\|, \theta_i \in \Theta, i = 1, \dots, Q \\ \text{s.t.} & \|\mathbf{B} - \mathbf{B}_q\|_F \leq \varepsilon \\ & \|\mathbf{B}^H \mathbf{v}(\bar{\theta}_k)\| \leq \gamma, \bar{\theta}_k \in \bar{\Theta}, k = 1, \dots, K \end{aligned} \quad (9)$$

where \mathbf{B}_q is the quiescent response beamspace matrix, $\varepsilon > 0$ is the parameter that bounds the in-sector signal distortion caused by the beamspace matrix \mathbf{B} as compared to \mathbf{B}_q , $\gamma > 0$ is the parameter of the user choice that characterizes the worst acceptable out-of-sector attenuation, $\bar{\Theta}$ combines a continuum of all out-of-sector directions, $\{\theta_i \in \Theta, i = 1, \dots, Q\}$ and $\{\bar{\theta}_k \in \bar{\Theta}, k = 1, \dots, K\}$ are grids of angles used to approximate the in-sector Θ and the out-of-sector $\bar{\Theta}$ by finite numbers Q and K of directions, respectively, $\|\cdot\|_F$ is the Frobenius

norm of a matrix, and $\|\cdot\|$ is the Euclidean norm.

An alternative robust approach is to minimize the difference between the desired and quiescent response beamspace matrices while keeping the in-sector jammers suppression higher than a certain desired level and, if needed, keeping the out-of-sector attenuation to an acceptable level. Hence, the corresponding optimization problem can be written as

$$\begin{aligned} \min_{\mathbf{B}} & \|\mathbf{B} - \mathbf{B}_q\|_F \\ \text{s.t.} & \|\mathbf{B}^H \tilde{\mathbf{v}}(\theta_i)\| \leq \delta, \theta_i \in \Theta, i = 1, \dots, Q \\ & \|\mathbf{B}^H \mathbf{v}(\bar{\theta}_k)\| \leq \gamma, \bar{\theta}_k \in \bar{\Theta}, k = 1, \dots, K \end{aligned} \quad (10)$$

where $\delta > 0$ is the parameter that characterizes the worst acceptable level of the jamming power radiation in the desired sector Θ . It is worth noting that the last set of constraints in (9) and (10) are needed only if there are interfering sources located in the out-of-sector area, and, therefore, they can be removed if only intentional jammer suppression is concerned.

As on-line computation becomes practical, it is meaningful to develop an approach that is data-adaptive for the beamspace design. This is particularly important when the jammers and/or the interfering sources are varying. To adaptively cancel out both types of sources, the data-adaptive formulation can be developed by minimizing the output power of the transformed vector $\tilde{\mathbf{y}}(\tau)$. This power can be denoted as

$$\mathbb{E}[\tilde{\mathbf{y}}^H(\tau)\tilde{\mathbf{y}}(\tau)] = \text{tr}\{\mathbb{E}[\tilde{\mathbf{y}}(t)\tilde{\mathbf{y}}^H(t)]\} = \text{tr}\{\mathbf{B}^H \mathbf{R}_y \mathbf{B}\} \quad (11)$$

where $\text{tr}\{\cdot\}$ denotes the trace of a matrix. Finally, the corresponding data-adaptive beamspace design can be cast as

$$\begin{aligned} \min_{\mathbf{B}} & \text{tr}\{\mathbf{B}^H \mathbf{R}_y \mathbf{B}\} \\ \text{s.t.} & \|\mathbf{B} - \mathbf{B}_q\|_F \leq \varepsilon \\ & \|\mathbf{B}^H \tilde{\mathbf{v}}(\theta_i)\| \leq \delta, \theta_i \in \Theta, i = 1, \dots, Q \\ & \|\mathbf{B}^H \mathbf{v}(\bar{\theta}_k)\| \leq \gamma, \bar{\theta}_k \in \bar{\Theta}, k = 1, \dots, K. \end{aligned} \quad (12)$$

The problems (9), (10), and (12) are convex and can be efficiently solved using second-order cone (SOC) programming. For given values of δ and γ , the feasibility of (12) is guaranteed if $\varepsilon \geq \varepsilon_{\min}$ is used where ε_{\min} is the minimum value of $\|\mathbf{B} - \mathbf{B}_q\|_F$ that can be calculated by solving (10).

It is worth noting that the capability of in-sector jammers suppression for MIMO radar is unique. PA radar is unable to achieve the goal of in-sector jammers suppression by utilizing the same way in spatial domain especially when the jammers and the desired targets are located at the same directions.

4. SIMULATION RESULTS

In our simulations, we use uniform linear arrays of $M = 16$ transmit and $N = 8$ receive antenna elements spaced half a wavelength apart. The presumed SOI area is $\Theta = [10^\circ, 25^\circ]$ and the out-of-sector area is $\bar{\Theta} = [-90^\circ, 0^\circ] \cup [35^\circ, 90^\circ]$. Two

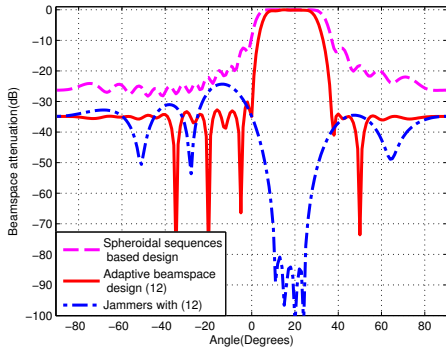


Fig. 1. Beamspace attenuation versus angle.

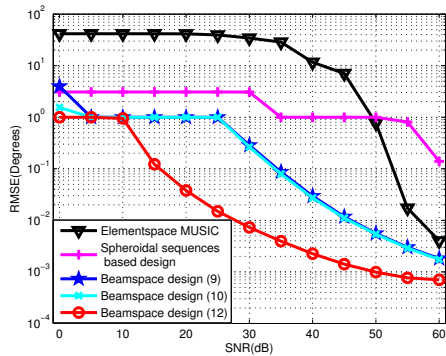


Fig. 2. RMSEs of DOA estimation versus SNR.

desired targets with DOAs $\theta_t = 16.5^\circ$ and 18.5° are located in the SOI, and four interfering sources are assumed to be located at $\theta = -35^\circ, -20^\circ, -5^\circ,$ and 50° , respectively. The signal-to-noise ratio (SNR) and interference-to-noise ratio (INR) are set to be equal to 0 dB and 40 dB, respectively. The CVX toolbox [15] is used to solve the problems (9), (10), and (12).

In the first example, we assume that uniformly distributed jammers spaced 1° apart from each other are present in the SOI. The jammer-to-noise ratio (JNR) is assumed to be equal to 50 dB. Other parameters employed are as follows: $D = 7$, $P = 500$, $\gamma = 0.2$, $\delta = 0.1$, and $\varepsilon = 1.467$. Fig. 1 shows the beamspace attenuation $g(\theta) \triangleq \|\mathbf{B}^H \mathbf{u}(\theta)\|^2 / \|\mathbf{u}(\theta)\|^2$ ($\mathbf{u}(\theta) = \mathbf{v}(\theta)$ for targets and $\mathbf{u}(\theta) = \tilde{\mathbf{v}}(\theta)$ for jammers) for the spheroidal sequences based algorithm and the proposed adaptive beamspace design in (12). It can be clearly seen that the proposed data-adaptive beamspace design shows good capability of suppressing the out-of-sector interference and the in-sector jammers, even if they have the same directions as the targets. There is almost no target attenuation within the SOI.

In the second example, we evaluate the suppression performance of the beamspace designs by comparing the DOA estimation performance versus SNR with that of the conven-

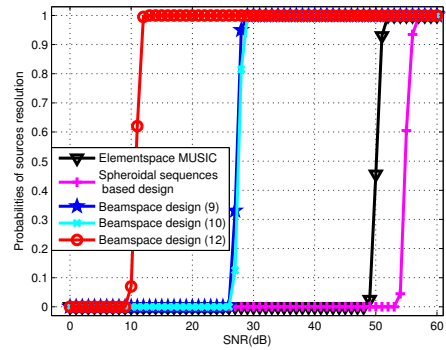


Fig. 3. Probabilities of source resolution versus SNR.

tional elementspace MUSIC and spheroidal sequences based algorithms. The same scenario and parameters are selected as used in the first example except that only the 5 jammers located between 15.5° and 19.5° are present. The results are averaged over 200 independent simulation runs. Fig. 2 displays the root-mean-square errors (RMSEs) of the MUSIC-based DOA estimators, and Fig. 3 shows the corresponding probabilities of source resolution for different designs. The target sources are regarded as resolved in the n th run if $\sum_{i=1}^2 |\hat{\theta}_i(n) - \theta_i| < 2^\circ$ where $\hat{\theta}_i(n)$ is the estimated DOA of the i th target in the n th run. It can be seen that the performance of all the proposed beamspace designs outperform that of the conventional methods. In the presence of powerful in-sector jammers and out-of-sector interfering sources, the conventional elementspace MUSIC and spheroidal sequences based algorithms can not accurately discriminate targets even if large SNR is employed. The proposed data-adaptive beamspace design gives the best RMSE and probabilities of source resolution only if the SNR is larger than 12 dB. The other two beamspace designs show approximately the same DOA estimation performance.

5. CONCLUSIONS

We have considered the jammers suppression problem for MIMO radar with colocated antennas, and have provided three RD beamspace designs to address the problem. Tradeoffs between the desired in-sector source distortion and the powerful jammer (possibly in-sector) attenuation are made when conducting the jammers suppression. We cast the designs as convex optimization problems using SOC programming, in which robustness/adaptiveness against the unknown in-sector jamming and out-of-sector interfering sources is incorporated. Moreover, we have investigated the MUSIC-based DOA estimation performance of the proposed designs. Simulation results show that the performance of the proposed designs outperforms that of the conventional methods. We have also shown that the capability of efficient in-sector jammers suppression using these designs is unique in MIMO radar.

6. REFERENCES

- [1] J. Li and P. Stoica, *MIMO Radar Signal Processing*. New York: Wiley, 2009.
- [2] A. M. Haimovich, R. S. Blum, and L. J. Cimini, "MIMO radar with widely separated antennas," *IEEE Signal Processing Magazine*, vol. 24, no. 1, pp. 116–129, Jan. 2008.
- [3] J. Li and P. Stoica, "MIMO radar with colocated antennas," *IEEE Signal Processing Magazine*, vol. 24, no. 5, pp. 106–114, Sep. 2007.
- [4] E. Fishler, A. Haimovich, R. S. Blum, L. Cimini, D. Chizhik, and R. Valenzuela, "Spatial diversity in radars: Models and detection performance," *IEEE Trans. Signal Processing*, vol. 54, no. 3, pp. 823–838, Mar. 2006.
- [5] D. R. Fuhrmann and G. S. Antonio, "Transmit beamforming for MIMO radar systems using signal cross-correlation," *IEEE Trans. Aerosp. Electron. Syst.*, vol. 44, no. 1, pp. 171–186, Jan. 2008.
- [6] P. Stoica, J. Li and Y. Xie, "On probing signal design for MIMO radar," *IEEE Trans. Signal Processing*, vol. 55, no. 8, pp. 4151–4161, Aug. 2007.
- [7] A. Hassanien and S. A. Vorobyov, "Phased-MIMO radar: A tradeoff between phased-array and MIMO radars," *IEEE Trans. Signal Processing*, vol. 58, no. 6, pp. 3137–3151, June 2010.
- [8] A. Hassanien and S. A. Vorobyov, "Transmit energy focusing for DOA estimation in MIMO radar with colocated antennas," *IEEE Trans. Signal Processing*, vol. 59, no. 6, pp. 2669–2682, June 2011.
- [9] A. Khabbazi-basmenj, A. Hassanien, S. A. Vorobyov, and M. W. Morency, "Efficient transmit beamspace design for search-free based DOA estimation in MIMO radar," *IEEE Trans. Signal Processing*, vol. 62, no. 6, pp. 1490–1500, Mar. 2014.
- [10] V. F. Mecca, D. Ramakrishnan, and J. L. Krolik, "MIMO radar space-time adaptive processing for multipath clutter mitigation," in *Proc. IEEE Workshop Sensor Array Multichannel Signal Processing*, Waltham, MA, 2006, pp. 249–253.
- [11] C-Y. Chen and P. P. Vaidyanathan, "MIMO radar space-time adaptive processing using prolate spheroidal waveform functions," *IEEE Trans. Signal Processing*, vol. 56, no. 2, pp. 623–635, Feb. 2008.
- [12] Y. Li, S. A. Vorobyov, and A. Hassanien, "Robust beamforming for jammers suppression in MIMO radar," *IEEE Radar Conf.*, Cincinnati, OH, May 2014.
- [13] R. O. Schmidt, "Multiple emitter location and signal parameter estimation," in *Proc. RADC Spectral Estimation Workshop*, Rome, NY, 1979, pp. 234–258.
- [14] A. Hassanien, S. A. Elkader, A. B. Gershman, and K. M. Wong, "Convex optimization based beamspace pre-processing with an improved robustness against out-of-sector sources," *IEEE Trans. Signal Processing*, vol. 54, no. 5, pp. 1587–1595, May 2006.
- [15] M. Grant and S. Boyd. (2013, Sept.). *CVX: Matlab software for disciplined convex programming* (version 2.0 beta) [online]. Available: <http://cvxr.com/cvx>

Publication VI

Yongzhe Li, Sergiy A. Vorobyov and Aboulnasr Hassanien. Robust beamforming for jammers suppression in MIMO radar. In *IEEE Radar Conference*, Cincinnati, OH, USA, pp. 0629–0634, May 2014.

© 2014 IEEE.

Reprinted with permission.

Robust Beamforming for Jammers Suppression in MIMO Radar

(Invited Paper)

Yongzhe Li^{*†}, Sergiy A. Vorobyov^{†‡}, and Aboulnasr Hassanien[‡]

^{*}Dept. of EE, University of Electronic Science and Technology of China, Chengdu, 611731, China

[†]Dept. of Signal Processing and Acoustics, Aalto University, PO Box 13000, FI-00076 Aalto, Finland

[‡]Dept. of Electrical and Computer Engineering, University of Alberta, Edmonton, AB T6G 2V4, Canada

Emails: lyzlyz888@gmail.com/yongzhe.li@aalto.fi, svor@ieee.org, hassanien@ieee.org

Abstract—Robust beamforming for multiple-input multiple-output (MIMO) radar in the background of powerful jamming signals is investigated in this paper. We design two minimum variance distortionless response (MVDR) type beamformers with adaptiveness/robustness against the powerful jammers for colocated MIMO radar. Specifically, the MVDR beamformer is firstly designed for known jammers in the sector-of-interest, which maintains distortionless response towards the direction of the target while imposing nulls towards the directions of jammers. Then the adaptive/robust MVDR beamformer is designed for the general case of unknown in-sector jammers and/or out-of-sector interfering sources. Convex optimization techniques are used in both of the designs. Moreover, we derive a closed-form solution to the simplified second design. Based on this solution, we derive efficient power estimates of the desired and/or interfering sources in the context of powerful jammers and non-ideal factors such as array calibration errors and target steering vector mismatches. We demonstrate that the capability of efficient jammers suppression using these designs is unique in MIMO radar.

I. INTRODUCTION

Multiple-input multiple-output (MIMO) radar has become the focus of intensive research [1]–[4]. Two configurations of MIMO radar have been developed in current literature. One is the MIMO radar with widely separated antennas [2], which exploits the spatial diversity of the target. This type of MIMO radar has been shown to be capable of improving the target detection and parameter estimation performance, and enhancing the ability to combat target scintillation [2], [4], [5]. The other is the MIMO radar with colocated antennas [3], which exploits the waveform diversity allowed by the transmit and receive antenna arrays. It has been shown that this type of MIMO radar facilitates improving the angular resolution and parameter identifiability, increasing the upper limit on the number of resolvable targets, extending the array aperture, and obtaining the desired transmit beampatterns [3], [6]–[10].

For MIMO radar, interfering sources can take different forms and have widely varying impacts on it. The terrain-scattered jamming is a typical interfering example that takes the form of high-power transmission and results in impairing the receiving system. It occurs when high-power jammer transmits its energy

into ground. The ground reflects the energy in a dispersive manner, hence the powerful jamming signal appears at the receive array as distributed source. This situation can be more serious when the powerful jammers are present in the same directions as the desired targets, which severely affects the performance of MIMO radar such as target detection ability, parameter estimation capability, etc. It worsens even more since the powerful jammers are generally unknown. Therefore, designing simple and efficient ways of jammers suppression becomes particularly important and imperative. Moreover, these suppression methods should be robust enough against the unknown jammers.

In current literature, space-time adaptive processing (STAP) techniques [11], [12] have been exploited to mitigate the clutter and the interference in MIMO radar systems, in which two-dimensional filters operating in both the spatial and temporal domains are employed in order to adaptively impose nulls towards them. For example, prolate spherical waveform functions are used to construct the clutter subspace in [11] for fully adaptive processing, and slow-time STAP is conducted in [12] to mitigate the clutter subject to multi-path propagation between the transmit and receive arrays. Although similar STAP techniques can be used to suppress the powerful jammers with small modifications, they are not robust when there exist array calibration errors and target steering vector mismatches. Moreover, they have large computational complexity due to their two-dimensional adaptive processing.

Another category of jammer suppression strategies that can be resorted to is the beamforming technique [7], [8], [13]–[17]. In the last two decades, robust adaptive beamforming has been thoroughly investigated for traditional phased-array (PA) radar. The well-known minimum variance distortionless response (MVDR) beamformer is obtained by minimizing the variance/power of the interference and noise at the output of the adaptive beamformer while ensuring the distortionless response of the beamformer towards the direction of the desired source. To the best of our knowledge, introducing robust adaptive MVDR beamforming to MIMO radar, and further studying the capability of efficient suppression on powerful jammers, however, have not received attention yet.

In this paper, we use beamforming techniques to implement the suppression of powerful jammers for colocated MIMO radar. We show that in MIMO radar the echoes reflected from

Y. Li's work is supported by China Scholarship Council while he is visiting Aalto University, and by the Fundamental Research Funds for the Central Universities of China under Contract ZYGX2010YB007, and the National Nature Science Foundation of China under Grant 61032010. This work is also supported in part by the Natural Science and Engineering Research Council (NSERC), Canada.

the targets and the intentionally radiated jamming signals have different spatial signatures even if they impinge on the receive array from the same spatial angle. Using this observation, we design two MVDR type beamformers with adaptiveness/robustness against powerful jammers for MIMO radar. We first design an MVDR beamformer for known jammers in the sector-of-interest (SOI) by maintaining distortionless response towards the direction of the target while enforcing nulls towards the directions of the jammers. Then we design another MVDR beamformer for the general case of unknown in-sector jammers and/or out-of-sector interfering sources. Both designs are cast as convex optimization problems. We propose to incorporate adaptiveness/robustness against the in-sector jammers and/or the out-of-sector interfering sources in these designs. Moreover, we derive a closed-form solution for the simplified second design. Based on this solution we further find an efficient source power estimate method in the background of powerful jammers and non-ideal factors such as array calibration errors and steering vector mismatches.

II. SYSTEM MODEL

Consider a MIMO radar system equipped with linear transmit and receive arrays which contain M transmit antenna elements and N receive antenna elements. Both the transmit and receive arrays are assumed to be close enough to each other such that they share the same spatial angle of a far-field target. Let $\Phi(t) = [\phi_1(t), \dots, \phi_M(t)]^T$ be the $M \times 1$ vector that contains the complex envelopes of the transmitted waveforms $\phi_i(t)$, $i = 1, \dots, M$ which are assumed to be orthogonal, i.e., $\int_{T_p} \phi_i(t)\phi_j^*(t)dt = \delta(i-j)$, $i, j = 1, \dots, M$, where T_p is the pulse duration and $\delta(\cdot)$ is the Kronecker delta function. Here $(\cdot)^T$ and $(\cdot)^*$ stand for the transpose and complex conjugate operations, respectively.

Let us assume that L sources including the desired and interfering ones are observed in the background of noise. Then the $N \times 1$ complex vector of the received observations can be expressed as

$$\mathbf{x}(t, \tau) = \sum_{l=1}^L \alpha_l(\tau) [\mathbf{a}^T(\theta_l) \Phi(t)] \mathbf{b}(\theta_l) + \mathbf{z}(t, \tau) \quad (1)$$

where τ is the slow time index, i.e., the pulse number, $\alpha_l(\tau)$ is the reflection coefficient of the l th source with variance σ_α^2 , θ_l is the spatial angle associated with the l th source, $\mathbf{a}(\theta)$ and $\mathbf{b}(\theta)$ are the steering vectors of the transmit and receive arrays, respectively, and $\mathbf{z}(t, \tau)$ is the $N \times 1$ zero-mean white Gaussian noise term. Note that $\alpha_l(\tau)$ is assumed to remain constant during the whole pulse, but varies independently from pulse to pulse, i.e., it obeys the Swerling II target model [18].

By matched filtering the received data to the M orthogonal waveforms at the receiving end, the $MN \times 1$ virtual data vector can be obtained as

$$\begin{aligned} \mathbf{y}(\tau) &= \text{vec} \left(\int_{T_p} \mathbf{x}(t, \tau) \Phi^H(t) dt \right) \\ &= \sum_{l=1}^L \alpha_l(\tau) [\mathbf{a}(\theta_l) \otimes \mathbf{b}(\theta_l)] + \tilde{\mathbf{z}}(\tau) \end{aligned} \quad (2)$$

where $\tilde{\mathbf{z}}(\tau) = \text{vec}(\int_{T_p} \mathbf{z}(t, \tau) \Phi^H(t) dt)$ is the $MN \times 1$ noise term whose covariance is given by $\sigma_z^2 \mathbf{I}_{MN}$ with \mathbf{I}_{MN} denoting the identity matrix of size $MN \times MN$, $\text{vec}(\cdot)$ is the operator that stacks the columns of a matrix into one column vector, \otimes denotes the Kronecker product, and $(\cdot)^H$ stands for the Hermitian transpose.

Let us assume that J powerful jammers are present and transmit their energy into ground, then the signal model (2) can be rewritten as

$$\begin{aligned} \mathbf{y}(\tau) &= \sum_{l=1}^L \alpha_l(\tau) [\mathbf{a}(\theta_l) \otimes \mathbf{b}(\theta_l)] \\ &\quad + \sum_{j=1}^J \beta_j(\tau) [\mathbf{1}_M \otimes \mathbf{b}(\theta_j)] + \tilde{\mathbf{z}}(\tau) \end{aligned} \quad (3)$$

where $\beta_j(\tau)$ is the signal of the j th jammer, θ_j is the presumed spatial angle associated with the j th jammer, and $\mathbf{1}_M$ denotes the $M \times 1$ vector of all ones.

Let $\mathbf{v}(\theta_l) \triangleq \mathbf{a}(\theta_l) \otimes \mathbf{b}(\theta_l)$ and $\tilde{\mathbf{v}}(\theta_j) \triangleq \mathbf{1}_M \otimes \mathbf{b}(\theta_j)$ be the virtual steering vectors of the l th target and the j th jammer, respectively, then (3) can be expressed as

$$\mathbf{y}(\tau) = \sum_{l=1}^L \alpha_l(\tau) \mathbf{v}(\theta_l) + \sum_{j=1}^J \beta_j(\tau) \tilde{\mathbf{v}}(\theta_j) + \tilde{\mathbf{z}}(\tau). \quad (4)$$

Note that the reason that the virtual steering vector of the jammer contains $\mathbf{1}_M$ is because the terrain-scattered jammer is independent of the transmitted waveforms.

III. ROBUST BEAMFORMING DESIGN FOR JAMMERS SUPPRESSION

We assume that the desired targets are located within a known SOI Θ [10] where powerful jamming sources are also present and can even have the same spatial angles as the targets. Meanwhile, we assume that the interfering sources are present outside the SOI.

The first beamforming design is for the case when all the in-sector jammers are known, for example, they can be estimated beforehand. To achieve the goal of jammers suppression, deep null notches should be formed towards the spatial directions of the jammers while maintaining distortionless response towards the direction of the target(s). Thus, the corresponding optimization problem can be written as

$$\min_{\mathbf{w}} \quad \mathbf{w}^H \mathbf{R} \mathbf{w} \quad (5a)$$

$$\text{s.t.} \quad \mathbf{w}^H \mathbf{v}(\theta_t) = 1 \quad (5b)$$

$$\mathbf{w}^H \tilde{\mathbf{v}}(\theta_j) = 0, \quad j = 1, \dots, J \quad (5c)$$

where \mathbf{R} is the covariance matrix of the interference plus jammer and noise, \mathbf{w} is the designed beamforming weight vector, and θ_t is the spatial angle of the desired target.

The constraints (5c) impose nulls towards the powerful jamming signals, and they are expected to annihilate all the jammer components of the received signal even if the jammers have the same spatial angle as the desired target. The principle of robust adaptive beamforming can be incorporated in the

considered case. Indeed, if there is an uncertainty about the in-sector target and jammer locations in the presence of the out-of-sector interfering signals, the distortionless response constraint (5b) and the null constraints (5c) can be extended to all steering vectors defined by a ball (or ellipse) centered around θ_i and θ_j [15]–[17].

The second beamforming design is based on the general case that the in-sector jammers and the out-of-sector interfering sources are unknown. Deep null notches should be formed towards all the possible directions of the jammers and, if needed, the out-of-sector interfering source attenuation should be kept to an acceptable level. Hence, the corresponding optimization problem can be written as

$$\min_{\mathbf{w}} \mathbf{w}^H \mathbf{R} \mathbf{w} \quad (6a)$$

$$\text{s.t. } \mathbf{w}^H \mathbf{v}(\theta_t) = 1 \quad (6b)$$

$$|\mathbf{w}^H \tilde{\mathbf{v}}(\theta_i)| \leq \delta, \theta_i \in \Theta, i = 1, \dots, Q \quad (6c)$$

$$|\mathbf{w}^H \mathbf{v}(\bar{\theta}_k)| \leq \gamma, \bar{\theta}_k \in \bar{\Theta}, k = 1, \dots, K \quad (6d)$$

where $\bar{\Theta}$ combines a continuum of all out-of-sector directions, $\{\bar{\theta}_k \in \bar{\Theta}, k = 1, \dots, K\}$ is the angular grid chosen to properly approximate the out-of-sector $\bar{\Theta}$ by a finite number K of directions, $\{\theta_i \in \Theta, i = 1, \dots, Q\}$ is a grid of angles used to approximate Θ by Q directions, $\gamma > 0$ is the parameter of the user choice that characterizes the worst acceptable out-of-sector attenuation of interfering targets, $\delta > 0$ is the parameter that characterizes the worst acceptable level of the jamming power radiation in the desired sector Θ , and $|\cdot|$ denotes the magnitude of a complex quantity.

Both of the MVDR beamforming designs (5) and (6) incorporate adaptiveness towards the out-of-sector interferences and robustness towards the in-sector jammers. The first design is simple and efficient for the case of known in-sector jammers whose spatial angles have been already known beforehand, while the second design adapts to the general case that the in-sector jammers are unknown, making it more robust than the first design. Although the robust in-sector jammers suppression and the out-of-sector interferences attenuation result in increased computational complexity, the latter design is a flexible and useful strategy. It overcomes the challenge that there is no prior information about the in-sector jammers and allows the jammers to be varying. Thus, in this sense, it serves as a universal strategy for powerful jammers suppression using MIMO radar. In addition, the out-of-sector attenuation facilitates the design that requires controlling the sidelobes in practice.

IV. SOURCE POWER ESTIMATION

The standard MVDR beamforming problem, i.e., the problem (5) without the constraint (5c), leads to the following closed-form solution [19]

$$\mathbf{w}_{\text{opt}} = \frac{\mathbf{R}^{-1} \mathbf{v}(\theta_t)}{\mathbf{v}^H(\theta_t) \mathbf{R}^{-1} \mathbf{v}(\theta_t)} \quad (7)$$

when $\mathbf{v}(\theta_t)$ is known. Using (7), the standard MVDR beamforming yields the estimate of the source power σ_0^2 as

$$\sigma_0^2 = \frac{1}{\mathbf{v}^H(\theta_t) \mathbf{R}^{-1} \mathbf{v}(\theta_t)}. \quad (8)$$

Powerful jamming source that locates at the same direction as the desired target results in serious performance degradation of the standard MVDR beamforming technique. It becomes even worse when the knowledge of $\mathbf{v}(\theta_t)$ is imprecise because the standard MVDR beamformer attempts to suppress the desired target as if it was an interfering source. This happens in practice especially when there are array calibration errors and mismatches between the presumed and actual target steering vectors. In what follows, we derive a solution of the simplified second proposed beamforming design with robustness against both the in-sector jammers and the aforementioned non-ideal factors simultaneously and, furthermore, provide the source power estimate for the robust MVDR beamforming design.

To simplify the derivation, we ignore the out-of-sector interfering source attenuation constraint (6d). Let us introduce a $MN \times Q$ matrix $\tilde{\mathbf{V}}$ whose i th column is defined as $\tilde{\mathbf{v}}(\theta_i)$, $i \in \{1, \dots, Q\}$, i.e., $\tilde{\mathbf{V}} \triangleq [\tilde{\mathbf{v}}(\theta_1), \dots, \tilde{\mathbf{v}}(\theta_Q)]$. Then the optimization problem (6) without (6d) can be expressed as

$$\min_{\mathbf{w}} \mathbf{w}^H \mathbf{R} \mathbf{w} \quad (9)$$

$$\text{s.t. } \mathbf{w}^H \mathbf{v}(\theta_t) = 1$$

$$\|\mathbf{w}^H \tilde{\mathbf{V}}\|_{\infty} \leq \delta$$

where $\|\cdot\|_{\infty}$ denotes the chebyshev norm.

Using the fact that $\|\mathbf{w}^H \tilde{\mathbf{V}}\|_{\infty} \geq \|\mathbf{w}^H \tilde{\mathbf{V}}\| / \sqrt{MN}$ where $\|\cdot\|$ denotes the Euclidean norm, and assuming that the mismatch between the actual target steering vector $\mathbf{v}(\theta)$ and the presumed target steering vector $\tilde{\mathbf{v}}(\theta)$ is bounded as $\|\tilde{\mathbf{v}}(\theta) - \mathbf{v}(\theta)\|^2 \leq \epsilon$, where ϵ is the given parameter that characterizes the worst allowable steering vectors error, then the optimization problem (9) can be approximated by the following strengthened optimization problem

$$\min_{\mathbf{w}} \mathbf{w}^H \mathbf{R} \mathbf{w} \quad (10a)$$

$$\text{s.t. } \mathbf{w}^H \tilde{\mathbf{v}}(\theta_t) = 1 \quad (10b)$$

$$\|\mathbf{w}^H \tilde{\mathbf{V}}\|^2 \leq \tilde{\delta} \quad (10c)$$

where $\tilde{\delta} \triangleq MN\delta^2$ is the new parameter that characterizes the worst acceptable level of the in-sector jamming power radiation for the new Euclidean norm based constraint.

Let $\lambda > 0$ and μ be the real-valued Lagrange multipliers with μ being arbitrary. Then we define the Lagrangian of the optimization problem (10) as

$$L(\mathbf{w}, \lambda, \mu) \quad (11)$$

$$= \mathbf{w}^H \mathbf{R} \mathbf{w} + \lambda \left(\|\mathbf{w}^H \tilde{\mathbf{V}}\|^2 - \tilde{\delta} \right) + \mu \left(-\Re \{ \mathbf{w}^H \tilde{\mathbf{v}}(\theta_t) \} + 1 \right)$$

where $\Re\{\cdot\}$ denotes the real part of a complex quantity. Let $\mathbf{R}_{\tilde{\mathbf{V}}} \triangleq \tilde{\mathbf{V}} \tilde{\mathbf{V}}^H$, then (11) can be rewritten as

$$L(\mathbf{w}, \lambda, \mu) \quad (12)$$

$$= \mathbf{w}^H \mathbf{R} \mathbf{w} + \lambda \left(\mathbf{w}^H \mathbf{R}_{\tilde{\mathbf{V}}} \mathbf{w} - \tilde{\delta} \right) + \mu \left(-\Re \{ \mathbf{w}^H \tilde{\mathbf{v}}(\theta_t) \} + 1 \right)$$

which satisfies the following inequality

$$L(\mathbf{w}, \lambda, \mu) \leq \mathbf{w}^H \mathbf{R} \mathbf{w} \quad \text{for any } \mathbf{w} \in D \quad (13)$$

where D is the feasible set defined by the constraints in (10). The equality in (13) holds on the boundary of D .

The solution of (10) can be derived under two conditions. The first condition is that

$$\frac{\bar{\mathbf{v}}^H(\theta_t) \mathbf{R}^{-1} \mathbf{R}_{\bar{\mathbf{V}}} \mathbf{R}^{-1} \bar{\mathbf{v}}(\theta_t)}{[\bar{\mathbf{v}}^H(\theta_t) \mathbf{R}^{-1} \bar{\mathbf{v}}(\theta_t)]^2} \leq \tilde{\delta} \quad (14)$$

and based on it we can derive the solution of (10) directly according to (7) by replacing the actual target steering vector with the presumed one, i.e.,

$$\bar{\mathbf{w}} = \frac{\mathbf{R}^{-1} \bar{\mathbf{v}}(\theta_t)}{\bar{\mathbf{v}}^H(\theta_t) \mathbf{R}^{-1} \bar{\mathbf{v}}(\theta_t)}. \quad (15)$$

This means that in this case λ is equal to 0 and hence the constraint (10c) is not necessary.

If (14) is not satisfied, then the second condition described by the following inequality

$$\frac{\bar{\mathbf{v}}^H(\theta_t) \mathbf{R}^{-1} \mathbf{R}_{\bar{\mathbf{V}}} \mathbf{R}^{-1} \bar{\mathbf{v}}(\theta_t)}{[\bar{\mathbf{v}}^H(\theta_t) \mathbf{R}^{-1} \bar{\mathbf{v}}(\theta_t)]^2} > \tilde{\delta} \quad (16)$$

holds, which sets the upper bound on $\tilde{\delta}$ and hence leads to a new solution. Realizing that (12) can be expressed as

$$\begin{aligned} L(\mathbf{w}, \lambda, \mu) &= \left[\mathbf{w} - \mu (\mathbf{R} + \lambda \mathbf{R}_{\bar{\mathbf{V}}})^{-1} \bar{\mathbf{v}}(\theta_t) \right]^H (\mathbf{R} + \lambda \mathbf{R}_{\bar{\mathbf{V}}}) \\ &\quad \times \left[\mathbf{w} - \mu (\mathbf{R} + \lambda \mathbf{R}_{\bar{\mathbf{V}}})^{-1} \bar{\mathbf{v}}(\theta_t) \right] - \mu^2 \bar{\mathbf{v}}(\theta_t)^H \\ &\quad \times (\mathbf{R} + \lambda \mathbf{R}_{\bar{\mathbf{V}}})^{-1} \bar{\mathbf{v}}(\theta_t) - \lambda \tilde{\delta} + 2\mu \end{aligned} \quad (17)$$

we find that the following solution

$$\bar{\mathbf{w}}_{\lambda, \mu} = \mu (\mathbf{R} + \lambda \mathbf{R}_{\bar{\mathbf{V}}})^{-1} \bar{\mathbf{v}}(\theta_t) \quad (18)$$

yields the minimum value of the Lagrangian (12) for fixed λ and μ , i.e.,

$$\begin{aligned} L(\bar{\mathbf{w}}_{\lambda, \mu}, \lambda, \mu) & \\ &= -\mu^2 \bar{\mathbf{v}}(\theta_t)^H (\mathbf{R} + \lambda \mathbf{R}_{\bar{\mathbf{V}}})^{-1} \bar{\mathbf{v}}(\theta_t) - \lambda \tilde{\delta} + 2\mu. \end{aligned} \quad (19)$$

The maximization of (19) with respect to μ is achieved by letting its derivative with respect to μ be equal to 0, which gives the following optimal value for μ

$$\bar{\mu} = \frac{1}{\bar{\mathbf{v}}(\theta_t)^H (\mathbf{R} + \lambda \mathbf{R}_{\bar{\mathbf{V}}})^{-1} \bar{\mathbf{v}}(\theta_t)}. \quad (20)$$

By substituting (20) into (19), the Lagrangian can be rewritten as

$$L(\bar{\mathbf{w}}_{\lambda, \mu}, \lambda, \bar{\mu}) = \frac{1}{\bar{\mathbf{v}}(\theta_t)^H (\mathbf{R} + \lambda \mathbf{R}_{\bar{\mathbf{V}}})^{-1} \bar{\mathbf{v}}(\theta_t)} - \lambda \tilde{\delta}. \quad (21)$$

Similarly, the maximization of (21) with respect to λ is achieved by letting its derivative with respect to λ be equal to 0. It leads to the following equality for the given parameter $\tilde{\delta}$

$$\tilde{\delta} = \frac{\bar{\mathbf{v}}(\theta_t)^H (\mathbf{R} + \bar{\lambda} \mathbf{R}_{\bar{\mathbf{V}}})^{-1} \mathbf{R}_{\bar{\mathbf{V}}} (\mathbf{R} + \bar{\lambda} \mathbf{R}_{\bar{\mathbf{V}}})^{-1} \bar{\mathbf{v}}(\theta_t)}{[\bar{\mathbf{v}}(\theta_t)^H (\mathbf{R} + \bar{\lambda} \mathbf{R}_{\bar{\mathbf{V}}})^{-1} \bar{\mathbf{v}}(\theta_t)]^2}. \quad (22)$$

The right-hand side of (22) is a monotonically decreasing function of $\bar{\lambda}$, meaning that $\bar{\lambda} > 0$ is unique and it can be achieved using an efficient searching algorithm. Hence, substituting (20) and $\bar{\lambda}$ that is found numerically as described above into (18), we obtain the solution of the optimization problem (10) under the condition (16) as

$$\bar{\mathbf{w}} = \frac{(\mathbf{R} + \bar{\lambda} \mathbf{R}_{\bar{\mathbf{V}}})^{-1} \bar{\mathbf{v}}(\theta_t)}{\bar{\mathbf{v}}(\theta_t)^H (\mathbf{R} + \bar{\lambda} \mathbf{R}_{\bar{\mathbf{V}}})^{-1} \bar{\mathbf{v}}(\theta_t)} \quad (23)$$

and the corresponding source power estimate as

$$\bar{\sigma}_0^2 = \frac{\bar{\mathbf{v}}(\theta_t)^H (\mathbf{R} + \bar{\lambda} \mathbf{R}_{\bar{\mathbf{V}}})^{-1} \mathbf{R} (\mathbf{R} + \bar{\lambda} \mathbf{R}_{\bar{\mathbf{V}}})^{-1} \bar{\mathbf{v}}(\theta_t)}{[\bar{\mathbf{v}}(\theta_t)^H (\mathbf{R} + \bar{\lambda} \mathbf{R}_{\bar{\mathbf{V}}})^{-1} \bar{\mathbf{v}}(\theta_t)]^2}. \quad (24)$$

The source power estimate (24) can be used for the first case when (14) is satisfied only if $\bar{\lambda} = 0$.

Note that throughout the derivation of the power estimate, we require \mathbf{R} and $\mathbf{R} + \bar{\lambda} \mathbf{R}_{\bar{\mathbf{V}}}$ to be positive definite in order to guarantee the invertibility. Generally, the matrix $\mathbf{R}_{\bar{\mathbf{V}}}$ is positive semidefinite due to the fact that $\text{rank}\{\mathbf{R}_{\bar{\mathbf{V}}}\} \leq \text{rank}\{\bar{\mathbf{V}}\}$, thus $\mathbf{R} + \bar{\lambda} \mathbf{R}_{\bar{\mathbf{V}}}$ will be close to singular when $\bar{\lambda}$ is large enough. To avoid this, we can employ a small diagonal loading to the matrix $\mathbf{R}_{\bar{\mathbf{V}}}$.

It is also worth noting that the equality (22) gives the lower bound on $\tilde{\delta}$, i.e., the limit when $\bar{\lambda}$ goes to infinity. Hence, (22) together with (14) imply that $\tilde{\delta}$ should be chosen from the following interval

$$\frac{1}{\bar{\mathbf{v}}(\theta_t)^H \mathbf{R}_{\bar{\mathbf{V}}}^+ \bar{\mathbf{v}}(\theta_t)} \leq \tilde{\delta} < \frac{\bar{\mathbf{v}}^H(\theta_t) \mathbf{R}^{-1} \mathbf{R}_{\bar{\mathbf{V}}} \mathbf{R}^{-1} \bar{\mathbf{v}}(\theta_t)}{[\bar{\mathbf{v}}^H(\theta_t) \mathbf{R}^{-1} \bar{\mathbf{v}}(\theta_t)]^2} \quad (25)$$

where $\mathbf{R}_{\bar{\mathbf{V}}}^+$ denotes the Moore-Penrose pseudoinverse of the matrix $\mathbf{R}_{\bar{\mathbf{V}}}$. As $\tilde{\delta}$ increases, the performance of source power estimate using the above-mentioned method approaches that of the standard MVDR beamformer, i.e., the performance of (8).

V. SIMULATION RESULTS

In our simulations, we use uniform linear arrays of $M = 10$ transmit and $N = 10$ receive antenna elements spaced half a wavelength apart from each other. The presumed SOI area is $\Theta = [10^\circ, 25^\circ]$ and the out-of-sector area is $\bar{\Theta} = [-90^\circ, 0^\circ] \cup [35^\circ, 90^\circ]$. We assume that there is one desired target located in the SOI with the direction-of-arrival (DOA) $\theta_t = 18^\circ$ and four interfering sources located outside the SOI with DOAs $\theta_l = -35^\circ, -20^\circ, 0^\circ, \text{ and } 50^\circ$, respectively. The signal-to-noise ratio (SNR), interference-to-noise ratio (INR), and jammer-to-noise ratio (JNR) are assumed to be equal to 5 dB, 40 dB, and 50 dB, respectively.

The jammer suppression performance of the two proposed MVDR beamformers is validated by showing the ideal beam-patterns and the source power estimates in the presence of powerful in-sector jammers as well as array calibration errors and target steering vector mismatches. Each beam-pattern is normalized to its maximal value. The mismatches are introduced by perturbing both the transmit and receive steering

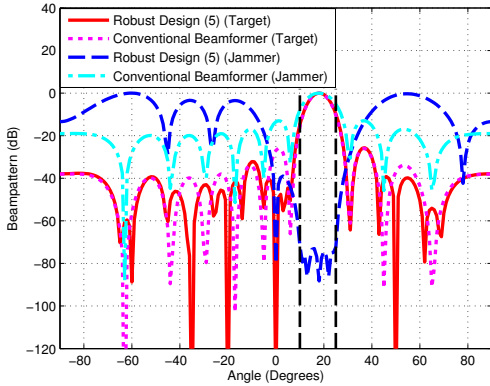


Fig. 1. Beampatterns versus angle for the first example.

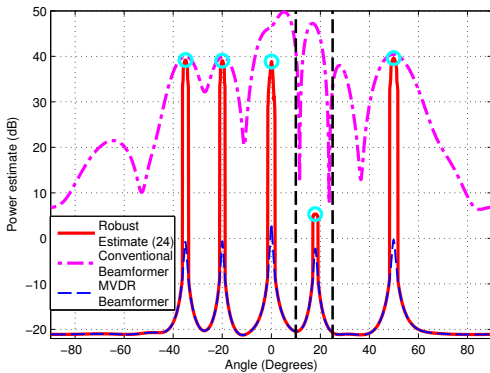


Fig. 2. Power estimates versus angle for the first example.

vectors of each incident source (the desired or interfering one) with a normalized vector whose elements are random independent variables that obey complex Gaussian distribution with mean 0 and variance 1. For each in-sector jammer, we add perturbations of the same Gaussian distribution to the elements of its corresponding receive steering vector. The obtained source power estimates are averaged over 100 independent simulation runs. The in-sector area is identified by two vertical dashed lines, and the power estimate peaks are marked by circles. The CVX toolbox [20] is used to solve the convex optimization problems (5) and (6).

In the first example, we assume that uniform distributed jammers are present in the SOI spaced 1° apart from each other. Fig. 1 shows the ideal beampatterns of both the target and the jammer using the MVDR beamforming design (5) and the conventional beamformer (Bartlett method) [21]. It can be seen that the design (5) is capable of suppressing the known jammers by imposing deep in-sector nulls towards their spatial directions, while the conventional beamforming method is invalid for the powerful in-sector jammers suppression. The desired target is not mitigated by the jammer suppression conducted in its direction. It can also be seen from Fig. 1 that the interfering sources located outside the SOI are adaptively

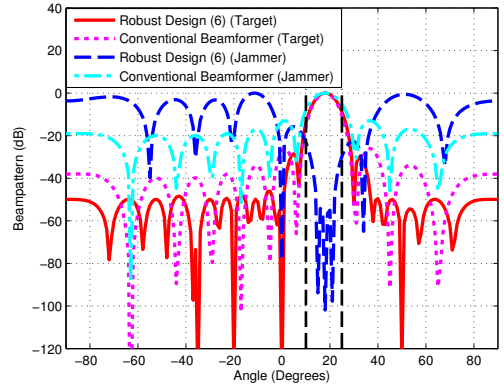


Fig. 3. Beampatterns versus angle for the second example.

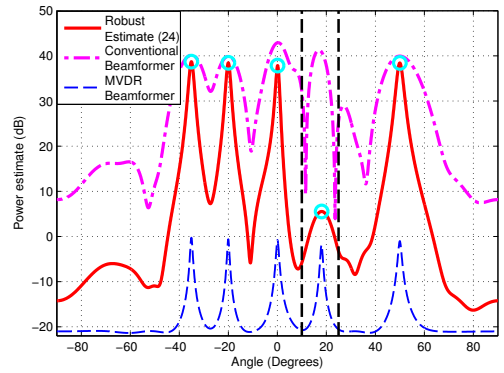


Fig. 4. Power estimates versus angle for the second example.

suppressed by the designed beamformer.

Fig. 2 shows the corresponding source power estimates. The parameter $\tilde{\delta}$ is selected to be equal to 0.0001. We compare the performance of the proposed source power estimate (24) with that of the standard MVDR beamformer associated with (8) and the conventional beamformer which gives the source power estimate as [21] $\hat{\sigma}_0^2 = \bar{\mathbf{v}}(\theta_t)^H \mathbf{R} \bar{\mathbf{v}}(\theta_t) / M^2 N^2$. It can be seen that the power estimates of the in-sector target and the out-of-sector interfering sources given by (24) are close to the accurate values. The target can still be well estimated even if its power is small (5 dB SNR versus 40 dB INR and 50 dB JNR). However, the standard MVDR beamforming and the conventional beamforming methods fail to estimate the power accurately in the background of powerful jamming signals and non-ideal factors. The former underestimates the power of all the sources, while the latter gives wrong power estimate peaks.

In the second example, we assume that there are three jamming signals with the DOAs $\theta_j = 15^\circ, 18^\circ, \text{ and } 21^\circ$, respectively. Fig. 3 shows the ideal beampatterns of both the target and the jammer using the MVDR beamforming design (6) and the conventional beamformer used also in the first example. We select the in-sector jammer suppression and out-of-sector interference attenuation parameters as $\delta = 0.0001$

and $\gamma = 0.0032$, respectively. It is shown that three deep nulls towards the directions of the in-sector jammers are formed adaptively using the proposed beamformer, and the out-of-sector sidelobe levels are suppressed below -50 dB. However, the conventional beamformer still has no effect on the in-sector jammers suppression and gives worse sidelobe levels.

The corresponding source power estimates are shown in Fig. 4. It is demonstrated again that the proposed source power estimate method shows much better performance than its two counterparts. The power estimates of all the sources that are above 0 dB (noise power) are denoted by the peaks with small-circle marks. It is shown that the presence of the in-sector jammer located at the same direction as the target does not affect the target power estimate obtained using the proposed estimate method. Moreover, this estimate method shows good robustness against the array calibration errors and target steering vector mismatches.

It is worth noting that the jammer present at the spatial angle $\theta_j = 0^\circ$ has the same virtual steering vector as the target with the same spatial angle, making it impossible to distinguish from the target using only beamforming technique when both are present in this direction. In our simulations, we show the case that the jammer is not present at $\theta_j = 0^\circ$. Successful suppression for this case can be achieved if the information of Doppler is considered, and it is similar to what has been done in STAP. Nevertheless, the MVDR beamforming designs are generally much easier than STAP techniques.

It is also worth noting that the PA radar is unable to suppress such jammers from the same sector while MIMO radar with the proposed beamforming techniques provide this capability. The reason lies in the fact that MIMO radar is capable of utilizing the spatial signature difference between the echoes of the targets and the jammers due to its waveform diversity. In this sense, the jammer suppression capability of MIMO radar is unique. This capability is of great significance since it enables the MIMO radar to easily suppress the jammers with robustness only in spatial domain, which immensely facilitates the application in practice.

VI. CONCLUSION

We have studied the problem of powerful jammers suppression for MIMO radar with colocated antennas, and have provided two MVDR type beamforming designs with robustness/adaptiveness against the powerful jammers in the SOI. We first have designed an MVDR beamformer for known jammers by maintaining distortionless response towards the direction of the target while imposing nulls towards the directions of the jammers located in the SOI. Then we have designed another MVDR beamformer for the general case that the in-sector jammers are unknown and, if needed, the out-of-sector interfering sources attenuation is also conducted. Both of the robust beamforming designs are cast as convex optimization problems. Furthermore, we have derived the closed-form solution to the simplified second design. Based on this solution, we have provided source power estimates in the background of powerful jamming signals and non-ideal factors such as array

calibration errors and target steering vector mismatches. It has been verified by the ideal beampatterns and the source power estimates that the robust MVDR beamforming designs are efficient, and they can serve as easier strategies for powerful jammers suppression compared to STAP techniques. Finally, we have demonstrated that the capability of efficient jammers suppression using these designs is unique in MIMO radar.

REFERENCES

- [1] J. Li and P. Stoica, *MIMO Radar Signal Processing*. New York: Wiley, 2009.
- [2] A. M. Haimovich, R. S. Blum, and L. J. Cimini, "MIMO radar with widely separated antennas," *IEEE Signal Processing Magazine*, vol. 24, no. 1, pp. 116–129, Jan. 2008.
- [3] J. Li and P. Stoica, "MIMO radar with colocated antennas," *IEEE Signal Processing Magazine*, vol. 24, no. 5, pp. 106–114, Sep. 2007.
- [4] E. Fishler, A. Haimovich, R. S. Blum, L. Cimini, D. Chizhik, and R. Valenzuela, "Spatial diversity in radars: Models and detection performance," *IEEE Trans. Signal Processing*, vol. 54, no. 3, pp. 823–838, Mar. 2006.
- [5] A. Hassanien, S. A. Vorobyov, and A. B. Gershman, "Moving target parameters estimation in non-coherent MIMO radar systems," *IEEE Trans. Signal Processing*, vol. 58, no. 6, pp. 3137–3151, June 2010.
- [6] D. R. Fuhrmann and G. S. Antonio, "Transmit beamforming for MIMO radar systems using signal cross-correlation," *IEEE Trans. Aerosp. Electron. Syst.*, vol. 44, no. 1, pp. 171–186, Jan. 2008.
- [7] P. Stoica, J. Li and Y. Xie, "On probing signal design for MIMO radar," *IEEE Trans. Signal Processing*, vol. 55, no. 8, pp. 4151–4161, Aug. 2007.
- [8] D. Wilcox and M. Sellathurai, "On MIMO radar subarrayed transmit beamforming," *IEEE Trans. Signal Processing*, vol. 60, no. 4, pp. 2076–2091, Apr. 2012.
- [9] A. Hassanien and S. A. Vorobyov, "Phased-MIMO radar: A tradeoff between phased-array and MIMO radars," *IEEE Trans. Signal Processing*, vol. 58, no. 6, pp. 3137–3151, June 2010.
- [10] A. Hassanien and S. A. Vorobyov, "Transmit energy focusing for DOA estimation in MIMO radar with colocated antennas," *IEEE Trans. Signal Processing*, vol. 59, no. 6, pp. 2669–2682, June 2011.
- [11] C.-Y. Chen and P. P. Vaidyanathan, "MIMO radar space-time adaptive processing using prolate spheroidal waveform functions," *IEEE Trans. Signal Processing*, vol. 56, no. 2, pp. 623–635, Feb. 2008.
- [12] V. F. Mecca, D. Ramakrishnan, and J. L. Krolik, "MIMO radar space-time adaptive processing for multipath clutter mitigation," in *Proc. IEEE Workshop Sensor Array Multichannel Signal Processing*, Waltham, MA, 2006, pp. 249–253.
- [13] H. Cox, R. Zeskind, and M. Owen, "Robust adaptive beamforming," *IEEE Trans. Acoustics, Speech and Signal Processing*, vol. 35, no. 10, pp. 1365–1376, Oct. 1987.
- [14] A. B. Gershman, "Robust adaptive beamforming in sensor arrays," *International Journal of Electronics and Communications*, vol. 53, no. 6, pp. 305–314, Dec. 1999.
- [15] S. A. Vorobyov, A. B. Gershman, and Z.-Q. Luo, "Robust adaptive beamforming using worst-case performance optimization: A solution to the signal mismatch problem," *IEEE Trans. Signal Processing*, vol. 51, no. 2, pp. 313–324, Feb. 2003.
- [16] S. A. Vorobyov, A. B. Gershman, Z.-Q. Luo, and N. Ma, "Adaptive beamforming with joint robustness against mismatched signal steering vector and interference nonstationarity," *IEEE Signal Processing Letters*, vol. 11, no. 2, pp. 108–111, Feb. 2004.
- [17] J. Li, P. Stoica, and Z. Wang, "Doubly constrained robust Capon beamformer," *IEEE Trans. Signal Processing*, vol. 52, no. 9, pp. 2407–2423, Sep. 2004.
- [18] M. I. Skolnik, *Introduction to radar systems*, 3rd ed. New York, NY: McGraw-Hill, 2001.
- [19] H. L. Van Trees, *Optimum Array Processing*. New York, NY: Wiley, 2002.
- [20] M. Grant and S. Boyd. (2013, Sep.). *CVX: Matlab software for disciplined convex programming* (version 2.0 beta) [online]. Available: <http://cvxr.com/cvx>
- [21] M. S. Barlett, *An Introduction to Stochastic Process*. New York: Cambridge Univ. Press, 1956.

Publication VII

Yongzhe Li and Sergiy A. Vorobyov. Fast algorithm for designing unimodular waveform(s) with good correlation properties. *IEEE Transactions on Signal Processing*, vol. 66, no. 5, pp. 1197–1212, March 2018.

© 2018 IEEE.

Reprinted with permission.

Fast Algorithms for Designing Unimodular Waveform(s) With Good Correlation Properties

Yongzhe Li ^{1b}, *Member, IEEE*, and Sergiy A. Vorobyov ^{1b}, *Fellow, IEEE*

Abstract—We develop new fast and efficient algorithms for designing single or multiple unimodular waveforms with good auto- and cross-correlation or weighted correlation properties, which are highly desired in radar and communication systems. The waveform design is based on the minimization of the integrated sidelobe level (ISL) and weighted ISL (WISL) of waveforms. As the corresponding problems can quickly grow to a large scale with increasing the code length and the number of waveforms, the main issue turns to be the development of fast large-scale optimization techniques. The difficulty is also that the corresponding optimization problems are nonconvex, but the required accuracy is high. Therefore, we formulate the ISL and WISL minimization problems as nonconvex quartic optimization problems in frequency domain, and then simplify them into quadratic problems via majorization-minimization technique, which is one of the basic techniques for addressing large-scale and/or nonconvex optimization problems. While designing our fast algorithms, we explore and use the inherent algebraic structures in objective functions to rewrite them into quartic forms, and in the case of WISL minimization, to derive additionally an alternative quartic form that allows us to apply the quartic-quadratic transformation. Our algorithms are applicable to large-scale unimodular waveform design problems as they are proved to have lower or comparable computational burden (analyzed theoretically) and faster convergence speed (confirmed by comprehensive simulations) than the state-of-the-art algorithms. In addition, the waveforms designed by our algorithms demonstrate better correlation properties compared to their counterparts.

Index Terms—Correlation, majorization-minimization, MIMO radar, waveform design.

I. INTRODUCTION

WAVEFORM/CODE design, as one of the major problems in radar signal processing [1]–[11], active sensing [12]–[14], and wireless communications [15], has attracted significant interest over the past several decades [16]–[21]. In radar signal processing and active sensing applications, waveform de-

sign plays an essential role because “excellent” waveforms can ensure higher localization accuracy [1], enhanced resolution capability [5], and improved delay-Doppler ambiguity of the potential target [22]. Moreover, designing waveforms with robustness or adaptiveness is also required for the scenarios with harsh environments that include heterogeneous clutter and/or active jammers [18]. In addition, with the advance of multiple-input multiple-output (MIMO) radar [23]–[26], the problem of joint multiple waveform design is gaining even more importance as it tends to grow to a large scale even faster (proportional to both the code length and number of waveforms).

To obtain waveforms with desirable characteristics, existing approaches usually resort to manipulations with correlation properties, such as the auto- and cross-correlations between different time lags of waveforms, which serve as the determinant factors for evaluating the quality of designed waveforms [7], [8]. Perfect auto- and cross-correlation properties indicate that the emitted waveforms are mutually uncorrelated to any time-delayed replica of them, meaning that the target located at the range bin of interest can be easily extracted after matched filtering, and the sidelobes from other range bins are unable to attenuate it. For example, in the applications of the spot and barrage noise jamming suppression [12] and synthetic aperture radar imaging [5], [8], waveforms with deep notches towards the time lags or frequency bands, where the jamming or clutter signals are located, are highly desired. On the other hand, it is preferred from hardware perspective that the designed waveforms maintain constant-modulus property, which can reduce the cost of developing advanced amplifiers.

There have been a number of waveform designs developed based on the consideration of correlation properties during the past decades [2], [5], [7], [8], [16]. The earlier techniques such as the maximal length sequence (also called M-sequence), P4, Chu, Kasami, and Gold sequences show good periodic correlation properties (see [16] and references therein), and some even approach the Welch lower bound [27] on periodic correlation levels. However, they are not designed to minimize the aperiodic correlation levels of waveforms, and therefore, perform far from the corresponding lower bound on aperiodic correlations. Other drawbacks of these techniques are inflexible code length, limited number of waveforms, nonarbitrary phase values, and shrunk feasibility set (or degrees of freedom) [17]. These weaknesses become especially negative when designing multiple waveforms under certain desirable conditions.

The integrated sidelobe level (ISL) [7], [17], which serves as an evaluation metric for the correlation levels of waveforms in terms of the accumulated sidelobes at all time lags, is typically used. If the receiver is fixed to be the matched filter, the focus of the waveform design methods is the waveform quality itself. Corresponding waveform designs use the fact that the matched

Manuscript received August 23, 2017; revised December 14, 2017; accepted December 14, 2017. Date of publication December 25, 2017; date of current version January 26, 2018. The associate editor coordinating the review of this manuscript and approving it for publication was Prof. Mathini Sellathurai. The work was supported in part by the Academy of Finland Research under Grant 299243. The work of Y. Li was supported in part by the Nokia Foundation under Grant 201710358. This paper was presented in part at the European Signal Processing Conference, Budapest, Hungary, August/September 2016, and in part at the IEEE International Conference on Acoustics, Speech, and Signal Processing, New Orleans, LA, USA, March 2017. (*Corresponding author: Sergiy A. Vorobyov.*)

The authors are with the Department of Signal Processing and Acoustics, Aalto University, Espoo FI-00076, Finland (e-mail: yongzhe.li@aalto.fi; svor@ieee.org).

Color versions of one or more of the figures in this paper are available online at <http://ieeexplore.ieee.org>.

Digital Object Identifier 10.1109/TSP.2017.2787104

filter can be implemented based on the correlation between the waveform and its delayed replica. If the receiver is not fixed and therefore has to be jointly optimized with the transmitted waveforms, the focus shifts to the so-called mismatched filter (also called instrumental variable filter [28]) design. Such designs add flexibility as they enable to consider constraints which are difficult to address otherwise. They make the receive filter to become generally mismatched mainly because of trading off the signal-to-noise ratio in order to improve the signal-to-interference-plus-noise ratio. The corresponding design techniques are usually based on alternating optimization where the minimum variance distortionless response (MVDR) filter design is involved. Once the waveforms are given, finding the optimal MVDR receive filter is technically and computationally simpler than designing the waveforms. Therefore, our focus here is to develop computationally efficient algorithms for addressing the core problem of waveform design when the optimal receive filter is the matched filter.

The computational complexity of algorithms is of crucial importance for unimodular waveform designs on the basis of ISL and/or weighted ISL (WISL) minimization. The work of [7] has proposed to design a single unimodular waveform in frequency domain using a cyclic procedure based on iterative calculations. A surrogate objective function minimized by a cyclic algorithm has been introduced, and the methods associated with the ISL and WISL minimizations therein have been named as CAN and WeCAN, respectively. These methods have been later extended to multiple waveform design in [8]. However, the corresponding ISL and WISL minimization problems can quickly grow to large scale with the increase of code length and number of waveforms. Moreover, they are non-convex and cannot be solved by classical large-scale optimization algorithms developed for convex problems with relatively simple objectives and constraints [29]. The objective functions based on the ISL and WISL metrics as well as the constant-modulus constraint to the desired waveforms are indeed complex to be dealt with, but the required accuracy of waveform design is high.

The aforementioned CAN and WeCAN [7], [8] use a cyclic procedure based on iterative calculations. Although large code length up to several thousands is allowed by them, the cost in terms of time consumption for both algorithms can reach several hours and even days when the code length and required number of waveforms grow large. This significant limitation restricts the design of waveforms in real time. Indeed, in large-scale optimization, the targeted computational complexity per iteration of an algorithm is linear in the dimension of the problem or at most quadratic [29]. To reduce the computational complexity, many relevant works [30]–[37] resort to the majorization-minimization (MaMi) technique [38], which serves as the basic technique for addressing large-scale and/or non-convex optimization problems with complex objectives. For example, the work of [30] has dealt with multistatic radar waveform design, where an information-theoretic criterion has been utilized, while the works of [31], [32] have been concerned with single- and multiple-waveform designs.

Another important characteristic of large-scale optimization algorithms is the convergence speed/rate [29]. Although the analytical bounds on convergence rate may be hard/impossible to derive even for some existing large-scale convex optimization algorithms, designing algorithms with provably faster convergence speed to tolerance than that of the other algorithms is possible. This motivates us to investigate the possibility of

achieving very fast convergence speed to a stationary point for the non-convex problems considered here.

In this paper,¹ we focus on the ISL and WISL minimization-based unimodular waveform designs for the match-filter receiver, aiming at developing fast algorithms of lower computational complexity and faster convergence speed than existing algorithms. The paper is based on a detailed study of inherent algebraic structures of the objective functions. Moreover, with respect to MaMi procedure, it also proposes better majorization functions which lead to algorithms with faster convergence speed. The principal goal is to enable the real-time waveform design with good correlation properties even when the code length and number of waveforms are large. Although MaMi framework is also used here as for example in [31] and [32], our work differs and contributes to the following main aspects. i) Our algorithm for non-convex quartic ISL minimization-based unimodular waveform design is generic in the sense that it can be used without changes and with reduced computations compared to [31] and [32]. ii) By means of exploring and using the inherent algebraic structures in the WISL expression, the objective of the WISL minimization-based waveform design problem is newly formulated in terms of a non-convex quartic form where Hadamard product is involved. It is then derived into an alternative quartic form that allows to further apply the quartic-quadratic transformation. Both the originally formulated (via Hadamard product) and the new eigenvalue decomposition based quartic forms are completely different from the objective forms in [31] and [32]. iii) Different from [31] and [32] as well as other existing works, we assume a general weighting matrix for WISL which can be indefinite. We also prove that it is not necessary to compute the corresponding eigenvalues for the eigenvalue decomposition based quartic form. iv) Different majorization functions from those of [31] and [32] within MaMi framework are used for both the ISL and WISL minimization problems. v) Our algorithms have lower or comparable computational burden per iteration, faster convergence speed, and demonstrate better correlation properties than the existing state-of-the-art algorithms including the ones in [31] and [32].

The paper is organized as follows. In Section II, the signal model and the ISL and WISL minimization-based unimodular waveform design problems are presented. In Section III, fast algorithms for the ISL and WISL minimization problems are developed and detailed. Simulation results are presented in Section IV, while the paper is concluded in Section V followed by Appendix that details some proofs and derivations.

Notations: We use bold uppercase, bold lowercase, and italic letters to denote matrices, column vectors, and scalars, respectively. Notations $(\cdot)^*$, $(\cdot)^T$, $(\cdot)^H$, $|\cdot|$, $\|\cdot\|$, $\|\cdot\|_F$, $\text{vec}(\cdot)$, $\text{tr}\{\cdot\}$, $\Re\{\cdot\}$, \otimes , \odot , and ∇ denote the conjugate, transpose, conjugate transpose, modulus, Euclidean norm, Frobenius norm, column-wise vectorization, maximum value, matrix trace, real part, Kronecker product, Hadamard product, and gradient operations, respectively. Moreover, notations δ_p , $\lfloor \cdot \rfloor$, \succeq , $\mathcal{O}(\cdot)$, $\arg(\cdot)$, $\lambda_{\max}(\cdot)$, and $\text{mod}(\cdot, \cdot)$ stand respectively for the Kronecker delta function (with respect to the index p), floor function, generalized inequality between matrices, order of complexity, argument of a complex value, largest eigenvalue of a matrix, and modulo operation with the first argument being the dividend, while $\mathcal{T}\{\cdot\}$ denotes the operation of constructing

¹Some preliminary results on the ISL and WISL minimization-based designs have been presented in [33] and [34], respectively.

a Hermitian Toeplitz matrix from a vector that coincides with the first column of the matrix, and $\text{diag}\{\cdot\}$ is the operator that picks up diagonal elements from a matrix and writes them into a vector (for matrix argument) or forms a diagonal matrix with main diagonal entries picked up from a vector (for vector argument). In addition, $\mathcal{U}_p\{\cdot\}$ and $\mathcal{D}_p\{\cdot\}$ are operators that respectively pick up the p th off-diagonal ($p = 0$ for the main diagonal) entries from the upper and lower triangular parts of a matrix and align them into a vector, $[\cdot]_{i,j}$ denotes the (i, j) th element of a matrix, \mathbf{I}_M is the $M \times M$ identity matrix, and $\mathbf{1}_M$ denotes an $M \times 1$ vector with all elements equal to 1.

II. SIGNAL MODEL AND PROBLEM FORMULATION

Consider a radar (or communication) system which emits M unimodular and mutually orthogonal waveforms. Each waveform is of code length P , and the whole waveform matrix \mathbf{Y} of size $P \times M$ is defined as $\mathbf{Y} \triangleq [y_1, \dots, y_M]$. Here the m th column \mathbf{y}_m corresponds to the m th launched waveform. Let the p th element of \mathbf{y}_m be $y_m(p) = e^{j\psi_m(p)}$ where $\psi_m(p)$ is an arbitrary phase value ranging between $-\pi$ and π . When the number of waveforms M reduces to 1, the waveform matrix \mathbf{Y} shrinks to a column vector.

The ISL metric for the set of waveforms $\{y_m(p)\}_{m=1, p=1}^{M, P}$ can be expressed as [8]

$$\zeta = \sum_{m=1}^M \sum_{\substack{p=-P+1 \\ p \neq 0}}^{P-1} |r_{mm}(p)|^2 + \sum_{m=1}^M \sum_{\substack{m'=1 \\ m' \neq m}}^M \sum_{p=-P+1}^{P-1} |r_{mm'}(p)|^2 \quad (1)$$

where

$$r_{mm'}(p) \triangleq \sum_{k=p+1}^P y_m(k)y_{m'}^*(k-p) = (r_{m'm}(-p))^* \\ m, m' \in \{1, \dots, M\}; p \in \{1, \dots, P-1\} \quad (2)$$

is the cross-correlation between the m th and m' th waveforms at the p th time lag. The first term on the right-hand side of (1) is associated with the auto-correlations, while the second term represents the cross-correlations of the waveforms.

Likewise, the WISL metric for the waveforms $\{y_m(p)\}_{m=1, p=1}^{M, P}$ can be expressed as [8]

$$\zeta_w = \sum_{m=1}^M \sum_{\substack{p=-P+1 \\ p \neq 0}}^{P-1} \gamma_p^2 |r_{mm}(p)|^2 + \sum_{m=1}^M \sum_{\substack{m'=1 \\ m' \neq m}}^M \\ \times \sum_{p=-P+1}^{P-1} \gamma_p^2 |r_{mm'}(p)|^2 \quad (3)$$

where $\{\gamma_p\}_{p=-P+1}^{P-1}$ are real-valued symmetric weights, i.e., $\gamma_p = \gamma_{-p}, \forall p$, used for controlling the sidelobe levels corresponding to different time lags. If γ_p takes zero value, it means that the sidelobe level associated with the p th time lag is not considered. If all the ISL controlling weights $\{\gamma_p\}_{p=-P+1}^{P-1}$ take the value 1, then ζ_w in (3) coincides with ζ in (1).

The basic unimodular waveform design problem is then formulated as synthesizing unimodular and mutually orthogonal waveforms $\{y_m(p)\}_{m=1, p=1}^{M, P}$ which have as good as possible auto- and cross-correlation or weighted correlation properties.

Using (3), the WISL minimization-based unimodular waveform design problem can be formally expressed as

$$\min_{\mathbf{Y}} \zeta_w \\ \text{s.t. } |y_m(p)| = 1, m = 1, \dots, M; p = 1, \dots, P \quad (4)$$

where the constraints ensure the constant-modulus property for each waveform element, while the orthogonality between waveforms is guaranteed by the objective. Obviously, if all the ISL controlling weights $\{\gamma_p\}_{p=-P+1}^{P-1}$ take the value 1, the problem (4) becomes that of the ISL minimization-based unimodular waveform design.

III. FAST WAVEFORM DESIGN ALGORITHMS

In this section, we develop fast algorithms for the ISL and WISL minimization-based unimodular waveform design problems. The inherent algebraic structures in the objective functions (1) and (3) are investigated and exploited within the MaMi framework. The strategy for applying MaMi is to design as accurate as possible majorization functions and then use them a number of times needed to arrive to a problem with closed-form computationally cheap solution. Since the problems are non-convex, the convergence to only a stationary point for MaMi-based algorithms is guaranteed [38], [39].

A. Fast ISL Minimization-Based Algorithm

The ISL ζ in (1) can be rewritten in the matrix form as

$$\zeta = \sum_{p=-P+1}^{P-1} \|\mathbf{R}_p - P\mathbf{I}_M \delta_p\|^2 \quad (5)$$

where \mathbf{R}_p is the following $M \times M$ waveform covariance matrix

$$\mathbf{R}_p \triangleq \begin{bmatrix} r_{11}(p) & r_{12}(p) & \dots & r_{1M}(p) \\ r_{21}(p) & r_{22}(p) & \dots & r_{2M}(p) \\ \vdots & \vdots & \ddots & \vdots \\ r_{M1}(p) & \dots & \dots & r_{MM}(p) \end{bmatrix} \quad (6)$$

whose elements are defined in (2).

Transforming (5) into frequency domain and performing some derivations, the ISL ζ can be expressed as [8]

$$\zeta = \frac{1}{2P} \sum_{p=1}^{2P} \|\tilde{\mathbf{y}}(\omega_p) \tilde{\mathbf{y}}^H(\omega_p) - P\mathbf{I}_M\|^2 \quad (7)$$

where

$$\tilde{\mathbf{y}}(\omega_p) \triangleq \sum_{n=1}^P \tilde{\mathbf{y}}_n e^{-j\omega_p n}, \omega_p \triangleq \frac{2\pi}{2P} p \quad (8)$$

with $\tilde{\mathbf{y}}_n$ being the transpose of the n th row of the waveform matrix \mathbf{Y} , i.e., $\tilde{\mathbf{y}}_n \triangleq [y_1(n), \dots, y_M(n)]^T$.

Expanding the norm in (7), after some elementary algebraic computations, the ISL ζ can be rewritten as

$$\zeta = \frac{1}{2P} \sum_{p=1}^{2P} \left(\|\tilde{\mathbf{y}}(\omega_p)\|^4 - 2P \|\tilde{\mathbf{y}}(\omega_p)\|^2 + P^2 M \right). \quad (9)$$

Moreover, introducing the $MP \times 1$ vectorized version of the waveform matrix \mathbf{Y} as $\mathbf{y} \triangleq \text{vec}(\mathbf{Y}) = [\mathbf{y}_1^T, \dots, \mathbf{y}_M^T]^T$ and the

$MP \times M$ matrix $\mathbf{A}_p \triangleq \mathbf{I}_M \otimes \mathbf{a}_p$ with \mathbf{a}_p defined as $\mathbf{a}_p \triangleq [1, e^{j\omega_p}, \dots, e^{j(P-1)\omega_p}]^T$ where $p = 1, \dots, 2P$, and using the facts that $\tilde{\mathbf{y}}(\omega_p) = \mathbf{A}_p^H \mathbf{y}$ and $\|\tilde{\mathbf{y}}(\omega_p)\|^2 = \tilde{\mathbf{y}}^H(\omega_p) \tilde{\mathbf{y}}(\omega_p)$, the ISL expression (9) can be further rewritten as

$$\zeta = \frac{1}{2P} \sum_{p=1}^{2P} \left((\mathbf{y}^H \mathbf{A}_p \mathbf{A}_p^H \mathbf{y})^2 - 2P(\mathbf{y}^H \mathbf{A}_p \mathbf{A}_p^H \mathbf{y}) + P^2 M \right). \quad (10)$$

Noticing that $\sum_{p=1}^{2P} \mathbf{A}_p \mathbf{A}_p^H = 2P \mathbf{I}_{MP}$ and using the fact that the desired waveforms are orthogonal and have constant modulus, i.e., $\|\mathbf{y}\|^2 = MP$, we can find that

$$\sum_{p=1}^{2P} \mathbf{y}^H \mathbf{A}_p \mathbf{A}_p^H \mathbf{y} = \mathbf{y}^H \left(\sum_{p=1}^{2P} \mathbf{A}_p \mathbf{A}_p^H \right) \mathbf{y} = 2MP^2. \quad (11)$$

Using (11) and excluding the immaterial optimization terms from (10), the optimization problem (4) can be rewritten as

$$\begin{aligned} \min_{\mathbf{y}} \quad & \sum_{p=1}^{2P} (\mathbf{y}^H \mathbf{A}_p \mathbf{A}_p^H \mathbf{y})^2 \\ \text{s.t.} \quad & |\mathbf{y}(p')| = 1, \quad p' = 1, \dots, MP \end{aligned} \quad (12)$$

where the objective function takes a quartic form with respect to \mathbf{y} .

Introducing the $MP \times MP$ and $M^2 P^2 \times M^2 P^2$, respectively, matrices $\tilde{\mathbf{Y}} \triangleq \mathbf{y} \mathbf{y}^H$ and

$$\Phi \triangleq \sum_{p=1}^{2P} \text{vec}(\mathbf{A}_p \mathbf{A}_p^H) (\text{vec}(\mathbf{A}_p \mathbf{A}_p^H))^H \quad (13)$$

and using the fact that $\mathbf{y}^H \mathbf{A}_p \mathbf{A}_p^H \mathbf{y} = \text{tr}\{\tilde{\mathbf{Y}}^H \mathbf{A}_p \mathbf{A}_p^H\} = (\text{vec}(\tilde{\mathbf{Y}}))^H \text{vec}(\mathbf{A}_p \mathbf{A}_p^H)$ obtained via the elementary properties of the trace and vectorization operations, the objective in (12) can be transformed from quartic into quadratic form as follows

$$\begin{aligned} \sum_{p=1}^{2P} (\mathbf{y}^H \mathbf{A}_p \mathbf{A}_p^H \mathbf{y})^2 &= \sum_{p=1}^{2P} (\text{tr}\{\tilde{\mathbf{Y}}^H \mathbf{A}_p \mathbf{A}_p^H\})^2 \\ &= \sum_{p=1}^{2P} (\text{vec}(\tilde{\mathbf{Y}}))^H \text{vec}(\mathbf{A}_p \mathbf{A}_p^H) (\text{vec}(\mathbf{A}_p \mathbf{A}_p^H))^H \text{vec}(\tilde{\mathbf{Y}}) \\ &= (\text{vec}(\tilde{\mathbf{Y}}))^H \Phi \text{vec}(\tilde{\mathbf{Y}}). \end{aligned} \quad (14)$$

Therefore, the problem (12) can be further rewritten as

$$\min_{\tilde{\mathbf{Y}}} (\text{vec}(\tilde{\mathbf{Y}}))^H \Phi \text{vec}(\tilde{\mathbf{Y}}) \quad (15a)$$

$$\text{s.t.} \quad \tilde{\mathbf{Y}} = \mathbf{y} \mathbf{y}^H, \quad (15b)$$

$$|\mathbf{y}(p')| = 1, \quad p' = 1, \dots, MP. \quad (15c)$$

Since the objective function (15a) takes a quadratic form, a proper majorized function can be applied. Before applying the majorant to (15a), we present the following general result that will be used later.

Lemma 1: If a real-valued function $f(\mathbf{x})$ with respect to complex variable \mathbf{x} is second-order differentiable, and there is a

matrix $\mathbf{G} \succeq 0$ satisfying the generalized inequality $\nabla^2 f(\mathbf{x}) \preceq \mathbf{G}$ for all \mathbf{x} , then for each point \mathbf{x}_0 , the following convex quadratic function

$$g(\mathbf{x}) = f(\mathbf{x}_0) + \Re\{\nabla^H f(\mathbf{x}_0)(\mathbf{x} - \mathbf{x}_0)\} + \frac{1}{2}(\mathbf{x} - \mathbf{x}_0)^H \mathbf{G}(\mathbf{x} - \mathbf{x}_0) \quad (16)$$

majorizes $f(\mathbf{x})$ at \mathbf{x}_0 .²

Proof: Using Taylor's theorem, the second-order expansion of $f(\mathbf{x})$ at the point \mathbf{x}_0 is given as

$$f(\mathbf{x}) = f(\mathbf{x}_0) + \Re\{\nabla^H f(\mathbf{x}_0)(\mathbf{x} - \mathbf{x}_0)\} + \frac{1}{2}(\mathbf{x} - \mathbf{x}_0)^H \nabla^2 f(\boldsymbol{\xi})(\mathbf{x} - \mathbf{x}_0) \quad (17)$$

where $\boldsymbol{\xi}$ is a point on the line connecting \mathbf{x}_0 and \mathbf{x} . Due to the fact that $\nabla^2 f(\boldsymbol{\xi}) \preceq \mathbf{G}$, the inequality $f(\mathbf{x}) \leq g(\mathbf{x})$ also holds true, where $g(\mathbf{x})$ is given by (16). ■

If $f(\mathbf{x})$ is a quadratic form, i.e., $f(\mathbf{x}) = \mathbf{x}^H \mathbf{Q} \mathbf{x}$, as it is the case for the objective function in (15), by substituting $\nabla f(\mathbf{x}_0) = 2\mathbf{Q} \mathbf{x}_0$ in (16), the majorant can be obtained as

$$g(\mathbf{x}) = \frac{1}{2} \mathbf{x}^H \mathbf{G} \mathbf{x} + \mathbf{x}_0^H \left(\frac{1}{2} \mathbf{G} - \mathbf{Q} \right) \mathbf{x}_0 + 2\Re\left\{ \mathbf{x}^H \left(\mathbf{Q} - \frac{1}{2} \mathbf{G} \right) \mathbf{x}_0 \right\}. \quad (18)$$

Let \mathbf{G} be the $M^2 P^2 \times M^2 P^2$ identity matrix magnified by the largest eigenvalue of the matrix Φ , i.e., $\mathbf{G} \triangleq \lambda_{\max}(\Phi) \mathbf{I}_{M^2 P^2}$. For such selection of \mathbf{G} , the generalized inequality $\mathbf{G} \succeq \Phi$ is guaranteed to hold. Then using (18), the objective function (15a) can be majorized by the following function

$$\begin{aligned} g_1(\tilde{\mathbf{Y}}, \tilde{\mathbf{Y}}^{(k)}) &= \frac{\lambda_{\max}(\Phi)}{2} (\text{vec}(\tilde{\mathbf{Y}}))^H \text{vec}(\tilde{\mathbf{Y}}) \\ &+ (\text{vec}(\tilde{\mathbf{Y}}^{(k)}))^H \left(\frac{\lambda_{\max}(\Phi)}{2} \mathbf{I}_{M^2 P^2} - \Phi \right) \text{vec}(\tilde{\mathbf{Y}}^{(k)}) \\ &+ 2\Re\left\{ (\text{vec}(\tilde{\mathbf{Y}}))^H \left(\Phi - \frac{\lambda_{\max}(\Phi)}{2} \mathbf{I}_{M^2 P^2} \right) \text{vec}(\tilde{\mathbf{Y}}^{(k)}) \right\} \end{aligned} \quad (19)$$

where the matrix $\tilde{\mathbf{Y}}^{(k)} \triangleq \mathbf{y}^{(k)} (\mathbf{y}^{(k)})^H$ is obtained at the k th iteration with $\mathbf{y}^{(k)} \triangleq \text{vec}\{\mathbf{Y}^{(k)}\}$ being the vectorized version of the waveform matrix $\mathbf{Y}^{(k)}$ at iteration k .

Using the elementary properties of the Kronecker product and vectorization operations, we can find that

$$\text{vec}(\tilde{\mathbf{Y}}) = \text{vec}(\mathbf{y} \mathbf{y}^H) = (\mathbf{y}^T \otimes \mathbf{I}_{MP})^H \mathbf{y}. \quad (20)$$

Furthermore, using (20) and the fact that the desired waveforms are orthogonal and unimodular, we obtain

$$(\text{vec}(\tilde{\mathbf{Y}}))^H \text{vec}(\tilde{\mathbf{Y}}) = \|\mathbf{y}\|^4 = M^2 P^2. \quad (21)$$

Moreover, using the definition (13) of the matrix Φ , the maximum eigenvalue of Φ is given as (see Appendix A for the proof)

$$\lambda_{\max}(\Phi) = 2MP^2. \quad (22)$$

Returning to (19) and using the facts (20)–(22), we can see that the first two terms on the right hand of (19) are constant and

²The one-dimension version of Lemma 1 appears in [39] as Theorem 3.1.

therefore immaterial for optimization. Thus, ignoring these two terms, the majorization problem for (15) can be written as

$$\begin{aligned} \min_{\tilde{\mathbf{Y}}} \quad & (\text{vec}(\tilde{\mathbf{Y}}))^{\text{H}} (\Phi - MP^2 \mathbf{I}_{M^2 P^2}) \text{vec}(\tilde{\mathbf{Y}}^{(k)}) \\ \text{s.t.} \quad & \tilde{\mathbf{Y}} = \mathbf{y}\mathbf{y}^{\text{H}} \\ & |\mathbf{y}(p')| = 1, p' = 1, \dots, MP. \end{aligned} \quad (23)$$

Using the definition (13) and the properties (20) and also

$$\text{vec}(\mathbf{A}_p \mathbf{A}_p^{\text{H}}) = (\mathbf{A}_p^{\text{T}} \otimes \mathbf{I}_{MP})^{\text{H}} \text{vec}(\mathbf{A}_p) \quad (24)$$

the objective function in (23), denoted hereafter as obj^{a} , can be expanded as

$$\begin{aligned} \text{obj}^{\text{a}} = & \sum_{p=1}^{2P} \left(\mathbf{y}^{\text{H}} (\mathbf{y}^{\text{T}} \otimes \mathbf{I}_{MP}) (\mathbf{A}_p^{\text{T}} \otimes \mathbf{I}_{MP})^{\text{H}} \text{vec}(\mathbf{A}_p) \right. \\ & \times (\text{vec}(\mathbf{A}_p))^{\text{H}} (\mathbf{A}_p^{\text{T}} \otimes \mathbf{I}_{MP}) ((\mathbf{y}^{(k)})^{\text{T}} \otimes \mathbf{I}_{MP})^{\text{H}} \mathbf{y}^{(k)}) \\ & \left. - MP^2 \mathbf{y}^{\text{H}} (\mathbf{y}^{\text{T}} \otimes \mathbf{I}_{MP}) ((\mathbf{y}^{(k)})^{\text{T}} \otimes \mathbf{I}_{MP})^{\text{H}} \mathbf{y}^{(k)} \right). \end{aligned} \quad (25)$$

Applying the mixed-product property of the Kronecker product to (25), the objective in (23) can be further derived as

$$\begin{aligned} \text{obj}^{\text{a}} = & \sum_{p=1}^{2P} \mathbf{y}^{\text{H}} ((\mathbf{y}^{\text{T}} \mathbf{A}_p^*) \otimes \mathbf{I}_{MP}) \text{vec}(\mathbf{A}_p) (\text{vec}(\mathbf{A}_p))^{\text{H}} ((\mathbf{A}_p^{\text{T}} \\ & \times (\mathbf{y}^{(k)*}) \otimes \mathbf{I}_{MP}) \mathbf{y}^{(k)} - MP^2 \mathbf{y}^{\text{H}} (\mathbf{y}^{\text{T}} (\mathbf{y}^{(k)*}) \mathbf{y}^{(k)}). \end{aligned} \quad (26)$$

It is straightforward to check that the equality $((\mathbf{y}^{\text{T}} \mathbf{A}_p^*) \otimes \mathbf{I}_{MP}) \text{vec}(\mathbf{A}_p) = \mathbf{A}_p \mathbf{A}_p^{\text{H}} \mathbf{y}$ holds. Applying this equality to (26), the objective in (23) can be rewritten as

$$\begin{aligned} \text{obj}^{\text{a}} = & \sum_{p=1}^{2P} \mathbf{y}^{\text{H}} \mathbf{A}_p ((\mathbf{y}^{(k)})^{\text{H}} \mathbf{A}_p \mathbf{A}_p^{\text{H}} \mathbf{y}^{(k)}) \mathbf{A}_p^{\text{H}} \mathbf{y} - MP^2 \mathbf{y}^{\text{H}} \\ & \times (\mathbf{y}^{(k)} (\mathbf{y}^{(k)})^{\text{H}}) \mathbf{y} = \mathbf{y}^{\text{H}} (\mathbf{A} \mathbf{A}^{\text{H}} - MP^2 \mathbf{y}^{(k)} (\mathbf{y}^{(k)})^{\text{H}}) \mathbf{y} \end{aligned} \quad (27)$$

where the $MP \times 2MP$ matrix \mathbf{A} and the $2MP \times 2MP$ matrix $\mathbf{A}^{(k)}$ are defined as $\mathbf{A} \triangleq [\mathbf{A}_1, \dots, \mathbf{A}_{2P}]$ and $\mathbf{A}^{(k)} \triangleq \text{diag}\{\boldsymbol{\mu}^{(k)} \otimes \mathbf{1}_M\}$, and the $2P \times 1$ vector $\boldsymbol{\mu}^{(k)}$ is defined as³

$$\boldsymbol{\mu}^{(k)} \triangleq |\tilde{\mathbf{A}}^{\text{H}} \mathbf{Y}^{(k)}|^2 \mathbf{1}_M \quad (28)$$

via the $P \times 2P$ matrix $\tilde{\mathbf{A}} \triangleq [\mathbf{a}_1, \dots, \mathbf{a}_{2P}]$.

Using (27), the problem (23) can be rewritten as

$$\begin{aligned} \min_{\mathbf{y}} \quad & \mathbf{y}^{\text{H}} (\mathbf{A} \mathbf{A}^{\text{H}} - MP^2 \mathbf{y}^{(k)} (\mathbf{y}^{(k)})^{\text{H}}) \mathbf{y} \\ \text{s.t.} \quad & |\mathbf{y}(p')| = 1, p' = 1, \dots, MP \end{aligned} \quad (29)$$

where the objective function takes a quadratic form, to which the majorant (18) can be applied again. Substituting the $2MP \times 2MP$ matrix \mathbf{G} , defined as $\mathbf{G} \triangleq \mu_{\max}^{(k)} \mathbf{A} \mathbf{A}^{\text{H}}$, into (18),

³In (28), $|\cdot|$ is applied to a matrix argument, which means that the magnitude is found for each element of the matrix, that is, the element-wise magnitude.

Algorithm 1: ISL Minimization-Based Algorithm.

```

1:  $k \leftarrow 0$ ,  $\mathbf{Y} \leftarrow$  unimodular sequence matrix with random
   phases.
2: repeat
3:   procedure ISLNEW( $\mathbf{Y}^{(k)}$ )
4:      $\boldsymbol{\mu}^{(k)} = |\tilde{\mathbf{A}}^{\text{H}} \mathbf{Y}^{(k)}|^2 \mathbf{1}_M$ 
5:      $\mathbf{v}^{(k)} = -\tilde{\mathbf{A}} (\boldsymbol{\mu}^{(k)} - \frac{1}{2} (\mu_{\max}^{(k)} + M^2 P^2) \mathbf{1}_{2P})$ 
6:      $\mathbf{T}^{(k)} = \mathcal{T}\{\mathbf{v}^{(k)}\}$ 
7:      $[\mathbf{Y}]_{m,p} = e^{j \cdot \arg([\mathbf{T}^{(k)} \mathbf{Y}^{(k)}]_{m,p})}$ ,  $\forall m, \forall p$ 
8:      $k \leftarrow k + 1$ 
9:   end procedure
10: until convergence

```

the objective (27) can be majorized by the following function

$$\begin{aligned} g_2(\mathbf{y}, \mathbf{y}^{(k)}) = & \frac{1}{2} \mu_{\max}^{(k)} \mathbf{y}^{\text{H}} \mathbf{A} \mathbf{A}^{\text{H}} \mathbf{y} + (\mathbf{y}^{(k)})^{\text{H}} (MP^2 \mathbf{y}^{(k)} (\mathbf{y}^{(k)})^{\text{H}} \\ & - \mathbf{A} (\boldsymbol{\Lambda}^{(k)} - \frac{1}{2} \mu_{\max}^{(k)} \mathbf{I}_{2MP}) \mathbf{A}^{\text{H}}) \mathbf{y}^{(k)} + 2\Re\{\mathbf{y}^{\text{H}} (\mathbf{A} (\boldsymbol{\Lambda}^{(k)} \\ & - \frac{1}{2} \mu_{\max}^{(k)} \mathbf{I}_{2MP}) \mathbf{A}^{\text{H}} - MP^2 \mathbf{y}^{(k)} (\mathbf{y}^{(k)})^{\text{H}}) \mathbf{y}^{(k)}\} \end{aligned} \quad (30)$$

where $\mu_{\max}^{(k)}$ is the largest element of $\boldsymbol{\Lambda}^{(k)}$, or equivalently, $\mu_{\max}^{(k)} \triangleq \max\{\boldsymbol{\mu}^{(k)}\}$. This scaling factor guaranties that the generalized inequality $\mathbf{G} \succeq \mathbf{A} \boldsymbol{\Lambda}^{(k)} \mathbf{A}^{\text{H}}$ holds.

Noticing that $\mathbf{A} \mathbf{A}^{\text{H}} = \sum_{p=1}^{2P} \mathbf{A}_p \mathbf{A}_p^{\text{H}} = 2P \mathbf{I}_{MP}$ and using the fact that the desired waveforms are orthogonal and have constant modulus, i.e., $\mathbf{y}^{\text{H}} \mathbf{y} = (\mathbf{y}^{(k)})^{\text{H}} \mathbf{y}^{(k)} = \|\mathbf{y}\|^2 = MP$, we can see that the first two terms in (30) are constant, and hence, immaterial for optimization. Ignoring these terms, the optimization problem (29) can be further majorized by the following problem

$$\begin{aligned} \min_{\mathbf{y}} \quad & \mathbf{y}^{\text{H}} \left(\mathbf{A} (\boldsymbol{\Lambda}^{(k)} - \frac{1}{2} \mu_{\max}^{(k)} \mathbf{I}_{2MP}) \mathbf{A}^{\text{H}} - M^2 P^3 \mathbf{I}_{MP} \right) \mathbf{y}^{(k)} \\ \text{s.t.} \quad & |\mathbf{y}(p')| = 1, p' = 1, \dots, MP. \end{aligned} \quad (31)$$

Using again the fact that the desired waveforms have constant modulus, the problem (31) can be equivalently rewritten as

$$\begin{aligned} \min_{\mathbf{Y}} \quad & \|\mathbf{Y} - \mathbf{T}^{(k)} \mathbf{Y}^{(k)}\| \\ \text{s.t.} \quad & |[\mathbf{Y}]_{m,p}| = 1, m = 1, \dots, M; p = 1, \dots, P \end{aligned} \quad (32)$$

where the $P \times P$ matrix $\mathbf{T}^{(k)} \triangleq \mathcal{T}\{\mathbf{v}^{(k)}\}$ is a Hermitian Toeplitz matrix constructed from the $P \times 1$ vector $\mathbf{v}^{(k)} \triangleq -\tilde{\mathbf{A}} (\boldsymbol{\mu}^{(k)} - \frac{1}{2} (\mu_{\max}^{(k)} + M^2 P^2) \mathbf{1}_{2P})$. The problem (32) has the following closed-form solution

$$[\mathbf{Y}]_{m,p} = \exp\{j \cdot \arg([\mathbf{T}^{(k)} \mathbf{Y}^{(k)}]_{m,p})\}, \forall m, \forall p. \quad (33)$$

Finally, according to the MaMi procedure and using the closed-form solution (33) to the majorization problem, the ISL minimization-based unimodular waveform design algorithm is summarized in Algorithm 1. There exist accelerated schemes for MaMi, such as the squared iterative method (SQUAREM) of [40], which can be straightforwardly applied to speed up

Algorithm 1. The SQUAREM scheme is an extension of the scalar Steffensen type method [41], [42] to vector fixed-point iteration empowered with the idea of “squaring” [43]. It is an “off-the-shelf” acceleration method that requires nothing extra to the parameter updating rules of an original algorithm, except possibly the computationally cheap projection to feasibility set, and it is guaranteed to converge [35], [40].

Different stopping criteria can be employed in Algorithm 1. For example, it can be the absolute ISL difference between the current and previous iterations normalized by the initial ISL, or it can be the norm of the difference between the waveform matrices obtained at the current and previous iterations.

In terms of the per iteration computational complexity of Algorithm 1, the straightforward calculation of $\boldsymbol{\mu}^{(k)}$ according to (28) requires $2MP(P+1)$ operations, the calculation of $\mathbf{v}^{(k)}$ costs $2P^2$ operations, while the computational burden of the matrix to matrix product $\mathbf{T}^{(k)}\mathbf{Y}^{(k)}$ in (33) is MP^2 operations. Therefore, the total computational complexity is $(3M+2)P^2+2MP$ operations. However, $\boldsymbol{\mu}^{(k)}$ and $\mathbf{v}^{(k)}$ can be computed by means of the fast Fourier transform (FFT) at the order of complexity $\mathcal{O}(MP \log P)$ and $\mathcal{O}(P \log P)$, respectively. Similarly, using the Toeplitz structure of $\mathbf{T}^{(k)}$, the product $\mathbf{T}^{(k)}\mathbf{Y}^{(k)}$ can also be calculated at a reduced complexity $\mathcal{O}(MP \log P)$, which is the highest in Algorithm 1. Thus, the order of complexity of Algorithm 1 is $\mathcal{O}(MP \log P)$, which is nearly linear in the dimension of the problem, as required in large-scale optimization.

B. Fast WISL Minimization-Based Algorithm

The WISL in (3) can be written in the matrix form as

$$\zeta_w = \gamma_0^2 \|\mathbf{R}_0 - P\mathbf{I}_M\|^2 + \sum_{\substack{p=-P+1 \\ p \neq 0}}^{P-1} \gamma_p^2 \|\mathbf{R}_p\| \quad (34)$$

where \mathbf{R}_p , $p \in \{-P+1, \dots, P-1\}$ are defined in (6).

In the frequency domain, (34) can be expressed as [8]

$$\zeta_w = \frac{1}{2P} \sum_{p=1}^{2P} \|\Psi(\omega_p) - \gamma_0 P\mathbf{I}_M\|^2 \quad (35)$$

where ω_p is defined in (8) and

$$\Psi(\omega_p) \triangleq \sum_{p=-P+1}^{P-1} \gamma_p \mathbf{R}_p e^{-j\omega_p n} \quad (36)$$

is the weighted spectral density matrix.

Let us define the $P \times P$ weighting matrix that has Toeplitz structure and is constructed by the weights $\{\gamma_p\}_{p=-P+1}^{P-1}$ as

$$\Gamma \triangleq \begin{bmatrix} \gamma_0 & \gamma_1 & \dots & \gamma_{P-1} \\ \gamma_{-1} & \gamma_0 & \ddots & \vdots \\ \vdots & \ddots & \ddots & \gamma_1 \\ \gamma_{-P+1} & \dots & \gamma_{-1} & \gamma_0 \end{bmatrix}. \quad (37)$$

Then the matrix $\Psi(\omega_p)$ in (36) can be rewritten in the vector-matrix form as

$$\begin{aligned} \Psi(\omega_p) &= \mathbf{Y}^H (\text{diag}\{\mathbf{a}_p\})^H \Gamma \text{diag}\{\mathbf{a}_p\} \mathbf{Y} \\ &= \mathbf{Y}^H ((\mathbf{a}_p \mathbf{a}_p^H) \odot \Gamma) \mathbf{Y}. \end{aligned} \quad (38)$$

Substituting (38) into (35), the WISL ζ_w can be expressed as

$$\zeta_w = \frac{1}{2P} \sum_{p=1}^{2P} \|\mathbf{Y}^H ((\mathbf{a}_p \mathbf{a}_p^H) \odot \Gamma) \mathbf{Y} - \gamma_0 P\mathbf{I}_M\|^2. \quad (39)$$

Expanding the squared norm in the sum of (39) yields

$$\begin{aligned} \zeta_w &= \frac{1}{2P} \sum_{p=1}^{2P} \left(\|\mathbf{Y}^H ((\mathbf{a}_p \mathbf{a}_p^H) \odot \Gamma) \mathbf{Y}\|^2 + \gamma_0^2 MP^2 \right. \\ &\quad \left. - 2\gamma_0 P \text{tr}\{\mathbf{Y}^H ((\mathbf{a}_p \mathbf{a}_p^H) \odot \Gamma) \mathbf{Y}\} \right). \end{aligned} \quad (40)$$

Using the facts that the desired waveforms are orthogonal and unimodular, i.e., $\text{tr}\{\mathbf{Y}^H \mathbf{Y}\} = \|\mathbf{Y}\|^2 = MP$, and also that $\sum_{p=1}^{2P} \mathbf{a}_p \mathbf{a}_p^H = 2P\mathbf{I}_P$, we find that

$$\begin{aligned} \sum_{p=1}^{2P} \text{tr}\{\mathbf{Y}^H ((\mathbf{a}_p \mathbf{a}_p^H) \odot \Gamma) \mathbf{Y}\} &= \text{tr}\left\{\mathbf{Y}^H \left(\sum_{p=1}^{2P} \mathbf{a}_p \mathbf{a}_p^H \odot \Gamma \right) \mathbf{Y}\right\} \\ &= 2P \text{tr}\{\mathbf{Y}^H (\mathbf{I}_P \odot \Gamma) \mathbf{Y}\} = 2\gamma_0 P \|\mathbf{Y}\|^2 = 2\gamma_0 MP^2. \end{aligned} \quad (41)$$

Therefore, the second and third terms of (40) are constant and immaterial for optimization. With this observation, the WISL minimization problem (4) can be rewritten as

$$\min_{\mathbf{Y}} \sum_{p=1}^{2P} \|\mathbf{Y}^H ((\mathbf{a}_p \mathbf{a}_p^H) \odot \Gamma) \mathbf{Y}\|^2 \quad (42a)$$

$$\text{s.t. } |y_m(p)| = 1, \quad m = 1, \dots, M; \quad p = 1, \dots, P. \quad (42b)$$

The Hadamard product of two matrices appears under the Frobenius norm in (42a), and the resulting matrix there is complex. Therefore, it cannot be rewritten into a proper quartic form with respect to \mathbf{y} by directly expanding the squared norm. Instead, it needs to be converted into an alternative quartic form. Towards this end, we consider the eigenvalue decomposition of Γ , which in general may be indefinite expressed as

$$\Gamma = \sum_{k=1}^K \lambda_k \mathbf{q}_k \mathbf{q}_k^H = \sum_{k=1}^K \mathbf{u}_k \mathbf{v}_k^H \quad (43)$$

where λ_k (real-valued) and \mathbf{q}_k are the k th eigenvalue and eigenvector, respectively, $\mathbf{u}_k \triangleq \sqrt{\lambda_k} \mathbf{q}_k$, \mathbf{v}_k equals $-\mathbf{u}_k$ when λ_k is negative, otherwise it is the same as \mathbf{u}_k , and K is the rank of Γ . Substituting (43) into (42a) and expanding the Frobenius norm, the objective function (42a), called hereafter as obj^b , can be rewritten as

$$\text{obj}^b = \sum_{p=1}^{2P} \sum_{k=1}^K \sum_{k'=1}^K \left| (\mathbf{v}_{k'} \odot \mathbf{a}_p)^H \mathbf{Y} \mathbf{Y}^H (\mathbf{u}_k \odot \mathbf{a}_p) \right|^2. \quad (44)$$

Applying the property $\mathbf{Y}^H (\mathbf{u}_k \odot \mathbf{a}_p) = (\mathbf{I}_M \otimes (\mathbf{a}_p \odot \mathbf{u}_k))^T \mathbf{y}^*$ (also holds if \mathbf{u}_k is replaced by $\mathbf{v}_{k'}$) where $\mathbf{y} = \text{vec}(\mathbf{Y})$ to (44) together with the mixed-product property of the Kronecker

product, the objective function (42a) can be rewritten as

$$\begin{aligned} \text{obj}^b &= \sum_{p=1}^{2P} \sum_{k=1}^K \sum_{k'=1}^K |\mathbf{y}^H (\mathbf{I}_M \otimes ((\mathbf{a}_p \mathbf{a}_p^H) \odot (\mathbf{u}_k \mathbf{v}_{k'}^H))) \mathbf{y}|^2 \\ &= \sum_{p=1}^{2P} \sum_{k=1}^K \sum_{k'=1}^K (\mathbf{y}^H ((\mathbf{A}_p \mathbf{A}_p^H) \odot \mathbf{\Gamma}_{kk'}^{\text{real}}) \mathbf{y})^2 \\ &\quad + (\mathbf{y}^H ((\mathbf{A}_p \mathbf{A}_p^H) \odot \mathbf{\Gamma}_{kk'}^{\text{img}}) \mathbf{y})^2 \end{aligned} \quad (45)$$

where the $MP \times MP$ Hermitian matrices $\mathbf{\Gamma}_{kk'}^{\text{real}}$ and $\mathbf{\Gamma}_{kk'}^{\text{img}}$ are defined as

$$\mathbf{\Gamma}_{kk'}^{\text{real}} \triangleq \mathbf{I}_M \otimes \frac{\mathbf{u}_k \mathbf{v}_{k'}^H + \mathbf{v}_{k'} \mathbf{u}_k^H}{2} \quad (46)$$

$$\mathbf{\Gamma}_{kk'}^{\text{img}} \triangleq \mathbf{I}_M \otimes \frac{\mathbf{u}_k \mathbf{v}_{k'}^H - \mathbf{v}_{k'} \mathbf{u}_k^H}{2i} \quad (47)$$

with $i \triangleq \sqrt{-1}$.

Substituting (45) to (42), the WISL minimization problem becomes

$$\begin{aligned} \min_{\mathbf{y}} \quad & \sum_{p=1}^{2P} \sum_{k=1}^K \sum_{k'=1}^K (\mathbf{y}^H ((\mathbf{A}_p \mathbf{A}_p^H) \odot \mathbf{\Gamma}_{kk'}^{\text{real}}) \mathbf{y})^2 \\ & + (\mathbf{y}^H ((\mathbf{A}_p \mathbf{A}_p^H) \odot \mathbf{\Gamma}_{kk'}^{\text{img}}) \mathbf{y})^2 \end{aligned} \quad (48a)$$

$$\text{s.t.} \quad |\mathbf{y}(p')| = 1, \quad p' = 1, \dots, MP. \quad (48b)$$

The objective function (48a) takes a proper quartic form with respect to \mathbf{y} that enables us to design an algorithm based on the MaMi approach.

By means of the trace and vectorization operations for matrices, and similar to the previous subsection, the objective (48a), denoted for brevity as obj^c , can be rewritten as

$$\begin{aligned} \text{obj}^c &= \sum_{p=1}^{2P} \left(\text{tr} \left\{ \tilde{\mathbf{Y}}^H ((\mathbf{A}_p \mathbf{A}_p^H) \odot \mathbf{\Gamma}_{kk'}^{\text{real}}) \right\} \right)^2 \\ &\quad + \left(\text{tr} \left\{ \tilde{\mathbf{Y}}^H ((\mathbf{A}_p \mathbf{A}_p^H) \odot \mathbf{\Gamma}_{kk'}^{\text{img}}) \right\} \right)^2 \\ &= (\text{vec}(\tilde{\mathbf{Y}}))^H \tilde{\mathbf{\Phi}} \text{vec}(\tilde{\mathbf{Y}}) \end{aligned} \quad (49)$$

where $\tilde{\mathbf{Y}} \triangleq \mathbf{y} \mathbf{y}^H$, $\tilde{\mathbf{\Phi}}$ is the $M^2 P^2 \times M^2 P^2$ matrix defined as

$$\tilde{\mathbf{\Phi}} \triangleq \tilde{\mathbf{\Phi}} \odot \bar{\mathbf{\Gamma}} \quad (50)$$

with

$$\tilde{\mathbf{\Phi}} \triangleq \sum_{p=1}^{2P} \text{vec}(\mathbf{A}_p \mathbf{A}_p^H) (\text{vec}(\mathbf{A}_p \mathbf{A}_p^H))^H \quad (51)$$

$$\begin{aligned} \bar{\mathbf{\Gamma}} &\triangleq \sum_{k=1}^K \sum_{k'=1}^K \text{vec}(\mathbf{\Gamma}_{kk'}^{\text{real}}) (\text{vec}(\mathbf{\Gamma}_{kk'}^{\text{real}}))^H \\ &\quad + \text{vec}(\mathbf{\Gamma}_{kk'}^{\text{img}}) (\text{vec}(\mathbf{\Gamma}_{kk'}^{\text{img}}))^H. \end{aligned} \quad (52)$$

Replacing the objective function (48a) with (49), the optimization problem (48) can be rewritten as

$$\min_{\tilde{\mathbf{Y}}} \quad (\text{vec}(\tilde{\mathbf{Y}}))^H \tilde{\mathbf{\Phi}} \text{vec}(\tilde{\mathbf{Y}}) \quad (53a)$$

$$\text{s.t.} \quad \tilde{\mathbf{Y}} = \mathbf{y} \mathbf{y}^H \quad (53b)$$

$$|\mathbf{y}(p')| = 1, \quad p' = 1, \dots, MP \quad (53c)$$

where (53a) takes a quadratic form, to which a majorant can be applied. Yet before applying the majorization procedure, we present the following result that will be used later.

Lemma 2: Given a set of $N \times 1$ arbitrary complex vectors $\{\mathbf{d}_k\}_{k=1}^K$ and an $N \times N$ arbitrary Hermitian matrix \mathbf{H} , the following generalized inequality

$$\sum_{k=1}^K (\mathbf{d}_k \mathbf{d}_k^H) \odot \mathbf{H} \preceq \lambda_{\max}(\mathbf{H}) \mathbf{D} \quad (54)$$

holds, where $\mathbf{D} \triangleq \text{diag}\{\sum_{k=1}^K |\mathbf{d}_k(1)|^2, \dots, \sum_{k=1}^K |\mathbf{d}_k(N)|^2\}$.

Proof: Let $\{\tilde{\lambda}_n\}_{n=1}^N$ and $\{\tilde{\mathbf{q}}_n\}_{n=1}^N$ be respectively the sets of eigenvalues (in descending order) and corresponding eigenvectors of the matrix \mathbf{H} , i.e., $\mathbf{H} = \sum_{n=1}^N \tilde{\lambda}_n \tilde{\mathbf{q}}_n \tilde{\mathbf{q}}_n^H$. Using this expression and some elementary properties of the Hadamard product, the inequality (54) can be proved as follows

$$\begin{aligned} \sum_{k=1}^K (\mathbf{d}_k \mathbf{d}_k^H) \odot \mathbf{H} &= \left(\sum_{k=1}^K \mathbf{d}_k \mathbf{d}_k^H \right) \odot \left(\sum_{n=1}^N \tilde{\lambda}_n \tilde{\mathbf{q}}_n \tilde{\mathbf{q}}_n^H \right) \\ &= \sum_{k=1}^K \sum_{n=1}^N \tilde{\lambda}_n (\mathbf{d}_k \mathbf{d}_k^H) \odot (\tilde{\mathbf{q}}_n \tilde{\mathbf{q}}_n^H) \\ &= \sum_{k=1}^K \sum_{n=1}^N \tilde{\lambda}_n (\mathbf{d}_k \odot \tilde{\mathbf{q}}_n) (\mathbf{d}_k \odot \tilde{\mathbf{q}}_n)^H \\ &\preceq \sum_{k=1}^K \sum_{n=1}^N \tilde{\lambda}_1 (\mathbf{d}_k \odot \tilde{\mathbf{q}}_n) (\mathbf{d}_k \odot \tilde{\mathbf{q}}_n)^H \\ &= \tilde{\lambda}_1 \left(\sum_{k=1}^K \mathbf{d}_k \mathbf{d}_k^H \right) \odot \left(\sum_{n=1}^N \tilde{\mathbf{q}}_n \tilde{\mathbf{q}}_n^H \right) \\ &= \tilde{\lambda}_1 \left(\sum_{k=1}^K \mathbf{d}_k \mathbf{d}_k^H \right) \odot \mathbf{I}_N \\ &= \lambda_{\max}(\mathbf{H}) \mathbf{D}. \end{aligned} \quad (55)$$

The proof is complete. \blacksquare

Applying Lemma 2 by taking $\mathbf{d}_k = \text{vec}(\mathbf{A}_p \mathbf{A}_p^H)$, $\mathbf{H} = \bar{\mathbf{\Gamma}}$, and $K = 2P$, we obtain the following generalized inequality

$$\tilde{\mathbf{\Phi}} \odot \bar{\mathbf{\Gamma}} \preceq \lambda_{\max}(\bar{\mathbf{\Gamma}}) \text{diag}\{\tilde{\mathbf{\Phi}}\}. \quad (56)$$

Note that for a given matrix $\mathbf{\Gamma}$ in (37), the largest eigenvalue of $\bar{\mathbf{\Gamma}}$ in (52), i.e., $\lambda_{\max}(\bar{\mathbf{\Gamma}})$, is fixed, and it can be found that

$$\lambda_{\max}(\bar{\mathbf{\Gamma}}) = M \lambda_{\max}^2(\mathbf{\Gamma}). \quad (57)$$

The proof of (57) can be found in Appendix B. Note also that for the majorization function computation it is more efficient and sufficient to approximate $\lambda_{\max}(\bar{\mathbf{\Gamma}})$ by any matrix norm of $\mathbf{\Gamma}$. In addition, the diagonal elements of $\tilde{\mathbf{\Phi}}$ take values either zero

or $2P$. Therefore, we can replace the matrix $\text{diag}\{\bar{\Phi}\}$ in (56) with an identity matrix magnified by $2P$ without disobeying the inequality.

Using (18) with $\mathbf{G} \triangleq \lambda_{\bar{\Phi}} \mathbf{I}_{M^2 P^2}$ (here $\lambda_{\bar{\Phi}} \triangleq 2P\lambda_{\max}(\bar{\Gamma})$) that satisfies $\mathbf{G} \succeq \bar{\Phi}$, the objective function (53a) can be majorized by the following function

$$\begin{aligned} \tilde{g}_1(\tilde{\mathbf{Y}}, \tilde{\mathbf{Y}}^{(k)}) &= \frac{\lambda_{\bar{\Phi}}}{2} (\text{vec}(\tilde{\mathbf{Y}}))^H \text{vec}(\tilde{\mathbf{Y}}) \\ &+ (\text{vec}(\tilde{\mathbf{Y}}^{(k)}))^H \left(\frac{\lambda_{\bar{\Phi}}}{2} \mathbf{I}_{M^2 P^2} - \bar{\Phi} \right) \text{vec}(\tilde{\mathbf{Y}}^{(k)}) \\ &+ 2\Re \left\{ (\text{vec}(\tilde{\mathbf{Y}}))^H \left(\bar{\Phi} - \frac{\lambda_{\bar{\Phi}}}{2} \mathbf{I}_{M^2 P^2} \right) \text{vec}(\tilde{\mathbf{Y}}^{(k)}) \right\}. \end{aligned} \quad (58)$$

Due to the property (21), the first and second terms in (58) are constant and therefore immaterial for optimization. Ignoring these terms, (53) can be majorized by the problem

$$\min_{\tilde{\mathbf{Y}}} (\text{vec}(\tilde{\mathbf{Y}}))^H \left(\bar{\Phi} - \frac{\lambda_{\bar{\Phi}}}{2} \mathbf{I}_{M^2 P^2} \right) \text{vec}(\tilde{\mathbf{Y}}^{(k)}) \quad (59a)$$

$$\text{s.t. } \tilde{\mathbf{Y}} = \mathbf{y}\mathbf{y}^H \quad (59b)$$

$$|y(p')| = 1, \quad p' = 1, \dots, MP. \quad (59c)$$

To further simplify (59a), we will need the following result that relates Hadamard to Kronecker products.

Lemma 3: Given two matrices \mathbf{F} and \mathbf{C} of the same size $N \times N$ and the $N \times N^2$ selection matrix $\mathbf{E} = [\bar{\mathbf{E}}_1, \dots, \bar{\mathbf{E}}_N]$ with $\bar{\mathbf{E}}_n$ being the n th $N \times N$ block matrix composed of all zeros except the n th element on the main diagonal equaling 1, i.e., $[\bar{\mathbf{E}}_n]_{n,n} = 1$, the following equality

$$\mathbf{F} \odot \mathbf{C} = \mathbf{E}(\mathbf{C} \otimes \mathbf{F})\mathbf{E}^H \quad (60)$$

holds. Under the condition that \sqrt{N} is an integer, $\bar{\mathbf{E}}_n$ can be decomposed as

$$\bar{\mathbf{E}}_n = \hat{\mathbf{E}}_{u(n)} \otimes \hat{\mathbf{E}}_{v(n)} \quad (61)$$

where the matrices $\hat{\mathbf{E}}_{u(n)}$ and $\hat{\mathbf{E}}_{v(n)}$ are constructed in the same way as $\bar{\mathbf{E}}_n$ but have the reduced size $\sqrt{N} \times \sqrt{N}$, and

$$u(n) \triangleq \left\lfloor \frac{n-1}{\sqrt{N}} \right\rfloor + 1, \quad n = 1, \dots, N \quad (62)$$

$$v(n) \triangleq \text{mod}(n-1, \sqrt{N}) + 1, \quad n = 1, \dots, N \quad (63)$$

are respectively the column and row indices of the element in a $\sqrt{N} \times \sqrt{N}$ matrix corresponding to the unique linear index n in its column-wise vectorization.

Proof: The proof of (60) appears in Lemma 1 of [44]. The remaining results (61)–(63) are the elementary properties of the selection matrix. ■

Applying Lemma 3 by taking $\mathbf{F} = \bar{\Phi}$, $\mathbf{C} = \bar{\Gamma}$, and $N = M^2 P^2$, and substituting (50) into (59a), the objective function (59a), denoted for brevity as obj^d , can be rewritten as

$$\begin{aligned} \text{obj}^d &= (\text{vec}(\tilde{\mathbf{Y}}))^H \left(\mathbf{E}(\bar{\Gamma} \otimes \bar{\Phi})\mathbf{E}^H - \frac{\lambda_{\bar{\Phi}}}{2} \mathbf{I}_{M^2 P^2} \right) \text{vec}(\tilde{\mathbf{Y}}^{(k)}) \\ &= (\text{vec}(\tilde{\mathbf{Y}}))^H \left(\sum_{n=1}^{M^2 P^2} \sum_{n'=1}^{M^2 P^2} [\bar{\Gamma}]_{n,n'} \bar{\mathbf{E}}_n \bar{\Phi} \bar{\mathbf{E}}_{n'}^H \right) \text{vec}(\tilde{\mathbf{Y}}^{(k)}) \\ &\quad - \frac{\lambda_{\bar{\Phi}}}{2} (\text{vec}(\tilde{\mathbf{Y}}))^H \text{vec}(\tilde{\mathbf{Y}}^{(k)}) \end{aligned} \quad (64)$$

where the latter expression in (64) is obtained by expanding the Kronecker product in the prior expression for the objective.

Using (52) and (61), and applying the properties (20) and (24), the objective (64) can be further rewritten as

$$\begin{aligned} \text{obj}^d &= \sum_{p=1}^{2P} \sum_{n=1}^{M^2 P^2} \sum_{n'=1}^{M^2 P^2} [\bar{\Gamma}]_{n,n'} \mathbf{y}^H (\mathbf{y}^T \otimes \mathbf{I}_{MP}) (\hat{\mathbf{E}}_{u(n)} \\ &\quad \otimes \hat{\mathbf{E}}_{v(n)}) (\mathbf{A}_p^T \otimes \mathbf{I}_{MP})^H \text{vec}(\mathbf{A}_p) (\text{vec}(\mathbf{A}_p))^H (\mathbf{A}_p^T \\ &\quad \otimes \mathbf{I}_{MP}) (\hat{\mathbf{E}}_{u(n')} \otimes \hat{\mathbf{E}}_{v(n')})^H ((\mathbf{y}^{(k)})^T \otimes \mathbf{I}_{MP})^H \mathbf{y}^{(k)} \\ &\quad - \frac{\lambda_{\bar{\Phi}}}{2} \mathbf{y}^H (\mathbf{y}^T \otimes \mathbf{I}_{MP}) ((\mathbf{y}^{(k)})^T \otimes \mathbf{I}_{MP})^H \mathbf{y}^{(k)}. \end{aligned} \quad (65)$$

Applying the mixed-product property of the Kronecker product together with the property $((\mathbf{y}^T \hat{\mathbf{E}}_{u(n)} \mathbf{A}_p^*) \otimes \hat{\mathbf{E}}_{v(n)}) \text{vec}(\mathbf{A}_p) = \hat{\mathbf{E}}_{v(n)} \mathbf{A}_p \mathbf{A}_p^H \hat{\mathbf{E}}_{u(n)} \mathbf{y}$ to (65), we obtain

$$\begin{aligned} \text{obj}^d &= \mathbf{y}^H \left(\sum_{p=1}^{2P} \sum_{n=1}^{M^2 P^2} \sum_{n'=1}^{M^2 P^2} [\bar{\Gamma}]_{n,n'} \hat{\mathbf{E}}_{v(n)} \mathbf{A}_p \left((\mathbf{y}^{(k)})^H \hat{\mathbf{E}}_{u(n')} \right. \right. \\ &\quad \left. \left. \times \mathbf{A}_p \mathbf{A}_p^H \hat{\mathbf{E}}_{v(n')} \mathbf{y}^{(k)} \right) \mathbf{A}_p^H \hat{\mathbf{E}}_{u(n)} - \frac{\lambda_{\bar{\Phi}}}{2} \mathbf{y}^{(k)} (\mathbf{y}^{(k)})^H \right) \mathbf{y} \\ &= \mathbf{y}^H \left(\mathbf{B}^{(k)} - \frac{\lambda_{\bar{\Phi}}}{2} \mathbf{y}^{(k)} (\mathbf{y}^{(k)})^H \right) \mathbf{y} \end{aligned} \quad (66)$$

where $\mathbf{y}^{(k)} \triangleq \text{vec}\{\mathbf{Y}^{(k)}\}$ and $\mathbf{B}^{(k)}$ is an $MP \times MP$ Hermitian matrix composed of M^2 block matrices, i.e.,

$$\mathbf{B}^{(k)} \triangleq \begin{bmatrix} \mathbf{B}_{11}^{(k)} & \dots & \mathbf{B}_{1M}^{(k)} \\ \vdots & \ddots & \vdots \\ \mathbf{B}_{M1}^{(k)} & \dots & \mathbf{B}_{MM}^{(k)} \end{bmatrix} \quad (67)$$

with the (m, m') th block

$$\mathbf{B}_{mm'}^{(k)} = 2PT \left(\boldsymbol{\rho}_{mm'}^{(k)}, \boldsymbol{\eta}_{mm'}^{(k)} \right) \quad (68)$$

being a $P \times P$ Toeplitz matrix whose first row and column coincide with the $P \times 1$ vectors $\boldsymbol{\rho}_{mm'}^{(k)}$ and $\boldsymbol{\eta}_{mm'}^{(k)}$, respectively.

Here, the $(p+1)$ th ($0 \leq p \leq P-1$) elements of $\boldsymbol{\rho}_{mm'}^{(k)}$ and $\boldsymbol{\eta}_{mm'}^{(k)}$ are respectively given by

$$\boldsymbol{\rho}_{mm'}^{(k)}(p+1) \triangleq \begin{cases} \gamma_p^2 \mathbf{1}_{P-p}^T \mathcal{U}_p(\mathbf{Z}_{mm'}^{(k)}), & p \in \Omega \\ 0, & p \in \bar{\Omega} \end{cases} \quad (69)$$

$$\boldsymbol{\eta}_{mm'}^{(k)}(p+1) \triangleq \begin{cases} \gamma_p^2 \mathbf{1}_{P-p}^T \mathcal{D}_p(\mathbf{Z}_{mm'}^{(k)}), & p \in \Omega \\ 0, & p \in \bar{\Omega} \end{cases} \quad (70)$$

where $\mathbf{Z}_{mm'}^{(k)} \triangleq \mathbf{y}_m^{(k)} (\mathbf{y}_{m'}^{(k)})^H$, $\Omega \triangleq \{0\} \cup \{p | \gamma_p \neq 0, p > 0\}$ is the set of non-negative indices associated with the non-zero ISL controlling weights (always including index $p = 0$ for simplicity), and $\bar{\Omega} \triangleq \{p | \gamma_p = 0, p > 0\}$ is the complementary set of Ω with the full set defined as $[0, P-1]$. The meanings of (69) and (70) are that the non-zero elements of $\boldsymbol{\rho}_{mm'}^{(k)}$ and $\boldsymbol{\eta}_{mm'}^{(k)}$ are expressed by the sum of the off-diagonal elements in the upper and lower triangular parts of $\mathbf{Z}_{mm'}^{(k)}$ magnified by γ_p^2 , respectively. Using (69) and (70), the calculations for zero-valued

Algorithm 2: The WISL Minimization-Based Algorithm.

```

1:  $k \leftarrow 0, \mathbf{y} \leftarrow$  unimodular sequence with random phases.
2:  $\lambda_{\tilde{\Phi}} \triangleq 2MP\lambda_{\max}^2(\mathbf{\Gamma})$ 
3: repeat
4:   procedure WISLNEW( $\mathbf{y}^{(k)}$ )
5:     Calculate  $\boldsymbol{\rho}_{mm'}^{(k)}, \boldsymbol{\eta}_{mm'}^{(k)}$  via (69) and (70),
6:        $m = 1, \dots, M; m' = m, \dots, M.$ 
7:      $\mathbf{B}_{mm'}^{(k)} = \left(\mathbf{B}_{m'm}^{(k)}\right)^H = 2P\mathcal{T}\left(\boldsymbol{\rho}_{mm'}^{(k)}, \boldsymbol{\eta}_{mm'}^{(k)}\right),$ 
8:        $m = 1, \dots, M; m' = m, \dots, M.$ 
9:     Construct  $\mathbf{B}^{(k)}$  via (67)
10:     $\tau^{(k)} = \|\mathbf{B}^{(k)} - \frac{1}{2}\lambda_{\tilde{\Phi}}\mathbf{y}^{(k)}(\mathbf{y}^{(k)})^H\|$ 
11:     $\mathbf{z}^{(k)} = \left(\frac{1}{2}(\tau^{(k)} + MP\lambda_{\tilde{\Phi}})\mathbf{I}_{MP} - \mathbf{B}^{(k)}\right)\mathbf{y}^{(k)}$ 
12:     $\mathbf{y}^{(k+1)}(p') = e^{j\arg(\mathbf{z}^{(k)}(p'))}, p' = 1, \dots, MP$ 
13:     $k \leftarrow k + 1$ 
14:   end procedure
15: until convergence

```

elements can be avoided. Note that $\mathbf{B}_{mm'}^{(k)} = \left(\mathbf{B}_{m'm}^{(k)}\right)^H$, therefore, only the upper (or lower) triangular part of $\mathbf{B}^{(k)}$ needs to be determined.

The objective function (66) takes a quadratic form, to which the majorant of (18) can be applied again. Let $\mathbf{G} \triangleq \tau^{(k)}\mathbf{I}_{MP}$, so that the generalized inequality $\mathbf{G} \succeq \mathbf{Q}$ is guaranteed for (18). Here we can use any matrix norm of $\mathbf{Q}^{(k)} \triangleq \mathbf{B}^{(k)} - \lambda_{\tilde{\Phi}}\mathbf{y}^{(k)}(\mathbf{y}^{(k)})^H/2$ for $\tau^{(k)}$ because it serves as an upper bound of the largest eigenvalue. Thus, the objective function (66) can be majorized by the following function

$$\tilde{g}_2(\mathbf{y}, \mathbf{y}^{(k)}) = \frac{\tau^{(k)}}{2}\mathbf{y}^H\mathbf{y} + (\mathbf{y}^{(k)})^H\left(\frac{\tau^{(k)} + MP\lambda_{\tilde{\Phi}}}{2}\mathbf{I}_{MP} - \mathbf{B}^{(k)}\right)\mathbf{y}^{(k)} + 2\Re\left\{\mathbf{y}^H\left(\mathbf{B}^{(k)} - \frac{\tau^{(k)} + MP\lambda_{\tilde{\Phi}}}{2}\mathbf{I}_{MP}\right)\mathbf{y}^{(k)}\right\}. \quad (71)$$

Similar to the majorant (30), the first two terms of (71) are constant and therefore immaterial for optimization. Ignoring these two terms, the problem (59) can be majorized by

$$\begin{aligned} \min_{\mathbf{y}} \quad & \mathbf{y}^H\left(\mathbf{B}^{(k)} - \frac{\tau^{(k)} + MP\lambda_{\tilde{\Phi}}}{2}\mathbf{I}_{MP}\right)\mathbf{y}^{(k)} \\ \text{s.t.} \quad & |\mathbf{y}(p')| = 1, p' = 1, \dots, MP. \end{aligned} \quad (72)$$

Due to the constant-modulus property of \mathbf{y} , the problem (72) is equivalent to the following optimization problem

$$\begin{aligned} \min_{\mathbf{y}} \quad & \|\mathbf{y} - \mathbf{z}^{(k)}\|^2 \\ \text{s.t.} \quad & |\mathbf{y}(p')| = 1, p' = 1, \dots, MP \end{aligned} \quad (73)$$

where $\mathbf{z}^{(k)} \triangleq \left(\frac{\tau^{(k)} + MP\lambda_{\tilde{\Phi}}}{2}\mathbf{I}_{MP} - \mathbf{B}^{(k)}\right)\mathbf{y}^{(k)}$. The problem (73) can be then solved in closed form as

$$\mathbf{y}(p') = \exp\{j \cdot \arg(\mathbf{z}^{(k)}(p'))\}, p' = 1, \dots, MP. \quad (74)$$

Finally, reshaping the so-obtained vector \mathbf{y} into a $P \times M$ matrix, we obtain the designed waveform matrix \mathbf{Y} . The WISL minimization-based unimodular waveform design algorithm is summarized in Algorithm 2.

To find the computational complexity of Algorithm 2, we assume that the set of Ω consists of N_P ($0 < N_P \leq P$) elements. It can be seen that both $\boldsymbol{\rho}_{mm'}^{(k)}$ in (69) and $\boldsymbol{\eta}_{mm'}^{(k)}$ in (70) can be calculated with at most $N_P P$ operations if the covariance matrix $\mathbf{Z}_{mm'}^{(k)}$ is given. The calculation of $\mathbf{Z}_{mm'}^{(k)}$ costs P^2 operations. Note that we only need to calculate for the subscripts $m = 1, \dots, M$ and $m' = m, \dots, M$, and then repeat the above summarized calculations $M(M-1)/2$ times. Finally, the calculation of the vector $\mathbf{z}^{(k)}$ needs $M^2 P^2$ operations. Consequently, the total number of operations is upper bounded by $((3M^2 - M)P^2 + (M^2 - M)N_P P)/2$. In other words, the computational complexity of Algorithm 2 is at most $\mathcal{O}((M-1)MP^2)$ which is smaller than quadratic in the problem size, and therefore suitable for large-scale optimization.⁴

The accelerated version of Algorithm 2 is obtained by a straightforward application of the SQUAREM acceleration scheme [40] as in the case of Algorithm 1.

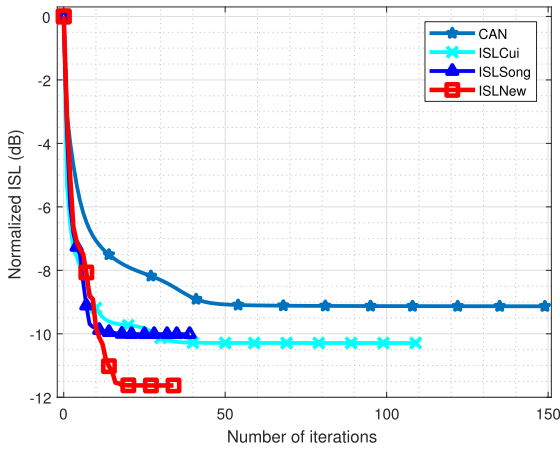
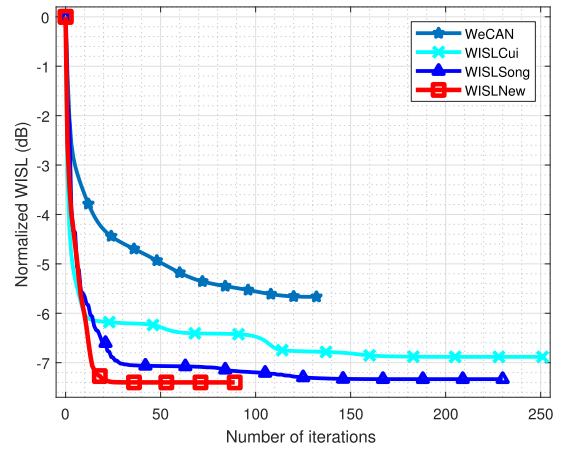
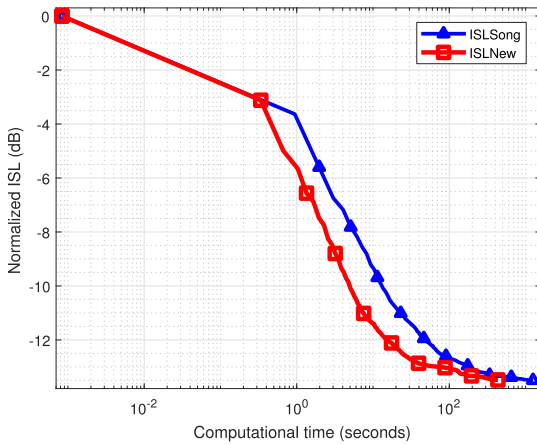
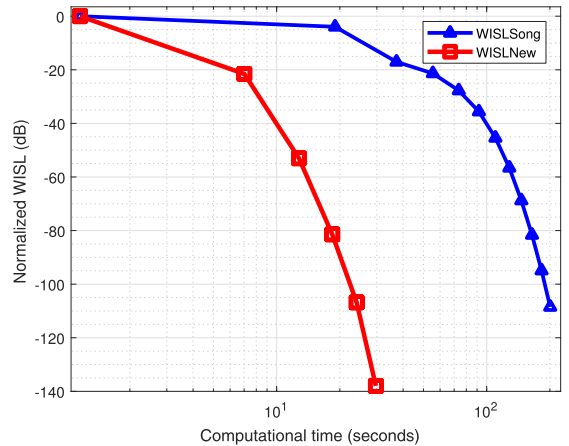
IV. SIMULATION RESULTS

In our simulations, we evaluate the performance of the proposed algorithms (Algorithms 1 and 2) and compare it with that of the existing ISL and WISL minimization-based algorithms. In particular, Algorithm 1 for ISL minimization (named hereafter as ISLNew) is compared with the CAN algorithm of [8], the (third) algorithm of [32] (named hereafter as ISLSong), and the algorithm of [45] (named hereafter as ISLCui with all weights equaling 1). Algorithm 2 for WISL minimization (named hereafter as WISLNew) is compared with the WeCAN algorithm of [8], the (second) algorithm of [32] (named hereafter as WISLSong), and the algorithm of [45] (named hereafter as WISLCui). The MaMi-based algorithms, including the ISLSong, ISLNew, WISLSong and WISLNew, are accelerated by the SQUAREM scheme [40].

We first investigate the convergence properties of the algorithms tested, and then conduct their performance evaluations in terms of the following characteristics: i) the minimum and average ISL/WISL values obtained after the algorithms converge to the preset tolerance (called ISL/WISL after convergence); ii) the average consumed time (in seconds); and iii) the average number of conducted iterations. Here all averaged results are obtained over 50 independent trials. Throughout all simulations, we generate sets of unimodular sequences with random phases as the initialization, and use the same initial sequence set in all algorithms for fair comparison. We conduct all comparisons based on the same hardware and software configurations (PC with 3.30 GHz Intel Xeon CPU E3-1230 and 16 GB RAM using MATLAB R2017a). The stopping criterion, defined as the absolute ISL/WISL difference between the current and previous iterations normalized by the initial ISL/WISL value, is employed in all simulation examples,⁵ and the preset stopping tolerance is 10^{-9} . In every example related to WISL minimization, the ISL controlling weights are set to be $\gamma_p = 1, p = -19, \dots, 19$, while the others are zeros. In addition, the ISL and WISL values

⁴Note that the overall computational complexity claimed in [32] has to be corrected to the same order as here. Further clarifications can be found in Section IV.

⁵We have also tested the other stopping criterion mentioned in Subsection III-A to confirm that convergence results are independent of a specific criterion. Thus, we only show the results for one stopping criterion here.

(a) Normalized ISL versus number of iterations for $M = 1$ and $P = 32$.(b) Normalized WISL versus number of iterations for $M = 2$ and $P = 32$.Fig. 1. Convergence evaluations of the ISL and WISL minimization-based algorithms for short code length $P = 32$.(a) Normalized ISL versus computational time for $M = 1$ and $P = 3000$.(b) Normalized WISL versus computational time for $M = 2$ and $P = 3000$.Fig. 2. Convergence evaluations of the ISL and WISL minimization-based algorithms for large code length $P = 3000$.

are shown in dBs and defined as $10 \log_{10}(\zeta)$ and $10 \log_{10}(\zeta_w)$, respectively.

Example 1: Convergence evaluation. In this example, we study the convergence properties of the waveform design algorithms in terms of the ISL/WISL values plotted versus the number of conducted iterations and the computational time. The ISL and WISL values at each iteration are normalized by the value obtained at initialization. The short code length of $P = 32$ and large code length of $P = 3000$ are tested for both the ISL and WISL evaluations, and the numbers of waveforms are set as $M = 1$ for the former and $M = 2$ for the latter.

The corresponding ISL convergence results versus the number of conducted iterations are shown in Fig. 1(a). It can be seen from the figure that for all the algorithms tested, the obtained ISL decreases monotonically as the number of iterations increases. Among the algorithms tested, the ISLNew algorithm shows the best convergence speed, i.e., it requires the smallest

number of iterations (around 30) to converge to the solution with -11.63 dB normalized ISL value that satisfies the preset tolerance parameter. The ISLSong algorithm shows the second best convergence speed with the consumption of about 40 iterations, while the ISLCui and CAN algorithms spend 110 and 512 iterations (only the first 150 are shown), respectively. Their normalized ISL values after convergence are -10.01 dB, -10.29 dB, and -9.43 dB, respectively. This example demonstrates the superiority of applying MaMi techniques with acceleration to the ISL minimization-based waveform design, and also verifies the advantage of the proposed ISLNew algorithm over the other algorithms.

Similar to the ISL convergence results, it can be seen from the results shown in Fig. 1(b) that the WISL values for all algorithms tested also decrease monotonically as the number of iterations increases. In this example, the WISLCui, WISLSong, and WISLNew algorithms show much faster convergence speed

TABLE I
ISL PERFORMANCE COMPARISONS (INCLUDING THE MINIMUM AND AVERAGE ISL VALUES, THE CONSUMED TIME, AND THE NUMBER OF CONDUCTED ITERATIONS) OF THE ALGORITHMS TESTED VERSUS CODE LENGTH FOR $M = 1$ WAVEFORM

	$P = 64, M = 1$				$P = 128, M = 1$				$P = 512, M = 1$				$P = 1024, M = 1$				$P = 2048, M = 1$			
	Min. ^a	Ave. ^b	Time	Iter. ^c	Min.	Ave.	Time	Iter.	Min.	Ave.	Time	Iter.	Min.	Ave.	Time	Iter.	Min.	Ave.	Time	Iter.
CAN	23.30	24.88	0.11	469	29.25	30.40	0.35	862	41.03	41.84	2.34	1766	47.17	47.75	82.03	2504	53.21	53.54	204.20	4009
ISLSong	22.47	24.02	0.03	93	28.43	29.47	0.11	138	40.56	40.92	3.18	359	46.63	46.87	23.38	596	52.38	52.74	121	792
ISLCui	23.09	24.08	1.39	168	28.86	29.65	7.3	279	40.76	40.99	649.12	978	–	–	hours	–	–	–	hours	–
ISLNew	22.46	24.00	0.02	85	28.32	29.39	0.08	127	40.44	40.91	2.92	342	46.49	46.79	19.87	578	52.22	52.69	109	765

^a Min.: Minimum ISL value (in dB). ^b Ave.: Average ISL value (in dB). ^c Iter.: Average number of conducted iterations.

TABLE II
ISL PERFORMANCE COMPARISONS (INCLUDING THE MINIMUM AND AVERAGE ISL VALUES, THE CONSUMED TIME, AND THE NUMBER OF CONDUCTED ITERATIONS) OF THE ALGORITHMS TESTED VERSUS LARGE CODE LENGTH FOR $M = 2$ WAVEFORMS

	$P = 1500, M = 2$				$P = 2000, M = 2$				$P = 3000, M = 2$				$P = 3500, M = 2$				$P = 4000, M = 2$			
	Min. ^a	Ave. ^b	Time	Iter. ^c	Min.	Ave.	Time	Iter.												
ISLSong	66.53	66.53	99.74	1084	69.03	69.03	177.67	1132	72.55	72.55	387.62	1199	73.89	73.89	552.53	1201	75.05	75.05	636.25	1051
ISLNew	66.53	66.53	92.08	1013	69.03	69.03	138.08	881	72.55	72.55	334.97	1007	73.89	73.89	495.11	1078	75.05	75.05	566.13	939

^a Min.: Minimum ISL value (in dB). ^b Ave.: Average ISL value (in dB). ^c Iter.: Average number of conducted iterations.

and achieve significantly lower WISL than the WeCAN algorithm. The proposed WISLNew algorithm shows the best performance. It consumes only 89 iterations for achieving WISL of -7.40 dB, while the WISLSong and WISLCui algorithms consume 230 and 251 iterations and obtain WISLs of -7.30 dB and -6.88 dB, respectively. The WeCAN algorithm obtains WISL of only -5.67 dB and spends 132 iterations. In addition, this example verifies that the WISLCui algorithm is more sensitive to the sparsity of ISL controlling weights than the MaMi-based algorithms, and it can result in very large number of iterations when non-sparse weights are present.

The ISL and WISL convergence results versus the computational time for the large code length of $P = 3000$ are shown in Fig. 2, where we only show the plots for the ISLSong, WISLSong and the proposed ISLNew and WISLNew algorithms. The non-competitive CAN, WeCAN, ISLCui, and WISLCui algorithms are excluded from the comparison because they lead to heavy time consumptions up to hours for the large code length tested. It can be seen from Figs. 2(a) and 2(b) that the proposed ISLNew and WISLNew algorithms outperform, respectively, ISLSong and WISLSong. The advantage is significant for the WISL evaluation, which is verified by the large gap between the two curves in Fig. 2(b). In short, we can conclude that our proposed ISLNew and WISLNew algorithms consistently show superiority over the ISLSong and WISLSong algorithms, respectively. This superiority is especially pronounced in the case of large code length. One of the reasons for this superiority is that better majorants are used for developing the proposed algorithms.

Example 2: Performance evaluation versus code lengths. In our second example, we evaluate the algorithms tested in terms of the performance characteristics listed in the beginning of this section. The sets of code lengths $\{64, 128, 512, 1024, 2048\}$ and $\{1500, 2000, 3000, 3500, 4000\}$ are used. The latter one represents large code lengths and is used for ISL evaluation only. In the case of WISL evaluation, the advantages are significant and visible even for relatively short code lengths represented by the former set. The numbers of waveforms are set as $M \in \{1, 2\}$ for ISL and $M = 2$ for WISL evaluations.

The results of the ISL evaluation tested for the first set of relatively short code lengths are shown in Table I. It can be seen that

the proposed ISLNew algorithm gives the best performance in terms of all performance characteristics for all code lengths. The ISLSong algorithm shows the second best performance which is slightly worse than that of ISLNew, while the CAN algorithm generally behaves the worst among the algorithms tested. It can be observed that the algorithms tested show minor differences in the obtained minimum and average ISL values. For example, the biggest gap between the best and worst minimum and average ISL values for all code lengths is 1.01 dB, and the smallest gap is nearly 0 dB. Indeed, the algorithms tested obtain nearly the same minimum and average ISL values (rounded off to two digits after the decimal place) when $M = 2$ (and more) waveforms are designed. This example indicates that all ISL minimization-based algorithms show no significant advantage over the benchmark CAN algorithm in terms of the obtained ISL values. It is mainly because they all converge to the lower bound of the minimum achievable ISL for each code length. The major differences between the algorithms tested are in the consumed time and number of conducted iterations. It can be seen from Table I that the ISLNew algorithm always consumes the shortest time and needs the smallest number of iterations compared to the other algorithms. For example, it generates waveform of code length 2048 within 109 seconds via 765 iterations, while the CAN and ISLSong algorithms spend about 204.20 and 121 seconds and require 4009 and 792 iterations, respectively. The ISLCui algorithm, however, costs significantly more time (7 to 10 times more than ISLNew for code lengths $P = 64$ and $P = 128$, and hundreds of time more for $P = 512$) as well as more iterations than the MaMi-based algorithms (ISLSong and ISLNew). It verifies its slow convergence speed and high computational complexity because of the necessity to update the waveform elements in sequence and re-calculate the waveform covariance and correlation matrices at each update. We do not show the results for the ISLCui algorithm for code length larger than 512 because of the high consumption of time (hours) as well as large number of iterations (thousands).

To further verify the advantages of the proposed ISLNew algorithm, we additionally evaluate the performance of the ISLSong and ISLNew algorithms over the second set of large code lengths ranging from 1500 to 4000. The results are shown in Table II. The non-competitive CAN and ISLCui algorithms

TABLE III

WISL PERFORMANCE COMPARISONS (INCLUDING THE MINIMUM AND AVERAGE WISL VALUES, THE CONSUMED TIME, AND THE NUMBER OF CONDUCTED ITERATIONS) OF THE ALGORITHMS TESTED VERSUS CODE LENGTH FOR $M = 2$ WAVEFORMS

	$P = 64, M = 2$				$P = 128, M = 2$				$P = 512, M = 2$				$P = 1024, M = 2$				$P = 2048, M = 2$			
	Min. ^a	Ave. ^b	Time	Iter. ^c	Min.	Ave.	Time	Iter.	Min.	Ave.	Time	Iter.	Min.	Ave.	Time	Iter.	Min.	Ave.	Time	Iter.
WeCAN	20.09	21.46	25.05	2534	18.73	19.53	13.01	494	19.66	20.44	26.68	107	20.32	20.47	95.12	107	20.32	20.90	289	94
WISLSong	11.73	14.52	3.45	557	-45.25	-32.73	0.94	55	-56.40	-31.61	10.73	22	-48.98	-45.94	44.43	22	-67.21	-30.64	203.37	23
WISLCui	12.32	14.61	18.55	662	-47.88	-46.69	2.54	30	-82.18	-69.05	18.69	6	-93.32	-82.31	124.06	5	-90.30	-85.83	779.21	4
WISLNew	11.29	14.19	0.92	269	-72.72	-48.12	0.22	28	-93.31	-77.66	1.29	7	-90.31	-77.66	4.05	6	-87.30	-62.36	20.90	5

^a Min.: Minimum WISL value (in dB). ^b Ave.: Average WISL value (in dB). ^c Iter.: Average number of conducted iterations.

TABLE IV

ISL PERFORMANCE COMPARISONS (INCLUDING THE MINIMUM AND AVERAGE ISL VALUES, THE CONSUMED TIME, AND THE NUMBER OF CONDUCTED ITERATIONS) OF THE ALGORITHMS TESTED VERSUS NUMBER OF WAVEFORMS WITH FIXED CODE LENGTH $P = 64$

	$P = 64, M = 3$				$P = 64, M = 4$				$P = 64, M = 5$				$P = 64, M = 6$				$P = 64, M = 7$			
	Min. ^a	Ave. ^b	Time	Iter. ^c	Min.	Ave.	Time	Iter.												
CAN	43.91	43.91	1.18	3532	46.92	46.92	0.65	1922	49.13	49.13	0.39	1115	50.89	50.89	0.33	908	52.36	52.36	0.38	1027
ISLSong	43.91	43.91	0.12	263	46.92	46.92	0.06	132	49.13	49.13	0.05	100	50.89	50.89	0.04	111	52.36	52.36	0.04	80
ISLCui	43.91	43.91	39.36	675	46.92	46.92	30.06	307	49.13	49.13	22.74	154	50.89	50.89	22.92	111	52.36	52.36	20.71	75
ISLNew	43.91	43.91	0.08	241	46.92	46.92	0.05	122	49.13	49.13	0.03	96	50.89	50.89	0.03	77	52.36	52.36	0.03	78

^a Min.: Minimum ISL value (in dB). ^b Ave.: Average ISL value (in dB). ^c Iter.: Average number of conducted iterations.

TABLE V

WISL PERFORMANCE COMPARISONS (INCLUDING THE MINIMUM AND AVERAGE WISL VALUES, THE CONSUMED TIME, AND THE NUMBER OF CONDUCTED ITERATIONS) OF THE ALGORITHMS TESTED VERSUS NUMBER OF WAVEFORM WITH FIXED CODE LENGTH $P = 64$

	$P = 64, M = 3$				$P = 64, M = 4$				$P = 64, M = 5$				$P = 64, M = 6$				$P = 64, M = 7$			
	Min. ^a	Ave. ^b	Time	Iter. ^c	Min.	Ave.	Time	Iter.	Min.	Ave.	Time	Iter.	Min.	Ave.	Time	Iter.	Min.	Ave.	Time	Iter.
WeCAN	31.45	32.37	9.28	737	39.56	40.05	6.64	424	43.60	43.74	4.45	243	46.14	46.24	4.11	185	47.99	48.06	6.13	237
WISLSong	30.72	31.49	4.21	362	37.76	38.49	14.48	735	41.88	42.06	20.87	697	44.33	44.40	50.13	1100	46.05	46.19	89.28	1419
WISLCui	28.51	30.81	35.29	618	38.15	38.58	87.87	918	41.79	41.97	193.20	1343	44.24	44.32	220.53	1094	45.87	46.13	354.73	1321
WISLNew	28.96	31.10	1.96	302	38.40	38.58	4.77	465	41.77	41.99	11.13	732	44.07	44.35	23.94	941	45.94	46.13	31.69	932

^a Min.: Minimum WISL value (in dB). ^b Ave.: Average WISL value (in dB). ^c Iter.: Average number of conducted iterations.

result in heavy time consumptions up to hours for the large code lengths tested, and therefore, are not included in the table. It can be seen that our proposed ISLNew algorithm outperforms the ISLSong algorithm in terms of the consumed time and the number of conducted iterations for all code lengths tested. The smallest and largest gaps on the time consumption between the two algorithms have respectively reached 7.64 (for $P = 1500$) and 70.12 seconds (for $P = 4000$), while the smallest and largest gaps on the number of conducted iterations have respectively reached 71 (for $P = 1500$) and 251 (for $P = 2000$). For each code length tested here under the preset convergence tolerance, the ISLSong and ISLNew algorithms show no performance difference in terms of the obtained minimum and average ISL values, since both of them nearly approach the lower bound on ISL given as $P^2 M(M-1)$ [17]. For example for $P = 2000$ and $M = 2$, the ISL is lower bounded by the value of $10 \log_{10}(2000^2 \cdot 2(2-1)) = 69.0309$ dB, which is the same as the corresponding ISL values in Table II rounded off to two digits after the decimal place.

For the WISL evaluation, it can be seen from Table III that the WISLNew algorithm generally outperforms the other three algorithms for all code lengths tested, while the WeCAN algorithm performs the worst. The WISLCui algorithm behaves better than the WISLSong algorithm from the perspective of minimum and average WISL values after convergence. However, it consumes much more time than the latter. Among all code lengths, the smallest average WISL values obtained af-

ter convergence by the WeCAN, WISLSong, WISLCui and WISLNew algorithms are respectively 19.53 dB, -45.94 dB, -85.83 dB and -77.66 dB, while the largest average WISL values are 21.46 dB, 14.52 dB, 14.61 dB and 14.19 dB (all for $P = 64$), respectively. The WeCAN algorithm generally consumes significantly more time, requires more iterations, and achieves worse WISL levels than the MaMi-based algorithms. It is mainly because WeCAN algorithm does not minimize the original WISL objective function, but instead it minimizes a surrogate one, which is less accurate compared to the majorization functions used by the MaMi-based algorithms. The advantages of the WISLNew and WISLSong algorithms over the WeCAN algorithm become a lot more obvious when the code length P is larger than 64, which verifies the fact that WeCAN is suitable only for the WISL minimization-based waveform design with short code length. Indeed, the WeCAN algorithm may converge very slowly when the set of ISL controlling weights is not sparse.

Focusing on the comparisons between the WISLSong, WISLCui, and WISLNew algorithms, we can also see from Table III that the WISLNew algorithm is superior to WISLSong, especially when the code length P is larger than 64. The biggest difference for the minimum WISL values obtained by the WISLSong and WISLNew algorithms reaches 41.33 dB, and it is 46.05 dB for the average WISL value. Moreover, the WISLNew algorithm always consumes less time and requires smaller number of iterations than WISLSong. This superiority

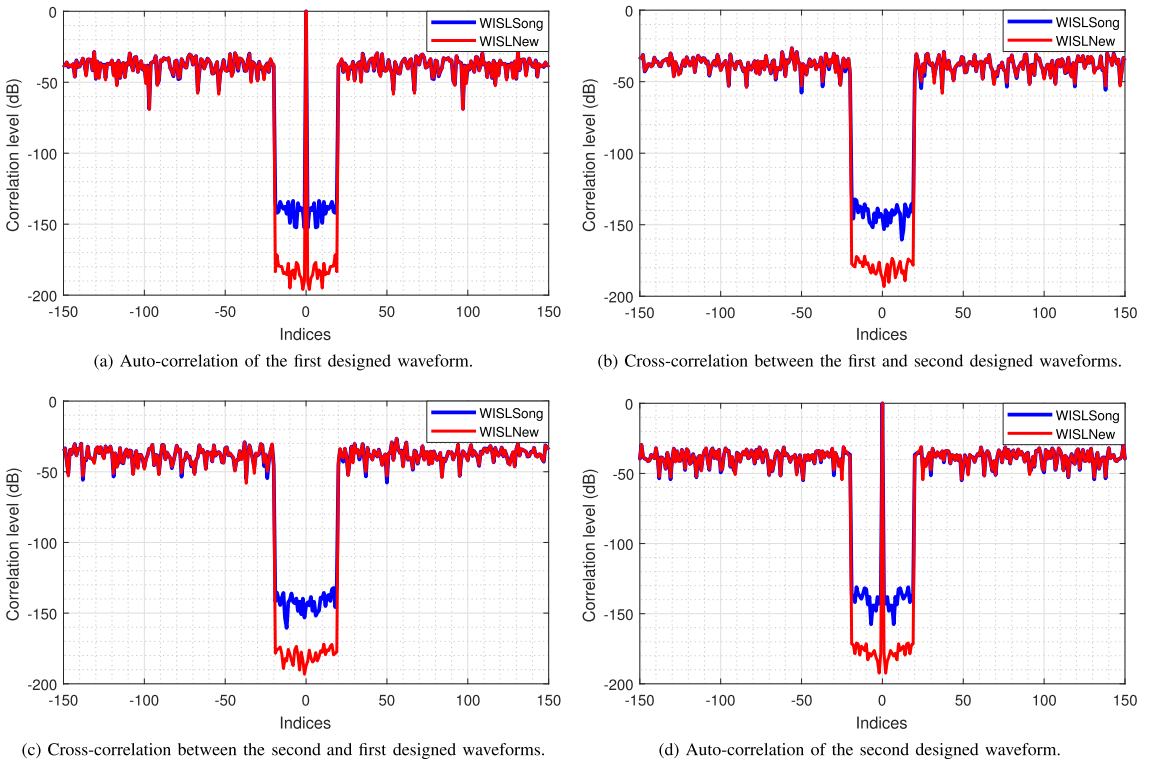


Fig. 3. Correlation property evaluation of the designed waveforms for the WISL minimization-based designs. Here the number of waveforms is $M = 2$, and the large code length is $P = 4096$. Correlation results with respect to time lags only within the range $[-150, 150]$ are shown.

becomes more obvious as the code length increases. In particular, the ratio of the time consumption by WISLNew compared to WISLSong decreases from 0.23 to 0.1, and the ratio of the number of conducted iterations decreases from 0.51 to 0.22 as the code length increases from 128 to 2048. Therefore, the proposed WISLNew algorithm is better suited for large-scale waveform design problems. As for the WISLCui algorithm, it always consumes significantly more time than the MaMi-based algorithms. Moreover, it even consumes more time than the WeCAN algorithm for large code lengths tested here. The resulted time consumption becomes much higher as the code length increases. In this example, about 13 minutes are consumed by the WISLCui algorithm for code length $P = 2048$, while only 3% of this time is required by the proposed WISLNew algorithm. The WISLCui algorithm requires almost the same number of iterations as the WISLNew algorithm for code length equal or larger than 128, but it requires around 2.5 times more iterations for the code length $P = 64$. This verifies the high computational complexity of the WISLCui algorithm and especially its sensitivity to the sparsity of ISL controlling weights. The minor advantage of WISLCui over WISLNew can be seen only for the average WISL values obtained for code lengths $P = 1024$ and $P = 2048$ when ISL controlling weights are sparse. Indeed, the WISLNew algorithm can achieve better or the same WISL levels as the WISLCui algorithm, and still consume much shorter time if the tolerance parameter is set lower.

Example 3: Performance evaluation versus number of waveforms. In our third example, we evaluate the performance of the algorithms tested in terms of the same performance characteristics as in the previous example versus the number of waveforms chosen from the set $\{3, 4, 5, 6, 7\}$ with fixed code length $P = 64$.

For the ISL evaluation, it can be seen from the results shown in Table IV that the proposed ISLNew algorithm maintains advantages over the other algorithms again. All algorithms obtain nearly the same minimum and average ISL values after convergence, but they differ from each other in terms of the consumed time and number of conducted iterations. Among all scenarios, the first one ($M = 3$) costs the most time and largest number of conducted iterations for all algorithms tested. The ISLNew algorithm consumes only 0.08 seconds and 241 iterations for this scenario, while the ISLCui algorithm consumes the worst time of 39.36 seconds, and the CAN needs the largest number of iterations (more than 3500). The ISLSong algorithm behaves slightly worse than the ISLNew but better than ISLCui and CAN for all scenarios.

For the WISL evaluation, it can be seen from the results shown in Table V that the proposed WISLNew algorithm again demonstrates advantages over the other algorithms in terms of all performance characteristics. To be explicit, the WISLNew algorithm takes around 2 to 3 times less time and 1.2 to 1.6 times less number of iterations compared to the WISLSong algorithm,

and it achieves slightly lower minimum and average WISL values after convergence for all code lengths. The WISLCui takes around two times more number of iterations than the WISLNew algorithm, and requires around 10 to 20 times more time. The WeCAN algorithm almost always demonstrates the worst minimum and average WISL values.

Example 4: Correlation level evaluation. In the last example, we present the auto- and cross-correlations for $M = 2$ waveforms designed by the WISLSong and WISLNew algorithms with large code length $P = 4096$. The corresponding results are shown in Fig. 3 where the sub-figures show the auto- and cross-correlations of the waveforms generated by the two algorithms. Here the correlation levels, defined as $20 \log_{10}(r_{m,m'}(p))$, $m, m' \in \{1, 2\}$; $p \in \{-4095, 4095\}$, are shown in dBs. To better display the results, we only show correlation levels for the time lags within the range $[-150, 150]$. The WISLCui and WeCAN algorithms for the large code length tested in this example require hours- or days-long time and show no better auto- and cross-correlations. Therefore, they are not shown in Fig. 3. Moreover, for the ISL minimization-based waveform design algorithms tested, the differences in auto- and cross-correlation plots are very minor. Therefore, we also omit to show the corresponding plots for the sake of brevity.

It can be seen from Fig. 3 that the auto-correlations associated with the time lags $[-19, -1] \cup [1, 19]$ and cross-correlations associated with the time lags $[-19, 19]$ for both generated waveform sets are well controlled, while the waveform correlations associated with other time lags are not explicitly controlled. Therefore, the latter results in much higher correlation levels. Under the condition of using the same tolerance parameter, the correlation levels corresponding to the time lags of interest obtained by the proposed WISLNew algorithm are significantly better than those obtained by the WISLSong algorithm. The largest gap between the obtained correlation levels by these two algorithms reaches about 50 dB. Moreover, the proposed WISLNew algorithm needs significantly shorter time than the WISLSong algorithm as it has been discussed above.

V. CONCLUSION

In this paper, we have developed two (one based on ISL and the other based on WISL minimization) new fast algorithms for designing single or multiple unimodular waveforms/codes with good auto- and cross-correlation or weighted correlation properties. Since the corresponding optimization problems are non-convex and may be large-scale, the proposed algorithms are developed based on the MaMi framework and utilize a number of newly found inherent algebraic structures in the objective functions of the corresponding optimization problems. These properties have enabled us to reduce the computational complexity of the algorithms to the level which is suitable for large-scale optimization. Moreover, the proposed algorithms also show faster convergence speed to the preset tolerance and provide waveforms of better qualities than those of the existing state-of-the-art algorithms.

APPENDIX

A. Proof of (22)

Proof: Using the definition of \mathbf{A}_p , that is, $\mathbf{A}_p \triangleq \mathbf{I}_M \otimes \mathbf{a}_p$, it can be seen that the matrix product $\mathbf{A}_p \mathbf{A}_p^H$ is block diagonal and

sparse containing $M(M-1)$ zero blocks of size $P \times P$. Recall that Φ in (13) is composed of the outer products of $2P$ vectors, which are the vectorized versions of $\mathbf{A}_p \mathbf{A}_p^H$, $p = 1, \dots, 2P$. Therefore, (13) contains many column-row vector pairs that have the same indices for corresponding columns and rows full of zeros. These pairs obviously do not contribute to the rank of Φ , and thus, do not affect non-zero eigenvalues of Φ , including $\lambda_{\max}(\Phi)$. Hence, for finding $\lambda_{\max}(\Phi)$, these pairs can be excluded. Then $\lambda_{\max}(\Phi)$ is the same as the maximum eigenvalue of the shrunk version of Φ given by

$$\Phi' = \sum_{p=1}^{2P} \text{vec}(\mathbf{1}_M^T \otimes (\mathbf{a}_p \mathbf{a}_p^H)) (\text{vec}(\mathbf{1}_M^T \otimes (\mathbf{a}_p \mathbf{a}_p^H)))^H. \quad (75)$$

Using the elementary properties of the vectorization operator and Kronecker product, (75) can be simplified as

$$\begin{aligned} \Phi' &= \sum_{p=1}^{2P} \left(\mathbf{1}_M \otimes \text{vec}(\mathbf{a}_p \mathbf{a}_p^H) \right) \left(\mathbf{1}_M^T \otimes (\text{vec}(\mathbf{a}_p \mathbf{a}_p^H))^H \right) \\ &= \sum_{p=1}^{2P} (\mathbf{1}_M \mathbf{1}_M^T) \otimes (\text{vec}(\mathbf{a}_p \mathbf{a}_p^H) (\text{vec}(\mathbf{a}_p \mathbf{a}_p^H))^H) \\ &= (\mathbf{1}_M \mathbf{1}_M^T) \otimes \sum_{p=1}^{2P} \text{vec}(\mathbf{a}_p \mathbf{a}_p^H) (\text{vec}(\mathbf{a}_p \mathbf{a}_p^H))^H \\ &= (\mathbf{1}_M \mathbf{1}_M^T) \otimes \Phi|_{M=1} \end{aligned} \quad (76)$$

where $\Phi|_{M=1}$ is the expression of Φ for $M = 1$. The component $\mathbf{1}_M \mathbf{1}_M^T$ in the Kronecker product of (76) is the rank-one matrix with its largest eigenvalue equal to M . Using the property of the Kronecker product about the eigenvalues [46] (see Theorem 4.2.12 therein), we can conclude that

$$\lambda_{\max}(\Phi') = \lambda_{\max}(\mathbf{1}_M \mathbf{1}_M^T) \lambda_{\max}(\Phi|_{M=1}) = 2MP^2 \quad (77)$$

where the fact that $\lambda_{\max}(\Phi|_{M=1}) = 2P^2$ is proved, for example, in [31]. Therefore, $\lambda_{\max}(\Phi) = \lambda_{\max}(\Phi') = 2MP^2$. The proof is complete. \blacksquare

B. Proof of (57)

Proof: Note that $\bar{\Gamma}$ in (52) is sparse and contains many column-row vector pairs that have the same indices for corresponding columns and rows full of zeros. Following the same logic as in Appendix A for the matrix Φ , we can conclude that

$$\lambda_{\max}(\bar{\Gamma}) = \lambda_{\max}(\mathbf{1}_M \mathbf{1}_M^T) \lambda_{\max}(\bar{\Gamma}|_{M=1}) = M \lambda_{\max}(\bar{\Gamma}|_{M=1}) \quad (78)$$

where $\bar{\Gamma}|_{M=1}$ is the expression of $\bar{\Gamma}$ for $M = 1$. Inserting the explicit forms of $\Gamma_{kk'}^{\text{real}}$ and $\Gamma_{kk'}^{\text{img}}$ given by (46) and (47), respectively, for $M = 1$ into (52), and using some elementary properties of the vectorization operator, the property $\text{vec}(\mathbf{u}_k \otimes \mathbf{v}_{k'}^H) = \mathbf{v}_{k'}^* \otimes \mathbf{u}_k$, and also the relationship between \mathbf{u}_k and \mathbf{v}_k given after (43), the matrix $\bar{\Gamma}|_{M=1}$ can be

simplified as

$$\begin{aligned}\bar{\Gamma}|_{M=1} &= \sum_{k=1}^K \sum_{k'=1}^K \frac{1}{4} \text{vec}(\mathbf{u}_k \mathbf{v}_{k'}^H + \mathbf{v}_{k'} \mathbf{u}_k^H) (\text{vec}(\mathbf{u}_k \mathbf{v}_{k'}^H \\ &\quad + \mathbf{v}_{k'} \mathbf{u}_k^H))^H + \frac{1}{4} (\text{vec}(\mathbf{u}_k \mathbf{v}_{k'}^H - \mathbf{v}_{k'} \mathbf{u}_k^H))^* \\ &\quad \times (\text{vec}(\mathbf{u}_k \mathbf{v}_{k'}^H - \mathbf{v}_{k'} \mathbf{u}_k^H))^T \\ &= \sum_{k=1}^K \sum_{k'=1}^K (\mathbf{u}_k \otimes \mathbf{v}_{k'}) (\mathbf{u}_k^H \otimes \mathbf{v}_{k'}^H).\end{aligned}\quad (79)$$

Note that (79) is the eigenvalue decomposition of $\bar{\Gamma}|_{M=1}$ which may be indefinite, and $\{(\mathbf{u}_k \otimes \mathbf{v}_{k'}) / \sqrt{\lambda_k \lambda_{k'}}\}_{k,k'=1}^K$ is the set of K^2 eigenvectors of $\bar{\Gamma}|_{M=1}$. Hence, $\lambda_{\max}(\bar{\Gamma}|_{M=1})$ equals the maximum value of the product $\lambda_k \lambda_{k'}$. Since λ_k and $\lambda_{k'}$, $k, k' \in \{1, \dots, K\}$ are real valued, we have $\max\{\lambda_k \lambda_{k'}\} = \max\{\lambda_k^2\}$. Without loss of generality, we denote by $\lambda_{\max}(\Gamma)$ the eigenvalue with the largest magnitude, then $\lambda_{\max}(\bar{\Gamma}|_{M=1}) = \max\{\lambda_k^2\} = \lambda_{\max}^2(\Gamma)$. Inserting the latter result into (78), we have $\lambda_{\max}(\bar{\Gamma}) = M \lambda_{\max}^2(\Gamma)$. The proof is complete. ■

REFERENCES

- [1] I. Bekkerman and J. Tabrikian, "Target detection and localization using MIMO radar and sonars," *IEEE Trans. Signal Process.*, vol. 54, no. 10, pp. 3873–3883, Oct. 2006.
- [2] P. Stoica, J. Li, and Y. Xie, "On probing signal design for MIMO radar," *IEEE Trans. Signal Process.*, vol. 55, no. 8, pp. 4151–4161, Aug. 2007.
- [3] Y. Yang and R. S. Blum, "MIMO radar waveform design based on mutual information and minimum mean-square error estimation," *IEEE Trans. Aerosp. Electron. Syst.*, vol. 43, no. 1, pp. 330–343, Jan. 2007.
- [4] C.-Y. Chen and P. P. Vaidyanathan, "MIMO radar ambiguity properties and optimization using frequency-hopping waveforms," *IEEE Trans. Signal Process.*, vol. 56, no. 12, pp. 5926–5936, Dec. 2008.
- [5] J. Li, P. Stoica, and X. Zheng, "Signal synthesis and receiver design for MIMO radar imaging," *IEEE Trans. Signal Process.*, vol. 56, no. 8, pp. 3959–3968, Aug. 2008.
- [6] A. De Maio, S. D. Nicola, Y. Huang, Z.-Q. Luo, and S. Zhang, "Design of phase codes for radar performance optimization with a similarity constraint," *IEEE Trans. Signal Process.*, vol. 57, no. 2, pp. 610–621, Feb. 2009.
- [7] P. Stoica, H. He, and J. Li, "New algorithms for designing unimodular sequences with good correlation properties," *IEEE Trans. Signal Process.*, vol. 57, no. 4, pp. 1415–1425, Apr. 2009.
- [8] H. Hao, P. Stoica, and J. Li, "Designing unimodular sequences sets with good correlations—Including an application to MIMO radar," *IEEE Trans. Signal Process.*, vol. 57, no. 11, pp. 4391–4405, Nov. 2009.
- [9] A. De Maio, Y. Huang, M. Piezzo, S. Zhang, and A. Farina, "Design of optimized radar codes with a peak to average power ratio constraint," *IEEE Trans. Signal Process.*, vol. 59, no. 6, pp. 2683–2697, Jun. 2011.
- [10] A. Aubry, A. De Maio, A. Farina, and M. Wicks, "Knowledge-aided (potentially cognitive) transmit signal and receive filter design in signal-dependent clutter," *IEEE Trans. Aerosp. Electron. Syst.*, vol. 49, no. 1, pp. 93–117, Jan. 2013.
- [11] S. D. Blunt and E. L. Mokole, "Overview of radar waveform diversity," *IEEE Aerosp. Electron. Syst. Mag.*, vol. 31, no. 11, pp. 2–42, Nov. 2016.
- [12] P. Stoica, H. He, and J. Li, "Optimization of the receive filter and transmit sequence for active sensing," *IEEE Trans. Signal Process.*, vol. 60, no. 4, pp. 1730–1740, Apr. 2012.
- [13] G. Krieger, "MIMO-SAR: Opportunities and pitfalls," *IEEE Trans. Geosci. Remote Sens.*, vol. 52, no. 5, pp. 2628–2645, May 2014.
- [14] W.-Q. Wang and J. Cai, "MIMO SAR using chirp diverse waveform for wide-swath remote sensing," *IEEE Trans. Aerosp. Electron. Syst.*, vol. 48, no. 4, pp. 3171–3185, Oct. 2012.
- [15] D. Tse and P. Viswanath, *Fundamentals of Wireless Communication*. Cambridge, U.K.: Cambridge Univ. Press, 2005.
- [16] N. Levanon and E. Mozeson, *Radar Signals*. Hoboken, NJ, USA: Wiley, 2004.
- [17] H. He, J. Li, and P. Stoica, *Waveform Design for Active Sensing Systems: A Computational Approach*. Cambridge, U.K.: Cambridge Univ. Press, 2012.
- [18] D. DeLong and E. M. Hofstetter, "On the design of optimum radar waveforms for clutter rejection," *IEEE Trans. Inf. Theory*, vol. IT-13, no. 3, pp. 454–463, Jul. 1967.
- [19] M. R. Bell, "Information theory and radar waveform design," *IEEE Trans. Inf. Theory*, vol. 39, no. 5, pp. 1578–1597, Sep. 1993.
- [20] H. Deng, "Polyphase code design for orthogonal netted radar systems," *IEEE Trans. Signal Process.*, vol. 52, no. 11, pp. 3126–3135, Nov. 2004.
- [21] M. C. Wicks, E. L. Mokole, S. D. Blunt, R. S. Schneible, and V. J. Amuso, *Principles of Waveform Diversity and Design*. Raleigh, NC, USA: SciTech Publ., 2010.
- [22] Y. Li, S. A. Vorobyov, and V. Koivunen, "Ambiguity function of the transmit beamspace-based MIMO radar," *IEEE Trans. Signal Process.*, vol. 63, no. 17, pp. 4445–4457, Sep. 2015.
- [23] A. M. Haimovich, R. S. Blum, and L. J. Cimini, "MIMO radar with widely separated antennas," *IEEE Signal Process. Mag.*, vol. 24, no. 1, pp. 116–129, Jan. 2008.
- [24] J. Li and P. Stoica, *MIMO Radar Signal Processing*. New York, NY, USA: Wiley, 2009.
- [25] A. Hassanien and S. A. Vorobyov, "Phased-MIMO radar: A tradeoff between phased-array and MIMO radars," *IEEE Trans. Signal Process.*, vol. 58, no. 6, pp. 3137–3151, Jun. 2010.
- [26] Q. He, R. S. Blum, and A. M. Haimovich, "Noncoherent MIMO radar for location and velocity estimation: More antennas means better performance," *IEEE Trans. Signal Process.*, vol. 58, no. 7, pp. 3661–3680, Jul. 2010.
- [27] L. R. Welch, "Lower bounds on the maximum cross correlation of signals," *IEEE Trans. Inf. Theory*, vol. IT-20, no. 3, pp. 397–399, May 1974.
- [28] P. Stoica, J. Li, and M. Xue, "Transmit codes and receive filters for radar," *IEEE Signal Process. Mag.*, vol. 25, no. 6, pp. 94–109, Nov. 2008.
- [29] Y. Nesterov, *Introductory Lectures on Convex Optimization: A Basic Course*. Norwell, MA, USA: Kluwer, 2004.
- [30] M. M. Naghsh, M. Modarres-Hashemi, S. ShahbazPanahi, M. Soltanalian, and P. Stoica, "Unified optimization framework for multi-static radar code design using information-theoretic criterion," *IEEE Trans. Signal Process.*, vol. 61, no. 21, pp. 5401–5416, Nov. 2013.
- [31] J. Song, P. Babu, and D. P. Palomar, "Optimization methods for designing sequences with low autocorrelation sidelobes," *IEEE Trans. Signal Process.*, vol. 63, no. 15, pp. 3998–4009, Aug. 2015.
- [32] J. Song, P. Babu, and D. P. Palomar, "Sequence set design with good correlations properties via majorization-minimization," *IEEE Trans. Signal Process.*, vol. 64, no. 11, pp. 2866–2879, Jun. 2016.
- [33] Y. Li, S. A. Vorobyov, and Z. He, "Design of multiple unimodular waveforms with low auto- and cross-correlations for radar via majorization-minimization," in *Proc. 24th Eur. Signal Process. Conf.*, Budapest, Hungary, Aug./Sep. 2016, pp. 2235–2239.
- [34] Y. Li and S. A. Vorobyov, "Efficient single/multiple unimodular waveform design with low weighted correlations," in *Proc. IEEE Int. Conf. Acoust., Speech, Signal Process.*, New Orleans, LA, USA, Mar. 2017, pp. 3226–3230.
- [35] L. Zhao, J. Song, P. Babu, and D. P. Palomar, "A unified framework for low autocorrelation sequence design via majorization-minimization," *IEEE Trans. Signal Process.*, vol. 65, no. 2, pp. 438–453, Jan. 2017.
- [36] M. Soltanalian, A. Gharanjik, B. Shankar, and B. Ottersten, "Grab-n-pull: A max-min fractional quadratic programming framework with applications in signal processing," *IEEE Trans. Signal Process.*, to be published. [Online]. Available: http://msol.people.uic.edu/papers/GnP_pre.pdf
- [37] A. KhabbaziBasmeh, F. Roemer, S. A. Vorobyov, and M. Haardt, "Sum-rate maximization in two-way AF MIMO relaying: Polynomial time solutions to a class of DC programming problems," *IEEE Trans. Signal Process.*, vol. 60, no. 10, pp. 5478–5493, Oct. 2012.
- [38] D. R. Hunter and K. Lange, "A tutorial on MM algorithms," *Amer. Statist.*, vol. 58, no. 1, pp. 30–37, Feb. 2004.
- [39] J. D. Leeuw, "Quadratic majorization," Jun. 2003. [Online]. Available: http://gifi.stat.ucla.edu/janspubs/2003/notes/deleeuw_U_03c.pdf
- [40] R. Varadhan and C. Roland, "Simple and globally convergent methods for accelerating the convergence of any EM algorithm," *Scand. J. Statist.*, vol. 35, no. 2, pp. 335–353, 2008.

[41] P. Henrici, *Elements of Numerical Analysis*. New York, NY, USA: Wiley, 1964.

[42] A. Cordero, J. L. Hueso, E. Martinez, and J. R. Torregrosa, "Steffensen type methods for solving nonlinear equations," *J. Comput. Appl. Math.*, vol. 236, no. 12, pp. 3058–3064, Jun. 2012.

[43] M. Raydan and B. F. Svaiter, "Relaxed steepest descent and Cauchy-Barzilai-Borwein method," *Comput. Optim. Appl.*, vol. 21, no. 2, pp. 155–167, Feb. 2002.

[44] S. Liu and G. Trenkler, "Hadamard, Khatri-Rao, Kronecker and other matrix products," *Int. J. Inf. Syst. Sci.*, vol. 4, no. 1, pp. 160–177, 2008.

[45] G. Cui, X. Yu, M. Piezzo, and L. Kong, "Constant modulus sequence set design with good correlation properties," *Signal Process.*, vol. 139, pp. 75–85, Oct. 2017.

[46] R. A. Horn and C. R. Johnson, *Topics in Matrix Analysis*. Cambridge, U.K.: Cambridge Univ. Press, 1991.



Yongzhe Li (S'12–M'17) received the B.Eng. and Ph.D. degrees in electronic engineering from the University of Electronic Science and Technology of China (UESTC), Chengdu, China, in 2008 and 2016, respectively. He is currently completing the D.Sc. degree at the Department of Signal Processing and Acoustics, Aalto University, Espoo, Finland. His research interests include statistical and array signal processing, radar signal processing, and fast optimization methods in signal processing.

Dr. Li was a recipient of the Distinguished Graduate Award of UESTC in 2008, the State Scholarship Award of China Scholarship Council (CSC) for 2013–2015, the Aalto Doctoral School Grant Award for 2016–2017, and the Nokia Foundation Grant Award in 2016.



Sergiy A. Vorobyov (M'02–SM'05–F'18) received the M.Sc. and Ph.D. degrees in systems and control from Kharkiv National University of Radio Electronics, Kharkiv, Ukraine, in 1994 and 1997, respectively.

He is currently a Professor with the Department of Signal Processing and Acoustics, Aalto University, Espoo, Finland. He was with the University of Alberta, Edmonton, AB, Canada, as an Assistant, Associate, and then Full Professor. Since his graduation, he also held various research and faculty positions with Kharkiv National University of Radio Electronics; the Institute of Physical and Chemical Research (RIKEN), Japan; McMaster University, Canada; Duisburg-Essen University and Darmstadt University of Technology, Germany; and the Joint Research Institute between Heriot-Watt University and Edinburgh University, U.K. His research interests include optimization and multilinear algebra methods in signal processing and communications; statistical and array signal processing; sparse signal processing; estimation and detection theory; sampling theory; and multiantenna, very large, cooperative, and cognitive systems.

Dr. Vorobyov is a recipient of the 2004 IEEE Signal Processing Society Best Paper Award, the 2007 Alberta Ingenuity New Faculty Award, the 2011 Carl Zeiss Award (Germany), the 2012 NSERC Discovery Accelerator Award, and other awards. Since 2016, he has been a Senior Area Editor for the IEEE SIGNAL PROCESSING LETTERS. He was an Associate Editor for the IEEE TRANSACTIONS ON SIGNAL PROCESSING in 2006–2010 and the IEEE SIGNAL PROCESSING LETTERS in 2007–2009. He was a member of the Sensor Array and Multichannel Signal Processing and the Signal Processing for Communications and Networking Technical Committees of the IEEE Signal Processing Society in 2007–2012 and 2010–2016, respectively. He was the Track Chair for Asilomar 2011, Pacific Grove, CA, USA; the Technical Cochair for IEEE CAMSAP 2011, San Juan, Puerto Rico; the Tutorial Chair for ISWCS 2013, Ilmenau, Germany; and the Technical Cochair for IEEE SAM 2018, Sheffield, U.K.

Publication VIII

Yongzhe Li and Sergiy A. Vorobyov. Efficient single/multiple unimodular waveform design with low weighted correlations for radar. In *IEEE International Conference on Acoustics, Speech, and Signal Processing (ICASSP)*, New Orleans, LA, USA, pp. 3226–3230, March 2017.

© 2017 IEEE.

Reprinted with permission.

EFFICIENT SINGLE/MULTIPLE UNIMODULAR WAVEFORM DESIGN WITH LOW WEIGHTED CORRELATIONS

Yongzhe Li and Sergiy A. Vorobyov

Dept. Signal Processing and Acoustics, Aalto University, P.O. Box 13000, FI-00076 Aalto, Finland

Emails: lyzlyz888@gmail.com/yongzhe.li@aalto.fi, svor@ieee.org

ABSTRACT

A new method for designing single/multiple unimodular waveforms with good weighted correlation properties, which is based on minimizing the weighted integrated sidelobe levels of waveforms, is developed. The main contributions of the paper lie in formulating the objective as a quartic form where Hadamard product of matrices is involved, converting the non-convex quartic optimization problem into a quadratic form and then solving it by means of majorization-minimization technique which seeks to find the solution iteratively. Corresponding algorithm enables good weighted correlations of the designed waveforms and shows fast convergence compared with existing methods.

Index Terms—Majorization-minimization, radar, waveform design, weighted correlations.

1. INTRODUCTION

Waveform design [1]–[4], which is a part of research areas such as radar signal processing [5]–[13], active sensing [14]–[16], communications [17], etc., has been a research field of significant interest for several decades. It plays an important role especially in radar signal processing since excellent waveforms can ensure good localization accuracy [5], high resolution [9], and superior delay-Doppler ambiguity of the potential target [18]. Besides, robust or adaptive waveform design can deal with heterogeneous clutter mitigation and active jammer suppression [3]. One of the most important factors that determine the quality of waveforms is the correlation property, i.e., the auto- and cross-correlations between different time lags of the designed waveforms. This property is of great importance for radar since perfect correlations indicate that the transmitted waveforms are uncorrelated to any of their time-delayed echoes, meaning that the target at the range bin of interest can be easily extracted after matched filtering, and the sidelobes from other range bins are unable to attenuate it. On the other hand, despite the rapid progress in developing modern hardware of amplifiers, waveforms with constant modulus are still preferable compared to other counterparts due to their constant energy at any time lag, which can reduce the cost of hardware.

There has been an extensive literature on waveform design

for radar applications. The integrated sidelobe level (ISL), which serves as an expression for characterizing waveform correlation properties and evaluating accumulated sidelobes at all non-zero time lags, is typically used. To design a single waveform via ISL minimization, [11] has proposed to design unimodular waveform in the frequency domain using a cyclic procedure of iterative calculations. A substitute objective function that is minimized by cyclic algorithm has been introduced. The methods associated with ISL and weighted ISL (WISL) minimization therein have been named as CAN and WeCAN, respectively. These methods have been later extended to multiple-input multiple-output radar case [12]. The work of [19] has dealt with the same ISL minimization problem as CAN but has addressed it via majorization-minimization (MaMi) technique [20]–[22]. WISL minimization problem for waveform design has been considered in [23].

In this paper, we aim at designing single or multiple waveforms with good weighted correlation properties. The WISL metric is used as the designing criterion for obtaining the optimal set of unimodular waveforms. We derive the objective of the formulated WISL minimization based problem in a non-convex quartic form, specifically, as the sum of two quartic components where Hadamard product of matrices is highly involved. We convert this quartic optimization problem into a quadratic form, and solve it by means of MaMi technique where majorized objective functions are properly selected. The solution to the WISL minimization based design problem is achieved efficiently in a way of iterative calculations. Corresponding algorithm which enables good weighted correlations of the designed waveforms and shows fast convergence is proposed.

2. PROBLEM FORMULATION

Consider designing a set of M unimodular waveforms, denoted by the $P \times M$ matrix $\mathbf{Y} \triangleq [\mathbf{y}_1, \dots, \mathbf{y}_M]$, whose m th column $\mathbf{y}_m \triangleq [y_m(1), \dots, y_m(P)]^T$ is the m th launched waveform of length P . Here, $(\cdot)^T$ stands for the transpose operation, and the elements of \mathbf{y}_m are denoted as $y_m(p) = e^{j\psi_m(p)}$, $p = 1, \dots, P$ with $\psi_m(p)$ being an arbitrary phase value ranging between $-\pi$ and π . The main problem of waveform design lies in synthesizing \mathbf{Y} which gives good weighted correlation properties.

The WISL of the waveform matrix \mathbf{Y} can be expressed as

$$\zeta = \sum_{m=1}^M \sum_{\substack{p=-P+1 \\ p \neq 0}}^{P-1} \gamma_p^2 |r_{mm}(p)|^2 + \sum_{m=1}^M \sum_{\substack{m'=1 \\ m' \neq m}}^M \sum_{p=-P+1}^{P-1} \gamma_p^2 |r_{mm'}(p)|^2 \quad (1)$$

where $r_{mm'}(p) \triangleq \sum_{k=p+1}^P y_m(k) y_{m'}^*(k-p)$ stands for the cross-correlation level of the m th and m' th waveforms at the p th time lag, $\{\gamma_p\}_{p=-P+1}^{P-1}$ are real-valued symmetric weights used to control the sidelobe levels corresponding to different time lags, i.e., $\gamma_p = \gamma_{-p}$, $p \in \{1, \dots, P-1\}$, and $|\cdot|$ and $(\cdot)^*$ are modulus and conjugation operators, respectively. Zero-valued element of γ_p means that the sidelobe level associated with the p th time lag is not considered. Therefore, the problem of unimodular waveform design associated with WISL minimization can be expressed as

$$\min_{\mathbf{y}} \zeta \quad \text{s.t. } |y_m(p)| = 1, \quad m = 1, \dots, M; \quad p = 1, \dots, P \quad (2)$$

where the constraint ensures the modularity of waveforms.

3. UNIMODULAR WAVEFORM DESIGN

After transforming (1) into frequency domain and performing some derivations, then the WISL ζ can be expressed as [12]

$$\zeta = \frac{1}{2P} \sum_{p=1}^{2P} \left\| \mathbf{Y}^H ((\mathbf{a}_p \mathbf{a}_p^H) \odot \mathbf{\Gamma}) \mathbf{Y} - \gamma_0 P \mathbf{I}_M \right\|^2 \quad (3)$$

where $\mathbf{a}_p \triangleq [1, e^{j\omega_p}, \dots, e^{j(P-1)\omega_p}]^T$, $p = 1, \dots, 2P$ with $\omega_p \triangleq \frac{2\pi}{2P}p$, $\mathbf{\Gamma}$ is a $P \times P$ Toeplitz matrix constructed by the weights $\{\gamma_p\}_{p=0}^{P-1}$, \odot and $(\cdot)^H$ are Hadamard product and Hermitian operators, respectively, and \mathbf{I}_M is an M -dimension identity matrix.

In order to solve (2) efficiently, we start by simplifying (3) and select to rewrite it into proper quadratic form. Expanding the square of norm in (3) yields the expression, i.e.,

$$\zeta = \frac{1}{2P} \sum_{p=1}^{2P} \left(\left\| \mathbf{Y}^H ((\mathbf{a}_p \mathbf{a}_p^H) \odot \mathbf{\Gamma}) \mathbf{Y} \right\|^2 + \gamma_0^2 MP^2 - 2\gamma_0 P \text{tr} \{ \mathbf{Y}^H ((\mathbf{a}_p \mathbf{a}_p^H) \odot \mathbf{\Gamma}) \mathbf{Y} \} \right). \quad (4)$$

Note that

$$\begin{aligned} \sum_{p=1}^{2P} \text{tr} \{ \mathbf{Y}^H ((\mathbf{a}_p \mathbf{a}_p^H) \odot \mathbf{\Gamma}) \mathbf{Y} \} &= \text{tr} \left\{ \mathbf{Y}^H \left(\sum_{p=1}^{2P} (\mathbf{a}_p \mathbf{a}_p^H) \odot \mathbf{\Gamma} \right) \mathbf{Y} \right\} \\ &= 2P \text{tr} \{ \mathbf{Y}^H (\mathbf{I}_P \odot \mathbf{\Gamma}) \mathbf{Y} \} = 2\gamma_0 P \|\mathbf{Y}\|^2 = 2\gamma_0 MP^2 \end{aligned} \quad (5)$$

where the properties $\sum_{p=1}^{2P} \mathbf{a}_p \mathbf{a}_p^H = 2P \mathbf{I}_P$ and $\text{tr} \{ \mathbf{Y}^H \mathbf{Y} \} = \|\mathbf{Y}\|^2$ have been used in the derivation. Therefore, we only need to consider the first component of the sum on the right hand side of (4).

Let $\mathbf{\Gamma} = \sum_{k=1}^K \lambda_k \mathbf{q}_k \mathbf{q}_k^H = \sum_{k=1}^K \mathbf{u}_k \mathbf{v}_k^H$ be the general eigenvalue decomposition of the weight matrix $\mathbf{\Gamma}$ which can be non-positive semi-definite, where λ_k and \mathbf{q}_k , $k \in \{1, \dots, K\}$ are the k th eigenvalue and eigenvector, respectively, $\mathbf{u}_k \triangleq \sqrt{\lambda_k} \mathbf{q}_k$ is a $P \times 1$ vector, \mathbf{v}_k equals $-\mathbf{u}_k$ when λ_k is negative, otherwise it is the same as \mathbf{u}_k , and K is the rank of $\mathbf{\Gamma}$. After some derivations, the first component of the sum in (4) can be further expressed as

$$\begin{aligned} \sum_{p=1}^{2P} \left\| \mathbf{Y}^H ((\mathbf{a}_p \mathbf{a}_p^H) \odot \mathbf{\Gamma}) \mathbf{Y} \right\|^2 &= \sum_{p=1}^{2P} \sum_{k=1}^K \sum_{k'=1}^K (\mathbf{y}^H ((\mathbf{A}_p \mathbf{A}_p^H) \odot \mathbf{\Gamma}_{kk'}^r) \mathbf{y})^2 + (\mathbf{y}^H ((\mathbf{A}_p \mathbf{A}_p^H) \odot \mathbf{\Gamma}_{kk'}^i) \mathbf{y})^2 \end{aligned} \quad (6)$$

where $\mathbf{A}_p \triangleq \mathbf{I}_M \otimes \mathbf{a}_p$, $\mathbf{y} \triangleq \text{vec}(\mathbf{Y}) = [\mathbf{y}_1^T, \dots, \mathbf{y}_M^T]^T$ is the $MP \times 1$ vectorized version of \mathbf{Y} , $\mathbf{\Gamma}_{kk'}^r \triangleq \mathbf{I}_M \otimes (\mathbf{u}_k \mathbf{v}_{k'}^H + \mathbf{v}_{k'} \mathbf{u}_k^H)/2$ and $\mathbf{\Gamma}_{kk'}^i \triangleq \mathbf{I}_M \otimes i(\mathbf{u}_k \mathbf{v}_{k'}^H - \mathbf{v}_{k'} \mathbf{u}_k^H)/2$.

Ignoring the constant summations for the latter two components of the sum in (4), the waveform design problem (2) can be rewritten as

$$\begin{aligned} \min_{\mathbf{y}} \quad & \sum_{p=1}^{2P} \sum_{k=1}^K \sum_{k'=1}^K (\mathbf{y}^H ((\mathbf{A}_p \mathbf{A}_p^H) \odot \mathbf{\Gamma}_{kk'}^r) \mathbf{y})^2 \\ & + (\mathbf{y}^H ((\mathbf{A}_p \mathbf{A}_p^H) \odot \mathbf{\Gamma}_{kk'}^i) \mathbf{y})^2 \end{aligned} \quad (7a)$$

$$\text{s.t. } |y_m(p)| = 1, \quad m = 1, \dots, M; \quad p = 1, \dots, P. \quad (7b)$$

The objective function (7a) takes a quartic form with respect to \mathbf{y} , and it can be transformed to the following form

$$\begin{aligned} \text{Obj} &= \sum_{p=1}^{2P} \sum_{k=1}^K \sum_{k'=1}^K \text{tr}^2 \{ \tilde{\mathbf{Y}}^H ((\mathbf{A}_p \mathbf{A}_p^H) \odot \mathbf{\Gamma}_{kk'}^r) \} \\ &+ \text{tr}^2 \{ \tilde{\mathbf{Y}}^H ((\mathbf{A}_p \mathbf{A}_p^H) \odot \mathbf{\Gamma}_{kk'}^i) \} \\ &= \text{vec}^H(\tilde{\mathbf{Y}}) \tilde{\mathbf{\Phi}} \text{vec}(\tilde{\mathbf{Y}}) \end{aligned} \quad (8)$$

where $\tilde{\mathbf{Y}} \triangleq \mathbf{y} \mathbf{y}^H$ and $\tilde{\mathbf{\Phi}}$ is defined as $\tilde{\mathbf{\Phi}} \triangleq \tilde{\mathbf{\Phi}} \odot \bar{\mathbf{\Gamma}}$ with

$$\tilde{\mathbf{\Phi}} \triangleq \sum_{p=1}^{2P} \text{vec}(\mathbf{A}_p \mathbf{A}_p^H) \text{vec}^H(\mathbf{A}_p \mathbf{A}_p^H) \quad (9)$$

$$\bar{\mathbf{\Gamma}} \triangleq \sum_{k=1}^K \sum_{k'=1}^K \text{vec}(\mathbf{\Gamma}_{kk'}^r) \text{vec}^H(\mathbf{\Gamma}_{kk'}^r) + \text{vec}(\mathbf{\Gamma}_{kk'}^i) \text{vec}^H(\mathbf{\Gamma}_{kk'}^i). \quad (10)$$

Then, the problem (7) can be rewritten as

$$\min_{\tilde{\mathbf{Y}}} \quad \text{vec}^H(\tilde{\mathbf{Y}}) \tilde{\mathbf{\Phi}} \text{vec}(\tilde{\mathbf{Y}}) \quad (11a)$$

$$\text{s.t. } \tilde{\mathbf{Y}} = \mathbf{y} \mathbf{y}^H \quad (11b)$$

$$|y(p')| = 1, \quad p' = 1, \dots, MP. \quad (11c)$$

Before applying majorization to (11a), we present the following result to be used later.

Given a set of N -dimension arbitrary complex vectors $\{\mathbf{d}_k\}_{k=1}^K$ and an $N \times N$ arbitrary Hermitian matrix \mathbf{H} , the following generalized inequality $\sum_{k=1}^K (\mathbf{d}_k \mathbf{d}_k^H) \odot \mathbf{H} \preceq \lambda_{\max}(\mathbf{H}) \mathbf{D}$ holds, where $\mathbf{D} \triangleq \text{diag} \{ \sum_{k=1}^K |\mathbf{d}_k(1)|^2, \dots, \dots$

$\sum_{k=1}^K \{\mathbf{d}_k(N)\}^2$ and $\lambda_{\max}(\cdot)$ denotes the largest eigenvalue of a matrix. The result that $\mathbf{x}^H \mathbf{Q} \mathbf{x}$ is majorized by the function $\mathbf{x}^H \mathbf{G} \mathbf{x} + 2\Re(\mathbf{x}^H (\mathbf{Q} - \mathbf{G}) \mathbf{x}_0) + \mathbf{x}_0^H (\mathbf{G} - \mathbf{Q}) \mathbf{x}_0$ at \mathbf{x}_0 when $\mathbf{G} \succeq \mathbf{Q}$ is also used in the following. They can be found in the associate full-size journal paper [24].

It can be shown that $\lambda_{\max}(\tilde{\Gamma})$ is a constant value, and the value of diagonal elements of the first component within the Hadamard product in $\tilde{\Phi}$ is either zero or $2P$. Therefore, we can select $\mathbf{G} \triangleq \lambda_{\tilde{\Phi}} \mathbf{I}_{M^2 P^2}$ (here $\lambda_{\tilde{\Phi}} \triangleq 2P \lambda_{\max}(\tilde{\Gamma})$) to satisfy the generalized inequality $\mathbf{G} \succeq \tilde{\Phi}$. Using the above-mentioned majorization results, the objective function (11a) can be majorized as

$$\begin{aligned} \tilde{g}_1(\tilde{\mathbf{Y}}, \tilde{\mathbf{Y}}^{(k)}) &= \lambda_{\tilde{\Phi}} \text{vec}^H(\tilde{\mathbf{Y}}) \text{vec}(\tilde{\mathbf{Y}}) \\ &+ 2\Re\left\{\text{vec}^H(\tilde{\mathbf{Y}}) (\tilde{\Phi} - \lambda_{\tilde{\Phi}} \mathbf{I}_{M^2 P^2}) \text{vec}(\tilde{\mathbf{Y}}^{(k)})\right\} \\ &+ \text{vec}^H(\tilde{\mathbf{Y}}^{(k)}) (\lambda_{\tilde{\Phi}} \mathbf{I}_{M^2 P^2} - \tilde{\Phi}) \text{vec}(\tilde{\mathbf{Y}}^{(k)}) \end{aligned} \quad (12)$$

where $\tilde{\mathbf{Y}}^{(k)} \triangleq \mathbf{y}^{(k)} (\mathbf{y}^{(k)})^H$. Note that $\text{vec}^H(\tilde{\mathbf{Y}}) \text{vec}(\tilde{\mathbf{Y}}) = \|\mathbf{y}\|^4 = M^2 P^2$. Hence, both summations for the first and third components in (12) are immaterial for optimization. The problem (11) can therefore be rewritten as

$$\begin{aligned} \min_{\tilde{\mathbf{Y}}} \quad & \text{vec}^H(\tilde{\mathbf{Y}}) (\tilde{\Phi} - \lambda_{\tilde{\Phi}} \mathbf{I}_{M^2 P^2}) \text{vec}(\tilde{\mathbf{Y}}^{(k)}) \\ \text{s.t.} \quad & \tilde{\mathbf{Y}} = \mathbf{y} \mathbf{y}^H \\ & |\mathbf{y}(p')| = 1, \quad p' = 1, \dots, MP. \end{aligned} \quad (13)$$

Using the explicit expression of $\tilde{\Phi}$, the properties $\text{vec}(\tilde{\mathbf{Y}}) = (\mathbf{y}^T \otimes \mathbf{I}_{MP})^H \mathbf{y}$ and $\text{vec}(\mathbf{A}_p \mathbf{A}_p^H) = (\mathbf{A}_p^T \otimes \mathbf{I}_{MP})^H \text{vec}(\mathbf{A}_p)$, and performing some manipulations between Hadamard and Kronecker products, the objective of (13) can be derived as

$$\begin{aligned} & \text{vec}^H(\tilde{\mathbf{Y}}) (\tilde{\Phi} - \lambda_{\tilde{\Phi}} \mathbf{I}_{M^2 P^2}) \text{vec}(\tilde{\mathbf{Y}}^{(k)}) \\ &= \mathbf{y}^H \left(\sum_{p=1}^{2P} (\tilde{\mathbf{a}}_p \tilde{\mathbf{a}}_p^H) \odot \Delta_p^{(k)} - \lambda_{\tilde{\Phi}} \mathbf{y}^{(k)} (\mathbf{y}^{(k)})^H \right) \mathbf{y} \end{aligned} \quad (14)$$

where $\tilde{\mathbf{a}}_p \triangleq \mathbf{1}_M \otimes \mathbf{a}_p$ and $\Delta_p^{(k)}$ is an $MP \times MP$ matrix whose (i, j) th element is expressed as

$$[\Delta_p^{(k)}]_{i,j} = \tilde{\gamma}_{i,j}^T \left((\mathbf{y}^{(k)} \odot \tilde{\mathbf{a}}_p^*) \otimes ((\mathbf{y}^{(k)})^* \odot \tilde{\mathbf{a}}_p) \right) \quad (15)$$

with the $M^2 P^2 \times 1$ vector $\tilde{\gamma}_{i,j}$ defined as

$$\begin{aligned} \tilde{\gamma}_{i,j} \triangleq & \left[[\tilde{\Gamma}]_{i,j}, [\tilde{\Gamma}]_{i,j+MP}, \dots, [\tilde{\Gamma}]_{i,j+(MP-1)MP}, \right. \\ & \left. \dots, [\tilde{\Gamma}]_{i+(MP-1)MP, j+(MP-1)MP} \right]^T. \end{aligned} \quad (16)$$

Therefore, the optimization problem (14) can be rewritten as

$$\begin{aligned} \min_{\mathbf{y}} \quad & \mathbf{y}^H \left(\sum_{p=1}^{2P} (\tilde{\mathbf{a}}_p \tilde{\mathbf{a}}_p^H) \odot \Delta_p^{(k)} - \lambda_{\tilde{\Phi}} \mathbf{y}^{(k)} (\mathbf{y}^{(k)})^H \right) \mathbf{y} \\ \text{s.t.} \quad & |\mathbf{y}(p')| = 1, \quad p' = 1, \dots, MP. \end{aligned} \quad (17)$$

Applying the majorization result (see the last paragraph on the previous page) to the component $((\tilde{\mathbf{a}}_p \tilde{\mathbf{a}}_p^H) \odot \Delta_p^{(k)})$ in (17),

we obtain that $((\tilde{\mathbf{a}}_p \tilde{\mathbf{a}}_p^H) \odot \Delta_p^{(k)}) \preceq \lambda_{\max}(\Delta_p^{(k)}) \mathbf{I}_{MP}$. Thus by selecting $\mathbf{G} \triangleq \sum_{p=1}^{2P} \lambda_{\max}(\Delta_p^{(k)}) \mathbf{I}_{MP}$, the objective of (17) can be majorized as

$$\begin{aligned} & \tilde{g}_2(\mathbf{y}, \mathbf{y}^{(k)}) \\ &= \sum_{p=1}^{2P} \lambda_{\max}(\Delta_p^{(k)}) \mathbf{y}^H \mathbf{y} + 2\Re \left\{ \mathbf{y}^H \left(\sum_{p=1}^{2P} (\tilde{\mathbf{a}}_p \tilde{\mathbf{a}}_p^H) \odot \Delta_p^{(k)} \right. \right. \\ & \quad \left. \left. - \lambda_{\tilde{\Phi}} \mathbf{y}^{(k)} (\mathbf{y}^{(k)})^H - \sum_{p=1}^{2P} \lambda_{\max}(\Delta_p^{(k)}) \mathbf{I}_{MP} \right) \mathbf{y}^{(k)} \right\} \\ &+ (\mathbf{y}^{(k)})^H \left(\sum_{p=1}^{2P} \lambda_{\max}(\Delta_p^{(k)}) \mathbf{I}_{MP} + \lambda_{\tilde{\Phi}} \mathbf{y}^{(k)} (\mathbf{y}^{(k)})^H \right. \\ & \quad \left. - \sum_{p=1}^{2P} (\tilde{\mathbf{a}}_p \tilde{\mathbf{a}}_p^H) \odot \Delta_p^{(k)} \right) \mathbf{y}^{(k)} \end{aligned} \quad (18)$$

where the summations for the first and third components of the sum in (18) do not need to be considered for optimization since they are constant. Therefore, (17) can be finally simplified into the following optimization problem

$$\begin{aligned} \min_{\mathbf{y}} \quad & \mathbf{y}^H \mathbf{z}^{(k)} \\ \text{s.t.} \quad & |\mathbf{y}(p')| = 1, \quad p' = 1, \dots, MP \end{aligned} \quad (19)$$

where the $MP \times 1$ vector $\mathbf{z}^{(k)}$ is defined as

$$\begin{aligned} \mathbf{z}^{(k)} \triangleq & \left(\sum_{p=1}^{2P} \lambda_{\max}(\Delta_p^{(k)}) + MP \lambda_{\tilde{\Phi}} \right) \mathbf{y}^{(k)} \\ & - \sum_{p=1}^{2P} ((\tilde{\mathbf{a}}_p \tilde{\mathbf{a}}_p^H) \odot \Delta_p^{(k)}) \mathbf{y}^{(k)}. \end{aligned} \quad (20)$$

Due to the constant modulus property of \mathbf{y} , (19) is equivalent to the following optimization problem

$$\begin{aligned} \min_{\mathbf{y}} \quad & \|\mathbf{y} - \mathbf{z}^{(k)}\| \\ \text{s.t.} \quad & |\mathbf{y}(p')| = 1, \quad p' = 1, \dots, MP \end{aligned} \quad (21)$$

which leads to the following closed-form solution

$$\mathbf{y}(p') = e^{j \arg(\mathbf{z}^{(k)}(p'))}, \quad p' = 1, \dots, MP. \quad (22)$$

Stacking \mathbf{y} into a $P \times M$ matrix, we obtain the final waveform matrix \mathbf{Y} . Based on the above derivations, we propose an original algorithm concluded in Algorithm 1 for solving (2). Note that the matrix $\Delta_p^{(k)}$ can be efficiently obtained in each iteration, for example, if needed, parallel computation can be used. We refer interested reader to the literature for accelerated schemes, for example, the SQUAREM scheme [25] used in [19], which can speed up the proposed Algorithm 1 as well.

4. SIMULATION RESULTS

We compare the performance of our proposed waveform design algorithm with that of the WeCAN algorithm (see [12]) and the method in [23] (named as WISLSong) accelerated by

Algorithm 1 WISL minimization via MaMi

- 1: $k \leftarrow 0$, $\mathbf{y} \leftarrow$ unimodular sequence with random phases.
 - 2: **repeat**
 - 3: **procedure** WISLMAMi($\mathbf{y}^{(k)}$)
 - 4: Calculate $\{\Delta_p^{(k)}\}_{p=1}^{2P}$ using (15).
 - 5: Calculate $\mathbf{z}^{(k)}$ using (20).
 - 6: $\mathbf{y}^{(k+1)}(p) = e^{j\arg(\mathbf{z}^{(k)}(p'))}$, $p' = 1, \dots, MP$.
 - 7: $k \leftarrow k + 1$
 - 8: **end procedure**
 - 9: **until** convergence
-

the SQUAREM scheme. We generate unimodular sequences with random phases as the initialization for each design, and the same initialized sequence is used for comparison. The SQUAREM scheme is also used to accelerate the proposed Algorithm 1. We select the absolute WISL difference between the current and previous iterations normalized to the initial WISL as the stopping criterion, and the tolerance is set to be 10^{-8} . All simulations for the tested methods are conducted using the same hardware and software platforms.

In the first example, we evaluate the convergence properties (running time versus code length) and the correlation properties (WISL versus time lags) of waveforms generated by the three designs tested for a single-waveform scenario, i.e., $M = 1$. The code length P is set from 20 to 100 with stepsize 10, and the controlling ISL weights are $\gamma_0 = 1$, $\gamma_p = 0.1991$, $p \in \{-9, \dots, -1\} \cup \{1, \dots, 9\}$, while the others are zeros (Γ is positive semi-definite as required by WeCAN). The results are averaged over 50 trials. It can be seen that our proposed design significantly outperforms the WeCAN design in convergence speed with respect to the consumed time and shows as better convergence property (within 1.3 seconds for all tested code length) as the method in [23] with SQUAREM acceleration (see Fig. 1(a)). Indeed, the WeCAN algorithm converges more slowly when the set of weights is not significantly sparse, while our algorithm is not sensitive to sparsity. Moreover, our proposed algorithm always achieves much lower WISL when it reaches the stopping tolerance (see Fig. 1(b)). This is mainly because our proposed design deals with the true objective of the corresponding WISL minimization problem, while the WeCAN design deals with a surrogate of it. For a fixed code length, the largest gaps between the achieved WISL by our proposed algorithm and the other two designs have reached about 40 dB and 55 dB, respectively.

In the second example, we present the correlations of $M = 2$ waveforms obtained by the three tested methods with code length of 32 for a multiple-waveform scenario. The controlling ISL weights are $\gamma_0 = 1$, $\gamma_p = 0.311$, $p \in \{-5, \dots, -1\} \cup \{1, \dots, 5\}$, while the others are zeros. The four sub figures in Fig. 2 stand for the auto- and cross-correlations of the two sets of waveforms generated by the methods tested. It can be seen that the auto-correlations associated with time lags $[-5, -1] \cup$

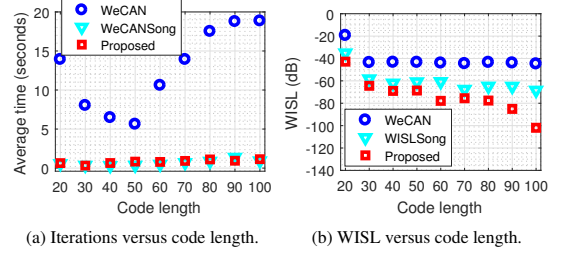


Fig. 1. Evaluations of consumed time and achieved WISL.

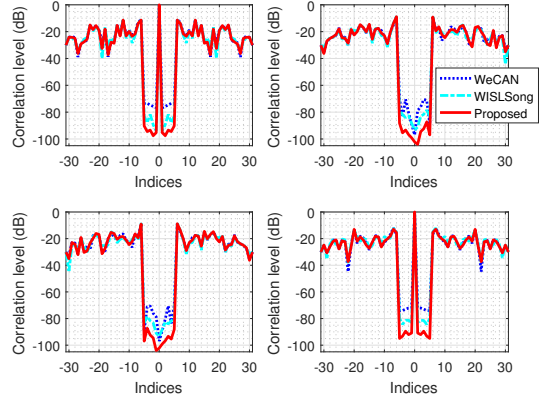


Fig. 2. Evaluation of correlation properties.

[1, 5] and cross-correlations associated with time lags $[-5, 5]$ for the three generated sets of waveforms are controlled, while waveform correlations associated with other time lags are not controlled, and therefore, show much higher correlation levels. Under the condition of the same convergence tolerance, the correlation levels corresponding to the time lags of interest by the proposed waveform design are better than those by the other two methods. The largest gaps between the obtained correlations by the proposed method and the other two have reached about 15 dB and 20 dB, respectively, and the WeCAN method shows the worst weighted correlations.

5. CONCLUSION

We have developed an efficient algorithm for designing single or multiple unimodular waveforms with good weighted correlations. WISL metric has been employed as the criterion for designing waveforms, and the waveform design has been formulated as a non-convex quartic problem where Hadamard product of matrices is involved. This quartic optimization problem has been converted into a quadratic form and then solved by means of MaMi technique where majorized objective functions are properly selected. The proposed algorithm has shown better weighted correlations of designed waveforms and faster convergence as compared to its counterparts.

6. REFERENCES

- [1] N. Levanon and E. Mozeson, *Radar Signals*. Hoboken, NJ, USA: Wiley, 2004.
- [2] M. C. Wicks, E. L. Mokole, S. D. Blunt, R. S. Schneible, and V. J. Amuso, *Principles of Waveform Diversity and Design*. Raleigh, NC, USA: SciTech Publishing, 2010.
- [3] D. DeLong and E. M. Hofstetter, "On the design of optimum radar waveforms for clutter rejection," *IEEE Trans. Inf. Theory*, vol. 13, no. 3, pp. 454–463, Jul. 1967.
- [4] M. R. Bell, "Information theory and radar waveform design," *IEEE Trans. Inf. Theory*, vol. 39, no. 5, pp. 1578–1597, Sep. 1993.
- [5] I. Bekkerman and J. Tabrikian, "Target detection and localization using MIMO radar and sonars," *IEEE Trans. Signal Process.*, vol. 54, no. 10, pp. 3873–3883, Oct. 2006.
- [6] P. Stoica, J. Li, and Y. Xie, "On probing signal design for MIMO radar," *IEEE Trans. Signal Process.*, vol. 55, no. 8, pp. 4151–4161, Aug. 2007.
- [7] Y. Yang and R. S. Blum, "MIMO radar waveform design based on mutual information and minimum mean-square error estimation," *IEEE Trans. Aerosp. Electron. Syst.*, vol. 43, no. 1, pp. 330–343, Jan. 2007.
- [8] C.-Y. Chen and P. P. Vaidyanathan, "MIMO radar ambiguity properties and optimization using frequency-hopping waveforms," *IEEE Trans. Signal Process.*, vol. 56, no. 12, pp. 5926–5936, Dec. 2008.
- [9] J. Li, P. Stoica, and X. Zheng, "Signal synthesis and receiver design for MIMO radar imaging," *IEEE Trans. Signal Process.*, vol. 56, no. 8, pp. 3959–3968, Aug. 2008.
- [10] A. De Maio, S. D. Nicola, Y. Huang, Z.-Q. Luo, and S. Zhang, "Design of phase codes for radar performance optimization with a similarity constraint," *IEEE Trans. Signal Process.*, vol. 57, no. 2, pp. 610–621, Feb. 2009.
- [11] P. Stoica, H. He, and J. Li, "New algorithms for designing unimodular sequences with good correlation properties," *IEEE Trans. Signal Process.*, vol. 57, no. 4, pp. 1415–1425, Apr. 2009.
- [12] H. Hao, P. Stoica, and J. Li, "Designing unimodular sequences sets with good correlations—Including an application to MIMO radar," *IEEE Trans. Signal Process.*, vol. 57, no. 11, pp. 4391–4405, Nov. 2009.
- [13] A. Aubry, A. De Maio, A. Farina, and M. Wicks, "Knowledge-aided (potentially cognitive) transmit signal and receive filter design in signal-dependent clutter," *IEEE Trans. Aerosp. Electron. Syst.*, vol. 49, no. 1, pp. 93–117, Jan. 2013.
- [14] P. Stoica, H. He, and J. Li, "Optimization of the receive filter and transmit sequence for active sensing," *IEEE Trans. Signal Process.*, vol. 60, no. 4, pp. 1730–1740, Apr. 2012.
- [15] G. Krieger, "MIMO-SAR: Opportunities and pitfalls," *IEEE Trans. Geosci. Remote Sens.*, vol. 52, no. 5, pp. 2628–2645, May 2014.
- [16] W.-Q. Wang and J. Cai, "MIMO SAR using chirp diverse waveform for wide-swath remote sensing," *IEEE Trans. Aerosp. Electron. Syst.*, vol. 48, no. 4, pp. 3171–3185, Oct. 2012.
- [17] D. Tse and P. Viswanath, *Fundamentals of wireless communication*. Cambridge, UK: Cambridge University Press, 2005.
- [18] Y. Li, S. A. Vorobyov, and V. Koivunen, "Ambiguity function of the transmit beamspace-based MIMO radar," *IEEE Trans. Signal Process.*, vol. 63, no. 17, pp. 4445–4457, Sep. 2015.
- [19] J. Song, P. Babu, and D. P. Palomar, "Optimization methods for designing sequences with low autocorrelation sidelobes," *IEEE Trans. Signal Process.*, vol. 63, no. 15, pp. 3998–4009, Aug. 2015.
- [20] D. R. Hunter and K. Lange, "A tutorial on MM algorithms," *Amer. Statist.*, vol. 58, no. 1, pp. 30–37, Feb. 2004.
- [21] M. W. Jacobson and J. A. Fessler, "An extended theoretical treatment of iteration-dependent Majorization-Mimization," *IEEE Trans. Signal Process.*, vol. 16, no. 10, pp. 2411–2422, Oct. 2007.
- [22] M. M. Naghsh, M. Modarres-Hashemi, S. Shahbaz-Panahi, M. Soltanalian, and P. Stoica, "Unified optimization framework for multi-static radar code design using information-theoretic criterion," *IEEE Trans. Signal Process.*, vol. 61, no. 21, pp. 5401–5416, Nov. 2013.
- [23] J. Song, P. Babu, and D. P. Palomar, "Sequence set design with good correlations properties via Majorization-Mimization," *IEEE Trans. Signal Process.*, vol. 64, no. 11, pp. 2866–2879, Jun. 2016.
- [24] Y. Li and S. A. Vorobyov, "Fast algorithms for designing single/multiple unimodular waveforms with good correlation properties," *submitted to IEEE Trans. Signal Process.*, 2017.
- [25] R. Varadhan and C. Roland, "Simple and globally convergent methods for accelerating the convergence of any EM algorithm," *Scand. J. Statist.*, vol. 35, no. 2, pp. 335–353, 2008.

Publication IX

Yongzhe Li, Sergiy A. Vorobyov and Zishu He. Design of multiple unimodular waveforms with low auto- and cross-correlations for radar via majorization-minimization. In *European Signal Processing Conference (EUSIPCO)*, Budapest, Hungary, pp. 2235–2239., August–September 2016.

© 2016 IEEE.

Reprinted with permission.

Design of Multiple Unimodular Waveforms With Low Auto- and Cross-Correlations for Radar via Majorization-Minimization

Yongzhe Li^{†‡}, Sergiy A. Vorobyov[†], and Zishu He[‡]

[†]Dept. Signal Processing and Acoustics, Aalto University, P.O. Box 13000, FI-00076 Aalto, Finland

[‡]Dept. EE, University of Electronic Science and Technology of China, Chengdu, 611731, China

lyzlyz888@gmail.com/yongzhe.li@aalto.fi, svor@ieee.org, zshe@uestc.edu.cn

Abstract—We develop a new efficient method for designing unimodular waveforms with good auto- and cross-correlation properties for multiple-input multiple-output (MIMO) radar. Our waveform design scheme is conducted based on minimization of the integrated sidelobe level of designed waveforms, which is formulated as a quartic non-convex optimization problem. We start from simplifying the quartic optimization problem and then transform it into a quadratic form. By means of the majorization-minimization technique that seeks to find the solution of a corresponding quadratic optimization problem, we resolve the design of waveforms for MIMO radar. Corresponding algorithms that enable good correlations of the designed waveforms and meanwhile show faster convergence as compared to their counterparts are proposed and then tested.

I. INTRODUCTION

Waveform design has become a research field of significant interest in multiple-input multiple-output (MIMO) radar since the emergence of MIMO radar concept [1]–[5]. The application of waveform design plays an important role in MIMO radar (also in single-input single-output radar) signal processing because high-quality waveform can guarantee good localization accuracy [6], high resolution [7], and improved delay-Doppler ambiguity of the potential target [8]. Moreover, in harsh environment such as in the presence of heterogeneous clutter and active jamming, robust or adaptive waveform designs are capable of suppressing them [9]. One of the most important factors that determine the quality of designed waveforms is the correlation property, i.e., the auto- and cross-correlations between different time lags of the waveforms. Perfect or low waveform correlations mean that the waveforms launched from radar platform are uncorrelated to any non-zero time-delayed version of themselves, which ensures that the target at the range bin of interest can be easily extracted after matched filtering, and the sidelobes from other range bins have almost no effect on its attenuation. Despite the application of correlated waveforms in MIMO radar [8], [10], [11], uncorrelated waveforms are still the most preferable and they can be easily converted to correlated ones by weighting on them. On the other hand, unimodular waveforms are still preferable compared to other counterparts due to their constant energy at any time lag, which significantly reduces the cost of hardware.

There has been an extensive literature on waveform design for radar applications [12]–[19]. The integrated sidelobe

level (ISL), which characterizes the correlation properties of waveforms and evaluates the accumulated sidelobes at all non-zero time lags, is the most commonly used metric. To design waveforms via ISL minimization, the work of [13] has proposed to produce unimodular waveforms in frequency domain using a cyclic procedure of iterative calculations. The methods associated with ISL and weighted ISL minimization therein were named CAN and WeCAN, respectively. These methods were later extended to MIMO radar case based on the same idea of using cyclic procedure of iterative calculations [5]. The work of [18] dealt with the same ISL minimization problem as CAN for designing a single waveform but solved it via majorization-minimization (MaMi) technique [20]. This technique has previously been used in [17] where the design of multiple waveforms were implemented from information-theoretic perspective. The recent work of [19] has extended [18] to the case of multiple waveforms.

In this paper, we develop an efficient method for designing a set of unimodular waveforms with good auto- and cross-correlation properties, which can be applied to MIMO radar. We conduct the waveform design based on ISL minimization of the waveforms. Using proper modeling and some transformations, we formulate the ISL minimization based design as a quartic non-convex optimization problem. We show how to simplify the quartic optimization problem and then transform it into a quadratic form. By means of the MaMi technique which majorizes the objective function of the quadratic optimization problem and seeks to find the corresponding solution via iterative calculations, we resolve the formulated waveform design for MIMO radar. Corresponding algorithms that enable good correlations of the designed waveforms and meanwhile show faster convergence as compared to the existing counterparts are proposed and tested in terms of simulations.

II. SIGNAL MODEL AND PROBLEM FORMULATION

Consider a MIMO radar equipped with M transmit antenna elements from which a set of M unimodular waveforms, denoted by the $P \times M$ matrix $\mathbf{Y} \triangleq [\mathbf{y}_1, \dots, \mathbf{y}_M]$, is launched within a pulse duration. Here \mathbf{y}_m , $m \in \{1, \dots, M\}$ stands for the $P \times 1$ emitted waveform vector associated with the m th antenna and P is the code length of each waveform. Let the p th ($p \in \{1, \dots, P\}$) element of \mathbf{y}_m that is associated with the

p th sub-pulse be $y_m(p) = e^{j\psi_m(p)}$ where $\psi_m(p)$ is an arbitrary phase value ranging between $-\pi$ and π . The main issue of the waveform design for MIMO radar lies in synthesizing sequences $\{y_m(p)\}_{m=1, p=1}^{M, P}$ which have good auto- and cross-correlation properties.

The ISL of the waveforms $\{y_m(p)\}_{m=1, p=1}^{M, P}$ is expressed as

$$\zeta = \sum_{m=1}^M \sum_{\substack{p=-P+1 \\ p \neq 0}}^{P-1} |r_{mm}(p)|^2 + \sum_{m=1}^M \sum_{\substack{m'=1 \\ m' \neq m}}^M \sum_{p=-P+1}^{P-1} |r_{mm'}(p)|^2 \quad (1)$$

where $r_{mm'}(p) \triangleq \sum_{k=p+1}^P y_m(k) y_{m'}^*(k-p)$, $m, m' \in \{1, \dots, M\}$; $p \in \{-1, \dots, P-1\}$ stands for the cross-correlation level of the m th and m' th waveforms at the p th time lag, and $|\cdot|$ and $(\cdot)^*$ are modulus and conjugation operators, respectively. Note that the first component of the sum on the right hand side of (1) stands for the ISL associated with auto-correlations and the latter represents the ISL associated with cross-correlations.

Using matrix expressions, the ISL ζ in (1) can be rewritten into the following compact form

$$\zeta = \sum_{p=-P+1}^{P-1} \|\mathbf{R}_p - P\mathbf{I}_M \delta_p\|^2 \quad (2)$$

where the $M \times M$ waveform correlation matrix \mathbf{R}_p , $p \in \{-P+1, \dots, 0, \dots, P-1\}$ is constructed as

$$\mathbf{R}_p \triangleq \begin{bmatrix} r_{11}(p) & r_{12}(p) & \dots & r_{1M}(p) \\ r_{21}(p) & r_{22}(p) & \dots & r_{2M}(p) \\ \vdots & \vdots & \ddots & \vdots \\ r_{M1}(p) & \dots & \dots & r_{MM}(p) \end{bmatrix} \quad (3)$$

δ_p is the Kronecker delta function whose value is 1 only when $p = 0$ while otherwise it is 0, \mathbf{I}_M is the $M \times M$ identity matrix, and $\|\cdot\|$ stands for the Frobenius norm of a matrix.

Transforming (2) into frequency domain and performing some derivations, the ISL can be expressed as [5]

$$\zeta = \frac{1}{2P} \sum_{p=1}^{2P} \|\tilde{\tilde{\mathbf{y}}}(\omega_p) \tilde{\tilde{\mathbf{y}}}^H(\omega_p) - P\mathbf{I}_M\|^2 \quad (4)$$

where $\omega_p \triangleq \frac{2\pi}{2P}p$ and $\tilde{\tilde{\mathbf{y}}}(\omega_p) \triangleq \sum_{n=1}^P \tilde{\mathbf{y}}_n e^{-j\omega_p n}$ with $\tilde{\mathbf{y}}_n$ constructed by the n th row of the waveform matrix \mathbf{Y} which is explicitly expressed as $\tilde{\mathbf{y}}_n \triangleq [y_1(n), \dots, y_M(n)]^T$. Here $(\cdot)^T$ and $(\cdot)^H$ are transpose and conjugate transpose operators, respectively.

Expanding the squared norm in (4), the ISL can be expressed in the following form

$$\zeta = \frac{1}{2P} \sum_{p=1}^{2P} \left(\|\tilde{\tilde{\mathbf{y}}}(\omega_p)\|^4 - 2P \|\tilde{\tilde{\mathbf{y}}}(\omega_p)\|^2 + P^2 M \right) \quad (5)$$

which can be further rewritten as the following compact form

$$\zeta = \frac{1}{2P} \sum_{p=1}^{2P} \left((\mathbf{y}^H \mathbf{A}_p \mathbf{A}_p^H \mathbf{y})^2 - 2P (\mathbf{y}^H \mathbf{A}_p \mathbf{A}_p^H \mathbf{y}) + P^2 M \right) \quad (6)$$

where $\mathbf{y} \triangleq \text{vec}(\mathbf{Y}) = [\mathbf{y}_1^T, \dots, \mathbf{y}_M^T]^T$ is the $MP \times 1$ vectorized version of the waveform matrix \mathbf{Y} , $\mathbf{A}_p \triangleq \mathbf{I}_M \otimes \mathbf{a}_p$ is an $MP \times M$ matrix with $\mathbf{a}_p \triangleq [1, e^{j\omega_p}, \dots, e^{j(P-1)\omega_p}]^T$, and $\text{vec}(\cdot)$ and \otimes are respectively vectorization and Kronecker product operators. Note that the results $\tilde{\tilde{\mathbf{y}}}(\omega_p) = \mathbf{A}_p^H \mathbf{y}$ and $\|\tilde{\tilde{\mathbf{y}}}(\omega_p)\|^2 = \tilde{\tilde{\mathbf{y}}}^H(\omega_p) \tilde{\tilde{\mathbf{y}}}(\omega_p)$ have been used to obtain (6) from (5).

We can finally express the waveform design problem associated with ISL minimization as

$$\min_{\mathbf{y}} \zeta \quad \text{s.t.} \quad |\mathbf{y}(p')| = 1, \quad p' = 1, \dots, MP. \quad (7)$$

III. WAVEFORM DESIGN VIA MAMI

In order to solve (7) efficiently, we start by simplifying (6). To begin, we note that the following train of equalities

$$\begin{aligned} \sum_{p=1}^{2P} (\mathbf{y}^H \mathbf{A}_p \mathbf{A}_p^H \mathbf{y}) &= \mathbf{y}^H \sum_{p=1}^{2P} (\mathbf{A}_p \mathbf{A}_p^H) \mathbf{y} \\ &= \|\mathbf{y}\|^2 = 2MP^2 \end{aligned} \quad (8)$$

holds because of the property $\sum_{p=1}^{2P} (\mathbf{A}_p \mathbf{A}_p^H) = 2P\mathbf{I}_{MP}$. Therefore, the latter two components of the sum in (6) are immaterial for optimization. After ignoring them in (6), the corresponding optimization problem can be rewritten as

$$\begin{aligned} \min_{\mathbf{y}} \quad & \sum_{p=1}^{2P} (\mathbf{y}^H \mathbf{A}_p \mathbf{A}_p^H \mathbf{y})^2 \\ \text{s.t.} \quad & |\mathbf{y}(p')| = 1, \quad p' = 1, \dots, MP. \end{aligned} \quad (9)$$

The objective function in (9) takes a quartic form with respect to \mathbf{y} , and it can be transformed into the following form

$$\begin{aligned} \sum_{p=1}^{2P} (\mathbf{y}^H \mathbf{A}_p \mathbf{A}_p^H \mathbf{y})^2 &= \sum_{p=1}^{2P} \text{tr}^2 \{ \tilde{\mathbf{Y}}^H \mathbf{A}_p \mathbf{A}_p^H \} \\ &= \sum_{p=1}^{2P} \text{vec}^H(\tilde{\mathbf{Y}}) \text{vec}(\mathbf{A}_p \mathbf{A}_p^H) \text{vec}^H(\mathbf{A}_p \mathbf{A}_p^H) \text{vec}(\tilde{\mathbf{Y}}) \\ &\triangleq \text{vec}^H(\tilde{\mathbf{Y}}) \Phi \text{vec}(\tilde{\mathbf{Y}}) \end{aligned} \quad (10)$$

where $\tilde{\mathbf{Y}} \triangleq \mathbf{y}\mathbf{y}^H$ is an $MP \times MP$ rank-1 matrix, $\Phi \triangleq \sum_{p=1}^{2P} \text{vec}(\mathbf{A}_p \mathbf{A}_p^H) \text{vec}^H(\mathbf{A}_p \mathbf{A}_p^H)$ is an $M^2 P^2 \times M^2 P^2$ matrix, and $\text{tr}\{\cdot\}$ stands for the matrix trace. The properties $\mathbf{y}^H \mathbf{A}_p \mathbf{A}_p^H \mathbf{y} = \text{tr}\{\tilde{\mathbf{Y}}^H \mathbf{A}_p \mathbf{A}_p^H\} = \text{vec}^H(\tilde{\mathbf{Y}}) \text{vec}(\mathbf{A}_p \mathbf{A}_p^H)$ have been used in the derivations of (10). Therefore, the optimization problem (9) can be further rewritten as

$$\min_{\tilde{\mathbf{Y}}} \text{vec}^H(\tilde{\mathbf{Y}}) \Phi \text{vec}(\tilde{\mathbf{Y}}) \quad (11a)$$

$$\text{s.t.} \quad \tilde{\mathbf{Y}} = \mathbf{y}\mathbf{y}^H \quad (11b)$$

$$|\mathbf{y}(p')| = 1, \quad p' = 1, \dots, MP. \quad (11c)$$

Before applying majorization to the objective function (11a), we present the following result to be used later [18].

The quadratic function $\mathbf{x}^H \mathbf{Q} \mathbf{x}$ is majorized by the function $\mathbf{x}^H \mathbf{G} \mathbf{x} + 2\Re\{\mathbf{x}^H (\mathbf{Q} - \mathbf{G}) \mathbf{x}_0\} + \mathbf{x}_0^H (\mathbf{G} - \mathbf{Q}) \mathbf{x}_0$ at \mathbf{x}_0 when the generalized inequality $\mathbf{G} \succeq \mathbf{Q}$ is satisfied. Here \mathbf{G} and \mathbf{Q} are Hermitian positive semidefinite matrices.

It can be shown that the largest eigenvalue of Φ , denoted by $\lambda_{\max}(\Phi)$, equals $2MP^2$. We omit the proof because of the space limitation. Therefore, we can select $\mathbf{G} \triangleq \lambda_{\max}(\Phi)\mathbf{I}_{M^2P^2}$ to guarantee the generalized inequality $\mathbf{G} \succeq \Phi$. Using the above-mentioned majorization result, the objective function (11a) can be majorized as

$$g_1(\tilde{\mathbf{Y}}, \tilde{\mathbf{Y}}^{(k)}) = \lambda_{\max}(\Phi)\text{vec}^H(\tilde{\mathbf{Y}})\text{vec}(\tilde{\mathbf{Y}}) + 2\Re\{\text{vec}^H(\tilde{\mathbf{Y}})(\Phi - \lambda_{\max}(\Phi)\mathbf{I}_{M^2P^2})\text{vec}(\tilde{\mathbf{Y}}^{(k)})\} + \text{vec}^H(\tilde{\mathbf{Y}}^{(k)})(\lambda_{\max}(\Phi)\mathbf{I}_{M^2P^2} - \Phi)\text{vec}(\tilde{\mathbf{Y}}^{(k)}) \quad (12)$$

where the matrix $\tilde{\mathbf{Y}}^{(k)} \triangleq \mathbf{y}^{(k)}(\mathbf{y}^{(k)})^H$ is obtained at the k th iteration and $\Re\{\cdot\}$ denotes the real part of a complex value. Note that $\text{vec}^H(\tilde{\mathbf{Y}})\text{vec}(\tilde{\mathbf{Y}}) = \|\mathbf{y}\|^4 = M^2P^2$. Hence, both the first and third components of the sum in (12) are constant terms which are immaterial for optimization. The problem (11) can be therefore rewritten as

$$\min_{\tilde{\mathbf{Y}}} \text{vec}^H(\tilde{\mathbf{Y}})(\Phi - \lambda_{\max}(\Phi)\mathbf{I}_{M^2P^2})\text{vec}(\tilde{\mathbf{Y}}^{(k)}) \quad (13a)$$

$$\text{s.t. } \tilde{\mathbf{Y}} = \mathbf{y}\mathbf{y}^H \quad (13b)$$

$$|\mathbf{y}(p')| = 1, \quad p' = 1, \dots, MP. \quad (13c)$$

Using the properties $\text{vec}(\tilde{\mathbf{Y}}) = \text{vec}(\mathbf{y}\mathbf{y}^H) = (\mathbf{y}^T \otimes \mathbf{I}_{MP})^H \mathbf{y}$ and $\text{vec}(\mathbf{A}_p \mathbf{A}_p^H) = (\mathbf{A}_p^T \otimes \mathbf{I}_{MP})^H \text{vec}(\mathbf{A}_p)$, and also substituting the explicit expressions of Φ and $\lambda_{\max}(\Phi)$, the objective function (13a) can be further transformed as

$$\begin{aligned} & \text{vec}^H(\tilde{\mathbf{Y}})(\Phi - \lambda_{\max}(\Phi)\mathbf{I}_{M^2P^2})\text{vec}(\tilde{\mathbf{Y}}^{(k)}) \\ &= \sum_{p=1}^{2P} \left(\mathbf{y}^H(\mathbf{y}^T \otimes \mathbf{I}_{MP})(\mathbf{A}_p^T \otimes \mathbf{I}_{MP})^H \text{vec}(\mathbf{A}_p)\text{vec}^H(\mathbf{A}_p) \right. \\ & \quad \times (\mathbf{A}_p^T \otimes \mathbf{I}_{MP})((\mathbf{y}^{(k)})^T \otimes \mathbf{I}_{MP})^H \mathbf{y}^{(k)} \\ & \quad \left. - 2MP^2 \mathbf{y}^H(\mathbf{y}^T \otimes \mathbf{I}_{MP})((\mathbf{y}^{(k)})^T \otimes \mathbf{I}_{MP})^H \mathbf{y}^{(k)} \right) \\ &= \sum_{p=1}^{2P} \mathbf{y}^H((\mathbf{y}^T \mathbf{A}_p^*) \otimes \mathbf{I}_{MP})\text{vec}(\mathbf{A}_p)\text{vec}^H(\mathbf{A}_p)((\mathbf{A}_p^T(\mathbf{y}^{(k)})^*) \\ & \quad \otimes \mathbf{I}_{MP})\mathbf{y}^{(k)} - 2MP^2 \mathbf{y}^H(\mathbf{y}^T(\mathbf{y}^{(k)})^*)\mathbf{y}^{(k)} \quad (14) \end{aligned}$$

$$= \sum_{p=1}^{2P} \mathbf{y}^H \mathbf{A}_p ((\mathbf{y}^{(k)})^H \mathbf{A}_p \mathbf{A}_p^H \mathbf{y}^{(k)}) \mathbf{A}_p^H \mathbf{y} - 2MP^2 \mathbf{y}^H (\mathbf{y}^{(k)} (\mathbf{y}^{(k)})^H) \mathbf{y} \quad (15)$$

where the mixed product property of Kronecker product and the property $((\mathbf{y}^T \mathbf{A}_p^*) \otimes \mathbf{I}_{MP})\text{vec}(\mathbf{A}_p) = \mathbf{A}_p \mathbf{A}_p^H \mathbf{y}$ are used to derive (14) and (15), respectively.

Stacking \mathbf{A}_p , $p = 1, \dots, 2P$ into a new $MP \times 2MP$ matrix \mathbf{A} , i.e., $\mathbf{A} \triangleq [\mathbf{A}_1, \dots, \mathbf{A}_{2P}]$, (15) can be further rewritten in the following compact form

$$\begin{aligned} & \sum_{p=1}^{2P} \mathbf{y}^H \mathbf{A}_p ((\mathbf{y}^{(k)})^H \mathbf{A}_p \mathbf{A}_p^H \mathbf{y}^{(k)}) \mathbf{A}_p^H \mathbf{y} \\ & \quad - 2MP^2 \mathbf{y}^H (\mathbf{y}^{(k)} (\mathbf{y}^{(k)})^H) \mathbf{y} \\ &= \mathbf{y}^H (\mathbf{A} \mathbf{A}^{(k)} \mathbf{A}^H - 2MP^2 \mathbf{y}^{(k)} (\mathbf{y}^{(k)})^H) \mathbf{y} \quad (16) \end{aligned}$$

where the $2MP \times 2MP$ diagonal matrix $\mathbf{A}^{(k)}$ is expressed as

$$\mathbf{A}^{(k)} \triangleq \text{diag}\left\{ \|\mathbf{a}_1^H \tilde{\mathbf{Y}}^{(k)}\|^2 \mathbf{1}_M^T, \dots, \|\mathbf{a}_{2P}^H \tilde{\mathbf{Y}}^{(k)}\|^2 \mathbf{1}_M^T \right\} \quad (17)$$

with $\mathbf{1}_M$ denoting a vector whose M elements are all ones. Therefore, the optimization problem (13) can be rewritten as

$$\min_{\mathbf{y}} \mathbf{y}^H (\mathbf{A} \mathbf{A}^{(k)} \mathbf{A}^H - 2MP^2 \mathbf{y}^{(k)} (\mathbf{y}^{(k)})^H) \mathbf{y} \quad (18a)$$

$$\text{s.t. } |\mathbf{y}(p')| = 1, \quad p' = 1, \dots, MP. \quad (18b)$$

Applying the previous majorization result to the first component of the quadratic objective function (18a) and selecting $\mathbf{G} \triangleq \mu_{\max}^{(k)} \mathbf{A} \mathbf{A}^H$ with $\mu_{\max}^{(k)} \triangleq \max\{\|\mathbf{a}_1^H \tilde{\mathbf{Y}}^{(k)}\|^2 \mathbf{1}_M^T, \dots, \|\mathbf{a}_{2P}^H \tilde{\mathbf{Y}}^{(k)}\|^2 \mathbf{1}_M^T\}$, we guarantee that $\mathbf{G} \succeq \mathbf{A} \mathbf{A}^{(k)} \mathbf{A}^H$. Therefore, the objective function (18a) is majorized as

$$\begin{aligned} & g_2(\mathbf{y}, \mathbf{y}^{(k)}) \\ &= \mu_{\max}^{(k)} \mathbf{y}^H \mathbf{A} \mathbf{A}^H \mathbf{y} + 2\Re\{\mathbf{y}^H (\mathbf{A} (\mathbf{A}^{(k)} - \mu_{\max}^{(k)} \mathbf{I}_{2MP}) \mathbf{A}^H \\ & \quad - 2MP^2 \mathbf{y}^{(k)} (\mathbf{y}^{(k)})^H) \mathbf{y}\} + (\mathbf{y}^{(k)})^H (2MP^2 \mathbf{y}^{(k)} \\ & \quad \times (\mathbf{y}^{(k)})^H - \mathbf{A} (\mathbf{A}^{(k)} - \mu_{\max}^{(k)} \mathbf{I}_{2MP}) \mathbf{A}^H) \mathbf{y}^{(k)}. \quad (19) \end{aligned}$$

Note that $\mathbf{A} \mathbf{A}^H = \sum_{p=1}^{2P} \mathbf{A}_p \mathbf{A}_p^H = 2P \mathbf{I}_{MP}$ and $\mathbf{y}^H \mathbf{y} = (\mathbf{y}^{(k)})^H \mathbf{y}^{(k)} = \|\mathbf{y}\|^2 = MP$. Hence the first and third components of the sum in (19) are immaterial for optimization. The optimization problem (18) can be finally simplified as

$$\begin{aligned} & \min_{\mathbf{y}} \mathbf{y}^H \mathbf{z}^{(k)} \\ & \text{s.t. } |\mathbf{y}(p')| = 1, \quad p' = 1, \dots, MP. \quad (20) \end{aligned}$$

where $\mathbf{z}^{(k)} \triangleq -\mathbf{A} \mathbf{A}^{(k)} \mathbf{A}^H \mathbf{y}^{(k)} + 2\mu_{\max}^{(k)} P \mathbf{y}^{(k)} + 2M^2 P^3 \mathbf{y}^{(k)}$. Due to the constant modulus property of \mathbf{y} , (20) is equivalent to the following optimization problem

$$\begin{aligned} & \min_{\mathbf{Y}} \|\mathbf{Y} - \mathbf{Z}\|^2 \\ & \text{s.t. } |[\mathbf{Y}]_{m,p}| = 1, \quad m = 1, \dots, M; p = 1, \dots, P \quad (21) \end{aligned}$$

where

$$\mathbf{Z}^{(k)} \triangleq -\mathbf{A} \mathbf{A}^{(k)} \mathbf{A}^H \mathbf{Y}^{(k)} + 2\mu_{\max}^{(k)} P \mathbf{Y}^{(k)} + 2M^2 P^3 \mathbf{Y}^{(k)} \quad (22)$$

with the waveform matrix $\mathbf{Y}^{(k)}$ achieved at the k th iteration and $[\cdot]_{m,p}$ standing for the (m, p) th element of a matrix. The solution of (21) can be found in the following closed form

$$[\mathbf{Y}]_{m,p} = e^{j \arg\left([\mathbf{Z}^{(k)}]_{m,p}\right)}, \quad m = 1, \dots, M; p = 1, \dots, P. \quad (23)$$

Note that (21) and (22) are written into matrix forms which facilitate our proposed algorithm in the following. Based on the above derivations, we propose an original algorithm for the ISL minimization problem (7) via MaMi technique summarized in Algorithm 1. To speed up the convergence of this algorithm, we can resort to accelerated schemes. For example, the schemes in [18] which lead to efficient accelerated methods can be used. Here we summarize also our algorithm accelerated by fix-point scheme in Algorithms 2. We refer interested readers to [18] for the proof of convergence.

Algorithm 1 ISL minimization via MaMi

```

1:  $k \leftarrow 0$ ,  $\mathbf{Y} \leftarrow P \times M$  unimodular sequence matrix with
   random phases.
2: repeat
3:   procedure ISLMAMi( $\mathbf{Y}^{(k)}$ )
4:      $\mu_{\max}^{(k)} = \max\{\|\mathbf{a}_p^H \hat{\mathbf{Y}}^{(k)}\|^2\}_{p=1}^{2P}$ 
5:      $\mathbf{Z}^{(k)} = -\mathbf{A}\mathbf{\Lambda}^{(k)}\mathbf{A}^H\mathbf{Y}^{(k)} + 2\mu_{\max}^{(k)}P\mathbf{Y}^{(k)}$ 
6:        $+ 2M^2P^3\mathbf{Y}^{(k)}$ 
7:      $[\mathbf{Y}^{(k+1)}]_{m,p} = e^{j\arg([\mathbf{Z}^{(k)}]_{m,p})}$ ,  $m = 1, \dots, M$ ;
8:        $p = 1, \dots, P$ .
9:    $k \leftarrow k + 1$ 
10:  end procedure
11: until convergence

```

IV. SIMULATION RESULTS

In our simulations, we compare the performance of our proposed waveform design algorithm with that of CAN (see [5]) and the method in [19] (named as CANSong), and also present correlation properties of the waveforms generated by them. We generate unimodular sequences with random phases as the initialization for each tested design, and the same initialized sequence is used when conducting comparison. The basic method of our work, i.e., Algorithm 1, and that of [19] (see Algorithm 3 therein) converge more slowly than the corresponding accelerated algorithms while giving similar minimized ISL performance. Therefore, we use the fix-point accelerated scheme. Two stopping criteria are employed in the conducted comparisons. One is the absolute ISL difference between the current and previous iterations normalized to the initial ISL, whose threshold is set to be 10^{-8} . The other is the norm of the difference between the waveform matrices obtained at the current and previous iterations, whose threshold is set to be 10^{-3} . All simulations for the tested methods are conducted based on the same hardware and software platforms, and are averaged by running 50 independent trials.

In the first example, we evaluate the convergence properties (i.e., running time versus code length) of the three tested waveform designs using the first (ISL based) stopping criterion. The number of designed waveforms is $M = 4$, and the code length P is varying from 20 to 200 with step size 20. Fig. 1 shows the performance comparison of the three waveform design. It can be seen from Fig. 1(a) that our proposed design and the design of [19] always outperform the CAN design in convergence rate in terms of the consumed time. It costs our proposed waveform design nearly the same running time as the design of [19] to obtain optimized waveforms when the code length is relatively smaller (i.e., from 20 to 80). However, our proposed design behaves increasingly better than the method of [19] when larger code length is selected, and indeed this superiority becomes obvious when both the code length and the number of waveforms are significantly large. Fig. 1(b) shows the corresponding achieved ISL of the three tested waveform

Algorithm 2 ISL minimization via accelerated MaMi

```

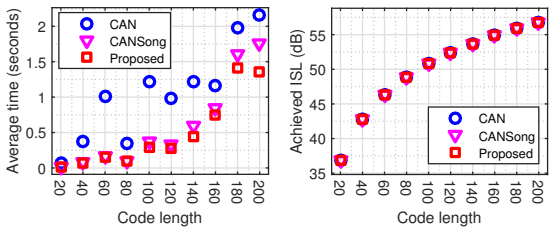
1:  $k \leftarrow 0$ ,  $\mathbf{Y} \leftarrow P \times M$  unimodular sequence matrix with
   random phases.
2: repeat
3:   procedure ISLAFMAMi( $\mathbf{Y}^{(k)}$ )
4:      $\hat{\mathbf{Y}} = \text{ISLMaMi}(\mathbf{Y}^{(k)})$ 
5:      $\hat{\hat{\mathbf{Y}}} = \text{ISLMaMi}(\hat{\mathbf{Y}})$ 
6:      $\hat{\hat{\Delta}} = \hat{\mathbf{y}} - \mathbf{y}^{(k)}$ ;  $\hat{\Delta} = \hat{\hat{\mathbf{Y}}} + \mathbf{Y}^{(k)} - 2\hat{\mathbf{Y}}$ 
7:      $\beta = -\|\hat{\Delta}\|/\|\hat{\hat{\Delta}}\|$ 
8:      $\mathbf{Z}^{(k)} = \mathbf{Y}^{(k)} - 2\beta\hat{\Delta} + \beta^2\hat{\hat{\Delta}}$ 
9:      $[\bar{\mathbf{Y}}^{(k)}]_{m,p} = e^{j\arg([\mathbf{Z}^{(k)}]_{m,p})}$ ,  $m = 1, \dots, M$ ;
10:        $p = 1, \dots, P$ .
11:   while ISL( $\bar{\mathbf{Y}}^{(k)}$ ) > ISL( $\mathbf{Y}^{(k)}$ ) do
12:      $\beta \leftarrow (\beta - 1)/2$ 
13:      $\mathbf{Z}^{(k)} = \mathbf{Y}^{(k)} - 2\beta\hat{\Delta} + \beta^2\hat{\hat{\Delta}}$ 
14:      $[\bar{\mathbf{Y}}^{(k)}]_{m,p} = e^{j\arg([\mathbf{Z}^{(k)}]_{m,p})}$ ,  $m = 1, \dots, M$ ;
15:        $p = 1, \dots, P$ .
16:   end while
17:    $\mathbf{Y}^{(k+1)} = \bar{\mathbf{Y}}^{(k)}$ 
18:    $k \leftarrow k + 1$ 
19: end procedure
20: until convergence

```

designs. It can be seen from Fig. 1(b) that the three designs nearly achieve the same ISL, where the results are shown with overlapping graphic shapes. Indeed, the ISLs achieved by our proposed design and that of [19] are better than that achieved by the CAN algorithm, however, the difference is quite small (less than 10^{-4} dB).

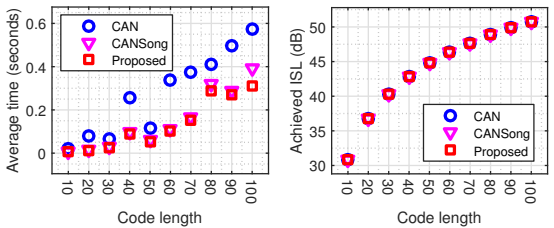
In the second example, we evaluate the convergence properties of the three tested designs using the second (waveform based) stopping criterion. The number of waveforms is $M = 2$, and the code length P is varying from 10 to 100 with step size 10. Fig. 2 shows the performance comparisons of the three waveform designs. Similar to Fig. 1, it can be seen from Fig. 2(a) that both our proposed design and the design of [19] outperform the CAN design in convergence rate with respect to the consumed time, and again our proposed design behaves increasingly better than that of [19] for larger code lengths. It can also be seen from Fig. 2(b) that the obtained ISL of the three tested designs are again quite close to each other, and the corresponding difference is smaller. Compared to the previous results, we remark that using the waveform based stopping criterion to obtain a desired ISL for all these waveform designs is generally faster than the case using the ISL based criterion.

In the third example, we present the correlation properties of waveforms optimized by the three tested designs using the ISL based stopping criterion. The corresponding waveform design parameters are $M = 2$ and $P = 256$. The normalized auto- and cross-correlations of the two designed waveforms are



(a) Running time versus code length. (b) Achieved ISL versus code length.

Fig. 1. Performance evaluation using the first stopping criterion.



(a) Running time versus code length. (b) Achieved ISL versus code length.

Fig. 2. Performance evaluation using the second stopping criterion.

shown in the sub figures of Fig. 3. It can be seen from Fig. 3 that the auto- and cross-correlations for the three tested designs are close to each other, which coincides with the ISL results in the previous two examples. The worst sidelobe level for the auto-correlation is about -23 dB, while the worst sidelobe level for the cross-correlations is around -20 dB.

V. CONCLUSION

An efficient method for designing multiple unimodular waveforms with good correlation properties that can be used for MIMO radar has been developed. We have employed ISL minimization of the waveforms as the designing criterion, and have formulated the ISL minimization based design as a quartic optimization problem. This quartic optimization problem has been converted into a quadratic form and then solved by means of MaMi technique. We have properly selected the majorized function for the objective function of the quadratic optimization problem, which is used by MaMi in order to find the corresponding solution. The proposed algorithms have shown good correlations of the designed waveforms and faster convergence as compared to its counterparts.

REFERENCES

- [1] P. Stoica, J. Li, and Y. Xie, "On probing signal design for MIMO radar," *IEEE Trans. Signal Process.*, vol. 55, no. 8, pp. 4151–4161, Aug. 2007.
- [2] Y. Yang and R. S. Blum, "MIMO radar waveform design based on mutual information and minimum mean-square error estimation," *IEEE Trans. Aerosp. Electron. Syst.*, vol. 43, no. 1, pp. 330–343, Jan. 2007.
- [3] B. Friedlander, "Waveform design for MIMO radars," *IEEE Trans. Aerosp. Electron. Syst.*, vol. 43, no. 3, pp. 1227–1238, Jul. 2007.
- [4] C.-Y. Chen and P. P. Vaidyanathan, "MIMO radar ambiguity properties and optimization using frequency-hopping waveforms," *IEEE Trans. Signal Process.*, vol. 56, no. 12, pp. 5926–5936, Dec. 2008.

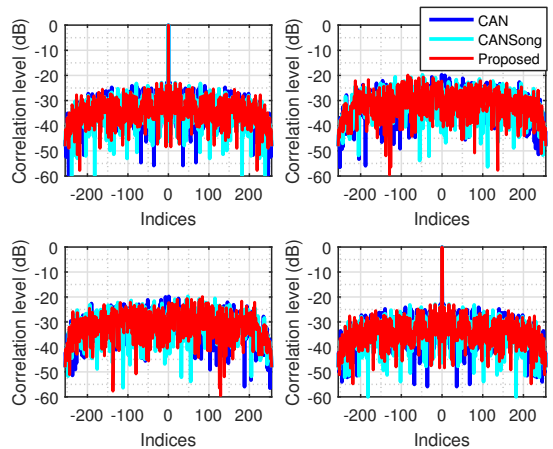


Fig. 3. Waveform correlations versus time lags.

- [5] H. He, P. Stoica, and J. Li, "Designing unimodular sequence sets with good correlations—Including an application to MIMO radar," *IEEE Trans. Signal Process.*, vol. 57, no. 11, pp. 4391–4405, Nov. 2009.
- [6] I. Bekkerman and J. Tabrikian, "Target detection and localization using MIMO radar and sonars," *IEEE Trans. Signal Process.*, vol. 54, no. 10, pp. 3873–3883, Oct. 2006.
- [7] J. Li, P. Stoica, and X. Zheng, "Signal synthesis and receiver design for MIMO radar imaging," *IEEE Trans. Signal Process.*, vol. 56, no. 8, pp. 3959–3968, Aug. 2008.
- [8] Y. Li, S. A. Vorobyov, and V. Koivunen, "Ambiguity function of the transmit beamspace-based MIMO radar," *IEEE Trans. Signal Process.*, vol. 63, no. 17, pp. 4445–4457, Sep. 2015.
- [9] D. DeLong and E. M. Hofstetter, "On the design of optimum radar waveforms for clutter rejection," *IEEE Trans. Inf. Theory*, vol. 13, no. 3, pp. 454–463, Jul. 1967.
- [10] A. Hassanien and S. A. Vorobyov, "Transmit energy focusing for DOA estimation in MIMO radar with colocated antennas," *IEEE Trans. Signal Process.*, vol. 59, no. 6, pp. 2669–2682, Jun. 2011.
- [11] S. Ahmed, J. S. Thompson, Y. R. Petillot, and B. Mulgrew, "Unconstrained synthesis of covariance matrix for MIMO radar transmit beampattern," *IEEE Trans. Signal Process.*, vol. 59, no. 8, pp. 3837–3849, Aug. 2011.
- [12] N. Levanon and E. Mozeson, *Radar Signals*. Hoboken, NJ, USA: Wiley, 2004.
- [13] P. Stoica, H. He, and J. Li, "New algorithms for designing unimodular sequences with good correlation properties," *IEEE Trans. Signal Process.*, vol. 57, no. 4, pp. 1415–1425, Apr. 2009.
- [14] A. De Maio, S. D. Nicola, Y. Huang, Z.-Q. Luo, and S. Zhang, "Design of phase codes for radar performance optimization with a similarity constraint," *IEEE Trans. Signal Process.*, vol. 57, no. 2, pp. 610–621, Feb. 2009.
- [15] A. Aubry, A. De Maio, A. Farina, and M. Wicks, "Knowledge-aided (potentially cognitive) transmit signal and receive filter design in signal-dependent clutter," *IEEE Trans. Aerosp. Electron. Syst.*, vol. 49, no. 1, pp. 93–117, Jan. 2013.
- [16] W. Rowe, P. Stoica, and J. Li, "Spectrally constrained waveform design," *IEEE Signal Process. Mag.*, vol. 31, no. 3, pp. 157–162, May 2014.
- [17] M. M. Naghsh, M. Modares-Hashemi, S. ShahbazPanahi, M. Soltanalian, and P. Stoica, "Unified optimization framework for multi-static radar code design using information-theoretic criteria," *IEEE Trans. Signal Process.*, vol. 61, no. 21, pp. 5401–5416, Nov. 2013.
- [18] J. Song, P. Babu, and D. P. Palomar, "Optimization methods for designing sequences with low autocorrelation sidelobes," *IEEE Trans. Signal Process.*, vol. 63, no. 15, pp. 3998–4009, Aug. 2015.
- [19] J. Song, P. Babu, and D. P. Palomar, "Sequence set design with good correlation properties via majorization-minimization," *IEEE Trans. Signal Process.*, vol. 64, no. 11, pp. 2886–2879, Jun. 2016.
- [20] D. R. Hunter and K. Lange, "A tutorial on MM algorithms," *Amer. Statist.*, vol. 58, no. 1, pp. 30–37, Feb. 2004.

Publication X

Yongzhe Li and Sergiy A. Vorobyov. Joint space-(slow) time transmission with unimodular waveforms and receive adaptive filter design for radar. In *IEEE International Conference on Acoustics, Speech, and Signal Processing (ICASSP)*, Calgary, AB, Canada, pp. 3276–3280, April 2018.

© 2018 IEEE.

Reprinted with permission.

JOINT SPACE-(SLOW) TIME TRANSMISSION WITH UNIMODULAR WAVEFORMS AND RECEIVE ADAPTIVE FILTER DESIGN FOR RADAR

Yongzhe Li and Sergiy A. Vorobyov

Dept. Signal Processing and Acoustics, Aalto University, P.O. Box 15400, FI-00076 Aalto, Finland

Emails: lyzlyz888@gmail.com/yongzhe.li@aalto.fi, svor@ieee.org

ABSTRACT

A novel computationally efficient method for jointly designing the space-(slow) time (SST) transmission with unimodular waveforms and receive adaptive filter is developed for different radar configurations. The range sidelobe effect and Doppler characteristics are considered. In particular, we develop a novel approach for jointly synthesizing unimodular SST waveforms and minimum variance distortionless response adaptive receive filter for two cases of known Doppler information and presence of uncertainties on clutter bins. The corresponding non-convex optimization problems are formulated and an efficient algorithm for addressing them is derived. The main ideas of the algorithm are to decouple composite objective function of the problems, generate a minorizing surrogate, and then solve the joint design problems iteratively, but in closed-form for each iteration, by means of minorization-maximization technique. The proposed algorithm demonstrates excellent performance and has fast convergence and low complexity.

Index Terms— Adaptive filter, joint waveform design, minorization-maximization, space-(slow) time, radar.

1. INTRODUCTION

Waveform design has been the research field of significant interest over several decades [1]–[4]. Many past works focus on designing fast-time waveform(s) to achieve various desirable properties [5]–[9]. These works improve the waveform quality when the receiver is fixed as the matched filter. However, in harsh environments involving heterogeneous clutter with Doppler uncertainties and/or active jamming, the receiver should be flexibly adaptive, and therefore, joint transmission and receive filter design (JTRFD) becomes necessary.

Recent works on JTRFD [10]–[16] can be divided into two categories. The first category concentrates on designing fast-time waveform transmission and receive filter with particular constraints on waveform characteristics, which essentially trade off the signal-to-noise ratio (SNR) for signal-to-clutter-plus-noise ratio (SCNR) [10]–[12]. The methods therein normally do not consider Doppler information processing. On the other hand, the methods in the second category focuses on synthesizing slow-time waveforms (for inter-pulse coding) at transmission while jointly enforcing the receive adaptive

filter [13]–[16]. As a result, they have the potential of coping with Doppler related issues, such as uncertainty, and therefore, can offer enhanced resolution, superior detection, etc. The latter newly emerged trend motivates us to further investigate the joint design with considerations on the range sidelobe effect of fast-time waveforms [17], and the multi-input multi-output (MIMO) waveform diversity with difficult constraints [18], [19]. It also motivates us to use space-time adaptive processing (STAP) technique [20], [21], so that the signal-to-interference-plus-noise ratio (SINR) performance could be improved through multi-dimension adaptive filter.

In this paper, we address the joint space-(slow) time (SST) transmission and receive adaptive filter design problem. We present a generic signal model suitable for different radar configurations while considering the intra-pulse compression (or range sidelobe) effect and Doppler characteristics. The SST waveforms are designed to have unit modulus by maximizing the output SINR, with which a minimum variance distortionless response (MVDR) STAP filter is associated. We devise an efficient approach based on simple iterative procedures, and find closed-form solutions to the sub-problems via minimization-majorization [22]. Our strategy is to minorize the composite objective function by properly designing surrogates defined in terms of quadratic form. Both cases of known Doppler information and uncertainties on clutter bins are studied. The solution to the latter case serves as a generic form for the former. Corresponding computationally efficient algorithms with good performance are proposed.

Notations: We use bold upper case, bold lower case, and italic letter to respectively denote matrices, column vectors, and scalars, except $\mathbf{1}_M$ defining a length- M vector of all ones. Notations $(\cdot)^T$, $(\cdot)^H$, \otimes , \odot , $\mathfrak{D}(\cdot)$, $\text{vec}(\cdot)$, $\mathbb{E}\{\cdot\}$, $|\cdot|$ and $\|\cdot\|$ are the transpose, conjugate transpose, Kronecker product, Hadamard product, diagonalization, column-wise vectorization, expectation, modulus, and Euclidean norm operators, respectively.

2. PROBLEM FORMULATION

Consider an airborne colocated MIMO radar equipped with M transmit and N receive elements. At each transmit element, a burst of L pulses encoded by an independent slow-time waveform, denoted by $\phi_m \triangleq [\phi_{m,1}, \dots, \phi_{m,L}]^T \in \mathbb{C}^{L \times 1}$ for the m th element, is launched within one radar coherent processing interval (CPI). An independent fast-time waveform

The research was supported in part by the Academy of Finland grant No. 299243.

of length P , denoted by $\mathbf{s}_m \in \mathbb{C}^{P \times 1}$ for the m th antenna, is repeatedly used for all intra-pulse modulations. We denote the SST and space-(fast) time (SFT) waveform matrices for transmission as $\Phi \triangleq [\phi_1, \dots, \phi_M]^T \in \mathbb{C}^{M \times L}$ and $\mathbf{S} \triangleq [\mathbf{s}_1, \dots, \mathbf{s}_M]^T \in \mathbb{C}^{M \times P}$, respectively, and define $\mathbf{R}_S^{(p)} \triangleq \mathbf{S} \mathbf{J}_p \mathbf{S}^H \in \mathbb{C}^{M \times M}$ as the waveform covariance matrix (for pulse compression) at time lag p ($0 \leq p \leq P-1$), with \mathbf{J}_p being the p th lower shift matrix of size $P \times P$ whose entries are ones on the p th off-diagonal ($p=0$ for the main diagonal) and zeros elsewhere.

At the receive end, after intra-pulse compression, i.e., matched filtering to \mathbf{S} at time lag p ($p=0$ for the target), and stacking the data into a vector, the received target vector $\mathbf{y}_t \in \mathbb{C}^{MNL \times 1}$ with a normalized Doppler frequency f_t for the target located at θ_t can be expressed as

$\mathbf{y}_t = \alpha_t \mathbf{a}_R(\theta_t) \otimes \mathcal{D}(\mathbf{d}(f_t)) \otimes ((\mathbf{R}_S^{(0)})^T \mathcal{D}(\mathbf{a}_T(\theta_t))) \phi$ (1) where α_t , $\mathbf{a}_T(\theta_t)$, $\mathbf{a}_R(\theta_t)$, and $\mathbf{d}(f_t)$ are the complex reflection coefficient, the transmit, receive, and Doppler steering vectors all for the target, respectively, and $\phi \triangleq \text{vec}(\Phi)$ is the vectorized version of Φ of length ML .

The observed clutter is a superposition of echoes from different uncorrelated scatters. Assuming that N_r ($N_r \leq L$) range rings interfere with the range-azimuth bin of interest where the target locates, and each ring consists of N_c discrete azimuth bins, the received clutter vector $\mathbf{y}_c \in \mathbb{C}^{MNL \times 1}$ can be expressed as

$$\mathbf{y}_c = \sum_{i'=0}^{N_r-1} \sum_{i=1}^{N_c} \xi_{ii'} \mathbf{a}_R(\theta_{ii'}) \otimes (\mathbf{J}_{i'} \mathcal{D}(\mathbf{d}(f_{ii'}))) \otimes ((\mathbf{R}_S^{(p)})^T \mathcal{D}(\mathbf{a}_T(\theta_{ii'}))) \phi$$
 (2)

where $\theta_{ii'}$, $f_{ii'}$, and $\xi_{ii'}$ are respectively the azimuth angle, normalized Doppler frequency, and complex reflection coefficient with zero mean, for the (i', i) th range-azimuth bin.

The overall vector \mathbf{y} of observations can be expressed as

$$\mathbf{y} = \mathbf{y}_t + \mathbf{y}_c + \mathbf{y}_{j+n}$$
 (3)

where $\mathbf{y}_{j+n} \in \mathbb{C}^{MNL \times 1}$ is the jamming plus noise vector which is assumed to be independent of the target and clutter components, and its covariance matrix is $\mathbf{R}_{j+n} \triangleq \mathbb{E}\{\mathbf{y}_{j+n} \mathbf{y}_{j+n}^H\}$. To simplify the notations, \mathbf{y}_t can be further expressed as $\mathbf{y}_t = \alpha_t \mathbf{T}_t \phi$, and \mathbf{y}_c as

$$\mathbf{y}_c = \sum_{i'=0}^{N_r-1} \sum_{i=1}^{N_c} \xi_{ii'} \mathbf{T}_{ii'}^{(p)} \phi = \sum_{i'=0}^{N_r-1} \sum_{i=1}^{N_c} \xi_{ii'} \tilde{\mathbf{T}}_{ii'}^{(p)} ((\tilde{\mathbf{d}}(f_{ii'}) \odot \phi)$$
 (4)

where $\tilde{\mathbf{d}}(f_{ii'}) \triangleq \mathbf{d}(f_{ii'}) \otimes \mathbf{1}_M$, $\mathbf{T}_t \triangleq \mathbf{a}_R(\theta_t) \otimes \mathcal{D}(\mathbf{d}(f_t)) \otimes ((\mathbf{R}_S^{(0)})^T \mathcal{D}(\mathbf{a}_T(\theta_t)))$, $\mathbf{T}_{ii'}^{(p)} \triangleq \mathbf{a}_R(\theta_{ii'}) \otimes (\mathbf{J}_{i'} \mathcal{D}(\mathbf{d}(f_{ii'}))) \otimes ((\mathbf{R}_S^{(p)})^T \mathcal{D}(\mathbf{a}_T(\theta_{ii'})))$, and $\tilde{\mathbf{T}}_{ii'}^{(p)} \triangleq \mathbf{a}_R(\theta_{ii'}) \otimes \mathbf{J}_{i'} \otimes ((\mathbf{R}_S^{(p)})^T \mathcal{D}(\mathbf{a}_T(\theta_{ii'})))$.

Using (4), the clutter covariance matrix $\mathbf{R}_c \triangleq \mathbb{E}\{\mathbf{y}_c \mathbf{y}_c^H\}$ for the case of known Doppler on clutter bins (i.e., $f_{ii'}$ is fixed), denoted in this case as \mathbf{R}_c^I , can be expressed as

$$\mathbf{R}_c^I = \sum_{i'=0}^{N_r-1} \sum_{i=1}^{N_c} \sigma_{ii'}^2 \mathbf{T}_{ii'}^{(p)} \phi \phi^H (\mathbf{T}_{ii'}^{(p)})^H$$
 (5)

with $\sigma_{ii'}^2 \triangleq \mathbb{E}\{|\xi_{ii'}|^2\}$. When $f_{ii'}$ is unknown, but rather distributed with a known probability density function (PDF) in the uncertainty interval $[\bar{f}_{ii'} - \epsilon_{ii'}/2, \bar{f}_{ii'} + \epsilon_{ii'}/2]$ with mean $\bar{f}_{ii'}$ and bounding parameter $\epsilon_{ii'}$, the clutter covariance matrix \mathbf{R}_c , denoted in this case as \mathbf{R}_c^H , can be expressed as

$$\mathbf{R}_c^H = \sum_{i'=0}^{N_r-1} \sum_{i=1}^{N_c} \sigma_{ii'}^2 \tilde{\mathbf{T}}_{ii'}^{(p)} (\phi \phi^H) \odot (\Upsilon_{ii'} \otimes \mathbf{1}_M \mathbf{1}_M^T) (\tilde{\mathbf{T}}_{ii'}^{(p)})^H$$
 (6)

where we used (4), and $\Upsilon_{ii'} \in \mathbb{C}^{L \times L}$ is a Hermitian matrix determined by the PDF of $f_{ii'}$ (see [13] for the example of uniform distribution).

Finally, the received data vector \mathbf{y} goes through the STAP filter with the weight vector $\mathbf{w} \in \mathbb{C}^{MNL \times 1}$. The output SINR at the filter can then be expressed as

$$\zeta = \frac{|\alpha_t|^2 \cdot |\mathbf{w}^H \mathbf{T}_t \phi|^2}{\mathbf{w}^H (\mathbf{R}_c + \mathbf{R}_{j+n}) \mathbf{w}}$$
 (7)

The problem considered here is the joint design of SST waveform(s) and receive adaptive filter under the constraint that the waveform(s) have constant modulus. The design objective is to maximize SINR in (7). Under the condition that the SFT waveform matrix \mathbf{S} is known, the above joint design problem can be written as the following optimization problem

$$\begin{aligned} \max_{\phi, \mathbf{w}} \quad & \zeta \\ \text{s.t.} \quad & |\phi(n)| = 1, n = 1, \dots, ML \end{aligned}$$
 (8)

where the constraints ensure the constant modulus property.

3. JOINT SST WAVEFORM AND ADAPTIVE RECEIVER DESIGN

Using (7), for given ϕ , the solution of the optimization problem (8) with respect to \mathbf{w} can be easily found, and it obeys the MVDR expression

$$\mathbf{w}_{\text{opt}}(\phi) = \frac{(\mathbf{R}_c + \mathbf{R}_{j+n})^{-1} \mathbf{T}_t \phi}{\phi^H \mathbf{T}_t^H (\mathbf{R}_c + \mathbf{R}_{j+n})^{-1} \mathbf{T}_t \phi}$$
 (9)

Inserting (9) into (7), the SINR metric ζ can be rewritten as

$$\zeta = |\alpha_t|^2 \cdot \phi^H \mathbf{T}_t^H (\mathbf{R}_c + \mathbf{R}_{j+n})^{-1} \mathbf{T}_t \phi$$
 (10)

Therefore, the optimization problem (8) with respect to ϕ only and for given \mathbf{w} can be written as

$$\begin{aligned} \max_{\phi} \quad & \phi^H \mathbf{T}_t^H (\mathbf{R}_c + \mathbf{R}_{j+n})^{-1} \mathbf{T}_t \phi \\ \text{s.t.} \quad & |\phi(n)| = 1, n = 1, \dots, ML. \end{aligned}$$
 (11)

The objective in (11) is a composite function of ϕ and $\mathbf{R}_c \in \{\mathbf{R}_c^I, \mathbf{R}_c^H\}$, where \mathbf{R}_c is also a function of ϕ . Before proceeding with solving (11), we present the following result.

Lemma 1. *The objective in (11) is minorized by*

$$\begin{aligned} g_1(\phi, \phi^{(k)}) &= (\phi^{(k)})^H \Psi(\phi^{(k)}) \phi^{(k)} + 2\Re\left\{(\phi^{(k)})^H \right. \\ &\times (\Psi(\phi^{(k)}))^H (\phi - \phi^{(k)})\left. \right\} - (\phi^{(k)})^H \mathbf{T}_t^H (\Omega(\phi^{(k)}))^H \\ &\times (\mathbf{R}_c(\phi) - \mathbf{R}_c(\phi^{(k)})) \Omega(\phi^{(k)}) \mathbf{T}_t \phi^{(k)} \end{aligned}$$
 (12)

where $\phi^{(k)}$ is the SST waveform vector obtained at iteration k , and $\Omega(\phi^{(k)}) \in \mathbb{C}^{MNL \times MNL}$ and $\Psi(\phi^{(k)}) \in \mathbb{C}^{NL \times NL}$ are both functions of ϕ , defined as $\Omega(\phi^{(k)}) \triangleq (\mathbf{R}_c(\phi^{(k)}) + \mathbf{R}_{j+n})^{-1}$ and $\Psi(\phi^{(k)}) \triangleq \mathbf{T}_t^H \Omega(\phi^{(k)}) \mathbf{T}_t$.

Proof. Using Taylor's theorem and considering the first order expansion of the objective in (11), it can be straightforwardly (but after some derivations that we omit due to space limitation) proved that (12) minorizes the objective in (11). \square

Let us consider first the case when \mathbf{R}_c is given by (5), i.e., $\mathbf{R}_c = \mathbf{R}_c^I$. Using Lemma 1 and inserting (5) into (12), after some derivations, we can rewrite the minorizing function as

$$g_1^I(\phi, \phi^{(k)}) = (\phi^{(k)})^H \Psi^I(\phi^{(k)}) \phi^{(k)} + 2\Re\left\{(\phi^{(k)})^H \times (\Psi^I(\phi^{(k)}))^H (\phi - \phi^{(k)})\right\} - \phi^H \mathbf{E}_c^I(\phi^{(k)}) \phi + (\phi^{(k)})^H \times \mathbf{E}_c^I(\phi^{(k)}) \phi^{(k)} \quad (13)$$

where $\Omega^I(\phi^{(k)}) \triangleq (\mathbf{R}_c^I(\phi^{(k)}) + \mathbf{R}_{j+n})^{-1}$, $\Psi^I(\phi^{(k)}) \triangleq \mathbf{T}_t^H \Omega^I(\phi^{(k)}) \mathbf{T}_t$, and

$$\mathbf{E}_c^I(\phi^{(k)}) \triangleq \sum_{i'=0}^{N_r-1} \sum_{i=1}^{N_c} \sigma_{ii'}^2 (\mathbf{T}_{ii'}^{(p)})^H \Omega^I(\phi^{(k)}) \times \mathbf{T}_t \phi^{(k)} (\phi^{(k)})^H \mathbf{T}_t^H (\Omega^I(\phi^{(k)}))^H \mathbf{T}_{ii'}^{(p)}. \quad (14)$$

Note that the third (negative) term in (13) is a quadratic form with respect to ϕ , to which we can apply a proper minorization function once more.

Before proceeding with further minorization of (13), we present the following lemma.

Lemma 2. *The quadratic function $f(\phi) = -\phi^H \mathbf{E}_c^I(\phi^{(k)}) \phi$ is minorized by the following function*

$$\tilde{g}(\phi, \phi^{(k)}) = -\frac{1}{2} \phi^H \mathbf{G}^{(k)} \phi - (\phi^{(k)})^H \left(\frac{1}{2} \mathbf{G}^{(k)} - \mathbf{E}_c^I(\phi^{(k)}) \right) \times \phi^{(k)} - 2\Re\left\{ \phi^H (\mathbf{E}_c^I(\phi^{(k)}) - \frac{1}{2} \mathbf{G}^{(k)}) \phi^{(k)} \right\} \quad (15)$$

if $\mathbf{G}^{(k)} \succeq \mathbf{E}_c^I(\phi^{(k)})$ is satisfied.

Proof. The result is equivalent to majorization of $-f(\phi)$, and it is proved in this form in [23]. \square

Applying Lemma 2 to (13), after some derivations, the minorization function $g_1^I(\phi, \phi^{(k)})$ can be rewritten as

$$g_2^I(\phi, \phi^{(k)}) = -\frac{1}{2} \phi^H \mathbf{G}^{(k)} \phi - 2\Re\left\{ \phi^H \left(\mathbf{E}_c^I(\phi^{(k)}) - \frac{1}{2} \mathbf{G}^{(k)} - \Psi^I(\phi^{(k)}) \right) \phi^{(k)} \right\} + (\phi^{(k)})^H \left(2\mathbf{E}_c^I(\phi^{(k)}) - \Psi^I(\phi^{(k)}) - \frac{1}{2} \mathbf{G}^{(k)} \right) \phi^{(k)}. \quad (16)$$

Choosing $\mathbf{G}^{(k)} = \lambda^{(k)} \mathbf{I}_{ML}$, where $\lambda^{(k)}$ is a properly selected magnitude (e.g., the largest eigenvalue of $\mathbf{E}_c^I(\phi^{(k)})$) such that $\mathbf{G}^{(k)} \succeq \mathbf{E}_c^I(\phi^{(k)})$. It is straightforward to see that the first and third terms in (16) are constant, and therefore, immaterial for optimization. Ignoring these terms, the minorization problem for (11) can be written as

$$\max_{\phi} \quad -\Re\left\{ \phi^H (\mathbf{E}_c^I(\phi^{(k)}) - \frac{1}{2} \mathbf{G}^{(k)} - \Psi^I(\phi^{(k)})) \phi^{(k)} \right\} \\ \text{s.t.} \quad |\phi(n)| = 1, n = 1, \dots, ML. \quad (17)$$

Using the constraint that ϕ has to have constant modulus and defining $\tau_I^{(k)} \triangleq (\mathbf{E}_c^I(\phi^{(k)}) - \frac{1}{2} \mathbf{G}^{(k)} - \Psi^I(\phi^{(k)})) \phi^{(k)}$, problem (17) can be equivalently written as

$$\min_{\phi} \quad \|\phi - \tau_I^{(k)}\| \quad \text{s.t.} \quad |\phi(n)| = 1, n = 1, \dots, ML \quad (18)$$

which can be solved in closed-form as

$$\phi(n) = \exp\{j \cdot \arg(\tau_I^{(k)}(n))\}, n = 1, \dots, ML. \quad (19)$$

For the case when $\mathbf{R}_c = \mathbf{R}_c^{\text{II}}$, i.e., \mathbf{R}_c is given by (6), the additional difficulty is that we need to deal with the Hadamard product. Let $\Upsilon_{ii'} = \sum_{k=1}^{K^{(ii')}} \lambda_k^{(ii')} \mathbf{q}_k^{(ii')} (\mathbf{q}_k^{(ii')})^H = \sum_{k=1}^{K^{(ii')}} \mathbf{u}_k^{(ii')} (\mathbf{u}_k^{(ii')})^H$ be the eigen decomposition of the matrix $\Upsilon_{ii'}$ in (6), with $K^{(ii')}$ being the rank of $\Upsilon_{ii'}$, $\lambda_k^{(ii')}$ (real-valued) and $\mathbf{q}_k^{(ii')}$ being the k th eigenvalue and eigenvector, respectively, and $\mathbf{u}_k^{(ii')} \triangleq (\lambda_k^{(ii')})^{1/2} \mathbf{q}_k^{(ii')} \in \mathbb{C}^{L \times 1}$. Then \mathbf{R}_c^{II} can be expressed as

$$\mathbf{R}_c^{\text{II}} = \sum_{i'=0}^{N_r-1} \sum_{i=1}^{N_c} \sum_{k=1}^{K^{(ii')}} \sigma_{ii'}^2 \tilde{\mathbf{T}}_{ii'}^{(p)} \mathbf{D}_k^{(ii')} \phi \phi^H (\mathbf{D}_k^{(ii')})^H (\tilde{\mathbf{T}}_{ii'}^{(p)})^H \quad (20)$$

where $\mathbf{D}_k^{(ii')} \triangleq \mathcal{D}(\mathbf{u}_k^{(ii')} \otimes \mathbf{1}_M) \in \mathbb{C}^{ML \times ML}$ is diagonal.

Applying the same minorization strategies as in the previous case, we obtain the corresponding minorization functions, denoted here by $g_1^{\text{II}}(\phi, \phi^{(k)})$ and $g_2^{\text{II}}(\phi, \phi^{(k)})$, by replacing matrices $\Omega^I(\phi^{(k)})$, $\Psi^I(\phi^{(k)})$, and $\mathbf{E}_c^I(\phi^{(k)})$ in (13) and (16) with $\Omega^{\text{II}}(\phi^{(k)}) \triangleq (\mathbf{R}_c^{\text{II}}(\phi^{(k)}) + \mathbf{R}_{j+n})^{-1}$, $\Psi^{\text{II}}(\phi^{(k)}) \triangleq \mathbf{T}_t^H \Omega^{\text{II}}(\phi^{(k)}) \mathbf{T}_t$, and

$$\mathbf{E}_c^{\text{II}}(\phi^{(k)}) \triangleq \sum_{i'=0}^{N_r-1} \sum_{i=1}^{N_c} \sum_{k=1}^{K^{(ii')}} \sigma_{ii'}^2 (\mathbf{D}_k^{(ii')})^H (\mathbf{T}_{ii'}^{(p)})^H \Omega^{\text{II}}(\phi^{(k)}) \times \mathbf{T}_t \phi^{(k)} (\phi^{(k)})^H \mathbf{T}_t^H (\Omega^{\text{II}}(\phi^{(k)}))^H \mathbf{T}_{ii'}^{(p)} \mathbf{D}_k^{(ii')}. \quad (21)$$

Then the minorization problem for (11) can be written as

$$\max_{\phi} \quad -\Re\left\{ \phi^H (\mathbf{E}_c^{\text{II}}(\phi^{(k)}) - \frac{1}{2} \mathbf{G}^{(k)} - \Psi^{\text{II}}(\phi^{(k)})) \phi^{(k)} \right\} \\ \text{s.t.} \quad |\phi(n)| = 1, n = 1, \dots, ML \quad (22)$$

and solved in closed-form as

$$\phi(n) = \exp\{j \cdot \arg(\tau_{\text{II}}^{(k)}(n))\}, n = 1, \dots, ML \quad (23)$$

where $\tau_{\text{II}}^{(k)} \triangleq (\mathbf{E}_c^{\text{II}}(\phi^{(k)}) - \frac{1}{2} \mathbf{G}^{(k)} - \Psi^{\text{II}}(\phi^{(k)})) \phi^{(k)}$ and $\mathbf{G}^{(k)}$ is chosen as in the routine used in the previous case. Note that the solution (23) boils down to solution (19), if $\mathbf{u}_k^{(ii')} = \mathbf{d}(f_{ii'})$ and $K^{(ii')} = 1, \forall i, i'$.

Finally, the algorithm for joint SST waveform and receive filter design is summarized in Algorithm 1. It can be accelerated using, for example, the squared iterative method (SQUAREM) of [24], the backtracking line search method (BLSM) [25], etc. We omit the corresponding convergence analyses for our proposed algorithm with accelerations here because of space limitation.

Algorithm 1 Joint Design Algorithm

- 1: Initialization: $\phi^{(0)}$; $\text{mod} \in \{I, II\}$
 - 2: **repeat** procedure with respect to $\phi^{(k)}$
 - 3: Calculate $\Omega^{\text{mod}}(\phi^{(k)})$, $\Psi^{\text{mod}}(\phi^{(k)})$, $\mathbf{E}_c^{\text{mod}}(\phi^{(k)})$
 - 4: Construct $\mathbf{G}^{(k)}$ via $\mathbf{E}_c^{\text{mod}}(\phi^{(k)})$
 - 5: $\tau_{\text{mod}}^{(k)} \triangleq (\mathbf{E}_c^{\text{mod}}(\phi^{(k)}) - \frac{1}{2}\mathbf{G}^{(k)} - \Psi^{\text{mod}}(\phi^{(k)}))\phi^{(k)}$
 - 6: $\phi(n) = \exp\{j \cdot \arg(\tau_{\text{mod}}^{(k)}(n))\}$, $n = 1, \dots, ML$
 - 7: $k \leftarrow k + 1$
 - 8: **until** convergence
 - 9: Calculate \mathbf{w}_{opt} , and $\phi_{\text{opt}} = \phi^{(k+1)}$
-

4. SIMULATION RESULTS

We evaluate the performance of the proposed algorithm for both modes. The radar platform is set to have $M = 4$ transmit and $N = 3$ receive antenna elements half-wavelength spaced between each other, with moving velocity of 125 m/s. The carrier wavelength is 0.25 m, and $L = 20$ pulses are emitted in one CPI with pulse repetition frequency of 500 Hz. The target is located at $\theta_t = 10^\circ$ with Doppler $f_t = 0.13$, and the SNR is set to 10 dB. Three acceleration schemes: i) SQUAREM [24]; ii) BLSM [25]; and iii) combination of i) and ii) are used. We choose the absolute SINR difference between the current and previous iterations normalized by SNR as the stopping criterion, and set the tolerance to 10^{-8} . Unimodular sequences with random phases are used as the initialization.

We first consider the scenario of homogeneous environment where $N_r = 10$ range rings interfere with the range-azimuth bin of interest, with each separated into $N_c = 181$ azimuth bins. The Doppler information of clutter bins is known (determined by their relative radial velocities), and the clutter-to-noise ratio (CNR) for each bin is set to 40 dB. Mode I of Algorithm 1 is exploited. It can be seen from Fig. 1 that our proposed algorithm shows good SINR behaviour in terms of the convergence speed. Both the original algorithm and its accelerations i), ii), and iii) demonstrate sharp SINR improvements for few iterations, starting from an initial SINR of 4.74 dB. The corresponding improvements after the first 25 iterations have reached 3.27 dB, 3.77 dB, 4.17 dB, and 4.48 dB (with completion rates 72%, 82%, 91%, and 98% compared to the maximum achievable SINR), respectively. Among the results shown, the smallest number (around 45) of consumed iterations after convergence to tolerance is achieved by acceleration iii), while the others (original and accelerations i) and ii) consume about 510, 225, 85 iterations, respectively.

We then consider the scenario with discrete heterogeneous environment with Doppler uncertainties on clutter bins. The corresponding parameters are: $N_r = 10$, $N_c = 3$, CNR=50 dB (for each discrete bin). The spatial directions of the three clutter sources at each ring are randomly distributed within the sectors $[-50^\circ, -30^\circ]$, $[-20^\circ, 10^\circ]$, and $[25^\circ, 35^\circ]$, respectively. The Doppler uncertainty parameters are: $f_{iiv} = 0$,

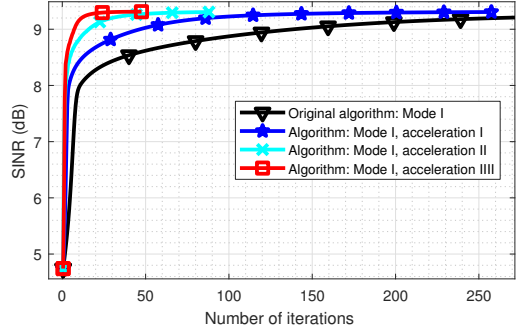


Fig. 1. SINR v.s. iterations: Example 1, cut at 270th iteration.

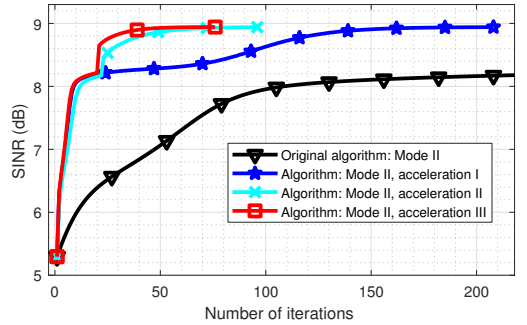


Fig. 2. SINR v.s. iterations: Example 2, cut at 220th iteration.

$\epsilon_{iiv} = 0.35$, $\forall i, i' \in \{1, 2, 3\}^2$, and Υ_{iiv} is determined by the PDF of uniform distribution (see [13]). Fig. 2 shows the corresponding SINR performance versus number of iterations consumed. It can be seen that the obtained SINRs for this scenario verify the effectiveness of our proposed algorithm. With the aid of accelerations, the obtained SINR levels are significantly improved after consuming around 10 iterations (above 8 dB), and the number of iterations has been reduced at most to about 70 (by acceleration III).

5. CONCLUSION

We have developed a novel approach for jointly synthesizing unimodular SST waveforms and MVDR-type STAP receive filter with considerations on the range sidelobe effect and Doppler characteristics. Two cases of known Doppler and presence of uncertainties on clutter bins have been considered. We have formulated the corresponding non-convex optimization problems and developed an efficient algorithm for addressing them by manipulating the composite objective of the problems and generating a minorizing surrogate containing a higher order quadratic term. Then the resulting minorized problems can be solved in closed-form via minorization-maximization technique. The proposed algorithm has low complexity, fast convergence, and it has demonstrated excellent performance throughout our simulations.

6. REFERENCES

- [1] N. Levanon and E. Mozeson, *Radar Signals*. Hoboken, NJ, USA: Wiley, 2004.
- [2] M. C. Wicks, E. L. Mokole, S. D. Blunt, R. S. Schneible, and V. J. Amuso, *Principles of Waveform Diversity and Design*. Raleigh, NC, USA: SciTech Publishing, 2010.
- [3] D. DeLong and E. M. Hofstetter, "On the design of optimum radar waveforms for clutter rejection," *IEEE Trans. Inf. Theory*, vol. 13, no. 3, pp. 454–463, Jul. 1967.
- [4] M. R. Bell, "Information theory and radar waveform design," *IEEE Trans. Inf. Theory*, vol. 39, no. 5, pp. 1578–1597, Sep. 1993.
- [5] P. Stoica, H. He, and J. Li, "New algorithms for designing unimodular sequences with good correlation properties," *IEEE Trans. Signal Process.*, vol. 57, no. 4, pp. 1415–1425, Apr. 2009.
- [6] H. Hao, P. Stoica, and J. Li, "Designing unimodular sequences sets with good correlations—Including an application to MIMO radar," *IEEE Trans. Signal Process.*, vol. 57, no. 11, pp. 4391–4405, Nov. 2009.
- [7] C.-Y. Chen and P. P. Vaidyanathan, "MIMO radar ambiguity properties and optimization using frequency-hopping waveforms," *IEEE Trans. Signal Process.*, vol. 56, no. 12, pp. 5926–5936, Dec. 2008.
- [8] Y. Yang and R. S. Blum, "MIMO radar waveform design based on mutual information and minimum mean-square error estimation," *IEEE Trans. Aerosp. Electron. Syst.*, vol. 43, no. 1, pp. 330–343, Jan. 2007.
- [9] Y. Li and S. A. Vorobyov, "Efficient single/multiple unimodular waveform design with low weighted correlations," in *Proc. IEEE Int. Conf. Acoust., Speech, Signal Process. (ICASSP)*, New Orleans, USA, Mar. 2017, pp. 3226–3230.
- [10] P. Stoica, J. Li, and M. Xue, "Transmit codes and receive filters for radar," *IEEE Signal Process. Mag.*, vol. 25, no. 6, pp. 94–109, Nov. 2008.
- [11] P. Stoica, H. He, and J. Li, "Optimization of the receive filter and transmit sequence for active sensing," *IEEE Trans. Signal Process.*, vol. 60, no. 4, pp. 1730–1740, Apr. 2012.
- [12] J. Li, P. Stoica, and X. Zheng, "Signal synthesis and receiver design for MIMO radar imaging," *IEEE Trans. Signal Process.*, vol. 56, no. 8, pp. 3959–3968, Aug. 2008.
- [13] A. Aubry, A. De Maio, A. Farina, and M. Wicks, "Knowledge-aided (potentially cognitive) transmit signal and receive filter design in signal-dependent clutter," *IEEE Trans. Aerosp. Electron. Syst.*, vol. 49, no. 1, pp. 93–117, Jan. 2013.
- [14] A. Aubry, A. De Maio, and M. M. Naghsh, "Optimizing radar waveform and Doppler filter bank via generalized fractional programming," *IEEE J. Sel. Topics Signal Process.*, vol. 9, no. 8, pp. 1387–1399, Dec. 2015.
- [15] A. Aubry, A. De Maio, Y. Huang, and M. Piezzo, "Robust design of radar Doppler filters," *IEEE Trans. Signal Process.*, vol. 64, no. 22, pp. 5848–5860, Nov. 2016.
- [16] G. Cui, X. Yu, V. Carotenuto, and L. Kong, "Space-time transmit code and receive filter design for colocated MIMO radar," *IEEE Trans. Signal Process.*, vol. 65, no. 5, pp. 1116–1129, Mar. 2017.
- [17] G. Hua and S. S. Abeysekera, "Receiver design for range and sidelobe suppression using MIMO and phased-array radar," *IEEE Trans. Signal Process.*, vol. 61, no. 6, pp. 1315–1326, Mar. 2013.
- [18] S. D. Blunt and E. L. Mokole, "Overview of radar waveform diversity," *IEEE Aerosp. Electron. Syst. Mag.*, vol. 31, no. 11, pp. 2–42, Nov. 2016.
- [19] Q. He, N. H. Lehmann, R. S. Blum, and A. M. Haimovich, "MIMO radar moving target detection in homogeneous clutter," *IEEE Trans. Aerosp. Electron. Syst.*, vol. 46, no. 3, pp. 1290–1301, Jul. 2010.
- [20] P. Setlur and M. Rangaswamy, "Waveform design for radar STAP in signal dependent interference," *IEEE Trans. Signal Process.*, vol. 53, no. 1, pp. 19–34, Jan. 2016.
- [21] S. D. Blunt, J. Metcalf, J. Jakabosky, J. Stiles, and B. Himed, "Multi-waveform space-time adaptive processing," *IEEE Trans. Aerosp. Electron. Syst.*, vol. 53, no. 1, pp. 385–404, Feb. 2017.
- [22] D. R. Hunter and K. Lange, "A tutorial on MM algorithms," *Amer. Statist.*, vol. 58, no. 1, pp. 30–37, Feb. 2004.
- [23] Y. Li and S. A. Vorobyov, "Fast algorithms for designing multiple unimodular waveforms with good correlation properties," *IEEE Trans. Signal Process.*, 2017, submitted for publication. [Online]. Available: <https://arxiv.org/pdf/1702.06821.pdf>
- [24] R. Varadhan and C. Roland, "Simple and globally convergent methods for accelerating the convergence of any EM algorithm," *Scand. J. Statist.*, vol. 35, no. 2, pp. 335–353, 2008.
- [25] J. Nocedal and S. Wright, *Numerical Optimization*, 2nd ed. New York, NY, USA: Springer, 2000.



ISBN 978-952-60-8240-0 (printed)
ISBN 978-952-60-8241-7 (pdf)
ISSN 1799-4934 (printed)
ISSN 1799-4942 (pdf)

Aalto University
School of Electrical Engineering
Department of Signal Processing and Acoustics
www.aalto.fi

**BUSINESS +
ECONOMY**

**ART +
DESIGN +
ARCHITECTURE**

**SCIENCE +
TECHNOLOGY**

CROSSOVER

**DOCTORAL
DISSERTATIONS**